

CHAPTER 1

LITERATURE REVIEW AND RESEARCH OVERVIEW

1.1. THE ENVIRONMENTAL SELENIUM PROBLEM

Selenium (*Se*) is a non-metallic element closely related to sulfur (*S*) and tellurium (*Te*) that was discovered over 200 years ago by the Swedish chemist Berzelius (Scott, 1973). It has beneficial uses in the glass industry, as an additive in brass and stainless steel to 5 improve machine-ability, and in anti-dandruff shampoo.

Se is an essential micro-nutrient in humans whose essentiality in mammals was discovered in 1957 (Schwarz and Foltz, 1957). It is necessary in some proteins, participates in antioxidant defense, is involved in thyroid hormone metabolism, and others. Not all human biological processes involving *Se* have been completely identified or understood (Navarro-10 Alarcón and López-Martínez, 2000; Rayman, 2000; Roman et al., 2014). Clinical trials are being performed based on the evidence that *Se* might be used as a cancer treatment or preventative or even to counteract the progression of HIV to AIDS (Rayman, 2000; Roman et al., 2014).

Se Toxicity.

The US Department of Agriculture (USDA) and the World Health Organization (WHO) both have recommended daily allowances (RDA) of approximately $20 \mu\text{g d}^{-1}$ to 15 $55 \mu\text{g d}^{-1}$ (age and gender dependent) which is the generally accepted minimum needed to prevent the onset of Keshan's disease, a type of congestive heart disease (USDA and US-DHHS, 2010; World Health Organization et al., 1996). Large *Se* doses are toxic (Navarro-20 Alarcón and López-Martínez, 2000; Roman et al., 2014) with EPA human health limits set at $4200 \mu\text{g L}^{-1}$ (USEPA, 2009). Less than toxic concentrations are known to cause adverse

health effects on the endocrine system, immune system, skin, nails, and hair. There are scattered places in the word where selenosis, or *Se* poisoning, affects mammals. The Hubei Province in China is the only location where natural human *Se* toxicity occurred (Spallholz and Hoffman, 2002).

5 *Se* toxicity is due partially to its ability to replace sulfur in many organic and inorganic compounds (Besser et al., 1989). *Se* accumulating plants, such as *Astragalus*, prince's plume, and some woody asters, may accumulate *Se* in concentrations up to 3000 mg kg⁻¹ of plant mass. These plants are not palatable by most grazing animals. The presence of these plants may promote nearby forage plants to accumulate more *Se* (USDA, Agricultural Research 10 Service, 2006). As early as 1934, *Se* was found to cause deaths and illnesses in livestock that eat high *Se* (Besser et al., 1989; Rohwer, 1931; Scott, 1973; USDA, Agricultural Research Service, 2006). Cows are more resistant to *Se* toxicity with fatal doses at 11.0 mg kg⁻¹ of body weight, while the fatal dose for horses is less than 4.4 mg kg⁻¹ of body weight (Painter, 1940). *Se* in fodder with doses between 5 mg kg⁻¹ to 40 mg kg⁻¹ of fodder weight 15 for long periods, can cause chronic poisoning in cows, also known as alkali disease (USDA, Agricultural Research Service, 2006).

Se is toxic to aquatic birds, primarily affecting reproduction. A study of aquatic birds and nests at Kesterson National Wildlife Refuge in California found embryo death rates at approximately 50% for some species. Of the eggs that hatched, many of the chicks 20 suffered from major abnormalities including skeletal and major organ defects. Selenium analysis of affected eggs found concentrations between 2.2 mg kg⁻¹ to 110 mg kg⁻¹ dry weight. Compared to the same species living in an area not affected by Se, birds living on Kesterson had *Se* concentrations 20 times higher and food organisms had *Se* concentrations about 12 to 130 times greater (Ohlendorf et al., 1986). In one controlled study it was found that

Se concentrations in feed as low as 8 mg kg^{-1} dry weight caused embryo malformations to increase by approximately 1% and concentrations at 10 mg kg^{-1} causing a 68% increase (Spallholz and Hoffman, 2002).

Se toxicity is also found in fish (Gillespie and Baumann, 1986; A. Lemly and G.

5 Smith, 1988), but the specific level is dependent on the species of fish and habitat. Besser et al. (1989) found that Selenomethionine, an organic *Se* compound, is preferentially bio-accumulated compared to selenite (SeO_3^{2-}) or (SeO_4^{2-}). This lead to their hypothesis that organic *Se* compounds may contribute disproportionately to toxicity in aquatic organisms.

At $1\text{ }\mu\text{g L}^{-1}$ to $5\text{ }\mu\text{g L}^{-1}$, *Se* can bio-accumulate in aquatic food-chains and become a concentrated, toxic, dietary source for fish. The additional strain of cold winters increases the mortality of *Se* contaminated fish (A. Dennis Lemly, 1993).

While not a widespread problem, there are areas in the world that have to deal with either *Se* deficiency or excess. Australia introduced *Se* supplements to improve livestock

health in the late 1970's and at the same time had some regions where *Se* toxicity has been

15 reported as the result of livestock feeding on *Se* accumulative plants. New Zealand has had to import Se-enriched Australian wheat to combat *Se* deficiencies in their population (Thomson and Robinson, 1996; Tinggi, 2003). In 1969, Finland had to enrich animal feeds with *Se* and in the early 1980's they introduce high-Se wheat to increase *Se* uptake in the diet of their population. China has seen the worst *Se* poisoning between 1961 and 1964 in

20 the Hubei Province. These were drought years that forced villagers to eat more vegetables and corn grown in high *Se* soil and less protein. During these years, the morbidity in the affected villages was almost 50% (Yang et al., 1983).

Issues with *Se* deficiency in the U.S. at the commercial level were first noted in turkey flocks in Ohio where there was a high mortality rate in chicks at 5-6 weeks of age (Scott et al.,

1967). Lambs and calves in the eastern U.S. suffered from nutritional muscular dystrophy. Supplementing the diet of the parent animal with *Se* concentrations as low as 0.1 mg kg^{-1} to 0.2 mg kg^{-1} of total diet prevented these defects . Even in 1973, the U.S. Food and Drug Administration (F.D.A.) was resistant to requests from livestock producers to add *Se* to the 5 diets of their livestock due to the claim that *Se* was a carcinogen (Scott, 1973). This claim has since been refuted and since 1974 *Se* is a required additive to the feed for livestock in the U.S (L. Jensen, 1999).

Se Toxicity in the Environment.

Se toxicity in the U.S. became a national issue at Kesterson Reservoir in the San 10 Joaquin Valley, California. While not the first incidence of *Se* toxicity in the U.S. it was the most publicized. Here, the inflows changed from primarily fresh water in 1978 to primarily irrigation runoff by 1981. This highly saline water carried the mobile SeO_4^{2-} which bio-accumulated in the fish and birds (Besser et al., 1989). In the years after the change in water source, the ecology of the reservoir changed such that the only fish and birds that 15 survived were those that were highly salt-tolerant. This was evident by frequent mass fish kills, disappearing waterfowl, and disfigured waterfowl (Clifton and Gilliom, 1989; Hamilton and A. Lemly, 1999; A Dennis Lemly, 2002; Saiki et al., 1993).

Various lakes and still water bodies have high *Se* concentrations. The Chesapeake Bay and estuary has recorded high *Se* concentrations due to irrigation runoff. While their 20 concentrations are low at approximately $0.15 \mu\text{g L}^{-1}$, the values are higher than the ocean water outside of the estuary (Takayanagi and Wong, 1984). The San Francisco Bay and Delta receive approximately 15,000 to 45,000 pounds of *Se* per year from various sources. These sources are primarily outflows from the California Central Valley which is one of the largest

agricultural centers in the United States (Luoma et al., 2000). Rainwater runoff was found to be a significant source of *Se* in two watersheds in Maryland (Lawson and Mason, 2001).

The Great Salt Lake, among it's other issues, has *Se* concerns with concentrations up to $1.68 \mu\text{g L}^{-1}$. The Great Salt Lake does remove *Se* through sedimentation and volatilization
5 at rates greater than 1,900 kg/year (Naftz et al., 2008; Oliver et al., 2009)

The Arkansas River is not the only river contaminated with *Se*. Belews River in North Carolina was contaminated with *Se* from a coal fired power plant disposing of ash waste into the river. *Se* concentrations in the river are still high 10 years after the source was removed. This shows that *Se* sources are persistent and decay slowly (A Dennis Lemly, 2002). The
10 San Joaquine River in California has *Se* concentrations at 286 to 869 mg L^{-1} (Clifton and Gilliom, 1989). Multiple studies have been performed in the San Joaquine River Valley to find efficient methods for removing *Se* from agricultural waters. A mass balance study of the Imperial and Brawley constructed wetlands have shown removal rates of 56-70% with volatilization estimated between 17-50% (Gersberg, 2006).

15 High *Se* levels in Colorado are of primary concern in the Lower Colorado River, Fountain Creek, Segments of the Upper Yampa River, North Fork of the Gunnison River, Lower Gunnison River, Upper South Platte River, and Lower Arkansas River. The largest impacts are seen on the Colorado, Gunnison, and Arkansas Rivers (State of Colorado, 2012).

The Gunnison River in Colorado has *Se* concentrations up to $25 \mu\text{g L}^{-1}$ (USBoR, 2008).
20 Donnelly and Timothy K. Gates (2005a) estimated *Se* returns to the Arkansas River in the LARV at $15.6 \text{ kg yr}^{-1} \text{ km}^{-1}$. The sources in the Donnelly study included groundwater and surfacewater returns.

Se Regulation in the United States.

The U.S. Federal and several state governments have moved to study and reduce the effects of *Se* toxicity. Shortly after the change in the Kesterson Reservoir ecology was evident, studies were initiated by the EPA to determine the cause. *Se* was considered one of 5 the major toxic factors. The National Irrigation Water Quality Prog (NIWQP) was initiated shortly thereafter to determine the concentrations of potentially toxic constituents, especially Se, in water, bottom sediment, and biota due to irrigation water runoff at multiple sites in the U.S. (Hamilton and A. Lemly, 1999). The current EPA aquatic life criteria chronic level for *Se* was set in 1990 at $5.0 \mu\text{g L}^{-1}$ (USEPA, 2009). The new draft criteria are under 10 consideration for *Se* that will redefine the criteria for still and moving water, lentic and lotic respectively, not acute and chronic as currently defined. The draft criteria are proposed to be set at $1.3 \mu\text{g L}^{-1}$ and $4.8 \mu\text{g L}^{-1}$ for still (lentic) and moving (lotic) water, respectively (Hamilton and A. Lemly, 1999; USEPA, 2009, 2014b).

Colorado and Kansas has set limits on *Se* concentrations that meet or exceed those 15 currently set by the EPA. Colorado's state wide limits for *Se* are $18.4 \mu\text{g L}^{-1}$ and $4.6 \mu\text{g L}^{-1}$ for acute and chronic conditions, respectively (State of Colorado, 2013). Each major river basin in Colorado has an additional regulation modifying the standards for specific stream segments. The chronic and acute condition standards for the entire Arkansas River are 5 $\mu\text{g L}^{-1}$ and $20 \mu\text{g L}^{-1}$, respectively, which reflects the standards set in 1995 to account for 20 the higher than average groundwater *Se* concentration. The USR and DSR have amended chronic condition standards of $16 \mu\text{g L}^{-1}$ and $19 \mu\text{g L}^{-1}$, respectively. These standards were emplaced to reflect existing *Se* concentrations exceeding the Arkansas River chronic standard of $5 \mu\text{g L}^{-1}$ (State of Colorado, 2014). Colorado and Kansas have identified *Se* pollution as an issue of concern and have included it on their 303(d) lists which identify which water bodies

are contaminated and the level of impact (Kansas Department of Health and Environment, 2014; State of Colorado, 2012).

1.2. MAJOR *Se* CYCLE PROCESSES IN THE ENVIRONMENT.

Se Sources.

5 As usual with most environmental contaminants, in the eyes of the public, the sources of greatest concern are industrial. Industrial sources include coal mining and combustion. Coal-fired power plants are of special concern because they concentrate the *Se* in the ash. Power plants that do not collect or or incorrectly dispose of ash run the risk of contaminating the environment with high does of *Se* (A Dennis Lemly, 2002). In fact, the same
10 technology that was implemented to reduce power plant emissions has increased the volume of *Se* enriched ash. Some of this ash is used in the concrete manufacturing industry. The EPA has reported the release of *Se* from fly ash concrete is immeasurable (USEPA, 2014a). Other sources include oil refinery waste, mining various precious and semi-precious minerals, and agricultural drainage.

15 *Se* is naturally occurring, and as such contamination of soils and waterways can be from completely natural causes. Such was the case with the *Se* poisoning in China. The *Se* came from coal deposits containing *Se* concentrations up to $80\,000 \mu\text{g g}^{-1}$ (ppm). These deposits were weathered and deposited large quantities of *Se* into the soil. Conditions were exacerbated by the villagers overuse of lime as a fertilizer (Yang et al., 1983).

20 Agricultural drainage is the *Se* source that is the least regulated. Power plants are required to meet requirements and are monitored by various regulatory agencies. This is because they have control over the concentration of *Se* from fly ash and its eventual disposal. Agricultural sources are not regulated by the quantity of *Se* discharged from fields because,

in most cases in the U.S., *Se* is not applied to the fields. In these cases, *Se* is naturally occurring and is released from the parent rock through oxidation reactions.

Major Environmental Processes.

With agricultural drainage, there are four major processes involved in the *Se* cycle:

- 5 reduction-oxidation reactions, sorption-desorption, biological uptake-decomposition, and volatilization. All processes are bi-directional, meaning, given the right conditions, a given process is reversible. Volatilization is reversible through *Se* dust deposition or *Se* contaminated rainfall, but these pathways have not been studied in the LARV (Lawson and Mason, 2001).

Figure 1.1 is a simple depiction of the *Se* cycle in a groundwater system.

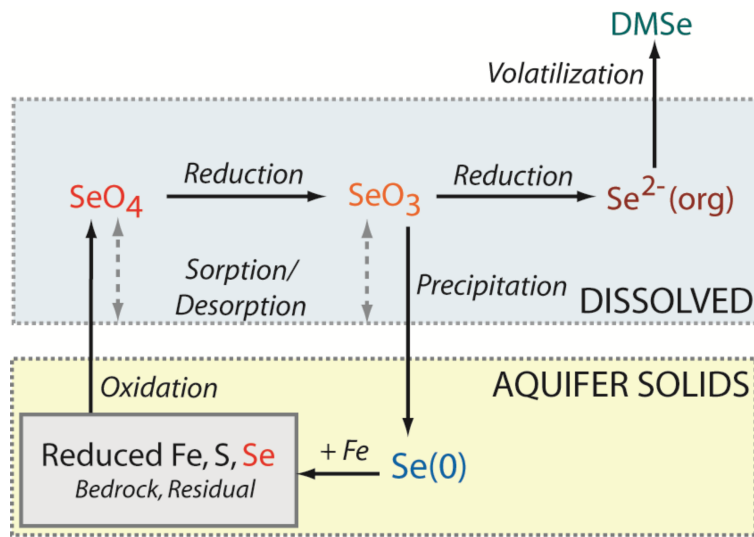


Figure 1.1. Oxidation-reduction transformations of *Se* species in a soil and groundwater system (Ryan T Bailey et al., 2012). DMSe, dimethyl-selenide.

- 10 This diagram become much more complicated once the nitrate (NO_3^{2-}) cycle is included as shown in Figure 1.2. This figure does not include volatilization pathways. NO_3^{2-} is primarily added to the system through fertilizers. The three primary commercial fertilizer components; nitrogen (*N*), PO_4^{3-} , and potash (K_2O) are found in various mixtures. Nitrogen, which includes NO_3^{2-} , ammonia, and other nitrogen bearing compounds, promotes plant

stem and leaf growth. PO_4^{3-} promotes plant root growth. K_2O promotes overall plant health. N is also introduced through the decomposition of plant roots and stems after harvest and through the application of manures (Ryan T Bailey et al., 2012).

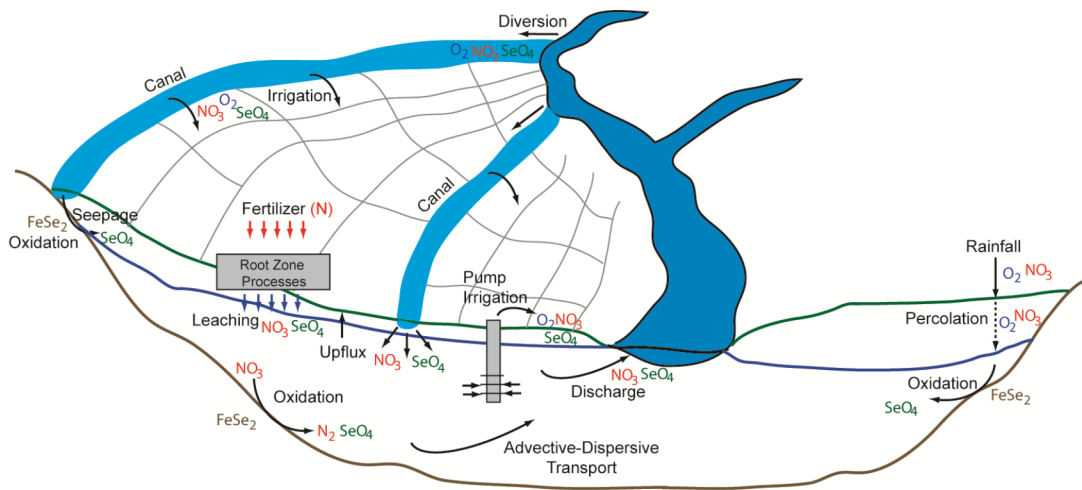


Figure 1.2. Conceptual model of the fate and transport of O_2 , NO_3^{2-} , and SO_4^{2-} in an irrigated stream-aquifer system subject to agricultural activities (e.g., irrigation and fertilizer loading) (Ryan T Bailey et al., 2012). Volatilization is not included in this diagram. The blue line denotes the water table, the green line is the ground surface.

Reduction-Oxidation Reactions

5 Reduction-oxidation (redox) reaction are the primary reaction method in groundwater and surface waters. Dissolved oxygen (O_2) and NO_3^- from fertilized fields leach into the groundwater table. O_2 is introduced into surface and groundwaters from the partial pressure of O_2 in the atmosphere. O_2 is consumed first in all oxidation reactions and usually does not last long enough to leach to the bedrock. The NO_3^- persists longer in the groundwater
10 and eventually moves, through advection and dispersion processes, to come in contact with the Se bearing parent bedrock. The NO_3^- oxidizes the Se , causing it to transform to the soluble and weekly adsorbing SeO_4^{2-} species.

Table 1.1 shows Se's common oxidation states and forms present in soils. Other oxidation states and forms exist, but are not common. Iron selenite is the most common form with very little elemental *Se* is found in soil and a wide range of organic *Se* compounds present (Painter, 1940).

Table 1.1. Selenium Oxidation States and Common Forms Present in Soil.

Oxidation State	Form	
	Name	Formula
6	selenate	SeO_4^{2-}
4	selenite	SeO_3^{2-}
0	elemental	Se
multiple	organic	multiple

For *Se* to move out of the SeO_4^{2-} species, all O_2 , NO_3^{2-} , and other strong oxidizing agents must be consumed from the water and the pH must be fairly high. Figure 1.3 is a Pourbaix diagram of *Se* which maps out the possible stable phases of *Se* in an aqueous system. The bottom scale is the pH range, the left side scale (pe) is the concentration of the standard reducing agent, the electron (e^-). The right side scale (Eh (V)) is the oxidation-reduction potential expressed in units of volts (V). The diagram shows that elemental *Se* converts to the SeO_4^{2-} species in low to moderate oxidizing environments along the spectrum of pH values that are common for surface and groundwaters. For SeO_4^{2-} to convert to the SeO_3^{2-} species, the pH will have to be higher and the oxidation potential fairly low. These conditions are not common in the groundwaters in the LARV.

Based on a Pourbaix diagram, in any given aqueous system, any number of the species combinations should exist based on chemical kinetics and reaction rates. The Pourbaix diagram does not include rate or kinetic limits between species. SeO_4^{2-} is kinetically limited for reduction to SeO_3^{2-} . This transformation is mediated by microbial processes (Lalvani, 2004). Some of these microbial processes have been recommended for *Se* remediation at

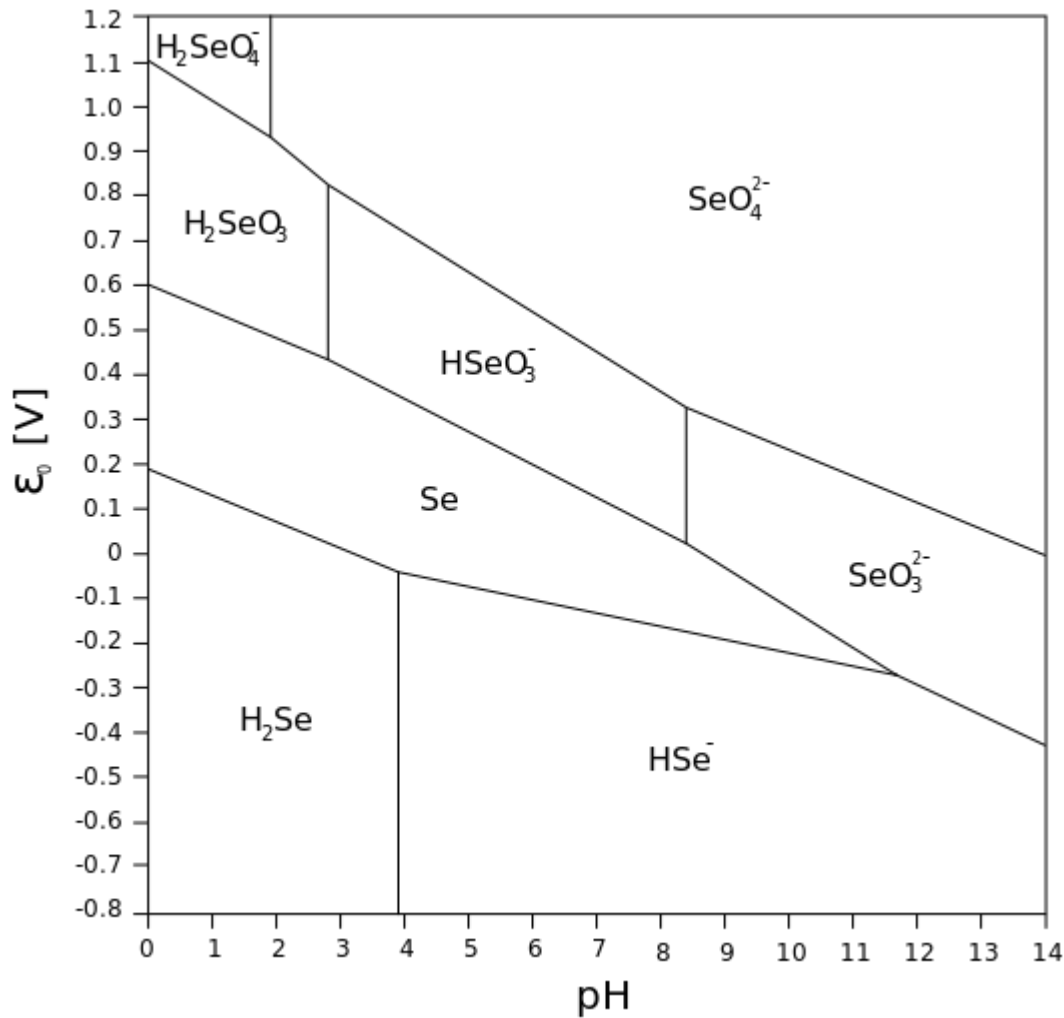


Figure 1.3. Selenium Pourbaix diagram.

mining sites (MSE Technology Applications, Inc., 2001). The magnitude of SeO_4^{2-} reduction via microbial processes in the LARV has not been studied.

Sorption Processes.

The second primary fertilizer, PO_4^{3-} , is a significant contributor to preventing the sorption of SeO_3^{2-} to soil particles. PO_4^{3-} is preferentially adsorbed due to its affinity for iron and aluminum at lower pH values and calcium at higher pH values, all three of which are present in clays common in the LARV. Besser et al. (1989) noted that, Se was more rapidly sorbed in fine-textured, highly organic pond sediments than sandy riverine sediments. Since

sandy sediments are primarily silica, which is a very weak adsorber, it follows that river sediments are not good adsorbers of either PO_4^{3-} or SeO_3^{2-} (Oram et al., 2008).

Biological Uptake of Se .

Biological uptake by plants is a major contributor to *Se* cycling. *Se* taken up as

5 SeO_4^{2-} by plants is stored in the stems and leaves. There is very little reduction of SeO_4^{2-} to SeO_3^{2-} or organic *Se* within the plant. The SeO_4^{2-} is then re-cycled into the system with the decomposition of the leaves that fall every year. This temporary storage of *Se* may serve as a buffer to the system. However, *Se* taken up as SeO_3^{2-} is not stored. It is converted to organic *Se* which is volatilized through plant transpiration processes. Besser et al.
10 (1989) noted that organic *Se* compounds were lost from the water column more rapidly than other *Se* species. The presence of sulfates in concentrations less than 80 mg L^{-1} promotes an increase in *Se* bio-accumulation and concentrations greater than 180 mg L^{-1} decreased *Se* uptake by organisms.

Se Volatilization

15 Volatilization of *Se* is through two possible pathways: chemical and biological. Chemical volatilization is very slow, as noted by Besser et al. (ibid.), when analysis of their sterile control groups reported no loss of *Se*. Biological pathways are again the preferred path for reduction of SeO_4^{2-} and SeO_3^{2-} to volatile organic *Se* species. A *Se* volatilization study per-

formed in California's Imperial Valley constructed wetlands showed that most of the *Se* was
20 retained in the sediments. These sediments are the fine-textured, highly organic type noted by Besser et al. (ibid.). Of the remaining *Se*, less than 1% was accumulated in plant tissues. This left 33-50% of the remaining *Se* unaccounted for. Gersberg (2006) reasoned that this unaccounted for *Se* was lost through volatilization. Other constructed wetland studies have

reported up to 69%. The constructed wetlands assessed in this study retained *Se* bearing water for approximately 18 days before discharging it back to the New River. The wetlands were planted with bulrush (*Schoenoplectus californicus*), tamarisk (*Tamarix spp.*), and wild grasses (Gersberg, 2006; P. I. Johnson et al., 2009).

5 The use of tamarisk is of special note with the study in this thesis because this plant, along with Russian olive (*Elaeagnus angustifolia*) is an invasive species that has overtaken much of the riparian area along the Arkansas River in Colorado (Nagler et al., 2010). Tamarisk has also been shown to perform as an effect pollutant accumulator (Sorensen et al., 2009). Table 1.2 is a summary of the common *Se* species and their characteristics in an
10 aqueous environment.

Table 1.2. Characteristics of *Se* Species.

<i>Se</i> Species	Oxidation State	Soluble	Adsorption	Oxidizing Conditions	Reducing Conditions	Toxic
Selenate	+6	yes	weak	Present	Absent	yes
Selenite	+4	yes	strong	Present	Absent	no
Selenium	0	no	none	Absent	Present	no
Selenide	-2	no	none	Absent	Present	yes

1.3. WATER BALANCE METHODS FOR ESTIMATING NPS RETURN FLOWS TO STREAMS

There are two basic water balance model types: regional and general. In the US, regional models consist primarily of the Thornthwaite-Mather, Palmer, and Thomas abcd models. The Thornthwaite-Mather model accounts for a regional water balance on a monthly
15 accounting procedure using the mean monthly temperature, monthly total precipitation, and the latitude of the region (Thornthwaite and Mather, 1955). This model takes into account snowfall and soil storage within the region of interest. The Palmer and Thomas abcd models are enhancements to the Thornthwaite-Mather model (Palmer, 1965; Thomas et al., 1983).

These methods are not valid for the water balance models generated in this thesis which is only concerned with the water contained in the river channel.

General water balance models use the general water balance equation (Equation 1) as a starting point and attempt to account for all gains and losses to the system. The general
5 model is well suited to systems where a large portion of the gains and losses are measurable or estimable. It is also applicable to use in studying soil, groundwater, atmospheric, and other systems. The model is not limited to natural systems as it is used in municipal and industrial mechanical system water balances.

$$\Delta S = \sum gains - \sum losses \quad (1)$$

1.4. MASS BALANCE METHODS FOR ESTIMATING NPS SOLUTE LOADING TO STREAMS

10 The general form of the mass balance model is based on the water balance model with the assumption that the mass is conservative. That is, the mass being modeled is not consumed or generated within the system boundary. The chemical mass balance approach has been used extensively to study the in-stream reactions and sediment dynamics of multiple natural and industrial materials (Christophersen and Wright, 1981; Elder, 1985;

15 Jain, 1996; Latimer et al., 1988; Plummer and Back, 1980; Yuretich and Batchelder, 1988).

Jain (1996) used monitoring points along a 25 km stretch of river to determine the effects of multiple industrial sites discharging dissolved and suspended metal into the river. These industries discharged into the main channel via direct addition to the river channel, addition to tributaries. Agricultural discharge was identified as the major non-point contributor.

20 McMahon and Woodside (1997) calculated the mass balance of nitrogen and phosphorus in eight sub-basins to determine the importance of agricultural non-point sources to

nutrient loading in a drainage basin encompassing large portions of the states of Virginia and North Carolina. They found that the highest in-stream loads were measured in agricultural drainages with point loads contributing approximately 3% of the total load.

Gersberg (2006) used mass balance methods to study the unloading of *Se* from the 5 Imperial Constructed Wetlands Demonstration Project in Southern California. This project is being used to determine the effectiveness of wetlands in remediating *Se* polluted waters from agricultural runoff. Two sub-sites were studied and removal rates of 56% and 70% were calculated based on a mass balance model which included monitoring the influx and out-flux of the sites and measuring the soil concentration over time. They found that between 33% 10 and 50% of the *Se* was lost to volatilization.

1.5. PREVIOUS RELATED STUDIES IN COLORADO's LOWER ARKANSAS RIVER VALLEY

The first significant *Se* study performed by Colorado State University determined that there was a multi-variate linear relationship between in-stream dissolved *Se* concentration and concentrations of SO_4^{2-} and NO_3^{2-} . This study also verified that *Se* was a significant 15 contaminant in the Downstream Study Region (DSR) of the Lower Arkansas River Valley (LARV) with in-stream concentrations between $1.6 \mu\text{g L}^{-1}$ to $43.2 \mu\text{g L}^{-1}$ (median concentration of $11 \mu\text{g L}^{-1}$) and alluvial groundwater concentrations between $<0.4 \mu\text{g L}^{-1}$ to $166 \mu\text{g L}^{-1}$ (median concentration of $11 \mu\text{g L}^{-1}$). They also determined that the *Se* was most likely originating from shale derived soils with groundwater concentrations between $<0.4 \mu\text{g L}^{-1}$ to 20 $3760 \mu\text{g L}^{-1}$. They performed a mass balance analysis over a one-year period and determined that approximately $15.6 \text{ kg km}^{-1} \text{ yr}^{-1}$ of *Se* returned to the Arkansas River. They estimated that 1086 kg yr^{-1} of *Se* was discharged from the river into irrigation canals and 959 kg yr^{-1} of *Se* was returned to the river (Donnelly and Timothy K. Gates, 2005b).

In a following study, Herting and Timothy K. Gates (2006) verified the in-stream and groundwater *Se* concentrations. They also took dissolved uranium (*U*) samples and found a linear relationship between dissolve *Se* and dissolved *U* in the groundwater which led them to conclude that the dissolved *Se* and *U* originated from marine shales. From these results,
5 they were able to generate a map of the region that identified the location of the *U* and *Se* rich shales in the DSR.

Mueller-Price and Timmothy K. Gates (2008) found that changes in stored dissolved *Se* in the river channel were "a major contributing factor to the calculation of NPS loads". They calculated the coefficient of variation (CV) of the DSR *Se* loads at 0.23. The CV
10 was used to describe the range of uncertainty associated with the models. They developed a stochastic model for the DSR Se mass loading and used Monte Carlo simulation techniques. They found the stochastic mean *Se* loading to the main stem of the DSR was $0.028 \text{ kg km}^{-1} \text{ d}^{-1}$, compared to the deterministic model mean of $0.038 \text{ kg km}^{-1} \text{ d}^{-1}$.

Timothy K. Gates et al. (2009) expanded the *Se* groundwater study to include the
15 Upstream Study Region (USR) in the LARV and found concentrations averaging about $57.7 \mu\text{g L}^{-1}$ for the USR and $33.0 \mu\text{g L}^{-1}$ for the DSR. They also identified relationships between the locations of *Se* concentrations and shale outcroppings, between dissolved *Se* and dissolved solids in the groundwater, between dissolved *Se* and *U*, and between dissolved
19 *Se* and NO_3^{2-} . Of particular note was their finding of the degree to which dissolved *Se* depends on oxidation and inhibited reduction which indicated prospects for reducing dissolved *Se* through
20

In a separate study, Miller et al. (2010) analyzed dissolved solids, dissolved *Se* , and dissolved *U* concentrations in surface water along the main stem of the Arkansas River from the headwaters near Leadville, Colorado, to the USGS gauge in Coolidge, Kansas, which is

near the Colorado-Kansas state line. They found that the in-stream *Se* concentration increase occurred upstream of Pueblo Reservoir. The variability in dissolved *Se* concentrations did not increase significantly between Avondale and Las Animas. They did find the highest instantaneous dissolved *Se* loads in the reach downstream of Fountain Creek and to Avondale. Instantaneous loads decreased from Avondale to the Catlin Canal diversion dam and then remained fairly constant to Coolidge, Kansas.

In his Ph.D. thesis, Cody (2010) found groundwater *Se* concentrations at $59.9 \mu\text{g L}^{-1}$ and $33.2 \mu\text{g L}^{-1}$ in the USR and DSR, respectively. He found that *Se* is "Strongly and significantly correlated with" many of the dissolved constituents in the groundwater. He also confirmed the correlation between the distance from *Se* and *U* bearing marine shales to the sample wells. He found that NO_3^{2-} is a significant contributor to *Se* dissolution from the marine shales through oxidation processes.

Ryan T Bailey et al. (2012) created a groundwater model to determine the effect of policy changes to groundwater *Se* concentrations . They found that by reducing NO_3^{2-} loads to the aquifer, *Se* loads to the Arkansas River could be greatly reduced. Another study found correlations between *Se* and specific conductivity in the two regions of the LARV discussed in this thesis. Non-linear estimating equations using power functions were developed for *Se* concentration in ground and surface water from specific conductivity (Cody, 2010).

1.6. GOALS AND OBJECTIVES OF THIS STUDY

The overall goal of this study is to estimate the magnitude, variability, and uncertainty of volumetric rates and dissolved *Se* loads in non-point source (NPS) groundwater return flows to two representative reaches of Colorado's Lower Arkansas River. The study is conducted at regional scales, i.e. along river reach lengths of tens of kilometers fed by

irrigated alluvial lands with areas of thousands of hectares, and addresses daily average return flow rates and *Se* loads from these lands. The aim is to describe current conditions in the irrigated stream-aquifer system and to provide support for the development of models for predicting the prospects for reducing return flow rates and *Se* loads through the use of 5 alternative land and water best management practices. The specific objectives of this study are as follows:

- (1) Develop and use a deterministic model to estimate the return water flow from unaccounted for non-point sources to the main channel of the Arkansas River.
- (2) Develop and use a deterministic model to estimate the return *Se* mass loading to 10 the main channel of the Arkansas River.
- (3) Develop and use a stochastic model to estimate the return flow and the uncertainty of the return flow from unaccounted for non-point sources to the Arkansas River using Monte Carlo simulation methods
- (4) Develop and use a stochastic model to estimate the return *Se* mass loading and the 15 uncertainty of the return *Se* mass loading from unaccounted for non-point sources to the Arkansas River using Monte Carlo simulation methods
- (5) Determine the sensitivity of the models to the various input variables.

This study does not address all of the major *Se* cycle processes. Chemical and biologically assisted *Se* volatilization, *Se* storage and chemistry within soil pore water, and 20 *Se* transport with suspended and bed sediments is not covered. It is our hope that the results of this study may justify studying some or all of these processes within river systems such as the Lower Arkansas River Valley.

CHAPTER 2

STUDY REGIONS

2.1. OVERVIEW OF THE LOWER ARKANSAS RIVER VALLEY IN COLORADO

The Upstream Study Reach (USR) extends from just west of Manzanola to near Las Animas and is representative of the hydrology, soil, crop, and irrigation conditions upstream of John Martin Reservoir. The Downstream Study Reach (DSR) is representative of the 5 conditions downstream of John Martin Reservoir. It extends from Lamar to the Colorado-Kansas state line. Both study reaches are located in the LARV which starts at the outlet of Pueblo Reservoir, approximately 10.5 km (6.5 mi) miles west of Pueblo, Colorado and extends into Kansas. This study is only concerned with the portions of the Arkansas River and LARV in Colorado. All portions of the LARV in Colorado are within Division 2 of the 10 Colorado Department of Water Resources (CDWR). Division 2 offices are located in Pueblo, Colorado. The CDWR is the state agency responsible for the legal administration of all surface and sub-surface waters in the State of Colorado. Figure 2.1 shows the location of the LARV, USR, DSR, and adjacent irrigated valley lands that contribute to the non-point source (NPS) return flows and loads to the study reaches in this thesis.

15 *Regional Geology of the LARV.*

The LARV is wide, with widths up to approximately 20 km (12.5 mi), but shallow with maximum elevation differences approaching 130 m (425 ft). The un-confined aquifer sits in alluvium made of a series of late Cambrian to Tertiary sedimentary formations (Darton, 1906). The bedrock underlying the alluvium consists primarily of marine-derived shales of 20 the Pierre, Niobrara, Carlisle, and Graneros series and limestones for most of the valley. As the river nears the Colorado-Kansas border, the bedrock is Dakota sandstone (Moore and

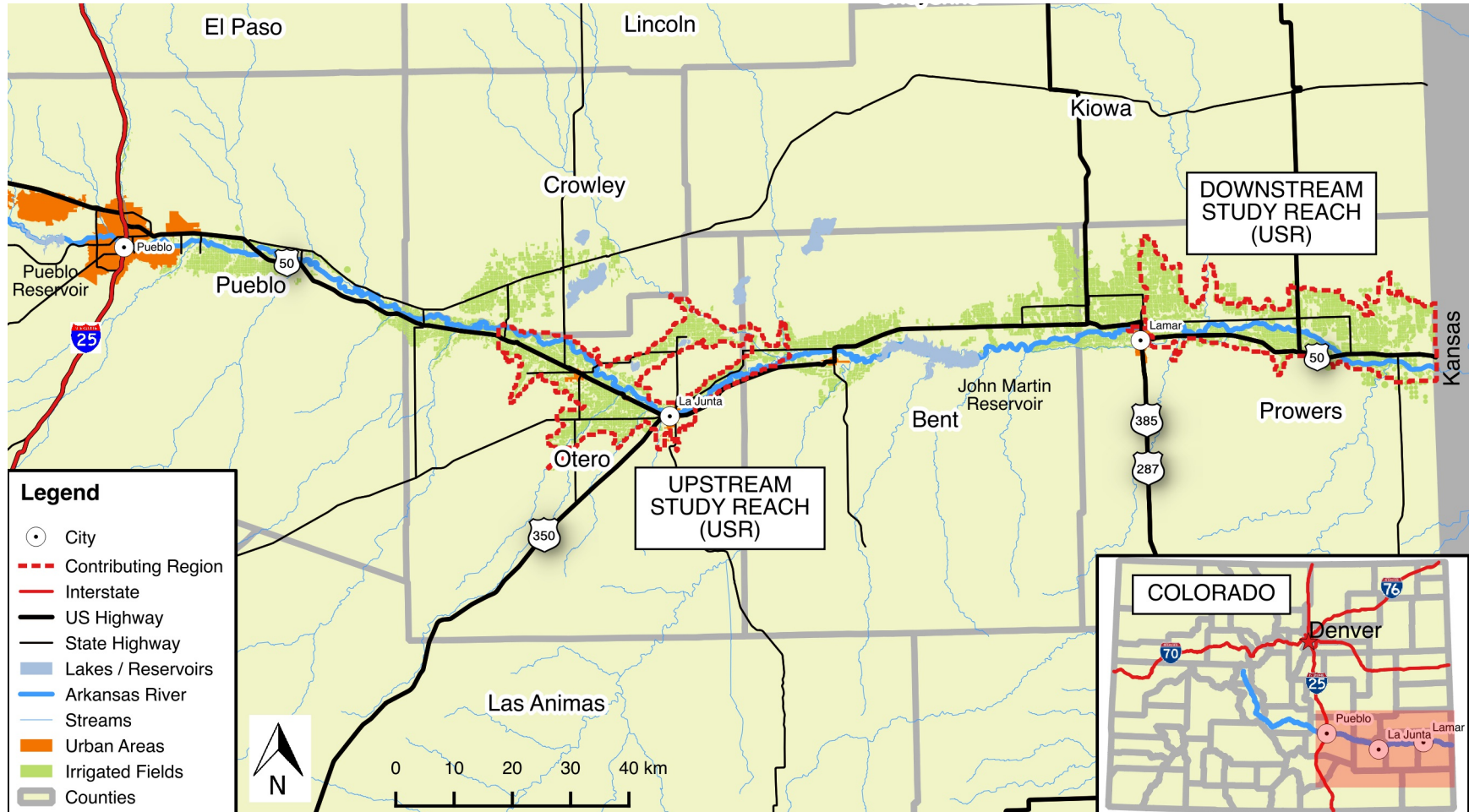


Figure 2.1. Lower Arkansas River Valley.

Wood, 1967) . The river is characterized as a shifting sand channel that meanders along the alluvial flood plain which is incised into the flood way. The alluvial aquifer and the Arkansas River and its tributaries have a strong hydraulic connection with the Arkansas River (Konikow and Bredehoeft, 1974).

5 Evidence indicates that the marine-derive shale bedrocks that underly most of the LARV and their weathered residuum yield a variety of salts, Se, and U under the dissolving action of natural and irrigation flows (Ryan T Bailey et al., 2012; Timothy K. Gates et al., 2009; Zielinski, Sigrid Asher-Bolinder, et al., 1995; Zielinski, Asher-Bolinder, et al., 1997). In the US, selenium is readily abundant in some, but not all areas west of the western Dakotas, 10 Nebraska, Kansas, and Oklahoma to the west cost (Painter, 1940). Figure 2.2 is a set of geochemical distribution maps developed by the U.S.G.S. Mineral Resources Program that shows the distribution of Se in the conterminous U.S. in the 0 cm to 5 cm layer, the top soil (A horizon) layer, and the parent rock (C horizon) layer (D. B. Smith et al., 2014).

Regional Climate and Hydrology of the LARV

15 Regionally, the climate is arid with large temperature fluctuations. Most of the rainfall comes during the growing season in the form of heavy thunderstorms. Summers are hot with an average high temperature of 93°F (34°C) and winters are cold, with an average low temperature of 14°C –10°C. Snowfall is usually light, but is prone to drifting with the low humidity and moderately high velocity, steady winter winds.

20 The historic stream flows show considerable seasonal variability. Most of the total annual flow is influenced primarily by snow melt and runoff in the Upper Arkansas River

Basin, above Pueblo Reservoir. Additionally, groundwater base flow, runoff from precipitation events in the Eastern Colorado plains, and releases from Pueblo and John Martin Reservoirs in compliance with operational rules contribute to flow rates (Miller et al., 2010).

Average annual precipitation within the LARV ranges between 31.52 cm (12.41 in) in
5 Pueblo, and varies eastwardly to 39.65 cm (15.61 in) in Holly. Figure 2.3 is a map of the LARV
with the Average Annual Precipitation from 1981 - 2010 as reported by the U.S.D.A N.R.C.S.
Average reference ET (ET_{Ref}) during the irrigation season (15 March - 15 November) is 1.3 m
(4.25 ft) based on data collected from CoAgMet weather stations over the period 1992 - 2008
(Clifford and Doesken, 2009). The Arkansas River riparian zone in the flood way is primarily
10 characterized by heavy growth of Russian Olive (*Elaeagnus angustifolia*), multiple species of
salt cedar (*Tamarix*), willows and other non-native species that are major contributors to
regional evapo-transpiration (ET) losses (Nagler et al., 2010).

Anthropogenic Factors for the LARB Study Regions.

Historically, prior to the advent of irrigated agriculture in the Ark River Basin during
15 the 19th century, groundwater recharge in the basin occurred primarily from infiltration
of precipitation through the unsaturated zone and from infiltration of surface water from
losing streams. By mid-1880s, the waters of the Arkansas R. and its tributaries were fully
appropriated for normal or average years (Abbott, 1985). In areas where surface water was
diverted for irrigation, infiltration of irrigation water from canals and fields became a primary
20 source of groundwater recharge. Natural recharge is about 0.08 inches/year in the southeast
corner of the state (Wolock, 2003).

The LARV river-aquifer system supplies water to towns and industries through shallow
aquifer wells. Water is returned either directly to the river after treatment or into the

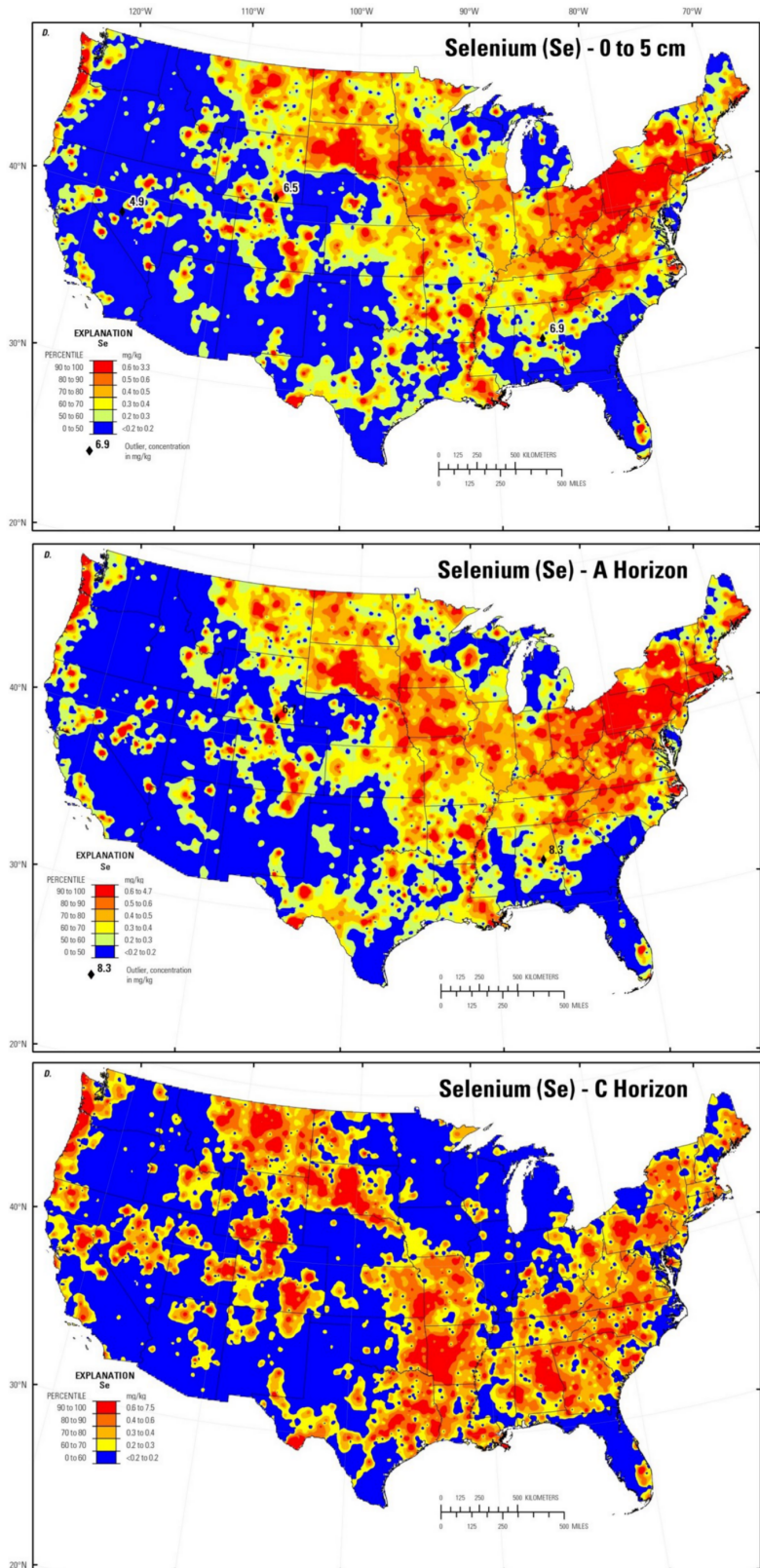


Figure 2.2. Distribution of Se in Soil in the Conterminous United States (D. B. Smith et al., 2014). This is a composite of three individual maps.

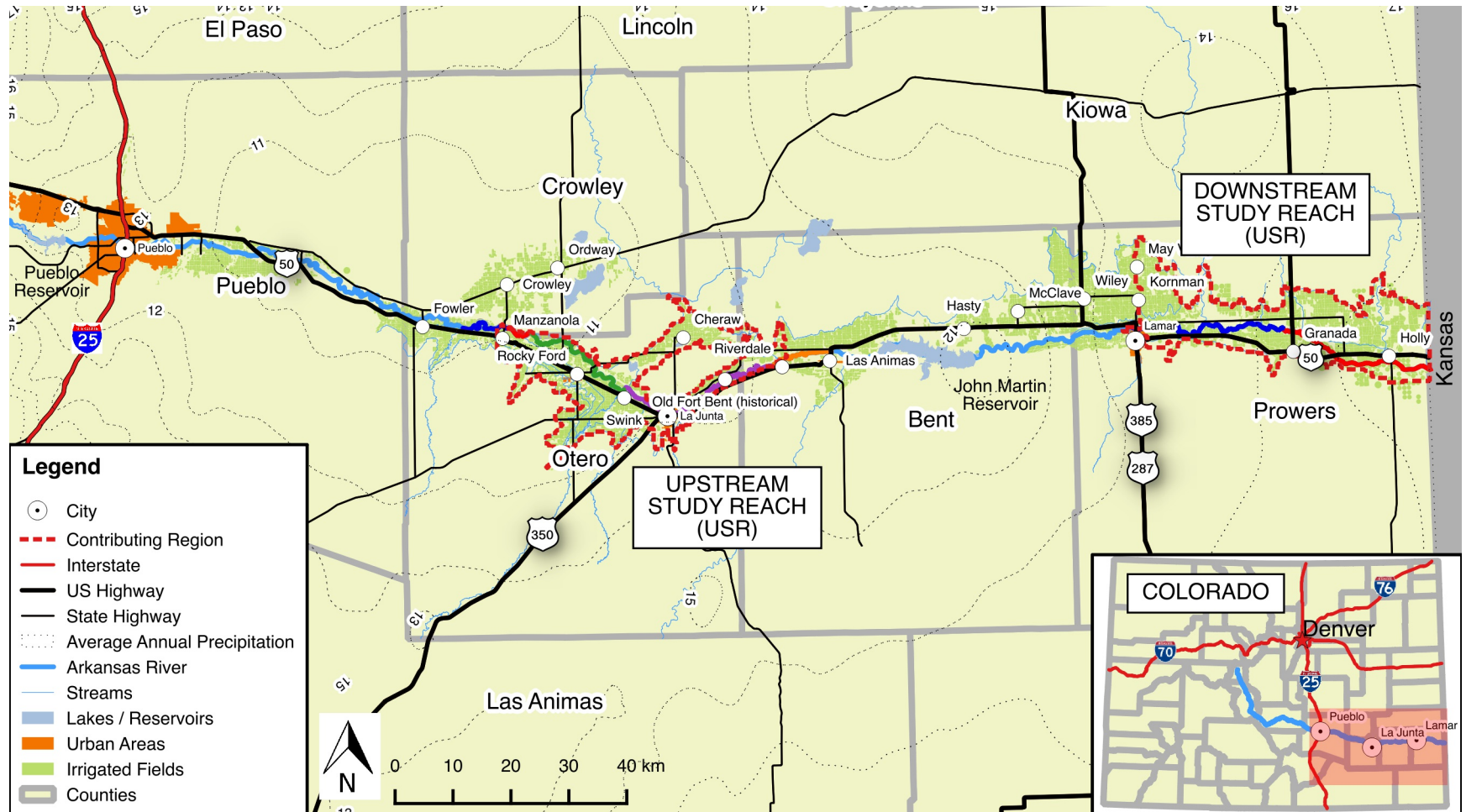


Figure 2.3. Precipitation in the LARV. Values on the isolines are reported as inches of average annual rainfall.

aquifer through groundwater seepage from treatment lagoons. Water supplied to these entities is a very small portion when compared to the demand from agriculture in the valley.

Agriculture is the primary industry in the LARV with approx 270,00 acres irrigated (R. T. Bailey et al., 2015; Miller et al., 2010). There are 25 main irrigation canals in the 5 LARV with diversion structures crossing the river. Many fields near the river drain excess irrigation water directly back to the river (Ryan T Bailey et al., 2012; Morway et al., 2013). There are also about 2,400 groundwater pumping wells that tap into the riparian aquifer, thereby taking water, albeit indirectly, from the river. The floodplain is characterized by heavy agriculture on fertile soils. The region is known for a wide variety of crops including but 10 not limited to alfalfa, corn, grass hay, wheat, sorghum, dry beans, cantaloupe, watermelon, and onions in order of cropped area (USDA NASS Colorado Field Office 2009). There are also a few diaries and cattle feed lots. Most fields are irrigated using surface-irrigation methods with less than about 5% irrigated with sprinklers or drip lines. Surface and sprinkler irrigation efficiencies are varied depending on the crop and location (Ryan T. Bailey, 2012)

15 refGates et al 2015

Precipitation in the LARV is substantially insufficient to support crop production by about 0.9 m (3 ft). It has been estimated that appropriated water rights in the LARV exceed the annual native river flow by as much as 40% in a low flow year (Cain, 1985; Sutherland and Knapp, 1988). Additional water is provided by releases from Pueblo and 20 John Martin Reservoirs which store water during the winter period. Some of this water is provided through trans-basin transfers through the Fryingpan-Arkansas Project.

Seepage from canals contributes significantly to the water quantity and quality in LARV aquifer. Canals are constructed at higher elevations, promoting the surface transport of water over long distances to fields. This elevation difference also places a higher hydraulic

gradient between the canal and aquifer. Canals, as a rule, are not constructed such that groundwater infiltrates into the canal channel. The entire process promotes the movement of water and dissolved constituents, including NO_3^{2-} , Se, U, and salts directly into the aquifer. Additionally, a significantly large quantity of the total canal length in the LARV is located
5 away from the river. This has two results. Since the aquifer is receiving recharge water from the canals, it acts as a reservoir, delaying the return of that water to the river channel. This result is seen during low flow conditions when the river channel still contains water, even though historic conditions would tell us otherwise. The second result is that dissolved constituents are introduced into the aquifer where it is the shallowest, along the edges of the
10 valley. This brings NO_3^{2-} and dissolved oxygen into contact with the Se bearing bedrock before either can be significantly depleted through other redox reactions (Ryan T. Bailey, 2012; Morway et al., 2013).

2.2. UPSTREAM STUDY REACH AND SURROUNDING REGION

The upstream boundary of the USR starts immediately downstream of the Catlin Canal diversion dam. The dam is approximately 4.5 miles (mi) (7 km) west of the intersection of U.S. Highway 50 and State Highway 207 in Manzanola and 4.5 mi (7 km) east of the 5 intersection of U.S. Highway 50 and State Highway 164 in Fowler. The USR extends along approximately 61.5 mi (99 km) of the river to where U.S. Highway 50 crosses the Arkansas River north of Las Animas. All portions of the USR are in CDWR Division 2, Water District 17 which extends from Fowler to Las Animas. There are three main tributaries, multiple minor tributaries, five main irrigation canals, and one return canal (for augmentation flow) 10 are present in the USR. Figure 2.4 shows the extent and approximate path of the USR and the irrigated region supplying return flow to the reach.

The USR is separated into five segments given designations from "A" to "E" (Figure 2.4). Segments are geographically separated by irrigation canal diversion dams. Segment B is the only segment that does not contain a stream gauge on the main stem of the river. 15 It is relatively short and has an additional diversion dam within its boundary. Typically, significantly different flows pass through the main channel of the river within each segment. Segments were defined to provide boundaries for river storage volume calculations. Within each segment, except for segment B, the water surface level is determined primarily by flowrate, hydraulic geometry, and hydraulic resistance. Knowledge of the water surface level 20 is necessary for estimating the river storage volume. A discussion of the river geometry analysis and storage volume calculation is provided in sections 3.2.

Figure 2.5 is a line diagram representing the major flow paths in the USR. This diagram is not to scale and depicts only the major canals and tributaries. The segments within the reach are color coded. Four canal diversion dams separate the segments. Points in

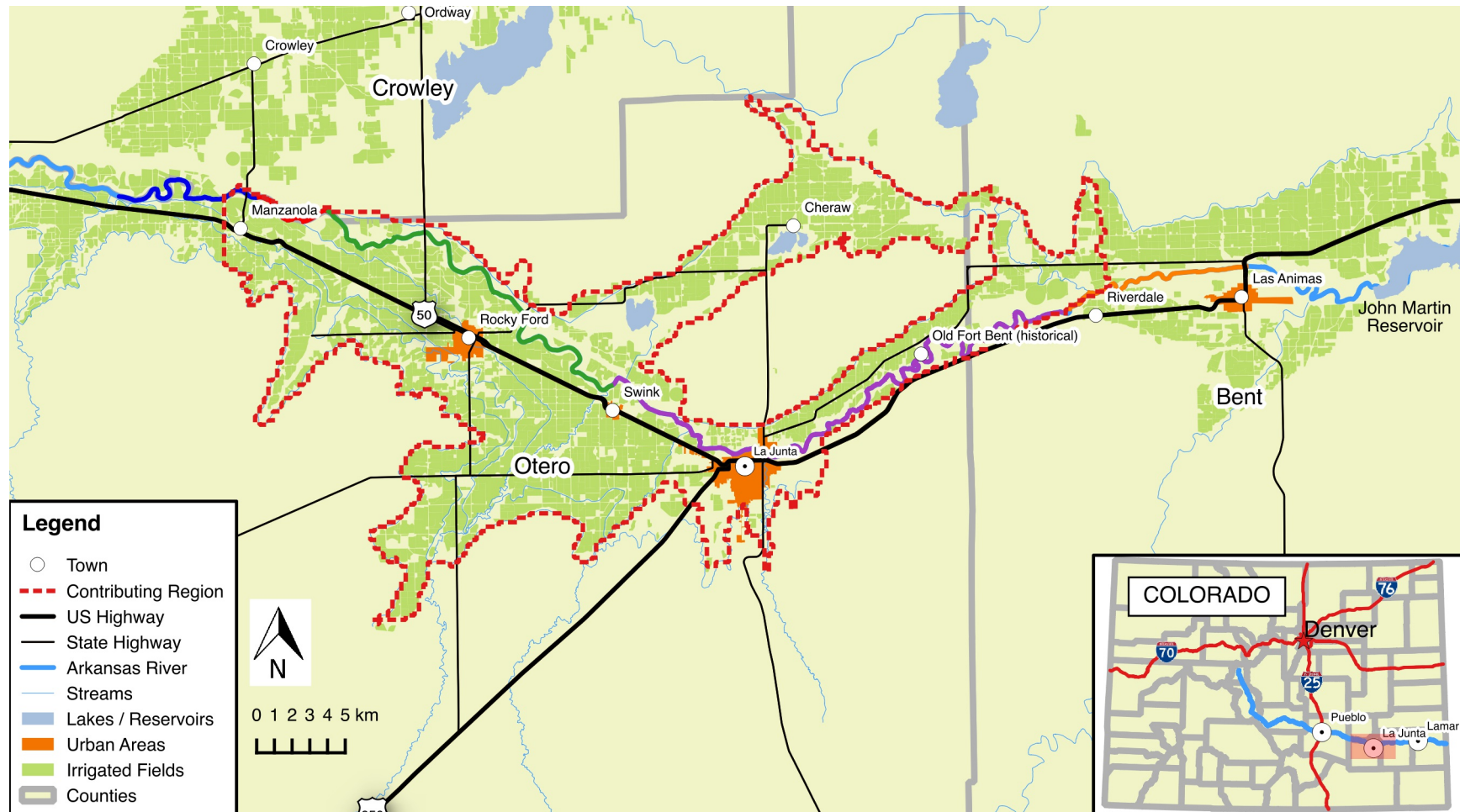


Figure 2.4. Upstream Study Reach. River segments within the USR are color coded.

Figure 2.5 designated as "Water Quality" are locations where CSU field technicians routinely took water samples for analysis. A discussion of the sampling and analysis methods is presented in section 3.1.

The main tributaries are perennial and supply water to the Arkansas River under 5 most conditions. These tributaries are Timpas Creek, Crooked Arroyo, and Horse Creek.

Most of the minor tributaries are usually dry and only convey water during larger rainfall events and flood conditions. All three major tributaries have a significant portion of their flows provided by agricultural runoff.

There are two minor tributaries that provide low volume, perennial flows to the 10 Arkansas River: King Arroyo and Anderson Arroyo. King Arroyo is assumed to be primarily

fed by La Junta Waste Water Treatment Plant (WWTP) effluent. The La Junta Water Treatment Plant (WTP) effluent spills into Anderson Arroyo. It is currently unknown what groundwater and other flows contribute to the discharge from King or Anderson Arroyos.

No discharge data are provided for the La Junta WTP due to the very low discharge rates.

15 The discharge from the La Junta WWTP is included in the models.

Patterson Hollow, a poorly-defined natural drainage, is depicted on the line graph as connected to the Arkansas River. Flows from the upper reach of Patterson Hollow are diverted to the Otero Canal. The reasons for the diversion are unknown, but it is speculated that the majority of the flows upstream of Otero Canal are irrigation returns and the diversion 20 was an attempt to re-use valuable irrigation water. Regardless, since Patterson Hollow, for the most part, was separated from the Arkansas River, it was not included in this study.

The five major canals diverting water from the Arkansas River along the USR are Holbrook Canal, Rocky Ford Canal, Fort Lyon Storage Canal, Fort Lyon Canal, and Jones Ditch. The Rocky Ford Return Canal is the only monitored canal returning augmentation

water to the Arkansas River in the USR. The Rocky Ford Return Canal diverts water from the Rocky Ford Canal and returns it directly to the Arkansas River. This system is in place to monitor and augment flows in conjunction with trans-basin flows used by the City of Aurora. The Otero and Rocky Ford Highline Canals run parallel to the USR. They divert
5 water from the Arkansas River upstream of the USR upstream boundary. Overflows from these two canals pass through the tributary gauge in Crooked Arroyo.

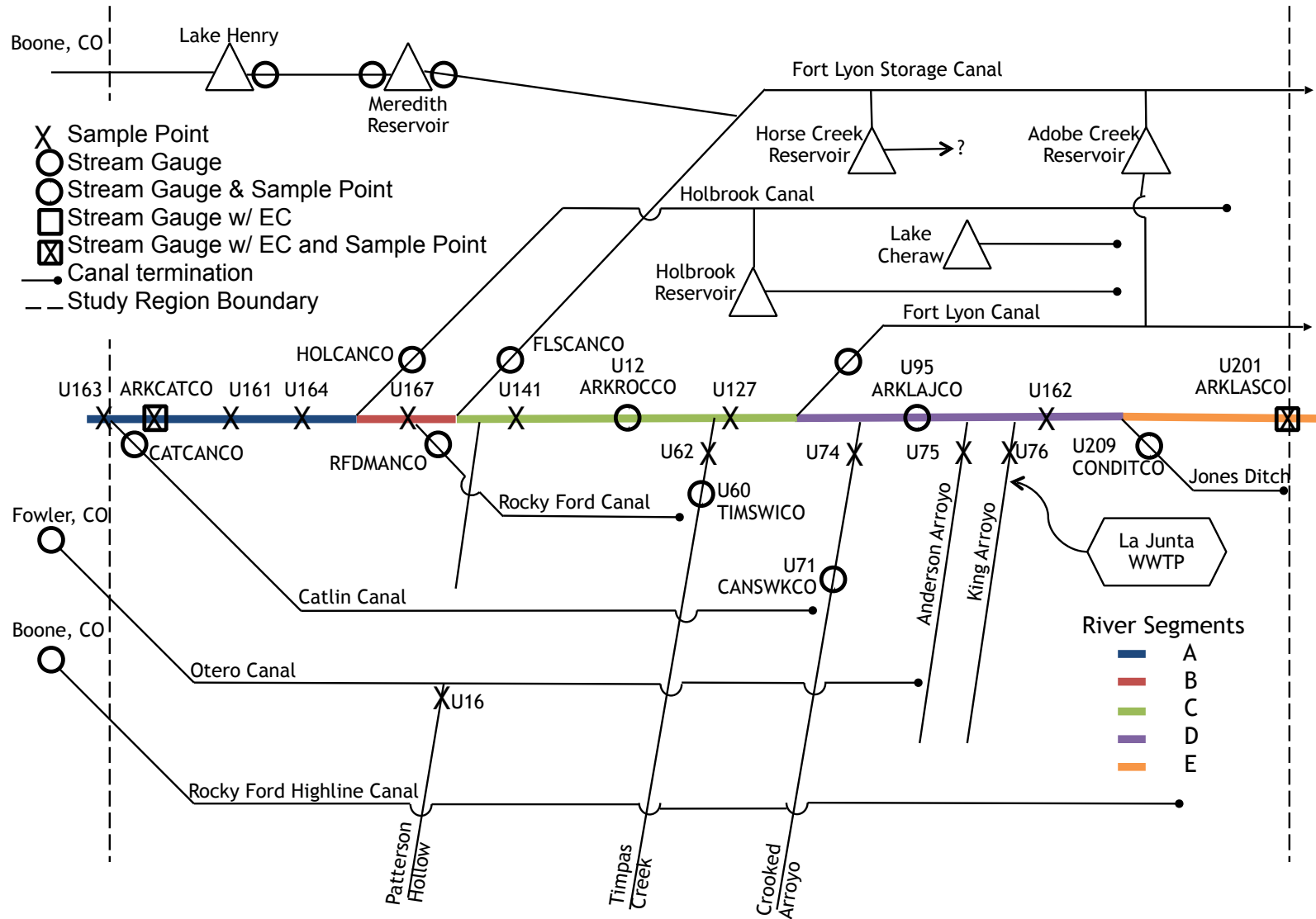


Figure 2.5. Upstream Study Reach Flow Diagram.

2.3. DOWNSTREAM STUDY REACH AND SURROUNDING REGION

The DSR begins at the U.S. Highway 50/U.S. Highway 287 Arkansas River crossing in Lamar, Colorado, and extends approximately 71 km to the Colorado/Kansas state line (Figure 2.6). Figure 2.7 is a line diagram representing the flow structure within the DSR.

5 Similar symbology is used on these maps as in Figures 2.4 and 2.5 for the USR. For a period of time, there were four tributaries and drains in the DSR where flows were measured manually gauged on an infrequent basis. The results of the this stream gauging activity do not affect the calculation or analysis of this study, but will be discussed in the conclusion.

The entirety of the DSR lies within CDWR Division 2, District 67 and contains two major

10 tributaries, multiple minor tributaries, and one irrigation canal.

The DSR is separated into Segment F and Segment G as shown in figure 2.6. The diversion dam for the Buffalo Ditch irrigation canal is the boundary between the two DSR segments. Field technicians have observed complete diversion of the Arkansas River at the Buffalo Ditch diversion with small but significant flows reappearing in the Arkansas River

15 channel only a few kilometers downstream. This leads to the speculation that significant portions of the downstream in-channel flow are from groundwater return flow.

The major tributaries within the DSR are Big Sandy Creek and Wild Horse Creek. CSU field technicians have observed that the stream gauge on Big Sandy Creek has been affected by beaver dams constructed downstream of the gauge and upstream of the culvert

20 passing under State Highway 196. The stream gauge on Wild Horse Creek is operated seasonally from April through November. CSU has made many visual flow observations in these creeks outside of the irrigation season. The off season flows are either extremely low or the stream is frozen.



Figure 2.6. Downstream Study Reach. River segments within the DSR are color coded.

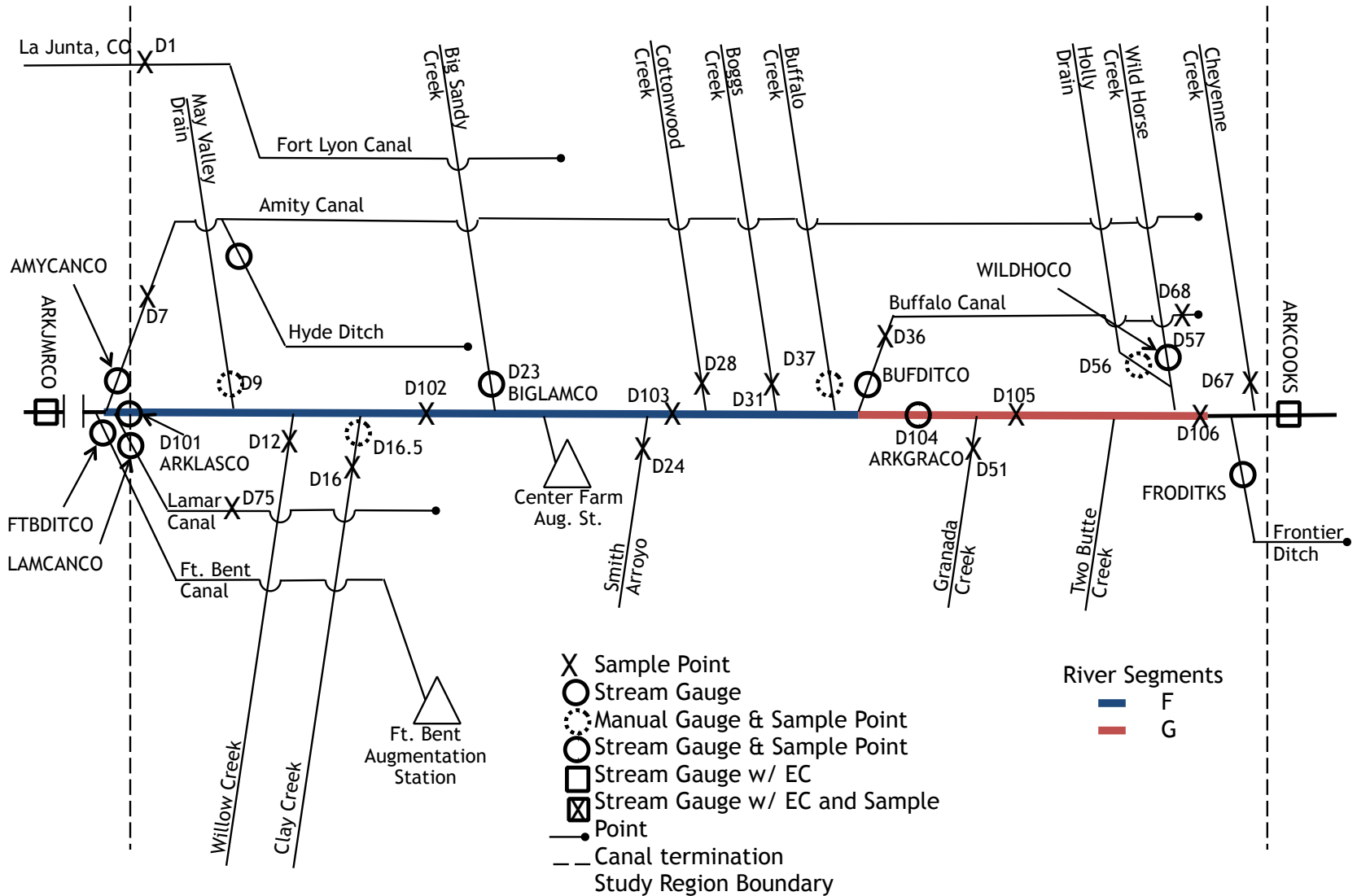


Figure 2.7. Downstream Study Reach Flow Diagram.

Unlike the USR, most of the minor tributaries in the DSR flow most of the year except in drought conditions. The primary source of water in the minor tributaries is irrigation runoff flowing into the streams through surface and subsurface flow paths. Most minor tributaries in the DSR do not have definitive entry points to the Arkansas River channel

5 resulting in doubt as to whether these flows reach the Arkansas River as surface water. It was assumed herein that the minor tributary flows enter the main stem primarily as groundwater. Minor surface return flows that do reach the Arkansas River are not gauged and most are difficult to access.

Buffalo Canal is the only functioning canal diversion within the DSR. There is historical and aerial imagery evidence for another diversion, but the Arkansas River has been routed around the structure and neither the CDWR nor the USGS maintain a flow gauge for the canal serviced by the diversion.

CHAPTER 3

DATA COLLECTION AND COMPIRATION

3.1. WATER QUALITY DATA COLLECTION

From June 2006 to July 2011 and April 2003 to August 2011, water quality samples were taken by CSU field personnel from the Arkansas River, tributaries, and drains in the USR and DSR, respectively. During the Se study periods, 18 surface water sampling trips 5 were made to the USR and 46 trips were made to the DSR. A total of 288 dissolved Se samples were taken and analyzed for dissolved Se and specific ions in the USR and 1,030 in the DSR during their respective study periods. Table 3.3 is a summary of the sample trips, the month and year of the trip, and the number of Se samples taken from the respective locations. Figures 3.1 and 3.2 show the dissolved Se sample locations in the USR and DSR, 10 respectively. Tables 3.1 and 3.2 list the sample locations and their location with the river reach and segment. The location of the sample point within the segment is only listed for samples collected on the Arkansas River with respect to the location of the stream gauge within the river segment. Sample points on tributaries and drains as noted in the tables.

Sample collection trips involved hours of preparation. Before leaving for the study 15 region(s), equipment and supplies were prepared. Peristaltic pumps were used for all surface water sample collection. Two Durham Geo TR-200 PSP peristaltic pumps were taken on each trip. The TR-200 is a single head, bi-directional, 12-volt battery operated, portable sampling pump capable of delivering flow rates up to 500 mL min^{-1} in both directions (Figure 3.3a). The pumps were cleaned, in-situ water quality instruments were calibrated, and sample 20 collection bottles were prepared. Peristaltic pumps were cleaned at the beginning and end of each sampling day and before sampling at each field sampling location. Figure 3.4 is a picture

Table 3.1. Upstream Study Region (USR) Sample Collection Point Information. A value of zero (0) indicates the location of the segment stream gauge. Negative distances indicate the point is upstream of the reference stream gauge location. Segment B does not contain a stream gauge on the river main stem.

River Segment Name	Sample Point	Dist from USR Upstream Boundary		Dist from River Segment Stream Gauge	
		mi	km	mi	km
A	U163	0	0	-2.7	-4.3
	U161	5.8	9.3	3.1	5
	U164	6.8	10.9	4.1	6.6
B	U167	9.2	14.8		
C	U141	14.7	23.7	-5.5	-8.9
	U12	20.2	32.5	0	0
	U60	26.1	42	5.9	9.5
	U127	26.4	42.5	6.2	10
D	U74	30.3	48.8	-3.5	5.6
	U95	33.8	54.4	0	0
	U162	44	70.8	10.2	16.4
	U209	52.8	85	19	30.6
E	U207	55.1	88.7	-6.6	-10.6
	U201	61.7	99.3	0	0

Table 3.2. Downstream Study Region (DSR) Se Sample Location Information. A value of zero (0) indicates the location of the segment stream gauge. Negative distances indicate the point is upstream of the reference stream gauge location.

River Segment Name	Sample Point	Dist from USR Upstream Boundary		Dist from River Segment Stream Gauge	
		mi	km	mi	km
F	D101C	0	0	0	0
	D102C	7.9	12.7	7.9	12.7
	D23	11.6	18.7	11.6	18.7
	D103C	17.6	28.3	17.6	28.3
	D36	23.4	37.7	23.4	37.7
G	D104C	24.9	40.1	0	0
	D105C	31.2	50.2	6.3	10.1
	D57	38.1	61.3	13.2	21.2
	D106C	38.9	62.6	14	22.5

Table 3.3. Summary of USR and DSR Water Sample Events.

Trip #	Date	USR Se Samples		DSR Se Samples	
		River	Trib. & Drain	River	Trib. & Drain
1	April 2003			12	14
2	June 2003			12	15
3	July 2003			7	15
4	July 2003			6	16
5	October 2003			6	15
6	January 2004			6	15
7	March 2004			6	15
8	May 2004			6	15
9	June 2004			6	15
10	July 2004			6	15
11	August 2004			6	15
12	November 2004			6	17
13	January 2005			6	15
14	March 2005			6	15
15	June 2005			6	17
16	July 2005			6	15
17	August 2005			6	17
18	December 2005			6	16
19	January 2006			6	16
20	March 2006			6	16
21	May 2006			6	16
22	June 2006	10	5	6	16
23	July 2006			6	16
24	August 2006			6	16
25	November 2006			6	16
26	March 2007			6	16
27	May 2007	10	5	6	16
28	June 2007			6	16
29	July 2007			6	16
30	August 2007			6	16
31	October 2007	10	4		
32	November 2007			6	16
33	January 2008			6	16
34	March 2008	10	4		
35	May 2008			6	16
36	June 2008	10	5		
37	July 2008			6	16
38	August 2008	10	5		
39	November 2008			6	16
40	January 2009	10	5		

Table 3.3. Summary of USR and DSR Water Sample Events. (Continued)

Trip #	Date	USR Se Samples		DSR Se Samples	
		River	Trib. & Drain	River	Trib. & Drain
41	(No Se Samples)				
42	March 2009			6	16
43	May 2009	10	5		
44	June 2009			6	16
45	July 2009	10	4		
46	August 2009			6	16
47	November 2009	10	4		
48	January 2010			6	16
49	March 2010	10	4	6	15
50	May 2010	9	4		
51	June 2010			6	16
52	July 2010	11	6		
53	August 2010	10	7	6	17
54	November 2010	12	7	8	19
55	March 2011	12	7	8	19
56	May 2011	15	9	8	17
57	July 2011	12	7		
58	August 2011			8	17
Totals		191	97	297	733

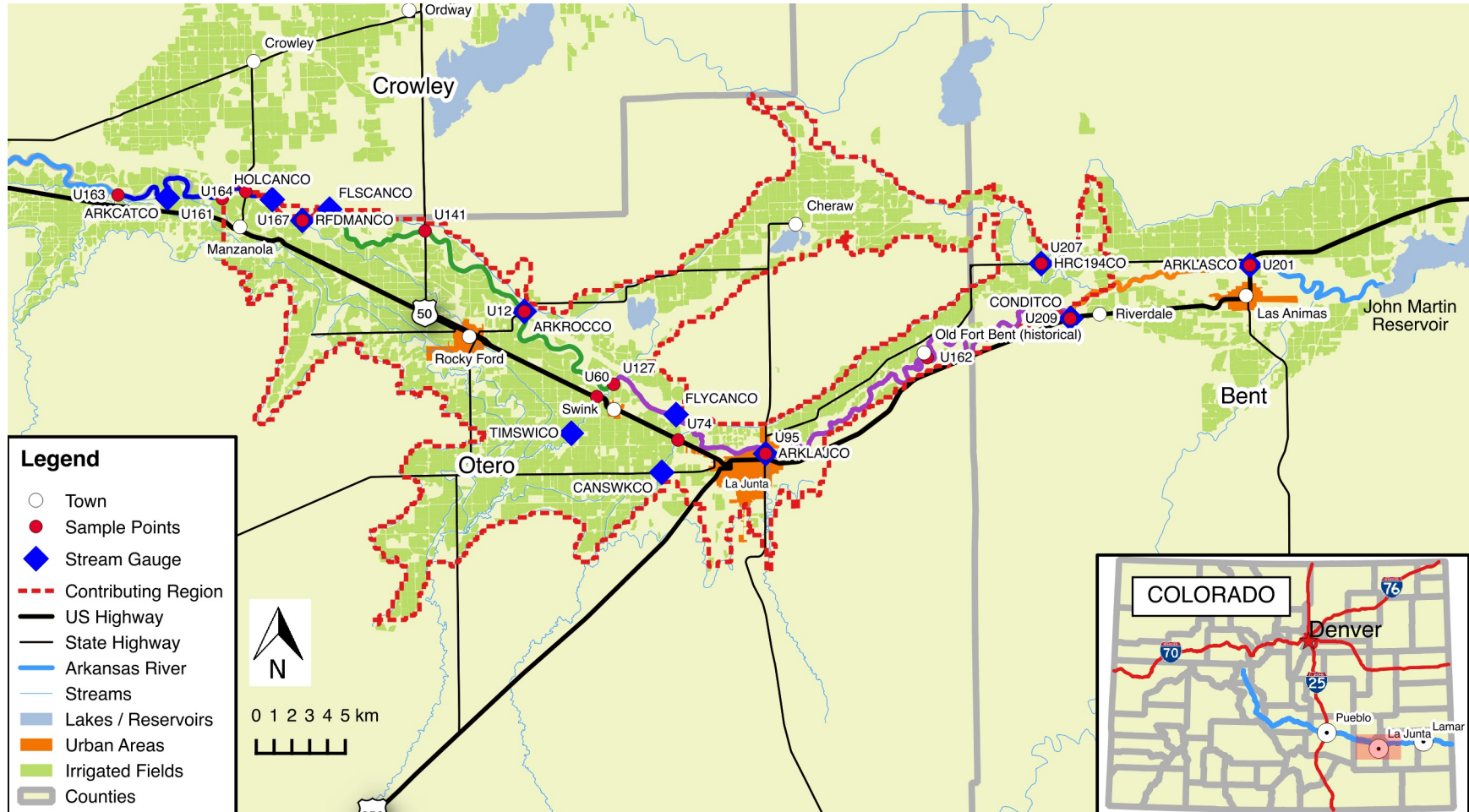


Figure 3.1. Dissolved Se sampling locations in the USR. Samples taken near, but not at stream gauge locations where shown.



Figure 3.2. Dissolved Se sampling locations in the DSR. Samples taken near, but not at stream gauge locations where shown.

of a typical vehicle setup with cleaning buckets, peristaltic pump, water quality sonde, and various other equipment items. Cleaning consisted of the following listed procedure:

(1) At the beginning of every sampling day, four, 5-gallon (gal) buckets with lids were prepared as follows:

5 (a) One bucket filled with approximately 2.5 gal tap water and approximately 20 mL of lab grade hydrochloric acid (HCl).

(b) One bucket filled with approximately 2.5 gal tap water and approximately 20 mL of LiquiNox®, a lab grade, phosphate and ammonia free, free rinsing detergent.

10 (c) Two buckets filled with approximately 2.5 gal deionized water.

(2) The acid solution was run through the pump for two minutes. This disinfected the pump tubing and prevented cross contamination.

(3) The detergent solution was run through the pump for two minutes. This removed any remaining soil particles from the pump tubing.

15 (4) Water from the first of the deionized water buckets was run through the pump for two minutes followed by the second bucket of deionized water for another two minutes. This rinsed all detergent from the pump tubing.

Two sample types were routinely taken at all locations during each trip. One sample type was for the analysis of specific ion concentrations as a general water quality panel.

20 A 250 mL-wide mouth, high density poly-ethylene (HDPE) bottle was used to collect and ship the specific ion samples. This bottle was pre-cleaned and shipped to CSU by Ward Laboratories, Inc. in Kearney, Nebraska, the laboratory that provided the bulk of the water quality analysis services. The second sample was taken for analysis of dissolved Se concentration using a 125 mL-wide mouth, HDPE bottle. This bottle was procured from multiple



(a) Durham Geo TR-200 PSP Peristaltic Pump.



(b) In Situ Water Quality Sonde and Data Logger. Measures temperature, specific conductivity, pH, oxidation-reduction potential, and dissolved oxygen concentration.

Figure 3.3. Water Quality Sampling Equipment.



Figure 3.4. Typical sample vehicle equipped for surface water sampling. Equipment includes peristaltic pump, water quality sonde, pump cleaning buckets, and various other equipment items. This picture is taken at sample site U162 which is on the National Park Service's Bent's Old Fort National Historic Site (fort in background).

sources and pre-cleaned to the US EPA's "Specifications and Guidance for Contaminant Free Sample Containers" (USEPA, 1992). Approximately 0.6 mL of a diluted nitric acid solution prepared with 33 mL of distilled water and 7 mL of ultra-pure nitric acid was added to each

bottle using a graduated pipette. This was done to preserve the sample by lowering the pH to less than 2 standard pH units. During the latter half of the sampling periods, samples for dissolved uranium (U) were gathered during most sampling trips. 250 mL-narrow mouth, pre-cleaned, pre-preserved with nitric acid, HDPE bottles were provided by TestAmerica Inc., the laboratory providing dissolved uranium analysis.

Blank samples of deionized water were prepared in the lab for each sample type before each trip at the beginning of each sampling day for each sample type. Blanks are intended to be free of the analyzed constituent and are used to test the samples for bias due to contamination. Trip blanks were taken in the lab before the begining of the sample trip. They accompanied field personnel during all sampling activities and were then shipped to their respective lab for analysis. Trip blanks were intended to demonstrate that there was no contamination due to transportation activities. Field blanks were taken in the field at the begining of the sampling day. These samples also accompanied the field personnel during sampling activities and were shipped to their respective lab for analysis. Field blanks were intended to demonstrate that there was no contamination in the sampling equipment. Any variation from non-detectable solute concentration in these blanks would indicate possible contamination of the water samples taken that day and further investigation would be required. None of the lab results from field or trip blanks reported values that would indicate sample contamination.

Two YSI, Inc. 600R sondes with attached YSI, Inc. 650 MDS display data loggers were used for in-situ measurements during each sample trip (Figure 3.3b). The sondes were equipped with a Rapid Pulse polarographic dissolved oxygen (DO) sensor capable of measuring DO from 0 mg L^{-1} to 50 mg L^{-1} , $\pm 2\%$; a thermistor capable of measuring temperature from -5°C to 50°C , $\pm 0.15^\circ\text{C}$; a glass combination electrode pH sensor capable of measuring

pH in the range of 0 to 14 units, ± 0.2 units; a platinum button oxidation-reduction potential (ORP) sensor capable of measuring in the range of -999 mV to 999 mV, ± 20 mV; and a four electrode, autoranging cell capable of measuring electrical conductivity (EC) as specific conductance at 25°C in the range of $0 \mu\text{S cm}^{-1}$ to $100\,000 \mu\text{S cm}^{-1}$, $\pm 0.5 + 1 \mu\text{S cm}^{-1}$. The equipment was serviced and calibrated by CSU field personnel before every trip to the study reaches and at the end of every sampling day. Sondes were sent to Geotech Environmental Equipment, Inc. annually for maintenance checks. Geotech Environmental Equipment, Inc. is an authorized dealer and service provider for YSI equipment with an office in Denver, Colorado.

At least one set of duplicate water samples was taken per sampling trip to theUSR and/or DSR. Duplicate, or replicate, samples were marked as 'A' and 'B' samples. The 'A' sample results were kept with the main data set and were used as the primary data set. 'B' sample results were kept separate and were used to determine the combined sampling methodology and lab analysis uncertainty. The sampling standard procedure was to take one duplicate set of surface water samples per day with a minimum of two duplicate surface water samples per sampling trip.

Each sampling event began with recording the site data on a form (log) similar to the one in Figure 3.5. In-situ water quality measurements were then taken using the YSI sonde. The data logger was used to read the data, but was not used as a recording device.

All data were recorded on the form shown as an example in Figure 3.5. The ranges at the bottom of the form are maximum acceptable ranges of values determined from previous sampling trips. Values outside of these ranges would indicate to field personnel that the equipment was damaged, had lost calibration, or operational error had occurred. The YSI sonde was allowed to rest in the water for a minimum of three minutes before recording

values. Usually, the sonde would rest in the water while water quality samples were taken. Samples were pumped through a disposable, in-line 0.45 micron, polyethersulfone filter into the sample bottles. Peristaltic pumps were used to extract all water samples from surface water sources. No air space was permitted in any of the sample bottles. Figure 3.6a shows 5 a trained sample collector at location U12 in the USR which is north of Rocky Ford on a bridge over the Arkansas River. The YSI sonde is not in this image, but is suspended in the river during sample collection. Figure 3.6b is the same sample collector at sample location U73 in the USR recording readings from the YSI sonde. Samples were stored on ice or in a refrigerator until they were shipped to their respective labs. Data was recorded onto the 10 data form from the YSI sonde immediately after collecting the water samples. The sonde was left in the water for an additional two to three minutes. Any changes in readings were recorded as a second entry. An example of a completed log is shown in Figure 3.7

Specific ion lab results from Ward Laboratories and dissolved U lab results from TestAmerica were not used directly in the analysis reported in this thesis. The Oscar E. 15 Olson Biochemistry Laboratories (Olson Labs) at South Dakota State University (SDSU) performed dissolved Se analysis using Official Methods of Analysis of AOAC International, 17th Edition, test number 996.16, Selenium in Feeds and Premixes. This test, a fluorometric test initially designed for testing animal feeds, provides repeatable analysis for dissolved Se near criteria levels. Double tests were completed on each sample and the average was 20 reported. The minimum reportable value was $0.4 \mu\text{g L}^{-1}$.

Late in 2011, the Olson Labs was closed by SDSU for funding reasons. Staff at Olson Labs assisted CSU staff in finding a new lab capable of continuing analyses using the same methods and to the same level of quality. South Dakota Agricultural Laboratories (SDAL) was chosen. Most of the staff and equipment from Olson Labs were employed at

Station No.:				Date:	
Location:				Time:	
	Left	Center	Right	Sample collector(s):	
Upstream				Pumping Note:	
Downstream					
Location Note:					
<input type="checkbox"/> Dry <input type="checkbox"/> Stagnant/Frozen <input type="checkbox"/> No Access _____					
Time (min)	Temp (°C)	Conductivity ($\mu\text{S}/\text{cm}$)	DO (mg/L)	pH	ORP (mv)
Range	(0-35)	(400-8000)	(0-18)	(4.8-10)	(-250-400)

Figure 3.5. Example water quality sample form.

the new SDAL providing CSU staff with ample reason to move all dissolved Se analyses to the new lab. Both Olson Labs and SDAL were certified by the USEPA for drinking water and subscribed to the proficiency testing and check sample programs for the USEPA for wastewaters .

ref. How?

5 The same procedures and techniques for sample gathering and analysis were used during the entire sampling periods. Newer or different techniques or procedures were considered, but was determined to have the possibility to compromise the consistency of the gathered data. Results from all lab analyses were recorded in a master database at CSU for later data extraction and analysis. The data includes results from over 4,500 sample sets.



(a) Sample location U12. The Se sample bottle is being filled with a peristaltic pump through a 0.45 micron filter. The specific ion sample bottle is filled, laying next to the pump.



(b) Sample location U73. Personnel is hand logging data from the YSI sonde.

Figure 3.6. Personnel performing water sample collection.

Approximately 95 and 1,035 of these sample sets were taken from surface water sites in the USR and DSR, respectively. Each sample set included in-situ measurements, a dissolved Se sample, a general specific ion panel, and a possible dissolved U sample. In-situ EC and temperature measurements taken at stream gauge sites with permanent water quality instrumentation were compared with the measured values reported at those sites. These sites record and report EC and water temperature measurements every 15-minutes. Minor deviations were expected due to instrument drift and calibration error, yet EC and temperature differences were found to be less than 1% for all in-situ measurements.

The water and mass balance models included in this study are among the many lines of research that have used this data. Because of the multiple uses of large data sets, great

Station No.: [U201]			Date: <i>16 May 16</i>		
Location: Arkansas River			Time: <i>1302</i>		
	Left	Center	Right	Sample collector(s): <i>KHM</i>	
Upstream				Pumping Note:	
Downstream		<i>X</i>			
Location Note:					
<input type="checkbox"/> Dry <input type="checkbox"/> Stagnant/Frozen					
<input type="checkbox"/> No Access _____					
Time (min)	Temp (°C)	Conductivity (µS/cm)	DO (mg/L)	pH	ORP (mv)
<i>4</i>	<i>19.40</i>	<i>1676</i>	<i>7.92</i>	<i>8.08</i>	<i>67.4</i>

Figure 3.7. Example completed water quality sample form.

care has been taken to ensure that data entry errors are rare. Data were copied into the database and randomly checked for transcription errors. Original lab reports were retained on file.

3.2. RIVER CROSS-SECTION GEOMETRY SURVEY

The Arkansas River was surveyed at twenty-one and thirteen locations in the USR and DSR, respectively. At these locations, cross-sections were surveyed and the data analyzed to determine the spatial distribution of the river geometry. The cross-sections are not equally spaced along the river segments. Cross-sections were surveyed at the extreme upstream and downstream end of each river segment. Intermediate cross-sections were located where both the landowner permitted access and the river was reasonably accessible. Additionally, the intermediate cross-sections were located where different cross-section profiles existed. This was done to capture a broadest possible range of cross-section profiles, thereby allowing for a more realistic characterization of the river geometry. Figures 3.9 and 3.10 show the locations of the surveyed cross-sections in the USR and DSR, respectively. Tables 3.4 and 3.5 describe the location of the survey point with respect to the river reach and segment. Survey locations within a river segment are with respect to the segment stream gauge location.

Industry standard survey techniques were used whenever possible. It was not possible to properly locate the instrument location in either the horizontal and vertical plane with respect to a local datum due to the remote location and the lack of available time. All data was collected with a total station (Figure 3.8a) and hand recorded into survey log books. Two back-sights were used at every surveyed cross-section. Both back-sights and the instrument location were located by using a hand held global positioning satellite (GPS) receiver (Figure 3.8b). The receiver was capable of determining the horizontal location to within ± 1 m and the vertical location to within ± 2 m. Licensed surveyors were not hired, retained, or consulted for this study.

Higher location and orientation accuracy could have been obtained by using survey grade GPS equipment or by referencing the instrument survey to an established benchmark.

Table 3.4. Upstream Study Region (USR) Survey Point Information. A value of zero (0) indicates the location of the segment stream gauge. Negative distances indicate the point is upstream of the reference stream gauge location. Segment B does not contain a stream gauge on the river main stem.

River Segment Name	Survey Point	Dist from USR Upstream Boundary		Dist from River Segment Stream Gauge	
		mi	km	mi	km
A	USS1	0	0	-2.7	-4.3
	USS2	2.7	4.3	0	0
	USS3	5.8	9.3	3.1	5
	USS4	7.8	12.6	5.1	8.2
B	USS6	9.2	14.8		
	USS7	9.3	14.9		
	USS8	10.2	16.4		
C	USS10	13.4	21.6	-6.8	-10.9
	USS11	18.1	29.1	-2.1	-3.4
	USS12	20.2	32.5	0	0
	USS13	24.4	39.3	4.2	6.8
	USS14	29.3	47.2	9.1	14.6
D	USS16	30	48.3	-3.8	-6.1
	USS17	32.6	52.5	-1.2	-1.9
	USS18	33.8	54.4	0	0
	USS19	35.9	57.8	2.1	3.4
	USS21	44	70.8	10.2	16.4
	USS22	46.4	74.7	12.6	20.3
	USS23	50.3	81	16.5	26.6
E	USS26	55.7	89.6	-6	-9.7
	USS27	61.7	99.3	0	0

For almost all surveyed cross-sections, benchmarks were not located within a reasonable distance. Attempting to tie into these benchmarks would result in an order of magnitude or more increase in the time required to complete the survey. There were also doubts as to whether the horizontal and vertical accuracy could be maintained due to the distance

- 5 between the nearest benchmarks and the survey sites and the surveyor's skill. Survey grade GPS equipment could have been used, but would have required either a larger team or a significantly increased risk of equipment tampering or theft. The available survey grade

Table 3.5. Downstream Study Region (DSR) River Cross-Section Survey Location Information. A value of zero (0) indicates the location of the segment stream gauge. Negative distances indicate the point is upstream of the reference stream gauge location.

River Segment Name	Survey Point	Dist from USR Upstream Boundary		Dist from River Segment Stream Gauge	
		mi	km	mi	km
F	DSS1	0	0	0	0
	DSS4	7.9	12.7	7.9	12.7
	DSS5	10.3	16.6	10.3	16.6
	DSS6	14.9	24	14.9	24
	DSS7	17.6	28.3	17.6	28.3
	DSS8	20.5	33	20.5	33
	DSS9	23.4	37.7	23.4	37.7
G	DSS10	23.5	37.8	-1.4	-2.3
	DSS13	29.3	47.2	4.4	7.1
	DSS14	31.2	50.2	6.3	10.1
	DSS15	33.9	54.6	9	14.5
	DSS16	37	59.5	12.1	19.5
	DSS17	38.9	62.6	14	22.5
	DSS20	46.2	74.4		



(a) Pentax PCS-315 Total Station.



(b) TopCon GMS-2 Sub-meter handheld GPS.

Figure 3.8. Survey Equipment.

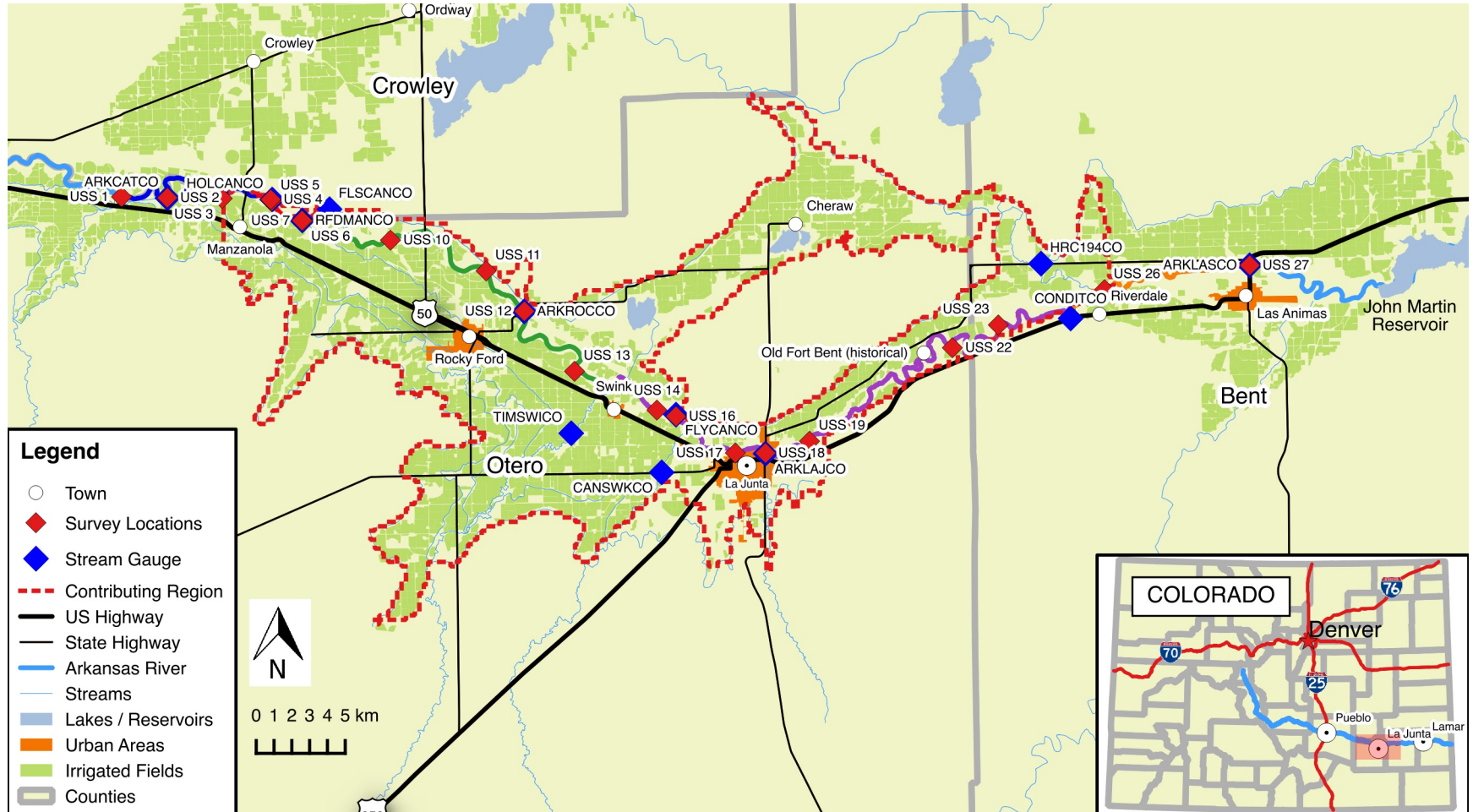


Figure 3.9. USR River Cross-section Survey Locations. Cross-sections are taken above and/or below the diversion structure and near gauge locations.

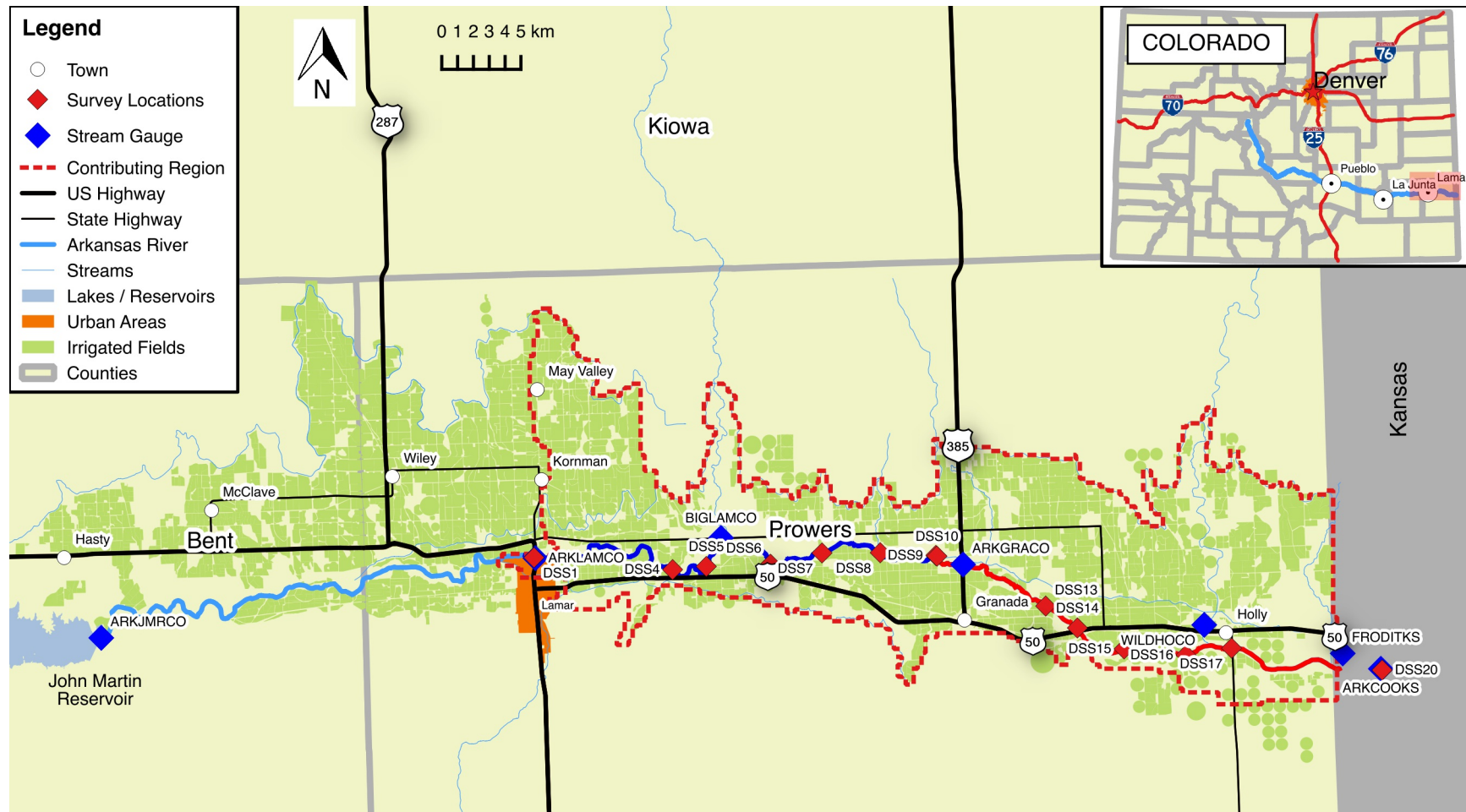


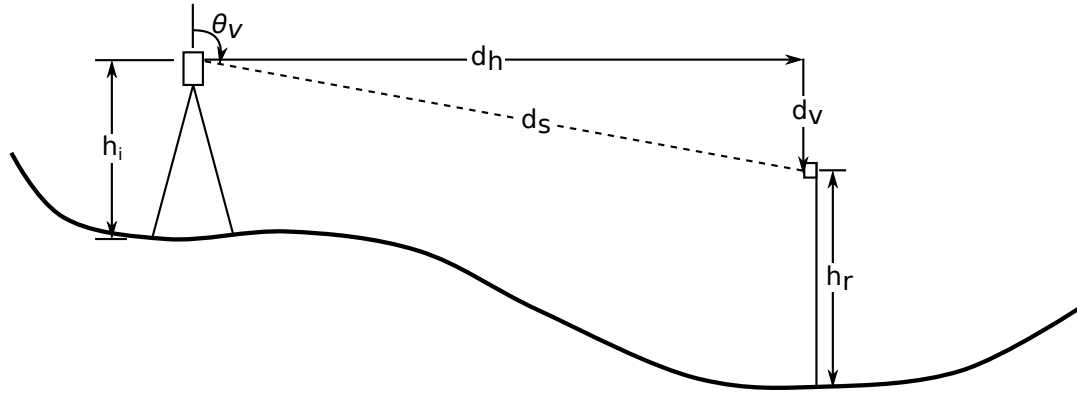
Figure 3.10. DSR River Cross-section Survey Locations. Cross-sections are taken above and/or below the diversion structure and near gauge locations.

GPS base station also had a limited range compared to the range required to access many of the locations. Since the goal of the survey was to determine the relationship between the depth and width of the river, it was determined that locating and orienting the survey data correctly was a secondary goal. For these reasons, it was determined that the level of
5 location and orientation accuracy obtained by using the hand held GPS receiver would be sufficient.

The data was collected in the form of horizontal angle, vertical angle, sight distance, rod height, and instrument height. The survey data was downloaded from the total station and entered into a spreadsheet for conversion to horizontal and vertical location relative to
10 the instrument. Values in the spreadsheet were checked against the survey log book. Points collected but not used to calculate the cross-section, such as the back-sight points, were marked so that they were not used in the cross-section analysis. These excluded points were used for other survey related calculations. The rod height for each measurement and the instrument height for the survey was transferred from the log book to the spreadsheet.

15 Coordinate geometry (COGO) techniques were used to convert from angle, sight distance, rod height, and instrument height measurements to horizontal and vertical distance measurements relative to the instrument as shown in figure 3.11. Vertical angles were measured using decimal degrees such that zero degrees (0°) was located above the instrument and 90° was horizontal. Horizontal angles were measured using decimal degrees such that
20 0° was located when the instrument was facing the first back-sight and positive angles were measured clockwise when viewed from above. The sight distance was measured using the instruments integrated laser distance measuring tool from the optics of the instrument to the rod prism with sub-millimeter accuracy. Horizontal and vertical distances to the ground location of the survey point from the ground location of the instrument were calculated as

shown in equations 2 and 3, respectively. The horizontal location was calculated as northing and easting with the line between the instrument and the first back-sight as the reference. Northing and easting distances were calculated with respect to the horizontal line between the instrument and the first backsight. Corrections were made to orient the points to the coordinate system, but this step was not necessary to provide the necessary results.



$$d_h = d_s \cdot \sin(\theta_v) \quad (2)$$

$$d_v = h_i - h_r + d_s \cdot \cos(\theta_v) \quad (3)$$

d_h = Horizontal distance from the instrument to the surveyed point.

d_v = Vertical distance from the instrument to the surveyed point.

d_s = Sight distance from the instrument optics to the rod prism.

θ_v = Vertical angle from the sight optics to the rod prism

Figure 3.11. Survey Measurement Definitions.

GPS location data for the instrument and back-sights was collected in the form of northing, easting, and elevation. Colorado State Plane-South, North American Datum 1983 (NAD83), U.S. feet was used as the horizontal datum and North American Vertical Datum 1988 (NAVD88) was used as the vertical datum. All survey units are U.S. Feet. Survey errors, also known as closing errors, were corrected for all points. Most survey locations were on soft soils. It was assumed that survey error would primarily consist of instrument location drift. Measurements were taken to both back-sights at the beginning and end of the

site survey. The northing, easting, and elevation difference between the measurements taken at the beginning and end of the site survey were spread equally and successively among all points. Since two back-sights were used, the total closing error was taken as the average of the closing errors for the two back-sights.

5 Correction of closing errors was required to obtain accurate stream depth and river top width values. Location and orientation error correction was not required and was only performed as a manner of good survey practice. Survey data points were translated from their position relative to the instrument to their position relative to the State Plane coordinate system by adding the northing, easting, and elevation values collected by the GPS receiver
10 at the instrument site. Orientation error corrections to make instrument North coincide with true North were made by adding a positive horizontal correction angle such that the corrected angle to the first back-sight, which was the zero back-sight, matched the angle between the two corresponding GPS northing and easting coordinate sets. Final survey locations should always have the most correct location and elevation relative to a given datum. Both the
15 back-sights and instrument location were marked with steel reinforcement bar (re-bar) and plastic caps (Figure 3.12), it may be possible for future surveys to be conducted at the same locations with the same back-sights.



Figure 3.12. Typical plastic cap on rebar used to locate instrument location and back-sights.

A least squares fit linear regression equation was fit to the relative location of all points along the surveyed cross-section (Figure 3.13). It was reasoned that a straight line through the data points would allow for a better approximation of the river's cross-section than connecting the points. The straight line would represent a true cross-section, whereas connecting the points would exaggerate the distance across the cross-section. The relative locations of the points as projected onto the best-fit line were entered into computer aided design and drafting (CADD) software (Figure 3.14). Horizontal lines, spaced 0.03 m (0.1 ft) apart from the bottom of the channel to 1.5 m (5 ft) from the bottom, were drawn from edge of bank to edge of bank. The vertical location of these lines was taken as the flow depth and the length of the line was taken as the river top width.

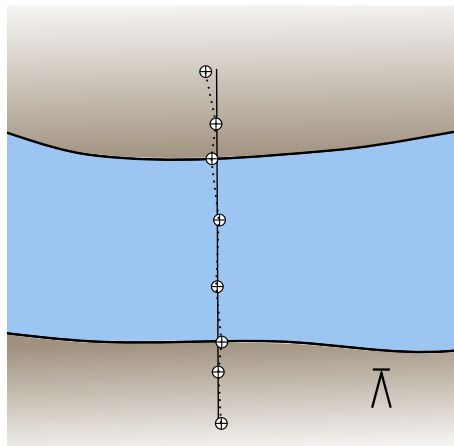


Figure 3.13. Depiction of the conversion of River Survey Locations to Linear Cross-Section. The crossed circles are the surveyed points. The instrument (total station) is in the lower right-hand corner. The dotted line depicts the cross section if no correction were made to linearize the survey cross section locations. The solid line is the cross-section line created from the best-fit line through the surveyed points. Surveyed points were translated perpendicular to the cross-section line to lie on the cross-section line across the river.



Figure 3.14. River Cross-Section as Draw in CADD Software. The black line is the channel cross-section with the left side representing the north bank of the Arkansas River (water flow is into the page). The blue horizontal line is the lowest point in the surveyed channel. All elevations were shifted such that the bottom point had a stream depth of zero. This particular cross section is at cross-section USS1. The horizontal and vertical scales are identical.

3.3. DATA COMPILED FROM OTHER SOURCES

The data collected in the field constituted a small portion of the total data required to perform water and mass balance calculations. Additional data were obtained from three sources: the USGS, the CDWR, and the Colorado Climate Center (CCC).

5 The USGS operates and maintains the largest network of stream gauges in the United States. USGS gauges in the LARV in Colorado are operated and maintained by the USGS Colorado Water Science Center. Their main office is Lakewood, Colorado, with one of their satellite offices in Pueblo, Colorado. Of the gauges listed in Tables 3.6 and 3.7 and shown in Figures 3.16 and 3.17, five are operated by the USGS. There is additional sensing
10 equipment owned and maintained by the USGS at some stream gauges owned and operated by the CDWR. Water temperature, air temperature, precipitation, and EC are the additional parameters typically measured and recorded by this equipment. EC is reported as specific conductance standardized to 25 °C and is the standard for EC used throughout this thesis. EC values are reported in units of micro-siemens per centimeter ($\mu\text{S cm}^{-1}$) and are converted
15 to units of deci-siemens per meter (dS m^{-1}).

The USGS and CDWR do not have typical gauge sites in the LARV. Gauge housing and locations vary as show in Figure 3.15. These figures are not all inclusive and other variations occur in the LARV. Both agencies were consistent in the flow measuring equipment deployed to the gauge sites. During the Se sampling time frame, all stream gauges were constant flow bubblers as described in the USGS Techniques of Water Resources Investigations
20 (TWRI) Report, Book 3, Section A, Chapter 7 (Sauer and Turnipseed, 2010). After all Se sampling was completed, the USGS and CDWR began upgrading some of the gauge sites with radar non-contact water level sensors. It is unknown how this will affect the comparison of the results of this thesis with any future work.

Table 3.6. Upstream Study Region (USR) Stream Gauge Information. Segment stream gauges record flow depth for surface area and river volume change calculations. A value of zero (0) indicates the location of the segment stream gauge. Negative distances indicate the point is upstream of the reference stream gauge location. Segment B does not contain a stream gauge on the river main stem.

River Segment	CDWR Stream Gauge Name	USGS Stream Gauge Name	Dist. from USR Upstream Boundary		Dist. from River Segment Stream Gauge	
			mi	km	mi	km
A	ARKCATCO		2.7	4.3	0	0
	HOLCANCO		7.8	12.6	5.1	8.2
B	RFDMANCO		9.2	14.8		
	FLSCANCO		10.2	16.4		
C	RFDRETCO		11.7	18.8	-8.5	-13.7
	ARKROCCO		20.2	32.5	0	0
	TIMSWICO	7121500	26.1	42	5.9	9.5
	FLYCANCO		29.3	47.2	9.1	14.6
D	CANSWKCO		30.3	18.8	-3.5	-5.6
	ARKLAJCO		33.8	54.4	0	0
	CONDITCO		52.8	85	19	30.6
E	HRC194CO		55.1	88.7	-6.6	-10.6
	ARKLASCO	7124000	61.7	99.3	0	0

Table 3.7. Downstream Study Region (DSR) Stream Gauge Information. River segment stream gauges record flow depth for surface area and river volume change calculations. A value of zero (0) indicates the location of the segment stream gauge. Negative distances indicate the point is upstream of the reference stream gauge location. Stream gauges ARKJMRCO, FRODITKS and ARKCOOKS although required for analysis, are not within the DSR.

River Segment	CDWR Stream Gauge Name	USGS Stream Gauge Name	Dist. from DSR Upstream Boundary		Dist. from River Segment Stream Gauge	
			mi	km	mi	km
	ARKJMRCO	07130500	-22	-35.4		
F	ARKLAMCO	07133000	0	0	0	0
	BIGLAMCO	07134100	11.6	18.7	11.6	18.7
	BUFDITCO		23.4	37.7	23.4	37.7
G	ARKGRACO	07134180	24.9	40.1	0	0
	WILDHOCO	07134990	38.1	61.3	13.2	21.2
	FRODITKS	07137000	43.5	70		
	ARKCOOKS	07137500	43.2	74.4		



(a) HRC194CO.



(b) BIGLAMCO.



(c) TIMSWICO



(d) FRODITKS



(e) ARKCOOKS

Figure 3.15. Range of Stream Gauge Equipment Housings in the LARV.

Data from the CDWR and USGS stream gauges are reported on web sites operated by the two agencies. Table 3.8 lists the gauge sites used in this study and notes the additional data besides streamflow collected at each gauge. Additional data are reported by the agency that owns and operates the gauge site. USGS instruments at a CDWR gauge site are recorded

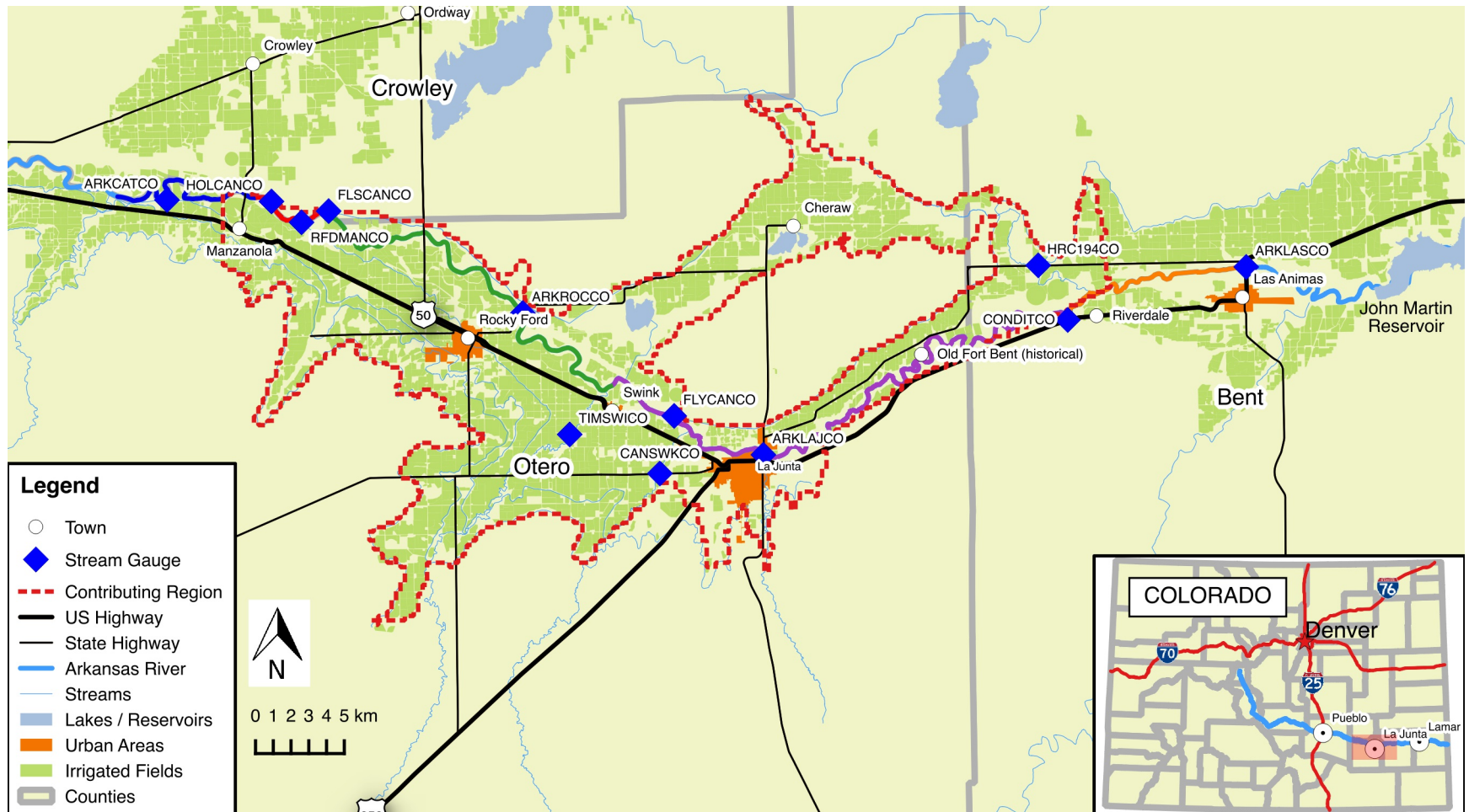


Figure 3.16. USR River River and Tributary Stream Gauge Locations.



Figure 3.17. DSR River River and Tributary Stream Gauge Locations.

and reported on the CDWR web site. Note that the CDWR gauge site ARKLAMCO, which is owned by the USGS, does not have any additional data collection instruments.

Table 3.8. Summary of Stream Gauges with Notation of Additional Data Collected.

Study Reach		Stream Gauge ID	Parameter		
	CDWR	USGS	Air Temp.	Water Temp.	EC
USR	ARKCATCO			X	X
	HOLCANCO				
	RFDMANCO				
	FLSCANCO				
	RFDRETCO				
	TIMSWICO				
	FLYCANCO				
	CANSWKCO				
	ARKLAJCO		X		
DSR	CONDITCO				
	HRC194CO				
	ARKLASCO	07124000		X	X
	ARKJMRCO	07130500		X	X
	ARKLAMCO	07124000			
	BIGLAMCO				
WILDHOCO	BUFDITCO				
	FRODITCKS				
	ARKCOOKS	07137500		X	X

Stream flow data were obtained as average daily flow for each stream gauge. Some average daily flow records were reported as being estimated or provisional. These data points were removed from the analysis. Average daily flow data were quality checked for unacceptable values. For each gauge, acceptable values were defined as those above zero and below the 99th percentile of all flows recorded at that gauge. Unacceptable values were removed from the data set.

All stream gauges report gauge height which is the vertical distance from the gauge site datum to the water surface (Figure 3.18). Gauge site datum is arbitrarily set, but is tied to a local survey benchmark. Flow depth is the depth from the bottom of the channel

to the water's surface. While both gauge height and flow depth measure the distance to the water's surface, their datums can, and frequently do vary. The Arkansas River is a shifting bed channel and as such, the channel bottom elevation varies with time at a gauge site. The rating table, which is used to convert flow depth to flow rate, is configured such that flow depths below the channel bottom have a flow rate of zero. The table is frequently updated with data obtained from routine re-calibration of the stream gauge.

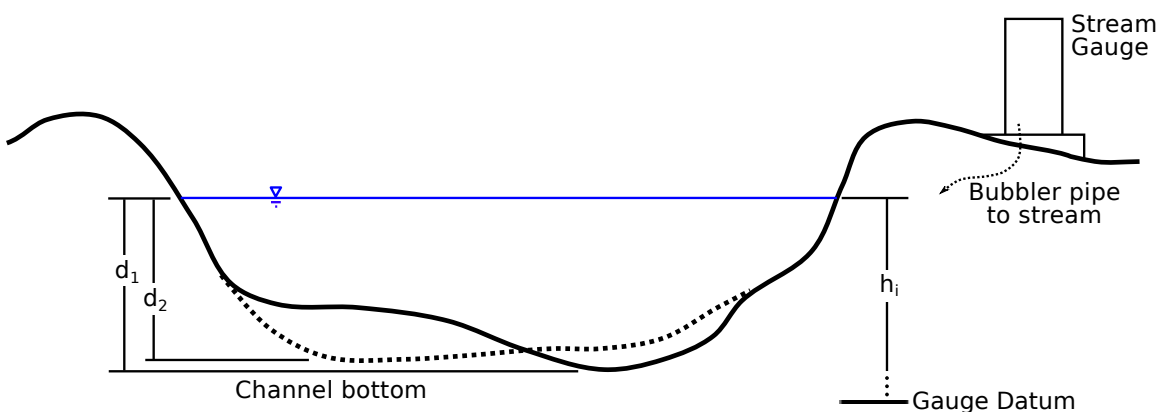


Figure 3.18. Depiction of Variable Channel Bottom and Fixed Gauge Datum. d_1 and d_2 are flow depths at different times. h_i is the stream gauge height measurement at any time.

Gauge height data is the directly measured value that is used to calculate flow rate. Flow rates are calculated from gauge height using a gauge site specific rating table produced in accordance with USGS standards and procedures (Rantz et al., 1982a,b). Gauge heights for the USGS and CDWR gauges were obtained from the respective regional offices. Historical recorded gauge heights are not reported on web sites as these data are considered to be precursors for stream flow rate calculations. Stream gauge data were provided as both average daily gauge height and as recorded gauge height. Recorded gauge height is the gauge height recorded in 15-minute increments during a calendar day. Average daily gauge height is the mean of the recorded gauge heights over a calendar day. All gauge heights were

provided in units of feet above the gauge datum. Gauge height units were converted to SI units of meters for this study to simplify calculations and discussion. Gauge height data were checked for accuracy by the source agency before being released to CSU staff.

Water temperature data were obtained as average daily temperature or as minimum
5 and maximum daily temperatures, depending on the gauge site. Average daily temperature is calculated as the mean of the minimum and maximum daily temperature. Water temperature data were provided in units of °C. Since frozen or partially-frozen river channels do not have the same gauge height to flow rate relationship as free running river channels, data corresponding to water temperatures below zero were removed from the data set.

10 EC data obtained from USGS and CDWR stream gauge sites were provided as average daily values for each recording gauge station. EC values recorded at the stations were compared to available EC values measured by CSU to cross-validate both data sets. Gauge station recorded EC values were quality controlled by removing the bottom and top 1% of EC values for each gauge. Changes in average daily EC between consecutive days were
15 checked for validity. Changes greater than 33% were analyzed to determine if the EC change was valid. The average daily flow rate and time of year were taken into consideration when determining if the questionable EC values were valid. EC values that exceeded the 33% change but were accompanied by large changes in EC or during peak irrigation seasons were considered valid EC values. Values considered to be invalid were removed from the data set.
20 EC values were provided in units of $\mu\text{S cm}^{-1}$.

Atmospheric data was required to determine the volume of water evaporated from the river's surface. The Colorado Agricultural Meteorological Network (CoAgMet) was chosen as the source for atmospheric data. The National Weather Service station sites in the study regions are located in populated areas or at airports and is only suitable for weather analysis.

CoAgMet station sites are more numerous, are located in agricultural areas, and are suitably equipped for evaporation and transpiration (*ET*) analysis. An example of one of the weather stations is shown in Figure 3.19. The CoAgMet network is operated by the Colorado Climate Center at CSU and consists of 86 weather stations throughout the state. Some stations are 5 only seasonally operational (Andales et al., 2009; Colorado Climate Center, 2012). Of the full-time sites, three are located in the USR and three are located in the DSR as shown in Figures 3.20 and 3.21, respectively. The CoAgMet weather stations in the USR are located such that they represent the upper, middle, and lower segments of the USR. The CoAgMet stations in the DSR are more tightly grouped toward the upstream end of the reach, but still 10 are considered representative of the study reach. The weather stations are primarily located in agricultural areas to provide agricultural researchers with data used for many different research applications. The data also are available to the public through a web site. This has aided farmers in determining irrigation timing and quantity (Andales et al., 2009). Table 3.9 is a list of the parameters measured at the CoAgMet stations and the typical instruments 15 used. Not all stations are identical. Instruments were replaced or upgraded by CCC staff when required with instruments that were available and equal to or better in quality than the instrument being replaced.

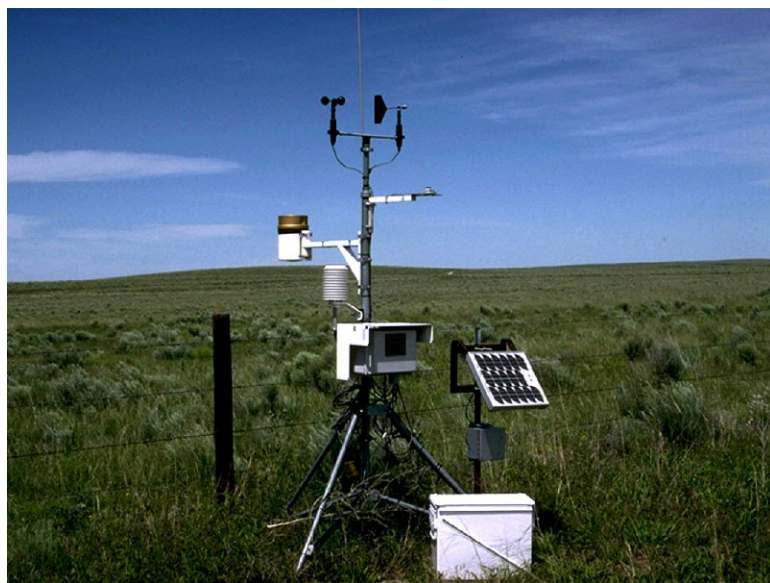


Figure 3.19. Typical CoAgMet Weather Station.

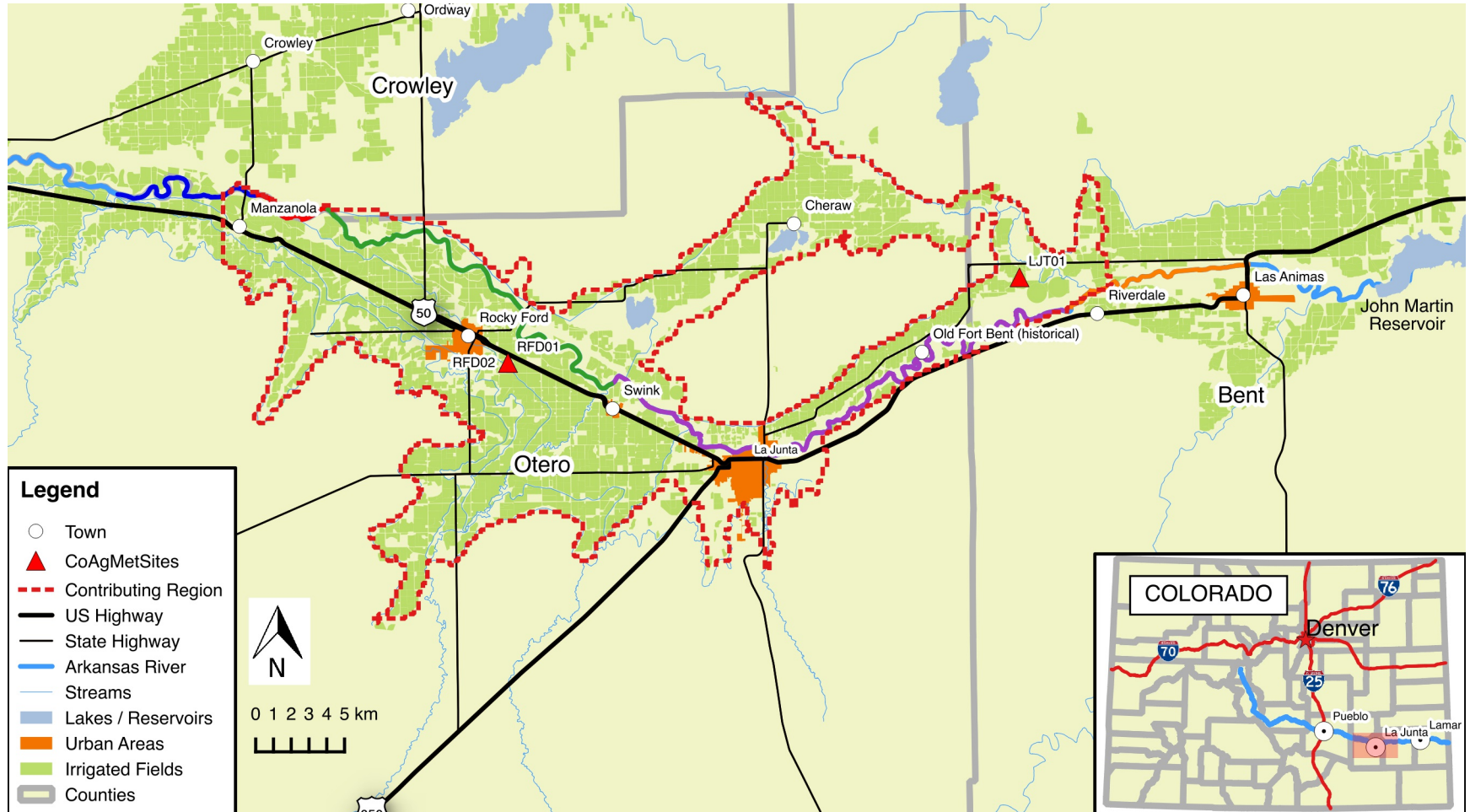


Figure 3.20. USR CoAgMet Weather Station Locations.



Figure 3.21. DSR CoAgMet Weather Station Locations.

Table 3.9. Typical Instrumentation at CoAgMet Weather Stations.

Measured Parameter	Typical Instrument
Temperature & Relative Humidity	Vaisala HMP45C Probe
Wind	R.M. Young Wind Sentry
Solar Radiation	Licor LI-200X Pyranometer
Precipitation	TE525 tipping bucket raingauge
Soil Temperature	CSI Model 107 Soil Temp Probe (thermistor)
Data Loggers	Campbell Scientific CR10, CR10X, and CR1000

Table 3.10 lists the weather stations in the LARV that were used in this study. This table lists the station name and location, the state of irrigation of the land surrounding the site, the date of first record, and a comparative estimate of the site estimated ET_{ref} to the actual ET_{ref} . The irrigation state of the land surrounding the site is used to determine the 5 comparative estimate of the site estimated ET_{ref} to the actual ET_{ref} . If the monitoring station is on irrigated land then the ET_{ref} values calculated based on site data are expected to be at or near the actual value of ET_{ref} for the site. If the station is on dry, or non-irrigated land, then calculated ET_{ref} values tend to over estimate the actual ET_{ref} .

CoAgMet provides both raw weather data from all weather stations and daily ET_{ref} 10 values calculated for select stations. Daily ET_{ref} values were obtained from the sites in the LARV. The American Society of Civil Engineers (ASCE) Environmental and Water Resources Institute (EWRI) standardized tall crop evapotranspiration reference Penman-Monteith equation was used by the Colorado Climate Center to calculate ET_{ref} . Values are obtained in units of mm d^{-1} .

15 The average daily ET_{ref} for a region surrounding a study reach was calculated as the mean of the stations reporting ET_{ref} for a given day. If a station or group of stations did not have data for a particular day in the study time frame, then those stations were not included in the calculation. An assumption was made that the ET_{ref} over the Arkansas

Table 3.10. CoAgMet Weather Stations used for analysis in the LARV.

Study		Station		Irrigation	Date of First Record	Comparative Est. of Site ET
Reach	ID	Name	Location			
USR	FWL01	Fowler	Fowler Golf Course	Full	17 Mar 2005	–
	LJT01	LaJunta	11 mi NE of LaJunta	Full	17 Mar 2005	Under
	RFD01	RockyFord	CSU Experiment Station, Rocky Ford	Full	6 Apr 1992	–
DSR	HLY01	Holly	5 mi NW of Holly	Part	27 Sep 2001	Over
	HLY02	Holly #2	8.5 mi NW of Holly	Full	21 May 2005	–
	LAM04	Lamar #4	4.5 mi NNE of Lamar	Full	11 May 2005	–

River within a study reach could be approximated as the mean of the reported values within the surrounding region.

The minimum daily relative humidity (RH_{min}) and wind speed at 2 m above ground surface (u_2) data were obtained from the same CoAgMet stations as the precipitation and
5 ET_{ref} data. RH_{min} values were reported as a fraction and values less than zero were removed from the data set. Wind speed values were reported as wind run, which is the total distance the air traveled during the calendar day and is reported in units of km d^{-1} . A small number of the wind run values in the obtained data set were less than zero and were removed. Historical average wind run values were not available to provide a method to sanitize the
10 wind run upper bound values. Wind run values were converted to average daily wind speed in units of m s^{-1} .

Precipitation data were collected from the same network of monitoring stations used to generate average daily ET_{ref} as daily values in units of mm d^{-1} . Data was not sanitized

before publication to the CoAgMet web site. A small number of total daily precipitation values in the obtained data set were less than zero or exceeded reasonable maximum values.

Daily total precipitation values less than zero or greater than 1.5 times the highest average precipitation reported by the National Weather Service were excluded. As with the ET_{ref}

5 data, the mean precipitation value over the surrounding region of a study reach for any given day only included those stations reporting data. Any additional data collected from the CoAgMet system was treated in a similar manner.

CHAPTER 4

EVALUATION OF NPS RETURN FLOW TO THE RIVER USING A WATER BALANCE MODEL

4.1. WATER BALANCE MODEL APPLIED TO THE LARV

The purpose of the water balance model is to determine the volume of unaccounted for water in each reach. We begin with a basic water balance model as described in most hydrology texts — (Wanielista et al., 1997).

$$\text{change in storage} = \text{inputs} - \text{outputs}$$

5 Adding the variables, both known and unknown, present in the LARV we have the following equation:

$$\frac{\Delta S}{\Delta t} = Q_{in,US} + \sum Q_{in} + P + R + B - Q_{out,DS} - \sum Q_{out} - E - T - F + X \quad (4)$$

Where:

$$\frac{\Delta S}{\Delta t} = \text{Stored volume change between time steps.}$$

$Q_{in,US}$ = Flow in the river entering the study reach at the upstream end.

$\sum Q_{in}$ = Flow gained by the river from tributaries and other gauged sources.

P = Volume of water gained to the river due to precipitation falling directly on the river's surface.

R = Volume of water gained to the river due to precipitation runoff from adjacent land.

B = Volume of water gained to the river due to subsurface flow.

$Q_{out,DS}$ = Flow in the river leaving the study reach at the downstream end.

$\sum Q_{out}$ Flow lost from the river to canals and other gauged sinks.

E = Volume of water lost from the river due to direct evaporation from the water's surface.

T = Volume of water lost from the river due to plant transpiration.

F = Volume of water lost from the river due to infiltration into the subsurface flow.

X = Water volume gains and losses to/from unknown sources and sinks.

The inclusion of the X term signifies one of two types of unknown values addressed in this thesis. There are known unknowns, which are directly addressed and unknown unknowns. Known unknowns are those values or terms which are known to exist, but the magnitude and sign of their effect is unknown and/or immeasurable. Unknown unknowns
5 are those values or terms which we do not know exist. Their existence and effect on a system are yet to be discovered. We assume with the current state of chemistry and physics, that the X term is insignificant. However, we cannot discount it from our analysis.

If we combine the terms that are unknown or unmeasured, we arrive at the following equation:

$$\frac{\Delta S}{\Delta t} = Q_{in,US} + \sum Q_{in} + P - Q_{out,DS} - \sum Q_{out} - E + Q_{UNPS} \quad (5)$$

Where:

$^{10} Q_{UNPS}$ = The sum of gains from non-point sources and losses to non-point sinks
= $Q_{UNPS} = R + B - T - F + Q_{U,in} - Q_{U,out} + X.$

There is no reasonable method for differentiating the components of Q_{UNPS} , therefore the abbreviation NPS in this thesis refers to both non-point sources and non-point sinks. Q_{UNPS} includes the non-point source gains from groundwater sources (B), non-point source losses to groundwater sinks (F), transpiration losses from plants in the river channel 5 (T), and gains from precipitation runoff from adjacent land (R). Additionally, this term includes ungauged flows leaving and entering the river. Ungauged gains to the river ($Q_{U,in}$) are suspected to be primarily in the form of irrigation drainage from adjacent farmland. Other sources could be due to errors in underestimating flows entering the river or overestimating flows leaving the river. Ungauged losses from the river ($Q_{U,out}$) are suspected to be 10 primarily in the form of minor or unauthorized withdrawals from the river channel. Of the ungauged flows, irrigation drainage from adjacent farmlands is assumed to be the largest contributor.

The two groundwater components of Q_{UNPS} are suspected of being the largest components of Q_{UNPS} . Water transfer between the aquifer and river happens continually whereas 15 $Q_{U,in}$, $Q_{U,out}$, R , and T are not continuous. $Q_{U,in}$ and $Q_{U,out}$ only occur periodically when individuals actively withdraw from the river or allow irrigation runoff to return to the river. R only occurs during rain events. Within the LARV, most rainwater is captured in irrigation canals. Only precipitation falling in the riparian zone is likely to reach the river. T only occurs during growing season. This value is also only considering the transpiration 20 happening within the river channel and does not include the riparian zone. Any losses due to transpiration in the riparian zone are first considered river losses to the aquifer (F).

Re-arranging equation (5) to solve for the unknown values produces equation 6. Due to the nearly identical method of calculating flow (Q) and it's associated error and uncertainty, these terms were associated with each other. Likewise, the precipitation (P) and

evaporation (E) terms were associated with each other.

$$Q_{UNPS} = \left(Q_{out,DS} + \sum Q_{out} - Q_{in,US} - \sum Q_{in} \right) + \frac{\Delta S}{\Delta t} - (P + E) \quad (6)$$

This model is further simplified to Equation 7 which combines terms that are calculated using similar methods to facilitate discussion.

$$Q_{UNPS} = \frac{\Delta S}{\Delta t} - \sum Q_{Surface} - \sum Q_{Atm} \quad (7)$$

Where:

$\frac{\Delta S}{\Delta t}$ = Reach storage change per time-step.

$\sum Q_{Surface}$ = Sum of flows added and removed from the reach per time-step.

$$= Q_{in,DS} + \sum Q_{in} - Q_{out,US} - \sum Q_{out}$$

Q_{Atm} = The sum of precipitation gains and evaporation losses, per time step.

$$= P - E$$

5

A time step of one day was established for all models calculated in this thesis. Most of the data from agencies is readily available in average daily format. While most of the data could also be obtained in hourly or quarter-hourly format, it was assumed that the additional information would not improve model accuracy.

4.2. STOCHASTIC AND DETERMINISTIC MODELS

Deterministic and stochastic models are used in both the unaccounted for water and mass balance models. Deterministic models are fully determined by the input parameters or variables. Randomness of any kind is not included. Stochastic models extend deterministic 5 models by including one or more random parameters. Given the same input parameter values, a stochastic model will produce different results with each iteration.

There are many recognized methods for solving stochastic models. Solutions to these models are not definite and the term "solve" must be taken loosely. Any individual solution from a stochastic model is one of a potentially infinite number of possible solutions. The 10 Monte Carlo (MC) simulation technique was used to obtain solutions for all stochastic models in this thesis. The MC technique is conceptually simple. The stochastic model is repetitively solved in a series of iterations. The combined solutions from all iterations are used to define the solution statistics of the model.

The number of iterations performed is determined by calculating and analyzing a set 15 of identifier statistic(s) after each run. Identifier statistic(s) are those that the modeler has determined to be of value in determining when to terminate the model. These statistics are monitored to identify when the change in the statistic has reached a predetermined threshold. It was determined that for the sake of simplicity, all of the models calculated in this thesis would use the same number of iterations. The USR mass balance model is the most 20 complex model as it has the largest number of input variables and uncertainty terms. The identifier statistics used were the mean, variance, and skewness which are the first, second, and third moments of the probability density. These were calculated for each iteration. The threshold between the observed iteration and the previous iteration was fixed at 0.1%. The identifier statistics reached the threshold in the following order: mean, variance, and

skewness. Skewness reached its break point shortly before the 500th iteration. A judgment call was made to increase the factor of safety. Therefore, the number of stochastic model iterations was fixed at 5,000. The fourth moment, kurtosis, was also calculated and analyzed for each iteration. It was found to be too sensitive as it did not consistently stay within the 5 accepted cutoff threshold of 0.1%. It is assumed that this sensitivity is due to the existence of a significant number of outliers that cause the distribution of results to be non-normal.

4.3. ERROR AND UNCERTAINTY.

Any problem that measures variable natural processes must account for parameter and model uncertainties (Vicens et al., 1975). Parameter uncertainty is derived from measurement error, spatial variability, and temporal variability (Herschy, 2002). Measurement 10 error is the difference between the true and measured values. Most of this error type is due to instrument measurement inaccuracies due to either error inherent in the instrument or from errors in calibration or measurement. Measurement errors inherent to the instrument are uncorrectable and cannot be accounted for within the model. Errors due to calibration 15 or measurement deviations are only correctable at the time of measurement or calibration and cannot be accounted for within the model.

Spatial variability is the difference in the true value at different points when measured at the same time. Data collected at a single given point in space may not be representative of the area it is assumed to represent due to spatial variability. This can manifest itself even 20 with very small distances between measurements. Temporal variability is the difference in the true value at the same point, but at different times. Data collected at a one time may not be representative of the time frame it is assumed to represent due to temporal variability (Timmothy K. Gates and Al-Zahrani, 1996). Again, this can be manifested even over small

time differences. Due to instrument error, the spatiotemporal variability of the measured object, and the inability to know the true value of the measurement, reported parameter values should be treated as random variables (C. T. Haan, 1989; Charles Thomas Haan, 2002).

5 Almost all of the data was obtained from outside agencies and was not collected by the research team. These agencies have data uncertainty ranges that account for all parameter uncertainties. These uncertainties are expressed in accordance with the ISO Guide to Expression of Uncertainty in Measurement (GUM) (ISO, 2008). While the GUM classifies uncertainty as either "Type A" or "Type B", the all of the data included in this
10 thesis has uncertainty evaluations described as "Type B". Type B evaluations usually use standard deviations and assumed probability distributions obtained from scientific judgment, available information, and possible variability of a measurement.

The data originators have provided uncertainty ranges which include instrument measurement random error and uncertainties due to temporal variations of the measured location. The root mean square method is used to estimate the uncertainty related to measurement of water quantity and water quality values (Harmel and P. K. Smith, 2007; ISO, 2008). Harmel and P. K. Smith (2007) describe this measurement uncertainty as the probably error range, and quantify upper and lower uncertainty boundaries for measured data points as the following when attempting to specify an expected range of expected values.

$$\sigma^2 = \left(\frac{O_i - UO_i(l)}{3.9} \right)^2 \quad \text{or} \quad \sigma^2 = \left(\frac{UO_i(u) - O_i}{3.9} \right)^2 \quad (8)$$

Where:

σ^2 = variance about measured data value O_i .

O_i = measured value.

UO_i = upper (u) and lower (l) uncertainty boundaries.

3.9 = number of standard deviations accounting for $> 99.99\%$ of a normal probability distribution

The data collected for this thesis is assumed to represent the mean of a normal distribution of possible values. The upper and lower bounds of the distributions are given as either a percent or value deviation from the mean. Equation 8 is re-written from the definition found in Harmel and P. K. Smith (2007) to that found in equation 9.

$$\sigma^2 = \left(\frac{\mu - (\mu - \mu p)}{3.9} \right)^2 \quad \text{or} \quad \sigma^2 = \left(\frac{(\mu + \mu p) - \mu}{3.9} \right)^2 \quad (9)$$

Where:

μ = the reported value (assumed to be the mean).

p = the reported percent deviation from μ .

5 Both of these equations in 9 simplify to equation 10. The standard deviation is shown as the calculated result due to the requirements of the modeling software.

$$\sigma = \frac{\mu p}{3.9} \quad (10)$$

When the upper and lower bounds are defined as a fixed value deviation from the reported value, then equation 8 becomes:

$$\sigma^2 = \left(\frac{\mu - (\mu - v)}{3.9} \right)^2 \quad \text{or} \quad \sigma^2 = \left(\frac{(\mu + v) - \mu}{3.9} \right)^2 \quad (11)$$

Where:

v = the reported value deviation from μ .

In this case, both equations in 11 simplify to:

$$\sigma = \frac{v}{3.9} \quad (12)$$

The difference between a model's calculated or estimated value and the reported value

5 is called a residual. The distribution of residuals is the model uncertainty. These distributions are uni-variate and do not have predefined shapes. There are a variety of statistical and graphical tools available to analyze unknown residual distributions to determine a best fit parametric distribution. The two graphical tools used in this thesis to analyze distributions are the histogram and the kernel density estimate.

10 Non-parametric distribution models are used as an aid for analyzing uni-variate data sets. Specifically, kernel density estimates (KDE) are used in conjunction with histograms to assist in visual analysis of the data. Figure 4.1 is an example of a random sample of one of the input data sets used in this thesis. The curve is the KDE. The short vertical lines between the histogram and the x-axis, called a rug, depict the data values. This figure
15 adequately displays the resulting differences between histograms and KDE. KDEs can more accurately depict data groupings that are lost in histogram bins. The histogram leads us to believe that the data has a strong tendency to be near zero, while the KDE shows that the majority of the data is between 0-20. Histograms can more accurately depict extremes

or cut-off values. In the figure, there are no values less than zero. The histogram clearly shows this while the KDE shows that there are values less than zero. Both histograms and KDE are used throughout this thesis to assist in the description of distributions. A rug is also presented with the histogram whenever the quantity of data allows for adequate data presentation. A rug is not included when the data set is too large to allow for discrete identification of data values.

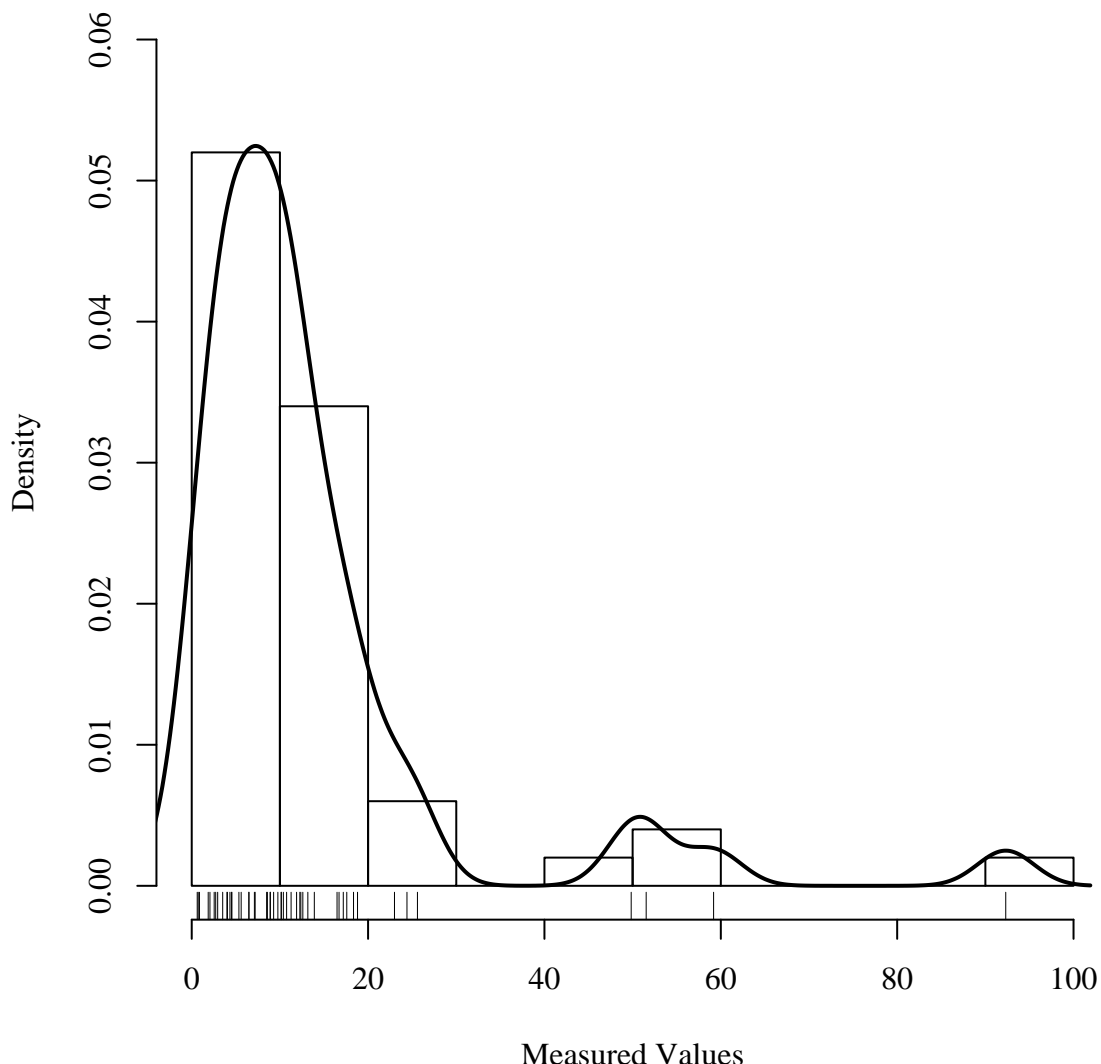


Figure 4.1. Example kernel density estimate. The data is a random sample of an input variable used in this thesis. The curve depicts the kernel density estimate. The short vertical lines between the histogram and the x-axis, called a rug, depict the data values.

Determining which parametric distribution best fits the uni-variate residual distribution requires the use of both the graphical and statistical tools. For each residual distribution, probable parametric distributions types were chosen for testing against the residual distribution. For each of these parametric distribution types, a best fit was generated using the

5 maximum likely-hood estimator (MLE) method. These MLE results were then analyzed using Kolmogorov-Smirnov (K-S), Cramer-von Mises (CvM), and Anderson-Darling (A-D) goodness-of-fit tests to determine which distribution type best fit the uni-variate residual distribution. All three tests are non-parametric tests of continuous uni-variate probability distributions. The K-S and CvM tests calculate the difference between the empirical cumulative density function (ECDF) of the test data and the cumulative density function (CDF) of

10 the tested reference distribution. The K-S and CvM tests use different algorithms to perform the calculation. Each of the goodness-of-fit tests has their own strength and weaknesses and as such, graphical tools are used to confirm or refute the statistical test results (D'Agostino and Stephens, 1986; Delignette-Muller and Dutang, 2014; Venables and Ripley, 2002).

4.4. RIVER STORAGE CHANGE

River reach estimated stored water volume changes ($\frac{\Delta S}{\Delta t}$) from equation 4 are the sum of the river segment stored water volume changes for each reach (Equation 13). The storage change for each segment is calculated independent of adjacent segments.

$$\frac{\Delta S}{\Delta t} = \sum \frac{\Delta S_i}{\Delta t} \quad (13)$$

Where:

ΔS = Water storage change in the river reach.

5

ΔS_i = Water storage change in river segment i .

Δt = Model time step = 1 day.

River reach volume changes are calculated between two consecutive time steps. Reach volume changes are calculated as the sum of the volume changes within the segments that compose the reach. River segment volume change between time steps is calculated as shown
10 in equation 14.

$$\frac{\Delta S_i}{\Delta t} = L_i \cdot \frac{\Delta A_i}{\Delta t} \quad (14)$$

Where:

$\frac{\Delta S_i}{\Delta t}$ = Segment storage change.

L_i = Segment length.

$\frac{\Delta A_i}{\Delta t}$ = Segment cross-section area change.

For the USR, Equation 13 includes the storage volume changes from all five segments of the USR as shown in Equation 15. Equation 16 shows the expanded form following

Equation 14.

$$\frac{\Delta S_{USR}}{\Delta t} = \frac{\Delta S_A}{\Delta t} + \frac{\Delta S_B}{\Delta t} + \frac{\Delta S_C}{\Delta t} + \frac{\Delta S_D}{\Delta t} + \frac{\Delta S_E}{\Delta t} \quad (15)$$

$$= L_A \cdot \frac{\Delta A_A}{\Delta t} + L_B \cdot \frac{\Delta A_B}{\Delta t} + L_C \cdot \frac{\Delta A_C}{\Delta t} + L_D \cdot \frac{\Delta A_D}{\Delta t} + L_E \cdot \frac{\Delta A_E}{\Delta t} \quad (16)$$

For the DSR, Equation 13 includes the storage volume changes from the two segments of the DSR as shown in Equation 17. Equation 18 shows the expanded form following Equation 14.

$$\frac{\Delta S_{DSR}}{\Delta t} = \frac{\Delta S_F}{\Delta t} + \frac{\Delta S_G}{\Delta t} \quad (17)$$

$$= L_F \cdot \frac{\Delta A_F}{\Delta t} + L_G \cdot \frac{\Delta A_G}{\Delta t} \quad (18)$$

Figure 4.2 shows the difference between a simplified example of a natural channel and the modeled channel. Although the river is variable in width and depth along its entire lengths, it is modeled as a trapezoidal prism with a constant length and with a cross-section that does not vary with respect to location. It was reasoned that this simplistic model would best approximate the average channel shape along the entire reach. The channel water surface elevation is assumed to be constant through each segment. This assumption is not true in nature, but we are not concerned with the water surface elevation, but with the flow depth. We are assuming that the flow depth remains relatively constant through a river segment. This assumes that all gains and losses to the river are accounted for either through flow gains and losses, evaporation, precipitation, or unaccounted for gains and losses as shown in equation 4.

Segment lengths, as reported in Table 4.1, are sufficiently short such that any surges due to irrigation canal gates changes, precipitation events, or other events pass through the

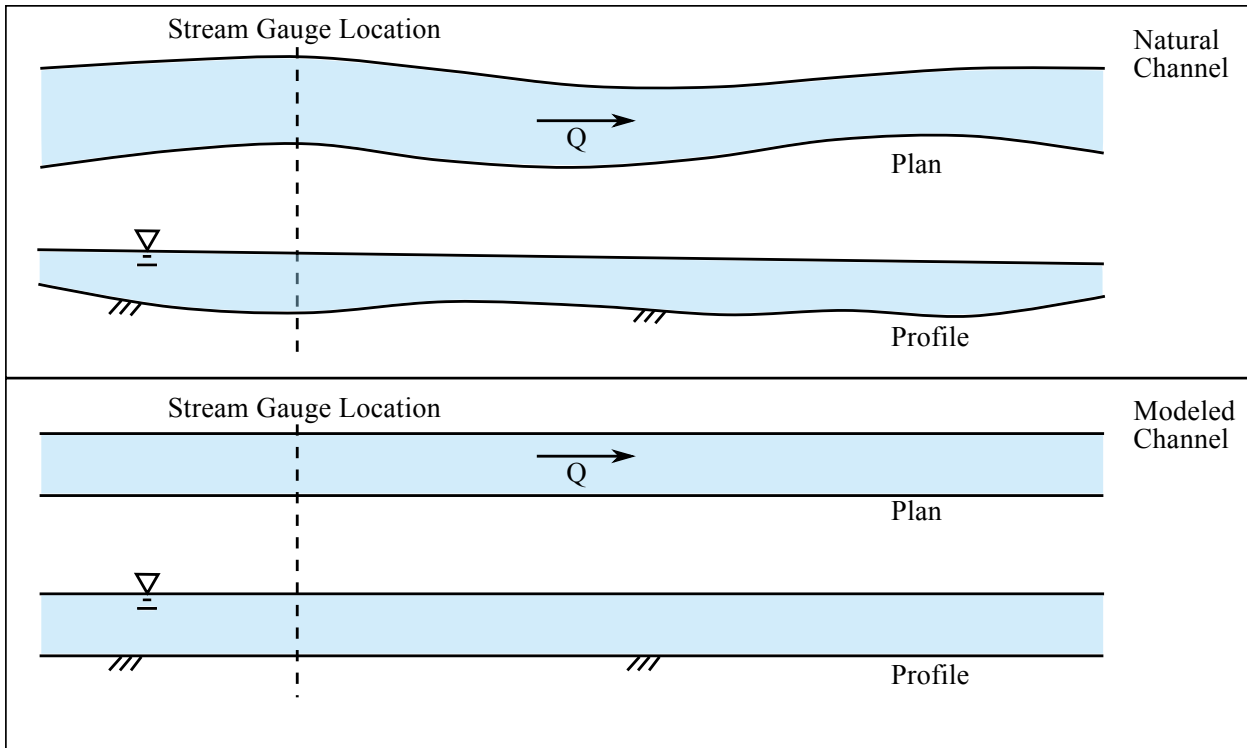


Figure 4.2. River Segment Model.

segment in less than a day. The total travel time is approximately 2-3 days and 1-2 days in the USR and DSR, respectively, based on USGS reported average stream velocity measurements taken in conjunction with stream gauge calibrations. River segment length (L_i) was measured to the nearest 0.1 km using publicly available satellite imagery, USGS hydrography data, and geographical information system (GIS) software. River segment length was calculated as the length of the thalweg between the segment endpoints. When the USGS thalweg did not follow along the river channel as shown in the satellite imagery, a new thalweg was drawn. Rough validation of these measurements was performed in the field by comparing the GIS calculated length of adjacent roadways to the actual driven distance as reported by a vehicle odometer. River lengths are assumed to be constant throughout the study time frame. Individual and combined variations in the channel path along a river segment were

assumed to be negligible.

Table 4.1. River Segment Lengths.

Study Reach	River Segment	Segment Length	
		km	mi
USR	A	12.5	7.8
	B	3.9	2.4
	C	30.7	19.1
	D	37.8	23.5
	E	14.3	8.9
DSR	F	37.6	23.4
	G	24.9	15.5

River segment cross-sectional area change ($\frac{\Delta A_i}{\Delta t}$) calculation is based on the trapezoidal area that approximates the difference between the cross-sectional area at two different

5 flow depths as depicted in Figures 4.3, 4.4 and in equation 19. While the cross sectional area difference isn't exactly a trapezoid, the difference for small differences in gauge height is insignificant.

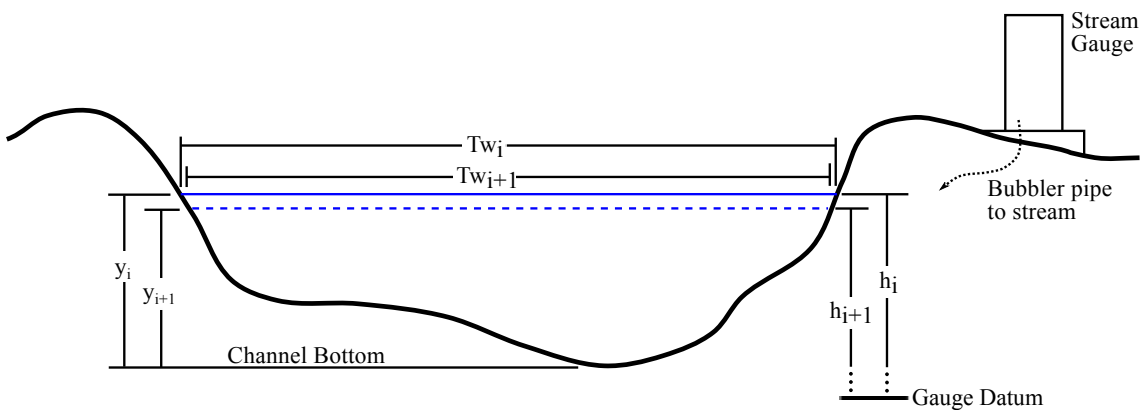


Figure 4.3. Average river segment cross-section area change.

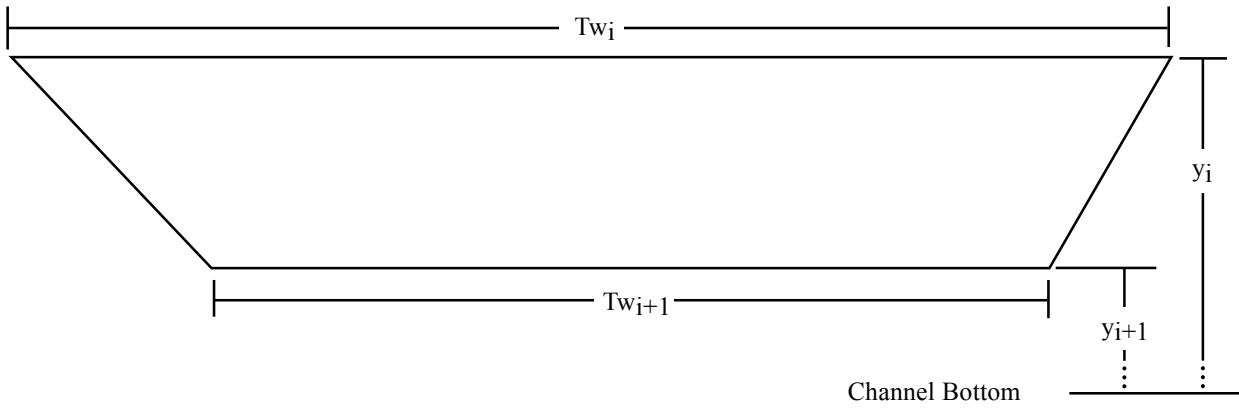


Figure 4.4. River cross-section area change diagram.

$$\begin{aligned}\frac{\Delta A_i}{\Delta t} &= \overline{Tw} \cdot \Delta y \\ \frac{\Delta A_i}{\Delta t} &= \frac{Tw_t + Tw_{t-1}}{2} \cdot (y_{t-1} - y_t)\end{aligned}\quad (19)$$

Where:

t = Current time step.

$t-1$ = Previous time step.

$\frac{\Delta A_i}{\Delta t}$ = Cross-section area change at river section i between time steps.

\overline{Tw} = Average river top width.

Δy = Change in flow depth from the previous time step.

Tw = River top width.

y = River flow depth.

Figure 4.3 shows a simplified river cross section at a stream gauge location. As previously discussed, stream gauges do not hold the channel bottom as their datum. They have an arbitrarily fixed datum that does not move unless reset by the gauge owner. The

difference between the stream gauge datum and the channel bottom is corrected using a constant correction factor calculated from the river survey. The gauge datum does not have a known marker where the elevation could be directly measured. Instead, the surveyed water surface elevation was recorded at the gauge location on both sides of the channel.

- 5 The flow depth value was calculated by finding the difference between the surveyed average water surface elevation and the surveyed channel bottom elevation. The flow depth was then compared to the stream gauge height reported for the same date and time as when the water surface elevation was surveyed. The difference between the reported value and the average of the surveyed values was taken as the correction factor for the gauge. This procedure was

10 repeated for each gauge.

Flow depth values as reported by the USGS and CDWR are measured values with an associated probability range as calculated in equation 10. The uncertainties are applied as shown in equation 20. A correction factor (C_i) is applied to each reported gauge depth to correct for the difference between the gauge datum and the channel bottom as measured

- 15 during the channel cross-section survey. Two separate uncertainties are applied. ε_{h1} is the uncertainty distribution as described by the gauge owner. This uncertainty is reported by both the USGS and CDWR as being normally distributed with extreme values at ± 0.01 ft (± 0.003 m) (Cobb, 1989). The second uncertainty term, ε_{h2} , is the result of personal observation of the river channel along its entire length. This term describes the variability in flow

20 depth. It was observed that the channel depth did not vary greatly along most of its length. There were particular areas where there were deeper pools, but these areas were noted to be more prone to ponding during low flow. It is assumed that the average effective flow depth only varies within a normal distribution with limits of ± 0.076 m (± 0.25 ft). There is the possibility that ε_{h1} could cause the storage change between the time steps to change from a

storage gain to a storage loss, or vice versa. This is acceptable as it is within the measurement limits of the instruments. Once $h + \varepsilon_{h1}$ has been calculated for the two successive time steps,

the relationship between the two time steps is fixed. If the river segment flow depth rises between time steps after this calculation, then that relationship must continue throughout

- 5 the rest of the volume change calculation. To facilitate this, it is assumed that ε_{h2} does not vary significantly within the study time frame and does not vary within a realization. The Arkansas River channel is sufficiently stable between consecutive days that this assumption is valid. A new ε_{h2} is drawn for each realization and remains constant for all time steps within the study time frame.

$$y_{i,t} = h_{i,t} + C_i + \varepsilon_{h1} + \varepsilon_{h2} \quad (20)$$

Where:

$y_{i,t}$ = Section i modeled average daily flow depth at time t .

$h_{i,t}$ = Section i reported average daily river gauge height at time t .

10 C_i = Section i river gauge height to flow depth correction term.

ε_{h1} = Reported river gauge height data uncertainty.

ε_{h2} = Estimated flow depth uncertainty.

Since the two uncertainty terms are both normal and additive to flow depth, they

were added to produce a new normal distribution with mean equal to the sum of the means of the two distributions and standard deviation equal to the sum of the standard deviations

- 15 of the two distributions. This additional step was taken to improve model calculation speed and to reduce the possible error of producing a total flow depth error that would cause a flow depth outside of the accepted range of 0.153 m to 1.53 m (0.5 ft to 5 ft). The uncertainty

distributions ε_{h1} and ε_{h2} are not dependent on location, therefore all flow depth calculations draw from the same distribution. The normal distribution resulting from the addition of the ε_{h1} and ε_{h2} has a mean of zero and standard deviation of 0.00707 m (0.02032 ft) (Equation 21).

$$y_{i,t} = h_{i,t} + C_i + \mathcal{N}(\mu = 0m, \sigma = 0.00707m) \quad (21)$$

River top width (Tw) is calculated using equation 22 (Buhman et al., 2002; Timmothy K. Gates and Al-Zahrani, 1996). The river channel does not have a fixed cross-section along it's length, therefore, the fitting parameters, β_1 and β_2 are not constant, but are from distributions of β_1 and β_2 . Equation 22 and the data from each survey cross-section was used to calculate a best fit equation using non-linear least squares regression. Regression results for each cross-section are presented in Table 4.2. There are an insufficient number of cross sections within each river segment to provide a statistically significant sample. This means that there is insufficient data available to generate independent fitting equations for each river segment. Therefore, the β_1 and β_2 values from each cross-section were combined to determine the distribution of β_1 and β_2 for the entire river reach. The combined distributions were tested to determine the best fit parametric distribution using the previously described method. The best fit distributions for β_1 and β_2 are presented in table 4.3. β_1 and β_2 values were analyzed for correlation which was found to be insignificant with a Pearson R value of 0.17. Visual analysis of the data points showed that there was no distinguishable pattern. Future cross-section surveys will expand the data set and may show that there is a correlation between β_1 and β_2 , but the available data does not support that conclusion. Also presented in Table 4.3 is the best fit distribution for the residuals. These distributions and

the distributions for β_1 and β_2 were analyzed to determine the best fit distribution using the methodology described in Section 4.3.

$$Tw_{i,t} = \beta_1 y_{i,t}^{\beta_2} + \varepsilon_{Tw} \quad (22)$$

Where:

$Tw_{i,t}$ = River segment i average daily top width at time step t .

$y_{i,t}$ = Calculated segment i average daily flow depth at time step t calculated using equation 20.

β_1 and β_2 = fitting parameter distributions.

ε_{Tw} = Calculated average daily flow depth uncertainty.

5 Non-linear regression models were used only when the specific model form, determined from known physical or geometrical relationships, was non-linear. R-squared values were not used to determine goodness-of-fit for non-linear regression models since they can have valid R-squared values that are negative or greater than one (Spiess and Neumeyer, 2010) and as such are outside of the boundary for comparing linear models. Pseudo or modified r-squared
10 calculations are available, yet these computations result in values that are comparable to the r-squared value for linear models, but have slightly different interpretations. Since non-linear regression models were used only when specific model forms could be predetermined, there was no need to compare different model forms estimating the same result.

Goodness-of-fit for non-linear regressions used in this thesis are purely for informational purposes. Since all non-linear models were based on known relationships, goodness-of-fit values only serve to show how well the data fits the model. In order to define non-linear regression model goodness-of-fit, the root mean squared error (RMSE) value was calculated.

Table 4.2. Arkansas River segment top width estimating coefficients.

Study Region	River Segment	Cross- Section	Fitting Parameter		Root Mean Squared Error
			β_1	β_2	
A		1	219.1	0.5098	21.57
		2	197.5	0.01573	0.07938
		3	205.2	0.7734	32.05
		4	211.5	0.008948	0.2069
B		5	59.4	0.9835	0.5002
		6	202	0.1382	12.48
		7	53.99	1.197	2.412
USR	C	10	141	0.5465	10.92
		11	187.2	0.5697	7.784
		12	277.9	0.01398	0.2358
		13	116.5	1.536	27.5
		14	110	0.917	1.986
D		16	49.37	1.115	1.5171
		17	57.68	1.288	1.469
		18	116.4	0.5197	17.42
		19	58.35	0.3868	6.382
		21	141	0.07095	0.7172
		22	63.82	0.6103	1.132
		23	109.3	0.07456	0.4762
		E	47.62	0.1682	0.5901
DSR		1	22.48	0.4006	0.8139
		2	41.61	1.390	3.953
		3	29.82	0.2265	1.821
		4	21.46	0.3801	2.541
		5	22.78	0.8004	5.715
		6	26.21	0.4153	1.681
		7	41.92	1.487	3.299
G		8	23.49	1.504	2.344
		9	33.54	1.106	3.676
		10	28.03	0.5790	2.003
		11	24.16	0.2103	1.693
		12	24.74	0.8992	2.617
		13	52.68	1.1850	5.757
		14	24.18	0.4764	0.9259

The RMSE represents the standard deviation of the differences between the predicted and observed values. The RMSE is scale dependent as the units are the same as the observed

value. The RMSE is also known as the standard deviation. This would cause an issue if models for different observed value units and scales were compared against each other. In this study, non-linear regression models are only used to estimate the cross-sectional width of a river segment and to estimate the selenium concentration at one location. Since all 5 cross-section analyses use the same measurement units, this allows us to compare the residual errors associated with the various cross sections without needing to consider scale or units.

The results of the top width equation for each cross-section, generated through non-linear regression, was compared to the observed results to visually compare the goodness-of-fit 10 for each cross-section. Figure 4.5 is an example

Table 4.3. River top width fitting parameter distributions.

Study	Fitting	Best Fit Distribution					
		Reach	Parameter	Dist.	Shape	p1*	p2*
USR	β_1			logistic		16.8	7.53
	β_2					-1.27	1.57
	Residual			logistic		1.99	0.99
DSR	β_1			logistic		28.2	4.84
	β_2					-0.43	0.65
	Residual			log-normal		0.87	0.57

* Distribution fitting parameters. For logistic, p1=location and p2=scale. For log-normal, p1=mean of the log scale and p2=standard dev. of the log scale

Values β_1 and β_2 are drawn from probability distributions. Calculated flow depth and river top width data pairs were used to determine the distributions from which β_1 and β_2 in equation 22 were drawn. These distributions were developed using non-linear, least-squares regression. Values below 0.15 m (0.5 ft) were removed from the regression analysis. Flow 15 values below this depth are not common and it was determined that these points would not allow for an accurate representation of the flow depth to river top width relationship for

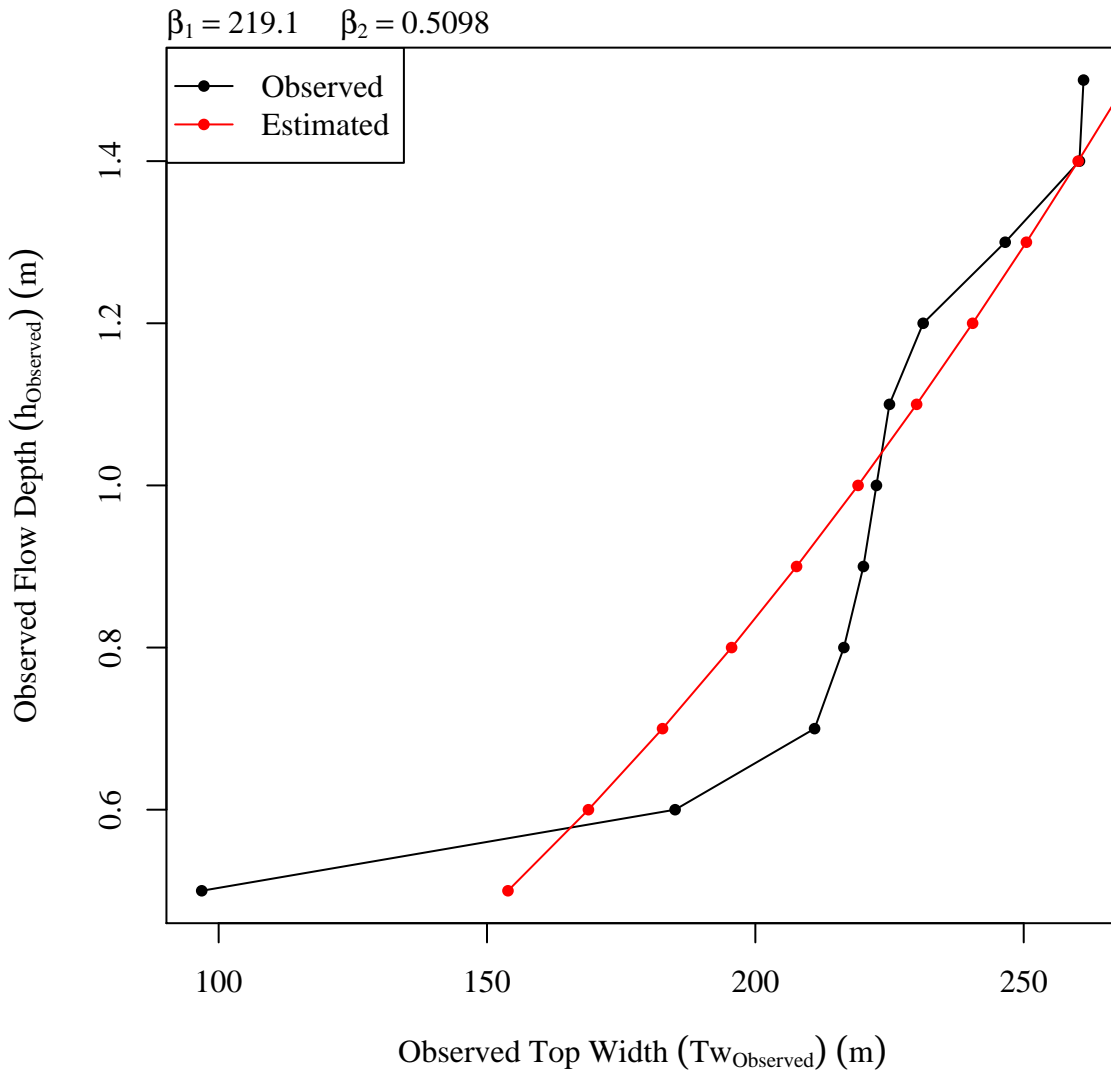


Figure 4.5. Example Flow Depth vs. River Top Width Relationship. The non-linear best fit line of the form in Equation 22 is red. The values are the two non-linear regression fitting parameters (β_1 and β_2) and the residual standard error for the fitting equation (σ). Similar figures for all cross-sections are found in the appendix.

the range of known flow depths. Values above 1.52 m (5.0 ft) were also removed from the regression analysis. Flow depths above this depth are above the banks of the primary river channel and are within the inner flood plain. Table 4.2 gives the resulting β_1 and β_2 values for each surveyed cross-section. Figure 4.5 is an example of the surveyed flow depth and river top width relationships and the derived non-linear relationship for cross-section 1 in

river segment A of the USR. Similar relationship plots for the other surveyed cross-sections are found in the appendix.

Figure 4.6 shows the distributions of β_1 and β_2 values and the various best-fit distributions in both the USR and DSR. Logistic, normal, exponential, Weibull, and log-normal 5 distributions were fitted to the data. Vertical tick marks in the x-axis margin are at the data values. Kernel density estimations were used as an alternative means to graphically represent the data density.

The resulting river shape parameter distributions are valid for the river reach for which they were calculated. Each river segment draws values from the shape parameter 10 distributions independently. Only one pair of shape parameters is drawn for each realization. It is assumed that the river geometry does not significantly change within the study time frame. Channel variability is modeled between the realizations.

Residuals from the non-linear regression analyses were combined into a single data set for uncertainty analysis. Combining this data set was a logical step following the combination 15 of the data that generated the residuals. Residuals were tested using the same tools and techniques used to test the river shape parameter distributions. USR and DSR channel shape residuals were found to have a log-normal distribution. Figure 4.7 presents the residuals distribution analyses for the USR and DSR. These figures are of the same type as those used to analyze the river shape parameter distributions, figure 4.6.

20 Residuals are the collection of the difference between the calculated regression model values and the measured values. Collectively, the distribution of the residuals describe the uncertainty of the regression model. In this case, the distribution of residuals describe the top width estimating uncertainty ε_{Tw} . Residuals should be tested for heteroskedasticity to determine if the model does not adequately predict the data. Heteroskedasticity is the

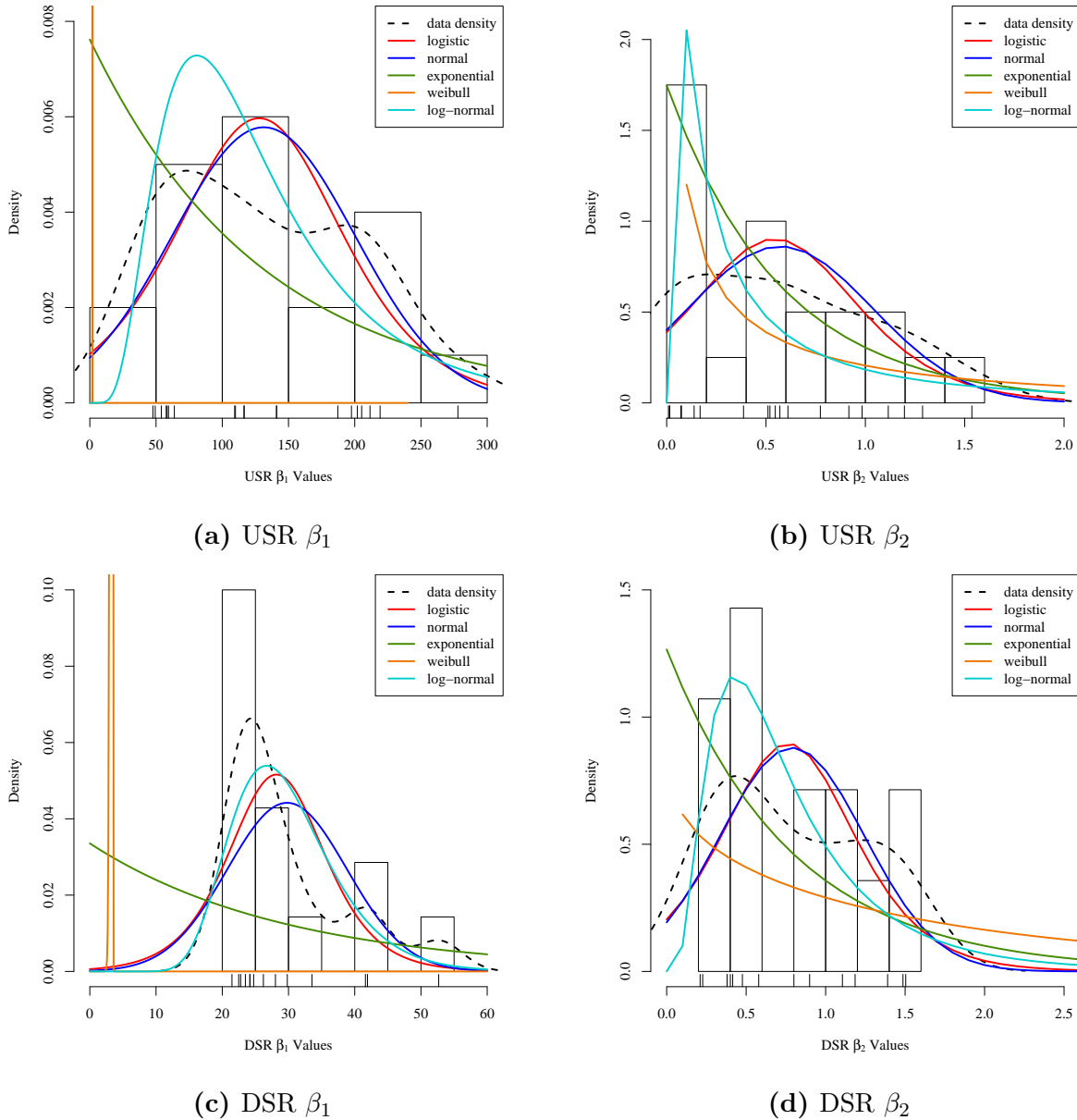
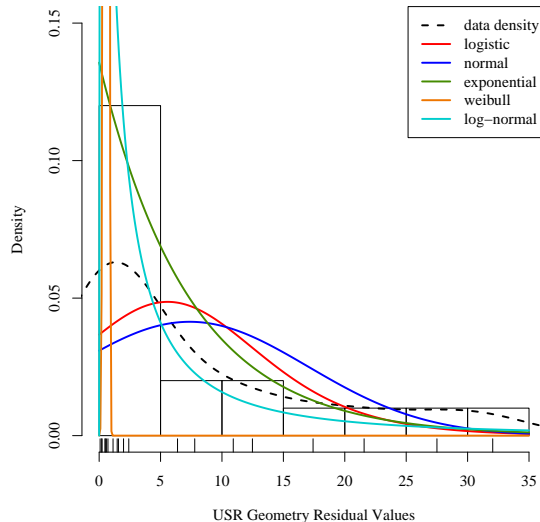
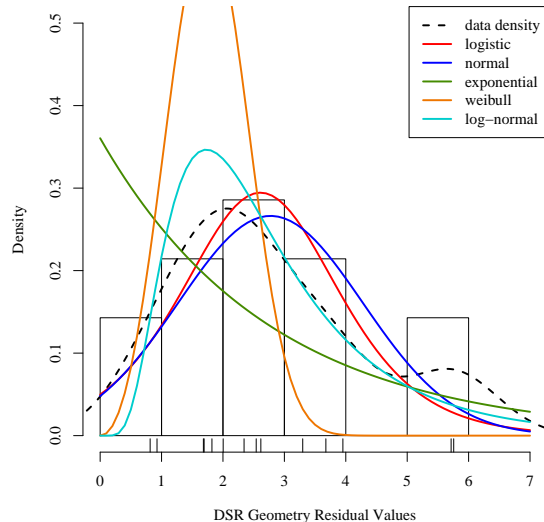


Figure 4.6. T_w Versus h Fitting Parameter β_1 and β_2 Distributions. The black dashed line is a kernel density plot representing a histogram where the bin size approaches zero. The colored curves are the best fit for the particular distribution type. Vertical tick marks in the x-axis are at the data values.

condition where the variability of a variable, in this case the residuals, is unequal across the range of the values and is usually indicative of under specification of the model. There are many tests for heteroskedasticity, but the most powerful is visual analysis of the plot of the residuals against the fitted, or calculated, values. When a small number of values is used to



(a) USR Residuals



(b) DSR Residuals

Figure 4.7. T_w versus H Residuals Distribution. The black dashed line is a kernel density plot representing a histogram where the bin size approaches zero. The colored curves are the best fit for the particular distribution type. Vertical tick marks in the x-axis are at the data values.

perform the regression, visual and computational analysis becomes difficult since patterns may appear that don't truly exist or patterns may not appear where they do exist. When heteroskedasticity was evident during model creation, the model was modified to remove the heteroskedasticity. Other methods are available to account for heteroskedasticity, but the most strongly recommended is model modification. Determining the parametric distribution that best fits the regressions is performed using the method described in section 4.3. Both visual and goodness-of-fit tests were applied to all residual regression analyses.

Results from the individual regression and residuals analyses are plotted with the source data to visually determine if the resulting best fit estimating equation or residuals distribution suitably fit the source data. An example of one of these figures is Figure 4.5 which plots a best fit regression equation alongside the source data. Figure 4.7 is representative of how the residual analysis results are visually analyzed. The best fit of several different distribution shapes are plotted over the histogram and KDE of the residuals or source data.

These types of figures are used throughout the analysis to visually verify that the calculated regression models and best-fit distributions actually fit the data.

Results from deterministic and stochastic models are presented throughout this thesis.

While both model types present results from the same source data, stochastic models, as

5 previously discussed, also include uncertainty in many forms. Stochastic model results are complex. They are time-series models where each time step is an independent distribution of the results. Figure is a very simple representation of a time-series. The top sub-figure shows a sine curve which represents the deterministic model. The second sub-figure shows one realization of the stochastic model which is the deterministic model with uncertainty added at each time step. For this example, the uncertainty is normally distributed within the

10 time step. The third sub-figure is 500 independent realizations shown on top of each other.

The fourth sub-figure shows the 500 realizations with three calculated lines representing stochastic model summary statistics time-series.

The middle line is the time-series that represents the mean value calculated for each

15 time-step. This is the stochastic model mean time-series. The top and bottom lines are the 97.5th and 2.5th percentile calculated for each time step. These are the stochastic model 97.5th percentile time-series and stochastic model 2.5th percentile time-series, respectively.

Collectively, these three time-series are called stochastic model summary statistics time-series. These three time-series show how the results and range of possible results vary with
20 time. All stochastic time-series graphs present only the three stochastic model summary statistics time-series. Values outside of these are not plotted so as to improve understanding and readability of the graphical results

Presenting individual values for stochastic model results requires further summary statistics of the calculated stochastic model summary statistics time-series. Without this

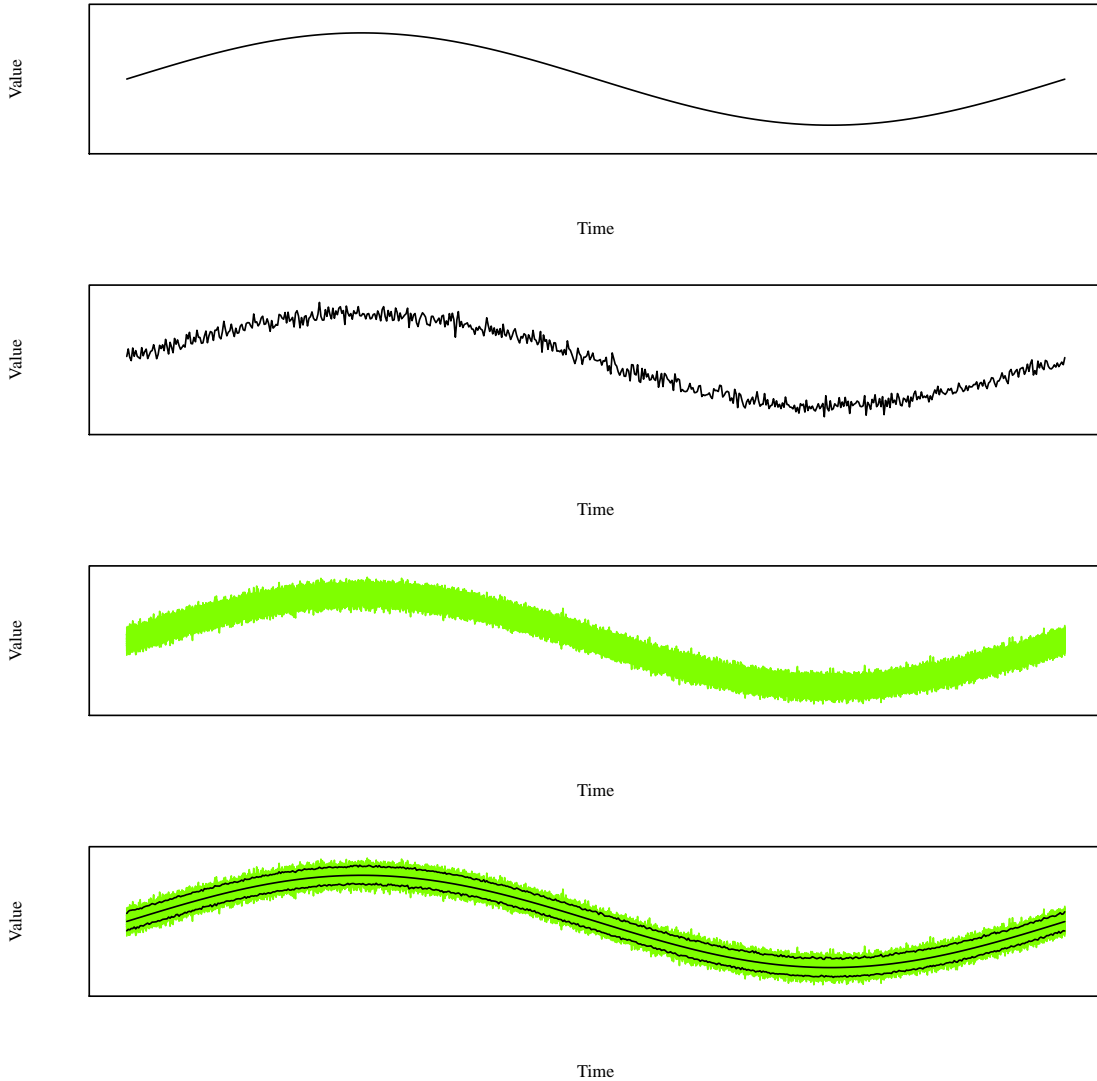


Figure 4.8. Stochastic model graphical results presentation description. The top sub-figure represents a simple deterministic time-series model. The second sub-figure represents a single stochastic time-series model. The third sub-figure represents 500 stochastic time-series. The fourth sub-figure shows the 500 stochastic time-series with the three stochastic model summary statistics time-series. The top line is the 97.5th percentile time-series, the middle line is the mean time-series, and the bottom line is the 2.5th percentile time-series.

further reduction, results would contain large quantities of values which are very difficult to present. The mean, 97.5th percentile, and 2.5th percentile are calculated for each of the summary statistics time-series to provide more readable results. The summary statistics for each of the stochastic model summary statistics time-series indicate the most likely value and
5 the range of possible values as presented in the example in Table 4.4. In this table, each row

of the bottom portion of the table presents one of the stochastic model summary statistic time-series results. In this example, values ' g ', ' h ', and ' i ' are the summary statistics for the stochastic model mean time-series.

Table 4.4 also includes the deterministic time-series summary statistics values. These
5 values are the 2.5th percentile, mean, and 97.5th percentile calculated from the deterministic model results and are presented in the upper half of the table. The deterministic model time-series summary statistics should be approximately the same as the stochastic model mean time-series summary statistics, which are values g , h , and i in the lower half of the table. This statement should be true if the deterministic model is a possible realization of
10 the stochastic model and if the distribution of the combined uncertainties in the stochastic model are approximately normally distributed.

Table 4.4. Example deterministic and stochastic model numerical results. The single row on the deterministic model side presents the summary statistics for the deterministic model (values a , b , and c). Each row on the stochastic model side presents the results for a specific stochastic model summary time-series. All values are presented in common units. The Pearson Correlation value (m) is calculated between the deterministic model time-series and the stochastic model mean time-series values at each time-step in the models.

Deterministic Model Time Series			
	2.5th Percentile	Mean	97.5th Percentile
	a	b	c
Stochastic Model Summary Statistics Time Series			
	2.5th Percentile	Mean	97.5th Percentile
97.5th Percentile	d	e	f
Mean	g	h	i
2.5th Percentile	j	k	l

Pearson Correlation = m

One goal of stochastic modeling is to have a deterministic model that resides within the stochastic. If the deterministic model isn't a possible realization of the stochastic model,

then there are significant stochastic model issues that need to be addressed. Ideally, the stochastic model mean time-series at each time step should be close to the deterministic model at that same time step. To determine if this relationship is true, the Pearson correlation between the stochastic model mean time-series and the deterministic model was calculated
5 and is included at the bottom of Table 4.4. Calculating the Pearson correlation requires assuming the two compared data sets are continuous and are linearly related. All input values and results in this thesis are continuous, either from zero to $+\infty$ or between $\pm\infty$.

Correlation values only provides a numerical value to describe the relationship between two values or data sets. It does not imply causality or linearity. We can infer causality
10 because the deterministic model is a subset of the stochastic model. In fact, the deterministic model was used to create the stochastic model. We cannot infer linearity. Figure attempts to answer the linearity issue through visual analysis. The black dots are the comparison of the stochastic mean time-series and the deterministic model. The red and blue dots are the comparison of the stochastic 97.5th and 2.5th percentile time-series as compared to the
15 deterministic model, respectively. The solid black line follows the equation $y=x$. This is where all of the black dots should lie if the stochastic mean time-series and deterministic models were in perfect agreement. The dashed line is the quadratic best fit line through the stochastic mean time-series.

River segment B in the USR does not have a flow gauge within its boundaries and
20 therefore has no reported flow depths. This segment has an additional irrigation diversion check structure within its boundaries, thereby sub-dividing segment B into two sub-segments, each with its own ungauged flow depth. Due to segment B being the shortest, composing only 3.9% of the USR's total length, and the additional variability of the possible flow depth, the average daily flow depth within segment B is taken as the mean of the reported flow

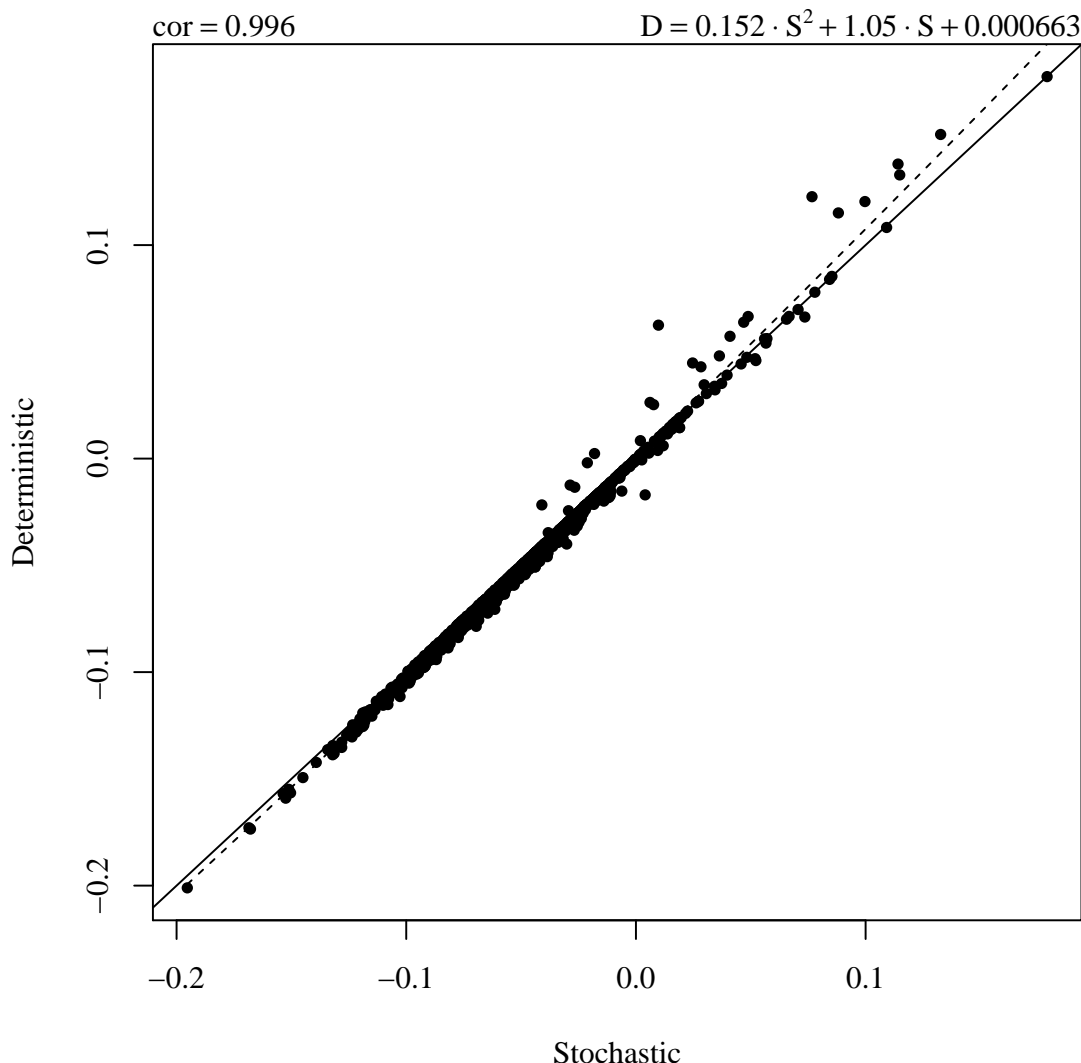
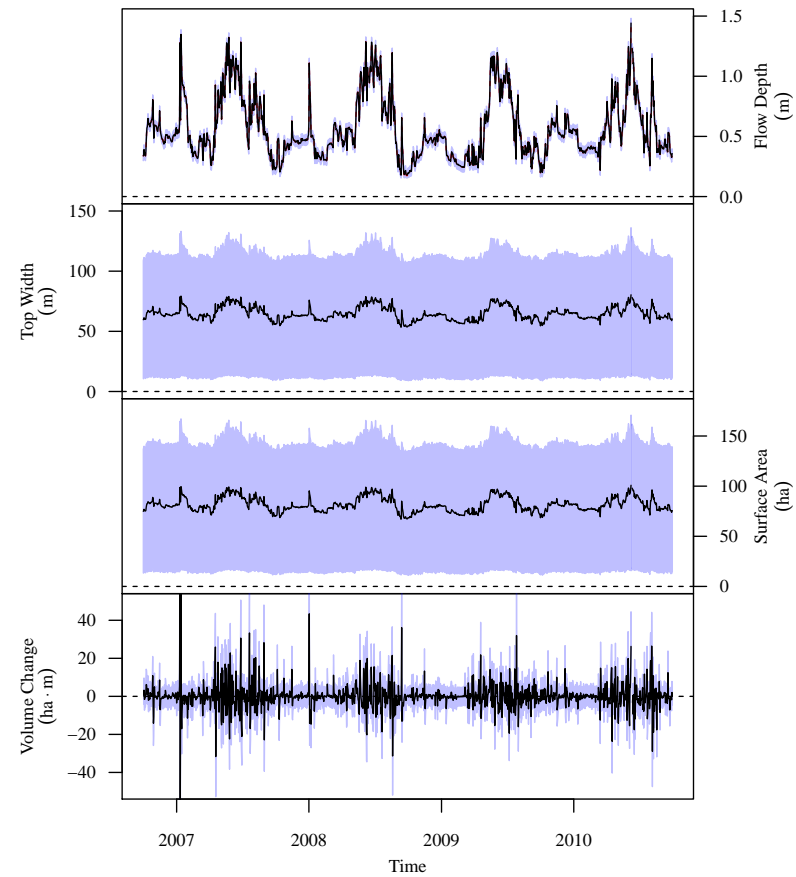


Figure 4.9. Example scatterplot comparing deterministic model time-series and stochastic model mean time-series results. The solid line is drawn such that $y = x$. The dashed line is the best-fit quadratic equation between the deterministic model time-series and the stochastic model mean time-series and the equation is in the top right. The Pearson Correlation is the top left number.

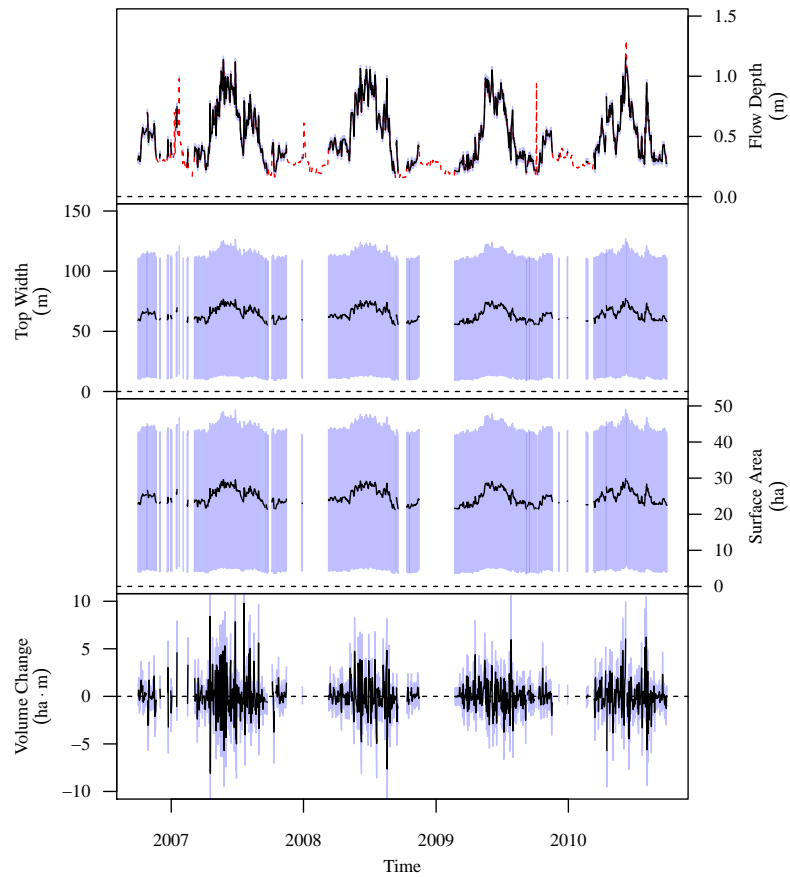
depths in segment A and C. Top width and volume change calculation follows the previously described methodology.

The time-series plots of all four stochastic geometric parameters for each study region river section segment is presented in Figures 4.10 and 4.11 for the USR and DSR, respectively. The black lines indicate the stochastic model mean time-series. The blue band indicates the 95% central inter-percentile range (CIR) of the stochastic values as defined by the stochastic model 2.5th percentile time-series and the stochastic model 97.5th percentile time-series.

5 The red dashed line in the flow depth portion of the figure indicates the reported flow depth values. It is plotted under the stochastic model mean time-series line and as such is only visible when either the stochastic model mean time-series value was not calculated due to missing data or when the two values deviate.

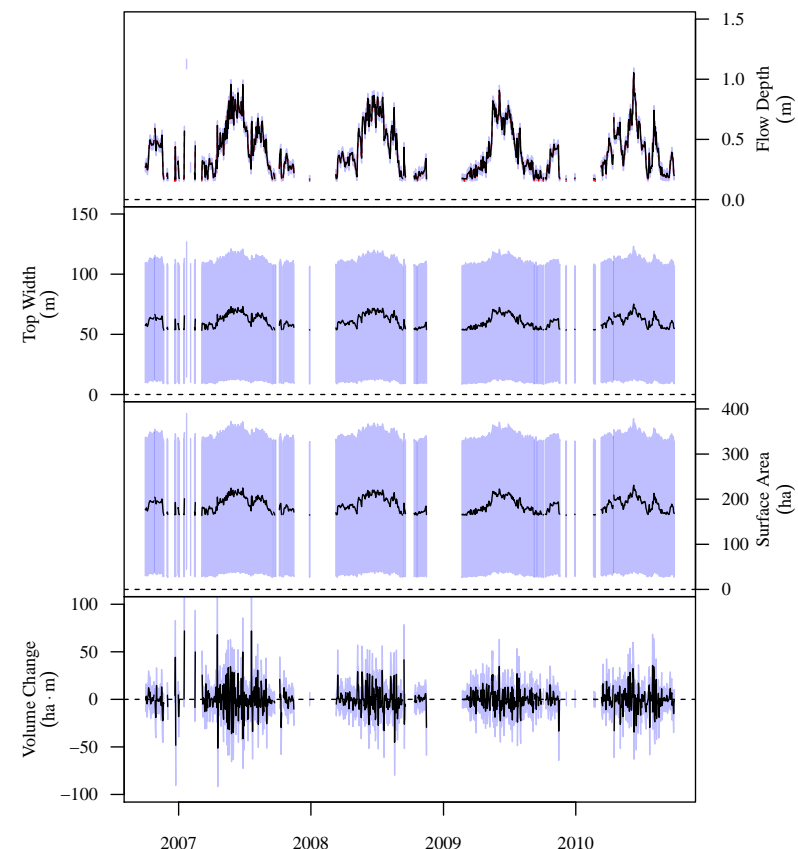


Segment A

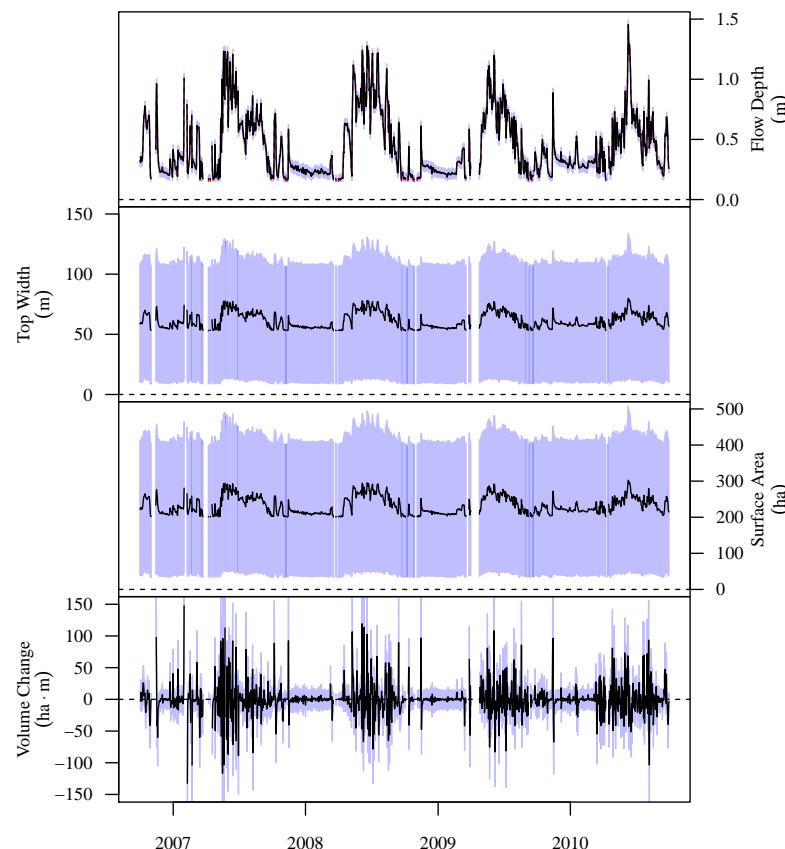


Segment B

Figure 4.10. USR and DSR stochastic geometric parameter time-series. The black lines indicate the stochastic model mean time-series. The blue band indicates the 95% central inter-percentile range (CIR) of the stochastic values. The red dashed line in the flow depth portion of the figure indicates the reported flow depth values.



Segment C



Segment D

Figure 4.10 (Cont). USR and DSR stochastic geometric parameter time-series.

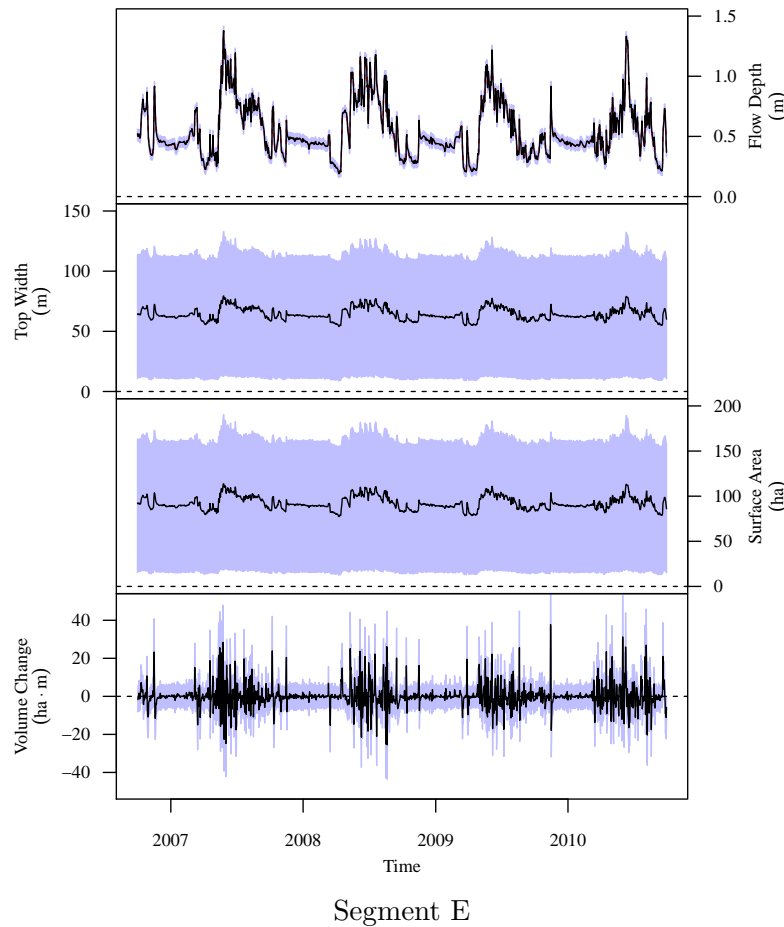
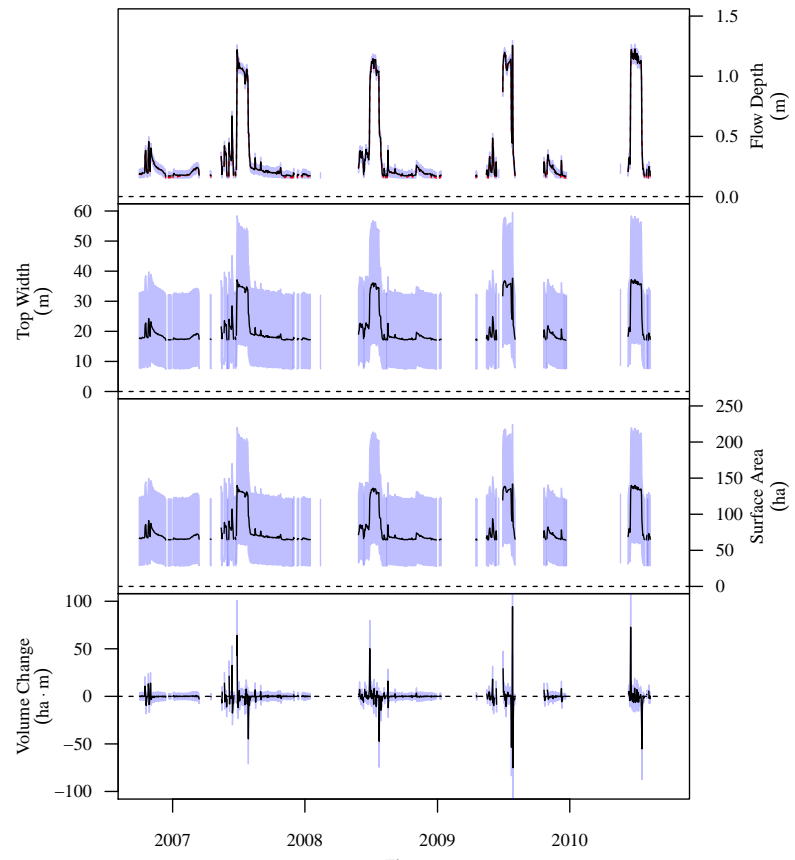
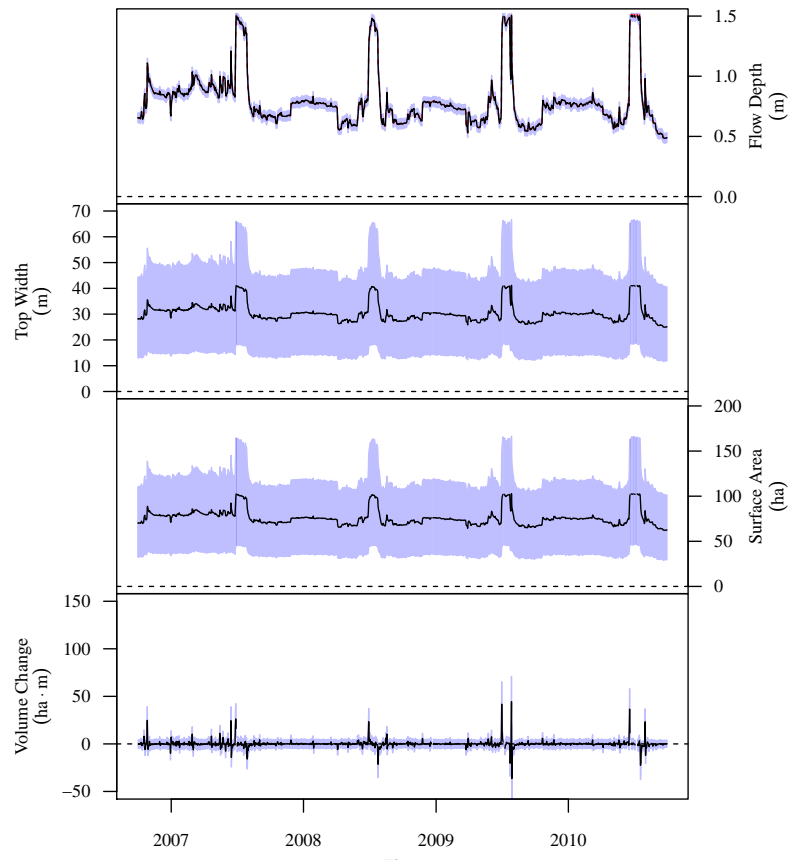


Figure 4.10 (Cont). USR and DSR stochastic geometric parameter time-series.



Segment F



Segment G

Figure 4.11. DSR stochastic geometric parameter time-series. The black lines indicate the stochastic model mean time-series. The blue band indicates the 95% central inter-percentile range (CIR) of the stochastic values. The red dashed line in the flow depth portion of the figure indicates the reported flow depth values.

Figures 4.10 and 4.11 were analyzed to verify that direct correlations existed between the flow depth and the calculated geometric parameters. Top width and surface area should increase and decrease in proportion with the increase and decrease in flow depth. Volume changes are based on two flow depth values and do not have a direct correlation to the flow
5 depth displayed in the figure. All of the river sections show the correct correlations between flow depth and the calculated river geometric parameters.

Tables 4.5 and 4.6 present the river segment average daily surface area deterministic model time-series and stochastic model summary statistic time-series results for the USR and DSR, respectively. Summary results for river segment average daily flow depth and
10 river segment average daily top width are not included as they are not direct precursors to the final model results. The surface area is directly used for precipitation and evaporation calculations.

Every one of these tables shows that the stochastic model tends to underestimate the river segment water surface area by approximately 38% in the USR and XX% in the
15 DSR. The correlation values indicate that the deterministic model time-series and stochastic model mean time-series are highly correlated. The corresponding correlation scatter-plots show that the relationships are linear. This is due to the way the river section average daily top width was estimated for the deterministic models. Since β_1 and β_2 are drawn from distributions and the deterministic model requires that none of the input values are
20 variable, the most likely values from the respective distributions were chosen as the fixed values. The β values from both study reaches are not normal, therefore the most likely value is not the mean and the values are not evenly distributed on either side of the likely value. The skewness of the β values is represented in the stochastic model. Calibrating the deterministic models to find the β values that approximate the stochastic model defeats the

Table 4.5. USR river segment surface area deterministic and stochastic model numerical results. Values are in hectares (ha) with values in parentheses in acres (ac).

USR river segment A

Deterministic Model Time Series			
	2.5th Percentile	Mean	97.5th Percentile
	106 (262)	134 (331)	167 (413)
Stochastic Model Summary Statistics Time Series			
Time Series	2.5th Percentile	Mean	97.5th Percentile
97.5th Percentile	135 (334)	143 (353)	159 (393)
Mean	70.1 (173)	81.6 (202)	96.3 (238)
2.5th Percentile	12.1 (29.9)	15 (37.1)	17.8 (44)
Pearson Correlation = 0.9984			

USR river segment B

Deterministic Model Time Series			
	2.5th Percentile	Mean	97.5th Percentile
	30.5 (75.4)	38.5 (95.1)	49 (121)
Stochastic Model Summary Statistics Time Series			
Time Series	2.5th Percentile	Mean	97.5th Percentile
97.5th Percentile	41.8 (103)	43.9 (108)	47.1 (116)
Mean	21.7 (53.6)	24.9 (61.5)	28.7 (70.9)
2.5th Percentile	3.74 (9.24)	4.64 (11.5)	5.58 (13.8)
Pearson Correlation = 0.9986			

purpose of the deterministic model, which is to estimate the most likely values. Sensitivity analysis which is discussed later, will show whether or not the river section average daily

Table 4.5 (Cont). USR river segment surface area deterministic and stochastic model numerical results.

USR river segment C

Deterministic Model Time Series

2.5th Percentile	Mean	97.5th Percentile
237 (586)	301 (744)	372 (919)

Stochastic Model Summary Statistics Time Series

Time Series	2.5th Percentile	Mean	97.5th Percentile
97.5th Percentile	326 (806)	343 (848)	364 (899)
Mean	165 (408)	189 (467)	218 (539)
2.5th Percentile	27.6 (68.2)	34.5 (85.3)	42.1 (104)
Pearson Correlation = 0.998			

USR river segment D

Deterministic Model Time Series

2.5th Percentile	Mean	97.5th Percentile
290 (717)	374 (924)	498 (1230)

Stochastic Model Summary Statistics Time Series

Time Series	2.5th Percentile	Mean	97.5th Percentile
97.5th Percentile	401 (991)	423 (1050)	473 (1170)
Mean	202 (499)	232 (573)	287 (709)
2.5th Percentile	33.9 (83.8)	42.1 (104)	53 (131)
Pearson Correlation = 0.9981			

surface area values are significant enough to warrant the effort required to calibrate them to the stochastic model.

Table 4.5 (Cont). USR river segment surface area deterministic and stochastic model numerical results.

USR river segment E			
Deterministic Model Time Series			
	2.5th Percentile	Mean	97.5th Percentile
	121 (299)	152 (376)	187 (462)
Stochastic Model Summary Statistics Time Series			
Time Series	2.5th Percentile	Mean	97.5th Percentile
97.5th Percentile	155 (383)	163 (403)	178 (440)
Mean	79.8 (197)	92.2 (228)	108 (267)
2.5th Percentile	13.8 (34.1)	16.7 (41.3)	19.7 (48.7)
Pearson Correlation = 0.9984			

Tables 4.7 and 4.8 present the river segment average daily surface area deterministic model time-series and stochastic model summary statistic time-series results for the USR and DSR, respectively. Summary results for river segment average daily flow depth and river segment average daily top width are not included as they are not direct precursors to the final model results. The surface area is directly used for precipitation and evaporation calculations.

The mean of the deterministic model time-series and the mean of the stochastic model mean time-series calculated average daily river segment water volume change are much closer to each other as reported in Tables 4.7 and 4.8. The stochastic model mean time-series underestimates the deterministic model time-series values by approximately 47%. The difference between the two models in terms of water volume is quite small, less than 1 ha m. The Pearson correlation values and their associated scatter-plots indicate that the

Table 4.6. DSR river segment surface area deterministic and stochastic model numerical results. Values are in hectares (ha) with values in parentheses in acres (ac).

DSR river segment F

Deterministic Model Time Series

2.5th Percentile	Mean	97.5th Percentile
0.0316 (0.0781)	0.0499 (0.123)	0.117 (0.289)

Stochastic Model Summary Statistics Time Series

Time Series	2.5th Percentile	Mean	97.5th Percentile
97.5th Percentile	120 (297)	139 (343)	214 (529)
Mean	64.5 (159)	79.2 (196)	137 (339)
2.5th Percentile	28.2 (69.7)	35.7 (88.2)	61.6 (152)
Pearson Correlation = 0.9999			

DSR river segment G

Deterministic Model Time Series

2.5th Percentile	Mean	97.5th Percentile
0.0475 (0.117)	0.0597 (0.148)	0.0903 (0.223)

Stochastic Model Summary Statistics Time Series

Time Series	2.5th Percentile	Mean	97.5th Percentile
97.5th Percentile	104 (257)	119 (294)	163 (403)
Mean	65.4 (162)	75.6 (187)	101 (250)
2.5th Percentile	30.9 (76.4)	35.7 (88.2)	46.1 (114)
Pearson Correlation = 0.9999			

results are strongly linearly related. The effects of uncertainty on river segment average river daily water volume change is much smaller than the effect on surface area. As with the surface area results, the significant portion of the difference between the deterministic

Table 4.7. USR river segment volume change deterministic and stochastic model numerical results. Values are in hectare-meters (ha m) and the values in parentheses are in acres (ac).

$$\frac{\Delta S_A}{\Delta t}$$

Deterministic Model Time Series

	2.5th Percentile	Mean	97.5th Percentile
	-20.3 (-165)	0.0233 (0.189)	24.2 (196)

Stochastic Model Summary Statistics Time Series

Time Series	2.5th Percentile	Mean	97.5th Percentile
97.5th Percentile	-2.59 (-21)	6.2 (50.3)	27 (219)
Mean	-12 (-97.3)	0.0144 (0.117)	14.7 (119)
2.5th Percentile	-23 (-186)	-6.32 (-51.2)	3.35 (27.2)
Pearson Correlation = 0.9997			

$$\frac{\Delta S_B}{\Delta t}$$

Deterministic Model Time Series

	2.5th Percentile	Mean	97.5th Percentile
	-5.08 (-41.2)	-0.0208 (-0.169)	5.57 (45.2)

Stochastic Model Summary Statistics Time Series

Time Series	2.5th Percentile	Mean	97.5th Percentile
97.5th Percentile	-0.771 (-6.25)	1.41 (11.4)	6.56 (53.2)
Mean	-3.3 (-26.8)	-0.0114 (-0.0924)	3.75 (30.4)
2.5th Percentile	-6.07 (-49.2)	-1.47 (-11.9)	0.854 (6.92)
Pearson Correlation = 0.9996			

model time-series and the stochastic model mean time-series is due to the estimation of the most likely values of β_1 and β_2 used in the deterministic models. At this point, adjusting or

Table 4.7 (Cont). USR river segment volume change deterministic and stochastic model numerical results.

$$\frac{\Delta S_C}{\Delta t}$$

Deterministic Model Time Series

	2.5th Percentile	Mean	97.5th Percentile
	-39.5 (-320)	-0.072 (-0.584)	45 (365)

Stochastic Model Summary Statistics Time Series

Time Series	2.5th Percentile	Mean	97.5th Percentile
97.5th Percentile	-5.39 (-43.7)	13.6 (110)	52.1 (422)
Mean	-24 (-195)	-0.0416 (-0.337)	27 (219)
2.5th Percentile	-48.2 (-391)	-14 (-113)	6.01 (48.7)
Pearson Correlation = 0.9994			

$$\frac{\Delta S_D}{\Delta t}$$

Deterministic Model Time Series

	2.5th Percentile	Mean	97.5th Percentile
	-83.3 (-675)	-0.291 (-2.36)	109 (884)

Stochastic Model Summary Statistics Time Series

Time Series	2.5th Percentile	Mean	97.5th Percentile
97.5th Percentile	-11.8 (-95.7)	19.2 (156)	115 (932)
Mean	-49.3 (-400)	-0.173 (-1.4)	64.6 (524)
2.5th Percentile	-91.2 (-739)	-20.1 (-163)	15.3 (124)
Pearson Correlation = 0.9995			

calibrating these values such that the results of the deterministic and stochastic models are more closely aligned seems unnecessary.

Table 4.7 (Cont). USR river segment volume change deterministic and stochastic model numerical results.

$\frac{\Delta S_E}{\Delta t}$			
Deterministic Model Time Series			
2.5th Percentile	Mean	97.5th Percentile	
-20 (-162)	-0.0177 (-0.143)	27.2 (221)	
Stochastic Model Summary Statistics Time Series			
Time Series	2.5th Percentile	Mean	97.5th Percentile
97.5th Percentile	-2.51 (-20.3)	6.74 (54.6)	30.1 (244)
Mean	-11.7 (-94.9)	-0.0106 (-0.0859)	16.3 (132)
2.5th Percentile	-23.2 (-188)	-6.96 (-56.4)	3.62 (29.3)
Pearson Correlation = 0.9997			

Figure 4.12 and 4.13 presents the river reach average daily river water storage change deterministic model time-series for the USR and DSR, respectively, as calculated using Equation 13. The left-hand figure is the deterministic model time-series. The right-hand figure is the stochastic model results with the black line representing the calculated stochastic model mean time-series and the blue band representing the space between the stochastic model 97.5th percentile time-series and the stochastic model 2.5th percentile time-series. The minimum and maximum range of values is not presented in this figure.

Tables xx presents the deterministic model time-series summary statistics and the summary statistics for each of the stochastic model summary statistics time-series for the river reach average daily water storage change in the USR and DSR.

Table 4.8. DSR river segment volume change deterministic and stochastic model numerical results. Values are in hectare-meters (ha m) and the values in parentheses are in acres (ac).

$$\frac{\Delta S_F}{\Delta t}$$

Deterministic Model Time Series

	2.5th Percentile	Mean	97.5th Percentile
	-6.87 (-55.7)	-0.0882 (-0.715)	6.36 (51.6)

Stochastic Model Summary Statistics Time Series

Time Series	2.5th Percentile	Mean	97.5th Percentile
97.5th Percentile	-3.27 (-26.5)	5.02 (40.7)	17.1 (139)
Mean	-9.68 (-78.5)	-0.125 (-1.01)	8.13 (65.9)
2.5th Percentile	-18.7 (-152)	-5.35 (-43.4)	2.2 (17.8)
Pearson Correlation = 0.9971			

$$\frac{\Delta S_G}{\Delta t}$$

Deterministic Model Time Series

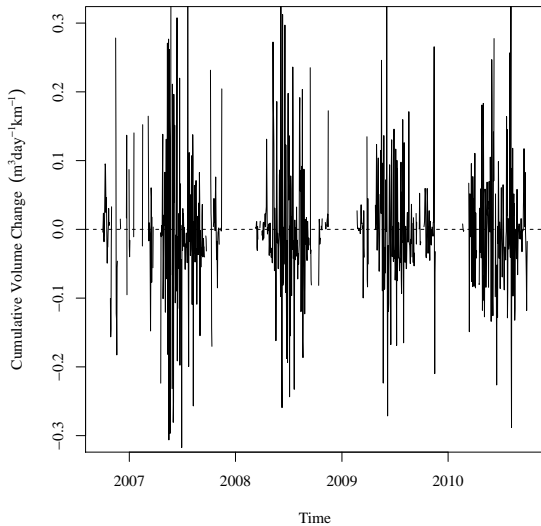
	2.5th Percentile	Mean	97.5th Percentile
	-3.53 (-28.6)	-0.00924 (-0.0749)	4.12 (33.4)

Stochastic Model Summary Statistics Time Series

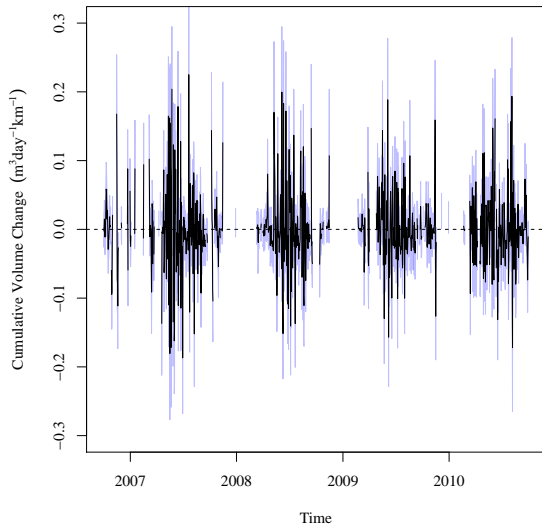
Time Series	2.5th Percentile	Mean	97.5th Percentile
97.5th Percentile	0.0845 (0.685)	4.64 (37.6)	10.9 (88.4)
Mean	-4.29 (-34.8)	-0.0109 (-0.0884)	5.1 (41.3)
2.5th Percentile	-10.4 (-84.3)	-4.7 (-38.1)	0.3 (2.43)
Pearson Correlation = 0.9986			

The figures show that there is a definite seasonal variation in the storage component.

Stored water changes are smallest during the cold months and are increasingly larger during

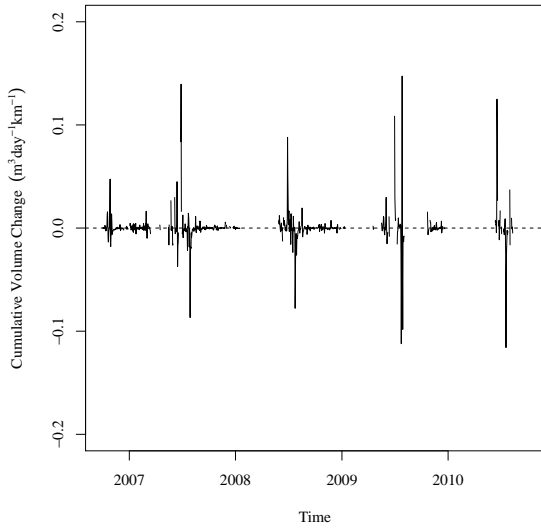


Deterministic Model.

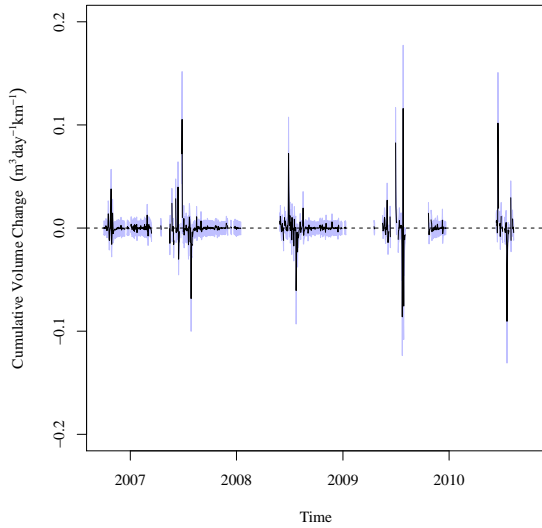


Stochastic Model.

Figure 4.12. USR Arkansas River water storage change contribution to the water model.



Deterministic Model.



Stochastic Model.

Figure 4.13. DSR Arkansas River water storage change contribution to the water model.

the growing season. This pattern is caused by irrigation practices in the Lower Arkansas River Basin (LARV). Stored irrigation water is released from reservoirs upstream of the LARV during the irrigation season as demands require. During the winter, there is very little to no irrigation occurring. This, combined with the low precipitation and no additional

Table 4.9. USR river reach average daily stored water volume change. Values in hectare-meters (ha m km^{-1}) and values in parentheses in acre-feet (ac ft mi^{-1})

$$\frac{\Delta S_{USR}}{\Delta t}$$

Deterministic Model Time Series

2.5th Percentile	Mean	97.5th Percentile
-0.187 (-13.1)	-0.000534 (-0.0374)	0.224 (15.7)

Stochastic Model Summary Statistics Time Series

Time Series	2.5th Percentile	Mean	97.5th Percentile
97.5th Percentile	-0.0508 (-3.56)	0.0331 (2.32)	0.207 (14.5)
Mean	-0.111 (-7.78)	-0.000283 (-0.0198)	0.131 (9.18)
2.5th Percentile	-0.172 (-12)	-0.0343 (-2.4)	0.0594 (4.16)
Pearson Correlation =	0.9996		

Table 4.10. DSR river reach average daily stored water volume change. Values in hectare-meters (ha m km^{-1}) and values in parentheses in acre-feet (ac ft mi^{-1})

$$\frac{\Delta S_{DSR}}{\Delta t}$$

Deterministic Model Time Series

2.5th Percentile	Mean	97.5th Percentile
-1.83e-05 (-0.00128)	1.17e-07 (8.2e-06)	1.92e-05 (0.00134)

Stochastic Model Summary Statistics Time Series

Time Series	2.5th Percentile	Mean	97.5th Percentile
97.5th Percentile	-0.00941 (-0.659)	0.0134 (0.939)	0.0526 (3.68)
Mean	-0.0253 (-1.77)	0.000122 (0.00855)	0.0287 (2.01)
2.5th Percentile	-0.045 (-3.15)	-0.0132 (-0.925)	0.0103 (0.721)
Pearson Correlation =	0.9979		

flow from snow-pack runoff, allow flows in the Arkansas River to reach base flow level when the river is at a natural equilibrium.

This pattern is not as pronounced in the DSR. This is most likely due to required flow rates being maintained at the Colorado-Kansas border. With the constant required flow, John Martin Reservoir releases only enough water to meet the required flow rate. This creates a flow regime that is nearly constant through most of the DSR.

5 Deviations are noted during peak irrigation season. These additional volume changes are most likely due to irrigation flows returning to the Arkansas River from fields irrigated from canal systems that procure and store water upstream of John Martin Reservoir. The Fort Lyon Storage Canal and Fort Lyon Canal are two examples of canal systems that perform this function. Water removed from the USR, stored, and added to the DSR is not
10 included in this study.

The distribution of all realizations within each time step was analyzed to determine a distribution type. This analysis was performed to determine if the assumption that the deterministic model results were representative of the stochastic model. Testing was performed by comparing K-S statistics for the best fit normal and logistic distributions. Log-normal,
15 logistic, exponential, gamma, and Weibull distributions were considered, but were not included in this analysis since they do not support the full range of possible values, $(-\infty, +\infty)$. The non-included distributions could have been scaled and shifted, but they are still limited in the range of possible values. In the USR and the DSR, all of the river water volume storage change stochastic model time steps are best fit by a logistic distribution.

20 The mean of the percent difference between the deterministic model time-series and stochastic model mean time-series is very low. This indicates that the deterministic model is representative of the stochastic model expected value. The high percent differences at the 2.5th and 97.5th percentile indicate that there is still a large range of uncertainty contained within the stochastic model that the deterministic model cannot replicate. The deterministic

model can be used to determine how changes can affect a reach over a span of time, but using it to estimate values for specific time steps is unwise as the differences noted at individual time steps is too large to account for.

4.5. GAUGED STREAM FLOWS AND DIVERTED CANAL FLOWS

Equation 4 contains the portion contained in equation 23 that describes the sum of all accountable surface water flows entering and leaving a defined reach. These flows include only the gauged river main stem flows, tributary stream flows, and diverted canal flows. Most 5 flows are reported as average daily flow rate. These flow rates, which are measured every 15 minutes, are calculated from the respective gauge's measured instantaneous stage height using stage-discharge tables. The only exception is with the average daily flow rate reported for the La Junta waste water treatment plant where the average daily flow is converted from the total daily discharge, reported in million gallons per day (mgd).

$$\sum Q_{Surface} = \left(Q_{out,DS} + \sum Q_{out} - Q_{in,US} - \sum Q_{in} \right) \quad (23)$$

Where:

$Q_{Surface}$ = sum of average daily flow rates in the study region.

Q_{in} = flow entering the study reach from a tributary.

Q_{out} = flow leaving the study reach to an irrigation canal.

10 $Q_{in,US}$ = flow entering the study reach in the main stem of the river at the upstream end of the reach.

$Q_{out,DS}$ = flow leaving the study reach in the main stem of the river at the downstream end of the reach.

Equation 23 is expanded as follows to contain all of the measured flows entering or leaving the main stem of the Arkansas River within the USR boundaries. The subscript for each flow in equation 24 is the CDWR symbol for a particular gauge site. See the map in Figure 3.1 for the gauge locations in the USR. The flows in this equation are ordered by

location along the main stem of the river, from upstream to downstream.

$$\begin{aligned} \sum Q_{Surface,USR} = & Q_{ARKCATCO} - Q_{HOLCANCO} - Q_{RFDMANCO} - Q_{FLSCANCO} \\ & + Q_{RFDRETCO} + Q_{TIMSWICO} - Q_{FLYCANCO} + Q_{CANSWKCO} \\ & + Q_{LAJWWTP} - Q_{CONDITCO} + Q_{HRC194CO} - Q_{ARKLASCO} \end{aligned} \quad (24)$$

Where each subscript is defined as the flow through the gauge described in Table 4.11. In this table, each of the flow variables in equation 24, designated by its CDWR gauge name, is grouped by the type of flow using the variables used in equation 23.

Table 4.11. Description of USR stream flow variables. The CDWR gauge name is the USR model variable sub-script. The variable group is the category to which the flow belongs.

CDWR Gauge Name	Variable Group	Description
<i>ARKCATCO</i>	$Q_{in,US}$	Arkansas River below the Catlin Canal diversion.
<i>HOLCANCO</i>	Q_{out}	Holbrook Canal
<i>RFDMANCO</i>	Q_{out}	Rocky Ford Canal
<i>FLSCANCO</i>	Q_{out}	Fort Lyon Storage Canal
<i>RFDRETCO</i>	Q_{in}	Rocky Ford Return Ditch
<i>TIMSWICO</i>	Q_{in}	Timpas Creek
<i>FLYCANCO</i>	Q_{out}	Fort Lyon Canal
<i>CANSWKCO</i>	Q_{in}	Crooked Arroyo
<i>LAJWWTP</i>	Q_{in}	Discharge from the La Junta WWTP
<i>CONDITCO</i>	Q_{out}	Consolidated Ditch (Jones Ditch)
<i>HRC194CO</i>	Q_{in}	Horse Creek at Colorado Highway 194
<i>ARKLASCO</i>	$Q_{out,DS}$	Arkansas River in Las Animas, Colorado

For the DSR, equation 23 is expanded as follows to contain all of the measured flows entering or leaving the main stem of the Arkansas River within its boundaries. The subscript for each flow in equation 25 is the CDWR symbol for a particular gauge site. See the map in Figure 3.2 for the gauge locations in the DSR. The flows in this equation are ordered by

location along the main stem of the river, from upstream to downstream.

$$\sum Q_{Surface,DSR} = Q_{ARKLAMCO} + Q_{BIGLAMCO} - Q_{BUFQUITCO} + Q_{WILDHOCO} - Q_{FRODITKS} - Q_{ARKCOOKS} \quad (25)$$

Where each subscript is defined as the flow through the gauge described in Table 4.12. In this table, each of the flow variables in equation 25, designated by its CDWR gauge name, is grouped by the type of flow using the variables used in equation 4.

Table 4.12. Description of DSR stream flow variables. The CDWR gauge name is the DSR model variable sub-script. The variable group is the category to which the flow belongs.

CDWR Gauge Name	Variable Group	Description
<i>ARKLAMCO</i>	$Q_{in,US}$	Arkansas River in Lamar, Colorado
<i>BIGLAMCO</i>	Q_{in}	Big Sandy Creek
<i>BUFQUITCO</i>	Q_{out}	Buffalo Ditch
<i>WILDHOCO</i>	Q_{in}	Wild Horse Creek
<i>FRODITKS</i>	Q_{out}	Frontier Ditch
<i>ARKCOOKS</i>	$Q_{out,DS}$	Arkansas River in Coolidge, Kansas

Equations 24 and 25 constitute the surface water flow portion of 23 for the USR
5 and DSR deterministic models, respectively. As with the other portions of the water balance models, converting these to be used in the stochastic models requires the addition of uncertainty terms.

$$Q_{stochastic} = Q_{reported} + \varepsilon_{Q_{reported}} \quad (26)$$

Where:

$Q_{stochastic}$ = flow rate through a gauge used in the stochastic model.

$Q_{reported}$ = flow rate through a gauge as reported by the USGS or CDWR.

$\varepsilon_{Q_{reported}}$ = reported gauge uncertainty for a specific stream gauge.

Using Equation 26 with very low flow values may result in negative flow rates. Therefore, $Q_{stochastic}$ was calculated using a truncated normal distribution where the minimum allowed value was $0 \text{ m}^3 \text{s}^{-1}$ ($0 \text{ ft}^3 \text{s}^{-1}$), the maximum allowed value was 1.25 times the maximum reported value for the specific stream gauge, and the mean value was the reported flow rate value. Truncation was performed using an algorithm within the statistical software that used re-sampling and replacement. Other methods were available, but they were deemed to be less reliable.

Stream flow data is provided as described in Section 3.3. The USGS provides three specific uncertainty distributions for average daily stream flow data which are described in every annual water data report (USGS, 2006, 2007, 2008, 2009, 2010, 2011, 2012). The USGS calls these uncertainty distributions "ratings of accuracy". These ratings are "excellent", "good", and "fair". The "excellent" rating indicates that "the daily discharges are within 5 percent of the true value". The distributions expand to 10% and 15% for "good" and "fair" ratings, respectively. There is a fourth rating used on some average daily stream flow data gathered in the LARV; "poor". This rating is not specific as it states that the values are more than 15% of the true value. For this thesis, we have refined the "poor" rating definition such that 95 percent of the values are within 20 percent of the true value. These ratings are as shown in Table 4.13 which was extracted from a USGS annual water data report.

Figures 4.14 and 4.15 present the stochastic and deterministic model results for each of the stream flow variables used in USR and DSR models, respectively. Each pair of figures presents the deterministic model results on the left and the stochastic model results on the right. The deterministic model figures show the flow rates as reported by the CDWR and USGS. The stochastic model figures present the stochastic model mean time-series and the band bounded by the stochastic model 2.5th percentile time-series and the stochastic model

Table 4.13. USGS Measured Field Parameter Accuracy Rating Table. This table was taken from the USGS annual water data report.

Measured field parameter	Ratings of accuracy (Based on combined fouling and calibration drift corrections applied to the record)			
	Excellent	Good	Fair	Poor
Water temperature	$\leq \pm 0.2^{\circ}\text{C}$	$> \pm 0.2 - 0.5^{\circ}\text{C}$	$> \pm 0.5 - 0.8^{\circ}\text{C}$	$> \pm 0.8^{\circ}\text{C}$
Specific conductance	$\leq \pm 3\%$	$> \pm 3 - 10\%$	$> \pm 10 - 15\%$	$> \pm 15\%$
Dissolved oxygen	$\leq \pm 0.3 \text{ mg/L}$ or $\leq \pm 5\%$, whichever is greater	$> \pm 0.3 - 0.5 \text{ mg/L}$ or $> \pm 5 - 10\%$, whichever is greater	$> \pm 0.5 - 0.8 \text{ mg/L}$ or $> \pm 10 - 15\%$, whichever is greater	$> \pm 0.8 \text{ mg/L}$ or $> \pm 15\%$, whichever is greater
pH	$\leq \pm 0.2$ units	$> \pm 0.2 - 0.5$ units	$> \pm 0.5 - 0.8$ units	$> \pm 0.8$ units
Turbidity	$\leq \pm 0.5$ turbidity units or $\leq \pm 5\%$, whichever is greater	$> \pm 0.5 - 1.0$ turbidity units or $> \pm 5 - 10\%$, whichever is greater	$> \pm 1.0 - 1.5$ turbidity units or $> \pm 10 - 15\%$, whichever is greater	$> \pm 1.5$ turbidity units or $> \pm 15\%$, whichever is greater

97.5th percentile time-series. These figures present results from each of the stream gauge in CDWR stream gauge name alphabetical order.

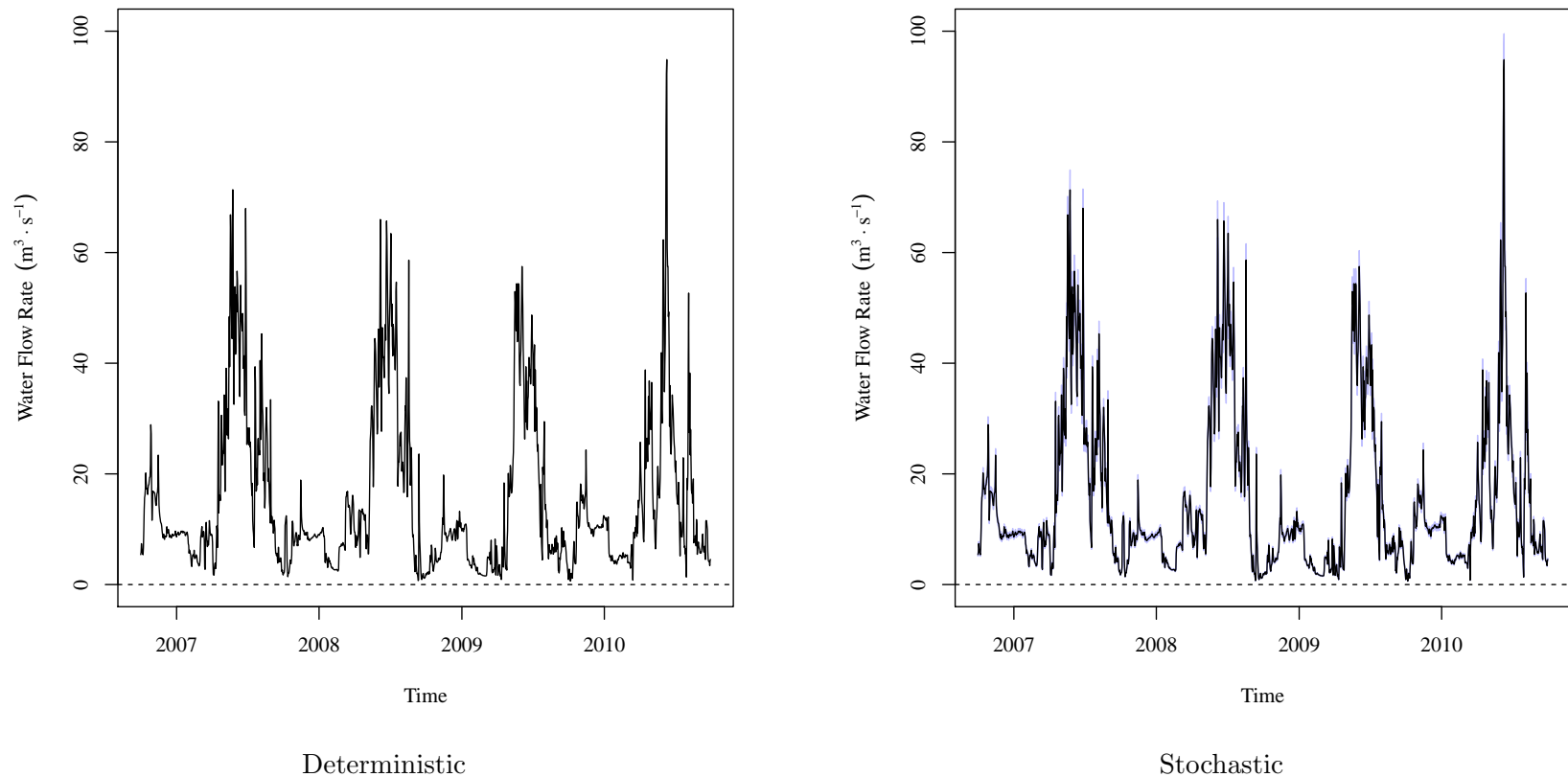


Figure 4.14. USR deterministic and stochastic model time-series average daily flow rate. The deterministic model time-series presents the data reported by the CDWR and USGS gauges. In the stochastic model time-series, the black lines indicate the stochastic model mean time-series. The blue band indicates the 95% central inter-percentile range (CIR) of the stochastic values. Results are presented in CDWR stream gauge name alphabetical order.

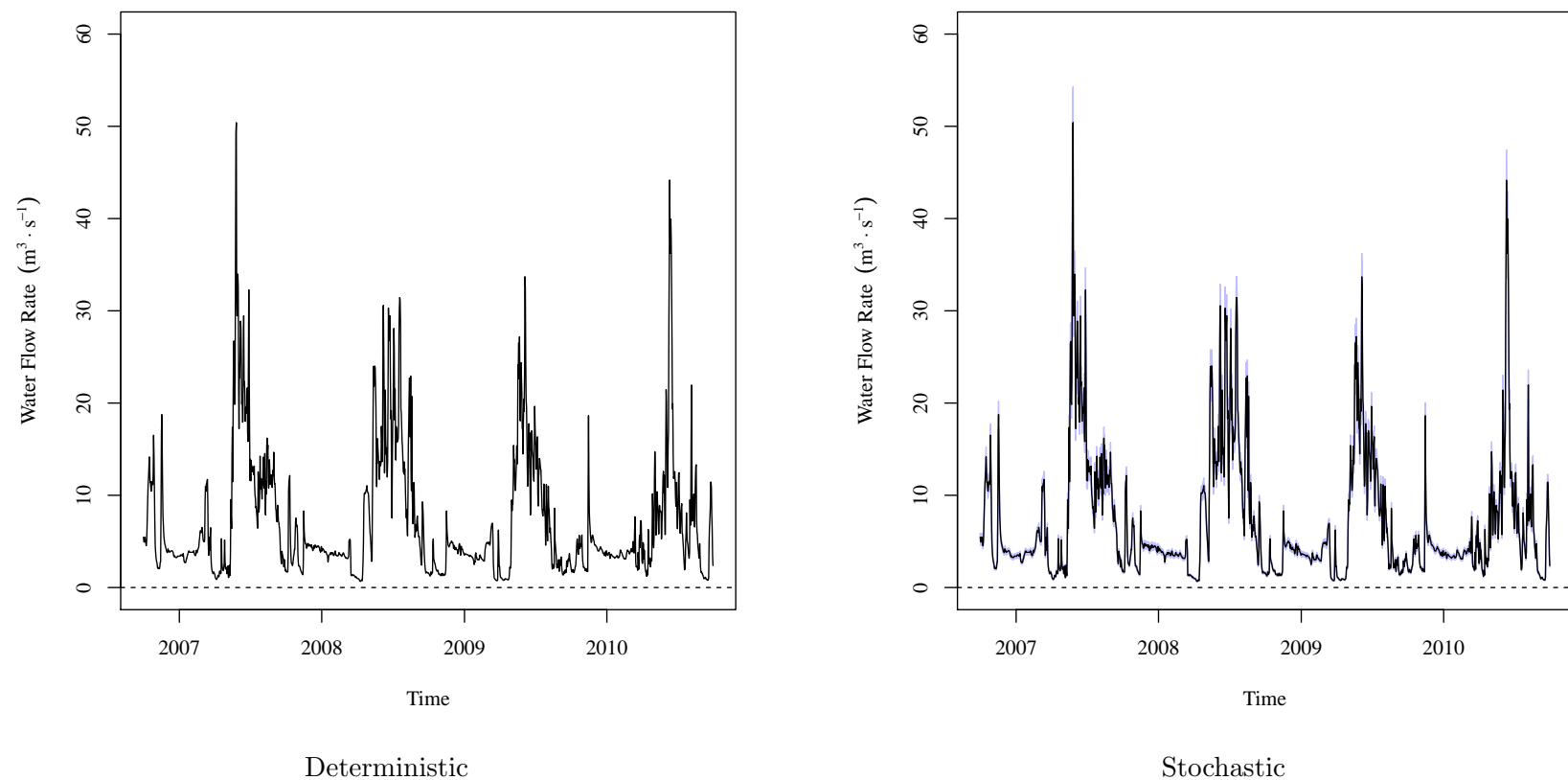
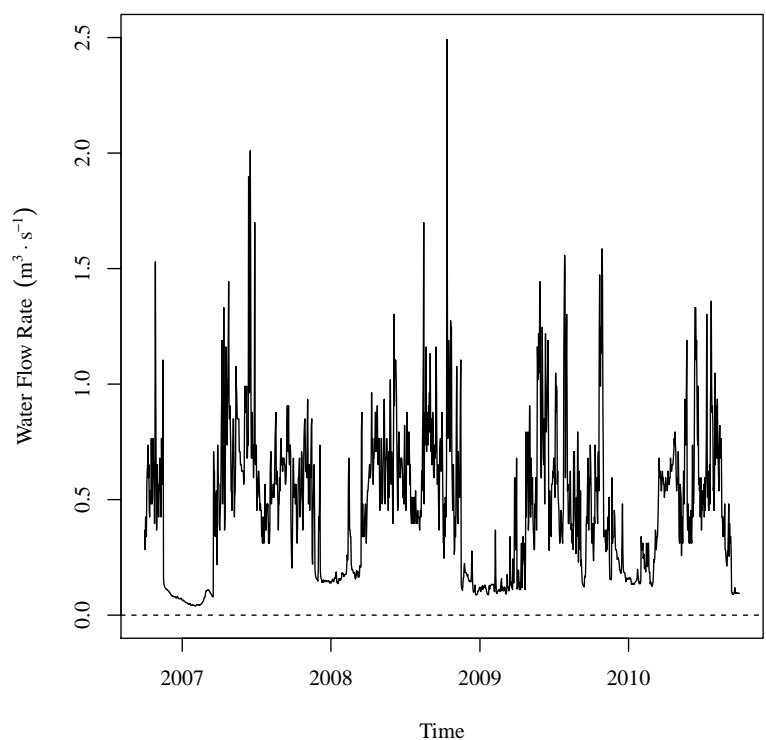
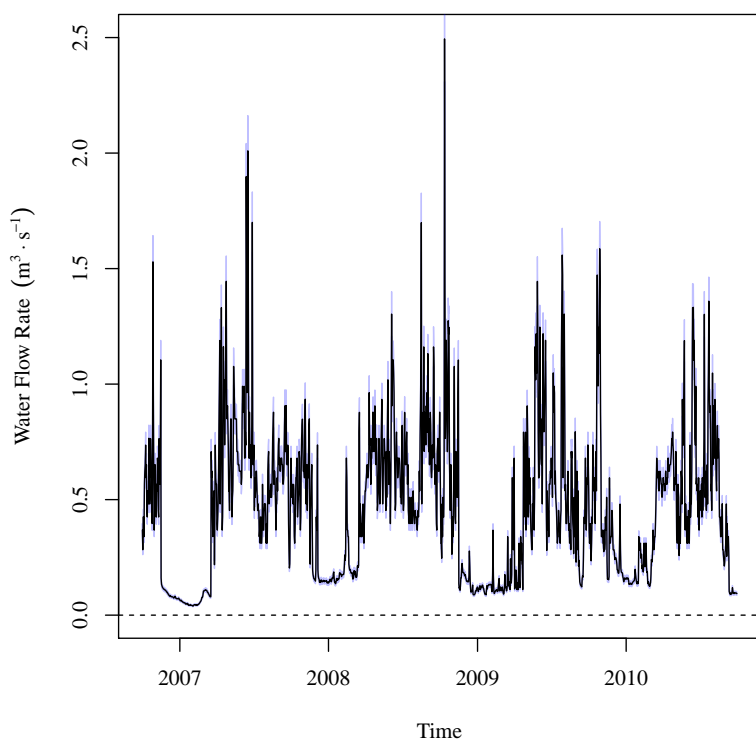


Figure 4.14 (Cont). USR deterministic and stochastic model time-series average daily flow rate.

$Q_{CANSWKCO}$



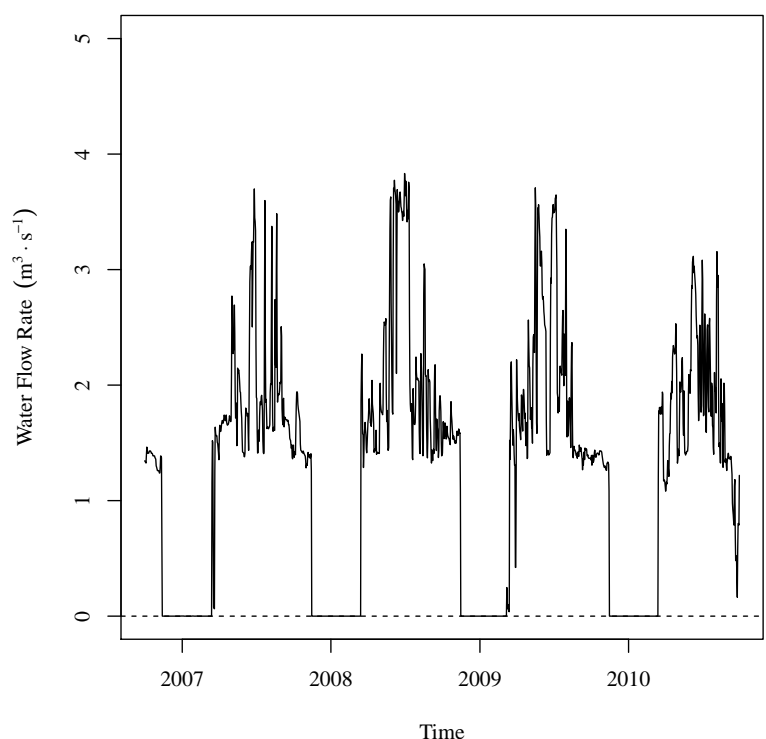
Deterministic



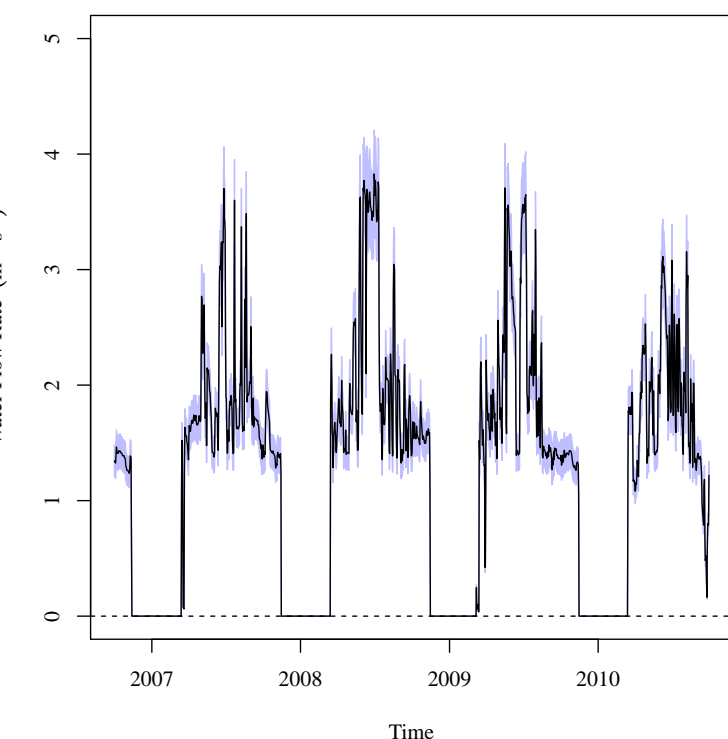
Stochastic

Figure 4.14 (Cont). USR deterministic and stochastic model time-series average daily flow rate.

$Q_{CONDITCO}$



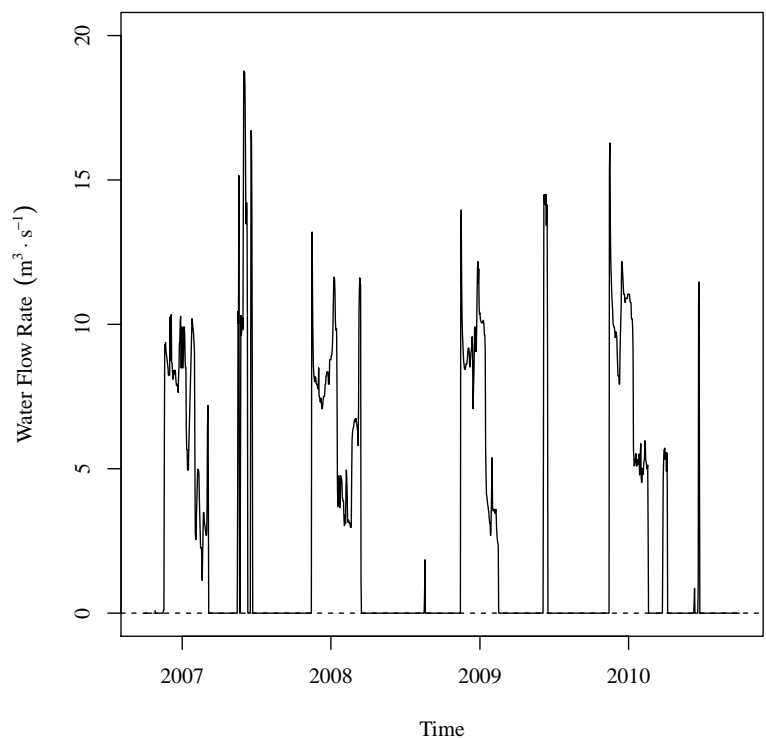
Deterministic



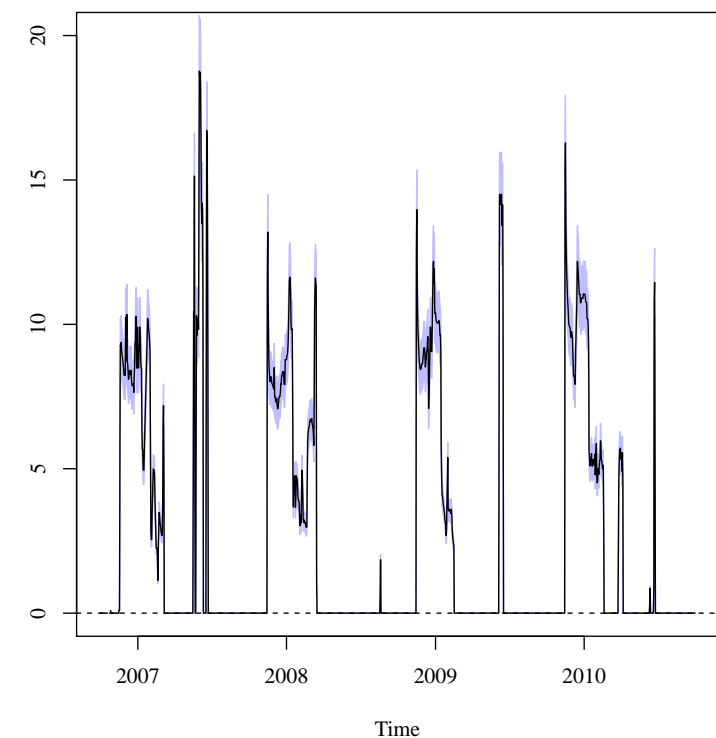
Stochastic

Figure 4.14 (Cont). USR deterministic and stochastic model time-series average daily flow rate.

$Q_{FLSCANCO}$



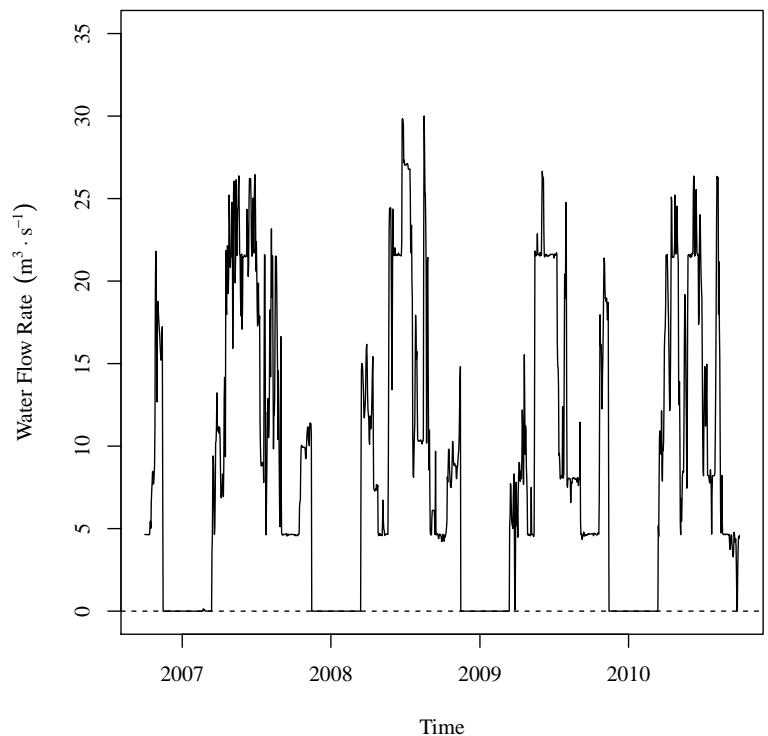
Deterministic



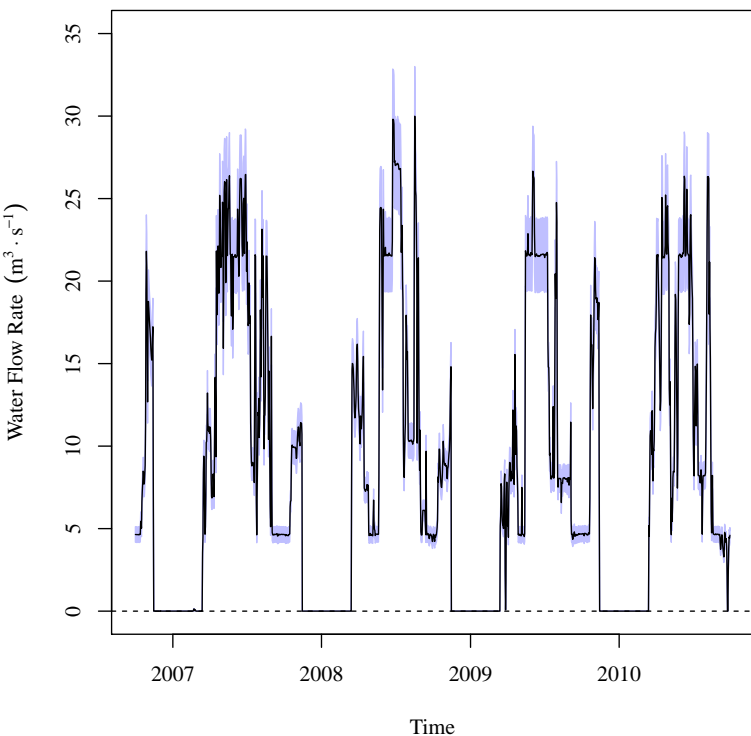
Stochastic

Figure 4.14 (Cont). USR deterministic and stochastic model time-series average daily flow rate.

$Q_{FLYCANCO}$



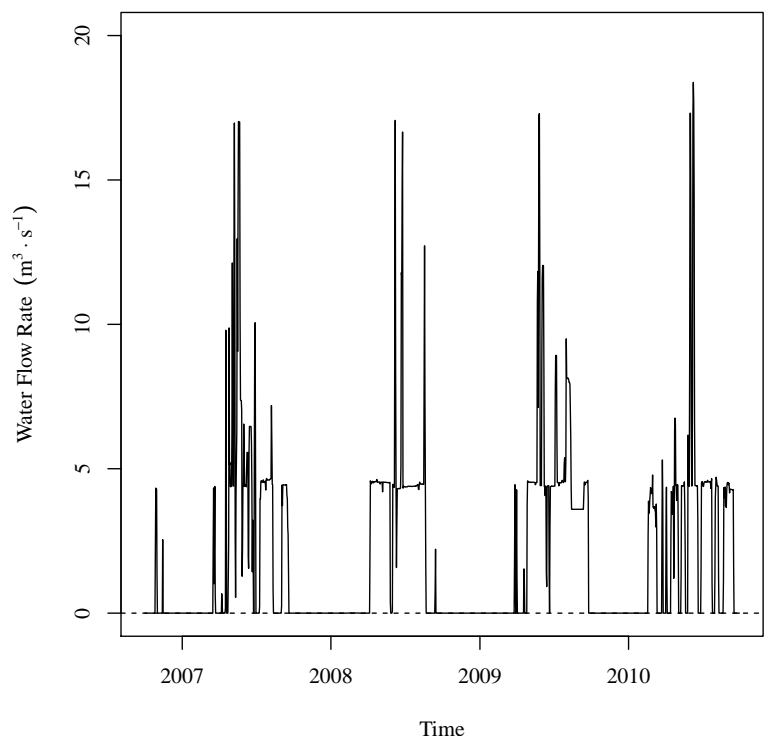
Deterministic



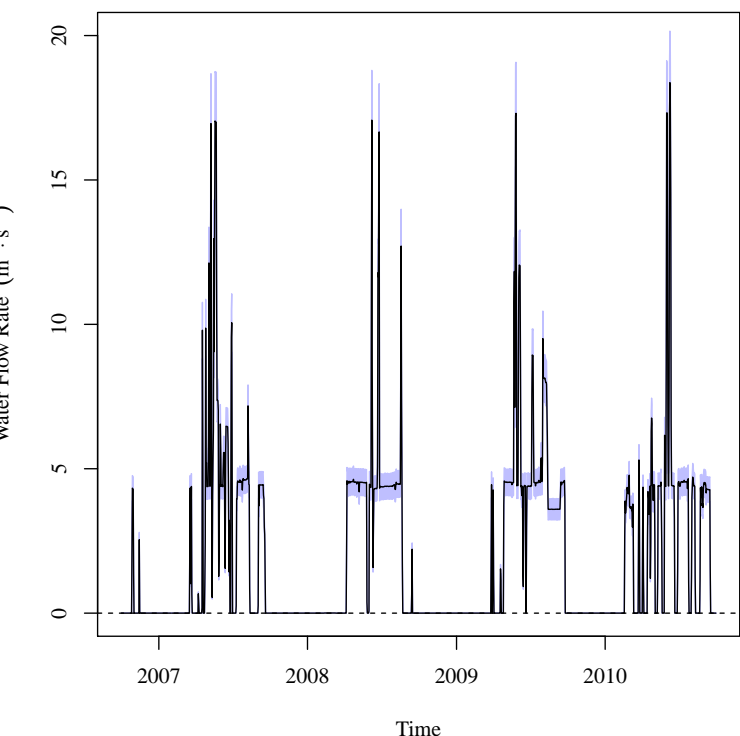
Stochastic

Figure 4.14 (Cont). USR deterministic and stochastic model time-series average daily flow rate.

$Q_{HOLCANCO}$



Deterministic

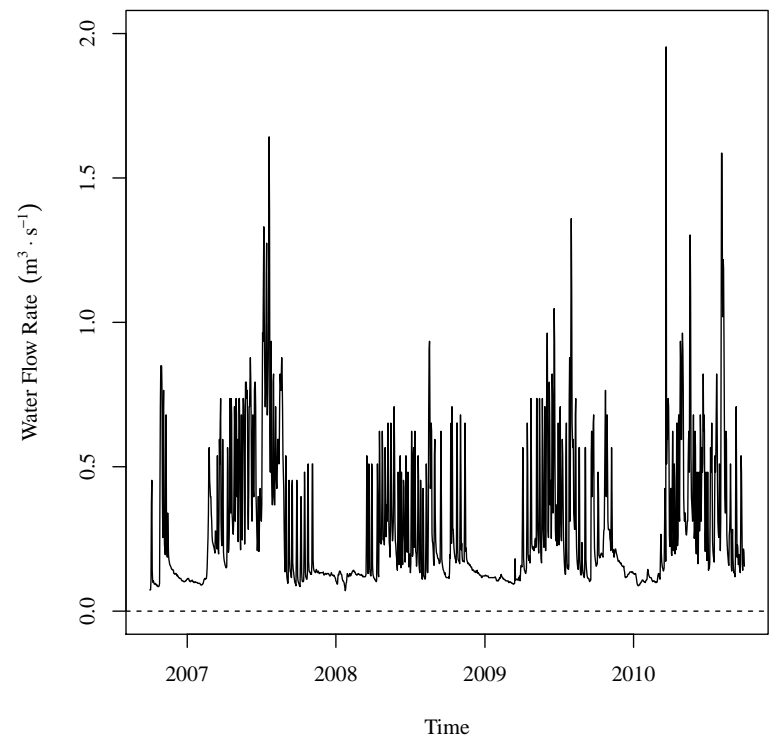


Stochastic

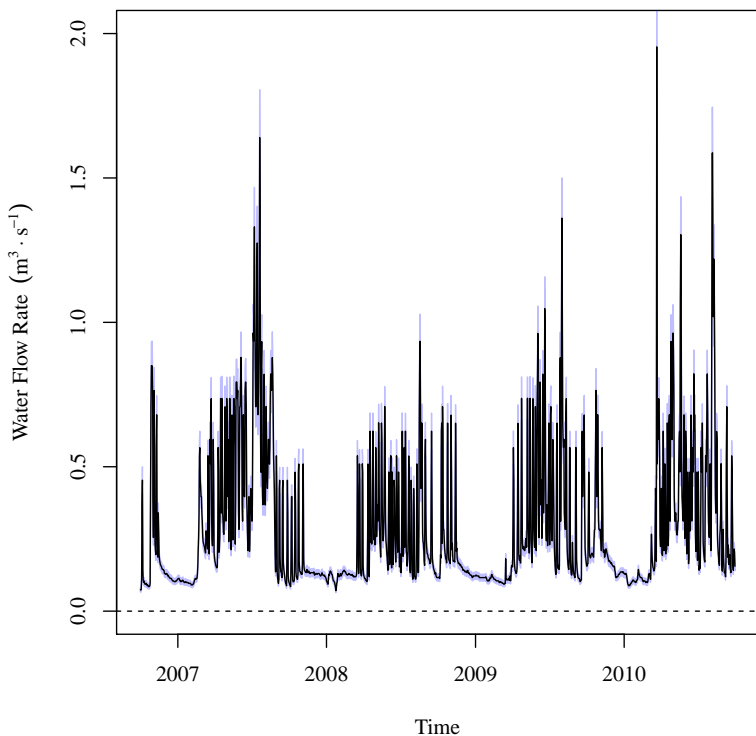
Figure 4.14 (Cont). USR deterministic and stochastic model time-series average daily flow rate.

$Q_{HRC194CO}$

9ct



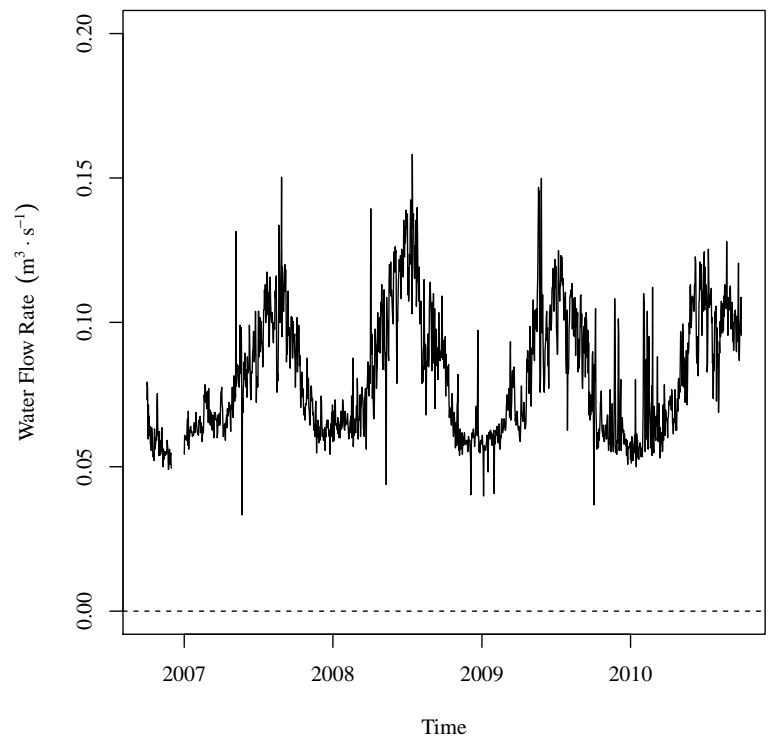
Deterministic



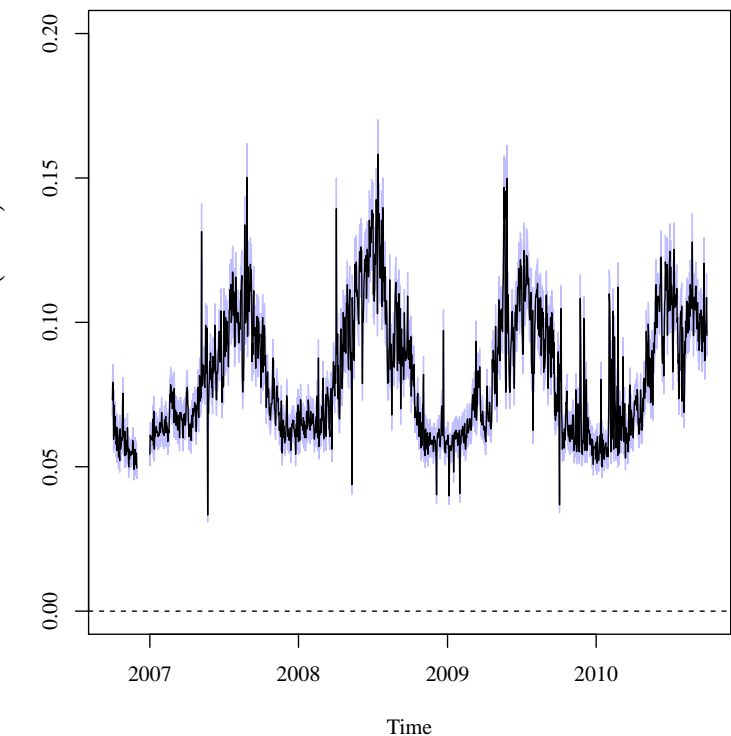
Stochastic

Figure 4.14 (Cont). USR deterministic and stochastic model time-series average daily flow rate.

$Q_{LAJWWTP}$



Deterministic



Stochastic

Figure 4.14 (Cont). USR deterministic and stochastic model time-series average daily flow rate.

$$Q_{RFDMANCO}$$

138

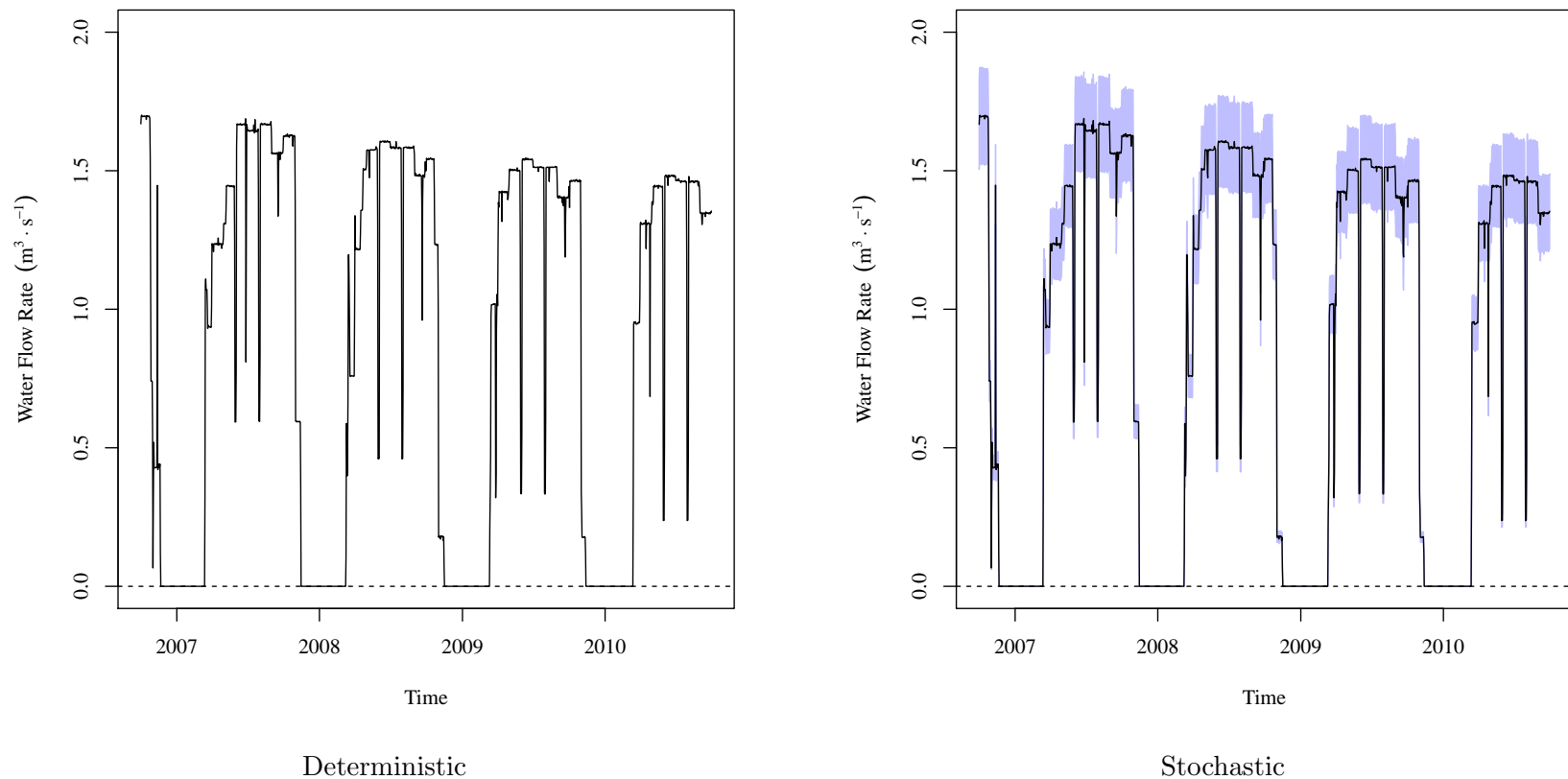
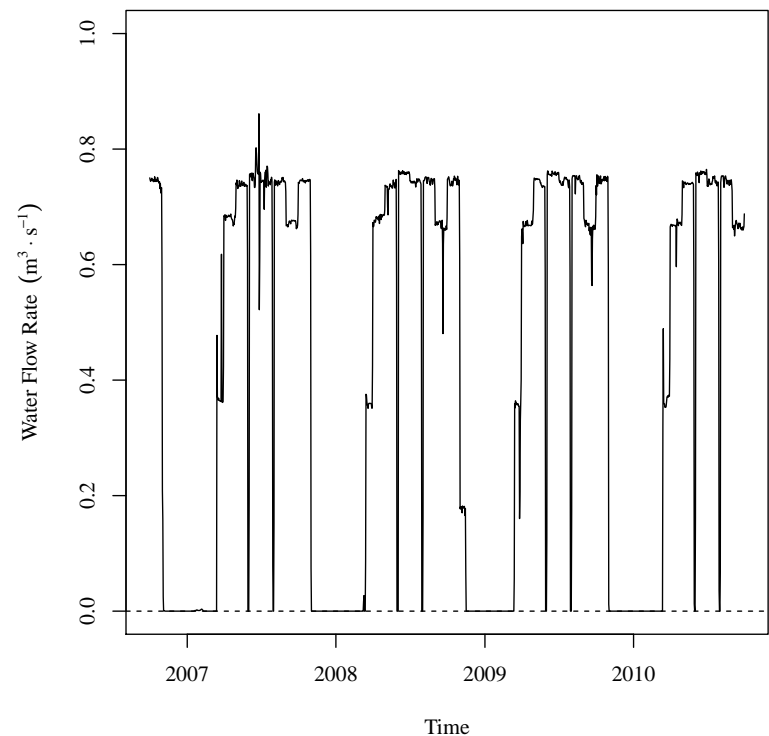


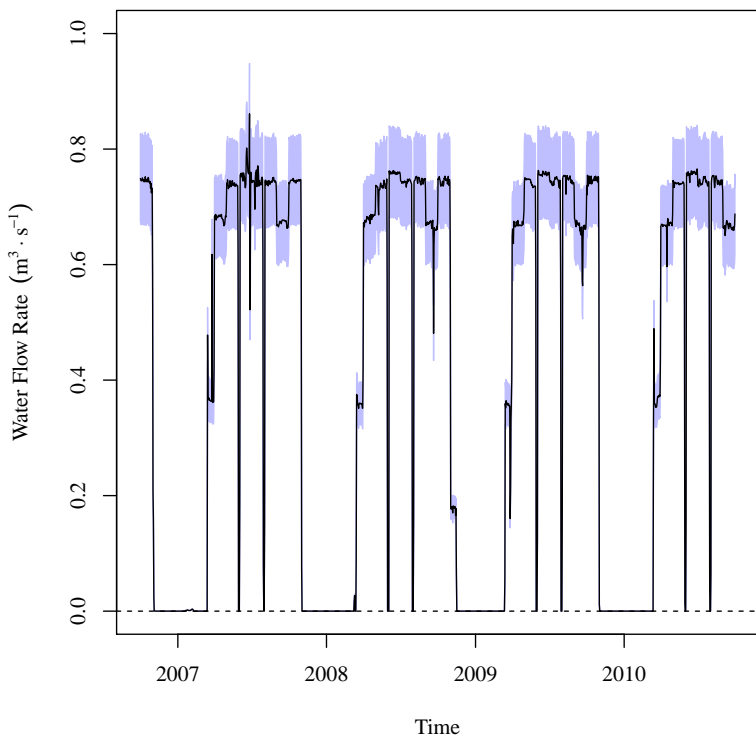
Figure 4.14 (Cont). USR deterministic and stochastic model time-series average daily flow rate.

$$Q_{RF DRETCO}$$

139



Deterministic



Stochastic

Figure 4.14 (Cont). USR deterministic and stochastic model time-series average daily flow rate.

$Q_{TMSWICO}$

0f1

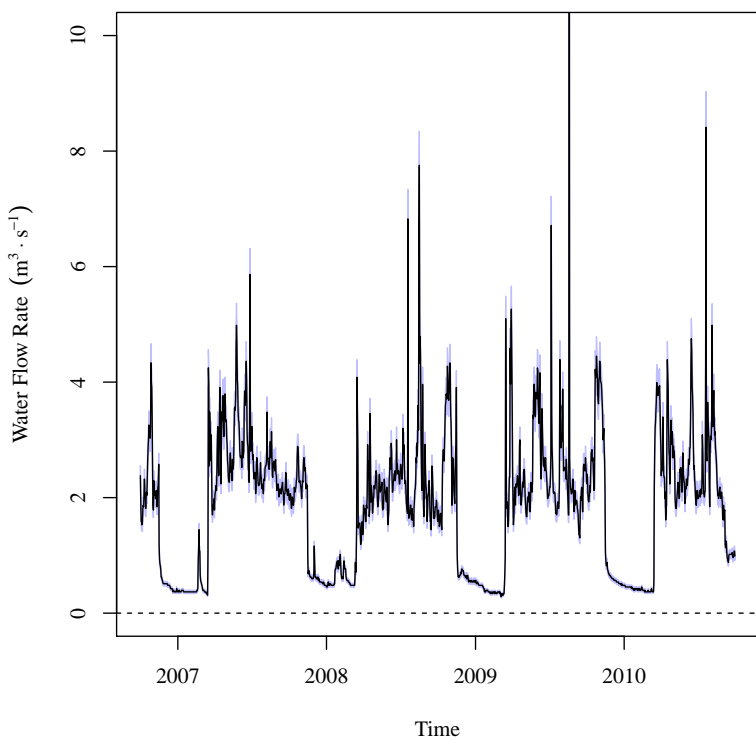
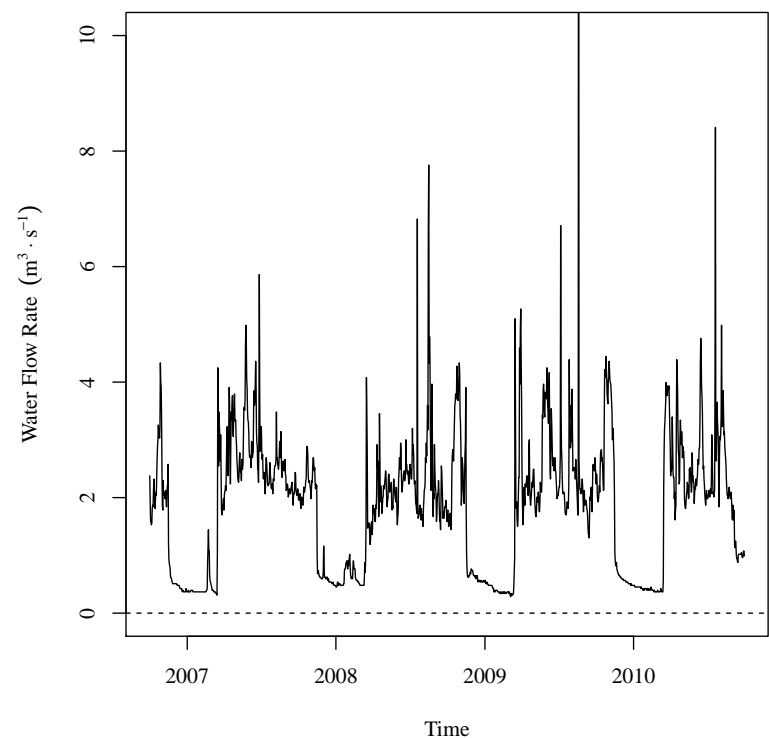
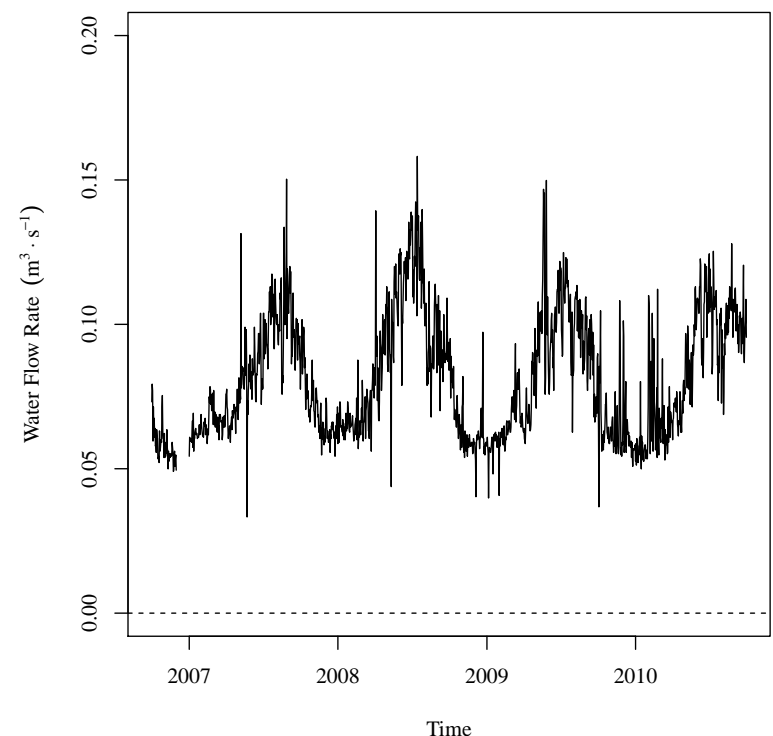
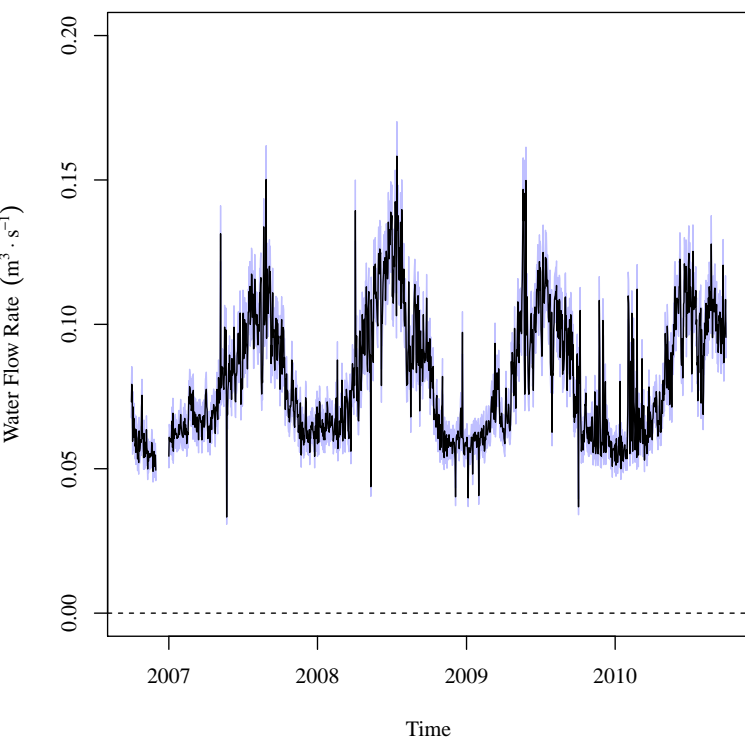


Figure 4.14 (Cont). USR deterministic and stochastic model time-series average daily flow rate.

$$Q_{LaJuntaWWTP}$$



Deterministic



Stochastic

Figure 4.14 (Cont). USR deterministic and stochastic model time-series average daily flow rate.

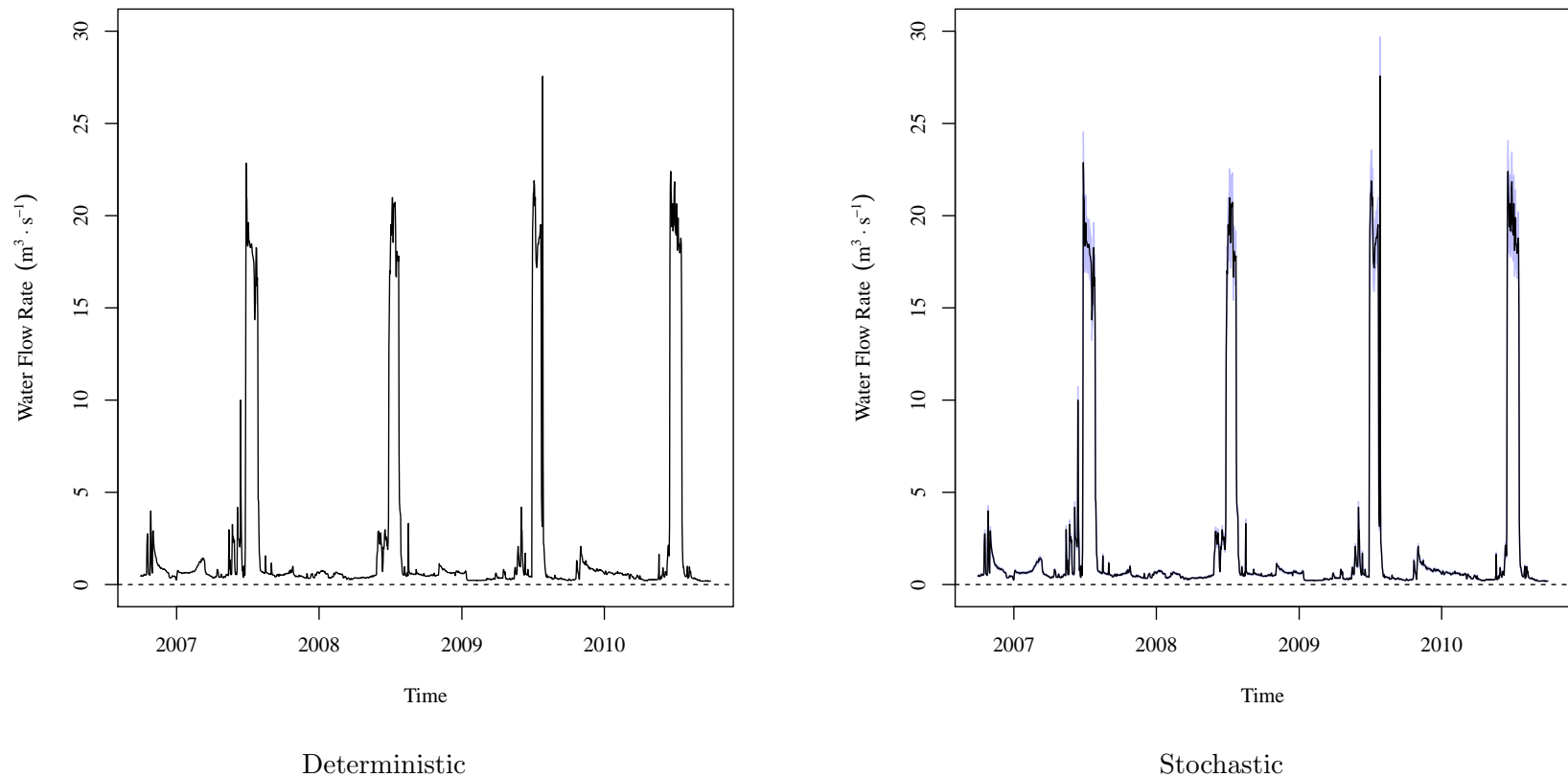


Figure 4.15. DSR deterministic and stochastic model time-series average daily flow rate. The deterministic model time-series presents the data reported by the CDWR and USGS gauges. In the stochastic model time-series, the black lines indicate the stochastic model mean time-series. The blue band indicates the 95% central inter-percentile range (CIR) of the stochastic values. Results are presented in CDWR stream gauge name alphabetical order.

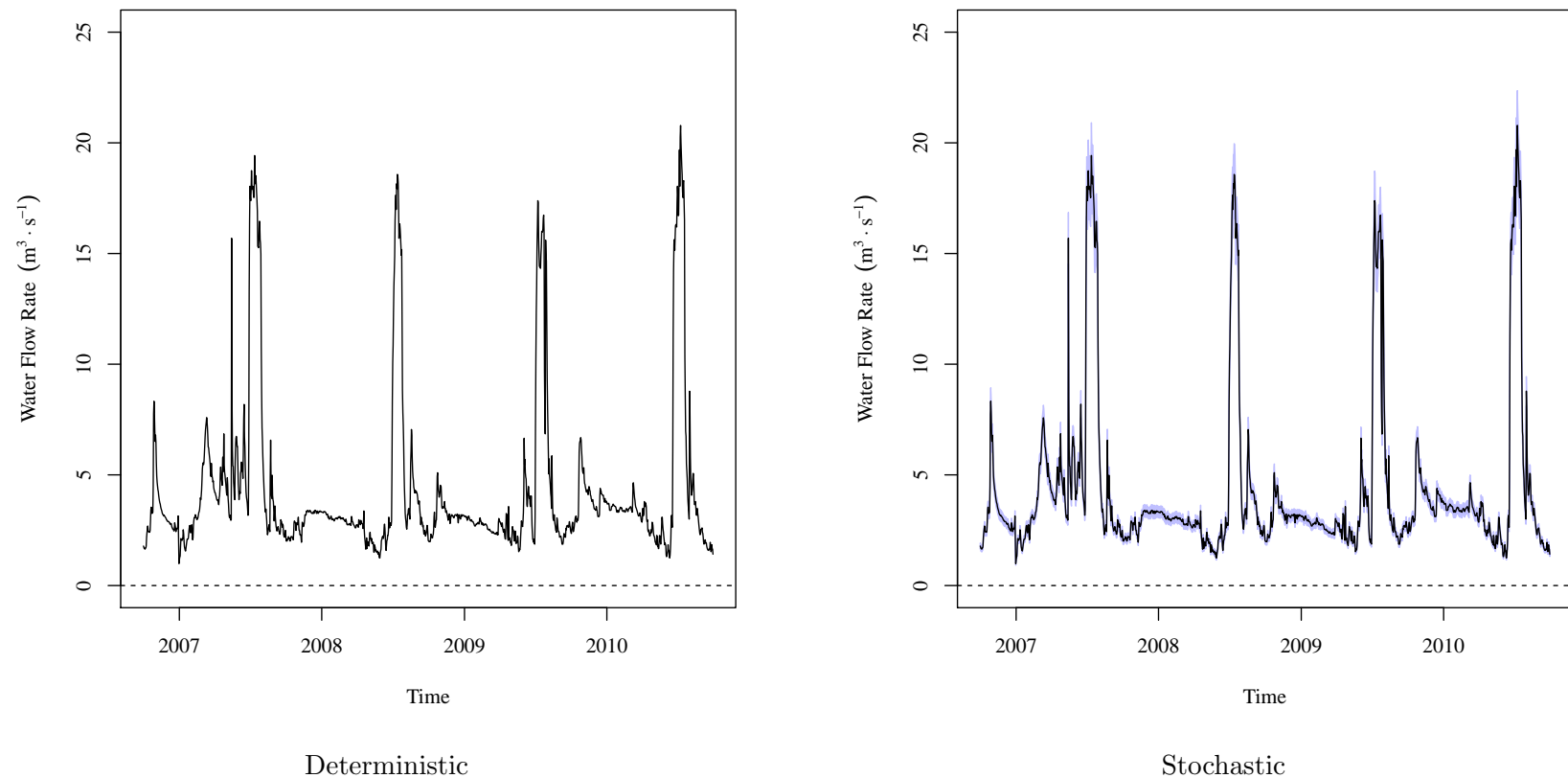


Figure 4.15 (Cont). DSR deterministic and stochastic model time-series average daily flow rate.

$Q_{BIGLAMCO}$

144

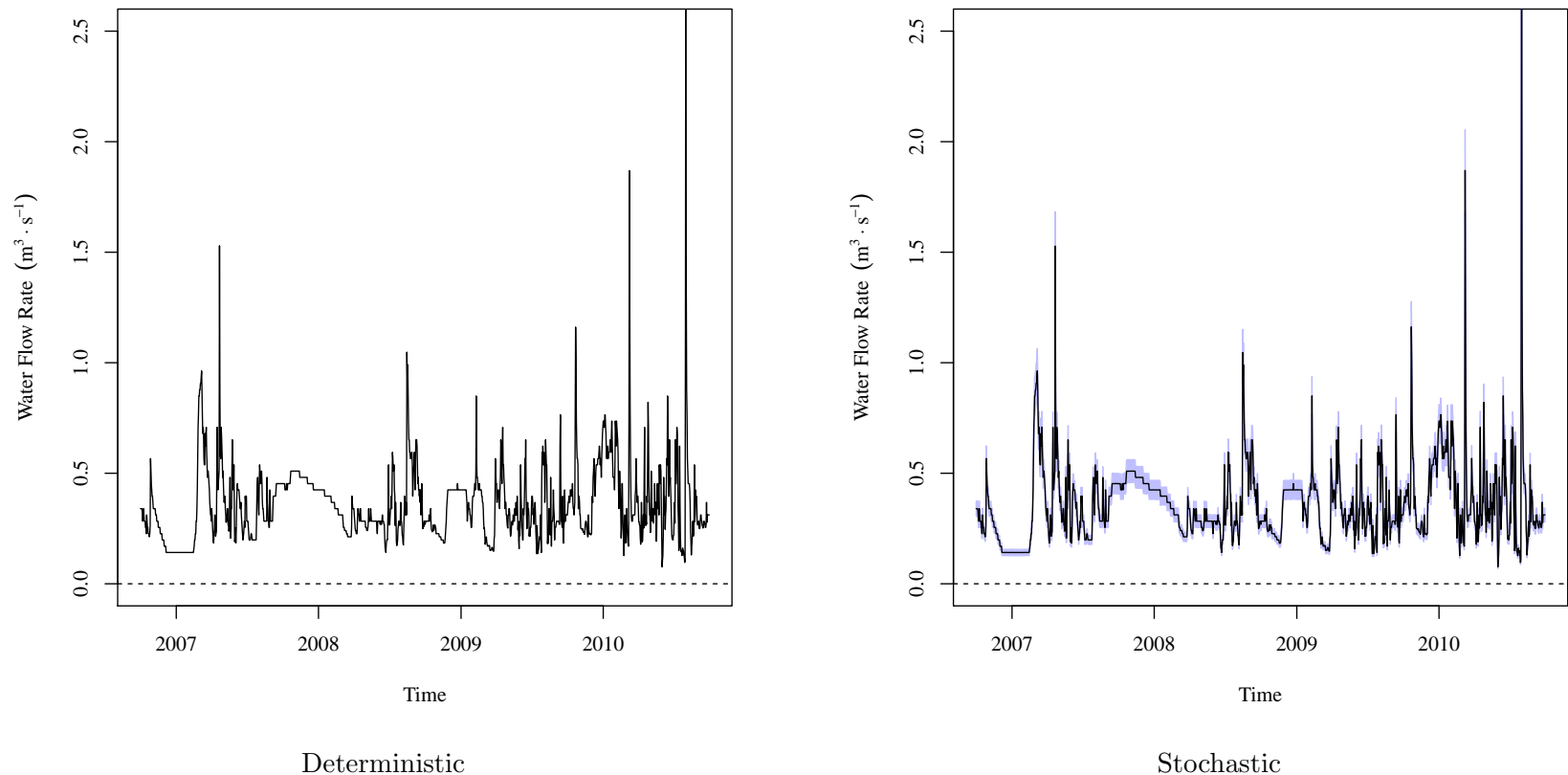
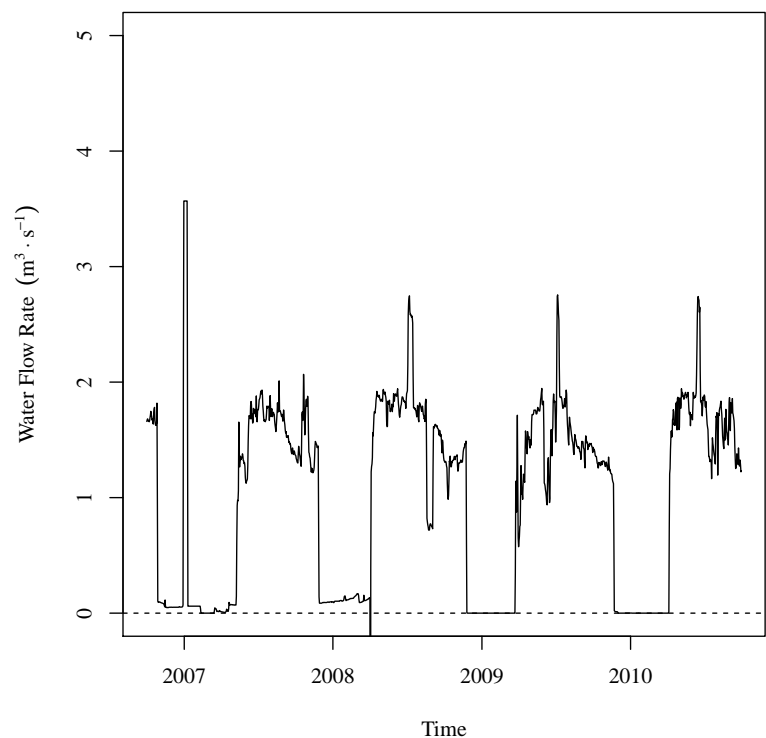


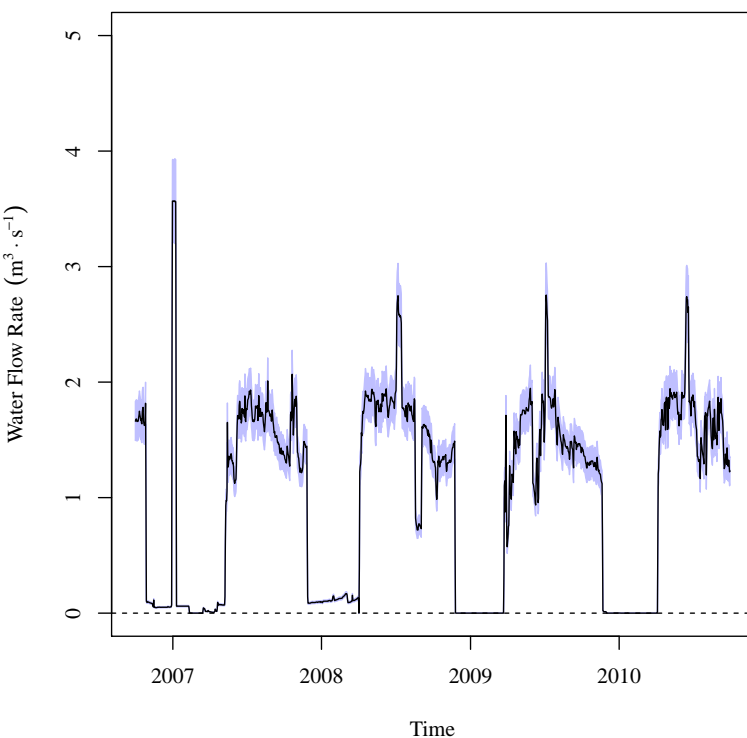
Figure 4.15 (Cont). DSR deterministic and stochastic model time-series average daily flow rate.

$Q_{BUF DITCO}$

971



Deterministic

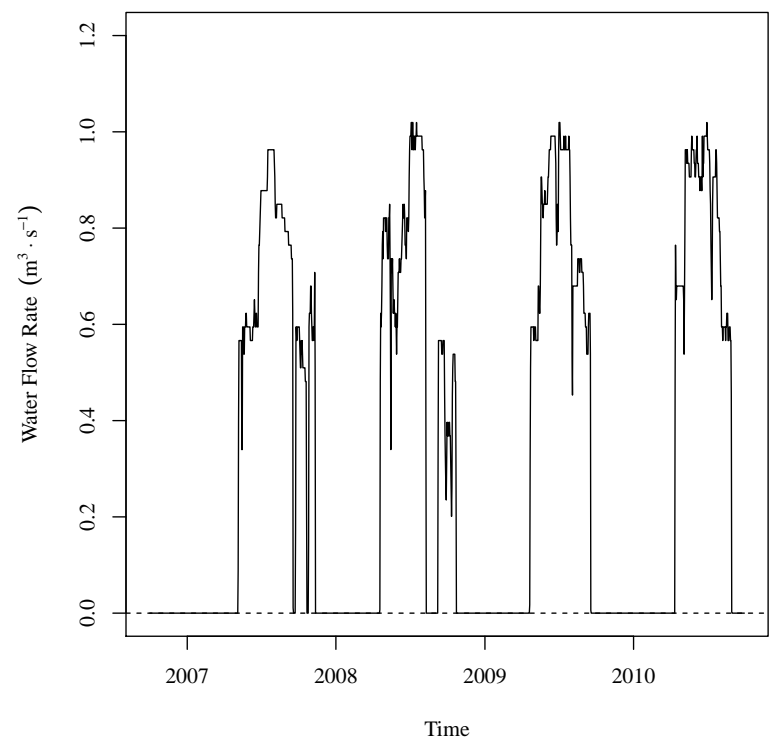


Stochastic

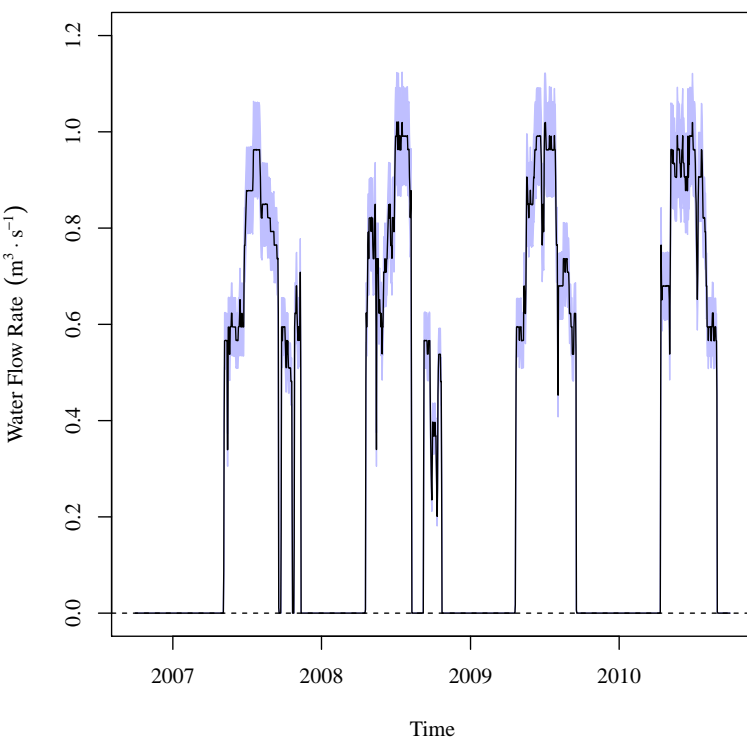
Figure 4.15 (Cont). DSR deterministic and stochastic model time-series average daily flow rate.

$Q_{FRODITKS}$

9f1



Deterministic



Stochastic

Figure 4.15 (Cont). DSR deterministic and stochastic model time-series average daily flow rate.

$$Q_{WILDHOCO}$$

LFI

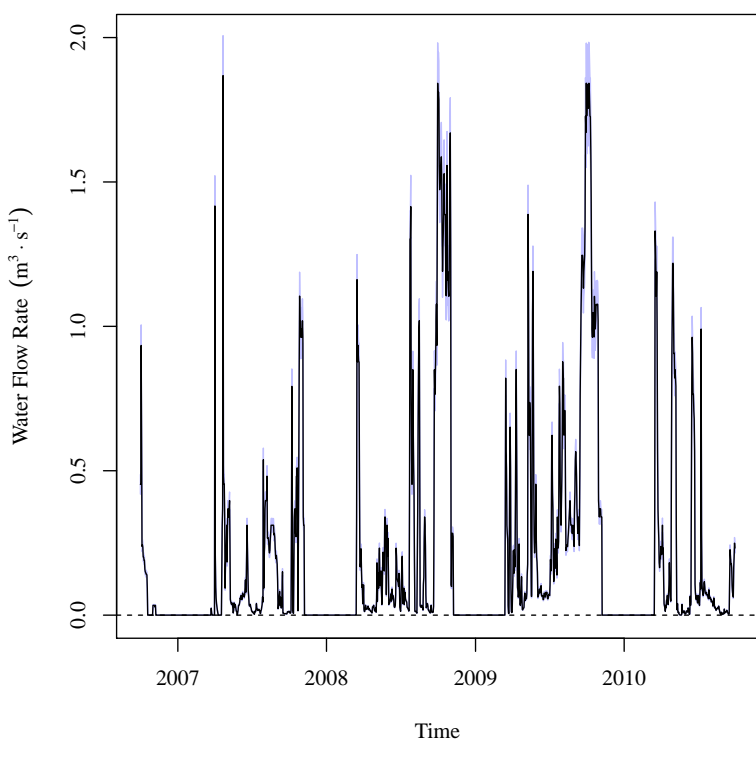
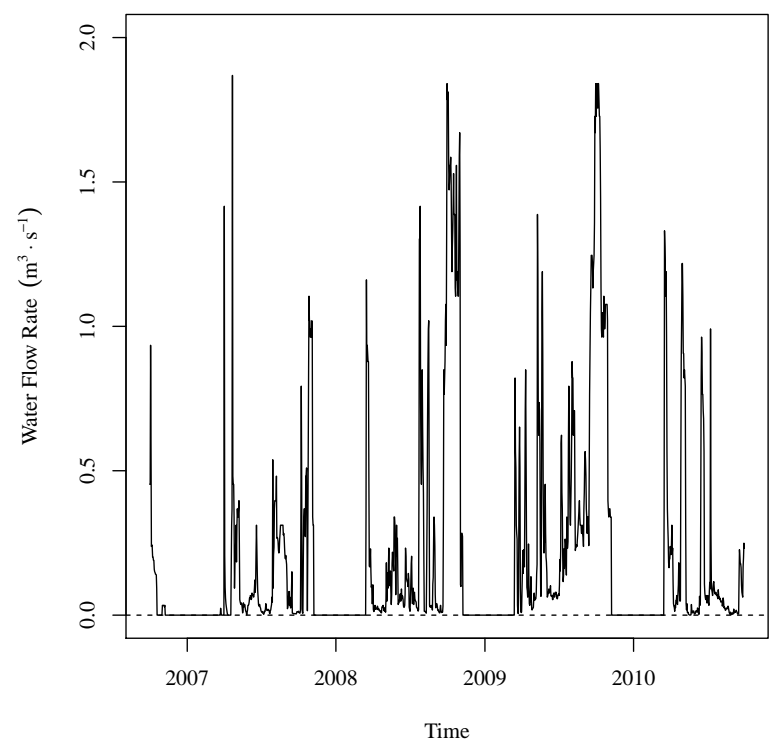


Figure 4.15 (Cont). DSR deterministic and stochastic model time-series average daily flow rate.

Both figures 4.14 and 4.15 show that the stochastic model mean time-series of each of the calculated stochastic model flow rates does not deviate significantly from the deterministic model time-series. Tables 4.14 and 4.15 present the numeric results associated with each of the figures. These tables show that the deterministic model time-series and stochastic
5 mean time-series are essentially identical. The 2.5th percentile, mean, and 97.5th percentile of the two models are identical or nearly identical for all flow rates. The Pearson Correlation values for the two models are 1 or very nearly 1 for all cases. These results show that for the average daily flow rate, the deterministic model is representative of the stochastic model

Table 4.14. USR deterministic and stochastic model time-series average daily flow rate numeric results. Results are presented in CDWR stream gauge name alphabetical order.

$Q_{ARKCATCO}$

Deterministic Model Time Series

2.5th Percentile	Mean	97.5th Percentile
1.7 (60)	15.3 (540)	53.7 (1900)

Stochastic Model Summary Statistics Time Series

Time Series	2.5th Percentile	Mean	97.5th Percentile
97.5th Percentile	1.78 (62.9)	16.1 (569)	56.3 (1990)
Mean	1.7 (60)	15.3 (540)	53.6 (1890)
2.5th Percentile	1.61 (56.9)	14.5 (512)	51 (1800)
Pearson Correlation = 1			

$Q_{ARKLASCO}$

Deterministic Model Time Series

2.5th Percentile	Mean	97.5th Percentile
0.906 (32)	7.14 (252)	26.7 (943)

Stochastic Model Summary Statistics Time Series

Time Series	2.5th Percentile	Mean	97.5th Percentile
97.5th Percentile	0.975 (34.4)	7.67 (271)	28.7 (1010)
Mean	0.906 (32)	7.14 (252)	26.7 (943)
2.5th Percentile	0.84 (29.7)	6.6 (233)	24.7 (872)
Pearson Correlation = 1			

Table 4.14 (Cont). USR deterministic and stochastic model time-series average daily flow rate numeric results.

$$Q_{CANSWKCO}$$

Deterministic Model Time Series

2.5th Percentile	Mean	97.5th Percentile
0.0538 (1.9)	0.457 (16.1)	1.19 (42)

Stochastic Model Summary Statistics Time Series

Time Series	2.5th Percentile	Mean	97.5th Percentile
97.5th Percentile	0.0578 (2.04)	0.492 (17.4)	1.28 (45.2)
Mean	0.0538 (1.9)	0.457 (16.1)	1.19 (42)
2.5th Percentile	0.0496 (1.75)	0.423 (14.9)	1.1 (38.8)
Pearson Correlation = 1			

$$Q_{CONDITCO}$$

Deterministic Model Time Series

2.5th Percentile	Mean	97.5th Percentile
0 (0)	1.25 (44.1)	3.53 (125)

Stochastic Model Summary Statistics Time Series

Time Series	2.5th Percentile	Mean	97.5th Percentile
97.5th Percentile	0 (0)	1.38 (48.7)	3.89 (137)
Mean	0 (0)	1.25 (44.1)	3.53 (125)
2.5th Percentile	0 (0)	1.13 (39.9)	3.18 (112)
Pearson Correlation = 1			

Table 4.14 (Cont). USR deterministic and stochastic model time-series average daily flow rate numeric results.

$$Q_{FLSCANCO}$$

Deterministic Model Time Series

2.5th Percentile	Mean	97.5th Percentile
0 (0)	2.54 (89.7)	11.8 (417)

Stochastic Model Summary Statistics Time Series

Time Series	2.5th Percentile	Mean	97.5th Percentile
97.5th Percentile	0 (0)	2.8 (98.9)	13 (459)
Mean	0 (0)	2.54 (89.7)	11.8 (417)
2.5th Percentile	0 (0)	2.29 (80.9)	10.6 (374)
Pearson Correlation = 1			

$$Q_{FLYCANCO}$$

Deterministic Model Time Series

2.5th Percentile	Mean	97.5th Percentile
0 (0)	8.5 (300)	26.2 (925)

Stochastic Model Summary Statistics Time Series

Time Series	2.5th Percentile	Mean	97.5th Percentile
97.5th Percentile	0 (0)	9.35 (330)	28.8 (1020)
Mean	0 (0)	8.5 (300)	26.2 (925)
2.5th Percentile	0 (0)	7.65 (270)	23.5 (830)
Pearson Correlation = 1			

Table 4.14 (Cont). USR deterministic and stochastic model time-series average daily flow rate numeric results.

$Q_{HOLCANO}$

Deterministic Model Time Series

2.5th Percentile	Mean	97.5th Percentile
0 (0)	1.96 (69.2)	9.84 (347)

Stochastic Model Summary Statistics Time Series

Time Series	2.5th Percentile	Mean	97.5th Percentile
97.5th Percentile	0 (0)	2.16 (76.3)	10.8 (381)
Mean	0 (0)	1.96 (69.2)	9.83 (347)
2.5th Percentile	0 (0)	1.77 (62.5)	8.85 (313)
Pearson Correlation = 1			

$Q_{HRC194CO}$

Deterministic Model Time Series

2.5th Percentile	Mean	97.5th Percentile
0.0934 (3.3)	0.291 (10.3)	0.878 (31)

Stochastic Model Summary Statistics Time Series

Time Series	2.5th Percentile	Mean	97.5th Percentile
97.5th Percentile	0.103 (3.64)	0.32 (11.3)	0.968 (34.2)
Mean	0.0934 (3.3)	0.291 (10.3)	0.878 (31)
2.5th Percentile	0.084 (2.97)	0.261 (9.22)	0.791 (27.9)
Pearson Correlation = 1			

Table 4.14 (Cont). USR deterministic and stochastic model time-series average daily flow rate numeric results.

$Q_{RFDMANCO}$

Deterministic Model Time Series

2.5th Percentile	Mean	97.5th Percentile
0 (0)	0.907 (32)	1.67 (59)

Stochastic Model Summary Statistics Time Series

Time Series	2.5th Percentile	Mean	97.5th Percentile
97.5th Percentile	0 (0)	0.998 (35.2)	1.84 (65)
Mean	0 (0)	0.907 (32)	1.67 (59)
2.5th Percentile	0 (0)	0.816 (28.8)	1.5 (53)
Pearson Correlation = 1			

$Q_{RFDRETCO}$

Deterministic Model Time Series

2.5th Percentile	Mean	97.5th Percentile
0 (0)	0.427 (15.1)	0.759 (26.8)

Stochastic Model Summary Statistics Time Series

Time Series	2.5th Percentile	Mean	97.5th Percentile
97.5th Percentile	0 (0)	0.47 (16.6)	0.836 (29.5)
Mean	0 (0)	0.427 (15.1)	0.759 (26.8)
2.5th Percentile	0 (0)	0.384 (13.6)	0.683 (24.1)
Pearson Correlation = 1			

Table 4.14 (Cont). USR deterministic and stochastic model time-series average daily flow rate numeric results.

$$Q_{TIMSWICO}$$

Deterministic Model Time Series

2.5th Percentile	Mean	97.5th Percentile
0.368 (13)	1.86 (65.7)	4.16 (147)

Stochastic Model Summary Statistics Time Series

Time Series	2.5th Percentile	Mean	97.5th Percentile
97.5th Percentile	0.395 (13.9)	2 (70.6)	4.47 (158)
Mean	0.368 (13)	1.86 (65.7)	4.16 (147)
2.5th Percentile	0.34 (12)	1.72 (60.7)	3.85 (136)
Pearson Correlation = 1			

$$Q_{LaJuntaWWTP}$$

Deterministic Model Time Series

2.5th Percentile	Mean	97.5th Percentile
0.0542 (1.91)	0.0808 (2.85)	0.125 (4.41)

Stochastic Model Summary Statistics Time Series

Time Series	2.5th Percentile	Mean	97.5th Percentile
97.5th Percentile	0.0582 (2.06)	0.0869 (3.07)	0.134 (4.73)
Mean	0.0542 (1.91)	0.0808 (2.85)	0.125 (4.41)
2.5th Percentile	0.0501 (1.77)	0.0747 (2.64)	0.115 (4.06)
Pearson Correlation = 1			

Table 4.15. DSR deterministic and stochastic model time-series average daily flow rate numeric results. Results are presented in CDWR stream gauge name alphabetical order.

$Q_{ARKLAMCO}$

Deterministic Model Time Series

2.5th Percentile	Mean	97.5th Percentile
0.221 (7.8)	2.1 (74.2)	19.4 (685)

Stochastic Model Summary Statistics Time Series

Time Series	2.5th Percentile	Mean	97.5th Percentile
97.5th Percentile	0.237 (8.37)	2.26 (79.8)	20.8 (735)
Mean	0.221 (7.8)	2.1 (74.2)	19.4 (685)
2.5th Percentile	0.204 (7.2)	1.95 (68.9)	17.9 (632)
Pearson Correlation = 1			

$Q_{ARKCOOKS}$

Deterministic Model Time Series

2.5th Percentile	Mean	97.5th Percentile
1.61 (56.9)	4.29 (151)	17.5 (618)

Stochastic Model Summary Statistics Time Series

Time Series	2.5th Percentile	Mean	97.5th Percentile
97.5th Percentile	1.73 (61.1)	4.61 (163)	18.8 (664)
Mean	1.61 (56.9)	4.29 (151)	17.5 (618)
2.5th Percentile	1.49 (52.6)	3.96 (140)	16.2 (572)
Pearson Correlation = 1			

Table 4.15 (Cont). DSR deterministic and stochastic model time-series average daily flow rate numeric results.

$$Q_{BIGLAMCO}$$

Deterministic Model Time Series

2.5th Percentile	Mean	97.5th Percentile
0.142 (5.01)	0.362 (12.8)	0.736 (26)

Stochastic Model Summary Statistics Time Series

Time Series	2.5th Percentile	Mean	97.5th Percentile
97.5th Percentile	0.156 (5.51)	0.398 (14.1)	0.81 (28.6)
Mean	0.142 (5.01)	0.362 (12.8)	0.736 (26)
2.5th Percentile	0.127 (4.48)	0.325 (11.5)	0.662 (23.4)
Pearson Correlation = 1			

$$Q_{BUFDITCO}$$

Deterministic Model Time Series

2.5th Percentile	Mean	97.5th Percentile
0 (0)	0.993 (35.1)	2.14 (75.6)

Stochastic Model Summary Statistics Time Series

Time Series	2.5th Percentile	Mean	97.5th Percentile
97.5th Percentile	0 (0)	1.1 (38.8)	2.36 (83.3)
Mean	0 (0)	0.996 (35.2)	2.14 (75.6)
2.5th Percentile	0 (0)	0.896 (31.6)	1.92 (67.8)
Pearson Correlation = 0.9923			

Table 4.15 (Cont). DSR deterministic and stochastic model time-series average daily flow rate numeric results.

$$Q_{WILDHOCO}$$

Deterministic Model Time Series

2.5th Percentile	Mean	97.5th Percentile
0 (0)	0.198 (6.99)	1.39 (49.1)

Stochastic Model Summary Statistics Time Series

Time Series	2.5th Percentile	Mean	97.5th Percentile
97.5th Percentile	0 (0)	0.213 (7.52)	1.49 (52.6)
Mean	0 (0)	0.198 (6.99)	1.39 (49.1)
2.5th Percentile	0 (0)	0.183 (6.46)	1.28 (45.2)
Pearson Correlation = 1			

$$Q_{FRODITKS}$$

Deterministic Model Time Series

2.5th Percentile	Mean	97.5th Percentile
0 (0)	0.319 (11.3)	0.991 (35)

Stochastic Model Summary Statistics Time Series

Time Series	2.5th Percentile	Mean	97.5th Percentile
97.5th Percentile	0 (0)	0.351 (12.4)	1.09 (38.5)
Mean	0 (0)	0.319 (11.3)	0.991 (35)
2.5th Percentile	0 (0)	0.287 (10.1)	0.891 (31.5)
Pearson Correlation = 1			

Average daily flow rates are not grouped and calculated by river segment. Figures 4.16 and 4.17 and Tables 4.16 and 4.17 present the results of the flow portion of the water balance model calculated as shown in Equations 24 and 25 for the USR and DSR, respectively. Figures 4.16 and 4.17 show the sum of the deterministic model flow rates in the left figure. The right figure shows the sum of the stochastic model flow rates. As with the other stochastic model figures, the black line depicts the stochastic model mean time-series and the blue region depicts the range of values between the stochastic model 97.5th percentile time-series and the stochastic model 2.5th percentile time-series. Values outside of this range are not included in the figures. The figures and associated tables are presented in units of $m^3 s^{-1} km^{-1}$ ($cfs mi^{-1}$). Standardizing the results to present values in units of storage per unit length allows for comparisons to be made between the two study reaches and between water balance model components. Positive values indicate that the respective reach gains water due to gauged surface water flows.

$$\sum Q_{Surface,USR}$$

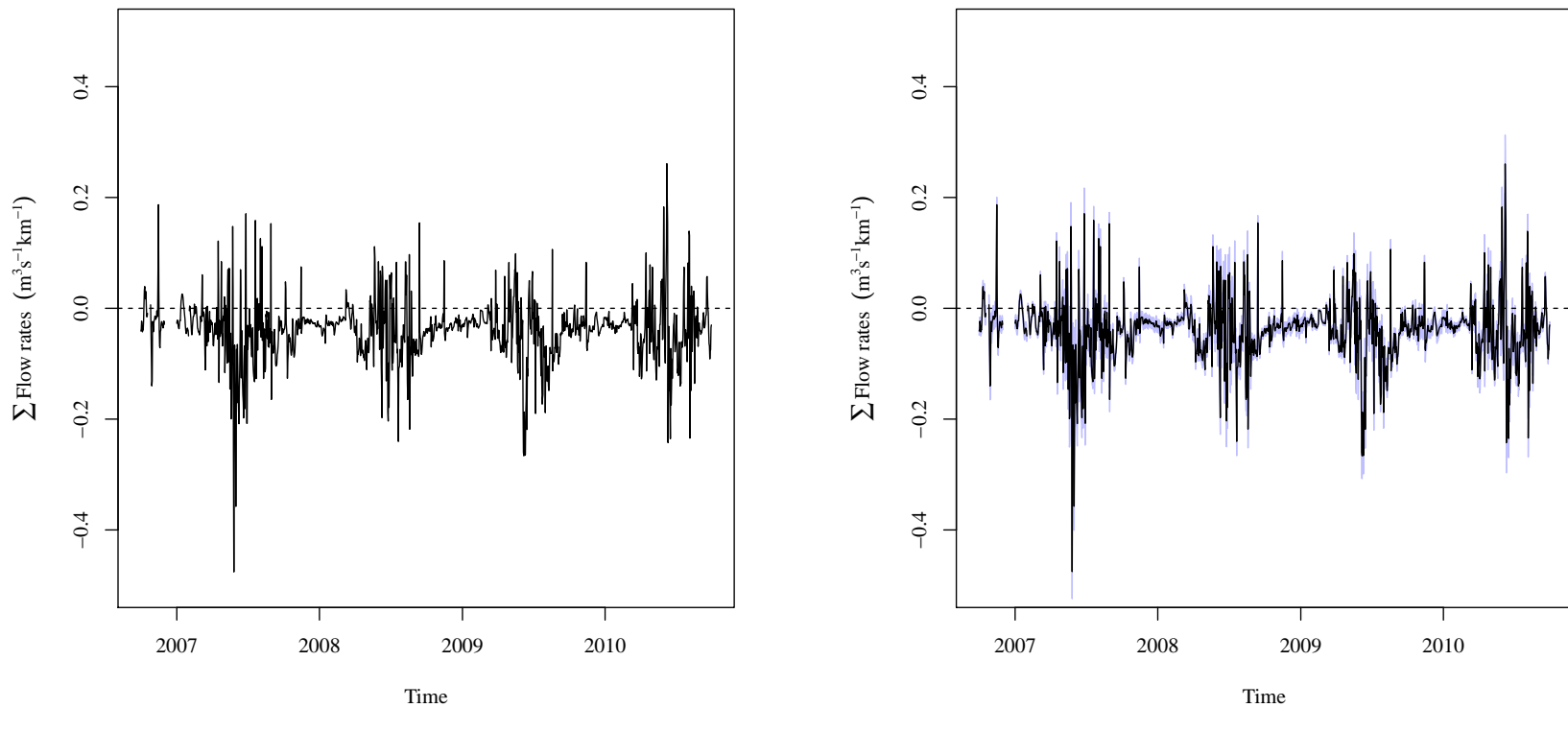


Figure 4.16. USR deterministic and stochastic model time-series reach flow rates. In the stochastic model time-series, the black lines indicate the stochastic model mean time-series. The blue band indicates the 95% central inter-percentile range (CIR) of the stochastic values.

$$\sum Q_{Surface, DSR}$$

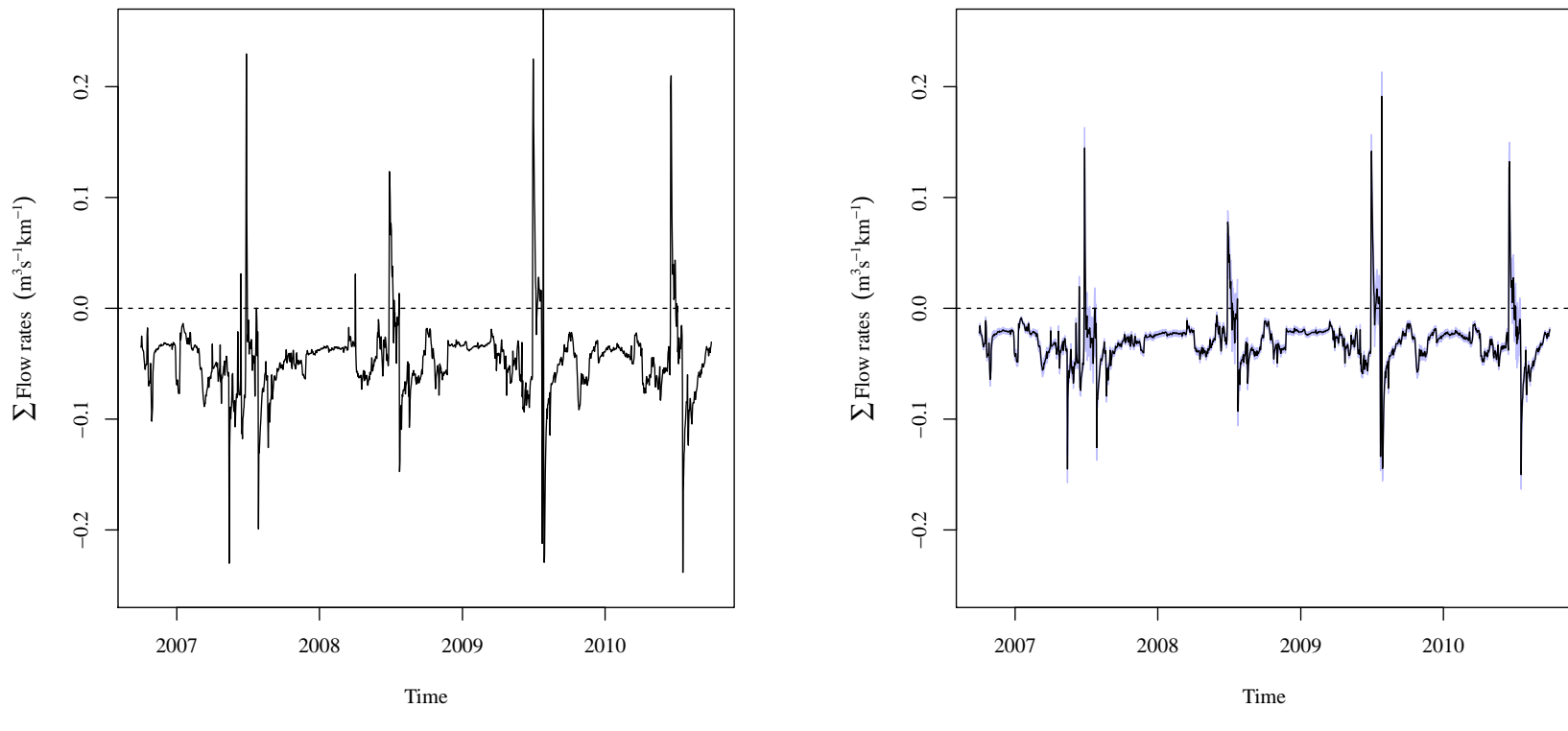


Figure 4.17. DSR deterministic and stochastic model time-series reach flow rates. In the stochastic model time-series, the black lines indicate the stochastic model mean time-series. The blue band indicates the 95% central inter-percentile range (CIR) of the stochastic values.

Table 4.16. USR deterministic and stochastic model reach total time-series average daily flow rate numeric results. Flow rates are presented in units of $\text{m}^3 \text{s}^{-1} \text{km}^{-1}$ (cfs mi^{-1}).

$$\sum Q_{\text{Surface}, \text{USR}}$$

Deterministic Model Time Series			
	2.5th Percentile	Mean	97.5th Percentile
	-0.174 (-9.89)	-0.0395 (-2.24)	0.0751 (4.27)
Stochastic Model Summary Statistics Time Series			
Time Series	2.5th Percentile	Mean	97.5th Percentile
97.5th Percentile	-0.141 (-8.01)	-0.0238 (-1.35)	0.103 (5.85)
Mean	-0.174 (-9.89)	-0.0395 (-2.24)	0.0751 (4.27)
2.5th Percentile	-0.211 (-12)	-0.0553 (-3.14)	0.0509 (2.89)
Pearson Correlation = 1			

Table 4.17. DSR deterministic and stochastic model reach total time-series average daily flow rate numeric results. Flow rates are presented in units of $\text{m}^3 \text{s}^{-1} \text{km}^{-1}$ (cfs mi^{-1}).

$$\sum Q_{\text{Surface}, \text{DSR}}$$

Deterministic Model Time Series			
	2.5th Percentile	Mean	97.5th Percentile
	-0.105 (-5.97)	-0.0469 (-2.67)	0.0182 (1.03)
Stochastic Model Summary Statistics Time Series			
Time Series	2.5th Percentile	Mean	97.5th Percentile
97.5th Percentile	-0.0979 (-5.56)	-0.0402 (-2.28)	0.0475 (2.7)
Mean	-0.105 (-5.97)	-0.0469 (-2.67)	0.0176 (1)
2.5th Percentile	-0.114 (-6.48)	-0.0536 (-3.05)	-0.013 (-0.739)
Pearson Correlation = 0.9989			

The individual gauged flow rate figures and the reach calculated sum of gauged flow rate figures show that there is a definite seasonal variation in the flow rates. This is as expected since the LARV water supply is highly dependent on irrigation waters provided by reservoir releases. The values in the reach tables show that the stochastic model mean 5 time-series closely follows the deterministic model time-series. The summary statistics of the two models and the Pearson Correlation between the two models are nearly identical. This shows that the gauge flow portion of the deterministic water balance model is a very good representation of the stochastic model.

Each of the time-steps of this portion of the USR stochastic model were analyzed to 10 determine the best fit distribution using K-S analysis. Of the tested possible distribution shapes, all of the time steps had logistic distributions. Visual analysis of the relationship between the date and the best fit distribution did not yield any significance. Similarly, visual analysis of the relationship between the resultant flow rate and the best fit distribution did 15 not yield any significance.

15 The DSR stochastic model underwent the same analysis. Of the tested possible distribution shapes, 98.3% of the time-steps were best fit by logistic distributions. The remaining 1.7% were best fit by normal distributions. Visual analysis of the comparison between the time-step date and the best fit distribution showed that all of the normally distributed time-steps are at the beginning of the study time frame. Visual analysis of the 20 comparison between the region volume change and the best fit distribution revealed that the few time-steps that were normally distributed, were characterized as low magnitude storage loss time-steps.

The reach flow summary time-series figures (4.14 and 4.14) show that there is a definite seasonal variation in the flow component. The surface water flow balance changes from being

a losing system to a gaining system during the irrigation season. This pattern is caused by irrigation practices in the Lower Arkansas River Basin (LARV). Excess irrigation water applied to fields runs off into tributaries which feed into the Arkansas River

The figures also show that the river is discharging more water than it receives. In 5 the USR, this matches the general observed trend where the upstream end of the reaches receives more water than the downstream ends discharges. This does not match the observed trend in the DSR where the flows at the upstream end appear to be less than or equal to the flows at the downstream end. In the DSR, this mismatch between the observed phenomenon and the measured values indicates that another process is a significant contributor to the 10 flow regime. Since the two reaches are in the same environment, it is reasonable to assume that the same phenomenon is present in the USR. It is suspected that groundwater from the riparian aquifer is the unaccounted for source in both the USR and DSR.

The reach flow summary time-series summary statistics tables (4.14 and 4.15) show that the deterministic model is very similar to the stochastic model mean time-series. The 15 similarity between the table values and the high Pearson Correlation lead to the determination that the deterministic model is representative of the stochastic model expected value.

4.6. ATMOSPHERIC CONTRIBUTIONS TO THE WATER BALANCE MODELS

Atmospheric effects on the river within the USR and DSR is limited to evaporation and precipitation as shown in Equation 27.

$$\sum Q_{Atm} = P - E \quad (27)$$

$$= P \cdot \sum A_i - E \cdot \sum A_i \quad (28)$$

Where:

$\sum Q_{Atm} =$ Total effects of precipitation and evaporation on the flow balance model,
expressed as a the change in volume per time-step.

$P =$ Reported total daily precipitation.

$E =$ Calculated total daily evaporation.

$\sum A_i =$ Sum of the river reach segment surface areas as previously calculated.

This equation is the form used earlier in this thesis. While it is the traditional form,

it assumes that P and E are expressed as flow. This is not the usual case. Both P and

5 E are usually expressed in units of depth per time-step. Multiplying these values by the
affected surface area results in a volume change per time-step (Equation ??). This may be
more appropriately labeled as the change in storage due to atmospheric effects per time-step
 $\left(\frac{\Delta S_{Atm}}{\Delta t}\right)$. This is a philosophical argument, and the decision was made to refer to the
atmospheric effects as shown in Equation ??.

10 Evaporation from natural water bodies is not directly measured. At best, evaporation
pans when used appropriately, are used to estimate evaporation from nearby natural bodies.

Yet, even these require the use of a calibrated coefficient before the data is relatively reliable.
For this thesis, evaporation data was gathered and treated as discussed in Section 3.3. This
data was provided as the total daily reference evapo-transpiration (ET_{ref}) as calculated using

15 the ASCE EWRI tall crop reference equation. This equation is identical to the Food and
Agriculture Organization of the United Nations (FAO) Penman-Montieth equation (Richard
G. Allen, Pereira, Raes, et al., 1988; Walter et al., 2000) and is calculated as follows with

variables in appropriate SI units:

$$ET_{ref} = \frac{0.408\Delta(R_n - G) + \gamma \frac{C_n}{T + 273} u_2(e_s - e_a)}{\Delta + \gamma(1 + C_d u_2)} \quad (29)$$

Where:

ET_{ref} = standardized reference crop evapotranspiration for short or tall surfaces.

R_n = calculated net radiation at the crop surface.

G = soil heat flux density at the soil surface.

T = mean daily air temperature at 1.5 to 2.5 meter height.

u_2 = mean daily wind speed at 2 meter height.

e_s = saturation vapor pressure at 1.5 to 2.5 meter height, calculated as the average of saturation vapor pressure at minimum and maximum air temperature.

e_a = mean actual vapor pressure at 1.5 to 2.5 meter height .

Δ = slope of the saturation vapor pressure-temperature curve.

γ = psychrometric constant .

C_n = numerator constant that changes with reference type.

C_d = denominator constant that changes with reference type.

This equation is quite complex and it was determined that independent calculation

would not be of any benefit. This equation also does not provide the necessary value of E , but of ET_{ref} , which is a reference value that describes the total of the evaporation (E) and transpiration (T) from a reference crop under ideal conditions. Converting ET_{ref} into E requires the use of conversion equations found in FAO56. The open water coefficient, K_w , is used to perform this conversion. The FAO has an extensive set of crop coefficients including

coefficients for open water for use on the FAO Penman-Montieth (FAO PM) equation.

$$E = K_w \cdot ET_{ref} \quad (30)$$

Where:

E = Evaporation

K_w = Open water coefficient

ET_{ref} = ASCE EWRI Standardized Reference Evapotranspiration Equation, tall crop equation.

The FAO developed the K_w values for the short reference crop ET_{ref} equation. Use

5 of crop coefficients developed for the short crop reference equation with the tall crop (alfalfa) reference equation is prohibited (Richard G. Allen, Pereira, Terry A. Howell, et al., 2011; Richard G. Allen, Pereira, Raes, et al., 1988). Equation 31 is used to convert crop coefficients for use between the two ET reference equation results (Richard G. Allen, Pereira, Raes, et al., 1988).

$$K_w = K_{ratio} \cdot K_{wt} \quad (31)$$

Where:

K_{ratio} = conversion factor, calculated using equation 32

10

K_{ws} = short crop based crop coefficient,

K_{wt} = tall crop based crop coefficient.

$$K_{ratio} = K_{ws} + [0.04(u_2 - 2) - 0.004(RH_{min} - 45)] \left(\frac{h}{3}\right)^{0.3} \quad (32)$$

Where:

$h = 0.5$ meters as the standard height for the tall crop reference.

There is no reported error associated with the use of equations 31 or 32. However, there are known uncertainties in the reported minimum daily relative humidity and average daily wind speed. Both relative humidity and wind speed uncertainties are based on equipment uncertainty and do not include any other sources of uncertainty. Precipitation, minimum daily relative humidity, and wind speed data error provided through the CoAgMet system was based solely on instrument accuracy and was reported as $\pm 1\%$ for precipitation, $\pm 2\%$ for minimum daily relative humidity, and $\pm 0.5 \text{ m s}^{-1}$ for wind speed. These values are based on the typical instruments installed at the various locations. Sensors vary somewhat between observation sites due to equipment replacement. Colorado Climate Network personnel have stated that replacement equipment either meets or exceeds the equipment on a typical observation site. The uncertainty distributions for these three weather measurements was assumed to be normal with 95% of the values within the reported range of the true value.

A preliminary analysis of this method resulted in K_{ratio} values shows a mean value of 1.097 and a standard deviation of 0.049. The K_{ratio} values are best fit by a logistic distribution with a location parameter of 1.099 and a scale parameter of 0.0266. Using the FAO K_{ws} value of 1.05 results in an average K_{wt} value of 0.95 using equation 31. Jensen suggests using $K_{ws} = 1.10$ based on data from Alamosa, Colorado, which results in an average K_{wt} value of 1.00.

This seems to suggest that unlike the short crop ET_{ref} equation, the tall crop ET_{ref} over estimates evaporation from a shallow water body. This seems plausible as surface area

is a significant factor in determining evaporation. A mature, 0.5 meter tall alfalfa crop has a large leaf area which could plausibly exceed the equivalent surface area of open water.

Atmospheric data obtained from CoAgMet does not have publicly defined uncertainty distributions. At the time this thesis, a study headed by Dr. José L. Chávez at Colorado State University was underway to evaluate the ASCE EWRI standardized alfalfa ET reference Penman-Montieth equation with relation to lysimetric data in Colorado. Preliminary findings provided by Dr. Chávez indicate an average daily reference ET mean bias error of -0.47 mm d^{-1} with a variability of $\pm 0.98 \text{ mm d}^{-1}$ when compared to lysimetric data. The bias error indicates that the reported ET_{ref} underestimates the actual ET. The measurement variability is reported as the root mean square error (RMSE), or standard deviation, of the measurement.

Figures 4.18 and 4.19 show the deterministic and stochastic model time-series of evaporation in mm for the USR and DSR respectively. Tables 4.18 and 4.19 present the associated summary statistics for the deterministic time-series and the summary statistics for the three calculated stochastic model time-series.

$$\overline{E}_{USR}$$

691

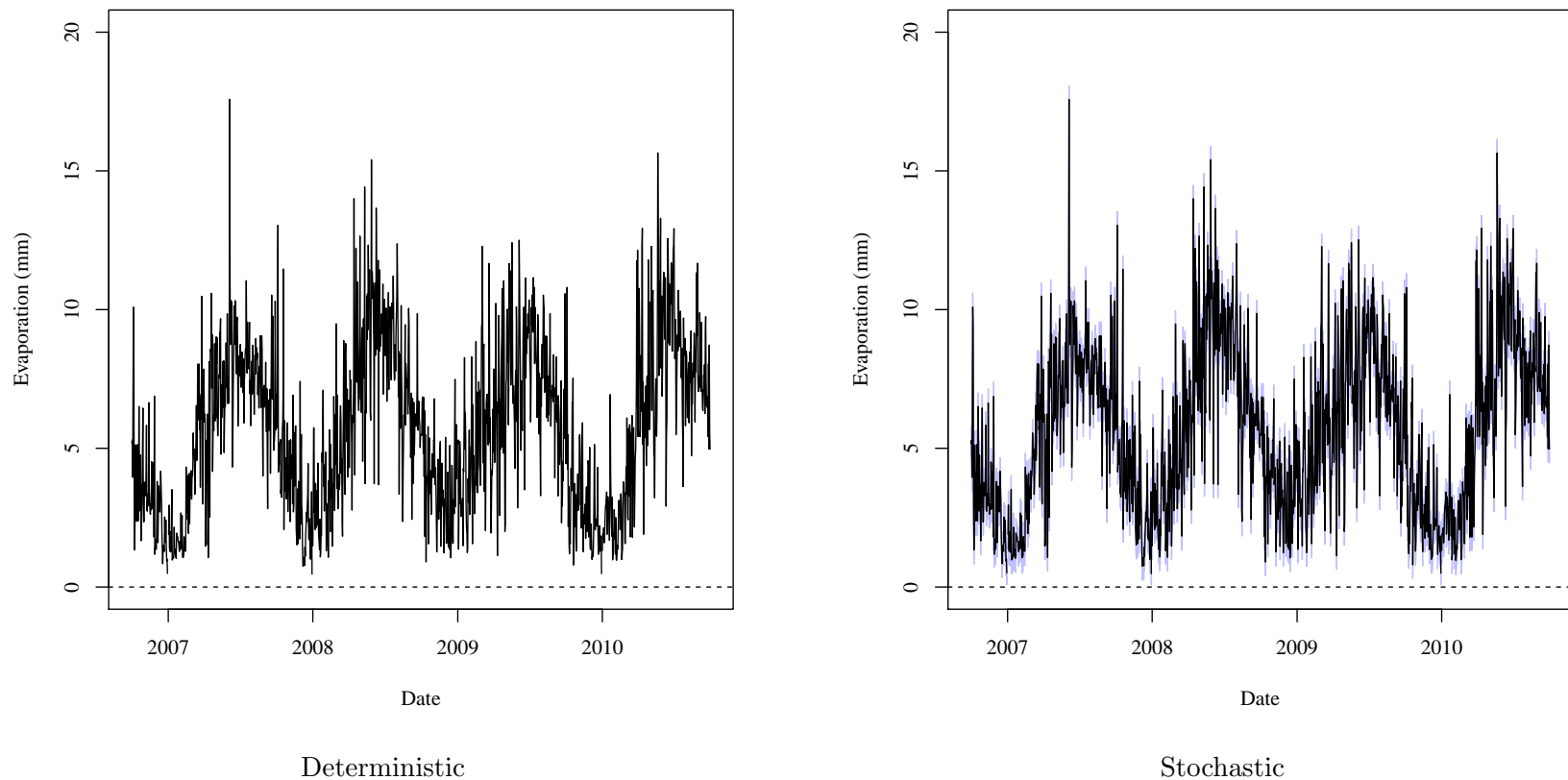


Figure 4.18. USR deterministic and stochastic model time-series total estimated evaporation. In the stochastic model time-series, the black lines indicate the stochastic model mean time-series. The blue band indicates the 95% central inter-percentile range (CIR) of the stochastic values.

0L1

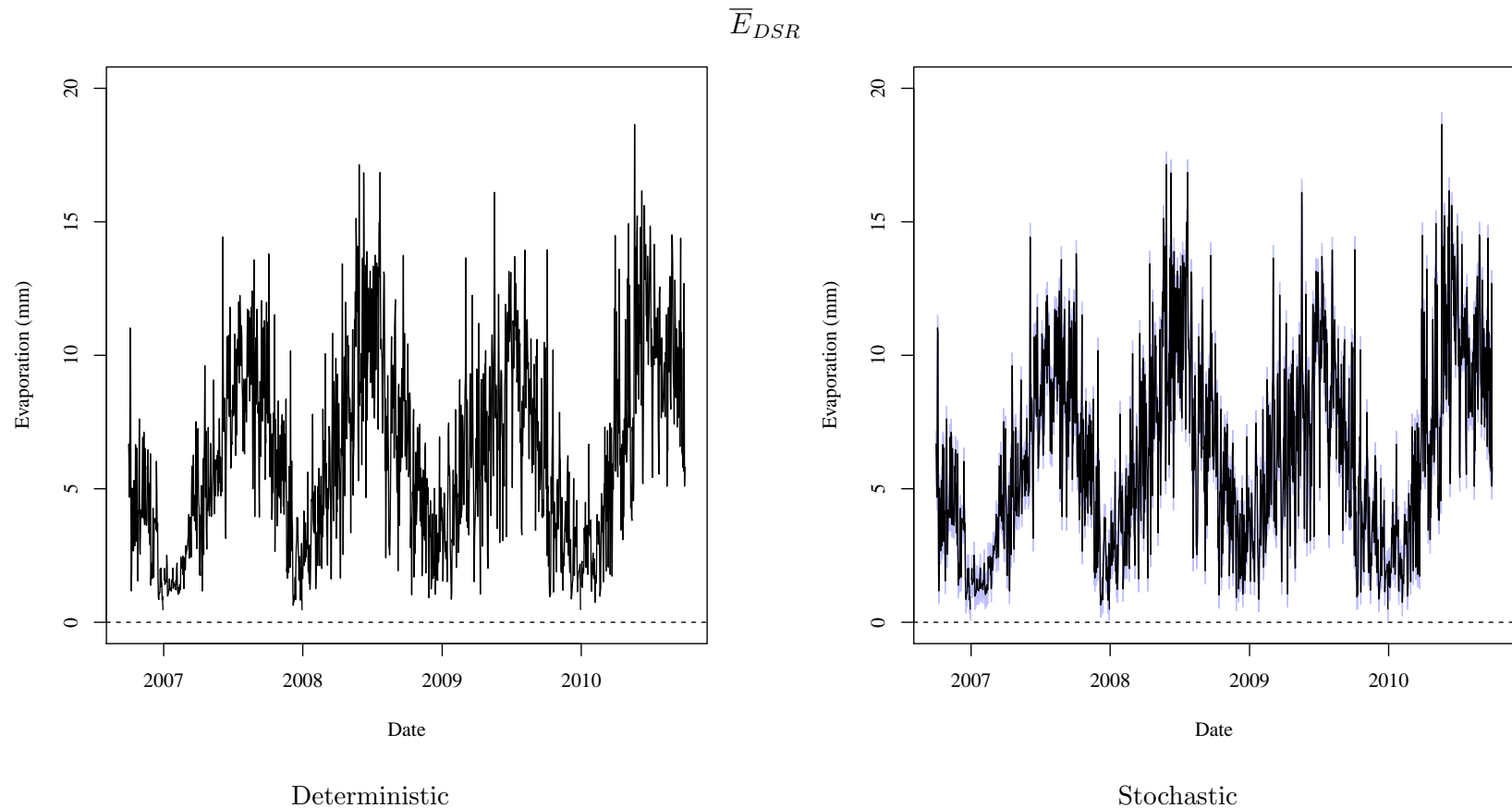


Figure 4.19. DSR deterministic and stochastic model time-series total estimated evaporation. In the stochastic model time-series, the black lines indicate the stochastic model mean time-series. The blue band indicates the 95% central inter-percentile range (CIR) of the stochastic values.

Table 4.18. USR deterministic and stochastic model time-series total estimated evaporation numeric results. Total daily evaporation rates are presented in units of mm (in).

$$\bar{E}_{USR}$$

Deterministic Model Time Series

2.5th Percentile	Mean	97.5th Percentile
1.16 (0.0457)	5.7 (0.224)	11.4 (0.449)

Stochastic Model Summary Statistics Time Series

Time Series	2.5th Percentile	Mean	97.5th Percentile
97.5th Percentile	1.68 (0.0661)	6.2 (0.244)	11.9 (0.469)
Mean	1.17 (0.0461)	5.7 (0.224)	11.4 (0.449)
2.5th Percentile	0.653 (0.0257)	5.21 (0.205)	10.9 (0.429)
Pearson Correlation = 1			

Table 4.19. DSR deterministic and stochastic model time-series total estimated evaporation numeric results. Total daily evaporation rates are presented in units of mm (in).

$$\bar{E}_{DSR}$$

Deterministic Model Time Series

2.5th Percentile	Mean	97.5th Percentile
1.13 (0.0445)	6.26 (0.246)	13.6 (0.535)

Stochastic Model Summary Statistics Time Series

Time Series	2.5th Percentile	Mean	97.5th Percentile
97.5th Percentile	1.63 (0.0642)	6.74 (0.265)	14.1 (0.555)
Mean	1.13 (0.0445)	6.26 (0.246)	13.6 (0.535)
2.5th Percentile	0.626 (0.0246)	5.77 (0.227)	13.2 (0.52)
Pearson Correlation = 1			

Precipitation in the study regions is not well defined. An assumption was made that precipitation was not uniformly distributed over either study region. Reports from field technicians, conversation with local residents, and personal experience indicate that most storms during the summer were isolated and relatively small. It was not known by the end 5 of this study whether weather radar data was available or could be used to more accurately estimate rainfall onto the Arkansas River water surface. It was assumed that, at best, 50% of any rain event would add water directly to the river. The reported precipitation depth value was modified by a factor of 0.5 to reflect the estimated average storm coverage for the region. The atmospheric contribution to the models is taken as the sum of the modified 10 precipitation and evaporation values with the assumption that all precipitation values are positive and all evaporation values are negative as shown in equation 33.

$$\sum Q_{Atm} = 0.5 \cdot \bar{P} \cdot \sum A_i - K_{wt} \cdot \overline{ET_{Ref}} \cdot \sum A_i \quad (33)$$

Where

Q_{Atm} = Total water volume gained (+) or lost (-) due to atmospheric contributions for a study region river section. Values calculated and presented as average daily flow rates.

\bar{P} = Regional average precipitation taken as the mean of the reporting regional rain gauges.

K_{wt} = Open water coefficient for the tall ET_{Ref} equation.

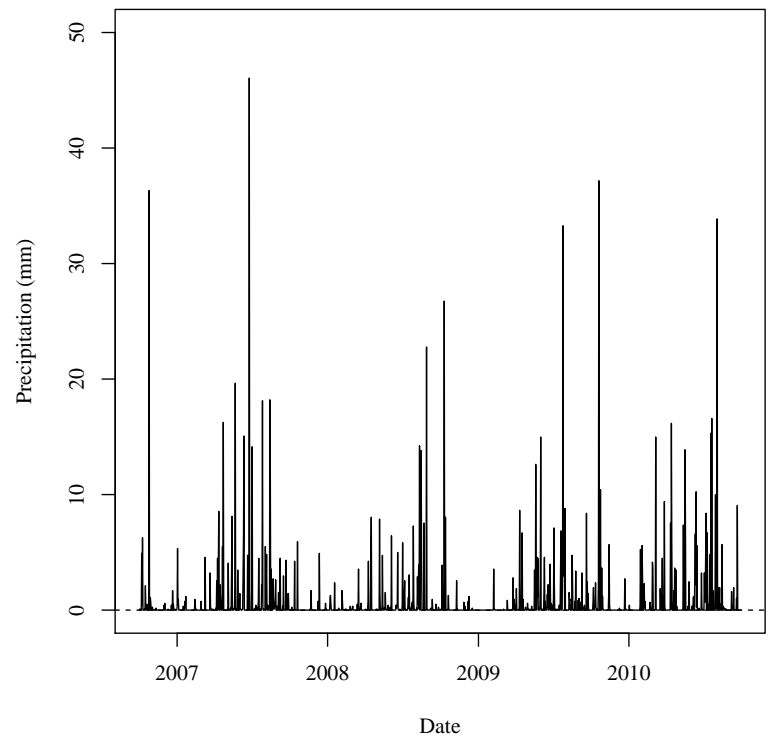
$\overline{ET_{ref}}$ = Regional average ET_{Ref} taken as the mean of the reporting regional reference ET gauges.

$\sum A_i$ = Sum of calculated reach surface areas within a study region river section.

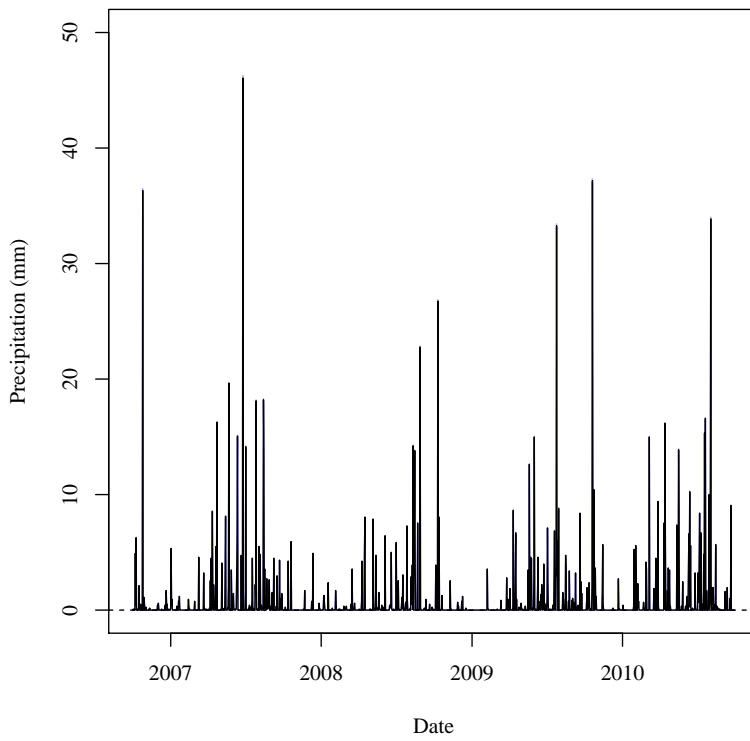
Figures 4.20 and 4.21 show the deterministic and stochastic model time-series of precipitation depth in mm for the USR and DSR respectively. Tables 4.20 and 4.21 present the associated summary statistics for the deterministic time-series and the summary statistics for the three calculated stochastic model time-series.

$$\overline{P}_{USR}$$

171



Deterministic



Stochastic

Figure 4.20. USR deterministic and stochastic model time-series total estimated precipitation. In the stochastic model time-series, the black lines indicate the stochastic model mean time-series. The blue band indicates the 95% central inter-percentile range (CIR) of the stochastic values.

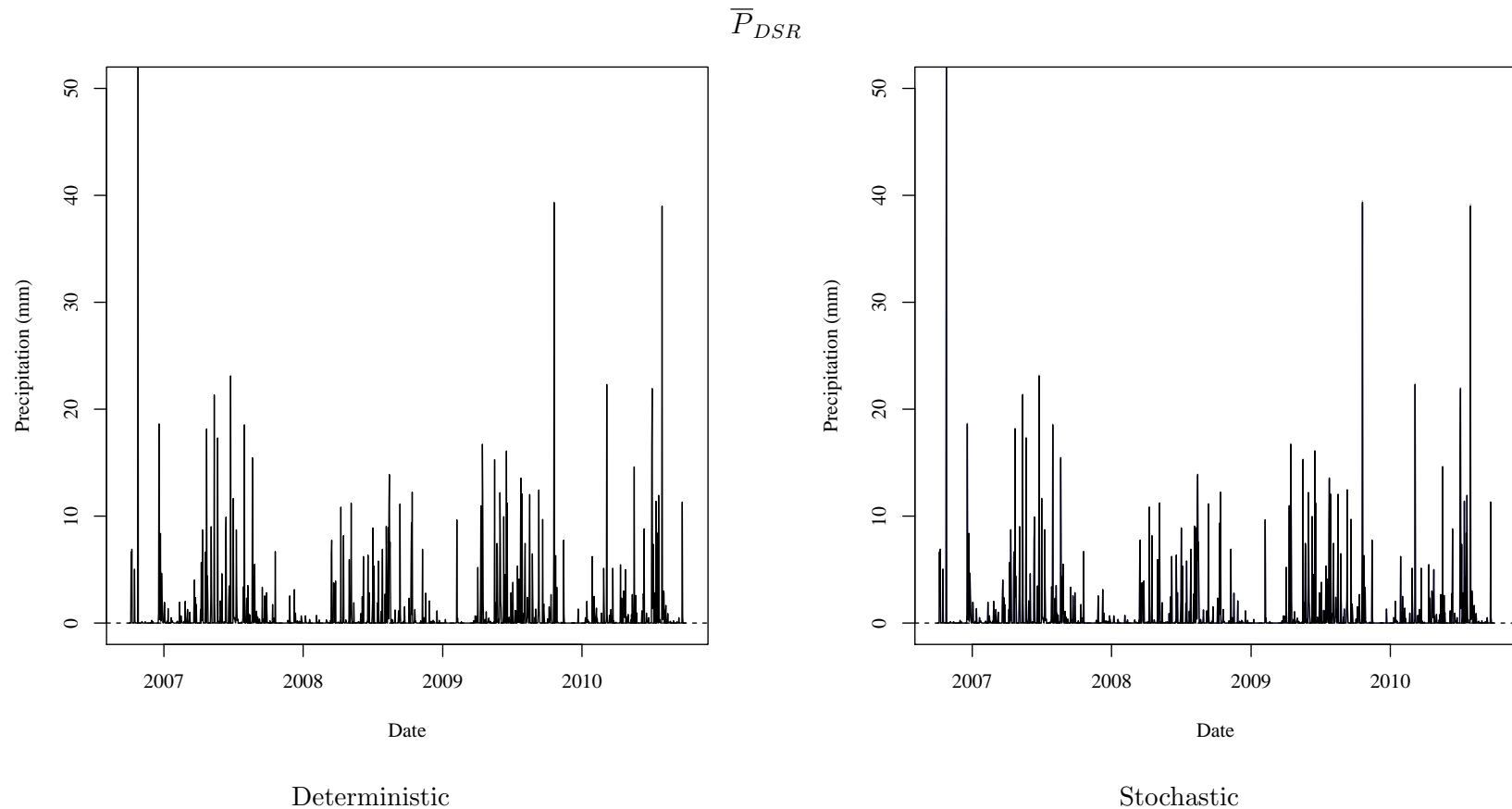


Figure 4.21. DSR deterministic and stochastic model time-series total estimated precipitation. In the stochastic model time-series, the black lines indicate the stochastic model mean time-series. The blue band indicates the 95% central inter-percentile range (CIR) of the stochastic values.

Table 4.20. USR deterministic and stochastic model time-series total estimated precipitation numeric results. Total daily precipitation rates are presented in units of mm (in).

$$\bar{P}_{USR}$$

Deterministic Model Time Series

2.5th Percentile	Mean	97.5th Percentile
0 (0)	0.832 (0.0328)	7.96 (0.313)

Stochastic Model Summary Statistics Time Series

Time Series	2.5th Percentile	Mean	97.5th Percentile
97.5th Percentile	0 (0)	0.836 (0.0329)	8 (0.315)
Mean	0 (0)	0.832 (0.0328)	7.96 (0.313)
2.5th Percentile	0 (0)	0.828 (0.0326)	7.92 (0.312)
Pearson Correlation = 1			

Table 4.21. DSR deterministic and stochastic model time-series total estimated precipitation numeric results. Total daily precipitation rates are presented in units of mm (in).

$$\bar{P}_{DSR}$$

Deterministic Model Time Series

2.5th Percentile	Mean	97.5th Percentile
0 (0)	0.944 (0.0372)	9.81 (0.386)

Stochastic Model Summary Statistics Time Series

Time Series	2.5th Percentile	Mean	97.5th Percentile
97.5th Percentile	0 (0)	0.949 (0.0374)	9.85 (0.388)
Mean	0 (0)	0.944 (0.0372)	9.81 (0.386)
2.5th Percentile	0 (0)	0.939 (0.037)	9.76 (0.384)
Pearson Correlation = 1			

The blue band in both P figures, which depicts the 95th CIR, is very small and is nearly indistinguishable from the stochastic mean time-series values. This indicates that the P measurement uncertainty is very small. A cyclical pattern is easily noted when observing the E and P values in both the USR and DSR. We note that both daily total E and P
5 are higher during warmer months and lower during cold months. The cyclical nature of the daily E agrees with common knowledge where evaporation rates are higher as average temperatures rise. The cyclical nature of the daily precipitation agrees with climate analyses by the National Weather Service which state that most of the precipitation in the LARV occurs with thunder storms during the warmer months.

10 It is interesting to note that during the 4 year time span calculated in this study annual average evaporation rates appear to increase and annual average precipitation rates appear to decrease. The time frame of this study is too short to conclude anything about the long term climate of the region. This observation may be useful when observing other results produced in this study.

15 The difference between the deterministic model time-series and the stochastic model mean time-series summary statistics as noted in the tables is very low for the E and P values in both the USR and DSR. This, and the very high Pearson Correlation values, indicate that the deterministic model accurately represents the expected value of the stochastic model.

20 The value $\sum A_i$, as used in equation 33, is the reach average daily surface area as previously calculated for the deterministic and stochastic models. These surface area values are calculated based on the calculated river top width values used to calculate the river volume change. No changes were made to the previous river geometry calculations before being used to estimate total precipitation gains to and evaporative losses from the river.

Total reach atmospheric contribution gains and losses in units of $\text{m}^3 \text{s}^{-1} \text{km}^{-1}$ are presented in Figures 4.22 and 4.23 for the USR and DSR, respectively. These figures show the volume of water gained or lost for each day scaled by the length of the respective reach for comparative purposes. For the USR and DSR, respectively, tables 4.22 and 4.23 present

5 the deterministic model time-series summary statistics and the summary statistics for the stochastic model mean time-series, the stochastic model 97.5th percentile time-series, and the stochastic model 2.5th percentile time-series.

$$\sum Q_{Atm,USR}$$

621

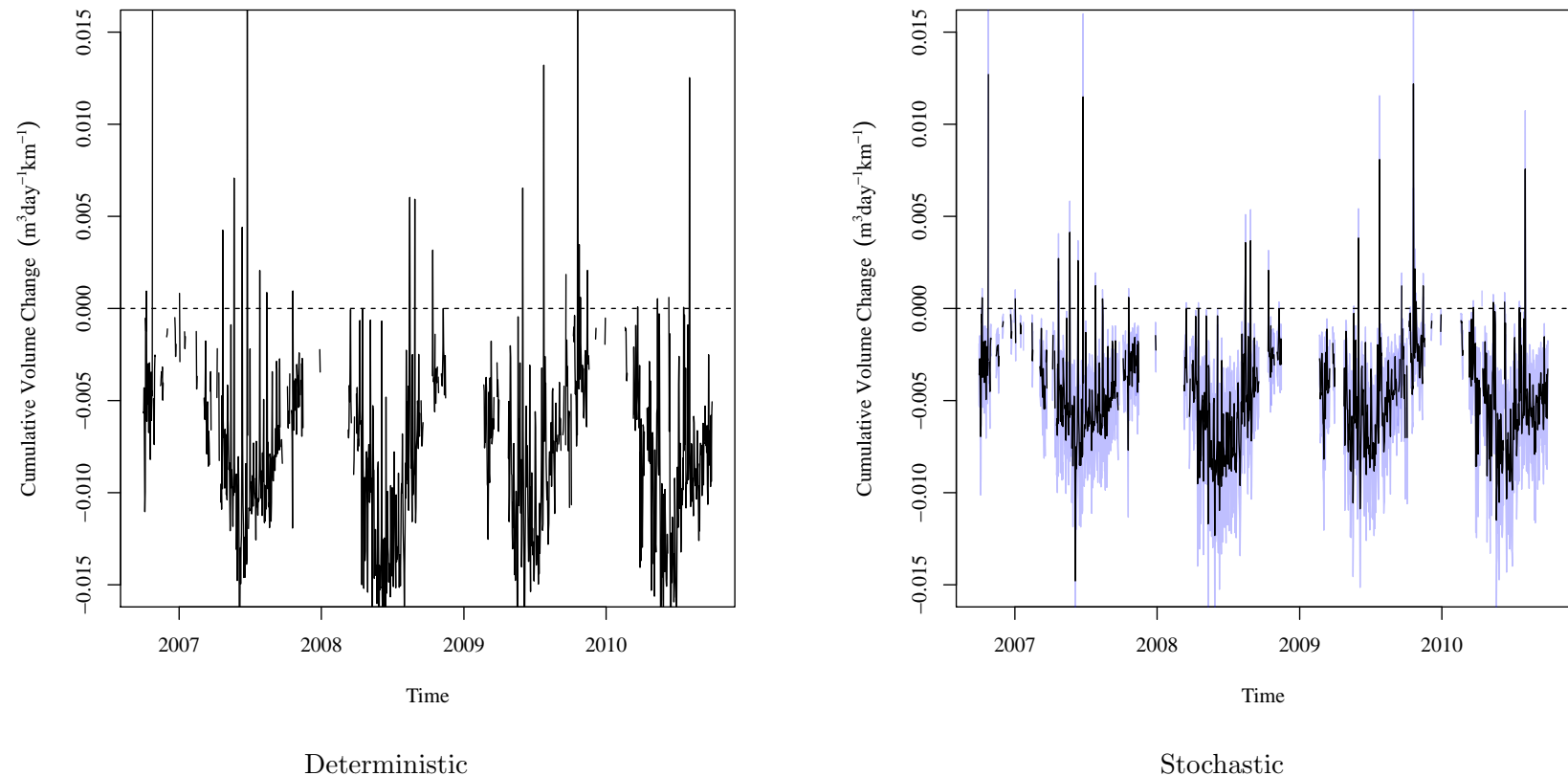


Figure 4.22. USR deterministic and stochastic model time-series total estimated atmospheric contribution to the water balance model. The blue band indicates the 95% central inter-percentile range (CIR) of the stochastic values.

$$\sum Q_{Atm, DSR}$$

081

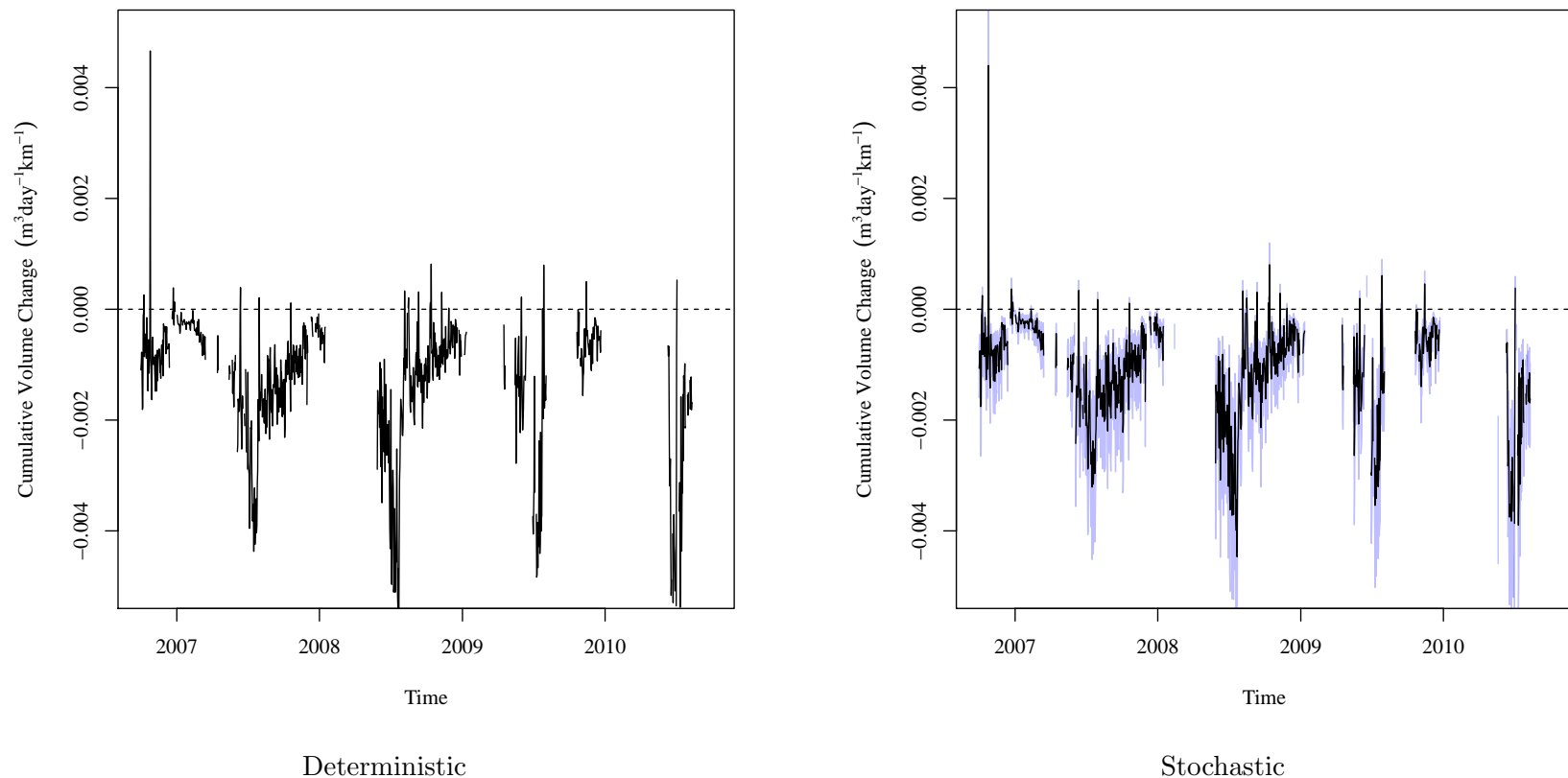


Figure 4.23. DSR deterministic and stochastic model time-series total estimated atmospheric contribution to the water balance model. In the stochastic model time-series, the black lines indicate the stochastic model mean time-series. The blue band indicates the 95% central inter-percentile range (CIR) of the stochastic values.

Table 4.22. USR deterministic and stochastic model time-series total estimated atmospheric contribution to the water balance model numeric results. Total daily contribution is presented in units of $\text{m}^3 \text{s}^{-1} \text{km}^{-1}$ (cfs mi^{-1}).

$$\sum Q_{Atm,USR}$$

Deterministic Model Time Series			
	2.5th Percentile	Mean	97.5th Percentile
	-0.0156 (-1.09)	-0.00777 (-0.544)	0.000635 (0.0445)

Stochastic Model Summary Statistics Time Series			
Time Series	2.5th Percentile	Mean	97.5th Percentile
97.5th Percentile	-0.00523 (-0.366)	-0.00254 (-0.178)	0.000881 (0.0617)
Mean	-0.00936 (-0.656)	-0.00473 (-0.331)	0.000398 (0.0279)
2.5th Percentile	-0.0131 (-0.918)	-0.00687 (-0.481)	3.19e-05 (0.00223)
Pearson Correlation =	0.9978		

The blue bands in Figures 4.22 and 4.23, which depict the 95th CIR, appear much wider than those shown in the respective P and E figures. This is entirely due to scaling as the volume of water in this calculation is small. The differences between the mean of the deterministic model time-series and the mean of the stochastic model mean time-series is 5 larger than the differences noted in the P and E tables. This is due to the uncertainty in calculating the average daily river reach surface area. While the percent differences between the summary statistics of the deterministic model time-series and the summary statistics of the stochastic model mean time-series are fairly large, that is due to the low magnitude of the values. The difference between the two sets of values, when expressed as flow rates, is 10 quite small. While the percent difference in the USR between the mean of the two time-series

Table 4.23. DSR deterministic and stochastic model time-series total estimated atmospheric contribution to the water balance model numeric results. Total daily contribution is presented in units of $\text{m}^3 \text{s}^{-1} \text{km}^{-1}$ (cfs mi^{-1}).

$$\sum Q_{Atm,DSR}$$

Deterministic Model Time Series			
	2.5th Percentile	Mean	97.5th Percentile
	-4.5e-06 (-0.000315)	-1.31e-06 (-9.18e-05)	1.8e-08 (1.26e-06)

Stochastic Model Summary Statistics Time Series			
Time Series	2.5th Percentile	Mean	97.5th Percentile
97.5th Percentile	-0.0032 (-0.224)	-0.00105 (-0.0735)	0.000176 (0.0123)
Mean	-0.0052 (-0.364)	-0.00177 (-0.124)	2.5e-05 (0.00175)
2.5th Percentile	-0.00737 (-0.516)	-0.00262 (-0.184)	-0.000111 (-0.00778)
Pearson Correlation =	0.9873		

is approximately 40%, the magnitude of the difference is approximately 3 L s^{-1} over a km of river length. This is a very small value and is not significant to the total model.

The figures show that there is a definite seasonal variation in the atmospheric component balance. This temporal relationship follows the same pattern identified with the evapo-

5 ration and precipitation time-series values. Losses are higher during the warmer months and lower during the colder months. It should be noted that while the figures for the USR and DSR have the same pattern, the magnitude of the losses is very different. This is due to the differences in river geometry. The USR is wider therefore losing more water to evaporation than in the DSR.

10 There figures appear to show that uncertainty with the atmospheric component is nearly equal to uncertainty with the storage component. This isn't true as the storage component is orders of magnitude larger than the atmospheric component. The low uncertainty

associated with the atmospheric component is due to the efforts by Dr. Chaávez and others to characterize evaporation and precipitation uncertainty.

The distribution of all realizations within each time step was analyzed to determine a distribution type. This analysis was performed to determine if the assumption that the 5 deterministic model results were representative of the stochastic model. Testing was performed by comparing K-S statistics for the best fit normal, log-normal, logistic, exponential, gamma, and Weibull distributions. In the USR and the DSR, 100% of all atmospheric component time steps best fit a normal distribution. This indicates that for both the USR and DSR, the distributions across the realizations are normal.

4.7. RESULTS OF CALCULATED UNACCOUNTED FOR RETURN FLOWS

The unaccounted for, non-point discharges and return flows are calculated from Equation 7. All portions of this equation are described in previous sections. Figures 4.24 and 4.25 show the deterministic and stochastic model time-series for the USR and DSR, respectively. The blue band in the stochastic model time-series depicts the 95th CIR. For the USR and DSR respectively, tables 4.24 and 4.25 present the deterministic model time-series summary statistics and the summary statistics for each of the three calculated stochastic model summary statistics time-series.

$$\sum Q_{UNPS,USR}$$

98I

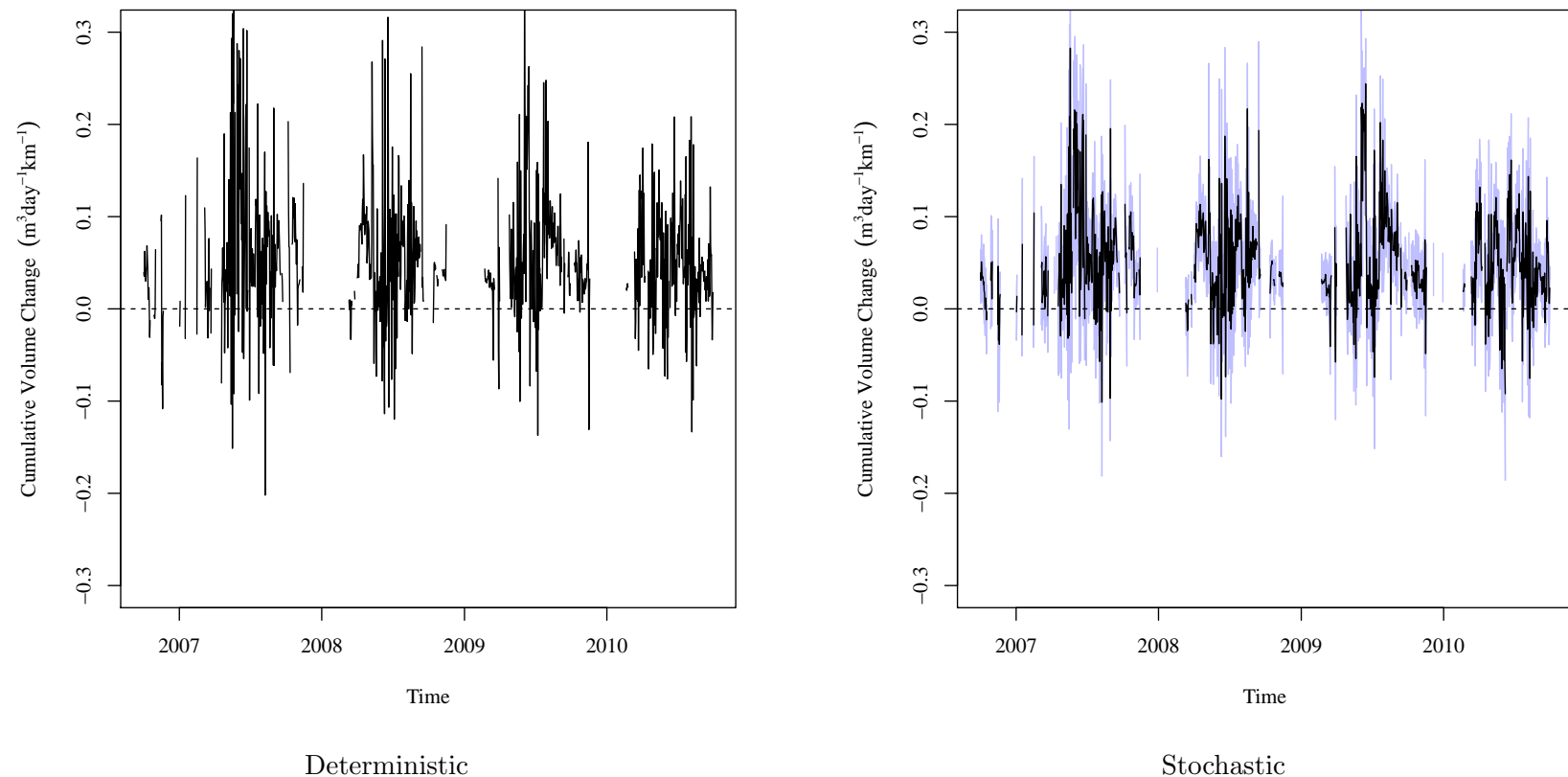


Figure 4.24. USR deterministic and stochastic model time-series total estimated unaccounted for non-point water gains and losses. In the stochastic model time-series, the black lines indicate the stochastic model mean time-series. The blue band indicates the 95% central inter-percentile range (CIR) of the stochastic values.

$$\sum Q_{UNPS, DSR}$$

981

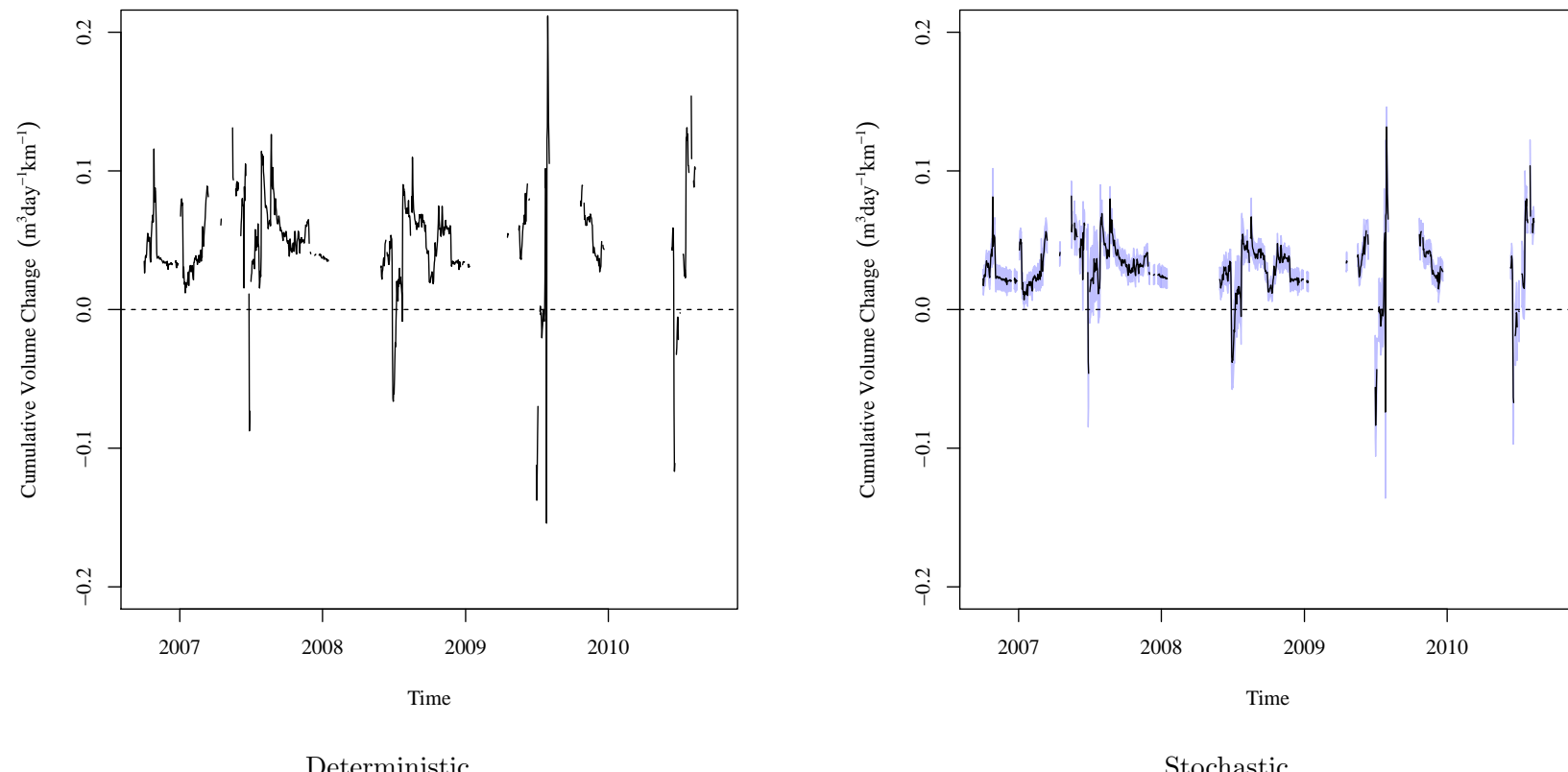


Figure 4.25. DSR deterministic and stochastic model time-series total estimated unaccounted for non-point water gains and losses. In the stochastic model time-series, the black lines indicate the stochastic model mean time-series. The blue band indicates the 95% central inter-percentile range (CIR) of the stochastic values.

Table 4.24. USR deterministic and stochastic model time-series total estimated unaccounted for non-point water gains and losses numeric results. Total daily contribution is presented in units of $\text{m}^3 \text{s}^{-1} \text{km}^{-1}$ (cfs mi^{-1}).

$$\sum Q_{UNPS,USR}$$

Deterministic Model Time Series

2.5th Percentile	Mean	97.5th Percentile
-0.0752 (-5.27)	0.0532 (3.73)	0.222 (15.6)

Stochastic Model Summary Statistics Time Series

Time Series	2.5th Percentile	Mean	97.5th Percentile
97.5th Percentile	0.00958 (0.671)	0.0905 (6.34)	0.257 (18)
Mean	-0.038 (-2.66)	0.0504 (3.53)	0.193 (13.5)
2.5th Percentile	-0.0977 (-6.84)	0.0102 (0.714)	0.119 (8.34)
Pearson Correlation =	0.8626		

The difference and percent difference between the mean of the deterministic model

time-series and the mean of the stochastic model mean time-series are low. The same cannot be said of the differences between the 95th CIR values for the two time-series as they are significantly different. This difference is due to the β_1 and β_2 values picked to represent

- 5 the most likely values for the deterministic model river top width calculations. The total stochastic model, which includes the 95th CIR, does include all of the values in the deterministic model time-series. This indicates that the deterministic model is a possible realization of the stochastic model. The differences between the deterministic model time-series and the stochastic model mean time series indicate that the deterministic model represents the
- 10 stochastic model fairly well for average conditions, over-estimates for high return flow conditions, and underestimates for low return flow or during discharge conditions. This deviation

Table 4.25. DSR deterministic and stochastic model time-series total estimated unaccounted for non-point water gains and losses numeric results. Total daily contribution is presented in units of $\text{m}^3 \text{s}^{-1} \text{km}^{-1}$ (cfs mi^{-1}).

$$\sum Q_{UNPS,DSR}$$

Deterministic Model Time Series			
	2.5th Percentile	Mean	97.5th Percentile
	-0.0426 (-2.98)	0.0461 (3.23)	0.127 (8.9)

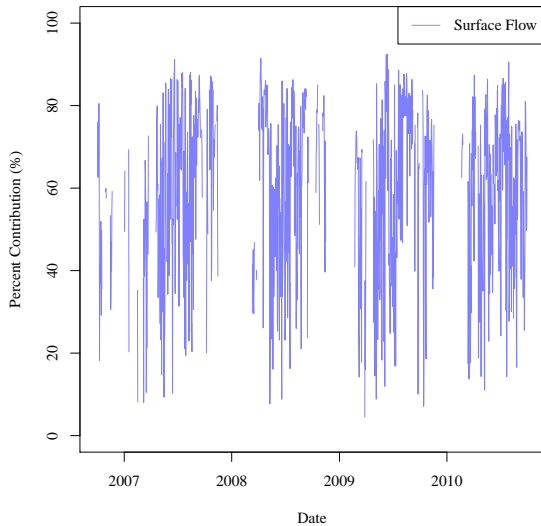
Stochastic Model Summary Statistics Time Series			
Time Series	2.5th Percentile	Mean	97.5th Percentile
97.5th Percentile	0.0129 (0.904)	0.0644 (4.51)	0.125 (8.76)
Mean	-0.0269 (-1.88)	0.0479 (3.36)	0.105 (7.35)
2.5th Percentile	-0.0634 (-4.44)	0.0317 (2.22)	0.0875 (6.13)
Pearson Correlation =	0.9114		

between the deterministic model time series and stochastic model mean time-series is also reflected in the Pearson Correlation values. These values are quite high and should be acceptable for most applications. Further calibration of the deterministic model river geometry values may be justified if they are found to be significant to the model as a whole during

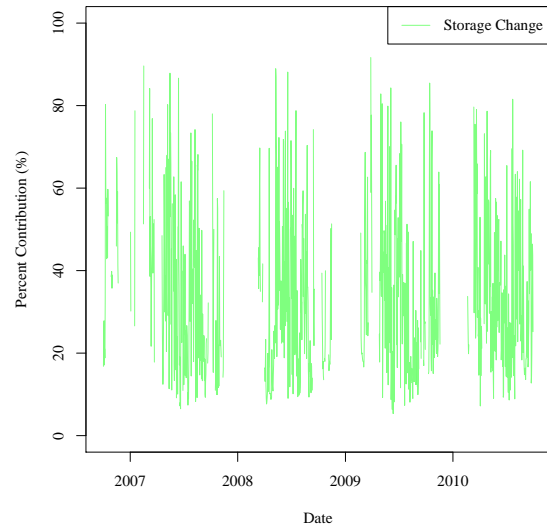
5 sensitivity analysis.

Figures 4.26 and 4.27 present the deterministic model results as fractions of the components of the USR and DSR water balance, respectively. Values are presented as percent of the total. Total values are calculated as the sum of the respective constituent components. The combined sub-figure combines the other sub-figures as a overlapping comparison.

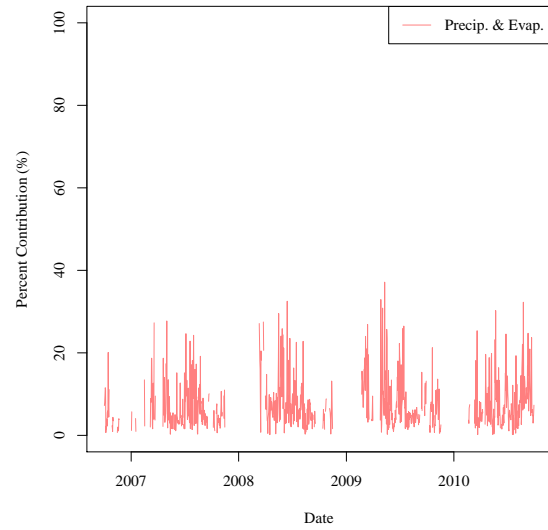
10 These figures show that the surface flow component of the water balance model $(\sum Q_{Surface})$ is the most significant portion in both the USR and DSR. They also show that the storage component $(\frac{\Delta S}{\Delta t})$, is more significant in the USR than the DSR. In both study regions, the atmospheric component, which is composed of the sum of precipitation



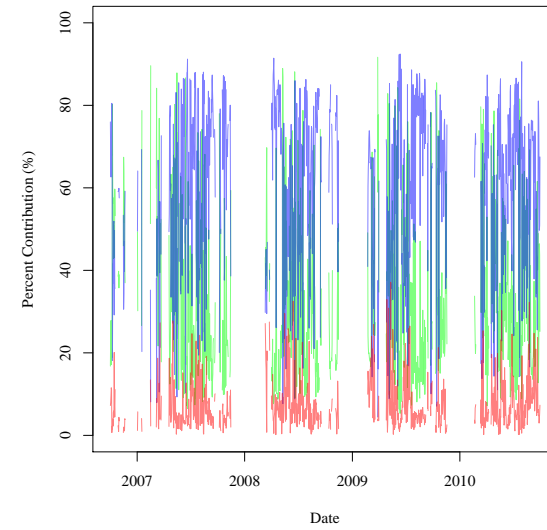
(a) Surface Water Portion.



(b) Storage Change Portion.



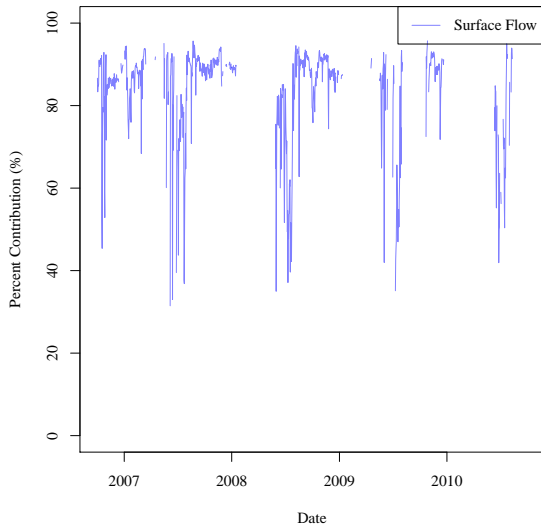
(c) Preip. & Evap. Portion.



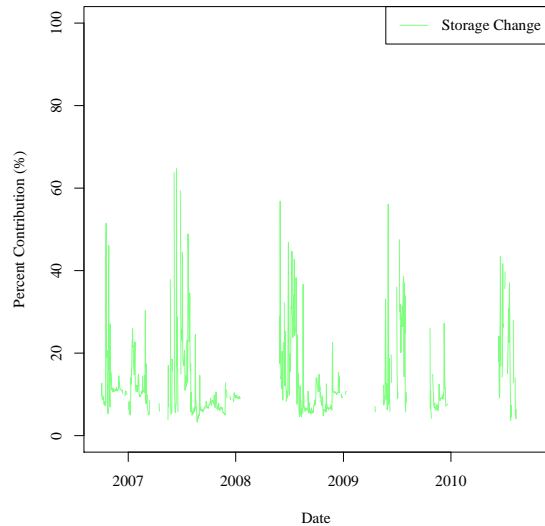
(d) Combined Contributions.

Figure 4.26. Time series of the major USR Arkansas River contributions to the water model.

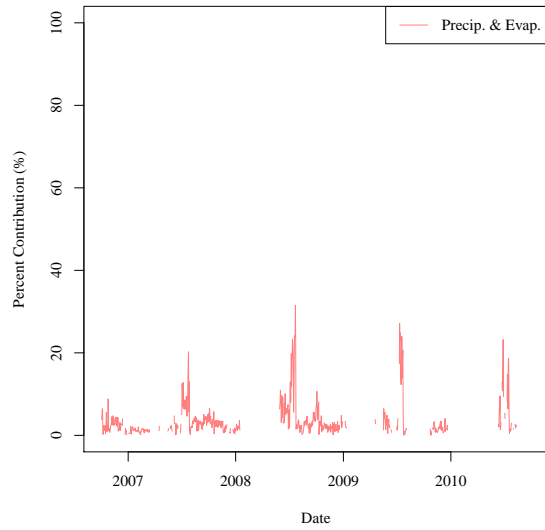
and evaporation ($\sum Q_{Atm}$), although a minor portion of their respective models, cannot be considered insignificant and therefore, cannot be removed from the model without significantly effecting the results. These figures also seem to show an inverse relationship between



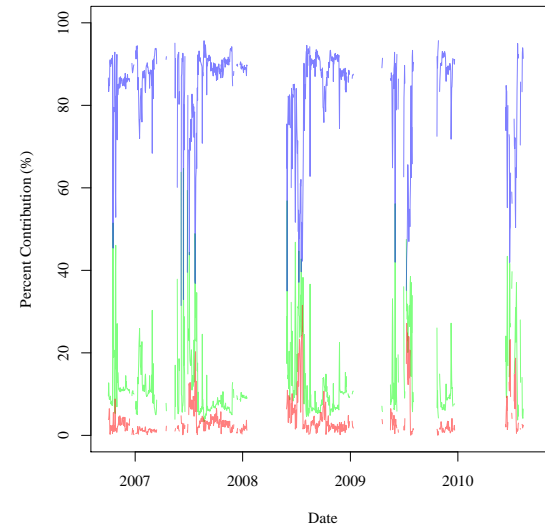
(a) Surface Water Portion.



(b) Storage Change Portion.



(c) Preip. & Evap. Portion.



(d) Combined Contributions.

Figure 4.27. Time series of the major DSR Arkansas River contributions to the water model.

the contribution of the flow portion and the contributions of the storage and atmospheric portions. The mechanism of this relationship is not understood at this time.

Table 4.26. Major Portion Contributions to the USR Models.

Model Portion	2.5%	Mean	97.5%
$\frac{\Delta S}{\Delta t}$	11.2	33.5	55.5
$\sum Q_{Surface}$	37.3	59.1	80.9
Q_{Atm}	3.83	7.38	14

Table 4.27. Major Portion Contributions to the DSR Models.

Model Portion	2.5%	Mean	97.5%
$\frac{\Delta S}{\Delta t}$	2.05	12.7	28.7
$\sum Q_{Total}$	67	83.6	94.7
Q_{Atm}	1.95	3.67	6.93

The typical method for calculating a river water balance includes negating daily storage change and the effects of evaporation and precipitation. This study assumed that these assumptions were false for the LARV and included major portions of the total effort to calculating daily changes in storage and the daily effects of evaporation and precipitation.

- 5 Neglecting the storage change component of the USR mass balance causes the largest change. Neglecting the atmospheric component would result in much smaller, but significant variations. In the DSR, only the atmospheric component is small enough that it could, but shouldn't be neglected. The mean difference calculated when the DSR atmospheric component is neglected is small, but the extremes calculated as the 2.5th and 97.5th percentile are
- 10 not insignificant. The major difference between the USR and DSR reaches is the average annual top width. The DSR passes much lower flows which translates to lower flow depths and smaller river top widths. Top width values are the major contributors to the atmospheric component.

Comparing the USR and DSR water balance model results shows that the unaccounted for flow are approximately equal between the study regions. Since the major assumption is that the unaccounted for flows are primarily groundwater flows, then we compare the two results as if they are groundwater flows.

5 This is directly observable in the DSR where the flow rate at the upstream end of the reach is visibly typically less than or equal to the flow rate at the downstream end. It has also been observed that there are flows present at the upstream end of the DSR when John Martin Reservoir, which is approximately 16 km (10 mi) upstream, is not actively discharging water to the river. There are no points along the river between the reservoir and
10 the upstream end of the DSR where water is discharged into the river channel. The water passing the upstream end of the DSR must be coming from groundwater sources.

Groundwater flows that are within an order of magnitude of each other are within acceptable limits. Groundwater flow rates are calculated as the product of the soil permeability and the head difference between two points. The major variation occurs with the
15 conductivity of soils. Nearly identical sandy soils, such as those found in the LARB can have permeability values that are an order of magnitude different. This is evidenced by tables of permeability of typical soils found in many groundwater texts.

The difference between the study regions is nearly negligible when looking at the mass balance models. these models have mean values that are nearly identical. This allows us to
20 conclude that the selenium dissolution and transport processes that are active in the USR are equal or approximately equal in magnitude to those in the DSR.

CHAPTER 5

EVALUATION OF NPS SELENIUM LOADING TO THE RIVER USING A MASS BALANCE MODEL

5.1. MASS BALANCE MODEL APPLIED TO THE LARV

The purpose of the mass balance model in this thesis is to determine the mass of unaccounted for dissolved selenium being transported into and out of the the study reaches in the LARV. The mass transport is called the mass loading, where mass loading refers to

5 mass entering the river channel and mass unloading refers to mass leaving the river channel.

The basic concept of the mass balance lies in Equation 34. This equation is generalized for any dissolved or suspended constituent. All references to loadings (L) in this thesis is specific to selenium.

$$L = Q \cdot C \quad (34)$$

Where:

L = Mass loading (when positive) or mass unloading (when negative).

Q = Water flow rate.

C = Concentration of the dissolved constituent under investigation.

Using this equation as a basis of understanding and applying it to Equation 4 in Chapter 4, we arrive at a very basic equation mass balance model (Equation 35).

$$\frac{\Delta S_M}{\Delta t} = \quad \quad \quad (35)$$

$$Q_{in,US} \cdot C_{in,US} + \sum (Q_{in} \cdot C_{in}) + P \cdot C_P + R \cdot C_R + B \cdot C_B \\ - Q_{out,DS} \cdot C_{out,DS} - \sum (Q_{out} \cdot C_{out}) - E \cdot C_E - T \cdot C_T \\ - F \cdot C_F + X \cdot C_X$$

The C terms are the concentration for the dissolved constituent at each of the model design points. Simplifying by using Equation 34 results in Equation 36.

$$\frac{\Delta S_M}{\Delta t} = L_{in,US} + \sum L_{in} + L_P + L_R + L_B - L_{out,DS} - \sum L_{out} - L_E - L_T - L_F + L_X \quad (36)$$

Where:

$\frac{\Delta S_M}{\Delta t}$ = Mass storage change in the study reach.

$L_{in,US}$ = Mass loading to the river along the main stem of the river at the upstream end of the study reach.

$\sum L_{in}$ = Sum of the mass loadings to the river from tributaries and other gauged sources.

L_P = Mass loading to the river from precipitation.

L_R = Mass loading to the river from precipitation runoff off of adjacent land.

L_B = Mass loading to the river from subsurface flow.

$L_{out,DS}$ = Mass unloading along the main stem of the river at the downstream end of the study reach.

$\sum L_{out}$ = Sum of the mass unloadings from the river to canals and other gauged sinks.

L_E = Mass unloading from the river due to evaporation.

L_T = Mass unloading from the river due to plant transpiration.

L_F = Mass unloading from the river due to infiltration into subsurface flow.

L_X = Mass loading/unloading to/from unknown sources and sinks.

Equation 36 is a direct application of the two equations. Some of the terms need

to be re-defined to be more appropriate for the situation. L_P is a possible process for

many dissolved constituents, but it is unknown whether or not it occurs in any significant magnitude when the constituent is dissolved selenium. Selenium does not naturally occur

5 in the atmosphere. It is transferred via biomethylation processes into the atmosphere. This

is the L_T term. While the transport directions are the same, the L_E term is the direct volatilization of dissolved selenium species into the atmosphere. At this time, volatilization

has been found to be an insignificant factor in the transport of dissolved selenium species

into the atmosphere.

10 Using the same justifications as used in the previous chapter, Equation 36 is simplified

to define the mass loading from and mass loading to unaccounted for non-point source

(L_{UNPS}). This equation includes two terms not previously used. $L_{U,in}$ and $L_{U,out}$ are subsets

of $\sum L_{in}$ and $\sum L_{out}$, respectively. They are the ungauged and non-point source river reach

gains and losses.

$$L_{UNPS} = \frac{\Delta S_M}{\Delta t} - \sum L_{Surface} \quad (37)$$

Where:

$$\begin{aligned} L_{UNPS} &= \text{The sum of mass gains from non-point sources and losses to non-point sinks} \\ &= L_R + L_B - L_T - L_F + L_{U,in} - L_{U,out} + L_P - L_E L_X. \end{aligned}$$

$$\begin{aligned} \sum L_{Surface} &= \text{The sum of the loadings passing through surface water flow gauges.} \\ &= (L_{in,US} + \sum L_{in} - L_{out,US} - \sum L_{out}) \end{aligned}$$

5.2. MASS STORAGE CHANGE

River water storage change calculations are developed and presented in Section 4.4.

5 Water storage change values between consecutive time steps are the basis for the calculations developed in this section. Stored selenium mass changes between two consecutive time steps is dependent on the change in river stored water volume and the concentration of selenium in the water. The stored selenium mass change in a given study region section is the sum of the stored selenium mass changes of the reaches within a study region river section. Individual
10 reach selenium storage changes are calculated using equation 38.

$$\frac{\Delta S_{M,i}}{\Delta t} = \frac{C_{in,i} + C_{out,i}}{2} \cdot \frac{\Delta S_i}{\Delta t} \quad (38)$$

Where:

$$\frac{\Delta S_{M,i}}{\Delta t} = \text{Stored volume change in study reach segment } i \text{ between time steps.}$$

$$C_{in,i} = \text{Calculated dissolved selenium concentration at the upstream end of segment } i.$$

$$C_{out,i} = \text{Calculated dissolved selenium concentration at the downstream end of segment } i.$$

$$\frac{\Delta S_i}{\Delta t} = \text{Stored water volume change for segment } i \text{ as calculated in Section ??}.$$

Ideally, the average selenate concentration should be calculated as the difference between the current calculation day stored mass and the prior calculation day stored mass. This requires that sufficient data is available to calculate the concentrations in the two consecutive calculation days. The actual stored water volume was not calculated and therefore 5 the stored selenium mass could not be calculated. The methodology shown in equation 38 was assumed to perform as an approximation of the stored selenium mass change between two consecutive days.

The stored water volume change is significantly larger than the average concentration. Therefore it was assumed that small but significant changes in selenium concentrations 10 between consecutive days would not significantly impact the stored selenium mass change.

5.2.1. *Solute Concentration Models*

One of the purposes of this thesis is to determine the selenium loading and unloading rate from unaccounted for sources/sinks. Elemental selenium does not exist in an aqueous form. The two dominant aqueous species are selenate and selenite. Of these two, selenate 15 is the most dominant to the extent that in most cases, selenite is immeasurable. Therefore, throughout this thesis, selenate is used as the surrogate for all aqueous selenium species. References in this thesis to dissolved selenium and aqueous selenium are in fact discussing aqueous selenate.

All concentrations discussed in this thesis refer only to dissolved selenium concentra- 20 tion. Therefore, the typical method of denoting concentration with the aqueous species in the subscript (i.e. C_{Se}) is not going to be used in this thesis. Instead, subscripts are being reserved to designate the location within a study region for which the concentration is used. As such, Tables 5.1 and 5.2 shows the symbolic relationship between the various gauged flow

and river segment storage changes and their associated dissolved selenium concentration for the USR and DSR, respectively. The concentration symbols use subscripts that designate the sample location as noted in Figures 3.1 and 3.2.

Table 5.1. USR gauged flow and river segment storage change symbolic relationship with dissolved selenium concentrations.

USR gauged flow and aqueous selenium concentration relationships.

Mass Loading Symbol	Gauged Flow Symbol	Concentration Symbol
$L_{ARKCATCO}$	$Q_{ARKCATCO}$	C_{U163}
$L_{ARKLASCO}$	$Q_{ARKLASCO}$	C_{U201}
$L_{CANSWKCO}$	$Q_{CANSWKCO}$	C_{U74}
$L_{CONDITCO}$	$Q_{CONDITCO}$	$C_{ARK,d=85.0}$
$L_{FLSCANCO}$	$Q_{FLSCANCO}$	$C_{ARK,d=16.4}$
$L_{FLYCANCO}$	$Q_{FLYCANCO}$	$C_{ARK,d=47.2}$
$L_{HOLCANCO}$	$Q_{HOLCANCO}$	$C_{ARK,d=12.5}$
$L_{HRC194CO}$	$Q_{HRC194CO}$	C_{U207}
$L_{RFDMANCO}$	$Q_{RFDMANCO}$	C_{U167}
$L_{RFDRETCO}$	$Q_{RFDRETCO}$	C_{U167}
$L_{TIMSWICO}$	$Q_{TIMSWICO}$	C_{U60}
$L_{LAJWWTP}$	$Q_{LAJWWTP}$	$C_{LAJWWTP}$

USR river segment water volume change and aqueous selenium concentration relationship.

Mass Loading Symbol	River Segment Volume Change	US Concentration Symbol	DS Concentration Symbol
$\frac{\Delta S_{M,A}}{\Delta t}$	$\frac{\Delta S_A}{\Delta t}$	C_{U163}	$C_{ARK,d=12.5}$
$\frac{\Delta S_{M,B}}{\Delta t}$	$\frac{\Delta S_B}{\Delta t}$	$C_{ARK,d=12.5}$	$C_{ARK,d=16.4}$
$\frac{\Delta S_{M,C}}{\Delta t}$	$\frac{\Delta S_C}{\Delta t}$	$C_{ARK,d=16.4}$	$C_{ARK,d=47.2}$
$\frac{\Delta S_{M,D}}{\Delta t}$	$\frac{\Delta S_D}{\Delta t}$	$C_{ARK,d=47.2}$	$C_{ARK,d=85.0}$
$\frac{\Delta S_{M,E}}{\Delta t}$	$\frac{\Delta S_E}{\Delta t}$	$C_{ARK,d=85.0}$	C_{U201}

The concentration associated with the $Q_{RFDRETCO}$ gauged flow is the same as that used for the $Q_{RFDMANCO}$ gauged flow. It was assumed that the two gauges would have the same dissolved selenium concentration due to their close proximity to each other. The concentrations in the USR with the designation $C_{ARK,d=x}$ are based on the concentrations for 5 all locations in the main stem of the Arkansas River. Since it is known that the concentration is not constant along the entire reach, a variable was needed to differentiate the concentration for the various irrigation canal diversions. It was found that there was a slight correlation between the distance between the sample point and the upstream end of the study region and the dissolved selenium concentration. Therefore, this distance was used and is noted in 10 the subscript as x , where x denotes the distance between the irrigation canal diversion and the upstream end of the study reach. The La Junta WWTP does not have a stream gauge nor were selenium analyses performed by the university for this location. Plant operators were kind enough to provide us with the total daily discharge from the plant in units of 15 million gallons per day (mgd). This value was converted to appropriate units as used in the previous chapter. They also provided the monthly selenium analyses results. These analyses were performed in accordance with State directives. University researchers did not question the validity of the discharge or selenium concentration results.

As can be observed in Figure 3.2, the flow gauge for Buffalo Ditch ($BUFDITCO$) has a sample location within close proximity on the channel. The concentrations associated 20 with this location ($D36$), were found to be inconsistent with concentrations at $D104C$. A chance encounter with the individual who owns the land immediately adjacent to the gauge location informed us that a small spring discharged from his property into Buffalo Ditch between the gauge location and the sample location. The landowner informed us that the spring discharged at approximately $0.056 \text{ m}^3 \text{ s}^{-1}$ (2 cfs). He also stated that the flow rate

Table 5.2. DSR gauged flow and river segment storage change symbolic relationship with dissolved selenium concentrations.

DSR gauged flow and aqueous selenium concentration relationships.

Mass Loading Symbol	Gauged Flow Symbol	Concentration Symbol
$L_{ARKLAMCO}$	$Q_{ARKLAMCO}$	C_{D101C}
$L_{ARKCOOKS}$	$Q_{ARKCOOKS}$	C_{D106C}
$L_{BIGLAMCO}$	$Q_{BIGLAMCO}$	C_{D23}
$L_{BUFDITCO}$	$Q_{BUFDITCO}$	$C_{ARK,d=37.7}$
$L_{FRODITKS}$	$Q_{FRODITKS}$	C_{D106C}
$L_{WILDHOCO}$	$Q_{WILDHOCO}$	C_{D57}

DSR river segment water volume change and aqueous selenium concentration relationship.

Mass Loading Symbol	River Segment Volume Change	US Concentration Symbol	DS Concentration Symbol
$\frac{\Delta S_{M,F}}{\Delta t}$	$\frac{\Delta S_F}{\Delta t}$	C_{D101C}	C_{D104C}
$\frac{\Delta S_{M,G}}{\Delta t}$	$\frac{\Delta S_G}{\Delta t}$	C_{D104C}	C_{D106C}

was fairly constant throughout the year. Since there was a significant variance between the measured concentrations at sample points $D36$ and $D104C$ and since there is a known discharge into the channel with an unknown concentration, it was determined that the gauged flow $Q_{BUFDITCO}$ would be associated with the concentration $C_{ARK,d=37.7}$.

5 Dissolved selenium samples were taken as discussed in Chapter 3. Samples were not taken for every time step in the study time frame. Concentration estimations for all sample locations except one were performed using linear regression. Linear regression models are defined as models where the functions of the predictor variables are not themselves variable. This is shown in equation 39. A regression model is considered linear if f_i does not contain

any fitting parameters (β_i).

$$\hat{y} = \beta_0 + \beta_1 f_1 + \beta_2 f_2 + \dots + \beta_n f_n \quad (39)$$

Where:

\hat{y} = fitted or predicted value

β_i = fitting parameters

f_i = functions of the predictor variables x_i

Whenever possible, ordinary least squares regression was used to generate best fit

5 equations with a given set of independent variables. Pearson's r-squared value is used as an initial goodness-of-fit value so that individual linear regression models can be evaluated both independently and comparatively with regards to how well they fit the data. R-squared values for linear models are positive, non-negative values less than one (1) with one (1) indicating a perfect fit. R-squared values account for the percent of the dependent variable
10 that can be accounted for in the independent variables. The adjusted r-squared value is calculated and compared to the r-squared value. This allows for some accounting for uncertainty when using multiple independent variables. If the two are considerably different, then the estimating model is missing an explanatory independent variable (R. A. Johnson and Wichern, 2007).

15 The f-statistic was also calculated and compared to the critical f-statistic for each estimating model. An f-statistic greater than the critical f-statistic indicates that at least one of the explanatory independent variables is linearly associated with the calculated dependent variable. When comparing estimating models for suitability, the model with the greater f-statistic is more suitable (ibid.). The model f-statistic is returned as part of the

statistics software linear regression summary. The critical f-statistic is calculated using the f-distribution and the desired significance level and the degrees of freedom.

The significance level, α , is closely tied to the desired confidence interval for this study. Considering the number and source of the input variables, it was considered desirable 5 to have all models calculated to account for 95% of the variability. This means that 5% of the variability in any model can be attributed to chance. With all models being two-tailed, the central inter-percentile range (CIR) was calculated for the range between 2.5% and 97.5% as a means to comprehend the daily change in variability. This takes the 5% unaccounted variability and distributes it to the two tails. The α is not changed on account 10 of the two-tailed nature of the models.

The two-sided p-value was used to determine if the estimating model independent variables were statistically significant. The p-values greater than α indicated that the independent variable was not significant and did not contribute significantly to describe the variability of the dependent variable. These variables were considered for removal during 15 linear regression model optimization.

The selenium concentration field data collection effort provided excellent data for specific locations at specific times. This data needed to be expanded to include as many intermediate locations and times as possible to provide a more complete set of results. The methodology for determining the dissolved selenium concentration at various locations in 20 both study region river sections is the same with only one exception. The set of starting independent variables, or starting terms, changes depending on the specific location, but the method of reducing the equation to the final equation is the same.

Estimating equations were calculated using multivariate linear ordinary least squares regression. The 'lm' function in the statistical software 'stats' package was used to fit linear models. Measured selenium concentration values were initially fitted to equations that included the average daily stream flow, EC, and water temperature values for the same day 5 as the selenium concentration sample was collected. Equations were then refined through a process that will be discussed.

All data points were included in the linear regression even if some terms were missing. The 'lm' function has an argument that allows the user to determine what should happen if missing data is encountered. All analyses were performed such that data points with 10 missing values were excluded from the analysis. As the number of terms was reduced during the equation refinement process, these excluded data points may or may not be included in the analysis. This allowed for the maximum number of data points without reforming the data set with each equation refinement iteration.

Determining which terms to include in each initial regression analysis began with 15 visual analysis of an enhanced scatter-plot matrix of the selenium concentration response vector and the independent variable terms. Figures 5.1 and 5.1 contain the scatter-plot matrices for all concentration points in the USR and DSR, respectively. The diagonal contains the variable names for the row and column. The lower triangle shows the individual variables when plotted against each other. Individual graphs are in appropriate units for 20 the investigated variables. Flow is in units of m^3s^{-1} , EC is in units of dS m^{-1} , and temperature is in units of $^{\circ}\text{C}$. The upper triangle presents the Pearson correlation value for the respective variable pair. Similar figures for the other regression analyses are included in the appendix.

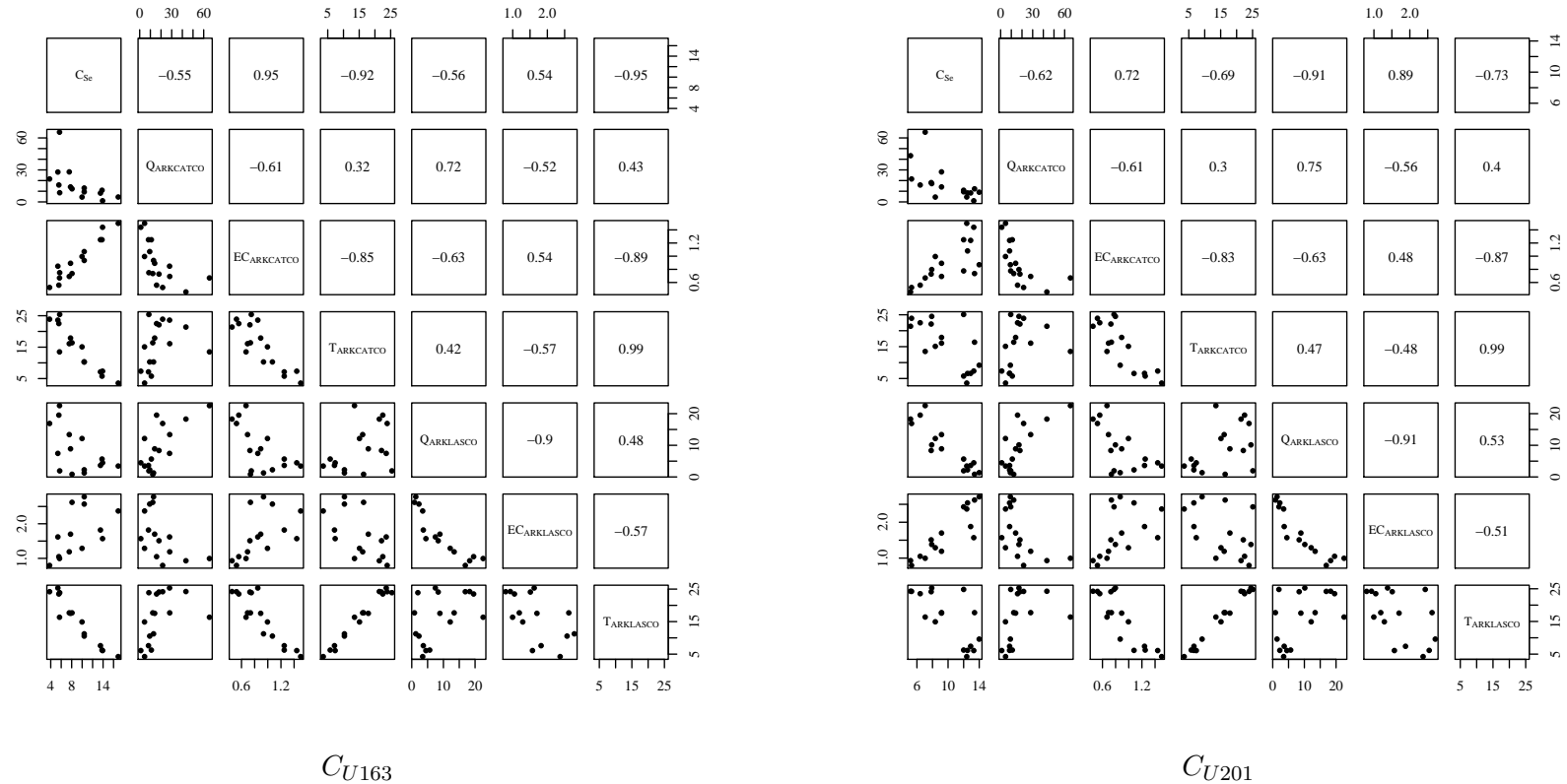


Figure 5.1. Scatter-plot matrices of the input variables used to estimate dissolved selenium concentrations in the USR. Variable names are plotted down the diagonal. Values in the upper triangle are Pearson correlation values for the intersecting variables. Scatter-plots for the intersecting variables are plotted in the lower triangle. Scales are in the units for the given variable. C_{Se} is in $\mu\text{g L}^{-1}$. Q values are in $\text{m}^3 \text{s}^{-1}$. EC values are in dS m^{-1} . T values are in $^{\circ}\text{C}$.

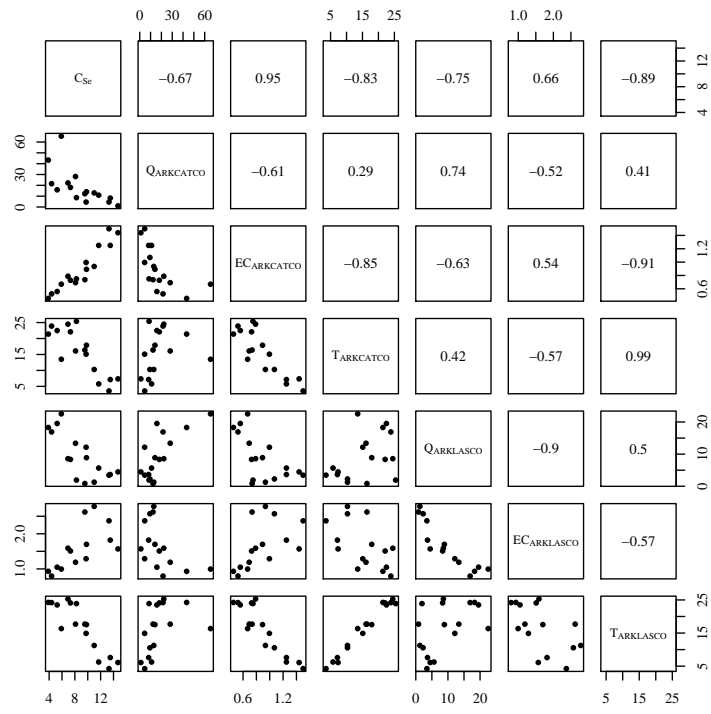
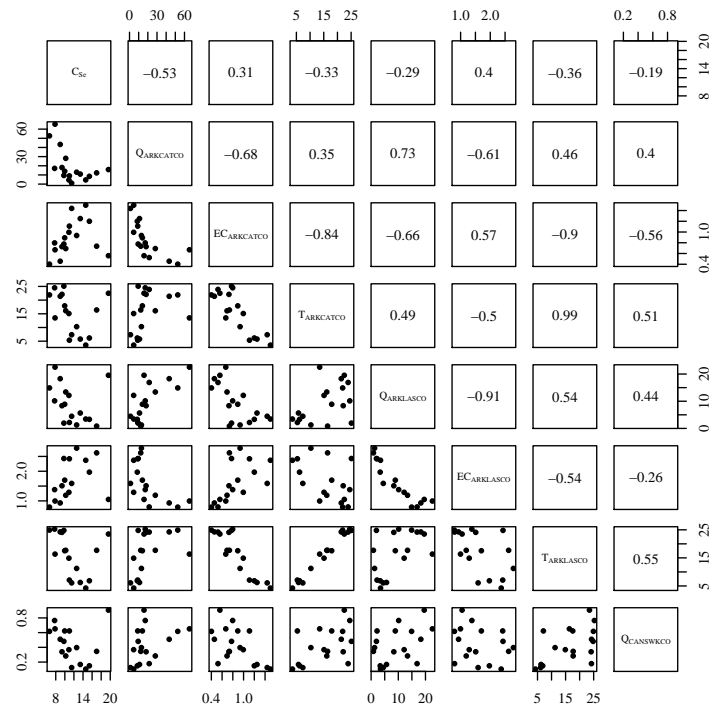
 C_{U167}  C_{U74}

Figure 5.1 (Cont). Scatter-plot matrices of the input variables used to estimate dissolved selenium concentrations in the USR.

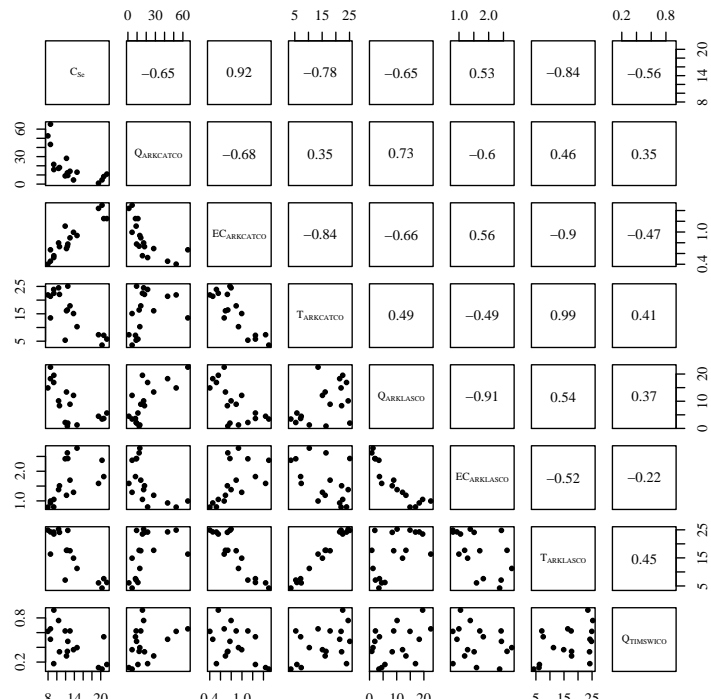
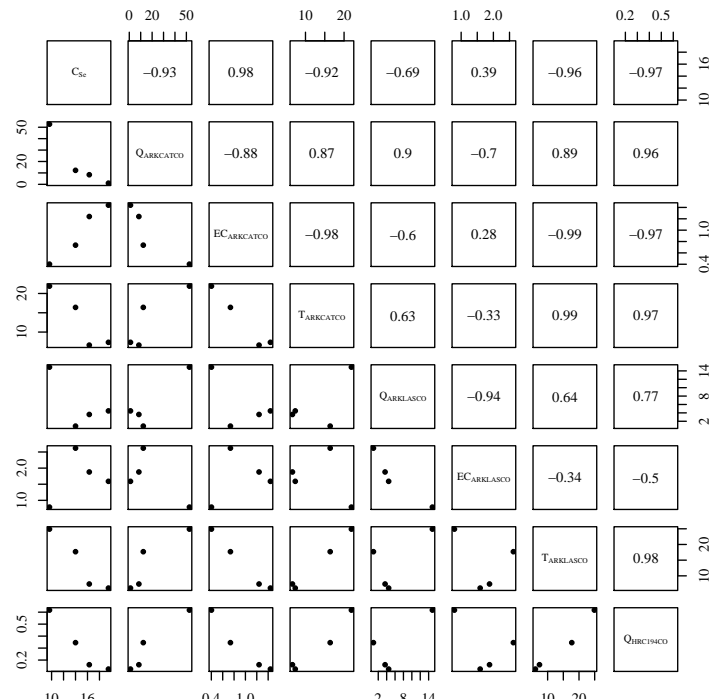
 C_{60}  C_{U209}

Figure 5.1 (Cont). Scatter-plot matrices of the input variables used to estimate dissolved selenium concentrations in the USR.

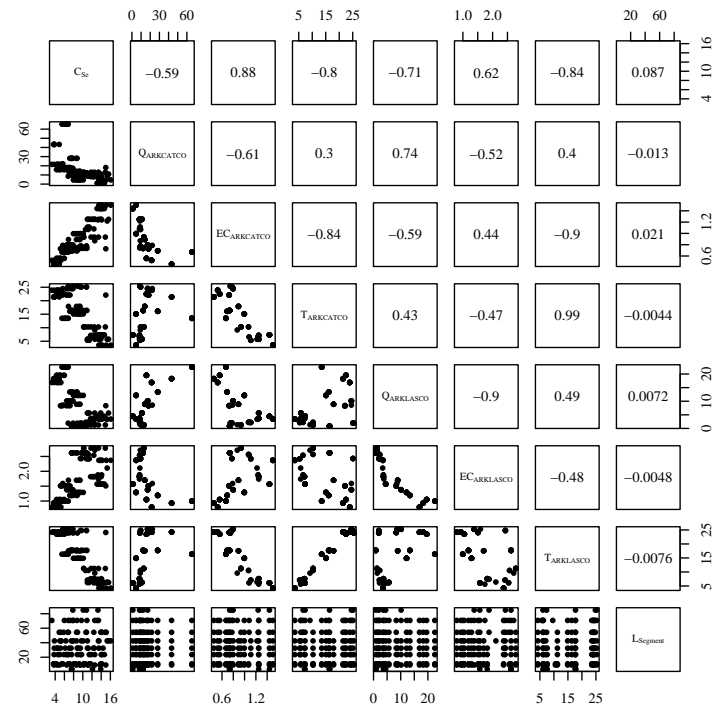
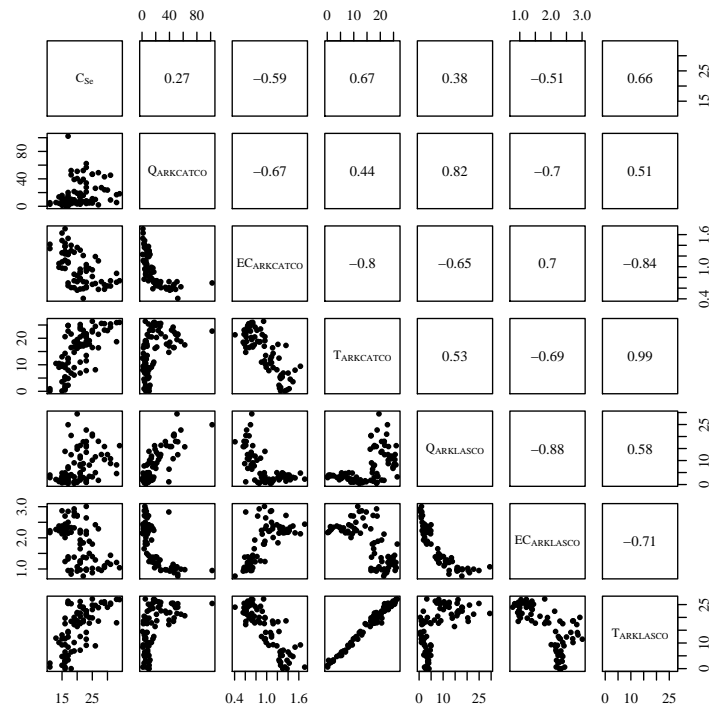
 $C_{ARK,d=x}$  $C_{LAJWWTP}$

Figure 5.1 (Cont). Scatter-plot matrices of the input variables used to estimate dissolved selenium concentrations in the USR.

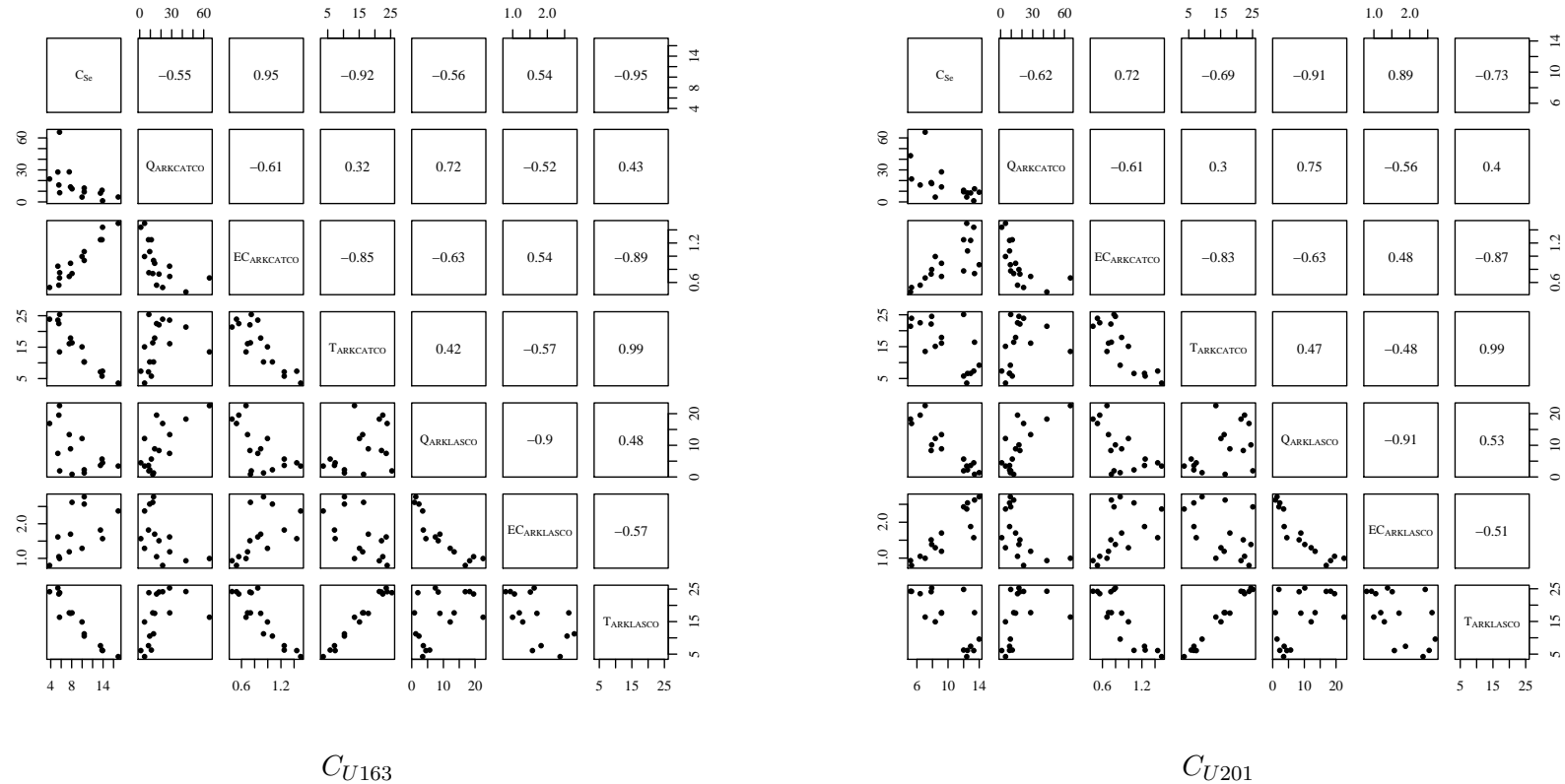


Figure 5.2. Scatter-plot matrices of the input variables used to estimate dissolved selenium concentrations in the DSR. Variable names are plotted down the diagonal. Values in the upper triangle are Pearson correlation values for the intersecting variables. Scatter-plots for the intersecting variables are plotted in the lower triangle. Scales are in the units for the given variable. C_{Se} is in $\mu\text{g L}^{-1}$. Q values are in $\text{m}^3 \text{s}^{-1}$. EC values are in dS m^{-1} . T values are in $^{\circ}\text{C}$.

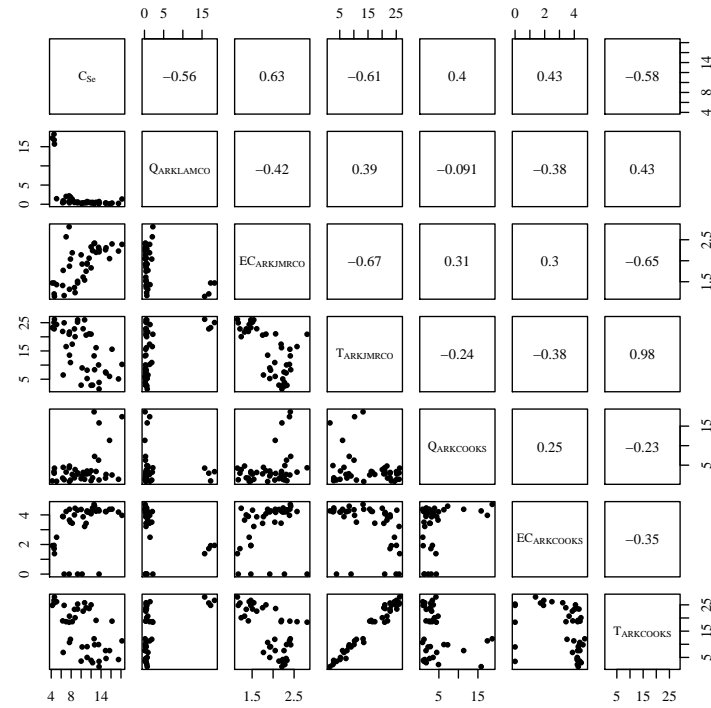
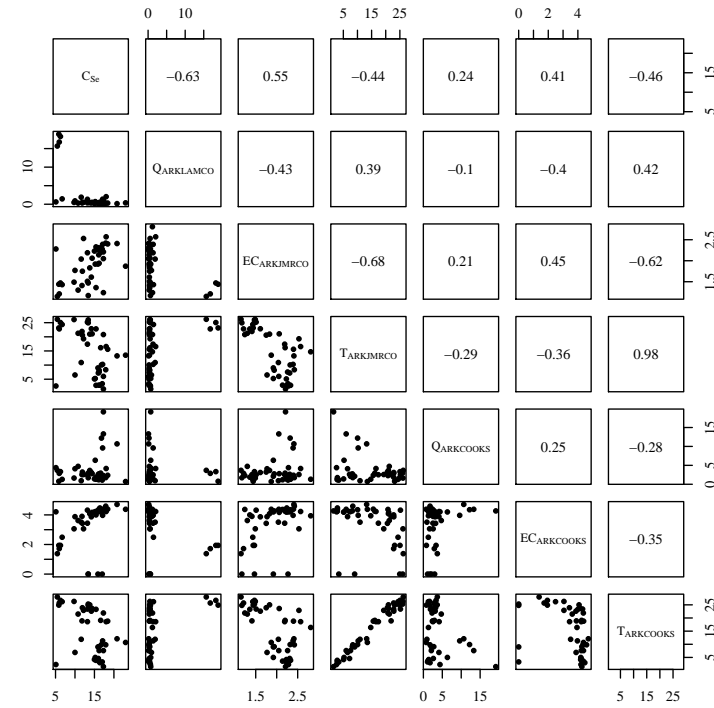
 C_{D101C}  C_{D106C}

Figure 5.2 (Cont). Scatter-plot matrices of the input variables used to estimate dissolved selenium concentrations in the DSR.

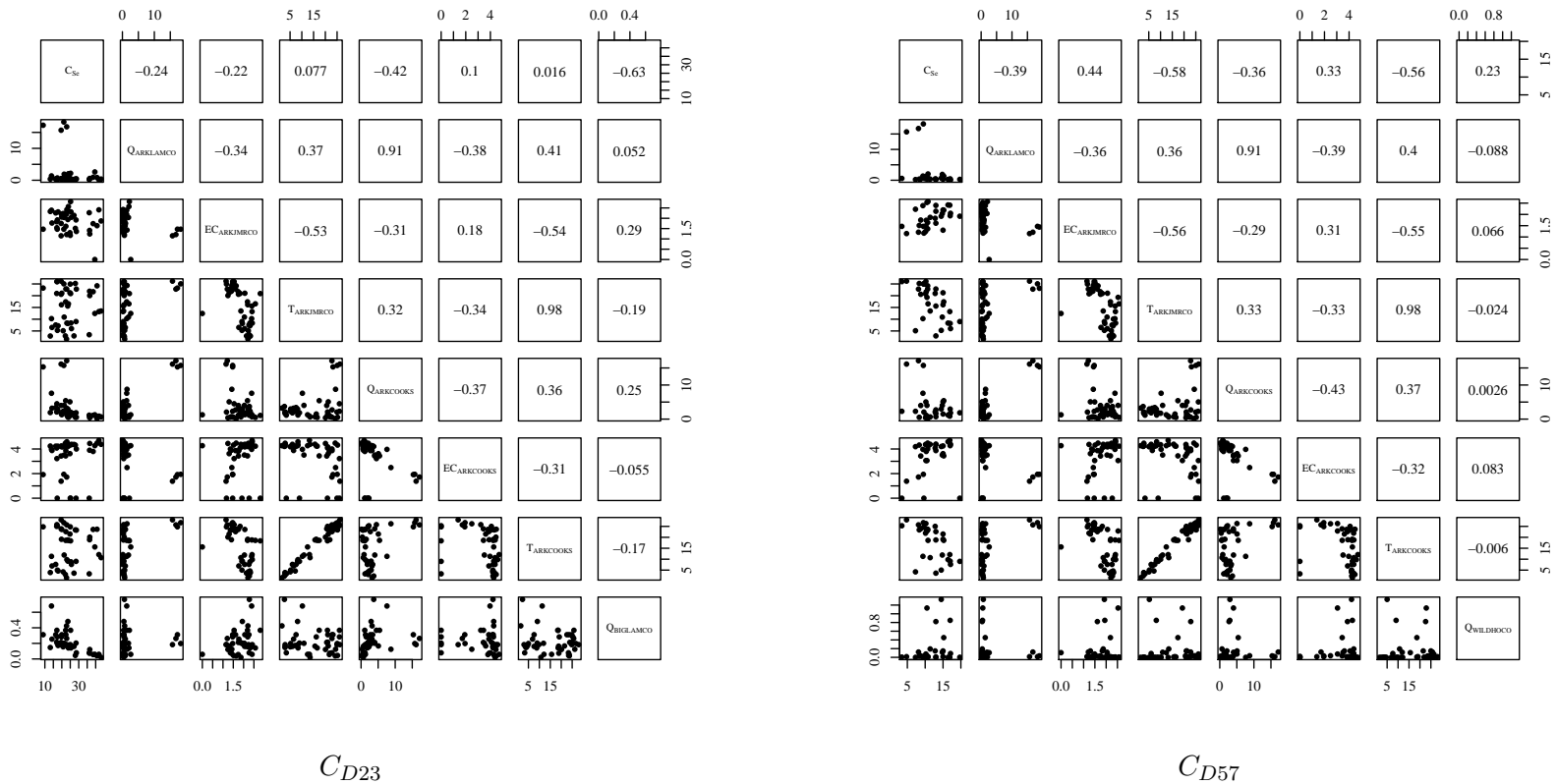
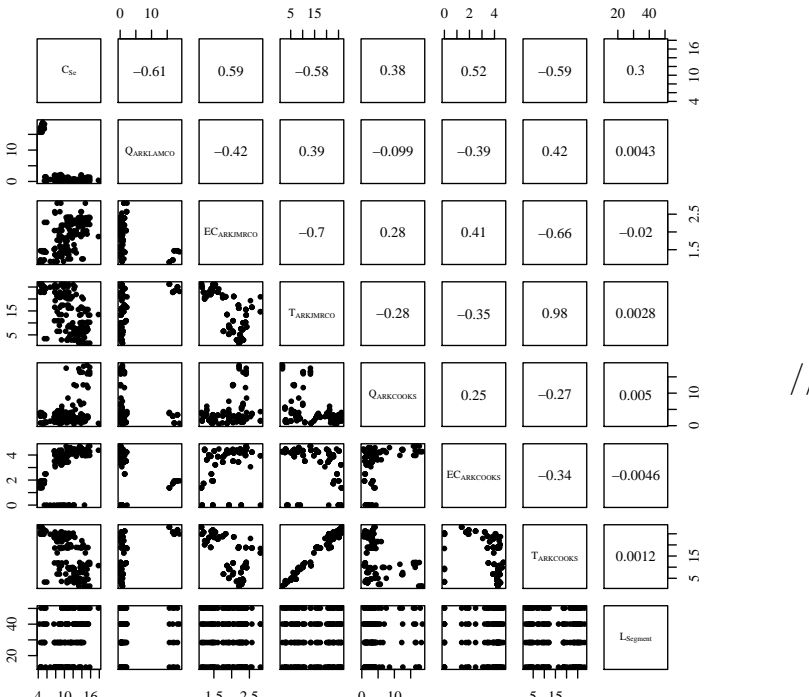


Figure 5.2 (Cont). Scatter-plot matrices of the input variables used to estimate dissolved selenium concentrations in the DSR.



$$C_{D23}$$

Figure 5.2 (Cont). Scatter-plot matrices of the input variables used to estimate dissolved selenium concentrations in the DSR.

In this case and as with most other regression analyses, there are strong correlations between terms which would indicate that removing all but the EC value would give an adequate estimation. The EC, which is related to the total salt concentration, is proportional to C_{Se} . However, temperature and flow are negatively correlated, compared with EC's 5 positive correlation with C_{Se} . An increase in flow volume dilutes the total salt load and therefore C_{Se} . Temperature affects the solubility of all salts. Including temperature allows the difference in solubility constants to be expressed. Also, flow has opposing correlations with EC and temperature. These trends show that although EC alone can be used to estimate C_{Se} , it may not be sufficient to completely describe how C_{Se} reacts to the 10 environment.

An initial regression form was used and individual terms were removed based on their individual p value. Only one variable was removed at a time and the new, reduced form was re-analyzed. This step-wise method was performed until the p value for the individual variables was less than an α of 0.05. Residual standard error values, r-squared values, 15 adjusted r-squared values, F-statistics, and p-values were collected for each analysis. If the statistics did not appear to support the conclusion that the final, reduced form linear mode was representative of the data, then the process was re-started with a different, more complex, initial regression form.

Tables 5.3 and 5.4 present the initial regression forms for the river sections in the 20 USR and DSR respectively. These initial regression forms presented do not include the resulting coefficients for the respective variables as they are insignificant to the results of this particular analysis and the complete model results.

Selenium concentration at the La Junta WWTP was not able to be sufficiently estimated using linear models. The La Junta water distribution system receives most of its

Table 5.3. USR Selenium Concentration Initial Regression Models.

Concentration	Initial regression model.
C_{U163}	$Q_{ARKCATCO} + EC_{ARKCATCO} + t_{ARKCATCO}$
C_{U201}	$Q_{ARKLASCO} + EC_{ARKLASCO} + t_{ARKLASCO}$
C_{U167}	$Q_{ARKCATCO} + EC_{ARKCATCO} + Q_{ARKLASCO}$ + $EC_{ARKLASCO} + t_{ARKLASCO}$
C_{U74}	$Q_{ARKCATCO} + EC_{ARKCATCO} + Q_{ARKLASCO}$ + $EC_{ARKLASCO} + t_{ARKLASCO} + Q_{CANSWKCO}$ + $Q_{ARKCATCO}Q_{CANSWKCO} + EC_{ARKCATCO}Q_{CANSWKCO}$ + $Q_{ARKLASCO}Q_{CANSWKCO} + EC_{ARKLASCO}Q_{CANSWKCO}$ + $t_{ARKLASCO}Q_{CANSWKCO}$
C_{U60}	$Q_{ARKCATCO} + EC_{ARKCATCO} + Q_{ARKLASCO}$ + $EC_{ARKLASCO} + t_{ARKLASCO} + Q_{TIMSWICO}$
C_{U207}	$Q_{ARKCATCO} + EC_{ARKCATCO} + Q_{ARKLASCO}$ + $EC_{ARKLASCO} + t_{ARKLASCO} + Q_{HRC194CO}$
$C_{ARK,d=x}$	$Q_{ARKCATCO} + EC_{ARKCATCO} + Q_{ARKLASCO}$ + $EC_{ARKLASCO} + t_{ARKLASCO} + d$
$C_{LAJWWTP}$	$\beta_1 \cdot Q_{WTP}^{\beta_2}$

water from wells. It was not known which aquifer supplied the city. It was assumed that the shallow river riparian aquifer was the city's water source as there are no known deep aquifers in the area. It was also assumed that the water treatment plant processes and waste water treatment plant processes could change the selenium concentration. The average daily flow

5 produced by the plant is the only variable available to estimate selenium concentrations.

Visual analysis of the scatter plot similar to Figure ?? showed that the relationship between the plant discharge rate and selenium concentration could not be easily defined. A non-linear model was used with the power function described in Table 5.3. This model produced fairly

Table 5.4. USR Selenium Concentration Initial Regression Models.

Concentration	Initial regression model.
C_{D101C}	$Q_{ARKLAMCO} + EC_{ARKJMRCO} + t_{ARKJMRCO}$ $+ Q_{ARKLAMCO}^2 + Q_{ARKLAMCO}EC_{ARKJMRCO}$ $+ Q_{ARKLAMCO}t_{ARKJMRCO} + EC_{ARKJMRCO}^2$ $+ EC_{ARKJMRCO}t_{ARKJMRCO} + t_{ARKJMRCO}^2$
C_{D106C}	$Q_{ARKCOOKS} + EC_{ARKCOOKS} + t_{ARKCOOKS}$ $+ Q_{ARKCOOKS}^2 + Q_{ARKCOOKS}EC_{ARKCOOKS}$ $+ Q_{ARKCOOKS}t_{ARKCOOKS} + EC_{ARKCOOKS}^2$ $+ EC_{ARKCOOKS}t_{ARKCOOKS} + t_{ARKCOOKS}^2$
C_{D23}	$Q_{ARKLAMCO} + EC_{ARKJMRCO} + Q_{ARKCOOKS}$ $+ EC_{ARKCOOKS} + t_{ARKCOOKS} + Q_{BIGLAMCO}$ $+ Q_{ARKLAMCO}Q_{BIGLAMCO} + EC_{ARKJMRCO}Q_{BIGLAMCO}$ $+ Q_{ARKCOOKS}Q_{BIGLAMCO} + EC_{ARKCOOKS}Q_{BIGLAMCO}$ $+ t_{ARKCOOKS}Q_{BIGLAMCO}$
C_{D57}	$Q_{ARKLAMCO} + EC_{ARKJMRCO} + t_{ARKJMRCO} + Q_{ARKCOOKS}$ $+ EC_{ARKCOOKS} + Q_{WILDHOCO} + Q_{ARKLAMCO}^2$ $+ Q_{ARKLAMCO}EC_{ARKJMRCO} + Q_{ARKLAMCO}t_{ARKJMRCO}$ $+ Q_{ARKLAMCO}Q_{ARKCOOKS} + Q_{ARKLAMCO}EC_{ARKCOOKS}$ $+ Q_{ARKLAMCO}Q_{WILDHOCO} + EC_{ARKJMRCO}^2$ $+ EC_{ARKJMRCO}t_{ARKJMRCO} + EC_{ARKJMRCO}Q_{ARKCOOKS}$ $+ EC_{ARKJMRCO}EC_{ARKCOOKS} + EC_{ARKJMRCO}Q_{WILDHOCO}$ $+ t_{ARKJMRCO}^2 + t_{ARKJMRCO}Q_{ARKCOOKS}$ $+ t_{ARKJMRCO}EC_{ARKCOOKS} + t_{ARKJMRCO}Q_{WILDHOCO}$ $+ Q_{ARKCOOKS}^2 + Q_{ARKCOOKS}EC_{ARKCOOKS}$ $+ Q_{ARKCOOKS}Q_{WILDHOCO} + EC_{ARKCOOKS}^2$ $+ EC_{ARKCOOKS}Q_{WILDHOCO} + Q_{WILDHOCO}^2$
$C_{ARK,d=x}$	$Q_{ARKLAMCO} + EC_{ARKJMRCO} + Q_{ARKCOOKS}$ $+ EC_{ARKCOOKS} + t_{ARKCOOKS} + d$

reasonable results. Better results could be obtained if average daily EC values of the plant discharge were available.

Tables 5.5 and 5.6 present the final, reduced regression equations with coefficients resulting from the regression analysis.

Table 5.5. USR Selenium Concentration Final Regression Models.

Concentration	Final regression model.
C_{U163}	$-0.05106 \cdot Q_{ARKCATCO} + 4.69 \cdot EC_{ARKCATCO}$ $-0.3063 \cdot t_{ARKCATCO} + 10.12$
C_{U201}	$-0.3138 \cdot Q_{ARKLASCO} - 0.1348 \cdot t_{ARKLASCO} + 14.91$
C_{U167}	$-0.3538 \cdot Q_{ARKLASCO} - 2.021 \cdot EC_{ARKLASCO}$ $-0.3306 \cdot t_{ARKLASCO} + 21.15$
C_{U74}	$-13.01 \cdot EC_{ARKCATCO} - 1.022 \cdot Q_{ARKLASCO} - 0.4132 \cdot t_{ARKLASCO}$ $-16.40 \cdot Q_{CANSWKCO} - 0.3138 \cdot Q_{ARKCATCO}Q_{CANSWKCO}$ $+2.0730Q_{ARKLASCO}Q_{CANSWKCO} + 39.40$
C_{U60}	$11.42 \cdot EC_{ARKCATCO} - 3.160 \cdot Q_{TIMSWICO} + 4.605$
C_{U207}	$-17.78 \cdot Q_{HRC194CO} + 20.41$
$C_{ARK,d=x}$	$4.710 \cdot EC_{ARKCATCO} - 0.1568 \cdot Q_{ARKLASCO} - 0.1491 \cdot t_{ARKLASCO}$ $+0.0203 \cdot d + 8.0831$
$C_{LAJWWTP}$	$19.18 \cdot Q_{WTP}^{0.07664}$

Tables 5.7 and 5.8 present the summary statistics from the regression analysis. The relative standard error with the degrees of freedom (RSE, DoF), multiple R-squared, adjusted R-squared, the F-statistic with the degrees of freedom (F-statistic, DoF), and the p-value generated by the statistical software after regression analyses are presented in these tables.

- 5 All fitted linear regression equations show statistics that indicate that they fit the measured data with a fairly high degree of accuracy.

Individual regression models were analyzed to determine if they were representative of the data. Figures 5.3 and 5.4 graphs used for each concentration point to make this analysis. For each sub-figure, the top left panel shows the residuals plotted against the fitted values.

- 10 All points should be evenly distributed in both directions. If the points are not symmetrical along the fitted values axis, then heteroscedasticity should be suspected. If the points are

Table 5.6. DSR Selenium Concentration Final Regression Models.

Concentration	Final regression model.
C_{D101C}	$3.429 \cdot EC_{ARKJMRCO} - 0.005623 \cdot Q_{ARKLAMCO} EC_{ARKJMRCO}$ $-0.07581 \cdot EC_{ARKJMRCO} t_{ARKJMRCO} + 6.355$
C_{D106C}	$-0.37 \cdot t_{ARKCOOKS} + 0.0627 \cdot EC_{ARKCOOKS} t_{ARKCOOKS} + 16.56$
C_{D23}	$0.08951 \cdot Q_{ARKLAMCO} - 0.9925 \cdot Q_{ARKCOOKS}$ $-1.376 \cdot Q_{BIGLAMCO} - 0.007387 \cdot Q_{ARKLAMCO} Q_{BIGLAMCO}$ $+0.006882 \cdot Q_{ARKCOOKS} Q_{BIGLAMCO} + 36.96$
C_{D57}	$-42.64 \cdot EC_{ARKJMRCO} - 3.309 \cdot t_{ARKJMRCO}$ $-14.18 \cdot EC_{ARKCOOKS} - 0.006969 \cdot Q_{ARKLAMCO} Q_{WILDHOCO}$ $+0.005895 \cdot Q_{ARKCOOKS} Q_{WILDHOCO}$ $-0.2522 \cdot Q_{WILDHOCO} EC_{ARKJMRCO}$ $+5.779 \cdot EC_{ARKJMRCO} EC_{ARKCOOKS}$ $+1.029 \cdot EC_{ARKJMRCO} t_{ARKJMRCO}$ $+0.2643 \cdot EC_{ARKCOOKS} t_{ARKJMRCO} - 112.7$
$C_{ARK,d=x}$	$-0.006576 \cdot Q_{ARKLAMCO} + 1.322 \cdot EC_{ARKJMRCO}$ $+0.003794 \cdot Q_{ARKCOOKS} + 0.4512 \cdot EC_{ARKCOOKS}$ $-0.07653 \cdot t_{ARKCOOKS} + 0.1066 \cdot d + 5.709$

Table 5.7. USR Selenium Concentration Regression Models Summary Statistics.

Concentration	RSE, DoF	Multiple R-squared	Adjusted R-squared	F-statistic, DoF	p-value
C_{U163}	0.5923, 11	0.9818	0.9769	198.3, 3 and 11	7.4×10^{-10}
C_{U201}	0.9467, 14	0.9145	0.9022	74.84, 2 and 14	3.3×10^{-8}
C_{U167}	0.7016, 10	0.9684	0.9589	102.1, 3 and 10	8.4×10^{-8}
C_{U74}	0.9868, 10	0.9501	0.9202	31.74, 6 and 10	6.0×10^{-6}
C_{U60}	1.749, 15	0.8633	0.845	47.35, 2 and 15	3.3×10^{-7}
$C_{ARK,d=x}$	1.196, 130	0.8808	0.8772	240.2, 4 and 130	$<2.2 \times 10^{-16}$
$C_{LAJWWTP}$	4.153, 85	NA	NA	NA	NA

RSE = Residual standard error

DoF = Degrees of Freedom

not symmetrical about either axis, then the regression model is missing an estimating term.

The bottom left panel shows a scale-location plot of the data. This panel shows the same information as the first panel with the exception that the square-root of the standardized

Table 5.8. DSR Selenium Concentration Regression Models Summary Statistics.

Concentration	RSE, DoF	Multiple R-squared	Adjusted R-squared	F-statistic, DoF	p-value
C_{D101C}	2.553, 38	0.5472	0.5114	15.31, 3 and 38	1.1×10^{-6}
C_{D106C}	3.534, 39	0.3404	0.3065	10.06, 2 and 36	3.0×10^{-4}
C_{D23}	5.701, 37	0.5819	0.5254	10.3, 5 and 37	3.5×10^{-6}
C_{D57}	2.337, 21	0.7278	0.6111	3.238, 9 and 21	2.7×10^{-4}
$C_{ARK,d=x}$	1.724, 156	0.7104	0.6993	63.78, 6 and 156	1.2×10^{-16}

RSE = Residual standard error

DoF = Degrees of Freedom

residuals is used. This reduces the effect of skewness on the analysis. Like the first panel, the points should be symmetrical along both axes. The top right panel shows a normal quantile-quantile (Q-Q) plot of the residuals. It is a reasonable assumption that residuals of a linear model are normally distributed. If the residuals are normally distributed, then the

5 points should fit closely to the line at $y = x$. The bottom right panel shows the residuals plotted against the leverage of the residuals. The dashed red lines show the Cook's distance which is a measure of the influence a particular data point has on the regression model. Points with a higher leverage have a higher influence on the model. Points with leverage values higher than the majority of the data may be outliers.

10 In all panels, potential outliers are indicated by having the index number of the data printed next to the point. If the same data points are indicated as outliers on most of the panels, then it is most likely true that they are outliers. None of the models had the outliers removed to improve the model. In fact, outliers were expected. Most of the dissolved selenium samples were collected during similar times in the year. Bias towards certain flow regimes and other factors are most likely present in the data. The outliers represent the samples taken outside of the normal sampling season and are more representative of the extremes. These outliers are necessary to the complete analysis and were not removed from the linear regression analyses.

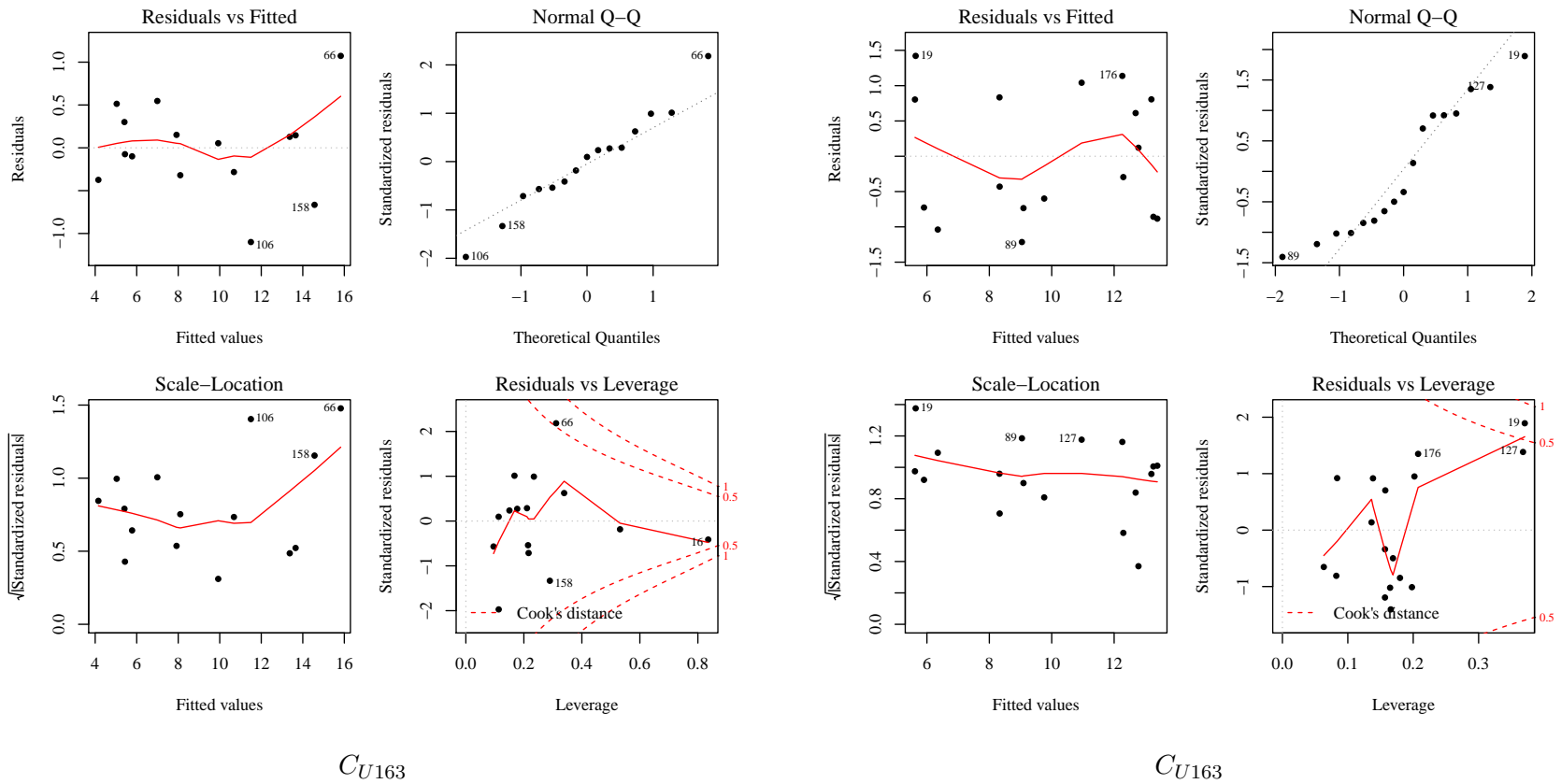
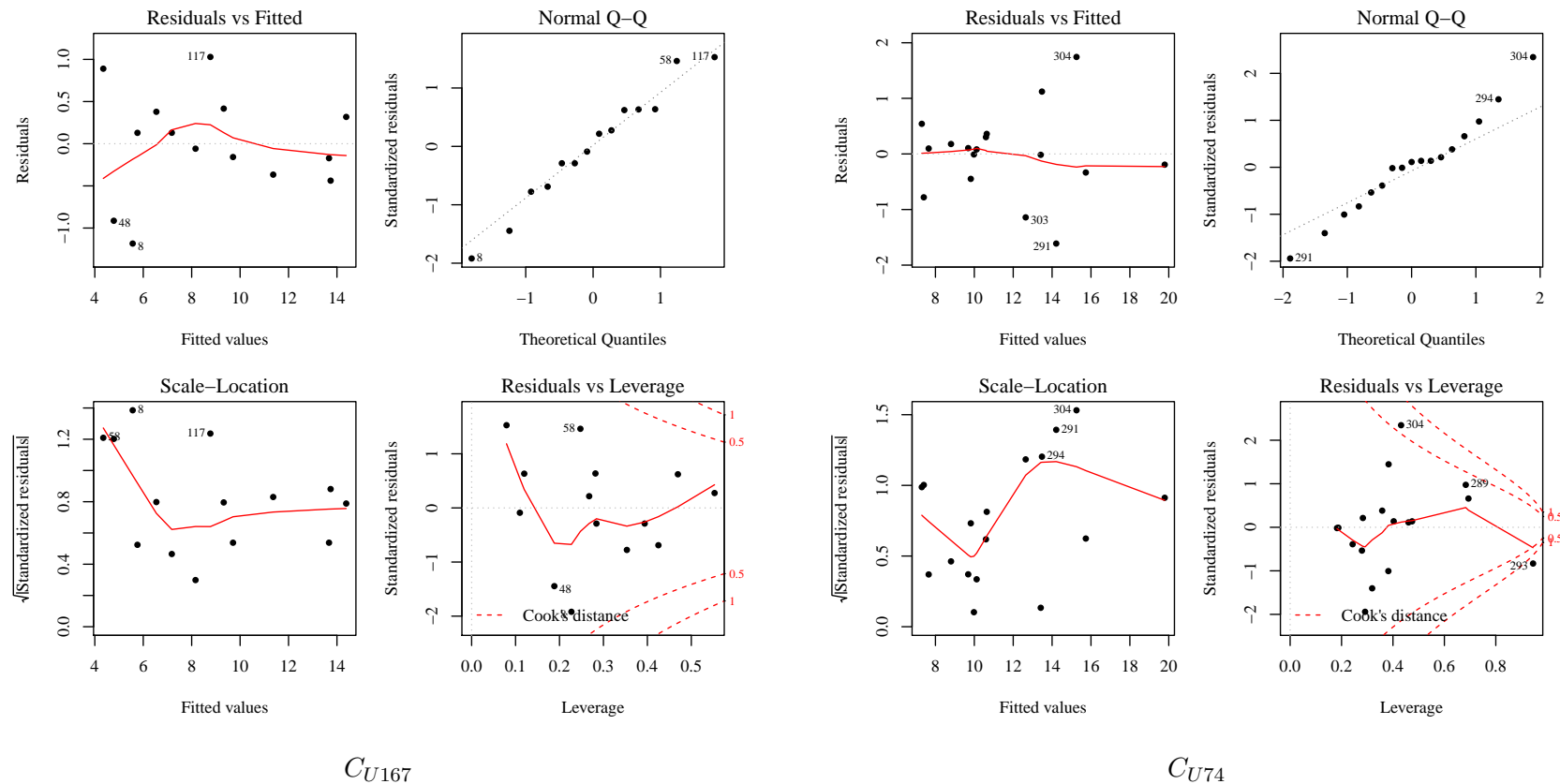
 C_{U163} C_{U163}

Figure 5.3. USR selenium concentration linear model analysis graphs. The black lines indicate the stochastic model mean time-series. The blue band indicates the 95% central inter-percentile range (CIR) of the stochastic values. The red dashed line in the flow depth portion of the figure indicates the reported flow depth values.

 C_{U167} C_{U74} **Figure 5.3 (Cont).** USR selenium concentration linear model analysis graphs.

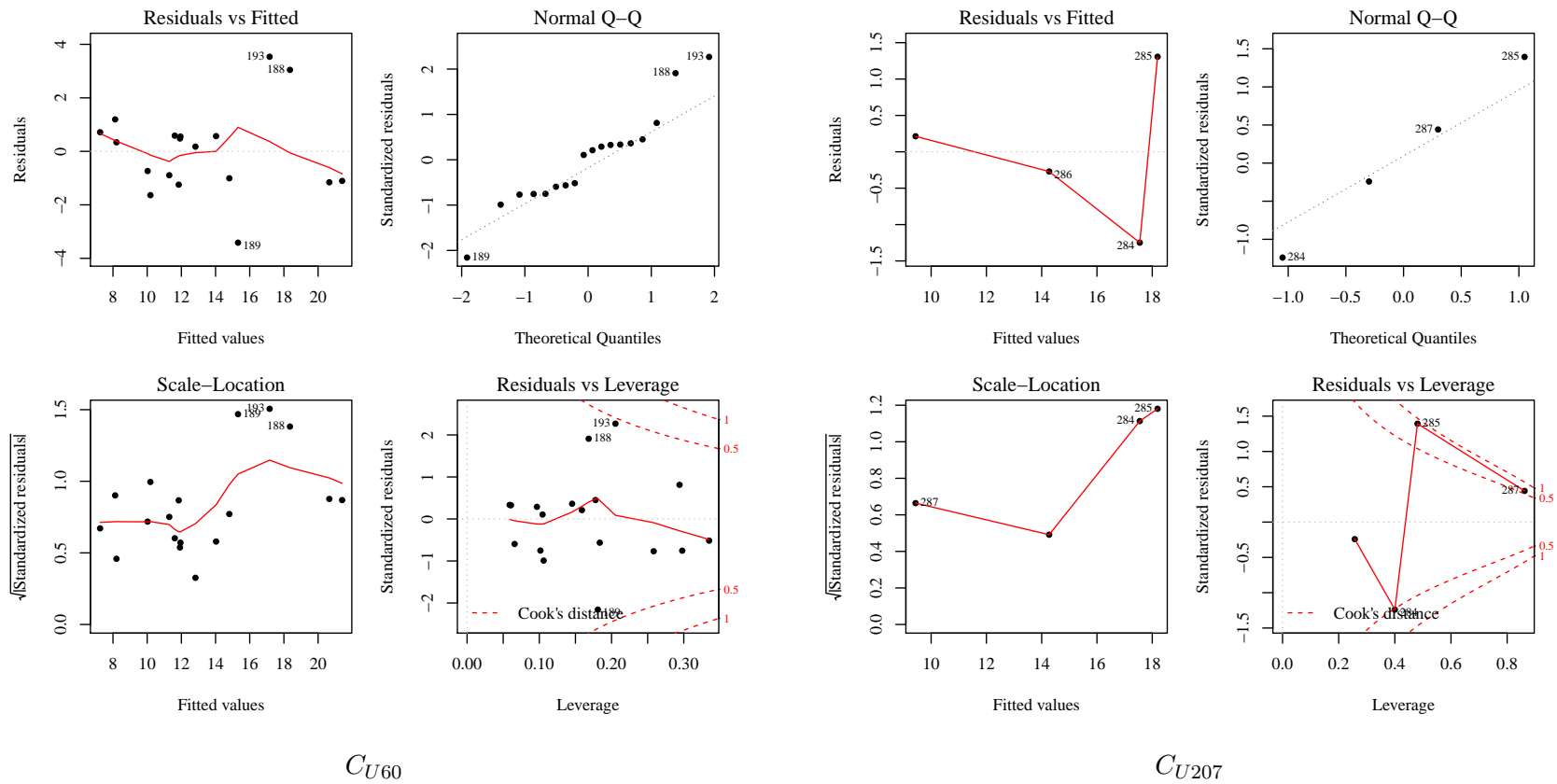


Figure 5.3 (Cont). USR selenium concentration linear model analysis graphs.

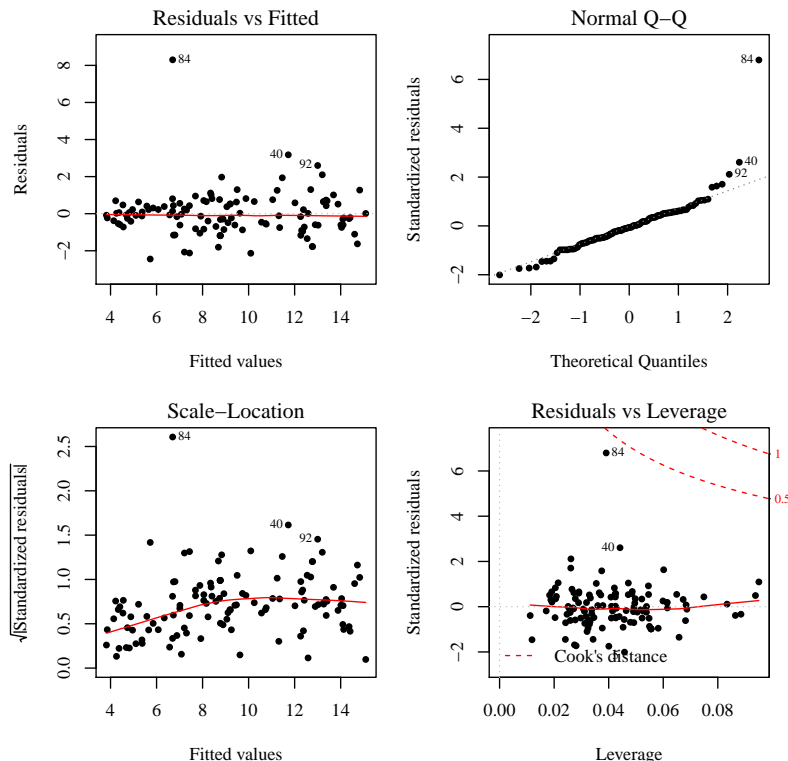


Figure 5.3 (Cont). USR selenium concentration linear model analysis graphs.

$$C_{ARK,d=x}$$

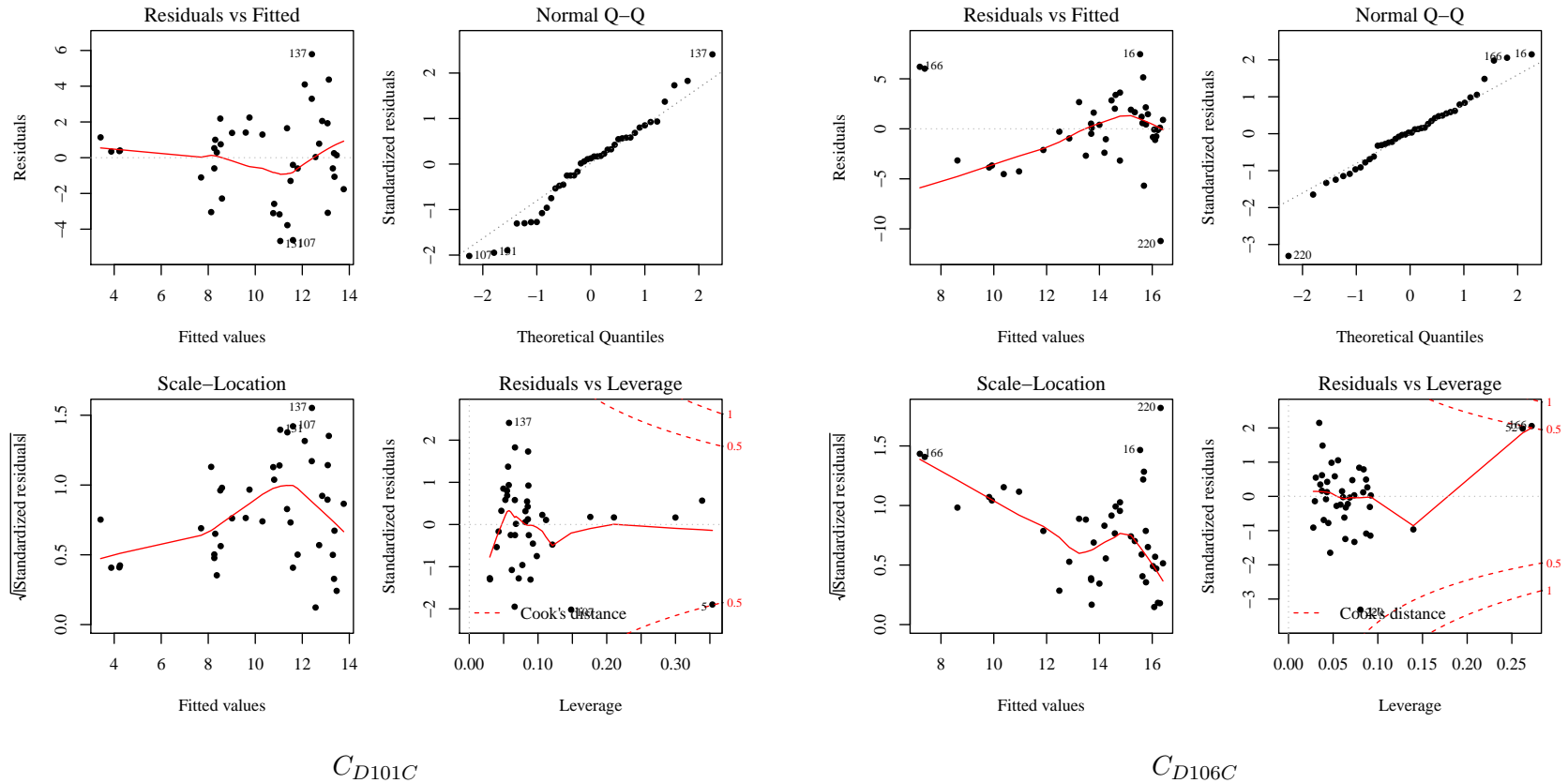


Figure 5.4. DSR selenium concentration linear model analysis graphs. The black lines indicate the stochastic model mean time-series. The blue band indicates the 95% central inter-percentile range (CIR) of the stochastic values. The red dashed line in the flow depth portion of the figure indicates the reported flow depth values.

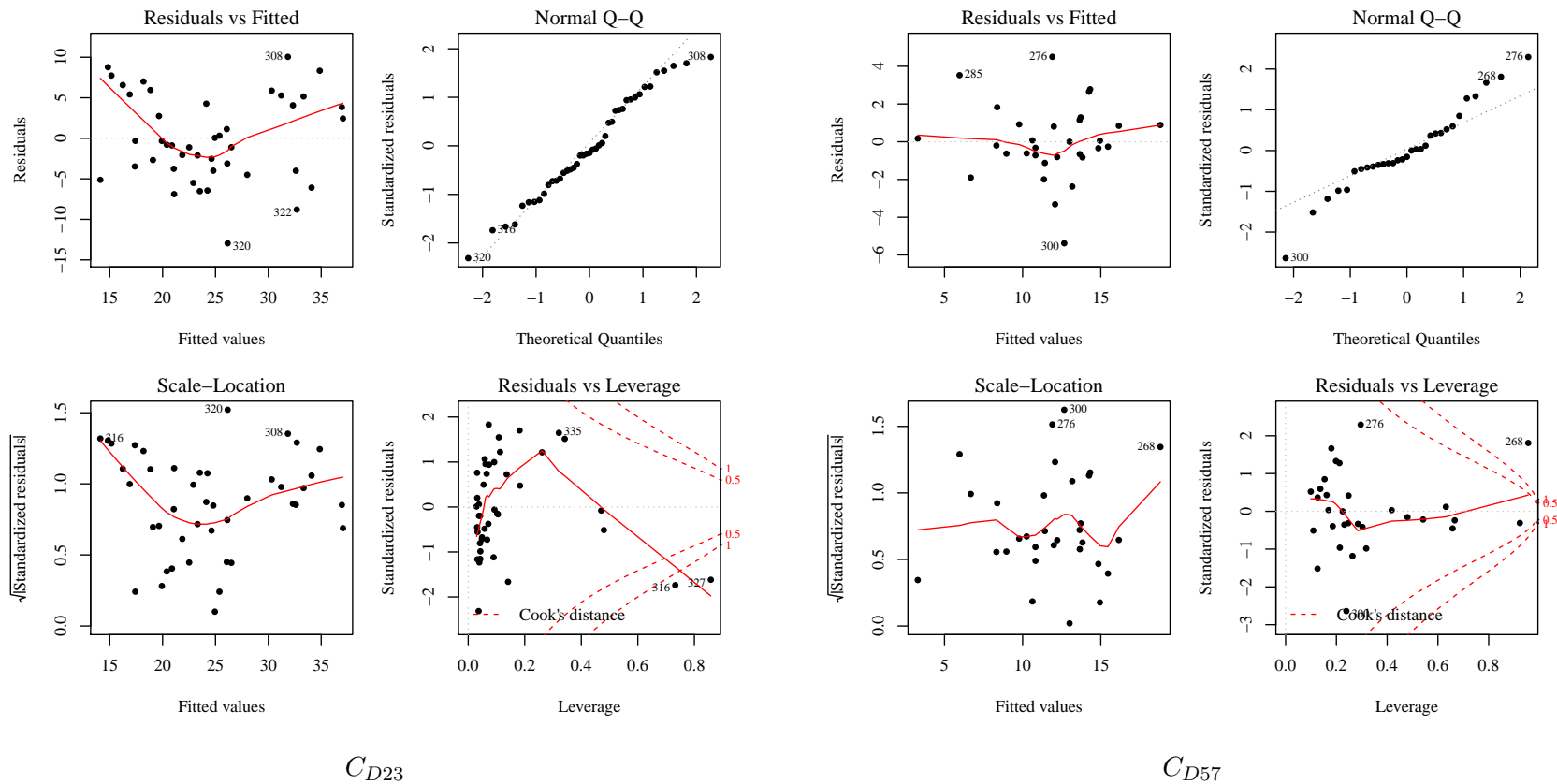
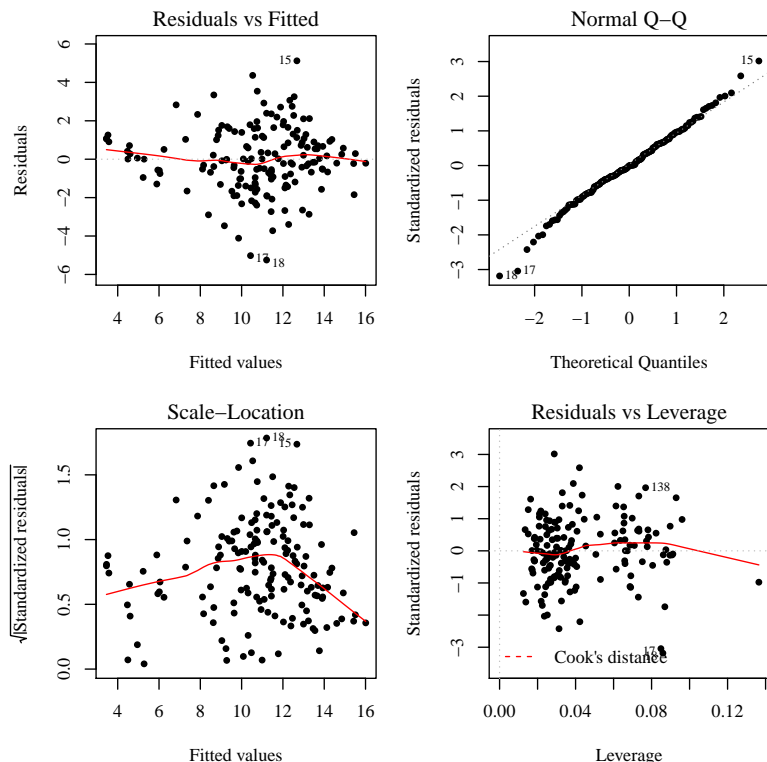


Figure 5.4 (Cont). DSR selenium concentration linear model analysis graphs.

C_{D23}

C_{D57}



$$C_{ARK,d=x}$$

Figure 5.4 (Cont). DSR selenium concentration linear model analysis graphs.

Since the dissolved selenium concentration at the La Junta WWTP is derived using a non-linear equation, the graphs used for linear models are not suitable. In order to prevent a biased comparison between linear and non-linear models and their respective goodness-of-fit, it was determined to judge the model results for the La Junta WWTP selenium

5 concentration on its own merits. The purpose of this model development was to determine which model provided the lowest root mean squared error while simultaneously ensuring that heteroskedasticity was not present. The final $C_{LAJWWTP}$ model was analyzed with the graphs shown in Figure 5.5. The upper sub-figures shows a plot of the fitted values versus the residuals. This plot would show if there was a correlation between these two values,

10 which is heteroskedasticity. The lower sub-figures shows an autocorrelation analysis of the residuals. In a well formed model, the residuals should not be correlated with themselves. Like heteroskedasticity, this indicates that there is a factor missing in the model. Figure 5.5 shows that both heteroskedasticity and autocorrelation are not significant factors in the final $C_{LAJWWTP}$ analysis.

15 The measured concentration values were compared to the predicted concentration values for all regression analyses. Figures 5.6 and 5.6 show the graphs used in this comparison. An $y = x$ line was plotted . Points below the line show that the estimating equation under-estimated the selenium concentration. The vertical distance between the point and the line corresponds to the estimate error, or residual. Similar figures for the other regression

20 analyses are presented in the appendix.

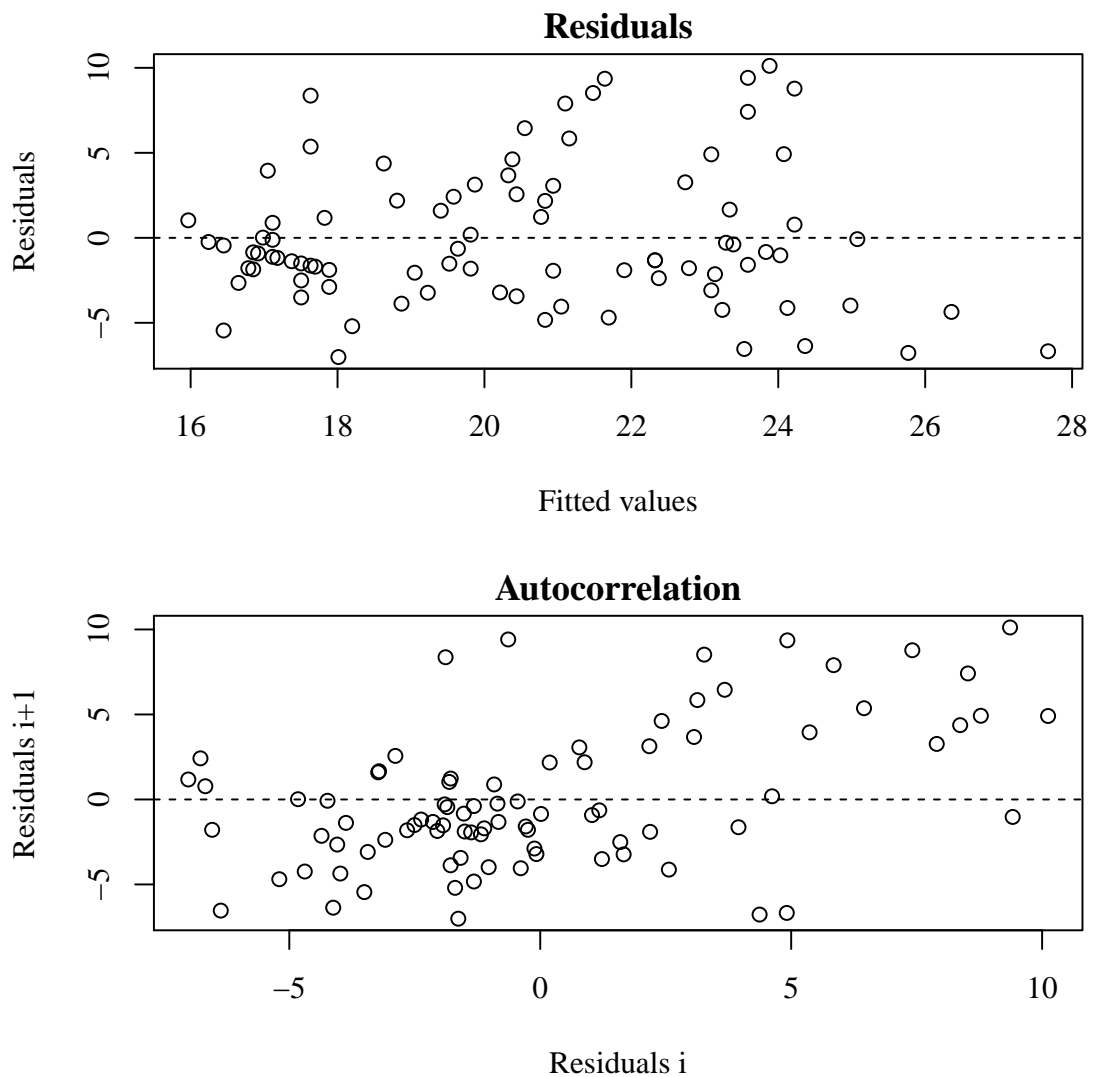


Figure 5.5. La Junta WWTP selenium concentration residuals analysis.

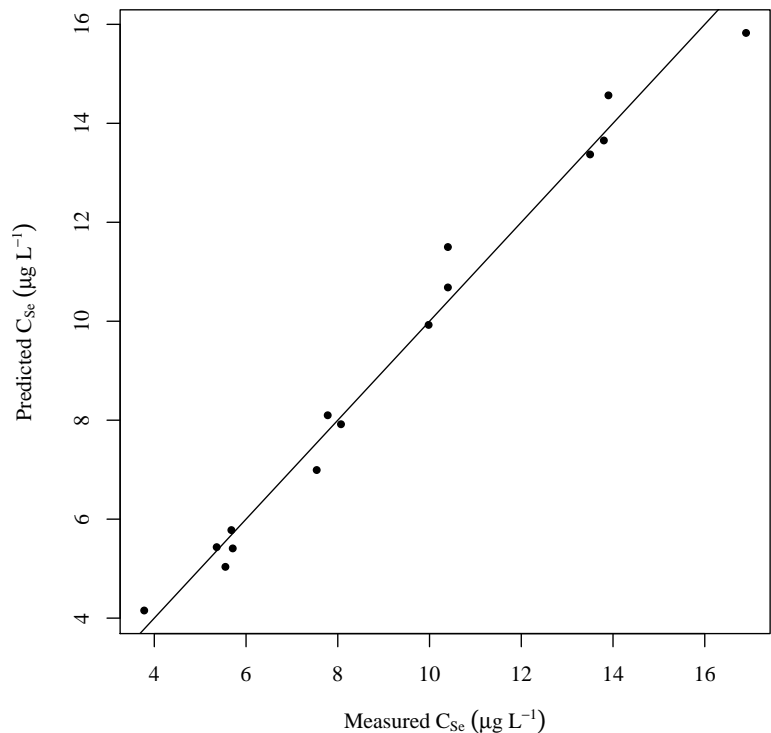
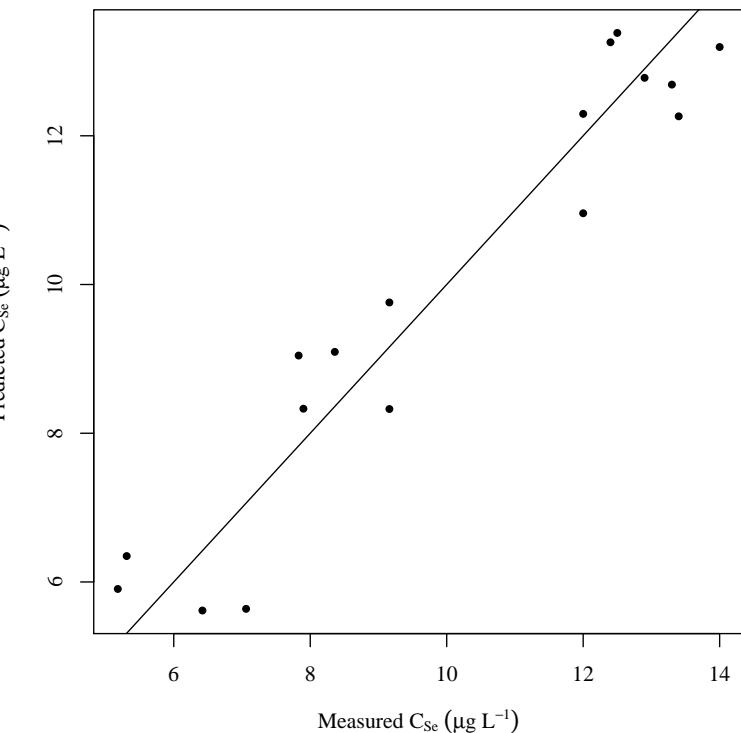
 C_{U163}  C_{U201}

Figure 5.6. USR measured vs. estimated selenium concentration comparison. The predicted values are calculated using the respective final regression equation. The diagonal line has a slope of 1 passing through the origin to show the over or under estimation. All concentrations are presented in $\mu\text{g L}^{-1}$.

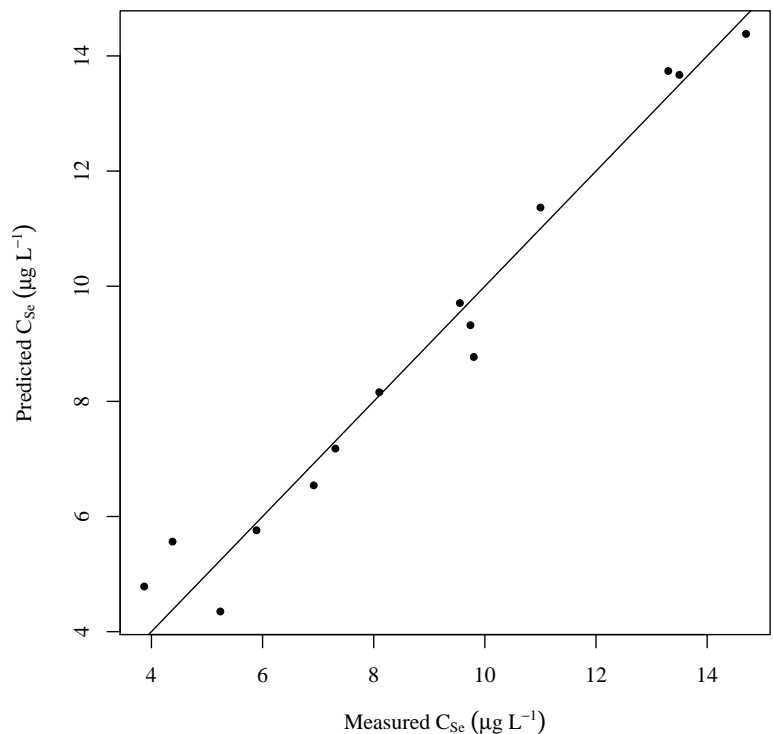
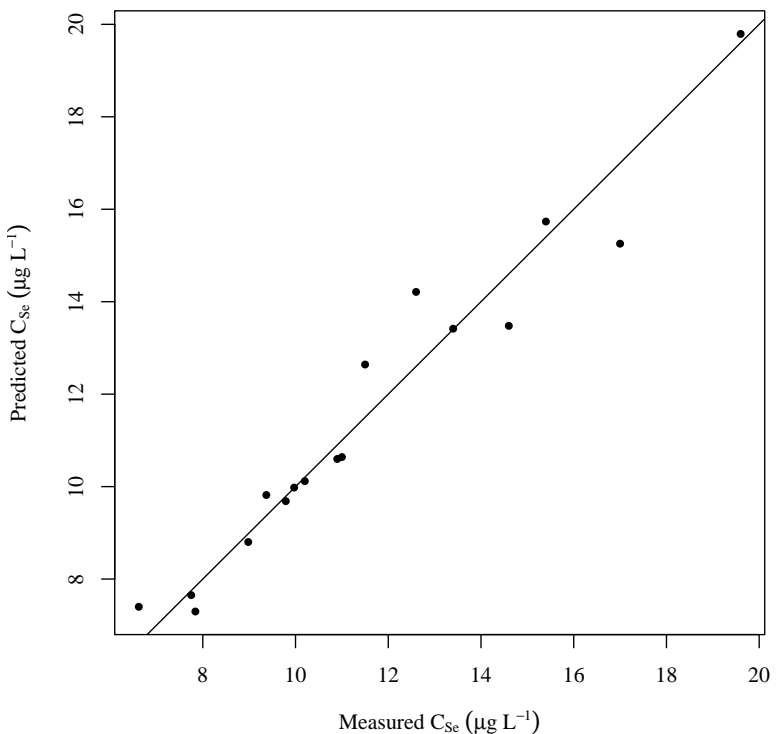
 C_{U167}  C_{U74}

Figure 5.6 (Cont). USR selenium concentration linear model analysis graphs.

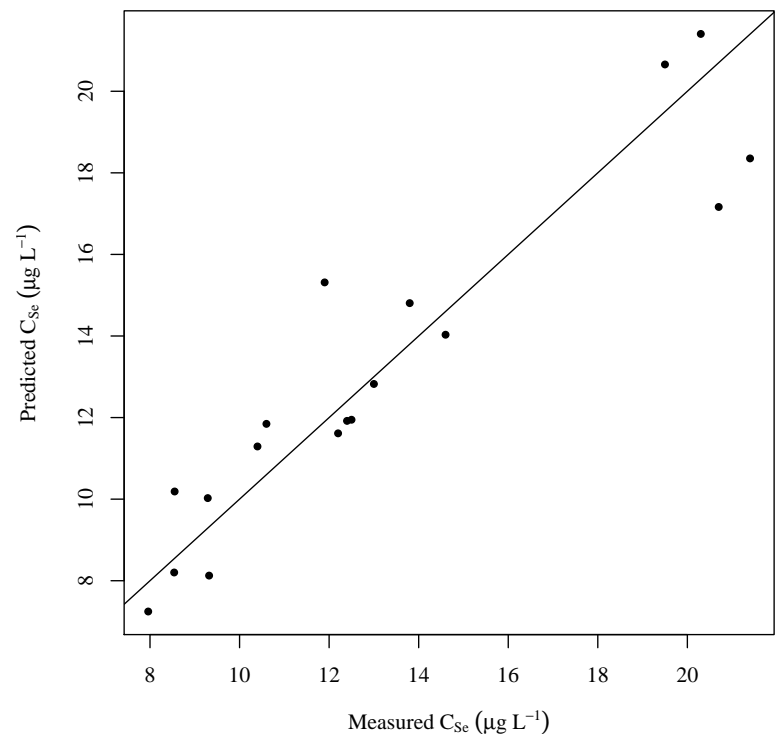
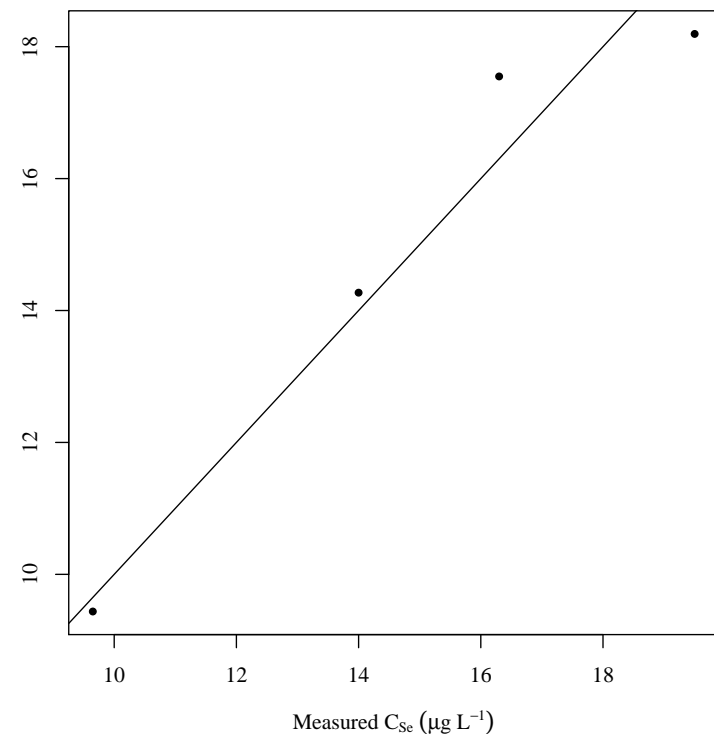
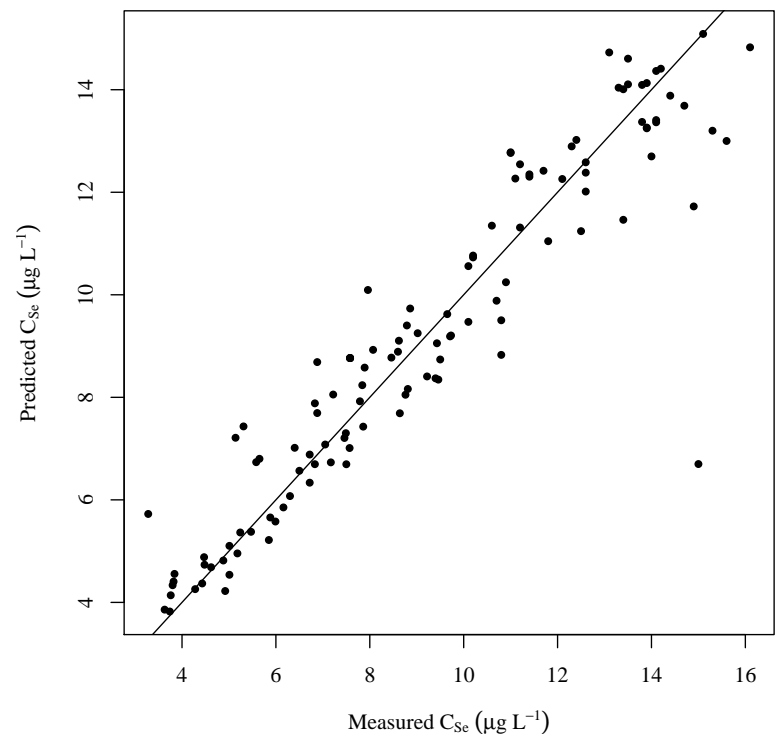
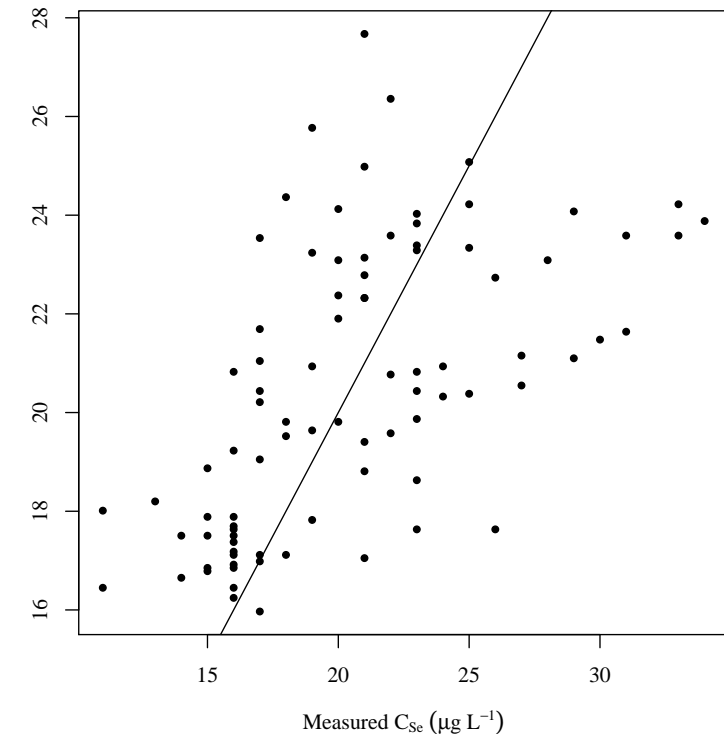
 C_{U60}  C_{U207}

Figure 5.6 (Cont). USR selenium concentration linear model analysis graphs.



$$C_{ARK,d=x}$$



$$C_{LAJWWTP}$$

Figure 5.6 (Cont). USR selenium concentration linear model analysis graphs.

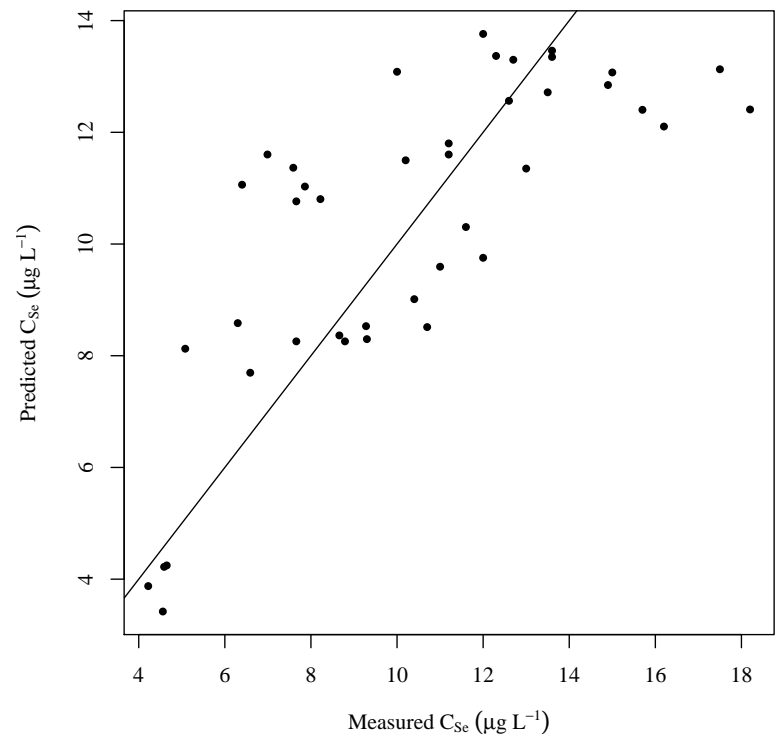
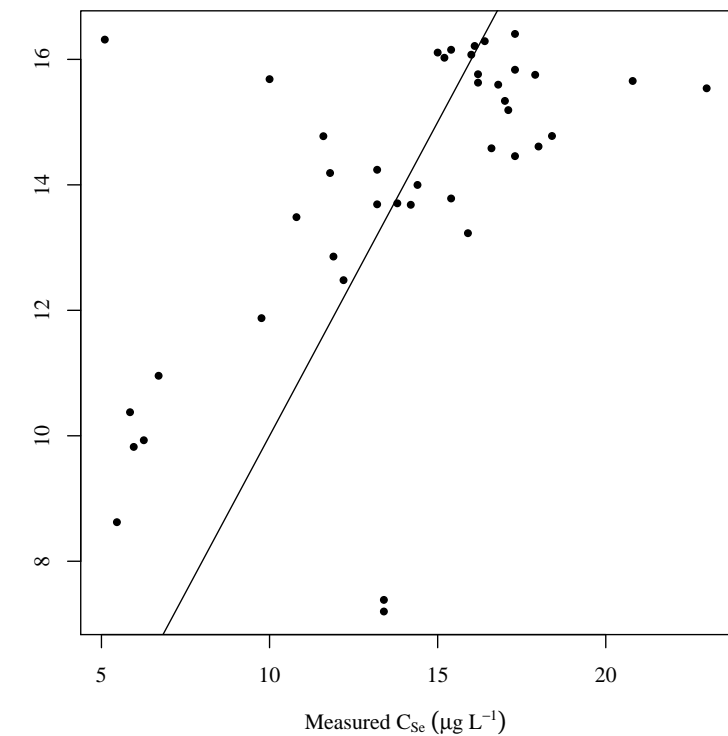
 C_{D101C}  C_{D106C}

Figure 5.7. DSR measured vs. estimated selenium concentration comparison. The predicted values are calculated using the respective final regression equation. The diagonal line has a slope of 1 passing through the origin to show the over or under estimation. All concentrations are presented in $\mu\text{g L}^{-1}$.

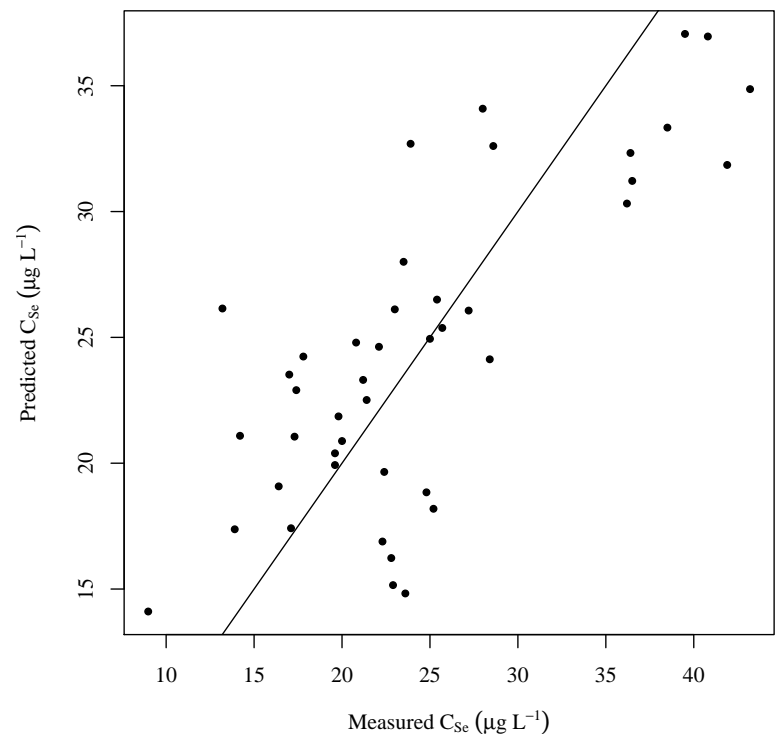
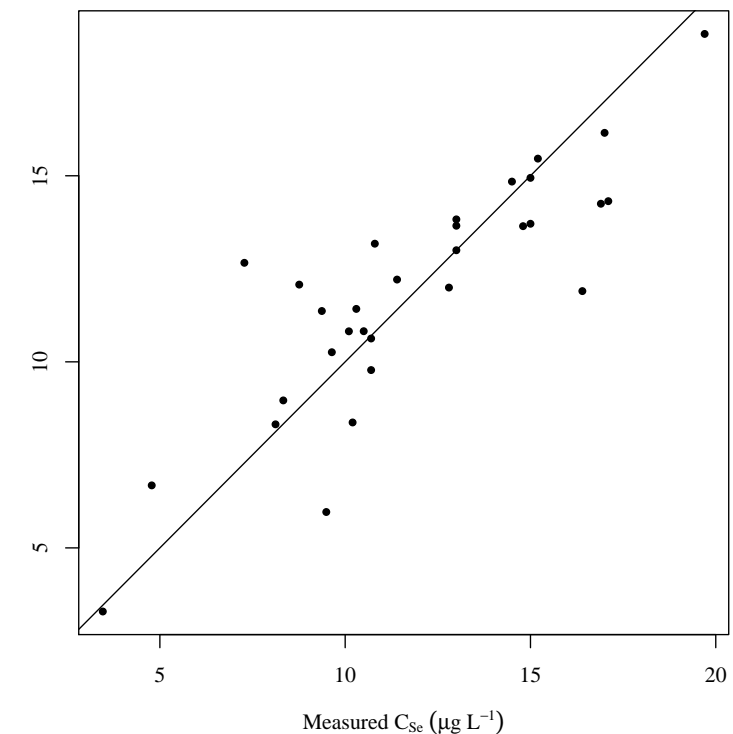
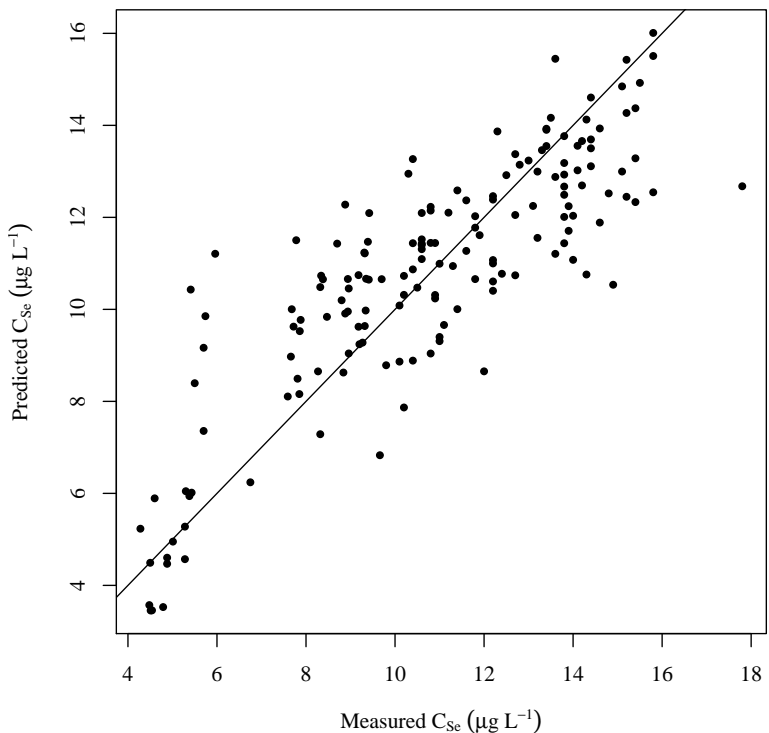
 C_{D23}  C_{D57}

Figure 5.7 (Cont). DSR selenium concentration linear model analysis graphs.



$$C_{ARK,d=x}$$

Figure 5.7 (Cont). DSR selenium concentration linear model analysis graphs.

Each of the dissolved selenium estimating equations is accompanied by two uncertainty values as shown in Equation 40. The uncertainty found in the regression equation ε_1 is due solely to the inability of the regression equation to accurately describe the measured dissolved selenium concentration values.

$$C_x + \varepsilon_1 + \varepsilon_2 \quad (40)$$

Where:

C_x = A calculated concentration value. X denotes any one of the concentration locations.

ε_1 = Uncertainty found in the regression equation.

ε_2 = Uncertainty in the measured dissolved selenium concentration lab values.

Selenium estimation calculation error, ε_1 was analyzed to determine the best fit distribution for each selenium estimating equation. Normal and logistic distributions were fit to the regression model residuals. Both of these distributions are unbounded and are simple to apply. They also fit the assumption that the linear model residuals are normally distributed. Logistic distributions were included because they are very similar to normal distributions, but with heavier tails. The best-fit normal and logistic distributions were compared to the regression model residuals by using Kolmogorov-Smirnov, Cramer von Mises, and Anderson-Darling goodness-of-fit tests. The results of these tests determined which of either the best fit normal distribution or best fit logistic distribution described the regression model residuals.

Results from the goodness-of-fit tests are presented in Tables 5.9 and 5.10 for the USR and DSR, respectively

Table 5.9. USR selenium concentration residuals goodness-of-fit test results. Kolmogorov-Smirnov (K-S), Cramer von Mises (CvM), and Anderson-Darling (AD) test statistics are presented for each regression model.

Concentration	Tested Distribution	Test Statistics		
		K-S	CvM	A-D
C_{U163}	Logistic*	0.107	0.022	0.151
	Normal	0.116	0.028	0.197
C_{U201}	Logistic*	0.180	0.129	0.766
	Normal	0.178	0.140	0.792
C_{U167}	Logistic*	0.091	0.020	0.165
	Normal	0.100	0.025	0.192
C_{U74}	Logistic*	0.136	0.053	0.315
	Normal	0.140	0.076	0.419
C_{U60}	Logistic*	0.128	0.076	0.476
	Normal	0.161	0.086	0.548
$C_{ARK,d=x}$	Logistic*	0.041	0.032	0.352
	Normal	0.109	0.354	2.47
$C_{LAJWWTP}$	Logistic*	0.090	0.163	1.22
	Normal	0.130	0.281	1.57

* = best fit distribution

Table 5.10. DSR selenium concentration residuals goodness-of-fit test results. Kolmogorov-Smirnov (K-S), Cramer von Mises (CvM), and Anderson-Darling (AD) test statistics are presented for each regression model.

Location	Tested Distribution	Test Statistics		
		K-S	CvM	A-D
C_{D101C}	Logistic	0.0923	0.038	0.263
	Normal*	0.090	0.378	0.259
C_{D106C}	Logistic*	0.082	0.289	0.199
	Normal	0.110	0.060	0.384
C_{D23}	Logistic	0.103	0.082	0.508
	Normal*	0.092	0.073	0.426
C_{D57}	Logistic*	0.117	0.058	0.340
	Normal	0.140	0.093	0.518
$C_{ARK,d=x}$	Logistic*	0.041	0.020	0.112
	Normal	0.043	0.050	0.319

* = best fit distribution

Table 5.11. USR selenium concentration residual distribution summary statistics.

Concentration	Best Fit Distribution	n	Parameter Estimate	
			Param. 1 ¹	Param. 2 ²
C_{U163}	Logistic	15	5.7×10^{-3}	0.2810
C_{U201}	Logistic	17	-3.0×10^{-2}	0.5365
C_{U167}	Logistic	14	1.5×10^{-2}	0.3383
C_{U74}	Logistic	17	1.7×10^{-3}	0.4049
C_{U60}	Logistic	18	-6.3×10^{-2}	0.8743
$C_{ARK,d=x}$	Logistic	135	-5.2×10^{-2}	0.5615
$C_{LAJWWTP}$	Logistic	87	-3.8×10^{-1}	2.313

¹ For normal distributions, mean. For logistic distributions, location.

² For normal distributions, standard deviation. For logistic distributions, scale.

The summaries of the fitted distributions are presented in Tables 5.11 and 5.12, for

the USR and DSR respectively. In all but one case, the location parameters are near zero.

The location parameter for logistic distributions and the mean parameter for normal distributions provide the same information; they describe the central tendency of the distribution.

- 5 For distributions that describe model error, the goal is to have this value near zero. The location parameter for the La Junta WWTP selenium concentration error distribution is a significant distance from zero. The selenium concentration lab results minimum detection level is $0.4 \mu\text{g L}^{-1}$ and the La Junta WWTP location parameter approaches this value. This indicates that the selenium concentration estimating model for the La Junta WWTP
- 10 is missing an estimating parameter. Unfortunately, no other parameters were available for the collected data.

Statistical plots of the residual distributions, shown in Figures 5.8 and 5.8, were created to visually analyze the data distribution and determine if the chosen distribution represented the data for the USR and DSR, respectively. These figures are diagnostic plots

15 that are produced by statistical software. They were not altered or customized. The top left panel shows a histogram of the residuals. The red curve is the chosen best-fit distribution.

Table 5.12. DSR selenium concentration residual distribution summary statistics.

Concentration	Best Fit Distribution	n	Parameter Estimate	
			Param. 1 ¹	Param. 2 ²
C_{D101C}	Normal	42	-1.7×10^{-17}	2.429
C_{D106C}	Logistic	42	7.5×10^{-2}	1.834
C_{D23}	Normal	43	-1.2×10^{-16}	5.289
C_{D57}	Logistic	31	-8.4×10^{-3}	1.026
$C_{ARK,d=x}$	Logistic	163	1.2×10^{-2}	0.9364

¹ = For normal distributions, mean. For logistic distributions, location.

² = For normal distributions, standard deviation. For logistic distributions, scale.

The bottom left panel shows the cumulative distribution function of the chosen distribution in red. The points represent the actual collected data. In a well fit distribution, the points should lie on or near the fitted distribution cumulative distribution function line. The top right panel shows the well known quantile-quantile plot. This is a visual test for normalcy.

- 5 The points should lie on or near the line $y = x$ if the distribution is normal. The focus on this panel is to see how well the tails fit a normal distribution. The bottom right panel is a probability-probability plot. This is also a visual test for normalcy and the points should lie on or near the line $y = x$ if the distribution is normal. The focus on this panel is to see how well the center of the data fits a normal distribution.

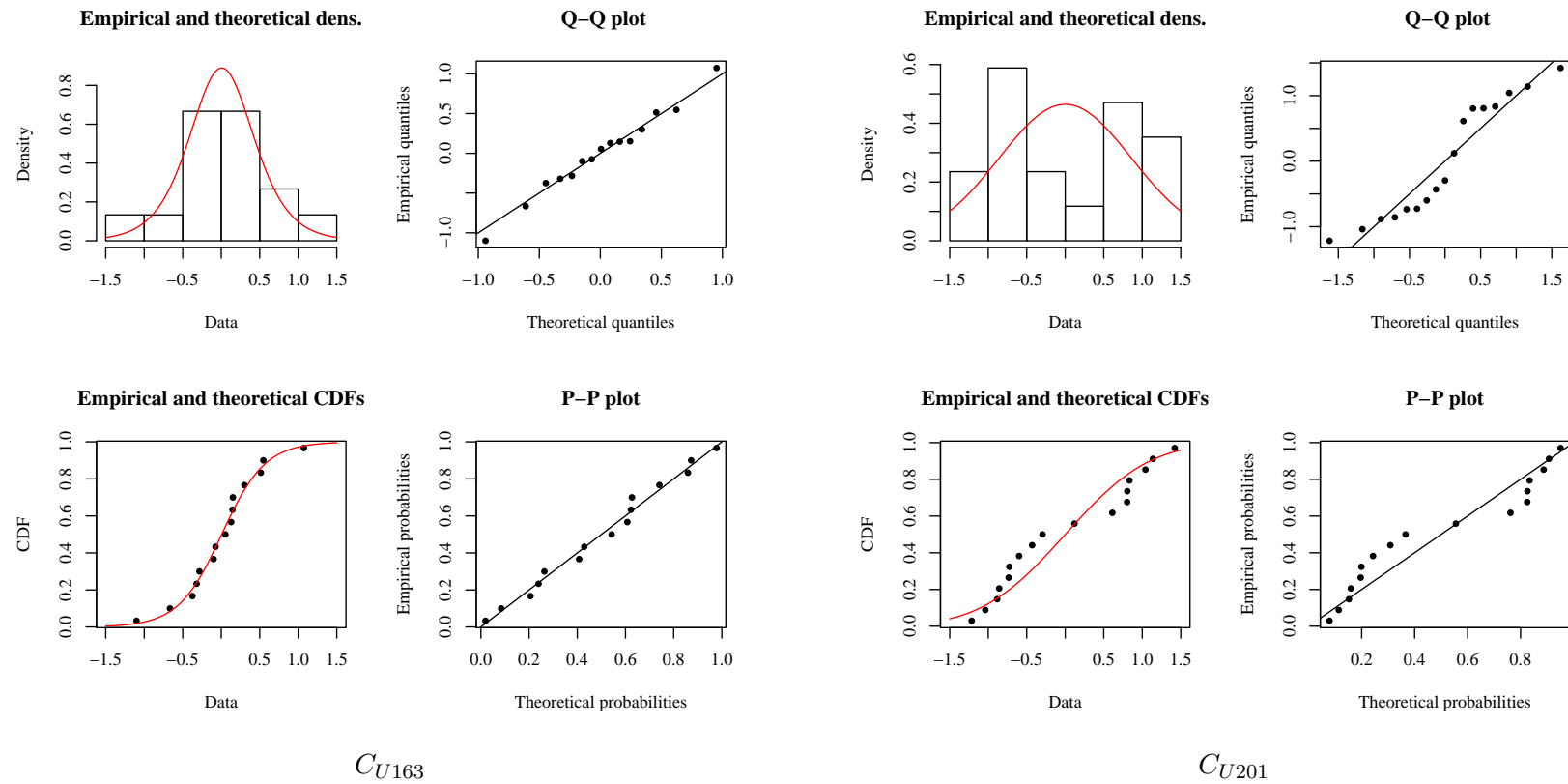


Figure 5.8. USR upstream boundary selenium estimate residual distribution analysis. The top left plot is a histogram of the residuals with the estimated logistic distribution plotted over top. The top right plot is a quantile-quantile (Q-Q). The bottom left is a plot of the theoretical cumulative distribution function (CDF) against the empirical CDF. The bottom right is a probability-probability plot.

C_{U163}

C_{U201}

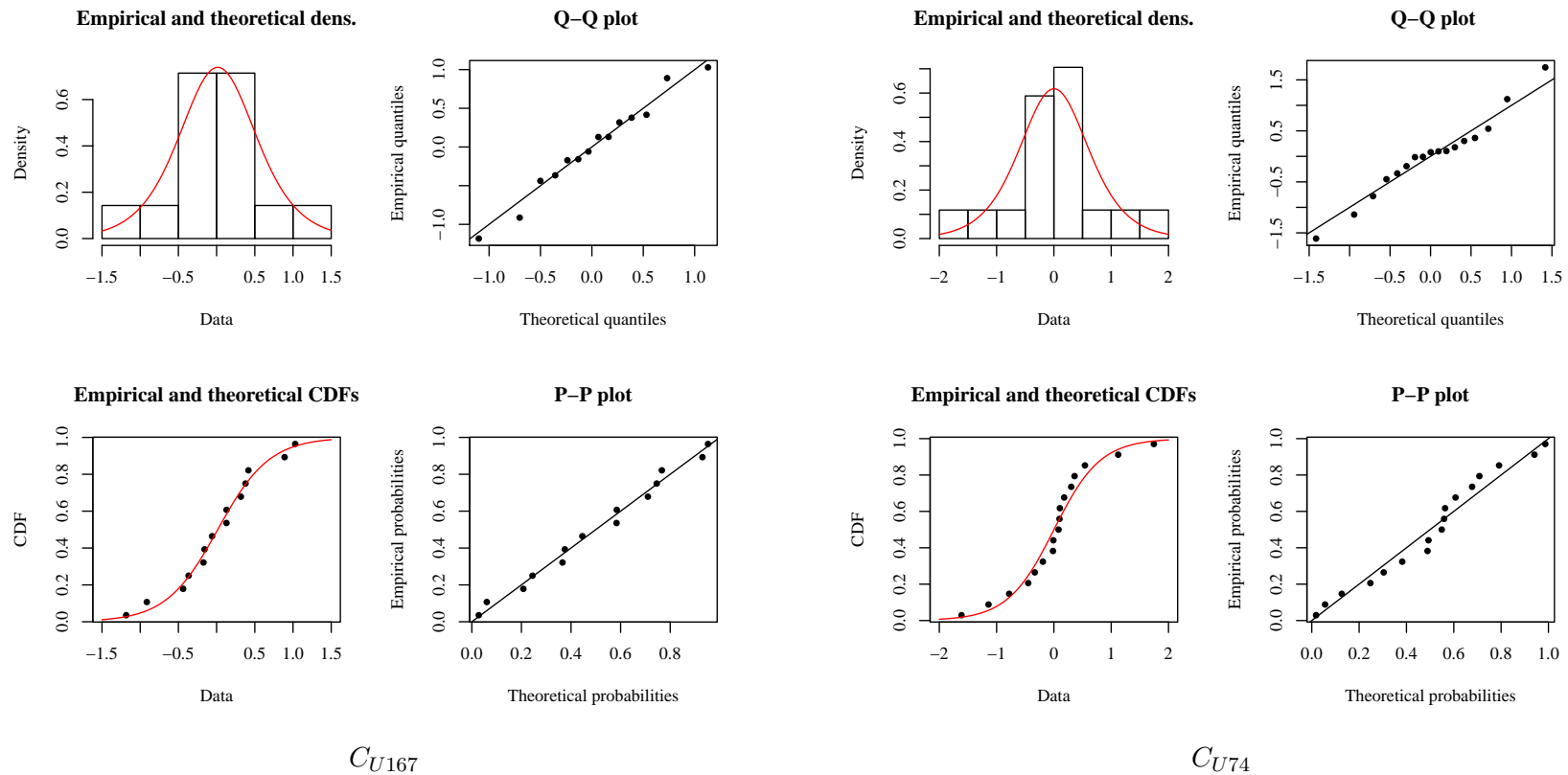


Figure 5.8 (Cont). USR upstream boundary selenium estimate residual distribution analysis.

C_{U167}

C_{U74}

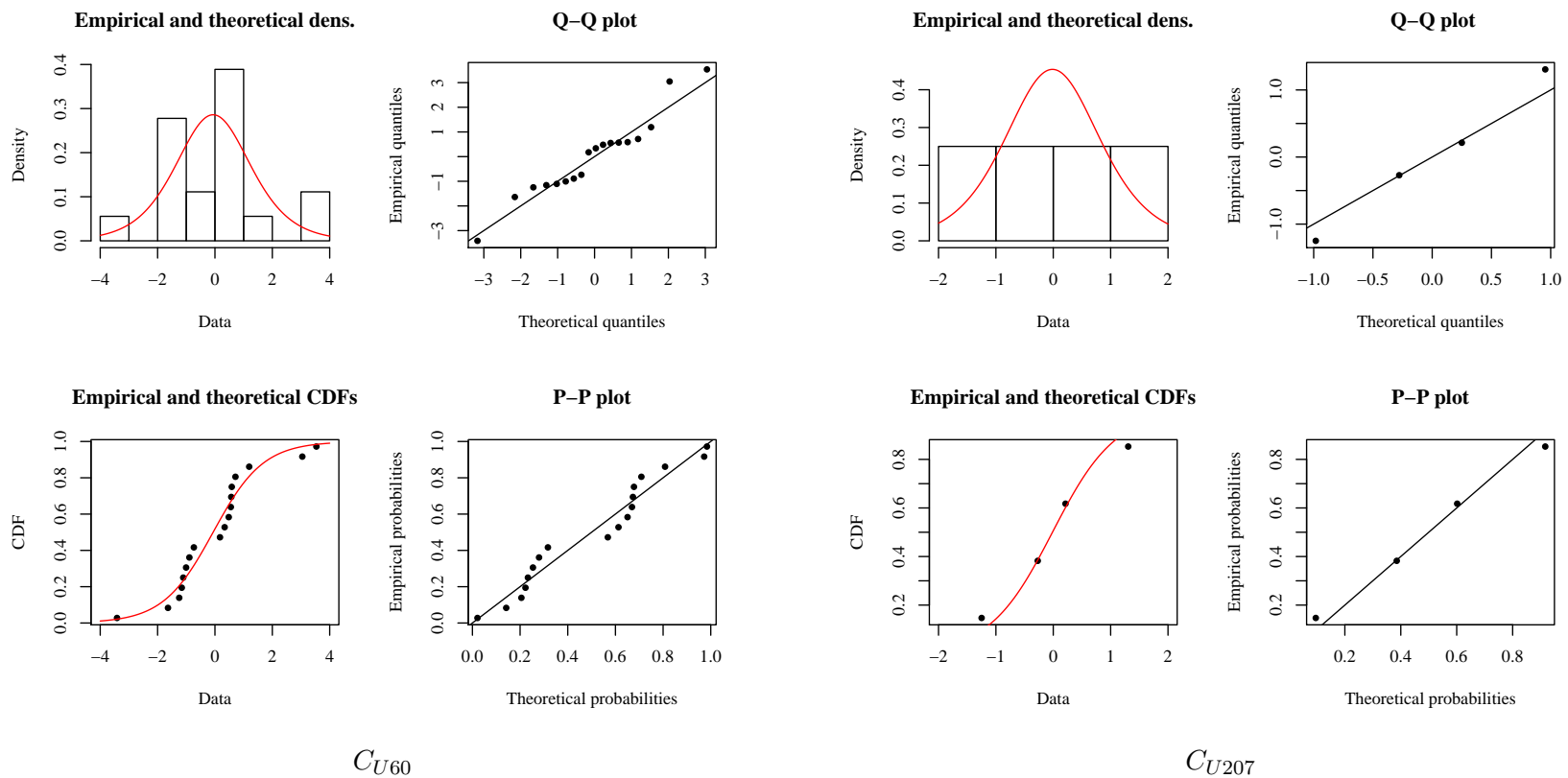


Figure 5.8 (Cont). USR upstream boundary selenium estimate residual distribution analysis.

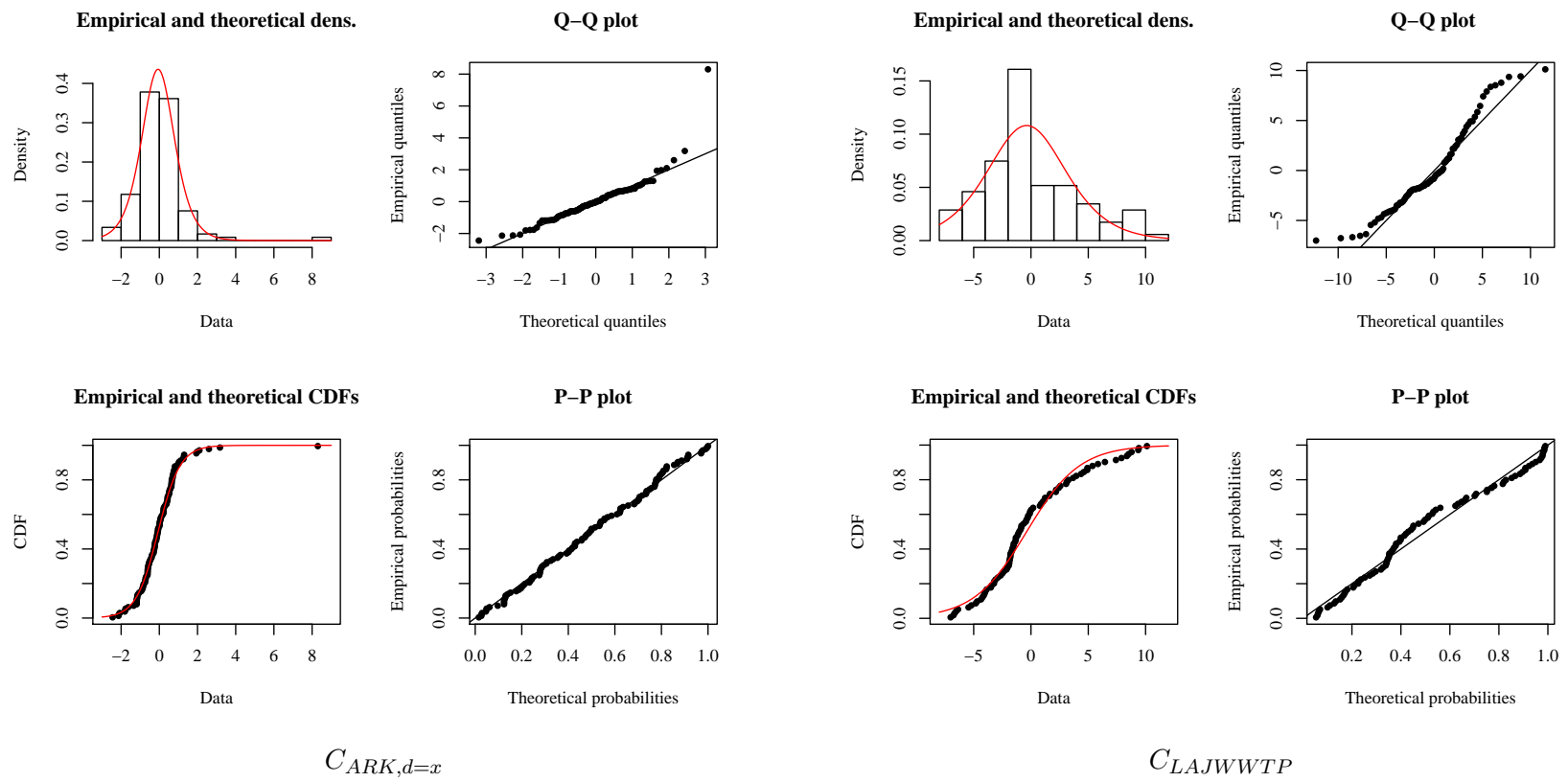


Figure 5.8 (Cont). USR upstream boundary selenium estimate residual distribution analysis.

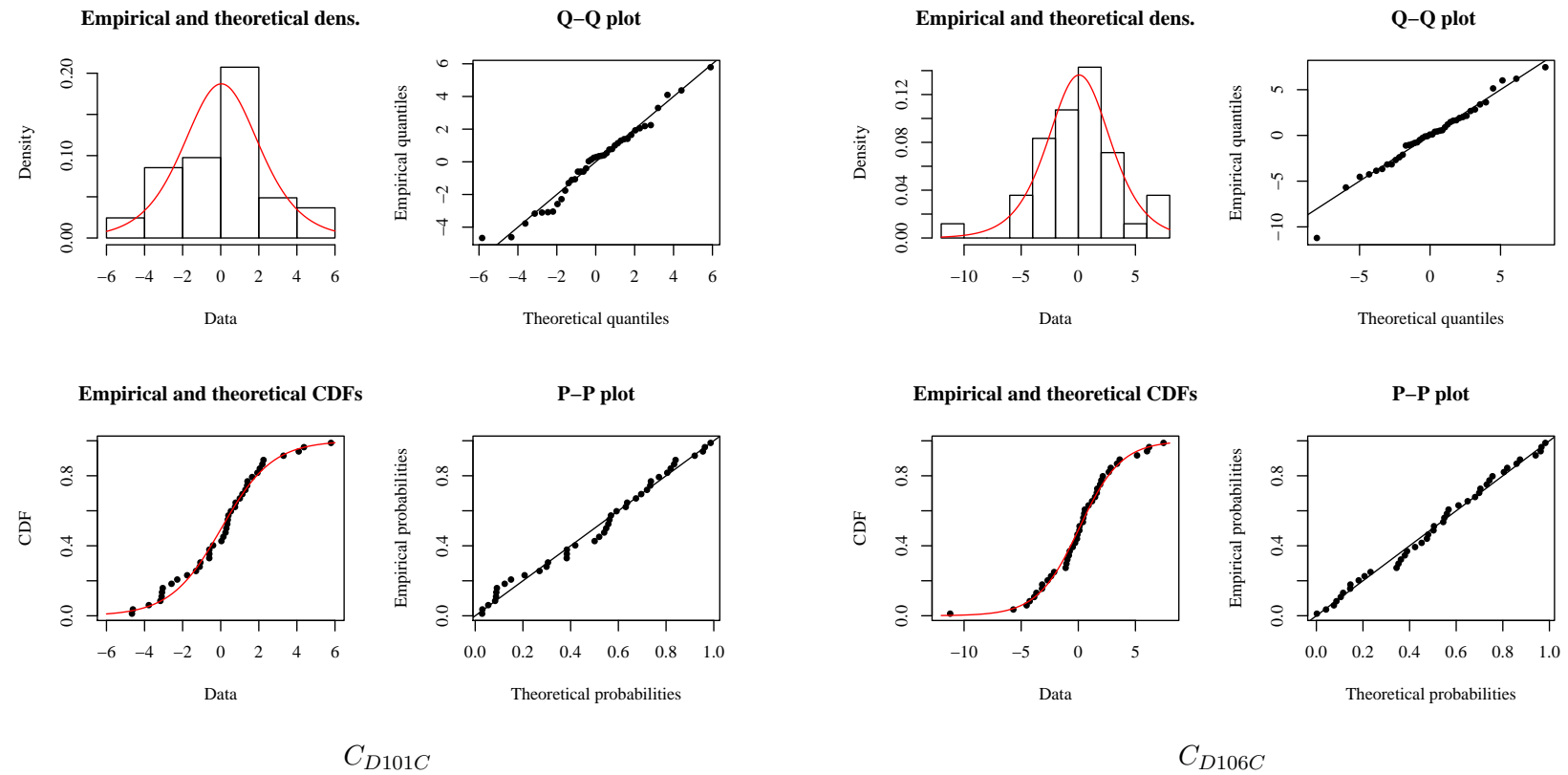


Figure 5.9. DSR upstream boundary selenium estimate residual distribution analysis. The top left plot is a histogram of the residuals with the estimated logistic distribution plotted over top. The top right plot is a quantile-quantile (Q-Q). The bottom left is a plot of the theoretical cumulative distribution function (CDF) against the empirical CDF. The bottom right is a probability-probability plot.

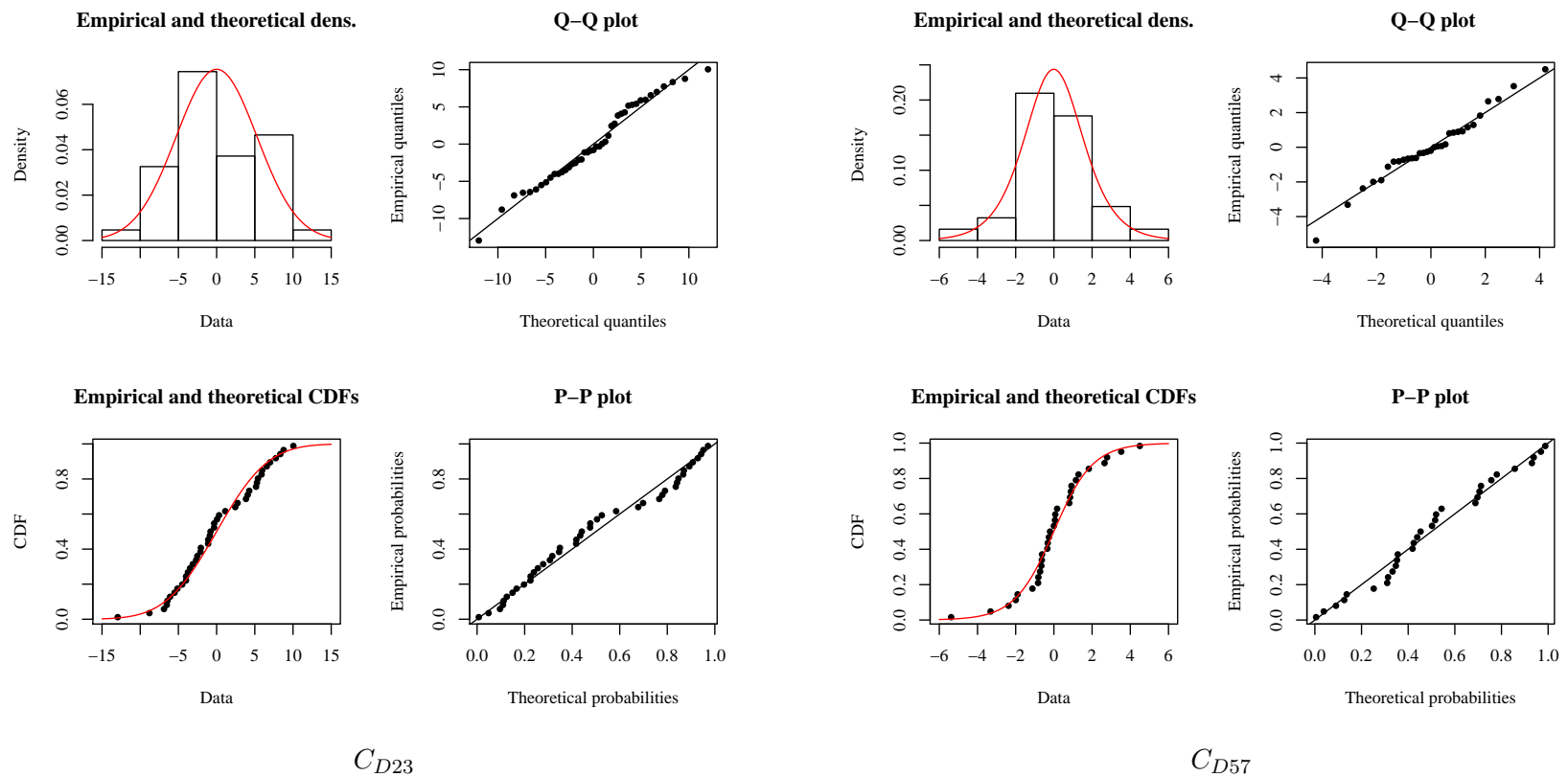
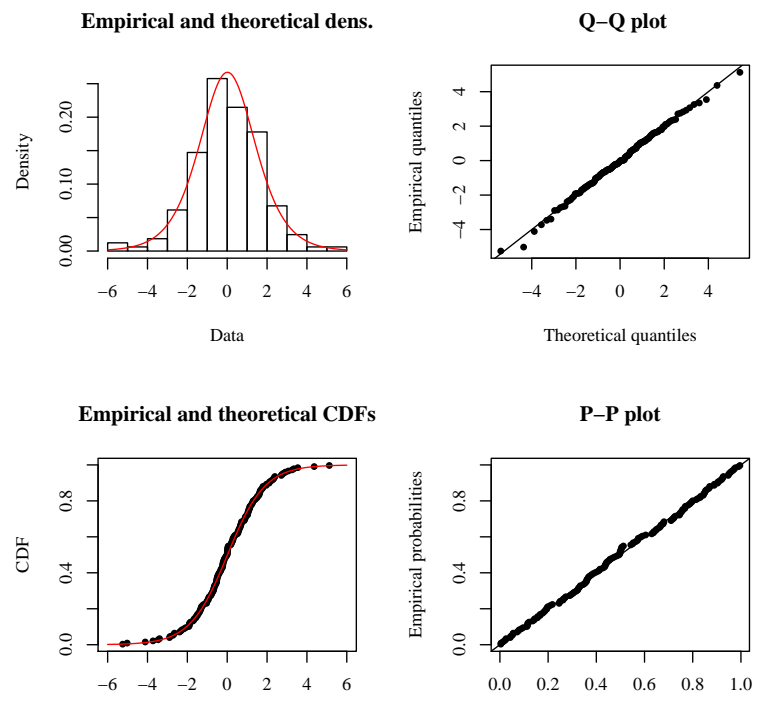


Figure 5.9 (Cont). DSR upstream boundary selenium estimate residual distribution analysis.



$$C_{ARK,d=x}$$

Figure 5.9 (Cont). DSR upstream boundary selenium estimate residual distribution analysis.

A number of the chosen residual distributions do not appear to fit the data. The residuals for the USR outlet appear to not be normally distributed. The distributions for CANSWKCO and TIMSWICO do not appear to be good fits. The data and distribution for HRC194CO does not have enough data to allow for a conclusive analysis. For the most 5 part, the lack of a good fit can be traced back to data collection. First, for the poorly fit distributions, there was insufficient data collected. Second, there was a tendency for the samples to be taken during the same time frame each year. If selenium concentration is seasonal, then the samples should have been taken relatively equally spaced throughout the year to capture the seasonal variation.

10 These selenium concentration error distributions were not discarded due to these findings. It was assumed that the error could be best described by the best fit distributions determined in this analysis. Future data should be included in future analyses to develop more accurate estimation models and error distribution.

To test statistical software's ability to generate the required distribution, residuals 15 were plotted as a histogram overlain with a kernel density estimate as shown in Figures 5.10 and 5.11 for the USR and DSR, respectively. The black line is the kernel density estimate of the residuals. The red line is the kernel density estimate of 5000 draws from the best fit regression model. In spite of the earlier findings that some of the best fit selenium concentration error distributions are not good fits, all graphs visually indicated that the 20 fitted distributions are not as poor as expected.

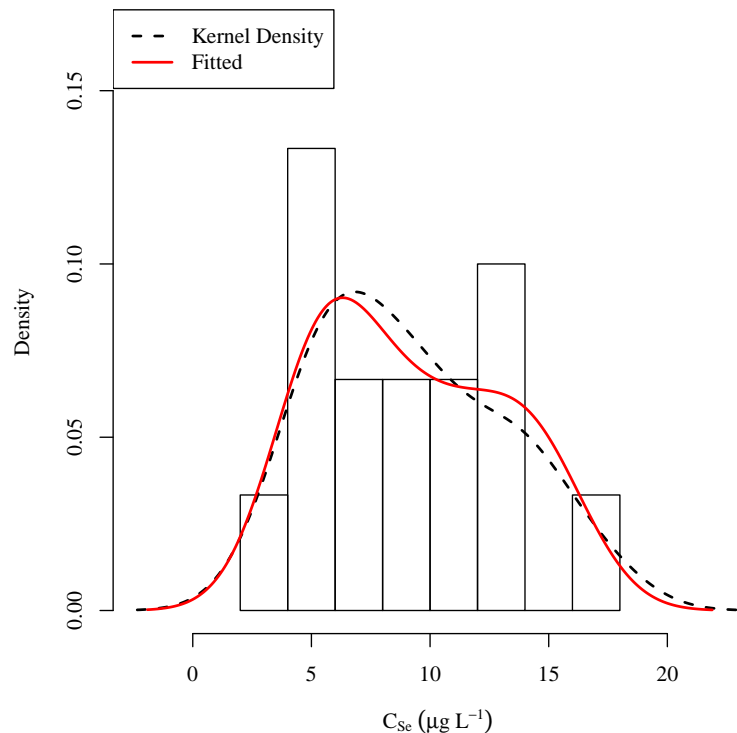
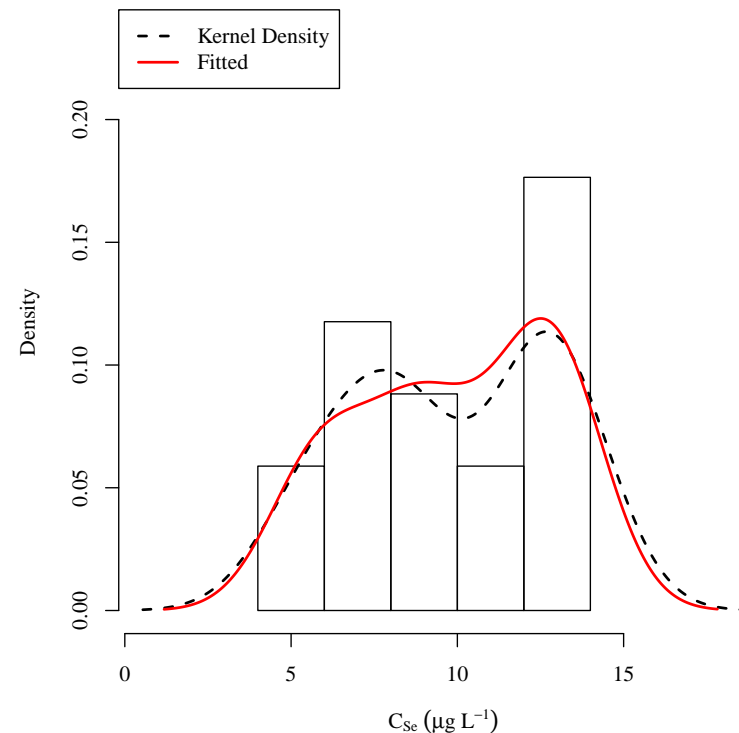
 C_{U163}  C_{U201}

Figure 5.10. USR selenium estimate residual histogram. The kernel density of the residuals is plotted over the histogram. Similar plots for the rest of the linear model analyses are included in the appendix.

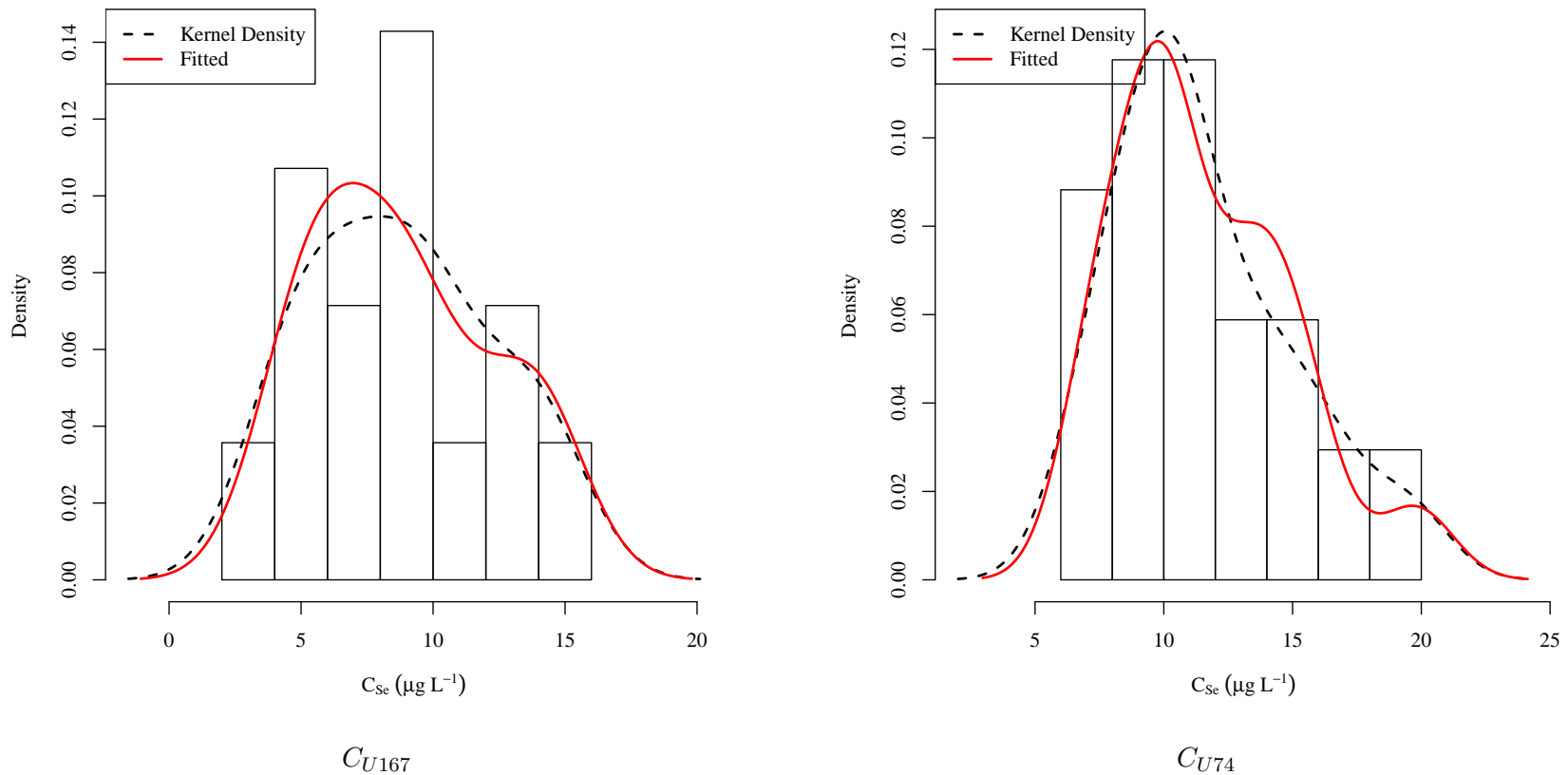


Figure 5.10 (Cont). USR selenium estimate residual histogram.

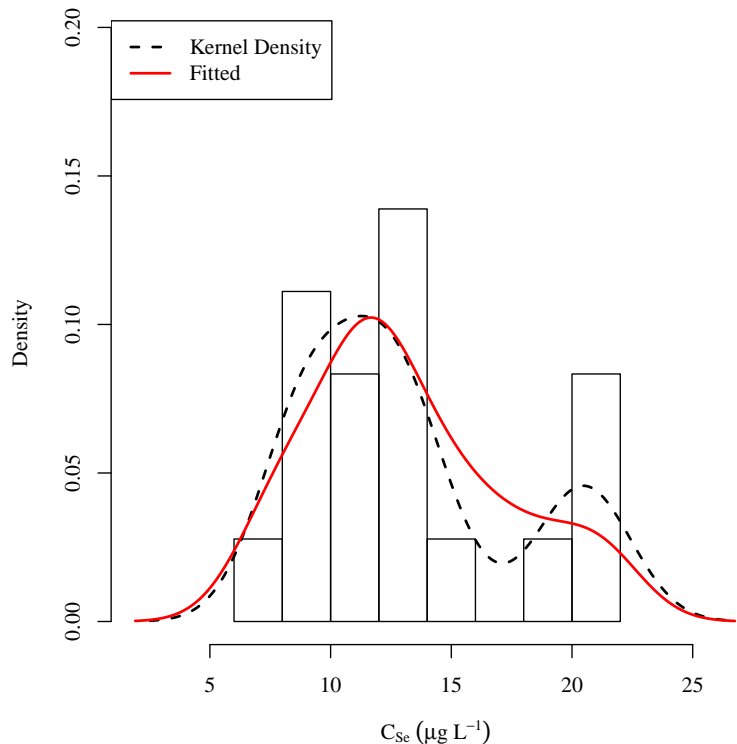
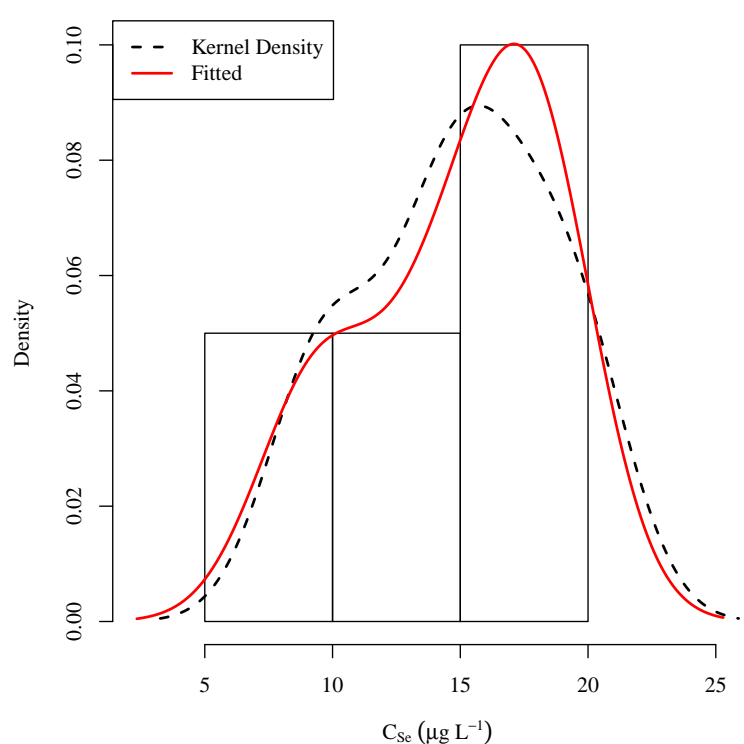
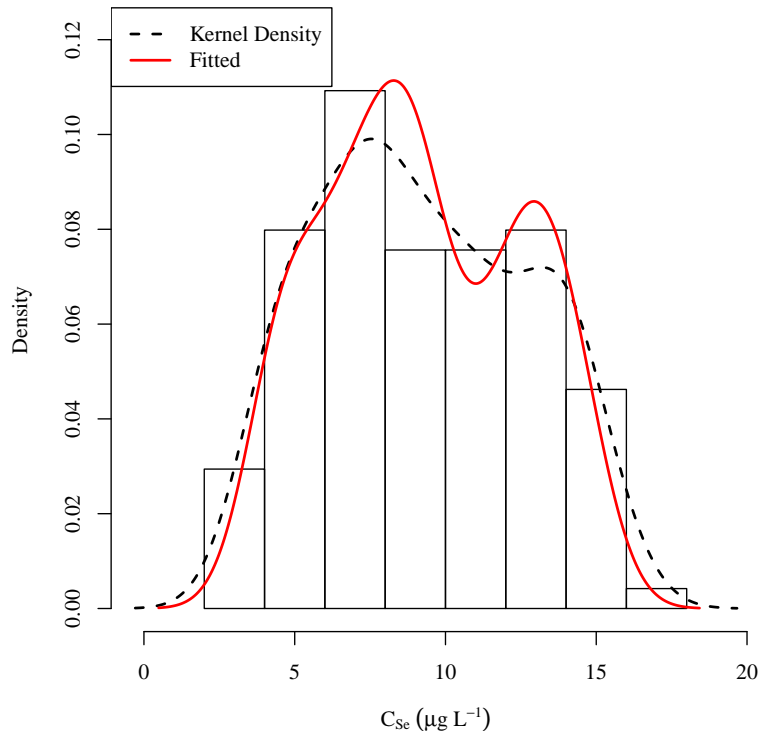
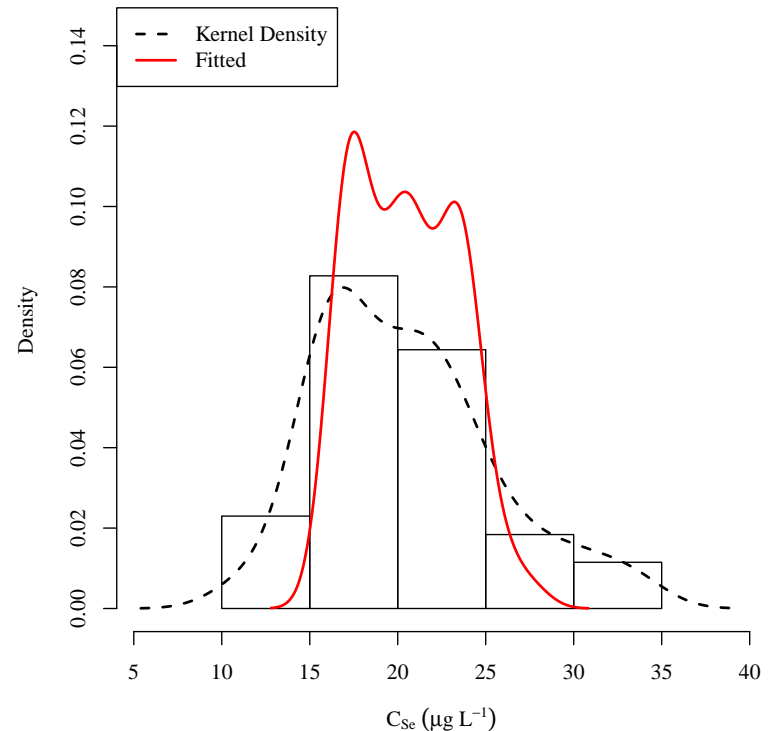
 C_{U60}  C_{U207}

Figure 5.10 (Cont). USR selenium estimate residual histogram.



$$C_{ARK,d=x}$$



$$C_{LAJWWTP}$$

Figure 5.10 (Cont). USR selenium estimate residual histogram.

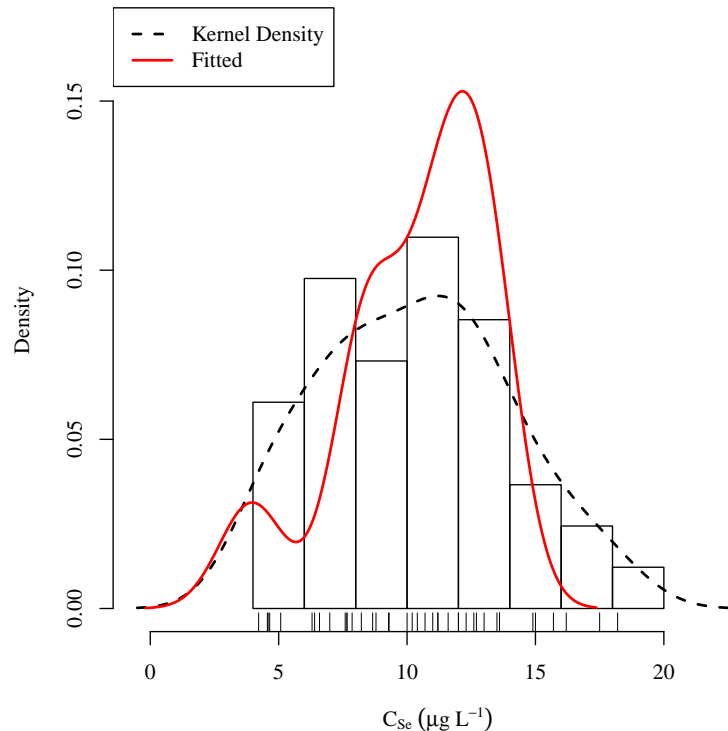
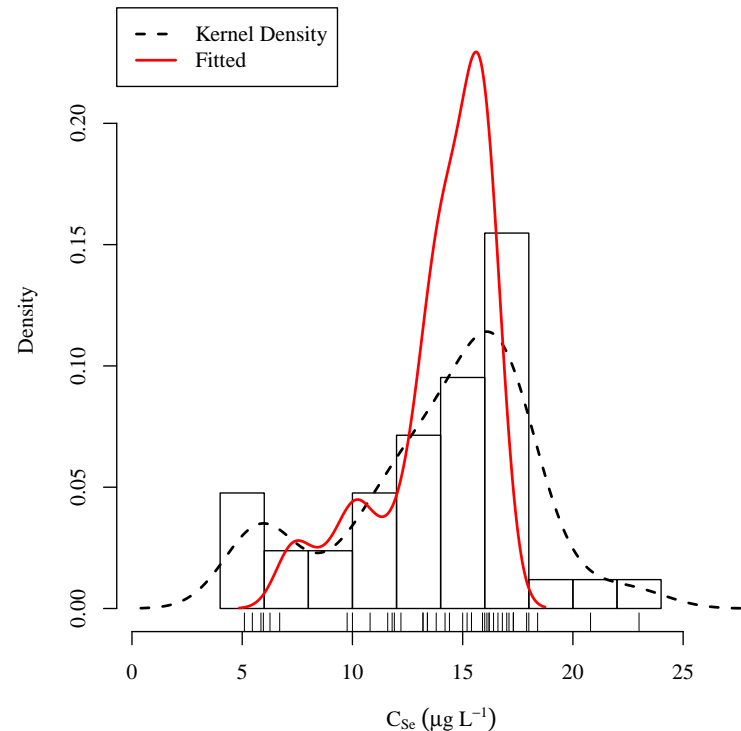
 C_{D101C}  C_{D106C}

Figure 5.11. DSR selenium estimate residual histogram. The kernel density of the residuals is plotted over the histogram. Similar plots for the rest of the linear model analyses are included in the appendix.

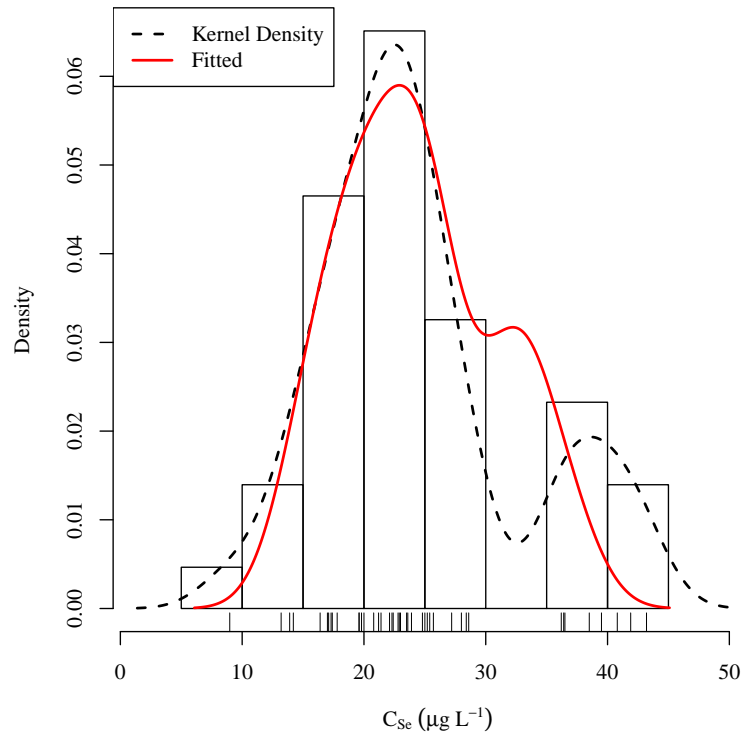
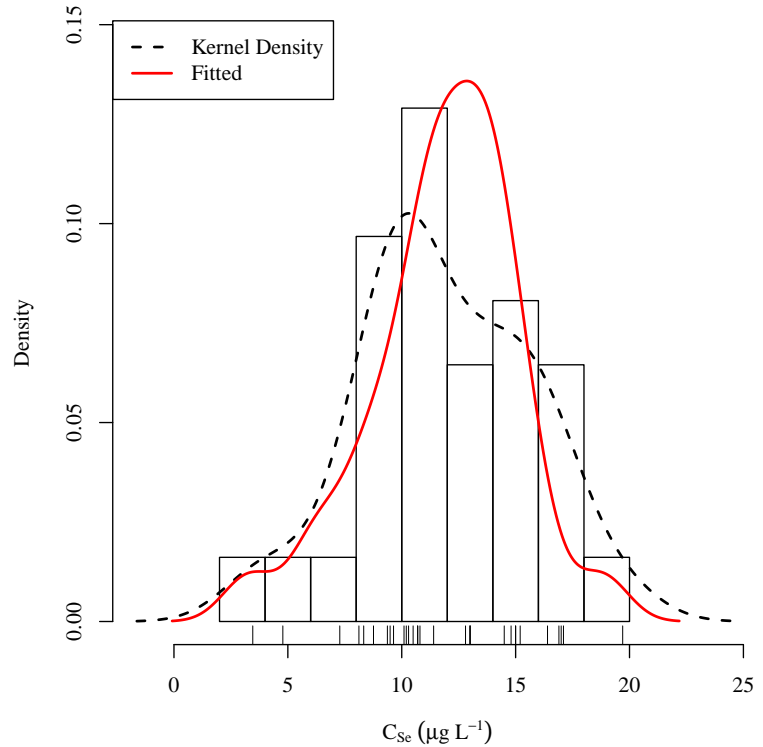
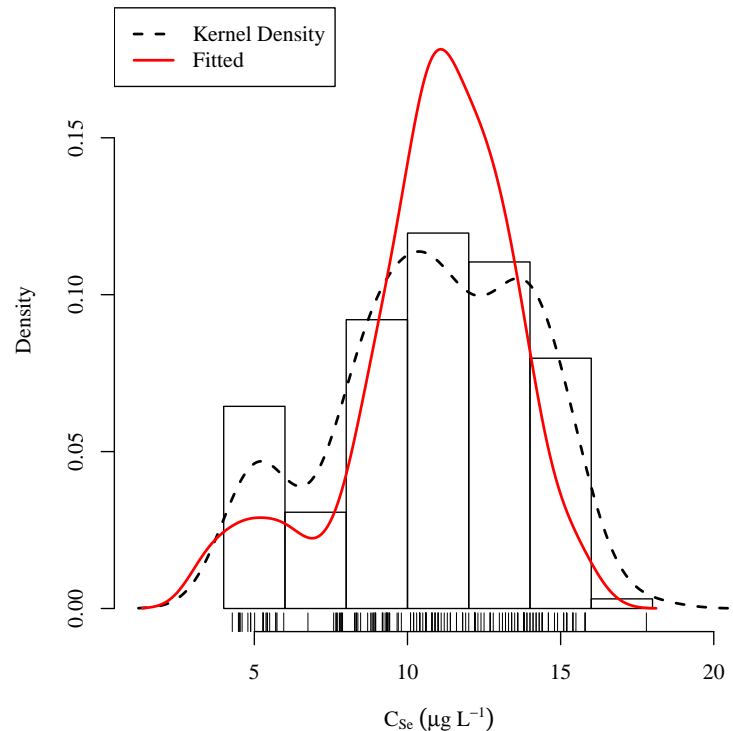
 C_{D23}  C_{D57}

Figure 5.11 (Cont). DSR selenium estimate residual histogram.



$$C_{ARK,d=x}$$

Figure 5.11 (Cont). DSR selenium estimate residual histogram.

The primary purpose of the next set of analyses was to determine if the computational code and assumptions used to generate the stochastic distributions of dissolved selenium concentrations were performed correctly. The first analysis was to compare the calculated dissolved selenium concentration values to the measured results from the collected field samples. Figure 5.12 is a box plot of the sampled selenium concentrations at the various sampling locations along the main stem of the river and the tributaries in the USR. The sample locations are arranged with the upstream on the left and the downstream on the right, in order. The value "n" above each sample location is the number of samples collected at each site. Concentrations are measured and reported in $\mu\text{g L}^{-1}$ of dissolved selenium. The boxes encompass the first to the third quartile. The whiskers extend to 1.5 times the inter quartile range. Blue tinted boxes indicate dissolved selenium concentrations within tributaries all other boxes are from samples collected within the main stem of the Ark R.

Concentrations for the Rocky Ford Return Ditch in the USR and Frontier Ditch in the DSR are not included. Both ditches are assumed to have the same dissolved selenium concentration as a nearby calculated location. The Rocky Ford Return Ditch (RFDRDTCO) uses the same concentration as the Rocky Ford Ditch (RFDCANCO) as it returns water from the main ditch to the Arkansas R. less than 1 km downstream of the main ditch head gate. The Frontier Ditch (FRODITKS) diverts water near the downstream end of the DSR and uses the concentrations calculated for this point.

Figure 5.13 is a box plot of the calculated estimated selenium concentration at the various key points in the USR mass balance model. The value "n" indicates the number of steps in the time series. The values used in the box plot are from the 1-D mean stochastic model. The blue tinted boxes indicate calculated dissolved selenium concentrations within

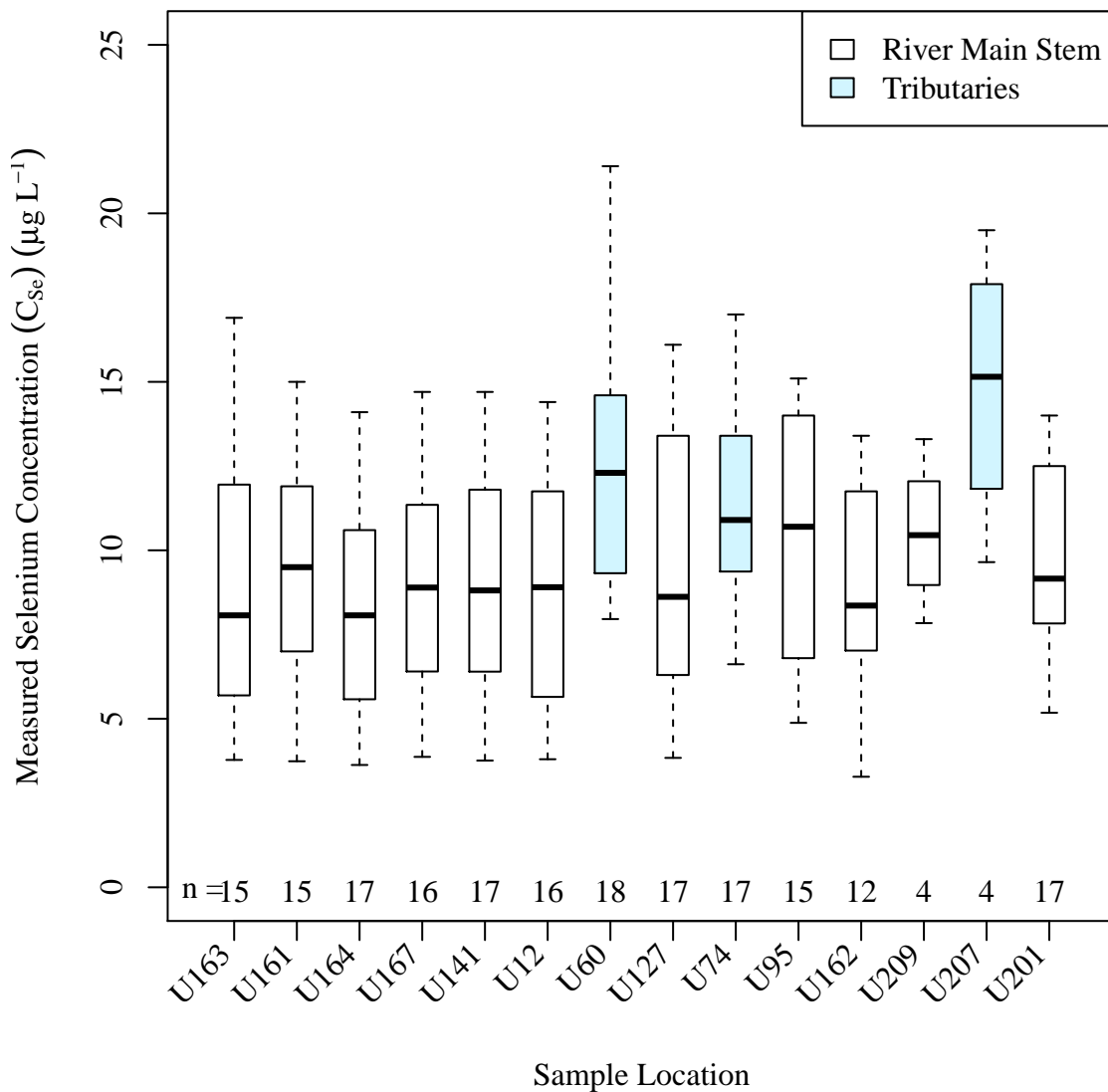


Figure 5.12. Measured Dissolved Selenium Concentrations in the USR.

tributaries and the tan tinted boxes indicate calculated dissolved selenium concentrations at the irrigation canal head gates.

Figure 5.14 is a box plot of the measured dissolved selenium concentrations at sample points in the main stem of the river and its main tributaries in the DSR. This plot is similar in fashion to figure 5.12.

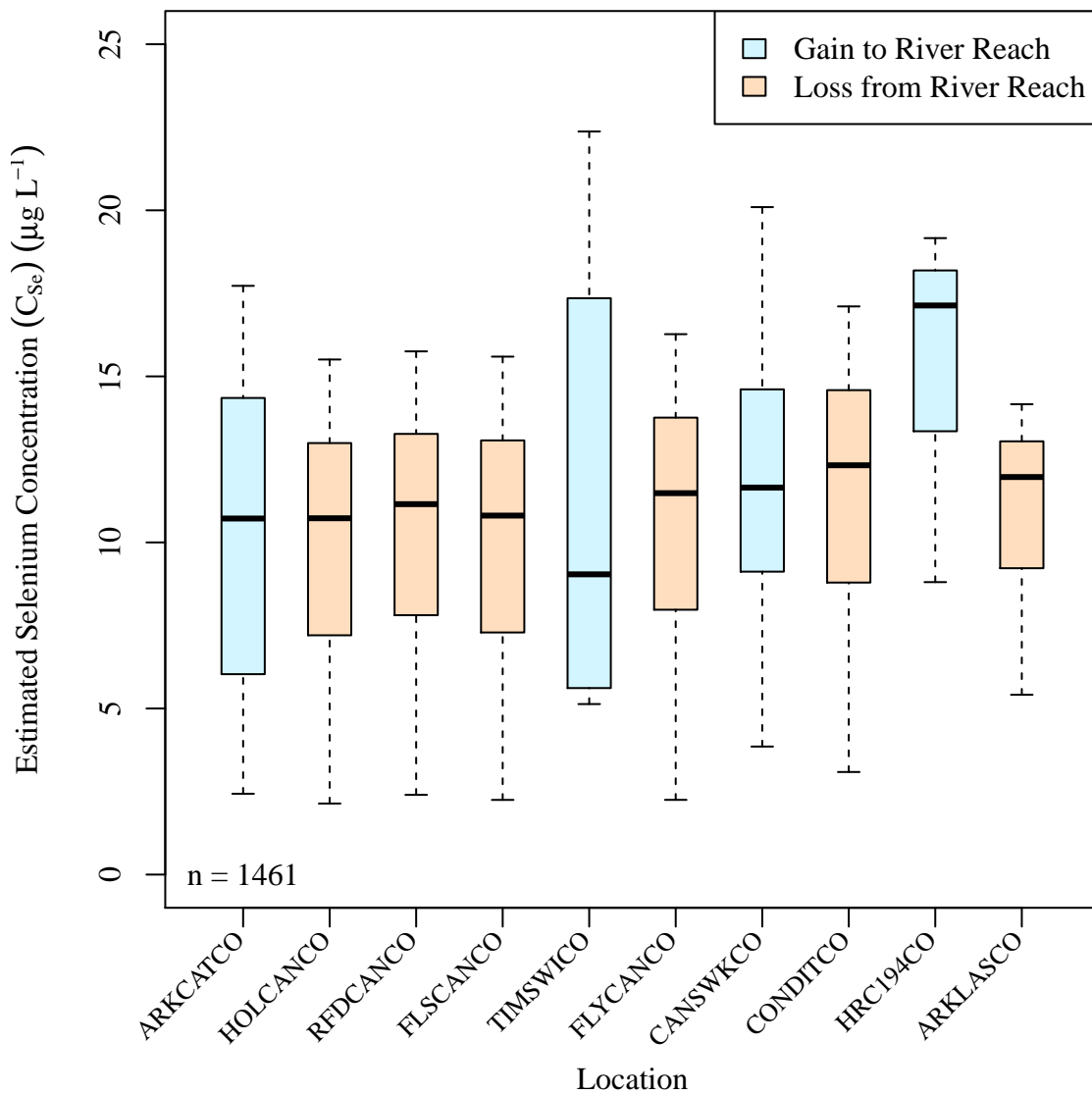


Figure 5.13. Calculated Dissolved Selenium Concentrations in the USR.

Figure 5.15 is a box plot of the measured dissolved selenium concentrations at sample points in the main stem of the river and its main tributaries in the DSR. This plot is similar in fashion to figure 5.13.

These four figures (5.12 to 5.15) compare the measured dissolved selenium concentration values with the estimated values. These figures are used along with tables ?? and ?? in chapter 2 to make this comparison. Study region sample locations along the Arkansas R. are

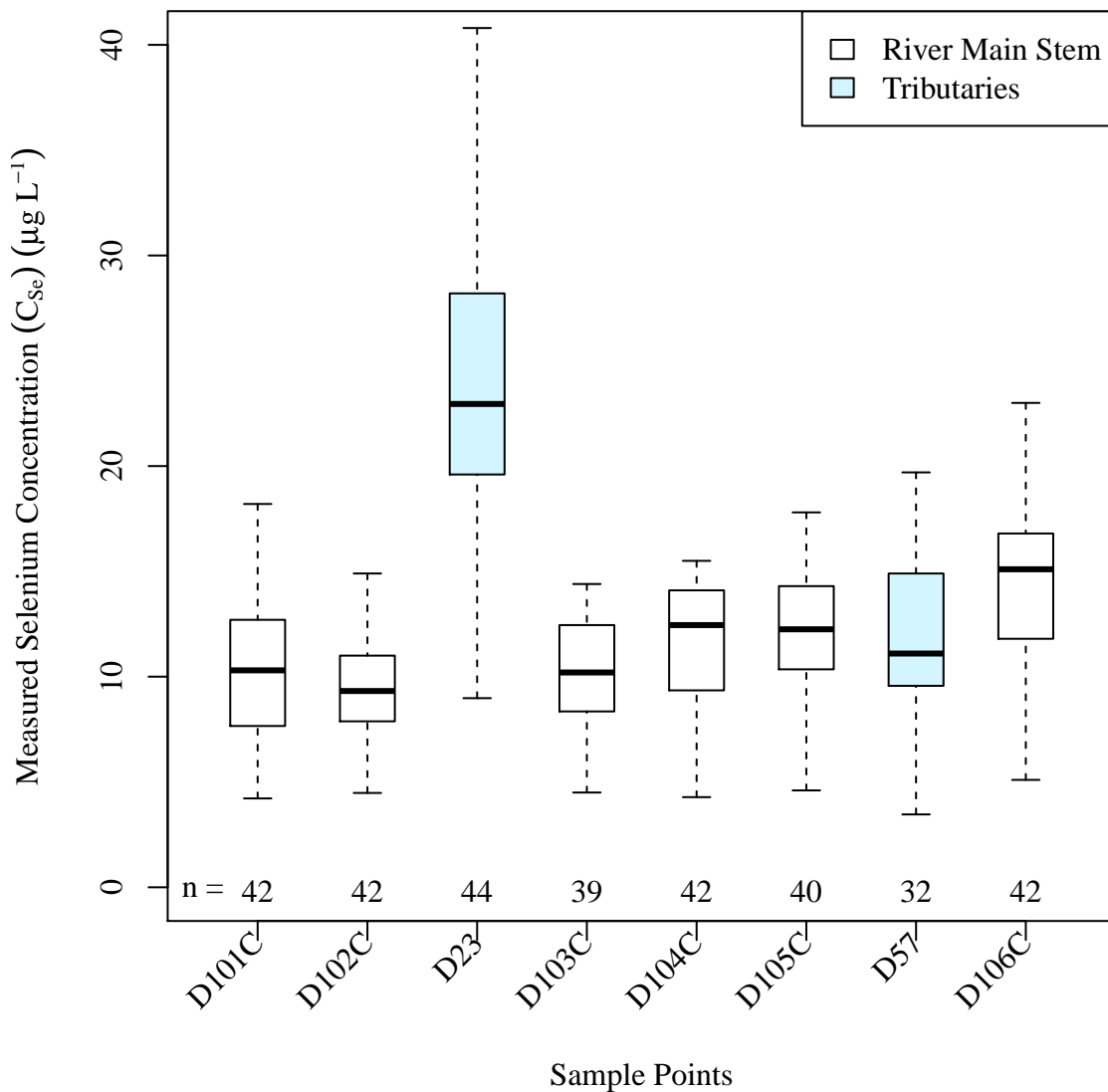


Figure 5.14. Measured Dissolved Selenium Concentrations in the DSR.

not necessarily located at the same places where calculated dissolved selenium concentrations are required.

In all cases but one, the graphs support the statement that the calculated selenium concentration values are representative of the actual recorded values. Timpas Creek (TIM-SWICO) in the USR appears to be the only exception. Here it appears that the calculated dissolved selenium concentrations are far lower than the measured values.

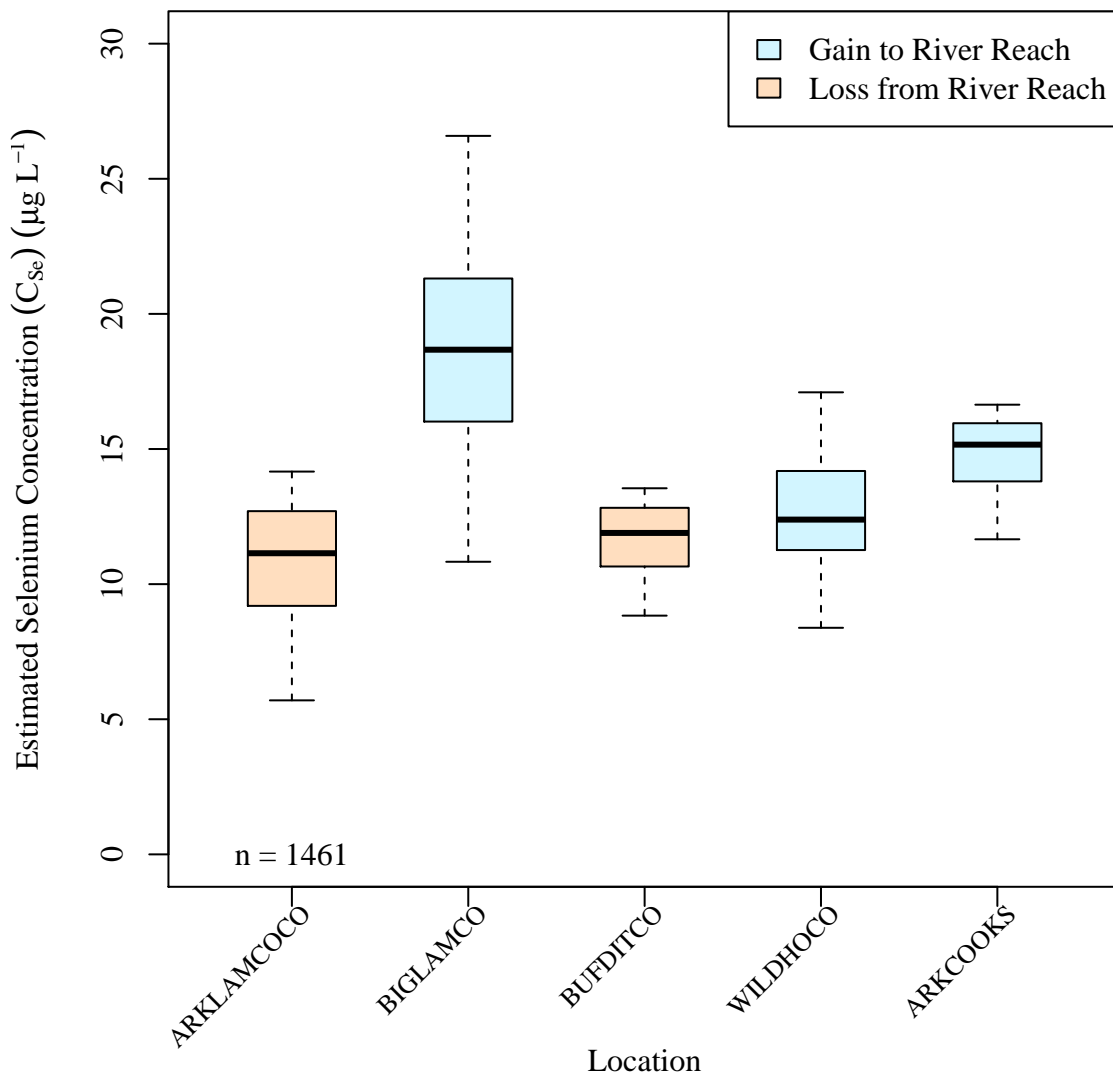


Figure 5.15. Calculated Dissolved Selenium Concentrations in the DSR.

This is possibly caused by three factors. The first is the sampling frequency. The sample results represented in figure 5.12 are not a uniform representation of the possible concentration values throughout a calendar year. The sample values more heavily consider three months, March, May, and July, and either minimal consider or ignore all other months.

5 The second is the nature of flows within Timpas Creek. The lower portion of the creek serves as a return flow channel for field irrigation runoff. The selenium concentration of the runoff and the effects of other water constituents are not known.

The second analysis was to compare the results between the deterministic model time-series and the stochastic model mean time-series results to determine if there is any unacceptable variance between the models. The distributions of the dissolved selenium concentrations calculated for both the deterministic and stochastic models were graphically

5 compared in Figures 5.16 and 5.17 for the USR and DSR, respectively. The histogram and the black KDE are of the calculated deterministic model values. The red dashed KDE represents the distribution of the stochastic model mean time-series. Similar figures for all calculated concentrations are provided in the appendix. The third factor is the uncertainty with which dissolved selenium concentrations were calculated for Timpas Creek.

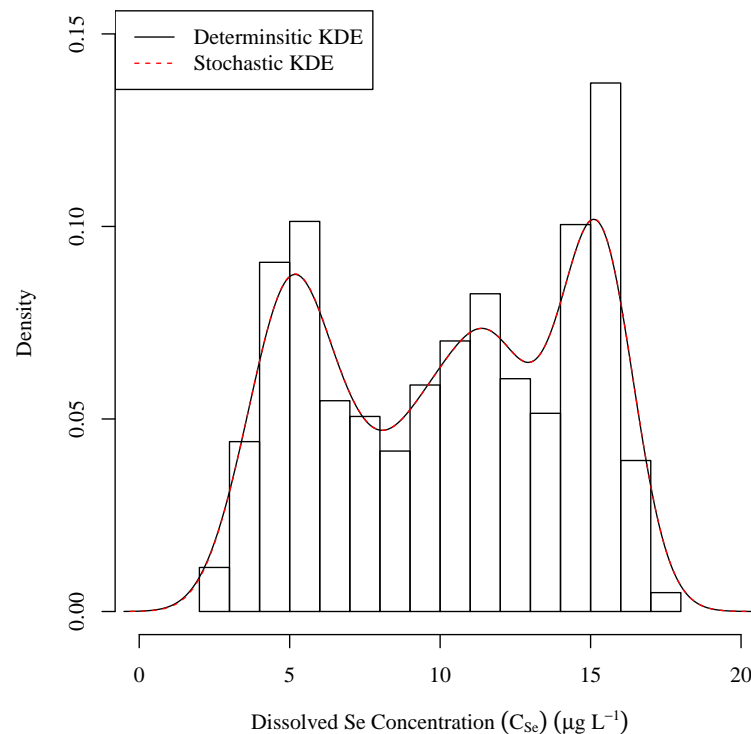
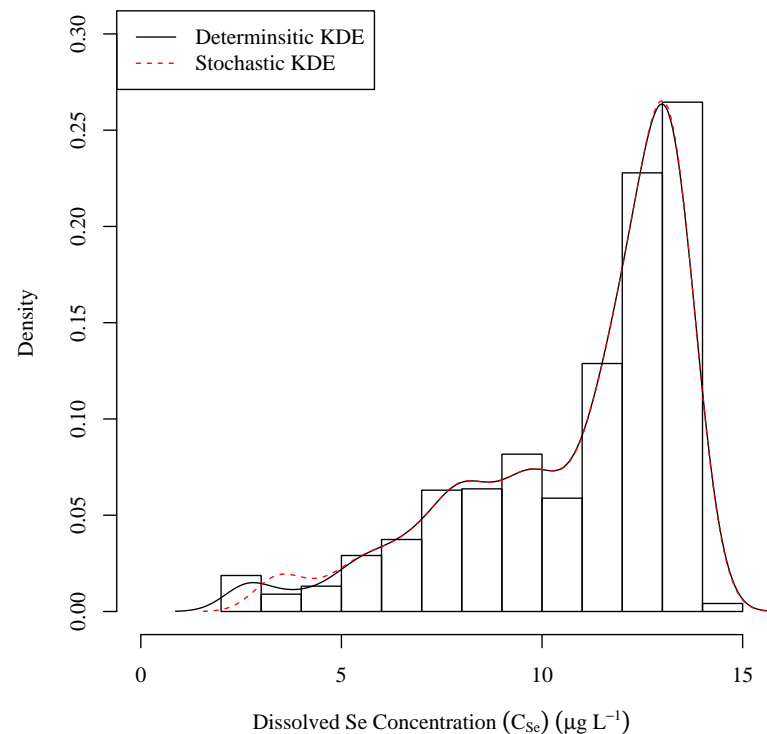

 C_{U163}

 C_{U201}

Figure 5.16. USR dissolved selenium concentration distribution analysis. The histogram and the black KDE are of the calculated deterministic model values. The red dashed KDE represents the distribution of the stochastic model mean time series.

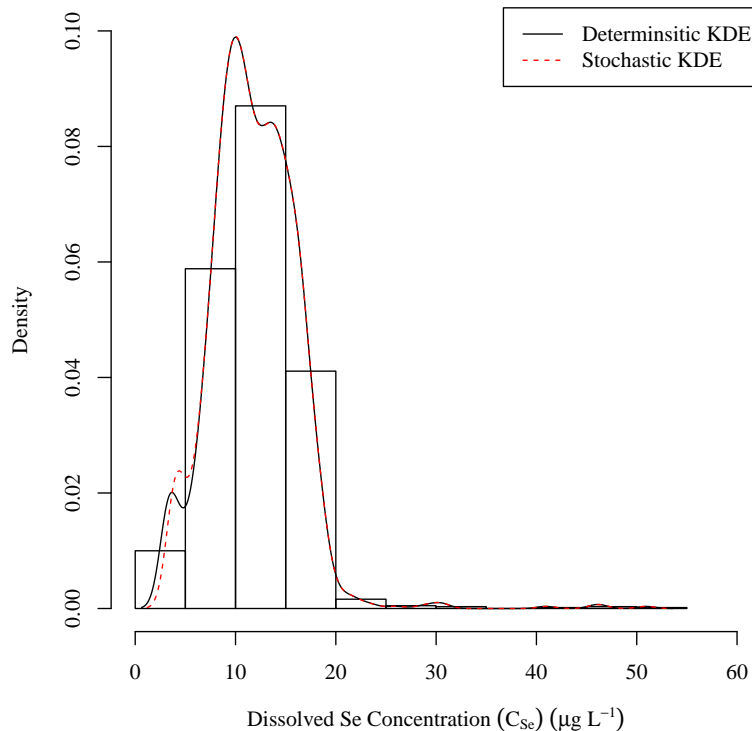
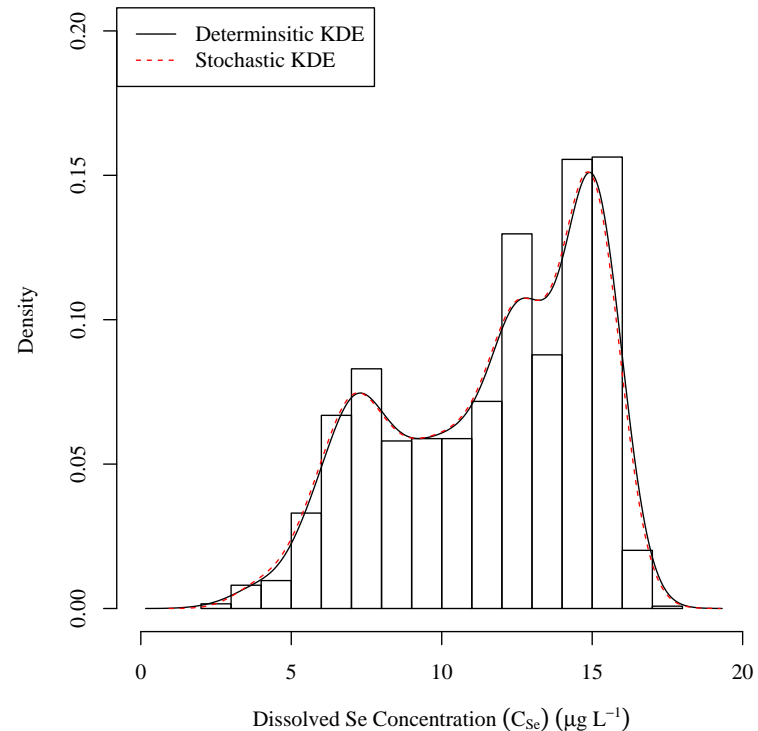
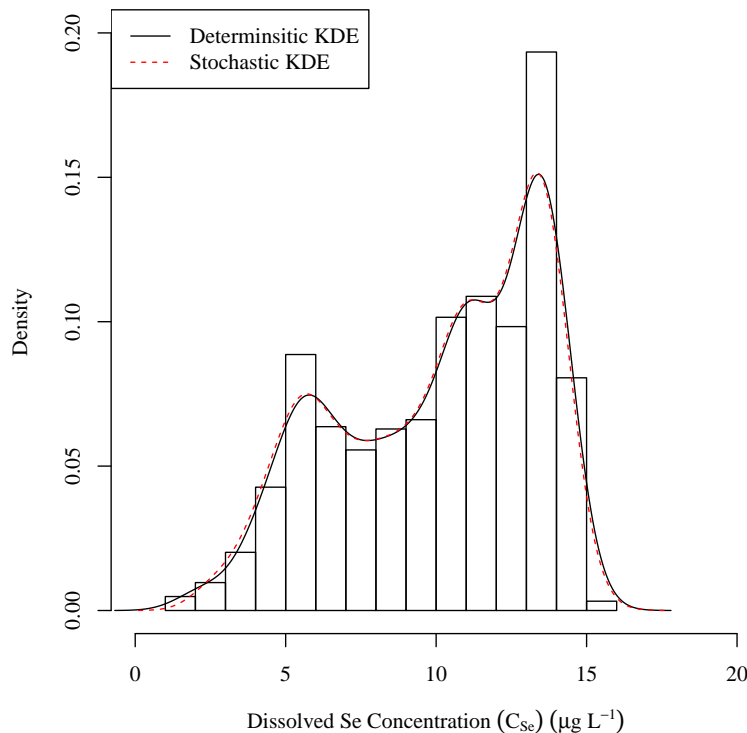
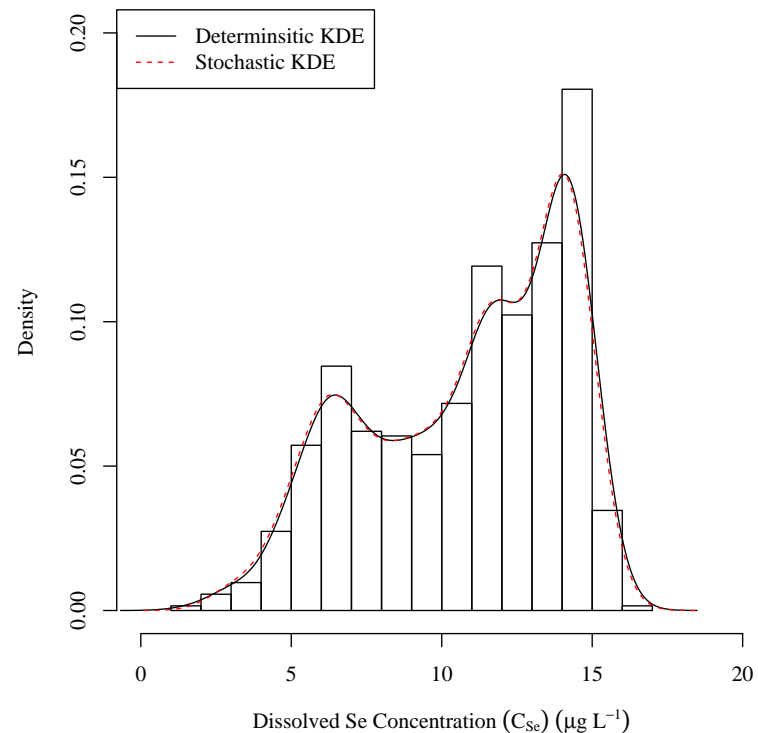
 C_{U74}  $C_{ARK,d=85.0}$

Figure 5.16 (Cont). USR selenium concentration linear model analysis graphs.

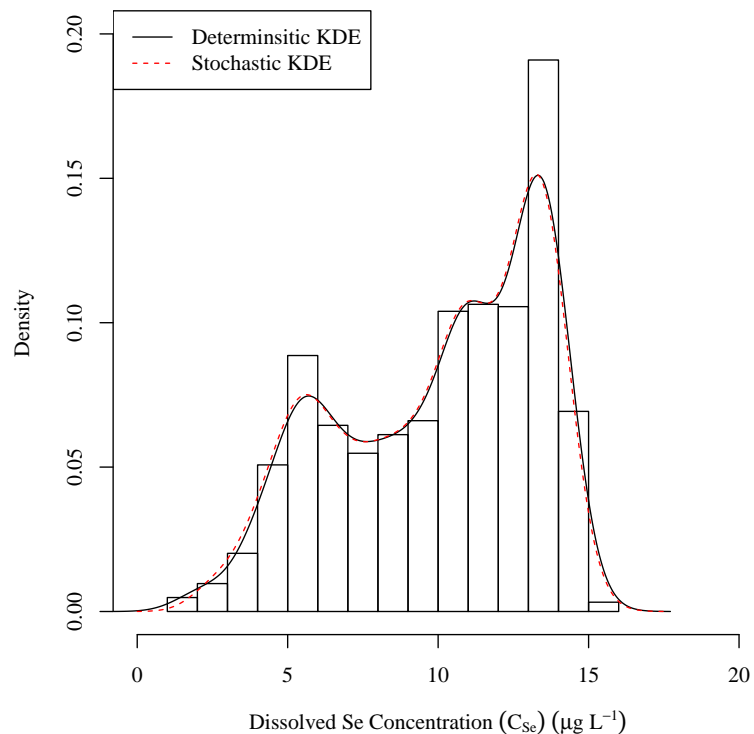


$$C_{ARK,d}=16.4$$



$$C_{ARK,d}=47.2$$

Figure 5.16 (Cont). USR selenium concentration linear model analysis graphs.



$$C_{ARK,d=12.5}$$

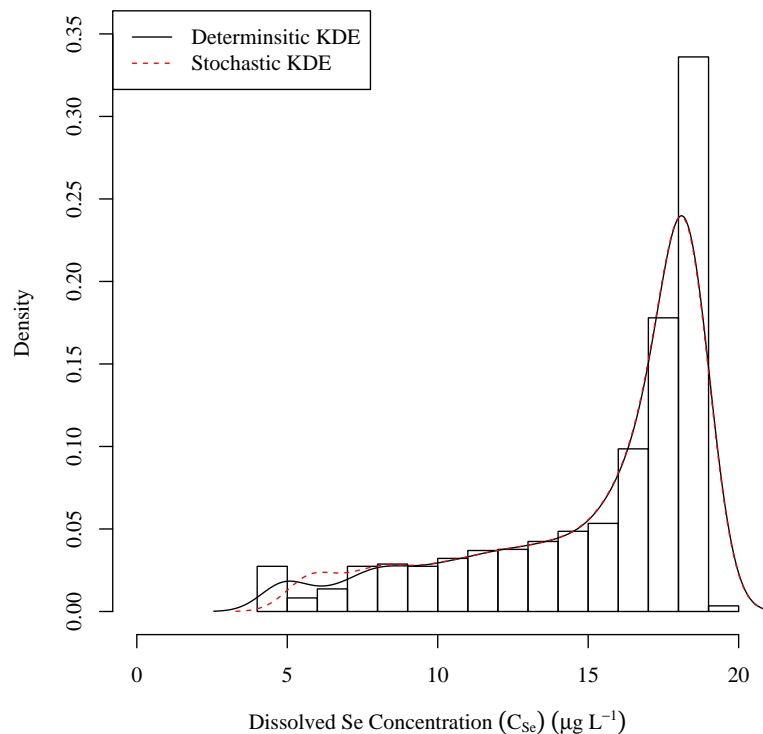


Figure 5.16 (Cont). USR selenium concentration linear model analysis graphs.

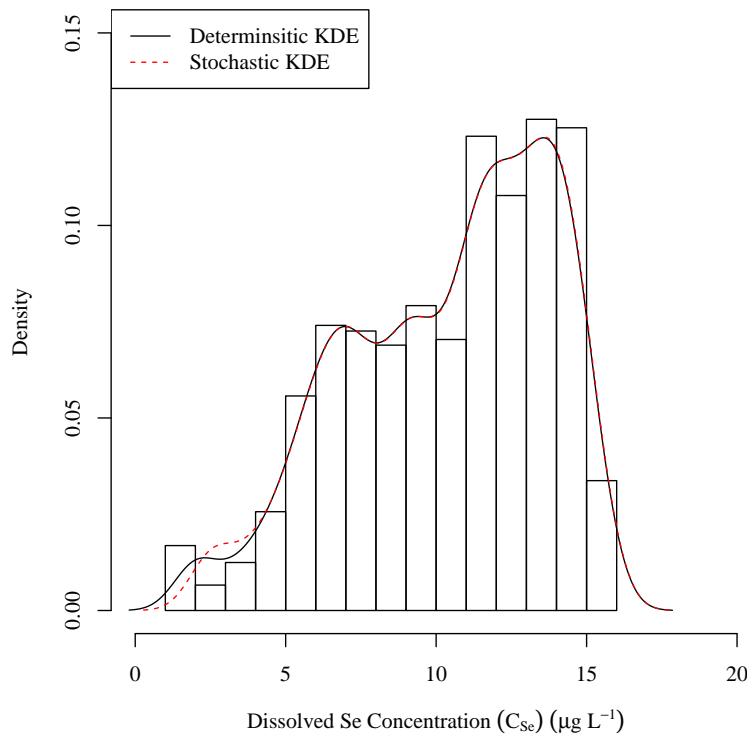
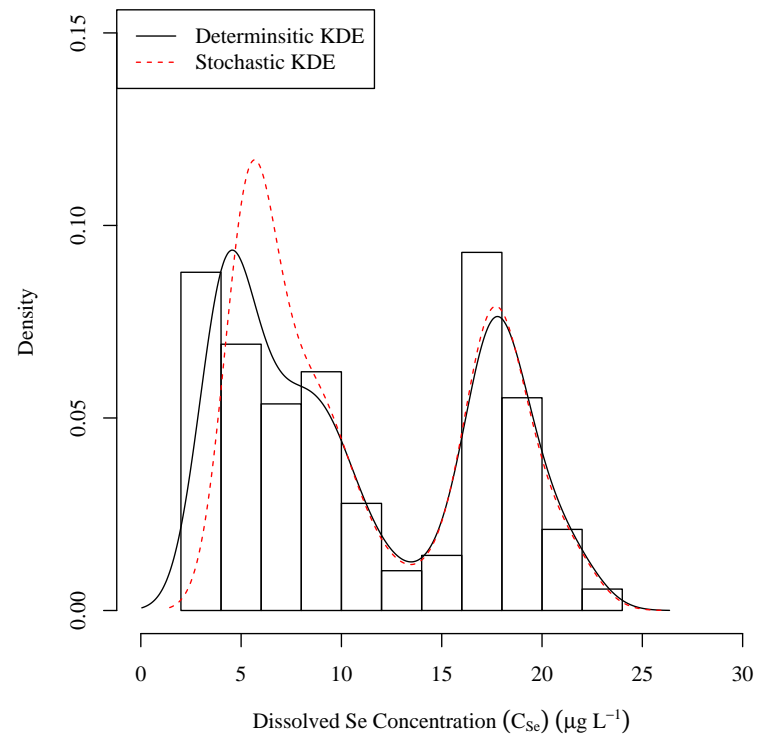
 C_{U167}  C_{60}

Figure 5.16 (Cont). USR selenium concentration linear model analysis graphs.

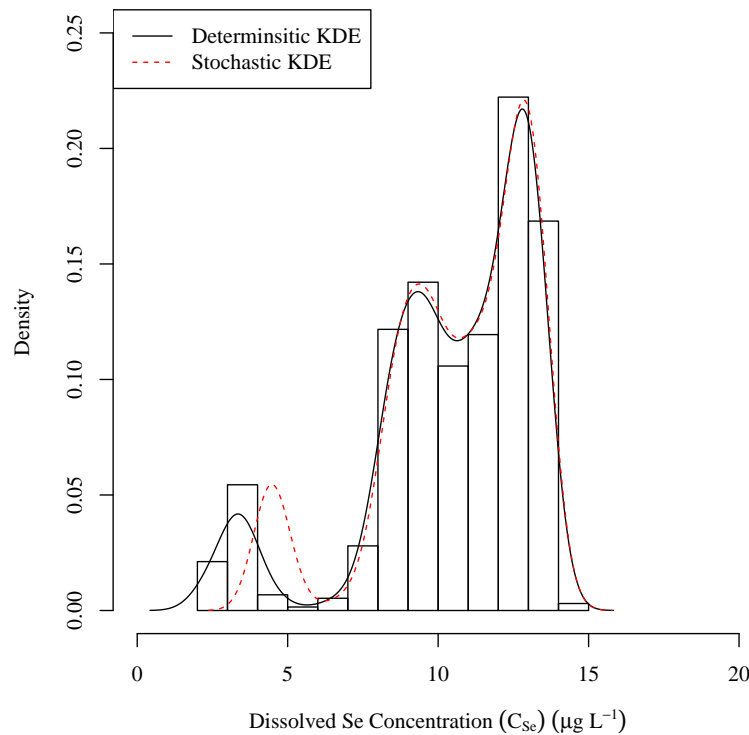
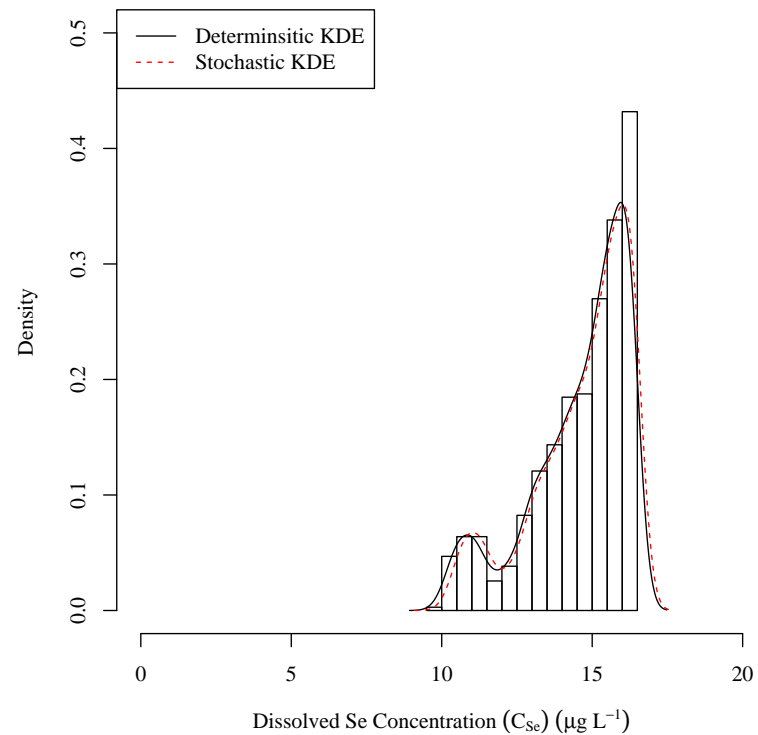

 C_{D101C}

 C_{D106C}

Figure 5.17. DSR dissolved selenium concentration distribution analysis. The histogram and the black KDE are of the calculated deterministic model values. The red dashed KDE represents the distribution of the stochastic model mean time series.

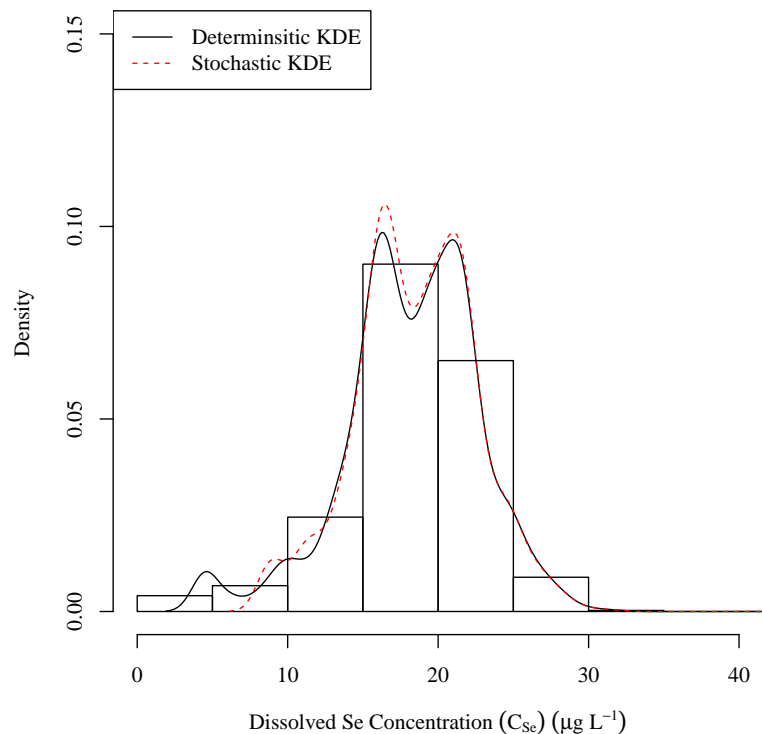
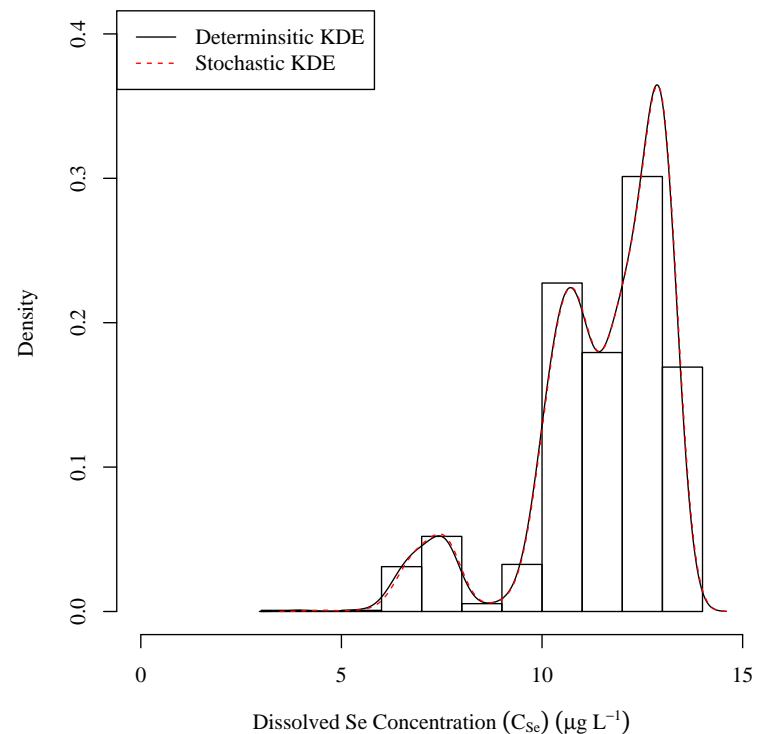
 C_{D23}  $C_{ARK,d=37.7}$

Figure 5.17 (Cont). DSR dissolved selenium concentration distribution analysis.

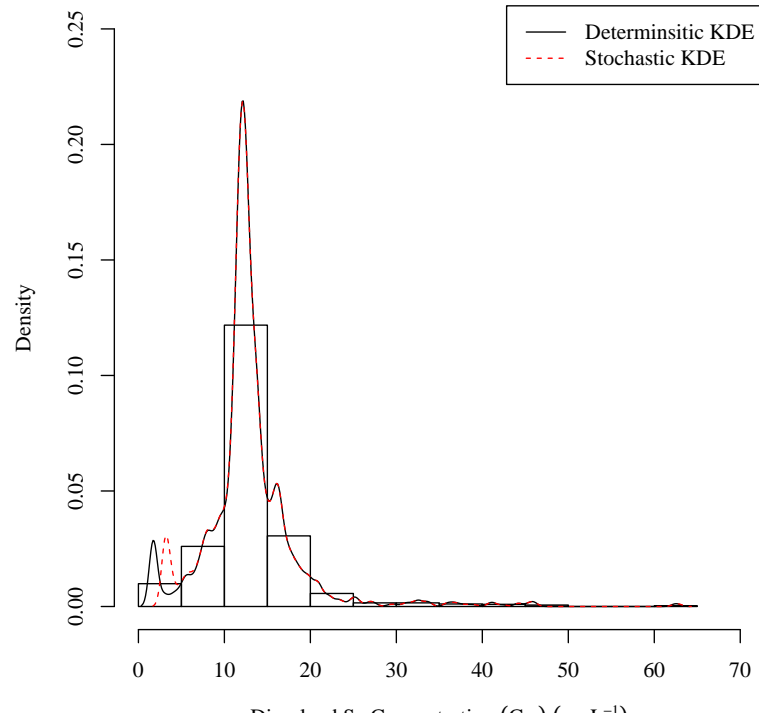
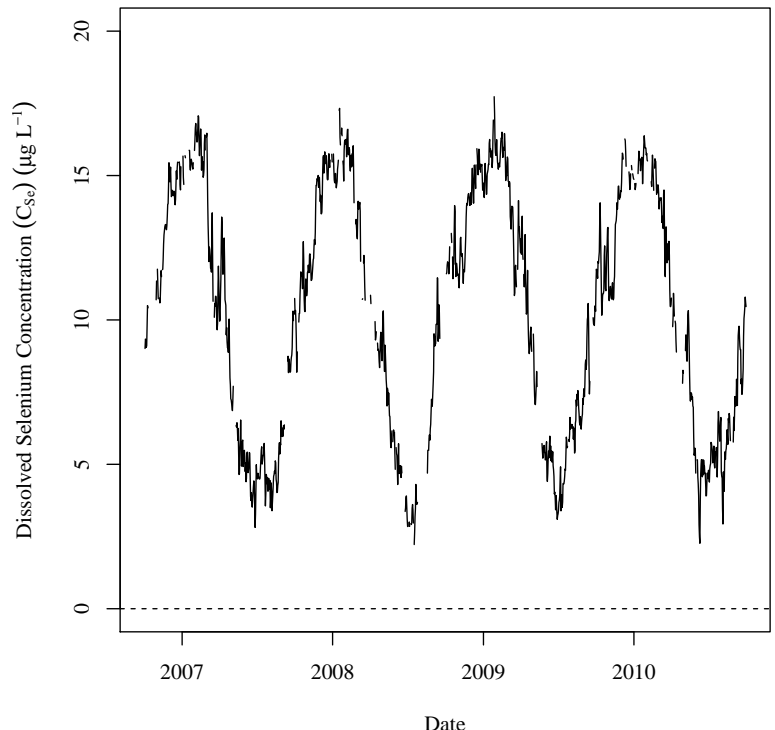
 C_{D57}

Figure 5.17 (Cont). DSR dissolved selenium concentration distribution analysis.

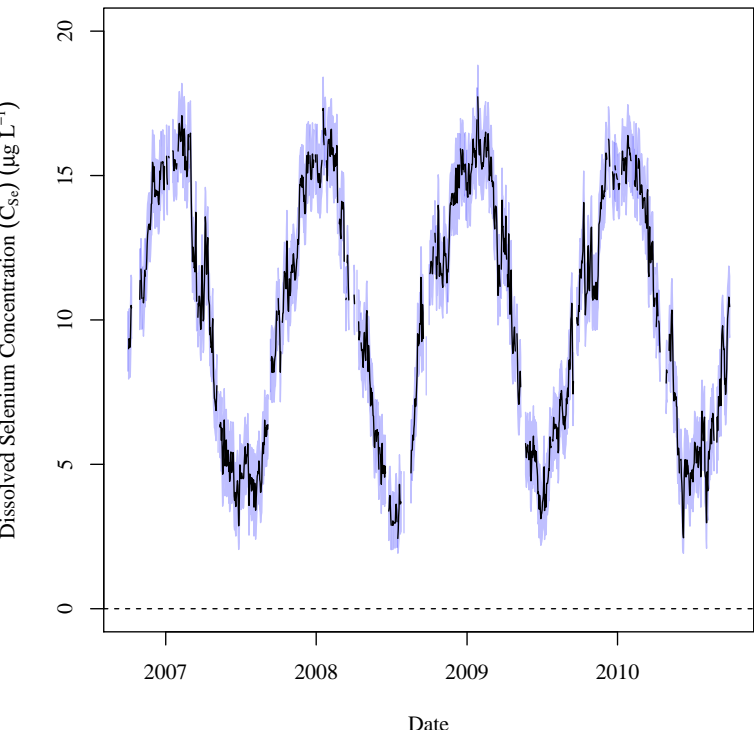
These figures show that the values used for the stochastic model and the deterministic model have very similar distributions. In some cases there are slight deviations between the two distributions at lower concentration values. This is due to the uncertainty assigned to the stochastic concentration estimates being more noticeable at lower calculated concentrations.

Time series plots of the concentration results from both the deterministic and stochastic models were prepared to visually analyze the relationship between the dissolved selenium concentration and the calendar date as shown in Figures 5.18 and 5.19 for the USR and DSR, respectively. Two sub-figures are provided. Sub-figure a is the deterministic model time series and sub-figure b is the stochastic model time series. The line is the mean of the realizations and the blue band is the 97.5th CIR.

C_{U163}



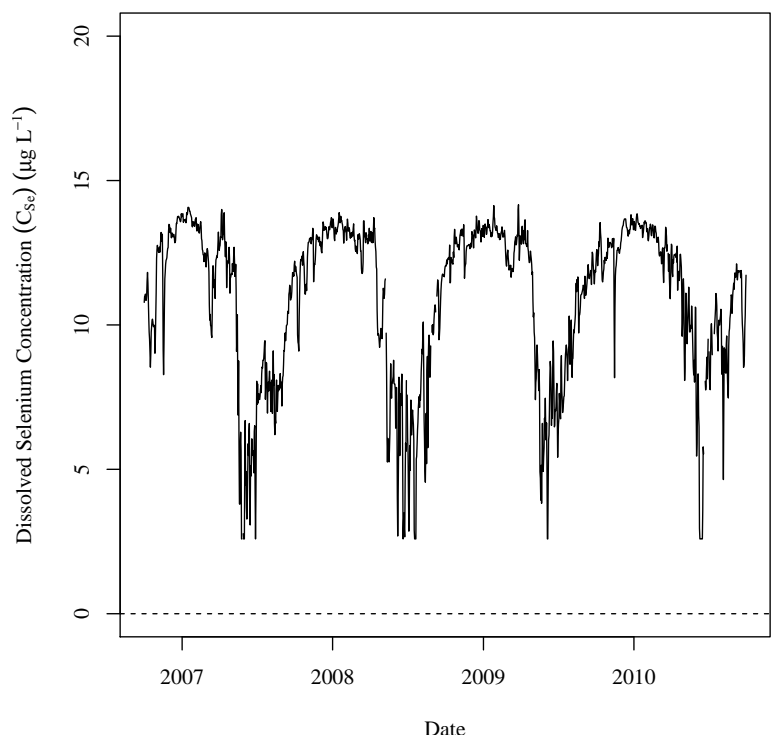
(a) Deterministic Model.



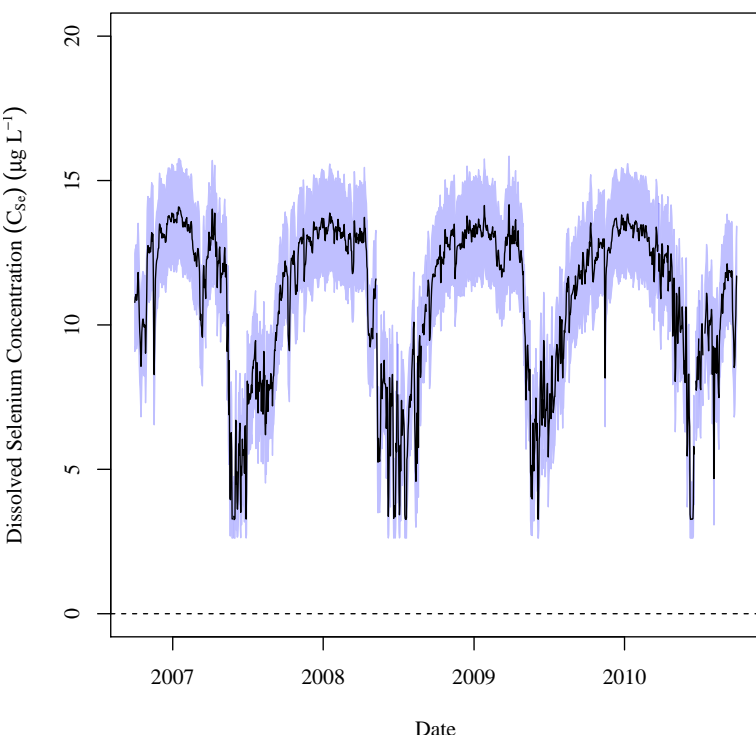
(b) Stochastic Model.

Figure 5.18. USR Deterministic and stochastic model time series of dissolved selenium concentration. For sub-figure b, the black line is the mean of the realizations and the blue band is the 97.5th CIR.

C_{U201}



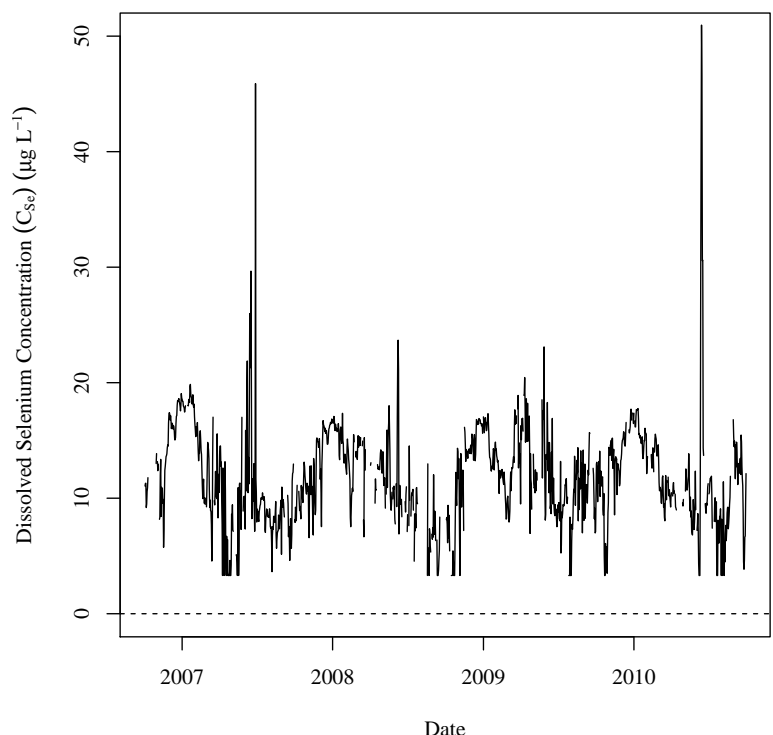
(a) Deterministic Model.



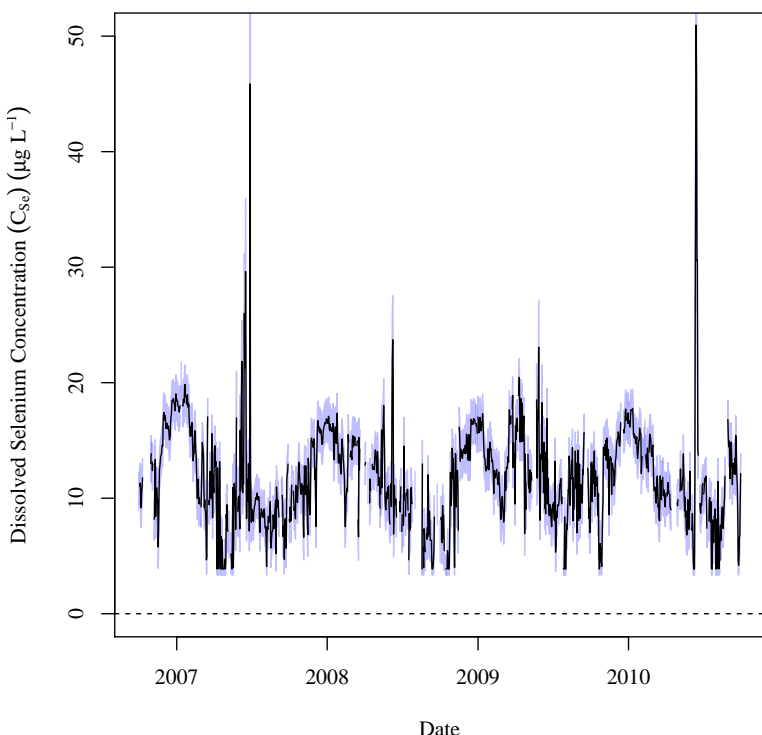
(b) Stochastic Model.

Figure 5.18 (Cont). USR Deterministic and stochastic model time series of dissolved selenium concentration.

C_{U74}



(a) Deterministic Model.

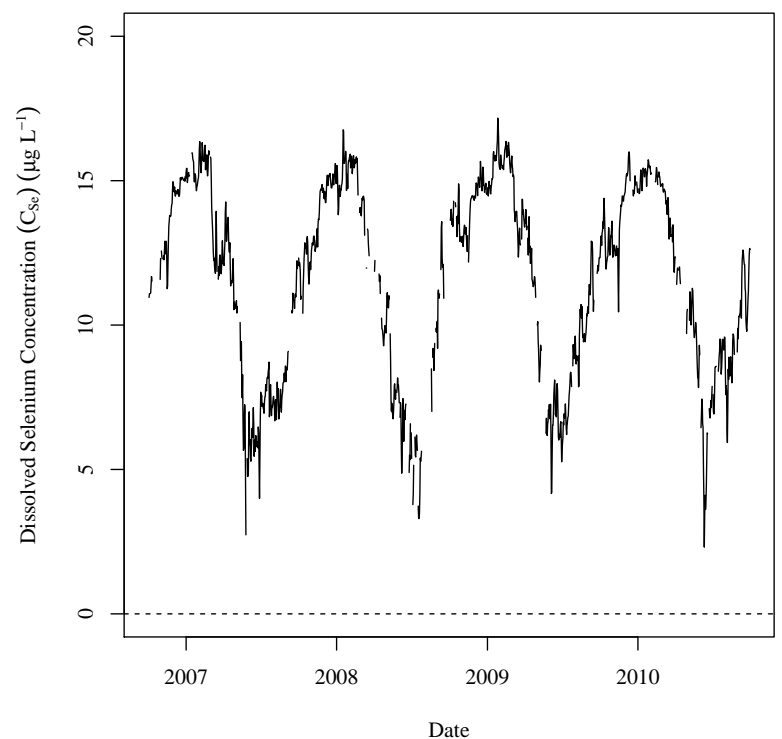


(b) Stochastic Model.

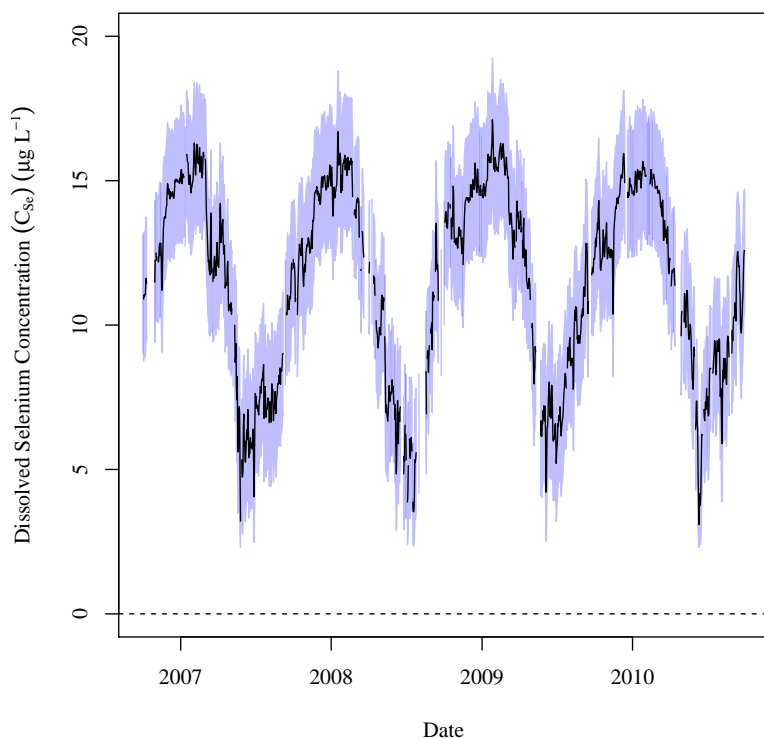
Figure 5.18 (Cont). USR Deterministic and stochastic model time series of dissolved selenium concentration.

$$C_{ARK,d=85.0}$$

271



(a) Deterministic Model.

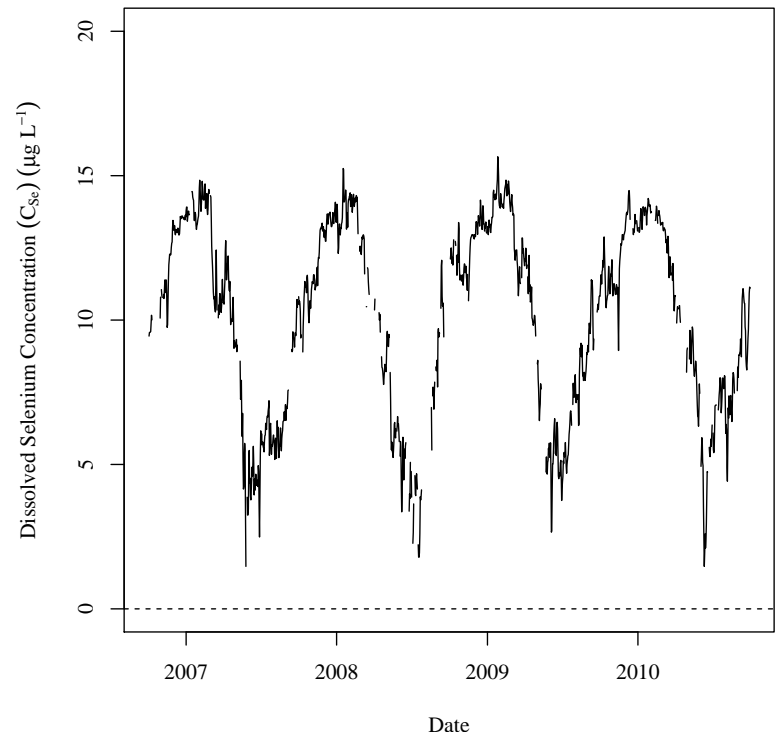


(b) Stochastic Model.

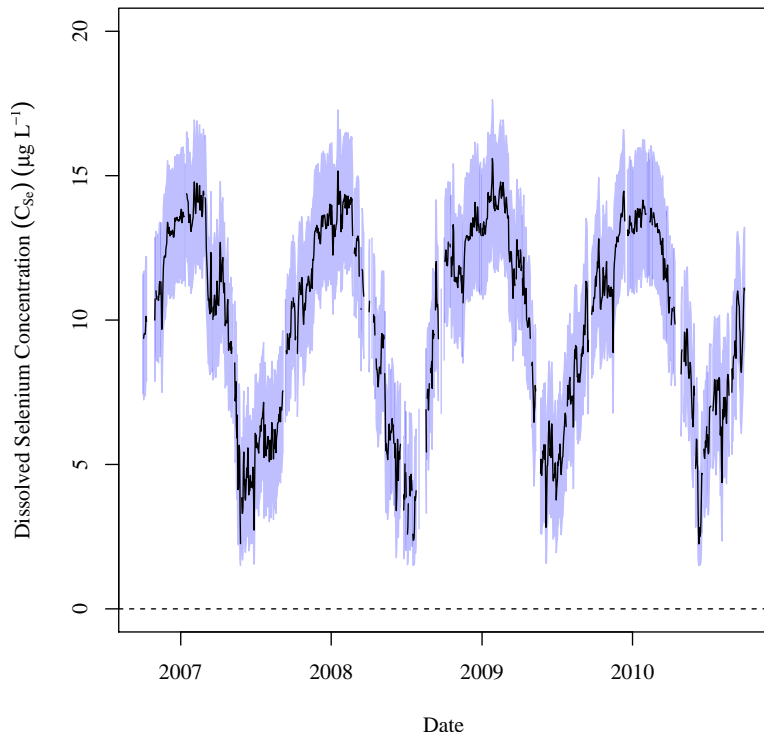
Figure 5.18 (Cont). USR Deterministic and stochastic model time series of dissolved selenium concentration.

$$C_{ARK,d=16.4}$$

272



(a) Deterministic Model.

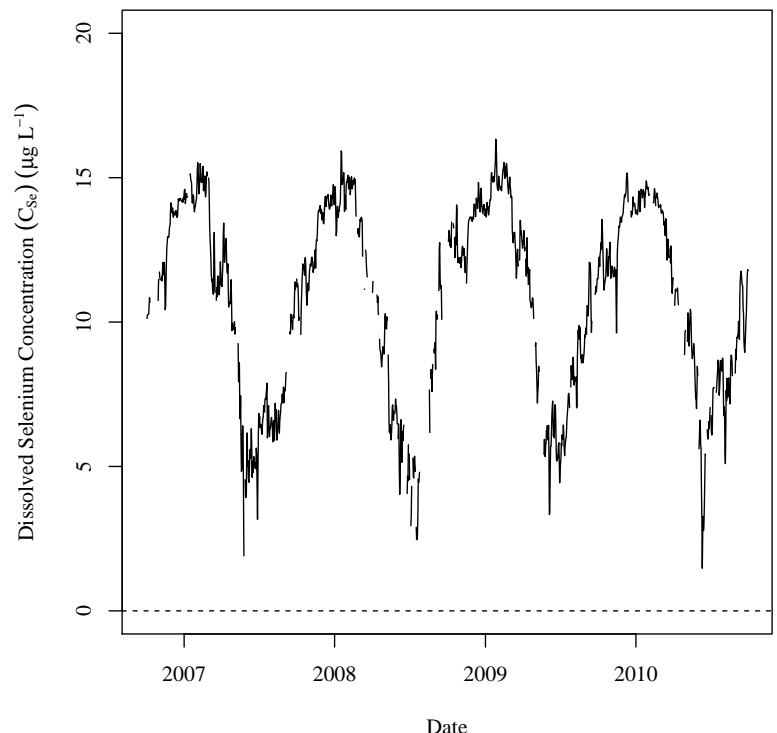


(b) Stochastic Model.

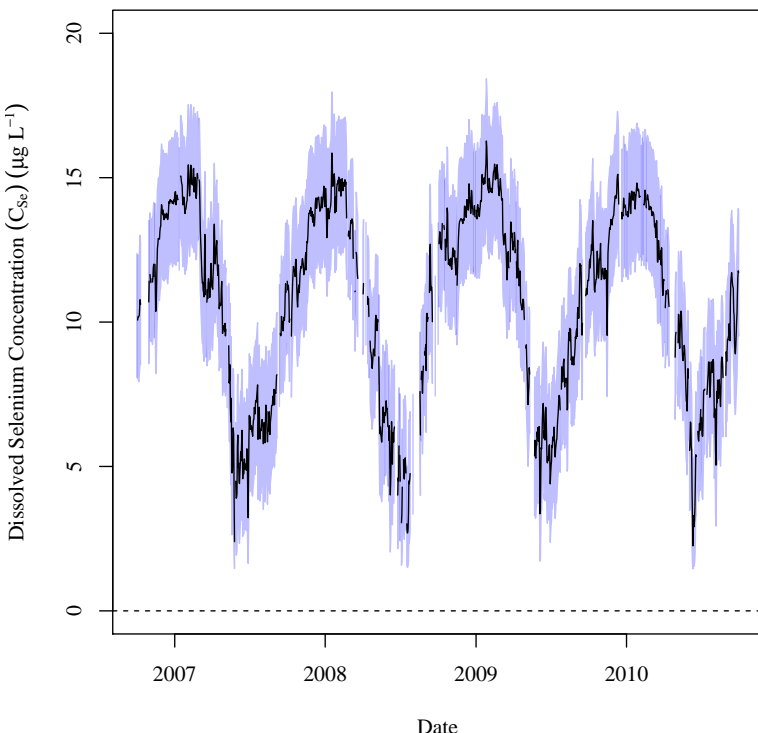
Figure 5.18 (Cont). USR Deterministic and stochastic model time series of dissolved selenium concentration.

$$C_{ARK,d=47.2}$$

273



(a) Deterministic Model.

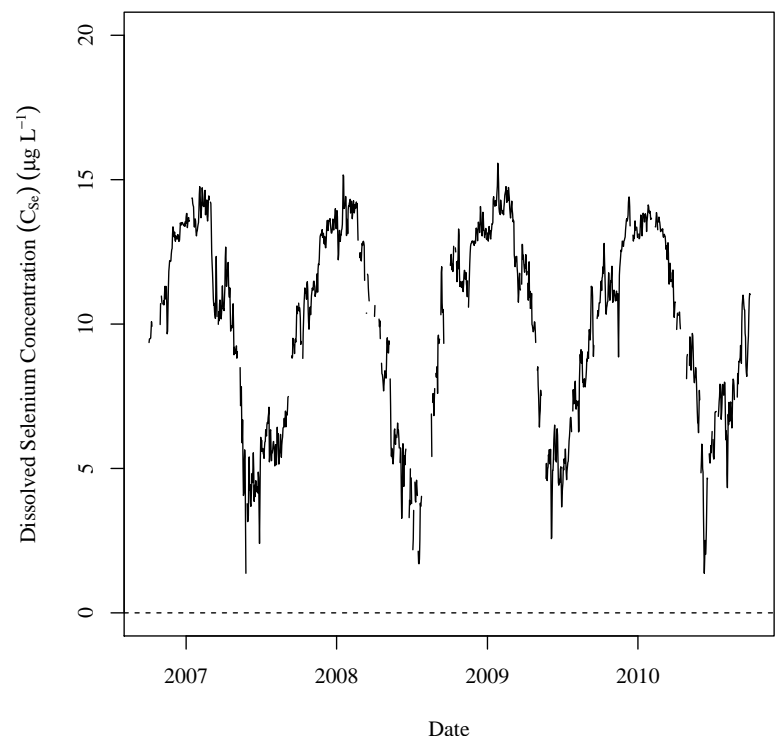


(b) Stochastic Model.

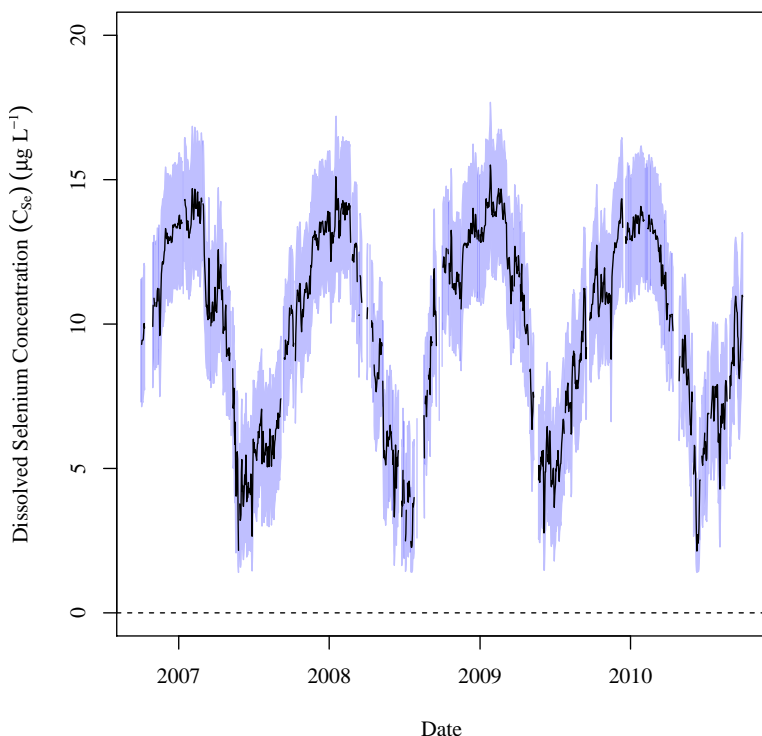
Figure 5.18 (Cont). USR Deterministic and stochastic model time series of dissolved selenium concentration.

$$C_{ARK,d=12.5}$$

274



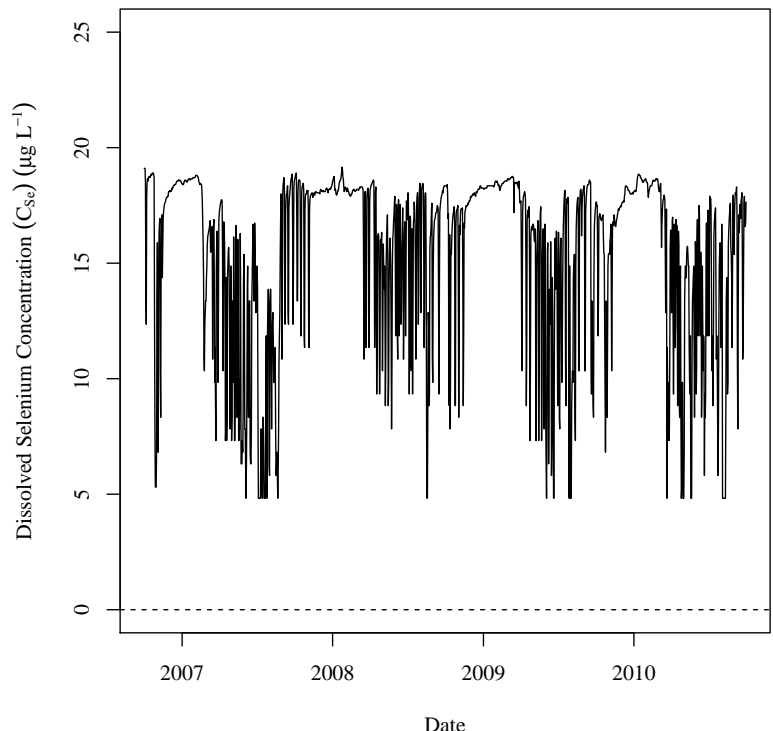
(a) Deterministic Model.



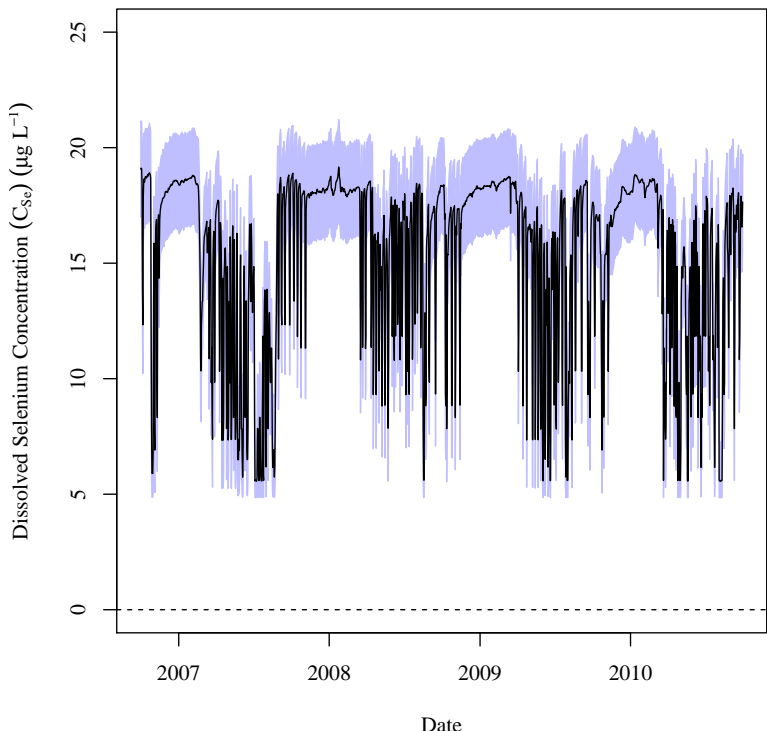
(b) Stochastic Model.

Figure 5.18 (Cont). USR Deterministic and stochastic model time series of dissolved selenium concentration.

C_{U207}



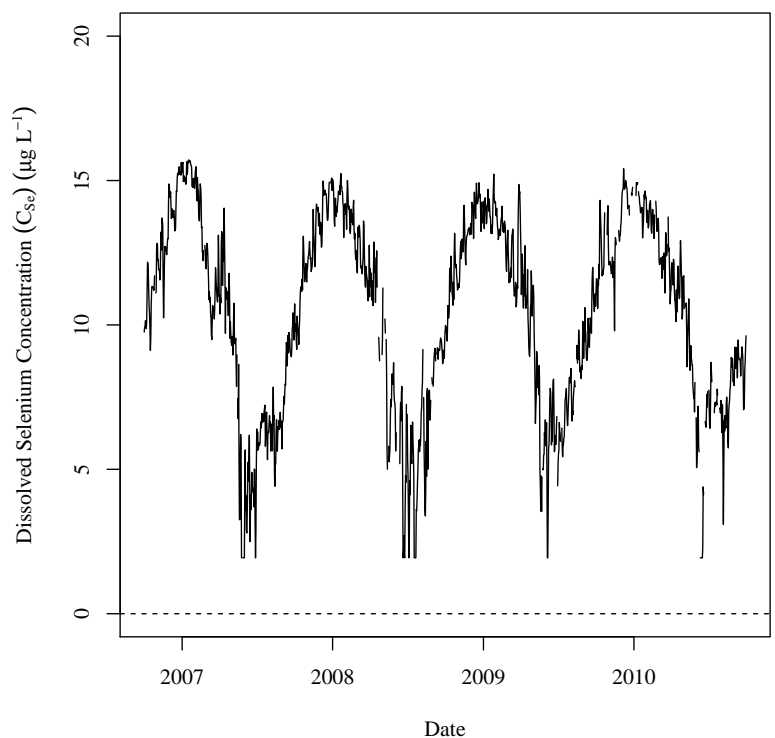
(a) Deterministic Model.



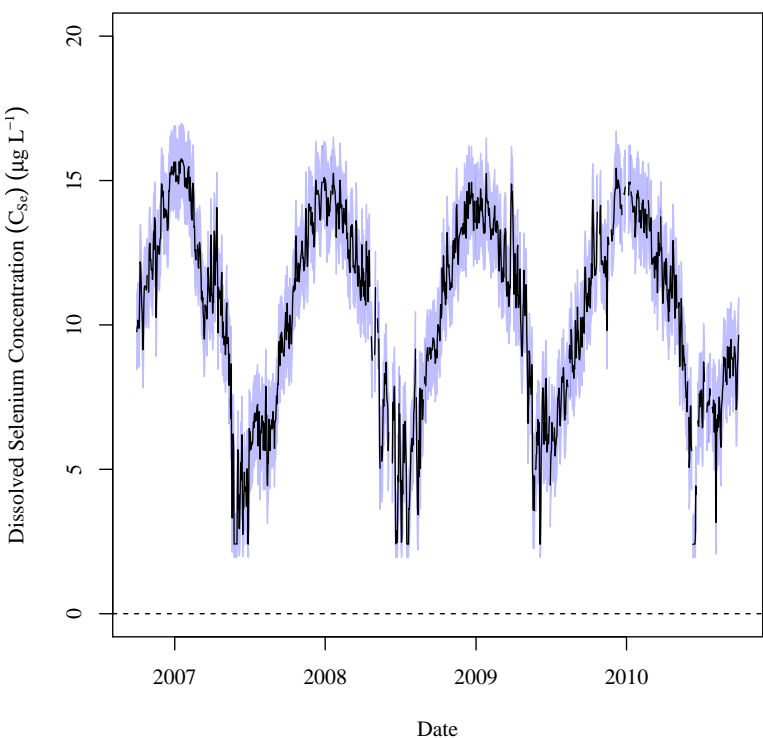
(b) Stochastic Model.

Figure 5.18 (Cont). USR Deterministic and stochastic model time series of dissolved selenium concentration.

C_{U167}

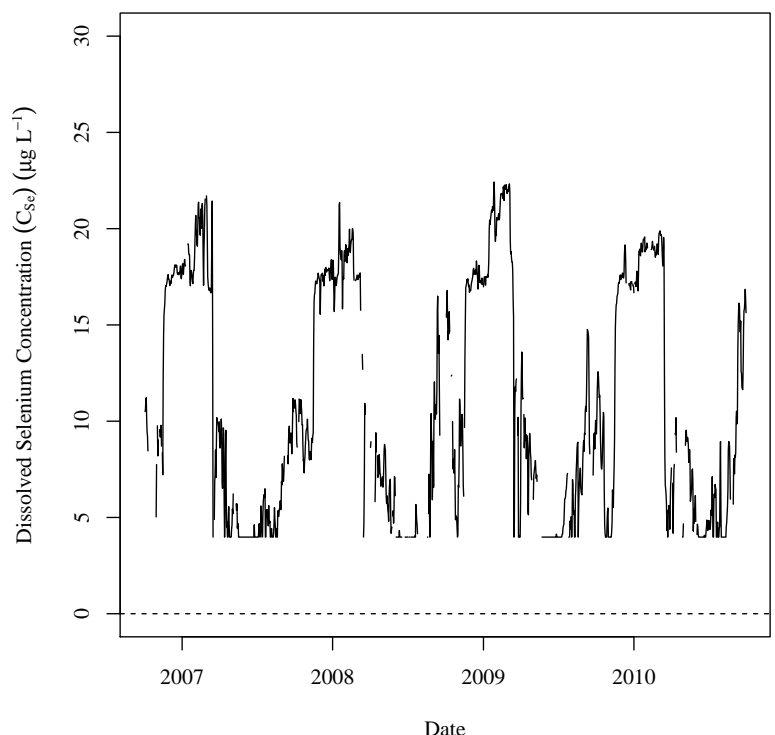


(a) Deterministic Model.

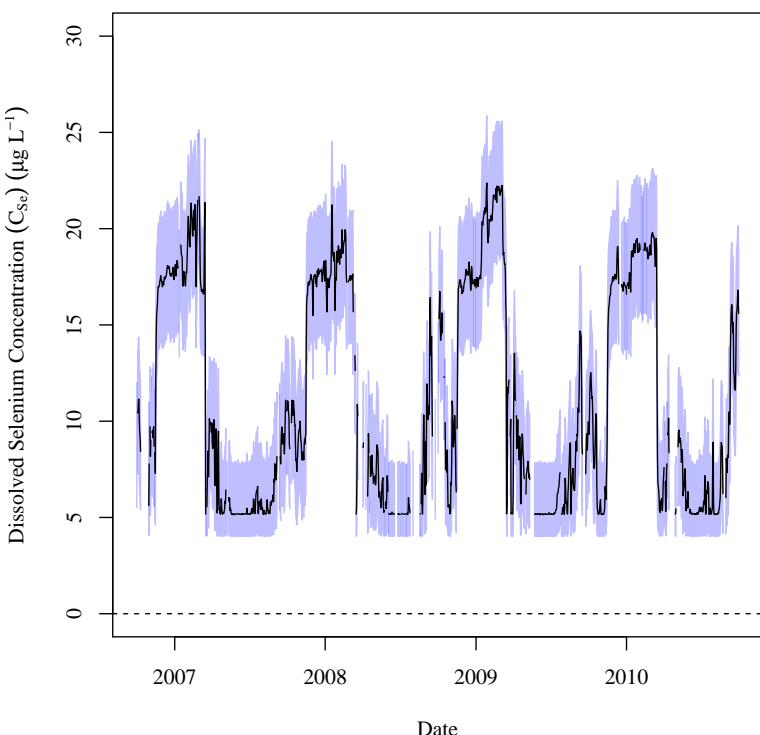


(b) Stochastic Model.

Figure 5.18 (Cont). USR Deterministic and stochastic model time series of dissolved selenium concentration.

C_{U60} 

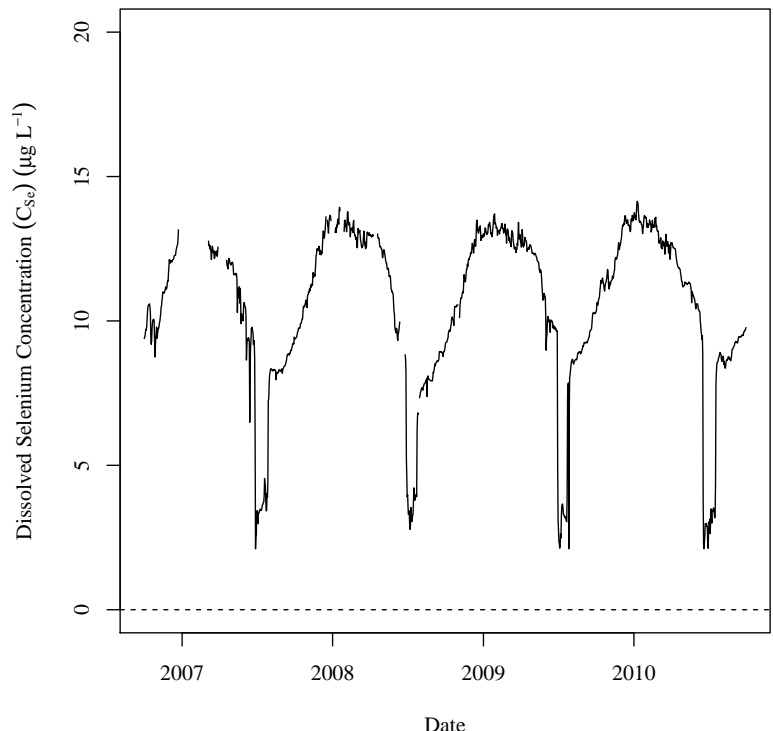
(a) Deterministic Model.



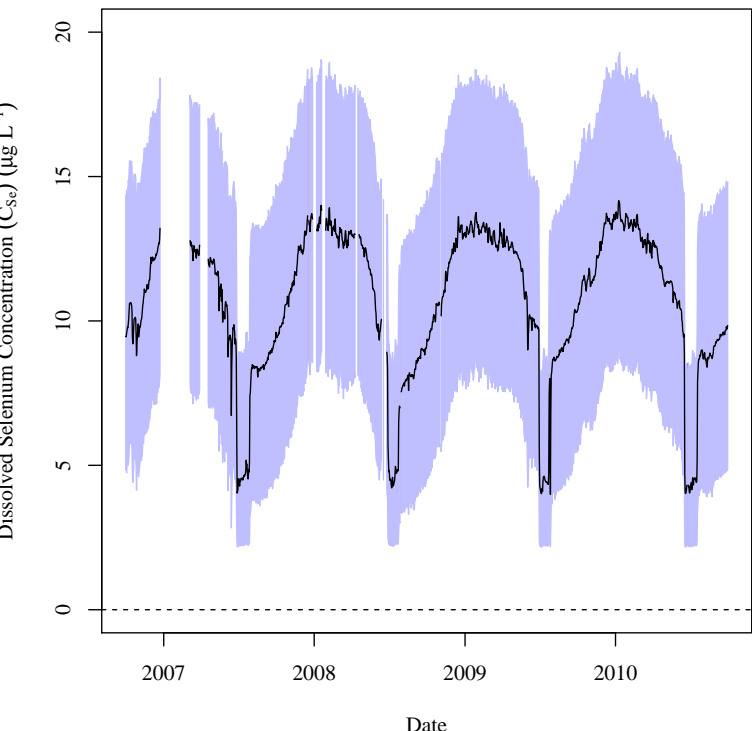
(b) Stochastic Model.

Figure 5.18 (Cont). USR Deterministic and stochastic model time series of dissolved selenium concentration.

C_{D101C}

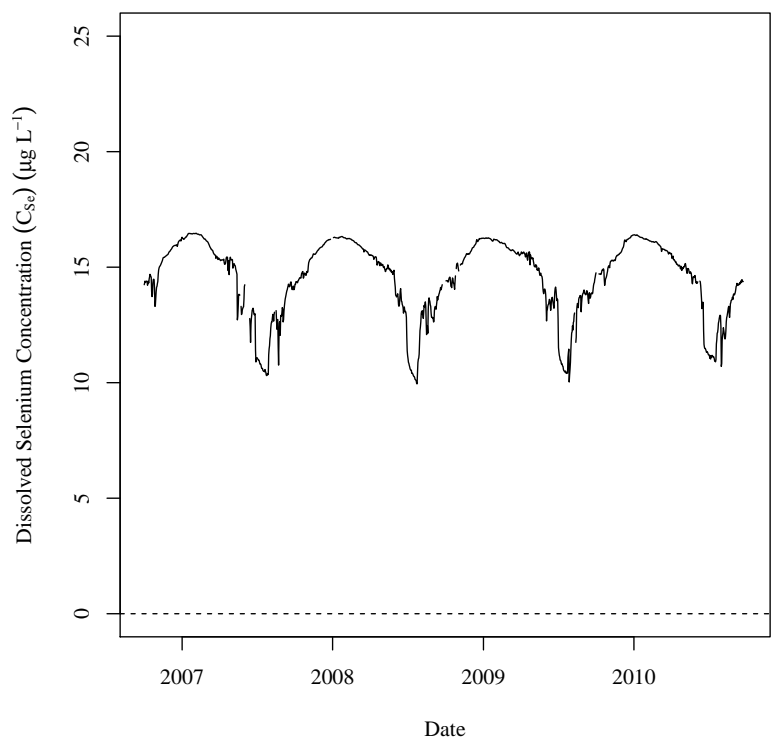


(a) Deterministic Model.

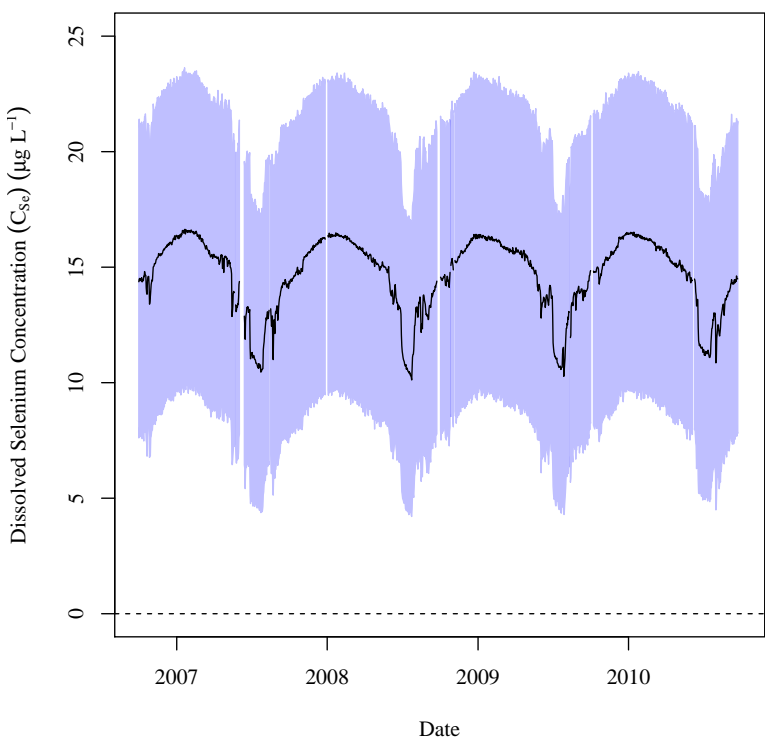


(b) Stochastic Model.

Figure 5.19. DSR Deterministic and stochastic model time series of dissolved selenium concentration. For sub-figure b, the black line is the mean of the realizations and the blue band is the 97.5th CIR.

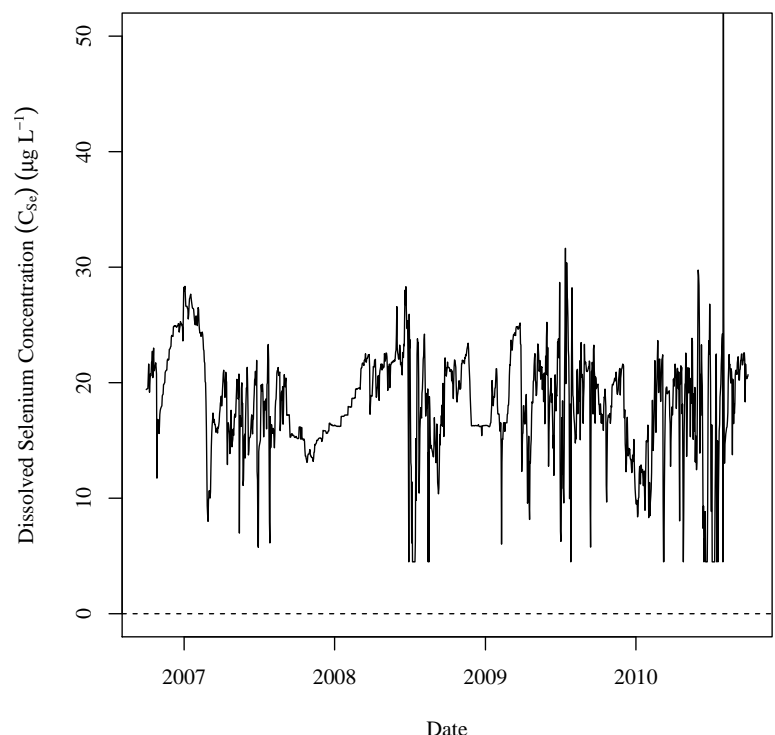
C_{D106C} 

(a) Deterministic Model.

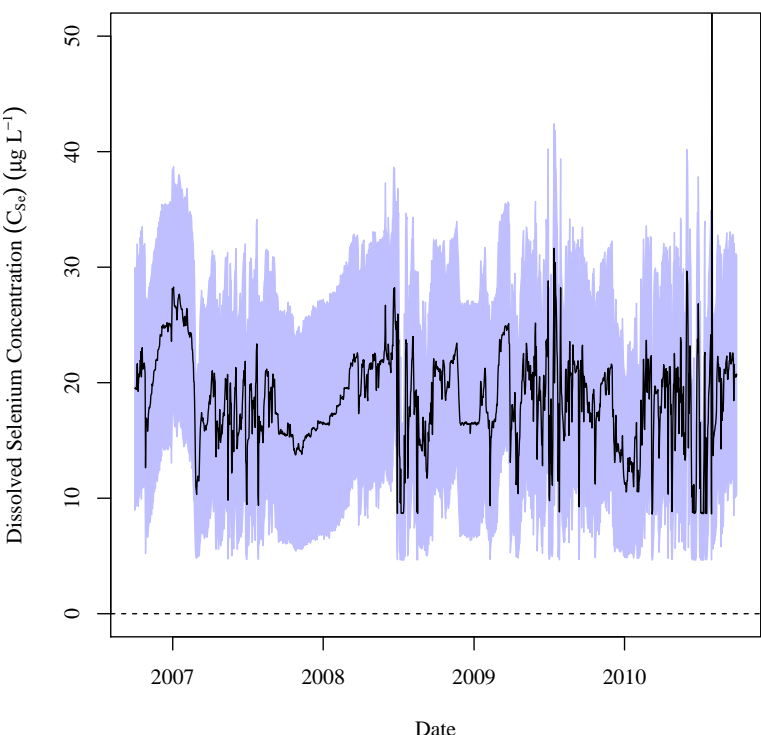


(b) Stochastic Model.

Figure 5.19 (Cont). DSR Deterministic and stochastic model time series of dissolved selenium concentration.

C_{D23} 

(a) Deterministic Model.

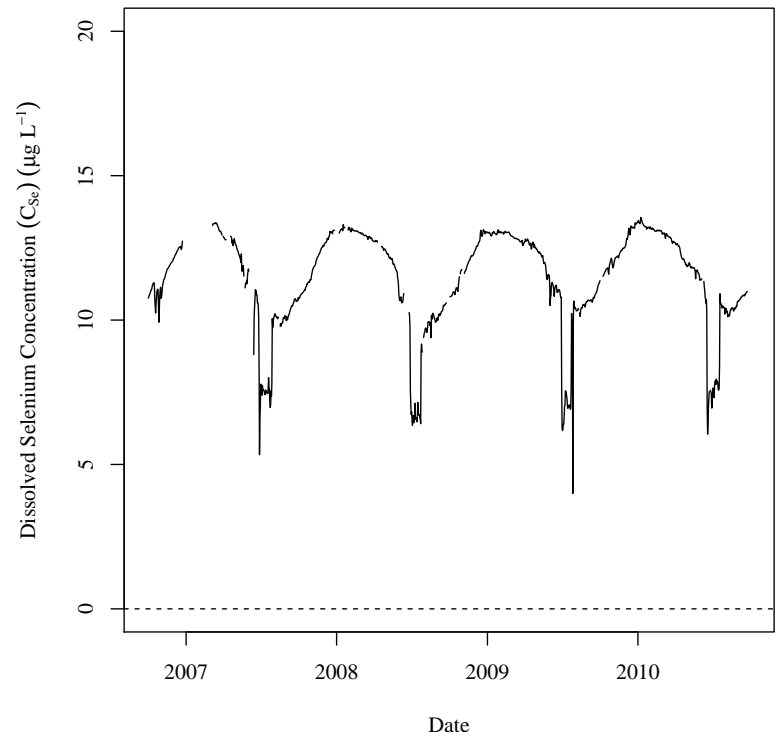


(b) Stochastic Model.

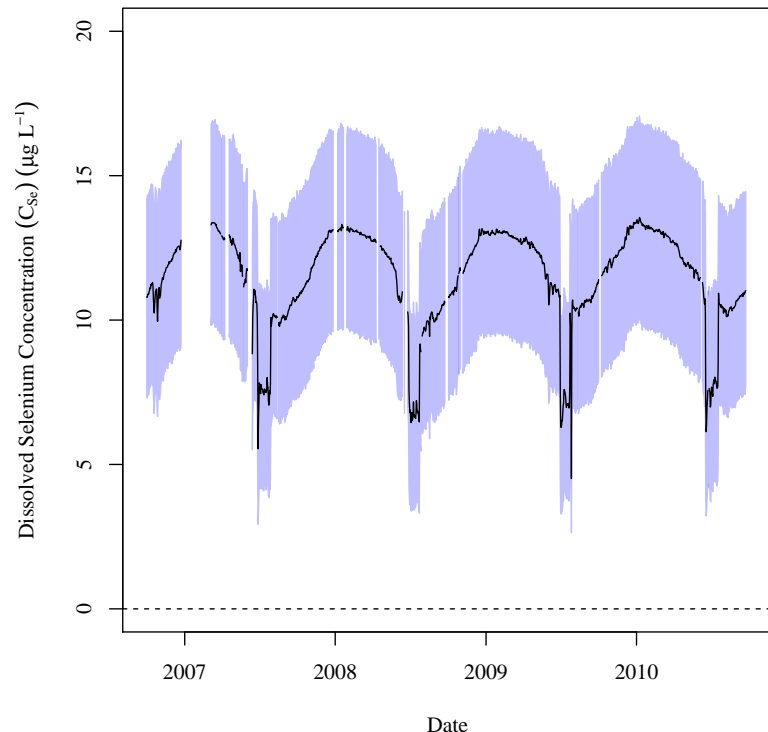
Figure 5.19 (Cont). DSR Deterministic and stochastic model time series of dissolved selenium concentration.

$$C_{ARK,d=7.7}$$

281



(a) Deterministic Model.

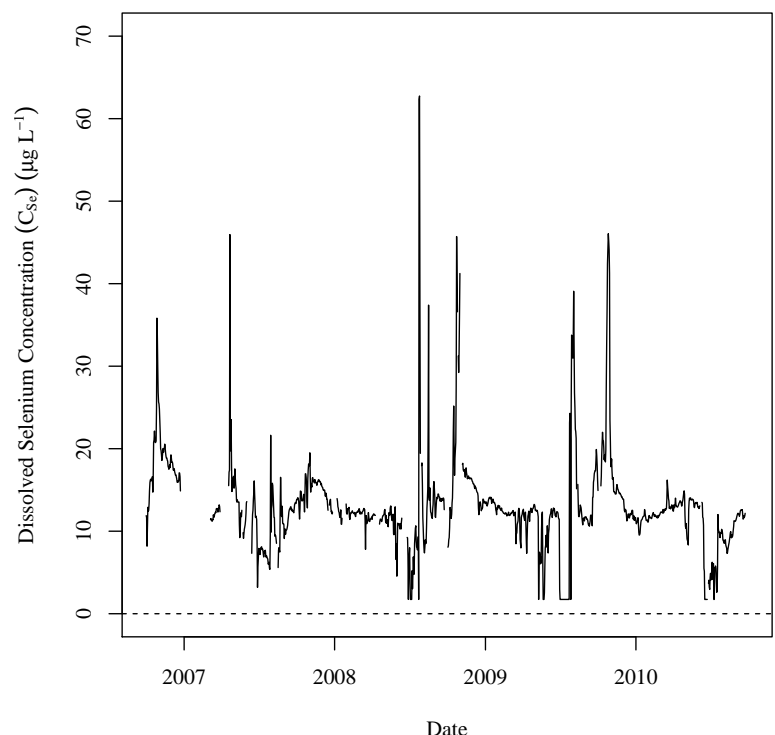


(b) Stochastic Model.

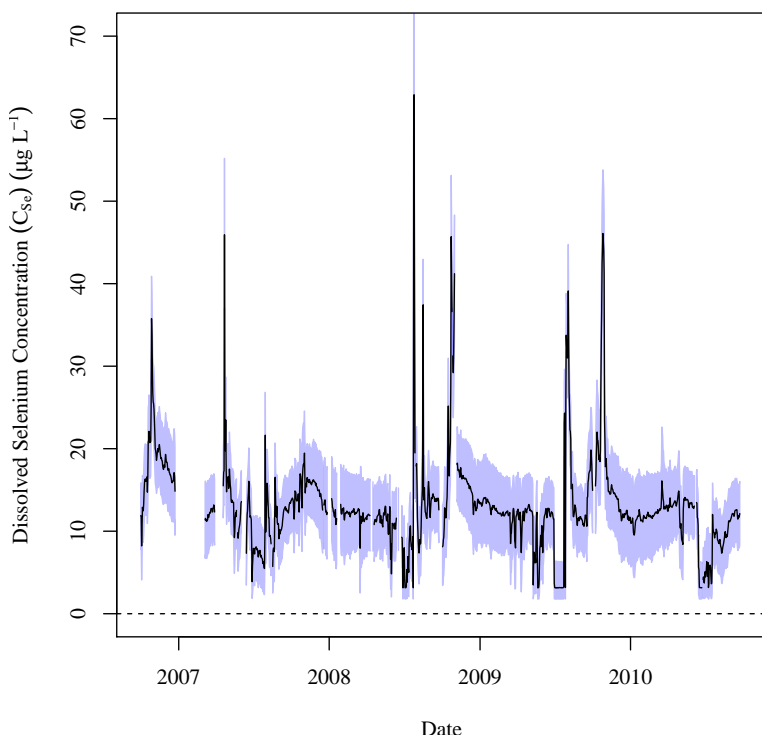
Figure 5.19 (Cont). DSR Deterministic and stochastic model time series of dissolved selenium concentration.

C_{U57}

282



(a) Deterministic Model.



(b) Stochastic Model.

Figure 5.19 (Cont). DSR Deterministic and stochastic model time series of dissolved selenium concentration.

These figures show a definite cyclical pattern for concentrations within the main stem of the Arkansas R. Although the pattern varies, it is interesting to note that higher concentrations are calculated during the colder months in all cases.

There were not any significant discrepancies between the calculated data and the measured data nor between the deterministic and stochastic models. The results and comparison of the results are presented in tables 5.13 and 5.14 for the USR and DSR, respectively. These tables present the mean, 2.5th, and 97.5th percentile of the deterministic time series results. These tables also present the mean, 2.5th, and 97.5th percentile of the 1-D stochastic mean time series results. The last column provides the percent difference between the two calculated mean values. Again, the stochastic and deterministic calculated dissolved selenium concentration resluts are not significantly different.

5.2.2. *Uncertainty of Lab Selenium Concentration Values*

Any sampling methodology is subject to error from a multitude of sources. The additional combined selenium concentration estimating error, ε_2 , includes error due to variations in field sampling technique, environmental variations, and lab analysis variations. The samples collected in this study were also subject to an additional unknown error due to environmental conditions during transport from the field to the lab. In some cases, samples reached the lab seven days after being taken in the field. Field technicians took great efforts to keep the samples chilled throughout the field collection process. At the end of a field sampling trip, samples were sent in a chilled insulated container by mail to the lab. The environmental conditions during this transport phase were not and could not be monitored.

Upon receipt at the lab, samples were stored in a refrigerator until they were analyzed. The temperature upon receipt was not recorded by any of the labs. The labs stored the

Table 5.13. USR dissolved selenium concentration results table. Values are in units of $\mu\text{g L}^{-1}$.

$$C_{U163}$$

Deterministic Model Time Series

2.5th Percentile	Mean	97.5th Percentile
3.49	10.3	16.3

Stochastic Model Summary Statistics Time Series

Time Series	2.5th Percentile	Mean	97.5th Percentile
97.5th Percentile	4.51	11.3	17.4
Mean	3.49	10.3	16.3
2.5th Percentile	2.48	9.2	15.2
Pearson Correlation = 1			

$$C_{U201}$$

Deterministic Model Time Series

2.5th Percentile	Mean	97.5th Percentile
3.81	10.9	13.7

Stochastic Model Summary Statistics Time Series

Time Series	2.5th Percentile	Mean	97.5th Percentile
97.5th Percentile	5.68	12.6	15.4
Mean	3.97	10.9	13.7
2.5th Percentile	2.71	9.25	12
Pearson Correlation = 0.9995			

samples in a refrigerator for a maximum of four days. It is not known what, if any, chemistry changes within the samples from the time the samples are taken to the time they are analyzed at the lab. It is also unknown if there is any difference due to minor variations in sampling technique.

Table 5.13 (Cont). USR dissolved selenium concentration results table.

C_{U74}

Deterministic Model Time Series

2.5th Percentile	Mean	97.5th Percentile
3.31	11.9	18.6

Stochastic Model Summary Statistics Time Series

Time Series	2.5th Percentile	Mean	97.5th Percentile
97.5th Percentile	5.14	13.7	20.7
Mean	3.89	11.9	18.6
2.5th Percentile	3.33	10.2	16.9
Pearson Correlation = 0.9997			

$C_{ARK,D=85.0}$

Deterministic Model Time Series

2.5th Percentile	Mean	97.5th Percentile
5.35	11.7	15.9

Stochastic Model Summary Statistics Time Series

Time Series	2.5th Percentile	Mean	97.5th Percentile
97.5th Percentile	7.42	13.7	18
Mean	5.32	11.6	15.9
2.5th Percentile	3.25	9.49	13.8
Pearson Correlation = 0.9999			

Preferably, these error sources could be accounted for on an individual basis. There were a number of factors that determined that this methodology would not work. Error analysis would have to be performed for each field technician. The total project data collection time frame spanned 10 years and included an unknown number of field technicians.

Table 5.13 (Cont). USR dissolved selenium concentration results table.

$$C_{ARK,D=16.4}$$

Deterministic Model Time Series

2.5th Percentile	Mean	97.5th Percentile
3.83	10.1	14.4

Stochastic Model Summary Statistics Time Series

Time Series	2.5th Percentile	Mean	97.5th Percentile
97.5th Percentile	5.89	12.2	16.5
Mean	3.82	10.1	14.3
2.5th Percentile	1.96	8	12.2
Pearson Correlation = 0.9999			

$$C_{ARK,D=47.2}$$

Deterministic Model Time Series

2.5th Percentile	Mean	97.5th Percentile
4.51	10.8	15.1

Stochastic Model Summary Statistics Time Series

Time Series	2.5th Percentile	Mean	97.5th Percentile
97.5th Percentile	6.6	12.9	17.2
Mean	4.49	10.8	15
2.5th Percentile	2.42	8.66	12.9
Pearson Correlation = 0.9999			

The data collection methodology previously described was not entirely adhered for the entire data collection time frame. Not all field technicians recorded what was later considered valuable information such as date and time of sample collection, field technician name, and sampling variances.

Table 5.13 (Cont). USR dissolved selenium concentration results table.

$$C_{ARK,D=12.5}$$

Deterministic Model Time Series

2.5th Percentile	Mean	97.5th Percentile
3.75	10.1	14.3

Stochastic Model Summary Statistics Time Series

Time Series	2.5th Percentile	Mean	97.5th Percentile
97.5th Percentile	5.82	12.1	16.4
Mean	3.74	10	14.3
2.5th Percentile	1.88	7.91	12.1
Pearson Correlation = 0.9999			

$$C_{U207}$$

Deterministic Model Time Series

2.5th Percentile	Mean	97.5th Percentile
4.82	15.4	18.8

Stochastic Model Summary Statistics Time Series

Time Series	2.5th Percentile	Mean	97.5th Percentile
97.5th Percentile	7.58	17.5	20.8
Mean	5.74	15.4	18.7
2.5th Percentile	4.86	13.3	16.7
Pearson Correlation = 0.9995			

The travel distance between the field locations and the lab is also a factor that cannot be overcome. Preferably, the lab would be located fairly close to either the university or the study region. At the start of the sampling time frame, there was no lab in Colorado capable of handling the required analysis with the additional physical, schedule, and fiscal requirements

Table 5.13 (Cont). USR dissolved selenium concentration results table.

C_{U167}

Deterministic Model Time Series

2.5th Percentile	Mean	97.5th Percentile
3.25	10.4	15.1

Stochastic Model Summary Statistics Time Series

Time Series	2.5th Percentile	Mean	97.5th Percentile
97.5th Percentile	4.71	11.8	16.4
Mean	3.32	10.5	15.1
2.5th Percentile	2.13	9.19	13.9
Pearson Correlation = 0.9998			

C_{U60}

Deterministic Model Time Series

2.5th Percentile	Mean	97.5th Percentile
3.98	11	21.3

Stochastic Model Summary Statistics Time Series

Time Series	2.5th Percentile	Mean	97.5th Percentile
97.5th Percentile	7.7	14.3	24.6
Mean	5.16	11.3	21.2
2.5th Percentile	4.02	8.68	17.9
Pearson Correlation = 0.9983			

imposed by the project supervisor. The additional distance made determining error due to transport time difficult to determine.

All dissolved selenium samples were treated with nitric acid to stabilize the sample for transport. The stabilization method and acceptable sample storage duration was discussed

Table 5.13 (Cont). USR dissolved selenium concentration results table.

$$C_{LAJWWTP}$$

Deterministic Model Time Series

2.5th Percentile	Mean	97.5th Percentile
16.1	19.7	25

Stochastic Model Summary Statistics Time Series

Time Series	2.5th Percentile	Mean	97.5th Percentile
97.5th Percentile	24.1	27.9	33.2
Mean	15.9	19.4	24.7
2.5th Percentile	8.05	11.2	16.2
Pearson Correlation = 0.9997			

at length with the lab before any sampling was undertaken. The samples were additionally preserved by storing and transporting them on ice. We were assured by the sampling lab that this additional preservation step would only serve to lengthen the time the sample would be considered viable.

5 The temperature variations experienced by the samples was not considered a factor during the sample collect time frame. On hind-sight, this could have easily been performed by adding a temperature transponder to the sample container before shipping. This technique might have brought transport temperature control issues to the technician's or the project supervisor's attention if the existed. Unfortunately, this information is not available and
10 we are left to assume that even though significant temperature variations may have existed, those variations did not significantly change the sample chemistry due to the applied sample preservation.

Field and lab blanks were used to determine if the samples were subjected to contamination from the environment or cross contamination from other samples. No lab or field

Table 5.14. DSR dissolved selenium concentration results table. Values are in units of $\mu\text{g L}^{-1}$.

C_{D101C}

Deterministic Model Time Series

2.5th Percentile	Mean	97.5th Percentile
3.07	10.5	13.6

Stochastic Model Summary Statistics Time Series

Time Series	2.5th Percentile	Mean	97.5th Percentile
97.5th Percentile	8.5	15.5	18.6
Mean	4.33	10.6	13.6
2.5th Percentile	2.21	6.02	8.68
Pearson Correlation = 0.997			

C_{D106C}

Deterministic Model Time Series

2.5th Percentile	Mean	97.5th Percentile
10.5	14.6	16.4

Stochastic Model Summary Statistics Time Series

Time Series	2.5th Percentile	Mean	97.5th Percentile
97.5th Percentile	17.3	21.4	23.3
Mean	10.7	14.7	16.5
2.5th Percentile	4.64	8.09	9.9
Pearson Correlation = 0.9996			

blanks exhibited any evidence of contamination. Since the blanks contained only de-ionized water, they did not have any chemical or physical markers to show whether they experienced unacceptable environmental conditions.

Table 5.14 (Cont). DSR dissolved selenium concentration results table.

$$C_{D23}$$

Deterministic Model Time Series

2.5th Percentile	Mean	97.5th Percentile
6.19	18.2	26.4

Stochastic Model Summary Statistics Time Series

Time Series	2.5th Percentile	Mean	97.5th Percentile
97.5th Percentile	18.3	28.8	36.8
Mean	9.6	18.5	26.4
2.5th Percentile	4.71	8.94	16
Pearson Correlation = 0.9928			

$$C_{ARK,d=37.7}$$

Deterministic Model Time Series

2.5th Percentile	Mean	97.5th Percentile
6.91	11.4	13.3

Stochastic Model Summary Statistics Time Series

Time Series	2.5th Percentile	Mean	97.5th Percentile
97.5th Percentile	10.3	14.9	16.8
Mean	6.96	11.5	13.3
2.5th Percentile	3.73	8.05	9.87
Pearson Correlation = 0.9999			

Lab analysis errors are known to exist and the lab states these ranges. Since the lab was USEPA certified and subscribed to USEPA proficiency testing, we can assume that the lab errors are as stated by the labs. Verification through a different lab was not performed

Table 5.14 (Cont). DSR dissolved selenium concentration results table.

$$C_{D57}$$

Deterministic Model Time Series

2.5th Percentile	Mean	97.5th Percentile
1.73	13.1	27.2

Stochastic Model Summary Statistics Time Series

Time Series	2.5th Percentile	Mean	97.5th Percentile
97.5th Percentile	6.32	17.5	33.4
Mean	3.17	13.1	27.2
2.5th Percentile	1.79	8.81	22.2
Pearson Correlation = 0.999			

at any time. Although the lab error range was known, it was not known if that error range could be influence by variances in the sampling technique or transport environment.

Combining all individual unaccountable errors into a single error term seemed to be the most pragmatic means to estimate the total error. The only data available to analyze 5 was the set of duplicate samples. As previously discussed at least two samples per sample trip were taken as duplicates. Duplicate samples were taken near the beginning and the end of the sampling trip. Only the 'A' sample was used for concentration estimation. The 'B' samples were taken to monitor for equipment malfunction, significant deviation in sampling methodology, and significant lab error. The 'A' and 'B' samples were taken using the same 10 equipment and transported in the same container from the sample location to the lab. Since they experienced the same environmental conditions, it was unreasonable to assume that this method could be used to estimate the error due to extreme transport environmental conditions. The samples were well preserved and it was assumed that temperature variations did not significantly affect the samples.

Lab results for the 'A' and 'B' samples from both the USR and DSR were complied into a single data set. Date, location, and all other identifying markers were removed from the data set to reduce potential bias due to prior knowledge of the individual samples. 'A' samples were assumed to be the expected value for the following samples.

Figure 5.20 shows the comparisons analyzed. The top graph plots the 'A' and 'B' sample concentrations against the difference from the mean of the 'A' and 'B' samples. The bottom graph plots the same data, but with respect to the percent difference from the mean of the 'A' and 'B' samples.

Figure 5.21 shows the 'A' and 'B' samples plotted against the difference and percent difference. This analysis was performed to determine if there was a correlation between the magnitude of the concentration and the magnitude of the difference. No such correlation was found.

The percent difference between the reported lab values and the mean duplicates was best fit with a logistic distribution. The logistic distribution had a location parameter of -0.067 and a scale parameter of 1.807. This comparison and distribution combination was chosen because it had the best fit when compared to others using Kolmogorov-Smirnov, Cramer-von Mises, and Anderson-Darling goodness-of-fit test statistics. The duplicate samples had a mean difference from the mean of their respective 'A' and 'B' samples of 0% with a standard deviation of 4.16%. This corresponds to 95% of the data within $\pm 10\%$ of the reported value

Calculated dissolved selenium concentrations at specific sites were constrained to fit between one-half of the minimum historically reported value and 1-1/2 of the maximum historically reported value. This range should allow for dissolved selenium concentration variations that are comparable to the values reported from the field samples. The range

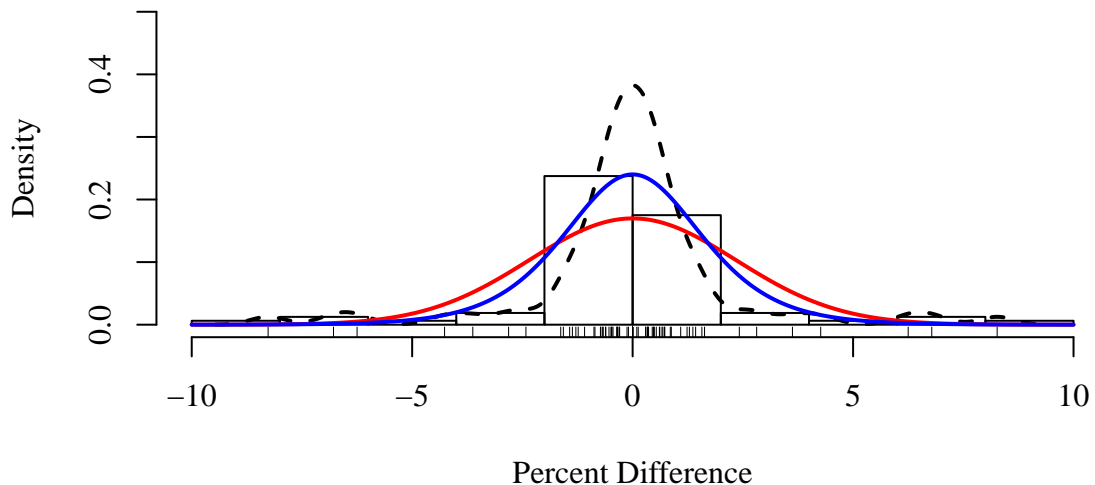
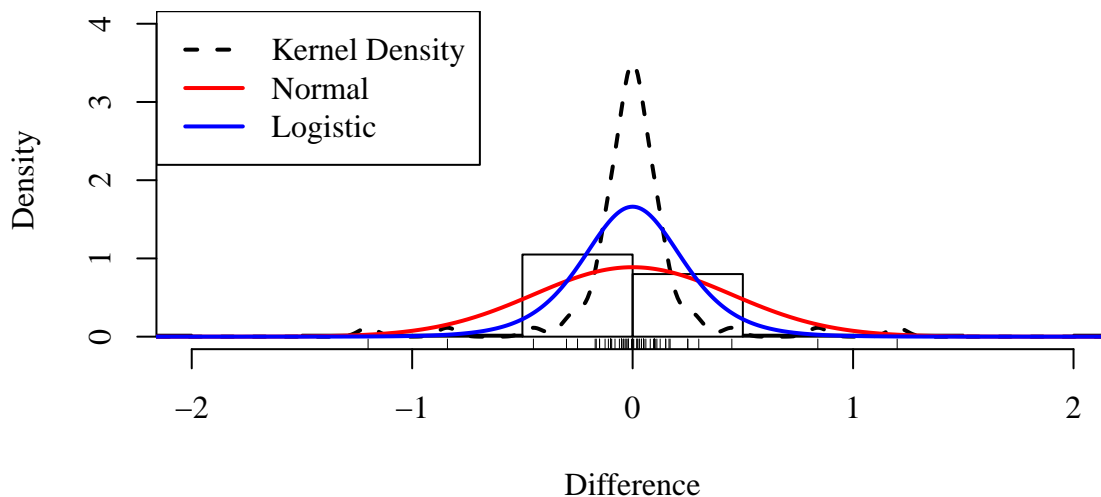


Figure 5.20. Dissolved Selenium Concentration Uncertainty. Each sub-figure shows the comparison of the lab reported dissolved selenium concentration and the mean for each pair of duplicate samples.

allowed for variation beyond the reported concentration range to allow for the possibility that concentrations beyond the range may possibly have existed at some time.

Visual analysis seems to indicate that using the percent difference distribution would lead to the best characterization of the selenium sample errors. This hypothesis was tested by 5 using Kolmogorov-Smirnov, Cramer von Mises, and Anderson-Darling goodness-of-fit tests.

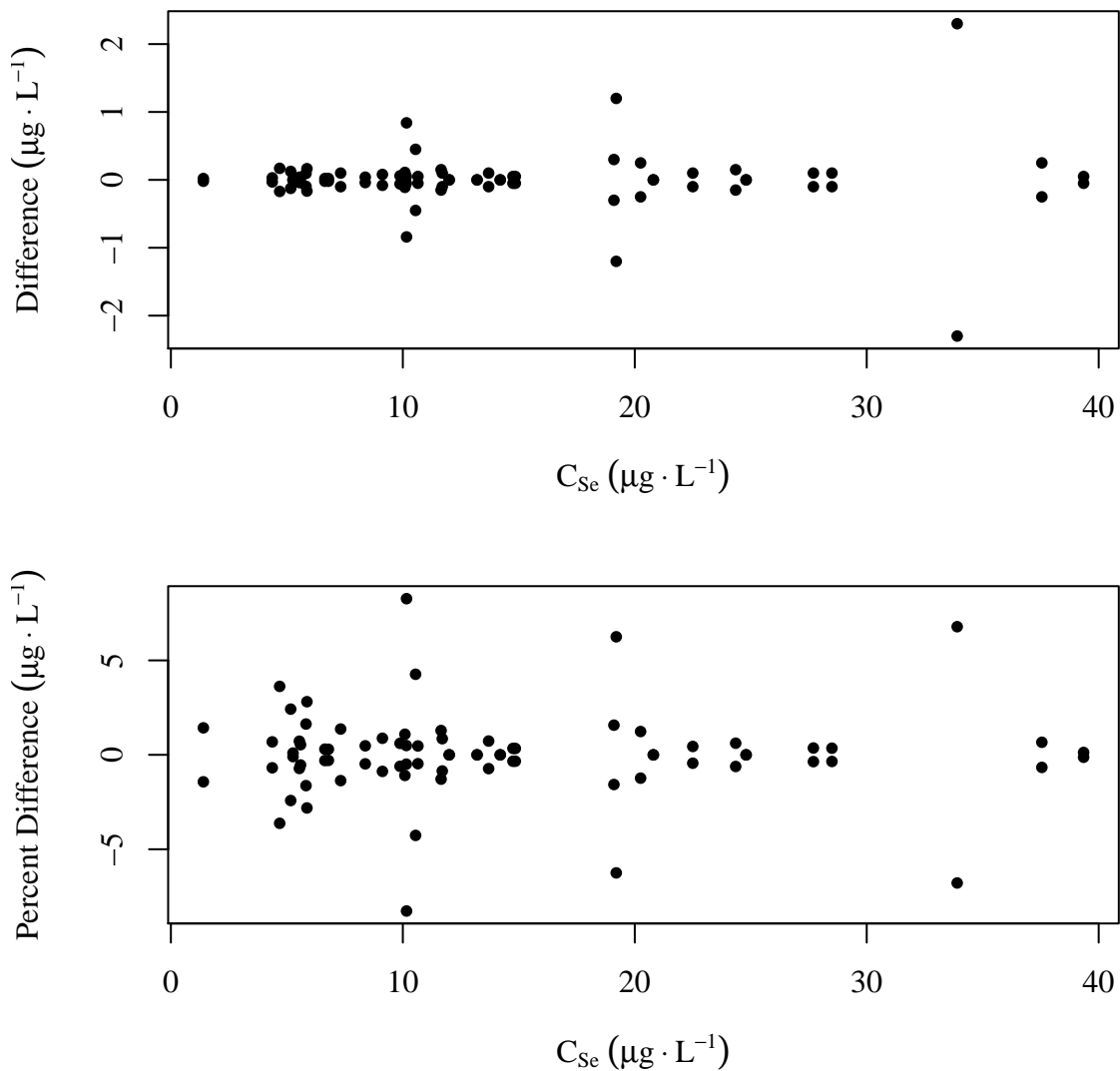


Figure 5.21. Dissolved Selenium Concentration Variation.

Results from these tests are presented in Table 5.15 (Cont). The logistic distribution of the percent difference calculation was shown to have the best fit calculation.

Given these results, the total field sampling and lab error distribution is described by a logistic distribution with a location parameter of -0.06693 and a scale parameter of 1.807.

5 The combined field sampling and lab error is bounded such that 95 % of the distribution lies in the range of approximately $\pm 6.6\%$ of the expected value.

Table 5.15 (Cont). Selenium combined error analysis goodness-of-fit test results.

Calculation	Distribution	Fit Test Result		
		K-S	CvM	A-D
Difference	normal	0.2876	2.598	13.48
	logistic	0.1644	0.8538	5.225
Percent Difference	normal	0.173	1.150	6.365
	logistic	0.1195	0.4139	2.729

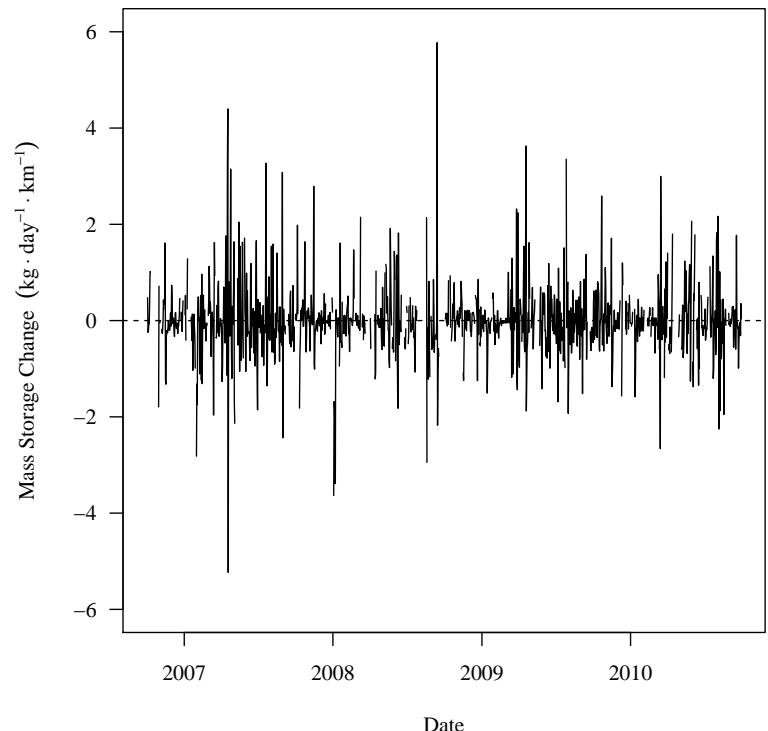
The combined field sampling and lab error is calculated independently from the selenium concentration estimation error previously described. The estimated selenium concentration, without the estimation estimation, is taken as the expected value for the combined field sampling and lab error.

5 5.2.3. Mass Storage Change Results

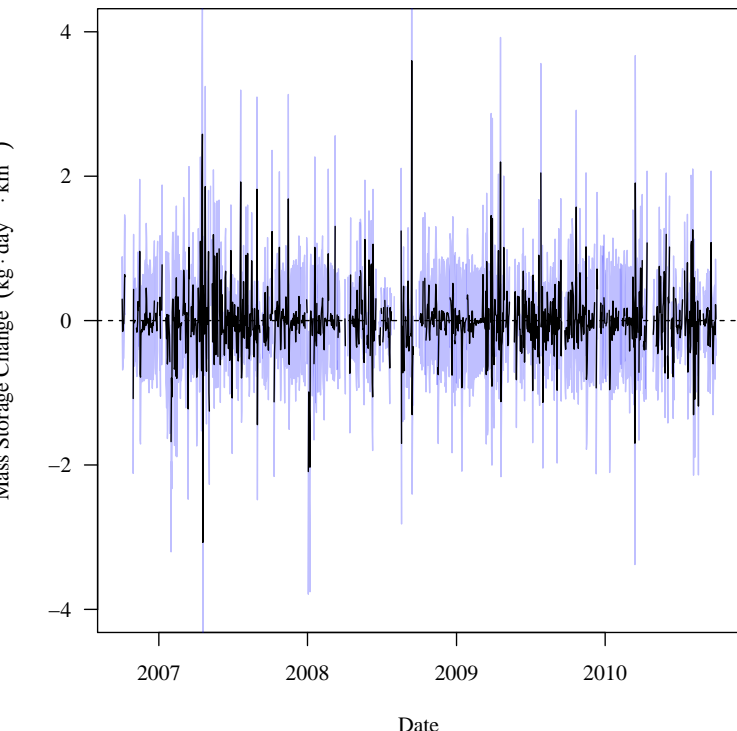
Figures 5.22 and 5.23 show the deterministic and stochastic time series of the mass storage change within each of the river segments in the USR and DSR, respectively. The black line in the stochastic model sub-figure is the mean of the realizations and the blue band is the 97.5th CIR. Results in these figures and tables 5.16 and 5.17 are presented in units 10 of $\text{kg d}^{-1} \text{km}^{-1}$. Standardizing values to mass storage per unit length allows for comparison between all river segments in both study reaches. This also allows for comparison between the mass storage change components and the mass transport components of the mass balance models.

$$\frac{\Delta S_{M,A}}{\Delta t}$$

297



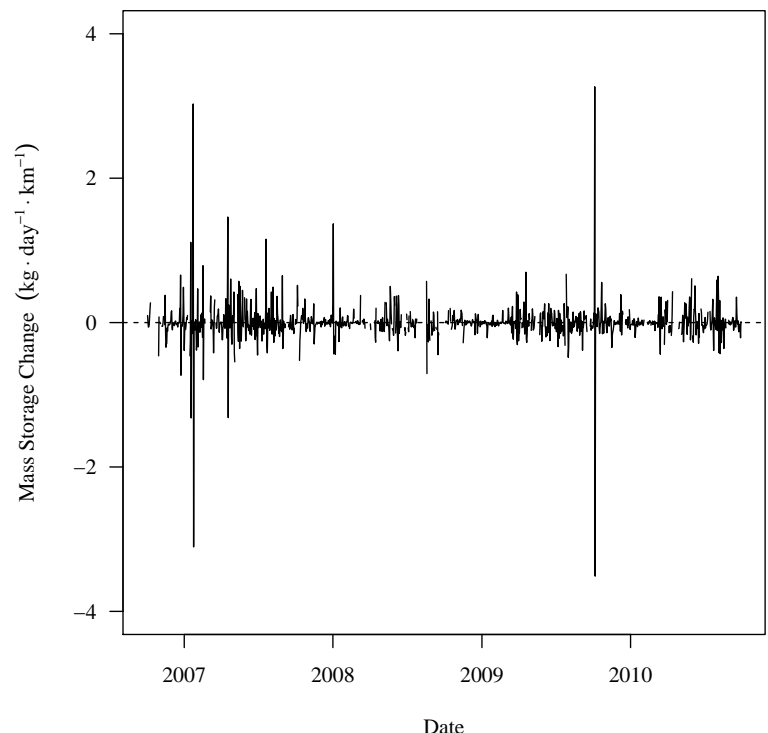
(a) Deterministic Model.



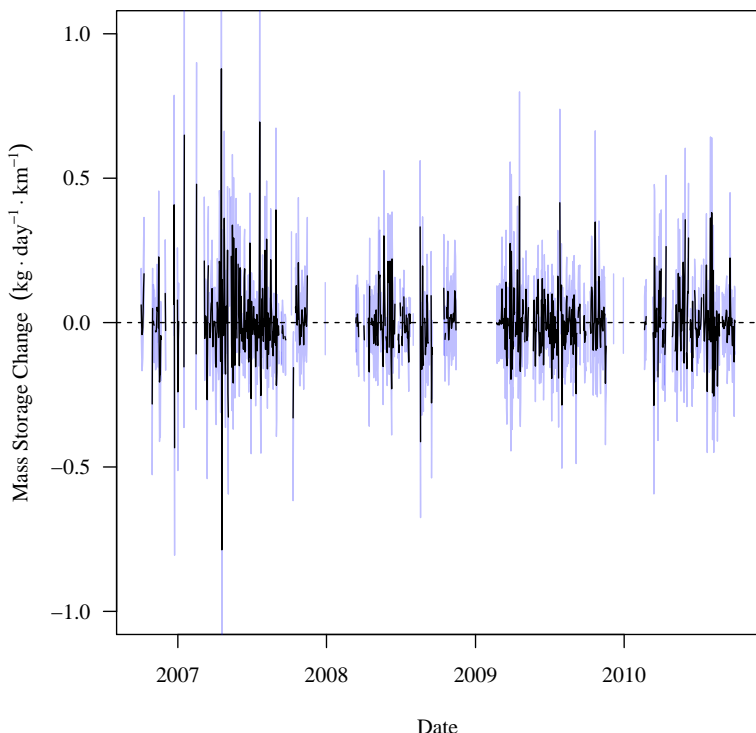
(b) Stochastic Model.

Figure 5.22. USR river segment deterministic and stochastic dissolved selenium mass storage change time series. For the stochastic model, the line is the mean of the realizations and the blue band is the 97.5th CIR.

$$\frac{\Delta S_{M,B}}{\Delta t}$$

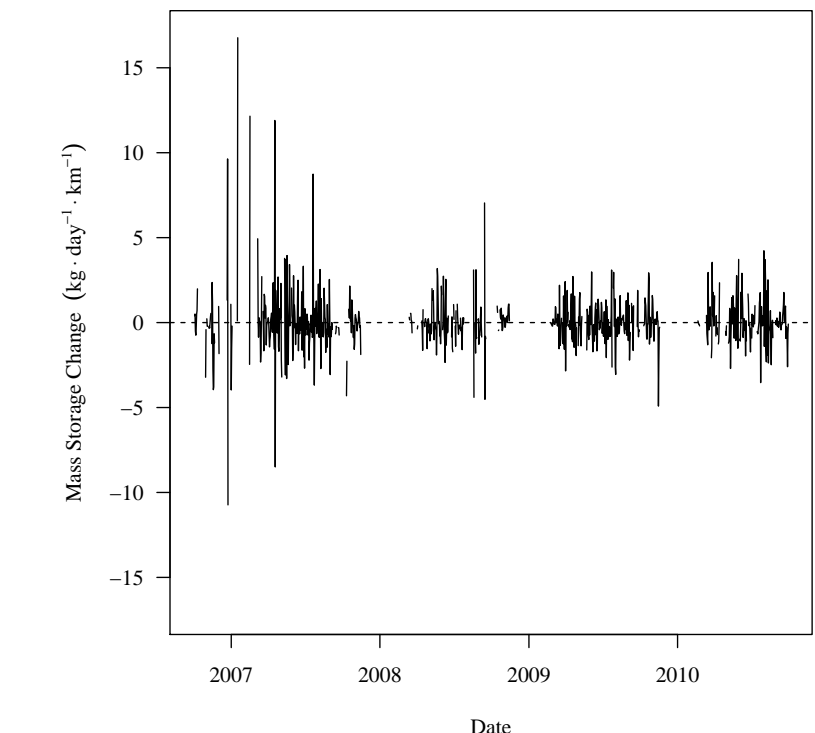


(a) Deterministic Model.

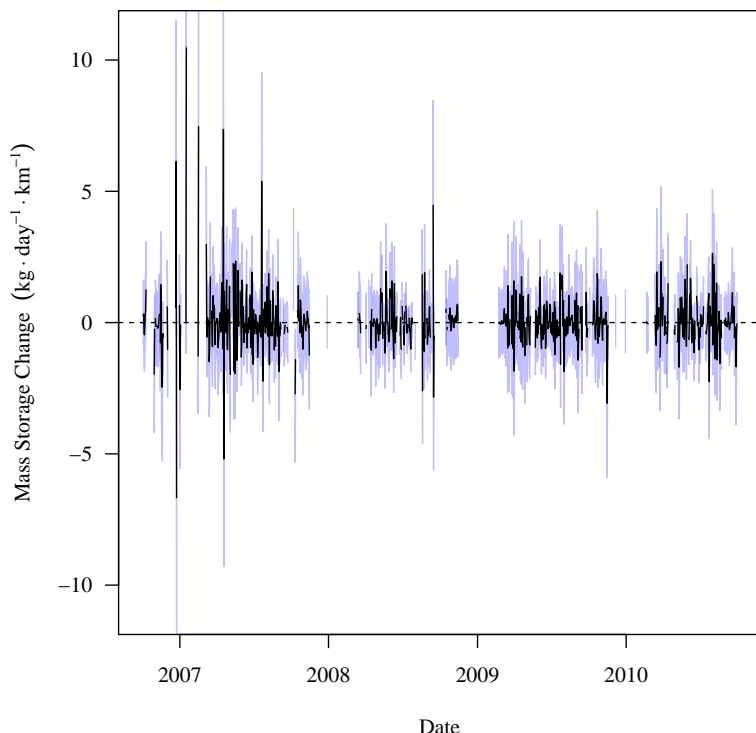


(b) Stochastic Model.

$$\frac{\Delta S_{M,C}}{\Delta t}$$

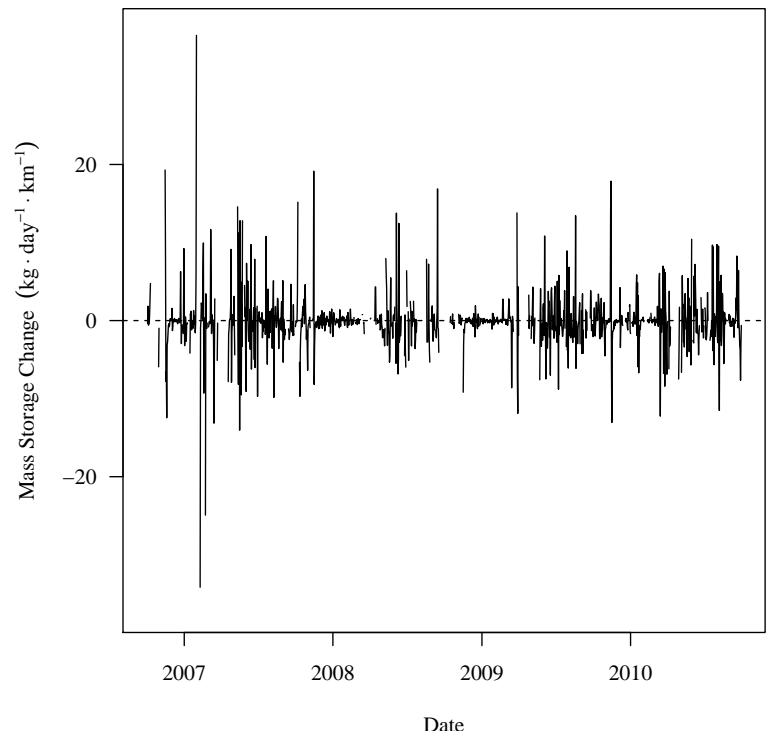


(a) Deterministic Model.

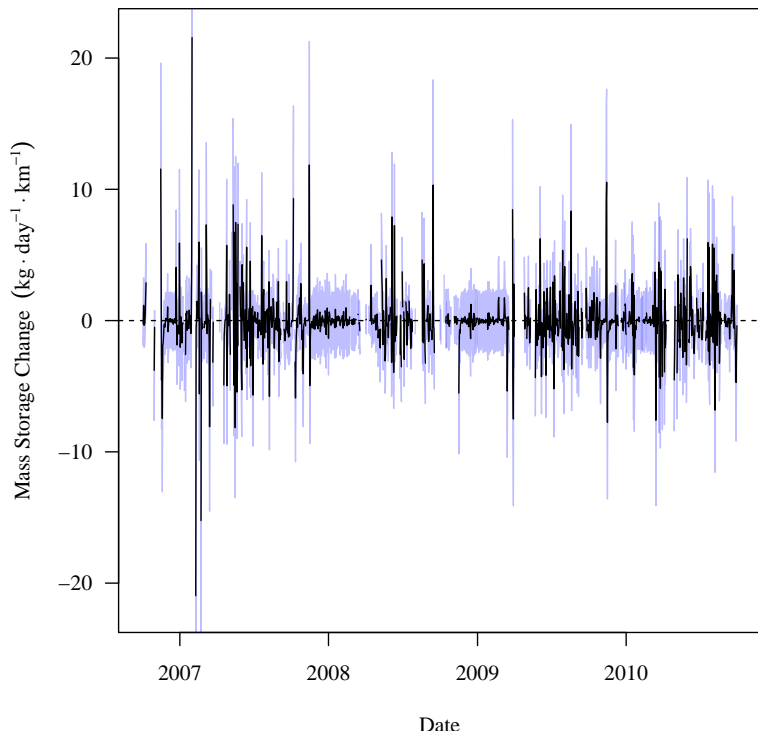


(b) Stochastic Model.

$$\frac{\Delta S_{M,D}}{\Delta t}$$



(a) Deterministic Model.



(b) Stochastic Model.

Figure 5.22 (Cont). USR river segment deterministic and stochastic dissolved selenium mass storage change time series.

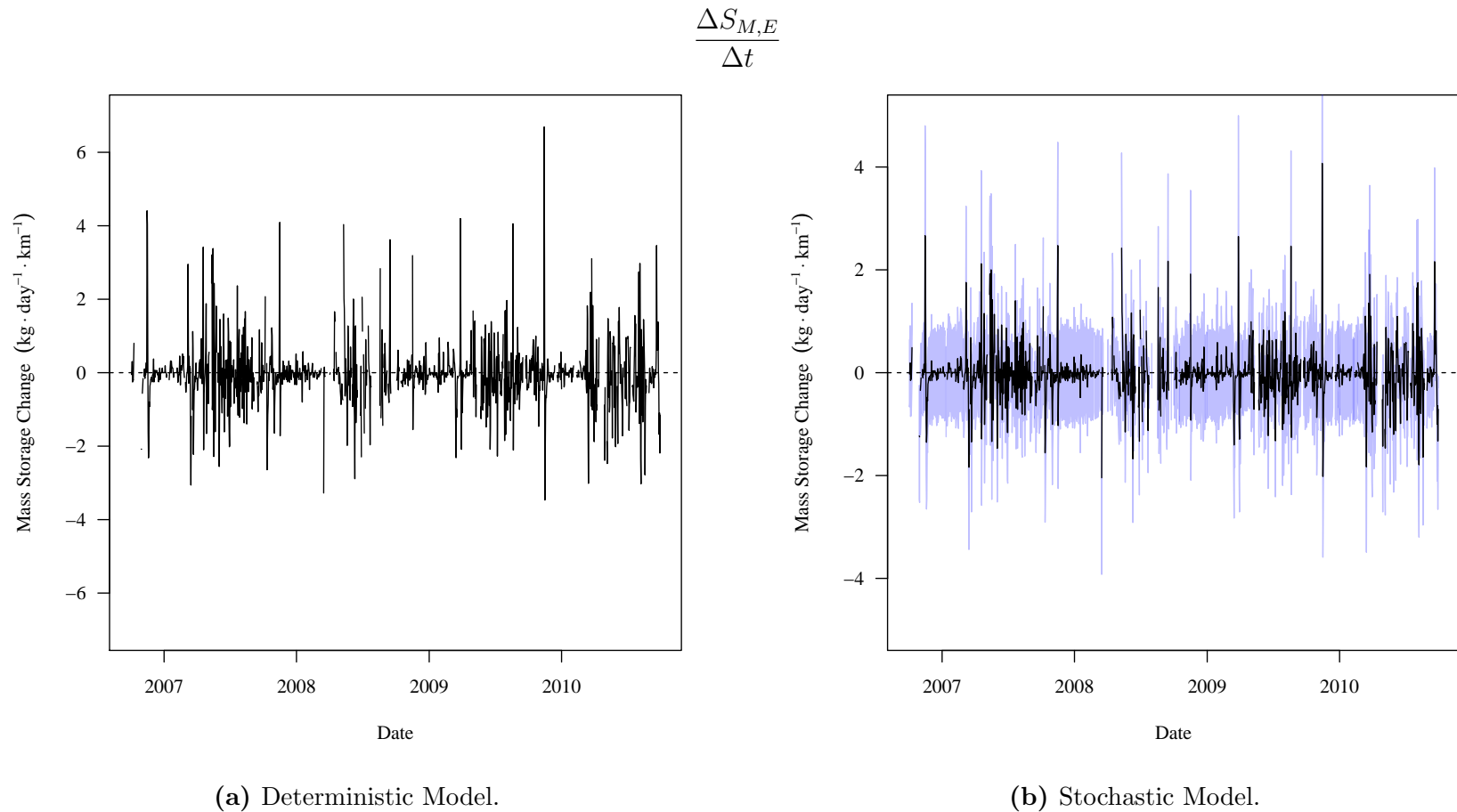
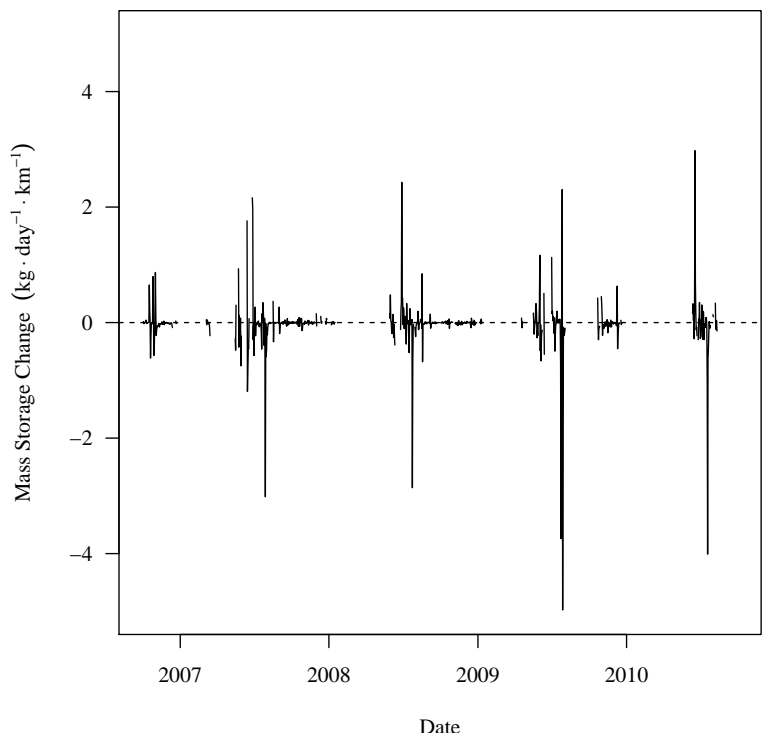
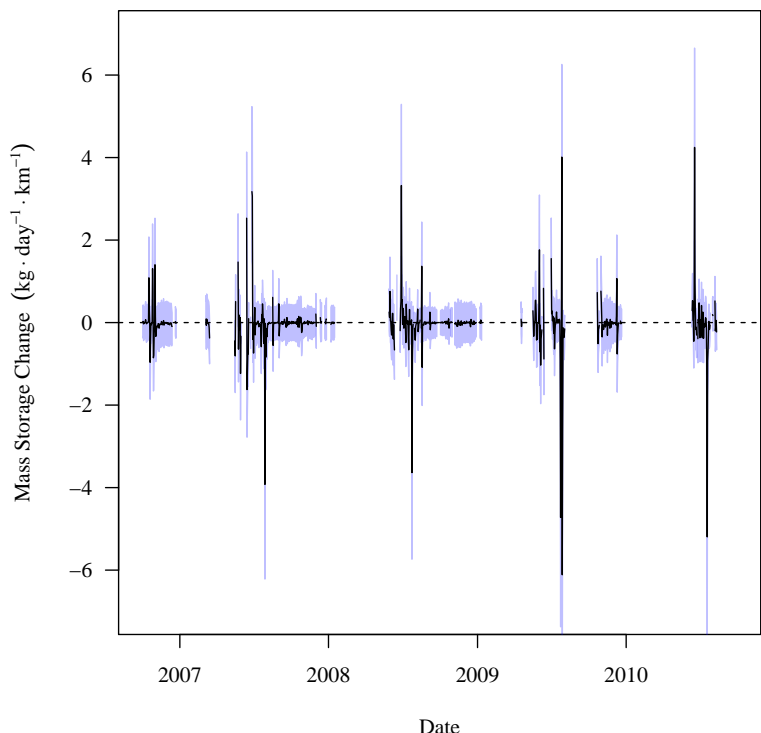


Figure 5.22 (Cont). USR river segment deterministic and stochastic dissolved selenium mass storage change time series.

$$\frac{\Delta S_{M,F}}{\Delta t}$$



(a) Deterministic Model.



(b) Stochastic Model.

Figure 5.23. USR river segment deterministic and stochastic dissolved selenium mass storage change time series. For the stochastic model, the line is the mean of the realizations and the blue band is the 97.5th CIR.

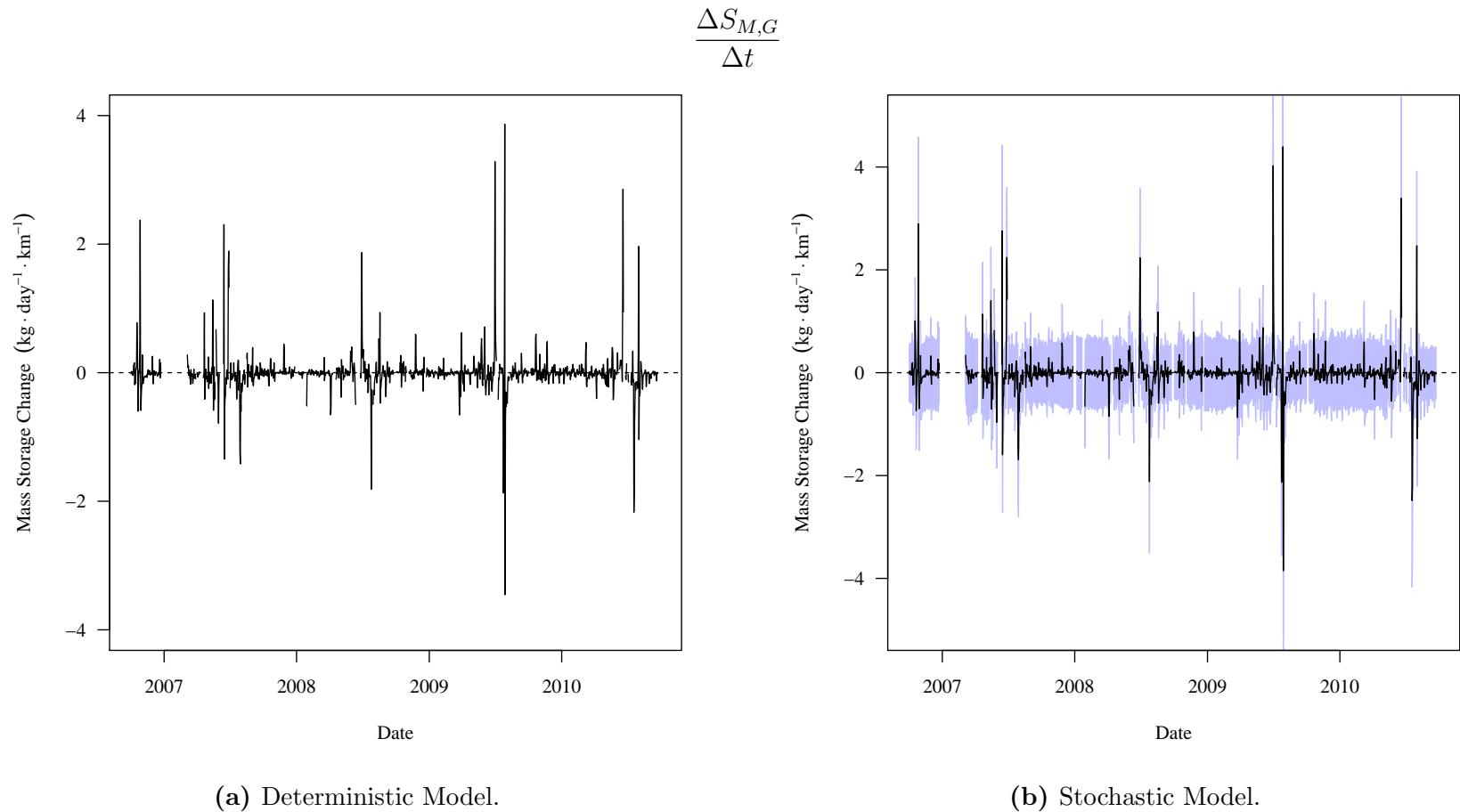


Figure 5.23 (Cont). USR river segment deterministic and stochastic dissolved selenium mass storage change time series.

Comparing the sub-figures provides for a visual goodness-of-fit analysis between the deterministic and stochastic models. All USR river segment stochastic models agree with the deterministic models. It should be noted that there is quite a fair amount of uncertainty associated with the values calculated for the stochastic model. This is the compounding of
5 uncertainties from the multiple input variables. This is as expected for a complex multi-variate model.

The calculated selenium storage change values for each reach were compared between the deterministic and stochastic models and are reported in tables 5.16 and 5.17 for the USR and DSR, respectively. All selenium storage change values in the figures and tables
10 are presented in units of $\text{kg d}^{-1} \text{ km}^{-1}$. This table is presented in a similar fashion to other comparison tables in this chapter.

These tables show that the deviation between the deterministic model time-series and the stochastic model mean time-series is low, but higher than the values calculated for the individual input variables. This is most likely indicative of the compounding of input
15 variable uncertainties. The percent deviation between the models for segment B in the USR is deceptive. Both the deterministic model time-series mean value and the stochastic model mean time-series mean value are near zero. This causes any deviation to appear large.

Table 5.16. USR river segment deterministic and stochastic dissolved selenium mass storage change results tables. Values are in units of $\text{kg d}^{-1} \text{ km}^{-1}$.

$$\frac{\Delta S_{M,A}}{\Delta t}$$

Deterministic Model Time Series

	2.5th Percentile	Mean	97.5th Percentile
	-1.44 (-3.17)	-0.0094 (-0.0207)	1.66 (3.66)

Stochastic Model Summary Statistics Time Series

Time Series	2.5th Percentile	Mean	97.5th Percentile
97.5th Percentile	-0.164 (-0.362)	0.575 (1.27)	1.96 (4.32)
Mean	-0.859 (-1.89)	-0.00538 (-0.0119)	1.01 (2.23)
2.5th Percentile	-1.84 (-4.06)	-0.597 (-1.32)	0.217 (0.478)
Pearson Correlation = 0.9995			

$$\frac{\Delta S_{M,B}}{\Delta t}$$

Deterministic Model Time Series

	2.5th Percentile	Mean	97.5th Percentile
	-0.345 (-0.761)	-3.08e-05 (-6.79e-05)	0.423 (0.933)

Stochastic Model Summary Statistics Time Series

Time Series	2.5th Percentile	Mean	97.5th Percentile
97.5th Percentile	-0.0487 (-0.107)	0.116 (0.256)	0.49 (1.08)
Mean	-0.216 (-0.476)	0.00232 (0.00511)	0.273 (0.602)
2.5th Percentile	-0.41 (-0.904)	-0.114 (-0.251)	0.064 (0.141)
Pearson Correlation = 0.9994			

Table 5.16 (Cont). USR river segment deterministic and stochastic dissolved selenium mass storage change results tables.

$$\frac{\Delta S_{M,C}}{\Delta t}$$

Deterministic Model Time Series

	2.5th Percentile	Mean	97.5th Percentile
	-2.7 (-5.95)	0.0261 (0.0575)	3.1 (6.83)

Stochastic Model Summary Statistics Time Series

Time Series	2.5th Percentile	Mean	97.5th Percentile
97.5th Percentile	-0.336 (-0.741)	1.18 (2.6)	3.81 (8.4)
Mean	-1.63 (-3.59)	0.0151 (0.0333)	1.88 (4.14)
2.5th Percentile	-3.61 (-7.96)	-1.17 (-2.58)	0.408 (0.899)
Pearson Correlation = 0.9993			

$$\frac{\Delta S_{M,D}}{\Delta t}$$

Deterministic Model Time Series

	2.5th Percentile	Mean	97.5th Percentile
	-7 (-15.4)	-0.0873 (-0.192)	8.82 (19.4)

Stochastic Model Summary Statistics Time Series

Time Series	2.5th Percentile	Mean	97.5th Percentile
97.5th Percentile	-1.01 (-2.23)	1.93 (4.25)	9.25 (20.4)
Mean	-4.27 (-9.41)	-0.0542 (-0.119)	5.3 (11.7)
2.5th Percentile	-8.28 (-18.3)	-2.1 (-4.63)	1.23 (2.71)
Pearson Correlation = 0.9995			

Table 5.16 (Cont). USR river segment deterministic and stochastic dissolved selenium mass storage change results tables.

$\frac{\Delta S_{M,E}}{\Delta t}$			
Deterministic Model Time Series			
	2.5th Percentile	Mean	97.5th Percentile
	-1.96 (-4.32)	-0.0439 (-0.0968)	1.83 (4.03)
Stochastic Model Summary Statistics Time Series			
Time Series	2.5th Percentile	Mean	97.5th Percentile
97.5th Percentile	-0.247 (-0.545)	0.697 (1.54)	2.24 (4.94)
Mean	-1.15 (-2.54)	-0.0256 (-0.0564)	1.14 (2.51)
2.5th Percentile	-2.19 (-4.83)	-0.773 (-1.7)	0.246 (0.542)
Pearson Correlation =	0.9996		

Table 5.17. DSR river segment deterministic and stochastic dissolved selenium mass storage change results tables. Values are in units of $\text{kg d}^{-1} \text{ km}^{-1}$.

$$\frac{\Delta S_{M,F}}{\Delta t}$$

Deterministic Model Time Series

	2.5th Percentile	Mean	97.5th Percentile
	-0.000593 (-0.00131)	-2.88e-05 (-6.35e-05)	0.000491 (0.00108)

Stochastic Model Summary Statistics Time Series

Time Series	2.5th Percentile	Mean	97.5th Percentile
97.5th Percentile	-0.323 (-0.712)	0.453 (0.999)	1.62 (3.57)
Mean	-0.886 (-1.95)	-0.0352 (-0.0776)	0.772 (1.7)
2.5th Percentile	-1.71 (-3.77)	-0.535 (-1.18)	0.255 (0.562)
Pearson Correlation = 0.9945			

$$\frac{\Delta S_{M,G}}{\Delta t}$$

Deterministic Model Time Series

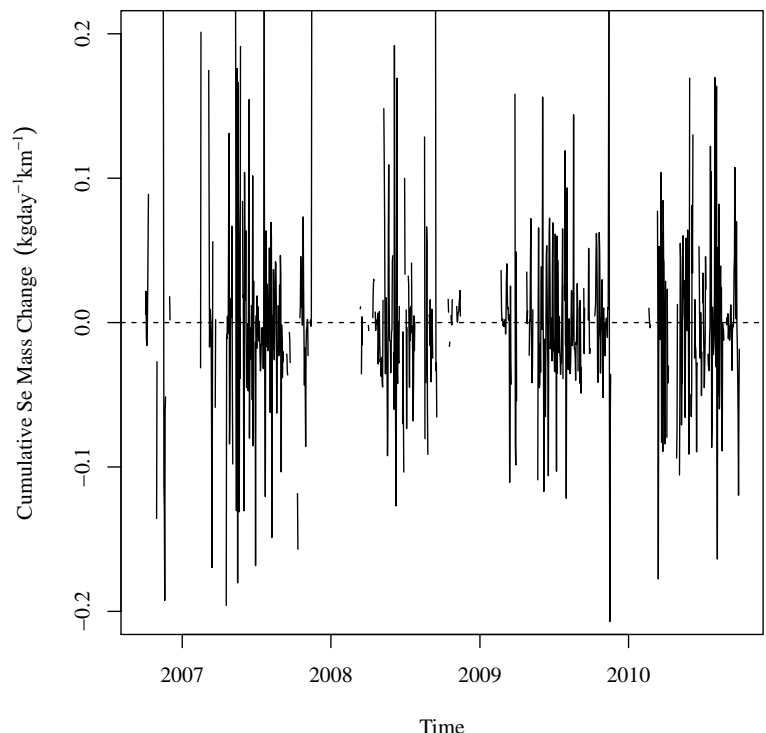
	2.5th Percentile	Mean	97.5th Percentile
	-0.000415 (-0.000915)	-6.06e-06 (-1.34e-05)	0.000486 (0.00107)

Stochastic Model Summary Statistics Time Series

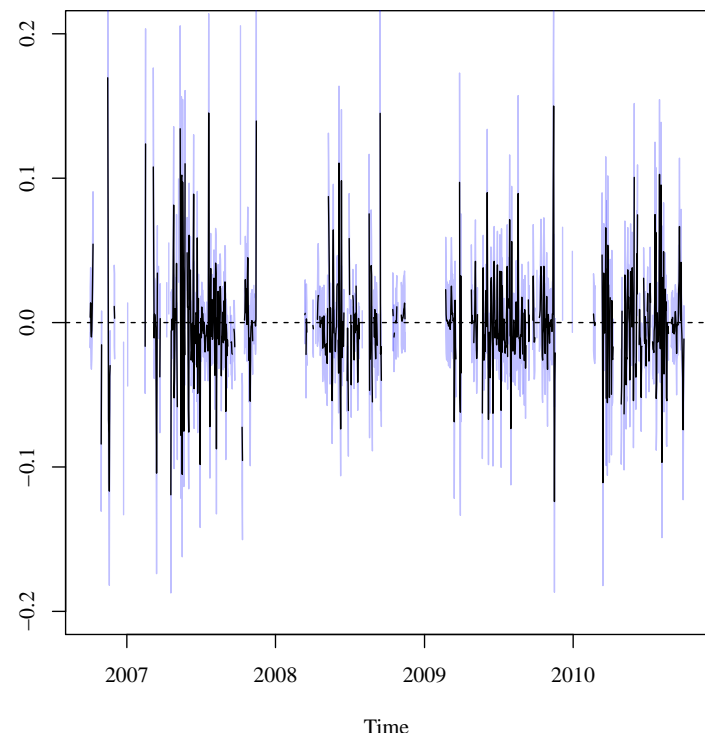
Time Series	2.5th Percentile	Mean	97.5th Percentile
97.5th Percentile	-0.00644 (-0.0142)	0.596 (1.31)	1.35 (2.98)
Mean	-0.52 (-1.15)	-0.00727 (-0.016)	0.611 (1.35)
2.5th Percentile	-1.27 (-2.8)	-0.617 (-1.36)	0.0425 (0.0937)
Pearson Correlation = 0.9986			

Figures 5.24 and 5.25 are the time-series of the deterministic and stochastic river reach selenium mass storage changes for the USR and DSR, respectively. The black line in the stochastic sub-figure is the mean for each time step. The blue band encompasses the 95% CIR for each time step. Values in these figures and associated tables are in units of
5 $\text{kg d}^{-1} \text{ km}^{-1}$. Standardizing the results allows for comparisons to be made between the two study reaches and between mass balance model components. Positive values indicate that the reach gained selenium during the given time step.

$$\frac{\Delta S_M}{\Delta t}$$



(a) Deterministic Model.

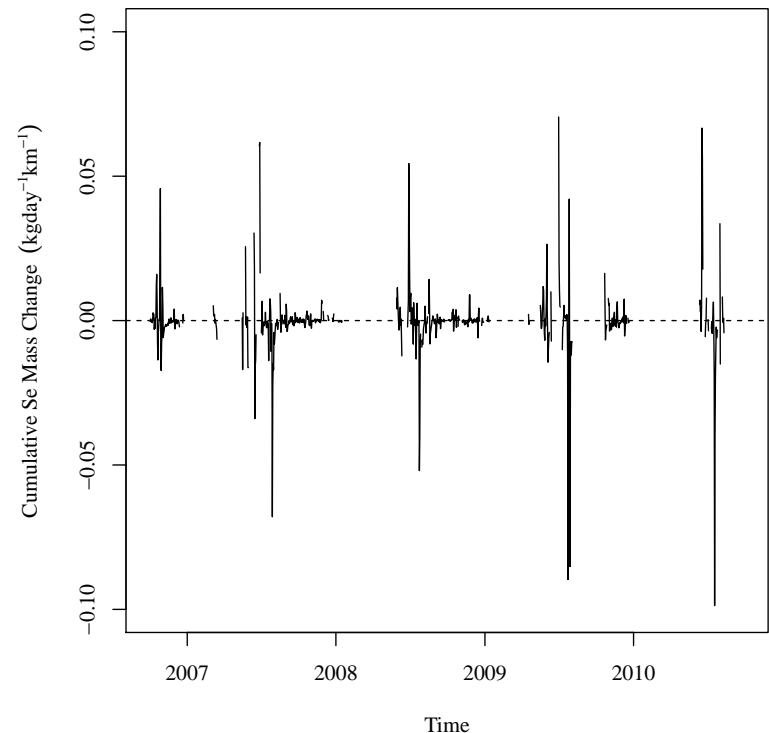


(b) Stochastic Model.

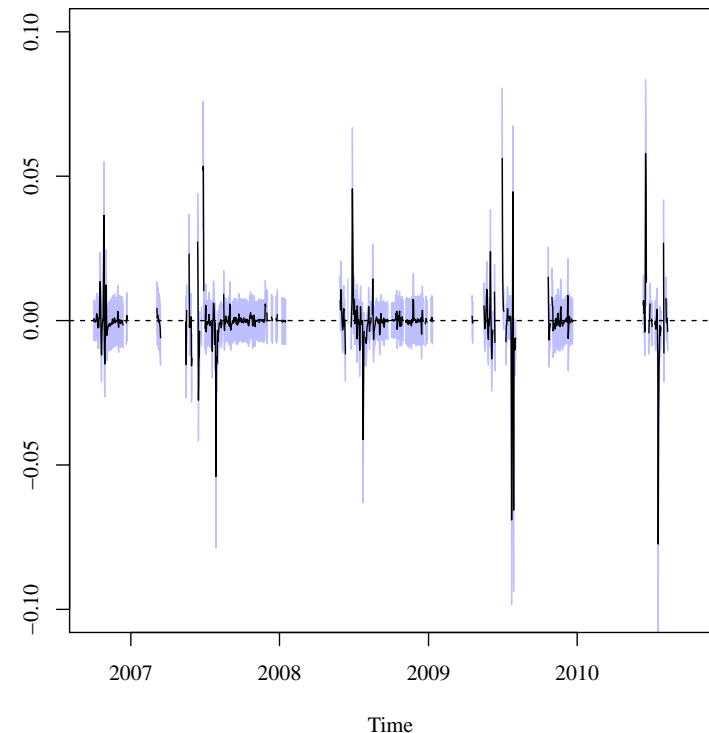
Figure 5.24. USR river reach deterministic and stochastic dissolved selenium mass storage change time series. For the stochastic model, the line is the mean of the realizations and the blue band is the 97.5th CIR.

$$\frac{\Delta S_M}{\Delta t}$$

TIE



(a) Deterministic Model.



(b) Stochastic Model.

Figure 5.25. DSR river reach deterministic and stochastic dissolved selenium mass storage change time series. For the stochastic model, the line is the mean of the realizations and the blue band is the 97.5th CIR.

Figures 5.24 and 5.25 show that there is a definite seasonal variation in the selenium storage component. This temporal relationship follows the same pattern identified with the water balance model storage component. There is a very strong visual relationship between the water balance model flow component and the mass balance model selenium transport 5 component. This is to be expected since the water balance storage component is the prime contributor to the mass balance selenium storage component. These figures also show that uncertainty with the selenium storage component is very large. This is to be expected since the mass balance models contain all of the uncertainty from the water balance model and the selenium concentration estimation linear models.

10 The distribution of all realizations within each time step was analyzed to determine a distribution type. This analysis was performed to determine if the assumption that the deterministic model results were representative of the stochastic model. Testing was performed by comparing K-S statistics for the best fit normal, log-normal, logistic, exponential, gamma, and Weibull distributions. In the USR, 43.7% of the time-steps are normally distributed and 56.3% are best fit by logistic distributions. In the DSR, 15.5% of the time-steps 15 are normally distributed and 84.5% are best fit by logistic distributions. This indicates that for both the USR and DSR, the distributions across the realizations have more data points in the tails.

Tables 5.18 and 5.19 present the summary statistics for the deterministic model time- 20 series and the three stochastic model summary statistics time-series for the USR and DSR, respectively. All values in these tables are in units of $\text{kg d}^{-1} \text{ km}^{-1}$

The mean of the percent difference between the deterministic and 1-D stochastic mean models is low, but not insignificant. This indicates that the deterministic model is

Table 5.18. USR river reach deterministic and stochastic dissolved selenium mass storage change time series summary statistics. Values are in units of $\text{kg d}^{-1} \text{ km}^{-1}$.

Deterministic Model Time Series

2.5th Percentile	Mean	97.5th Percentile
-0.12 (-0.265)	-0.00131 (-0.00289)	0.16 (0.353)

Stochastic Model Summary Statistics Time Series

Time Series	2.5th Percentile	Mean	97.5th Percentile
97.5th Percentile	-0.0319 (-0.0703)	0.0238 (0.0525)	0.15 (0.331)
Mean	-0.0729 (-0.161)	-0.000772 (-0.0017)	0.096 (0.212)
2.5th Percentile	-0.114 (-0.251)	-0.0258 (-0.0569)	0.0405 (0.0893)
Pearson Correlation =	0.9996		

Table 5.19. DSR river reach deterministic and stochastic dissolved selenium mass storage change time series summary statistics. Values are in units of $\text{kg d}^{-1} \text{ km}^{-1}$.

Deterministic Model Time Series

2.5th Percentile	Mean	97.5th Percentile
-1.68e-05 (-3.7e-05)	-3.02e-07 (-6.66e-07)	1.78e-05 (3.92e-05)

Stochastic Model Summary Statistics Time Series

Time Series	2.5th Percentile	Mean	97.5th Percentile
97.5th Percentile	-0.00853 (-0.0188)	0.0122 (0.0269)	0.0417 (0.0919)
Mean	-0.0228 (-0.0503)	-0.000339 (-0.000747)	0.0235 (0.0518)
2.5th Percentile	-0.0389 (-0.0858)	-0.0129 (-0.0284)	0.00968 (0.0213)
Pearson Correlation =	0.9965		

fairly representative of the stochastic model expected value. The high percent differences at the 2.5th and 97.5th percentile indicate that there is still a large range of uncertainty contained within the stochastic model that the deterministic model cannot replicate. The deterministic model can be used to determine how changes can affect a reach over a span of

time, but using it to estimate values for specific time steps is unwise as the differences noted at individual time steps is too large to account for.

5.3. MASS TRANSPORT IN GAUGED STREAMS AND DIVERTED CANALS

The combined river reach loading transported through surface water gauges ($L_{Surface}$)

is calculated as shown in Equation 41 which contains all portions of the mass balance model
 that transport selenium in and out of the river channel through a flow gauge. This equation
 5 is a part of Equation 37. Selenium surface transport rates for individual stream gauges are
 calculated as positive values regardless of whether they discharge to or receive water from
 the main stem of the river. Each of the loadings uses Equation 34 with the flow gauge and
 dissolved selenium concentration relationships as described in Tables 5.1 and 5.2

$$\sum L_{Surface} = L_{in,US} + \sum L_{in} - L_{out,DS} - \sum L_{out} \quad (41)$$

$\sum L_{Surface}$ = Sum of all loadings transported through surface water gauges.

$L_{out,DS}$ = Loading being discharged at the downstream end of the reach.

$\sum L_{out}$ = Sum of loadings being discharged through the reach irrigation canals.

$L_{in,US}$ = Loading being received at the upstream end of the reach.

$\sum L_{in}$ = Sum of loadings being received through the reach tributaries.

Figures 5.22 and 5.23 show the deterministic and stochastic time series of the mass

storage change within each of the river segments in the USR and DSR, respectively. The

black line in the stochastic model sub-figure is the mean of the realizations and the blue band

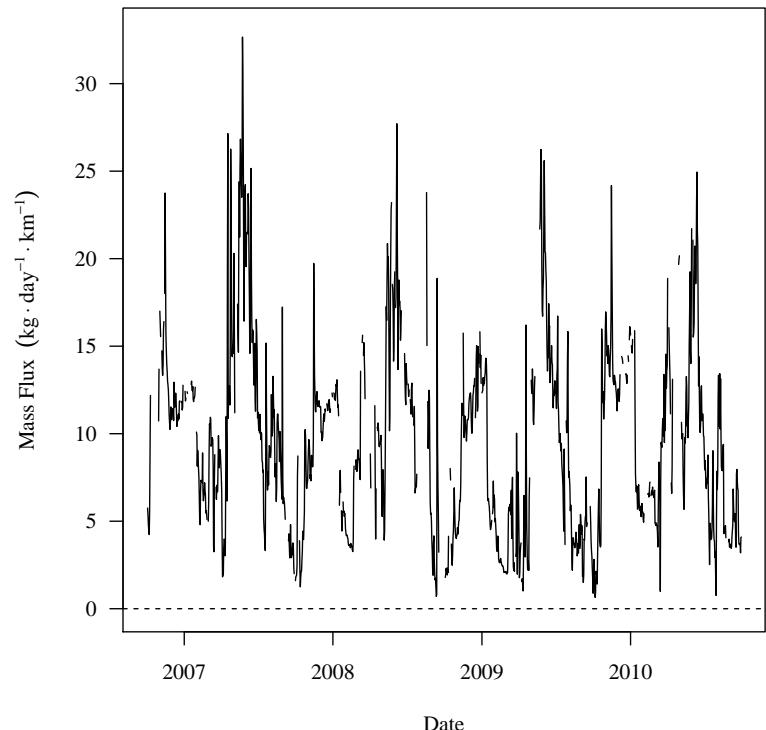
is the 97.5th CIR. Results in these figures and tables 5.16 and 5.17 are presented in units

15 of $\text{kg d}^{-1} \text{km}^{-1}$. Standardizing values to mass storage per unit length allows for comparison

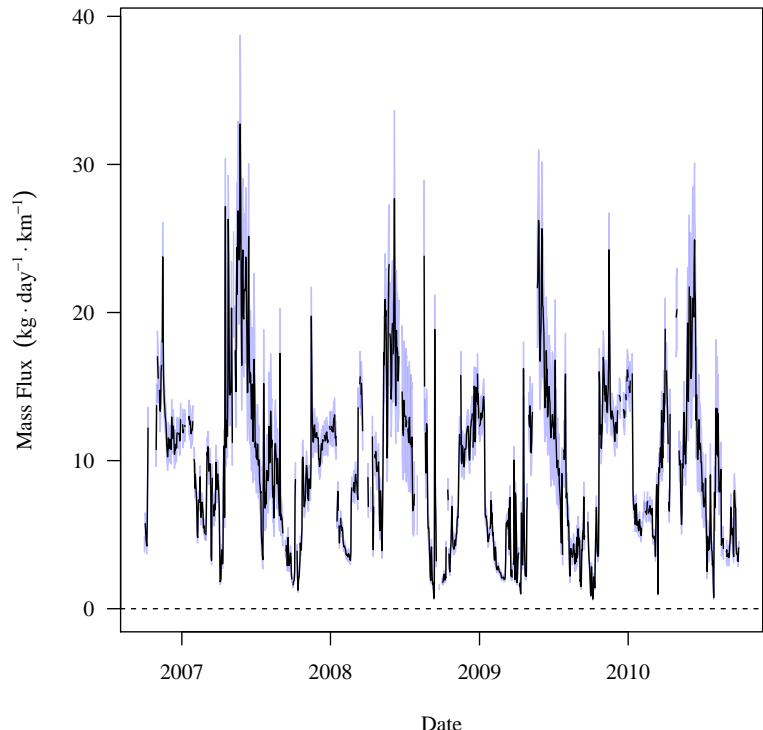
between all river segments in both study reaches. This also allows for comparison between

the mass storage change components and the mass transport components of the mass balance

models.

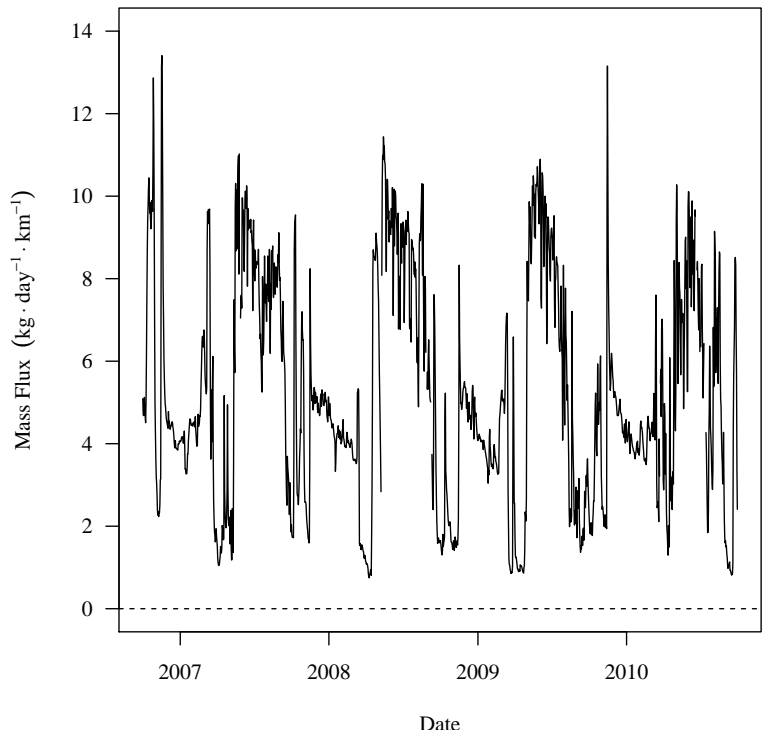


(a) Deterministic Model.

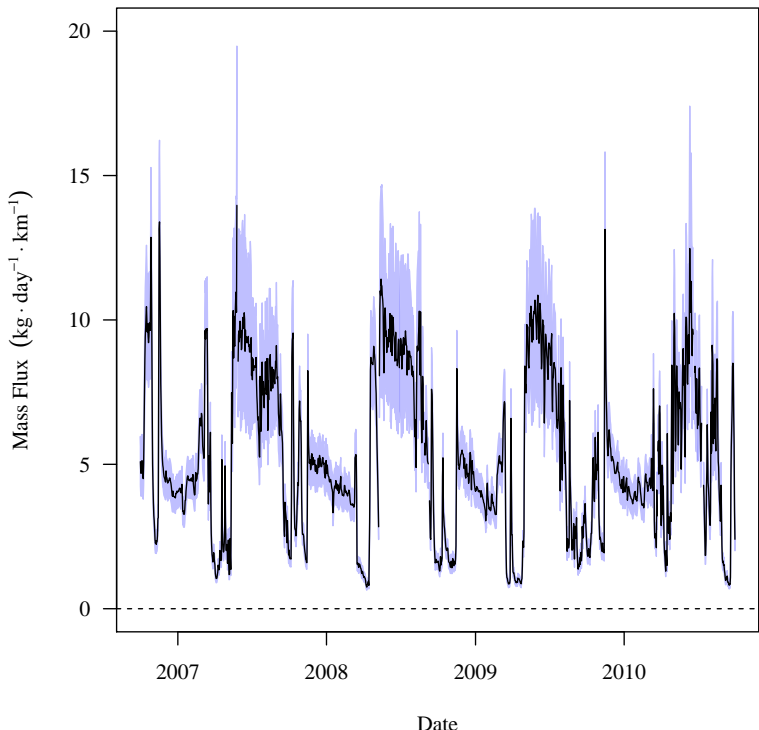


(b) Stochastic Model.

Figure 5.26. USR tributary and irrigation canal stream gauge deterministic and stochastic dissolved selenium mass transport time-series. For the stochastic model, the line is the mean of the realizations and the blue band is the 97.5th CIR.

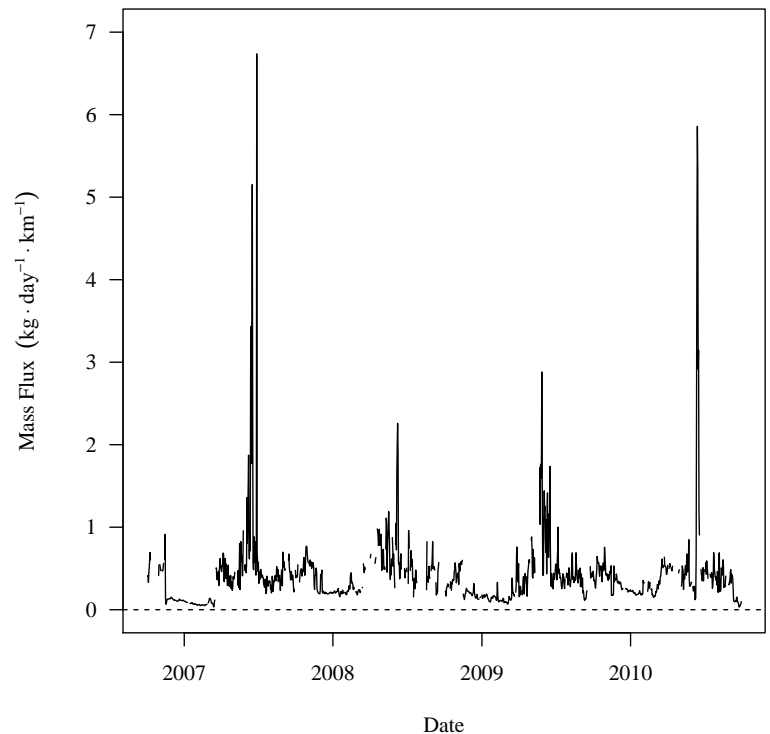


(a) Deterministic Model.

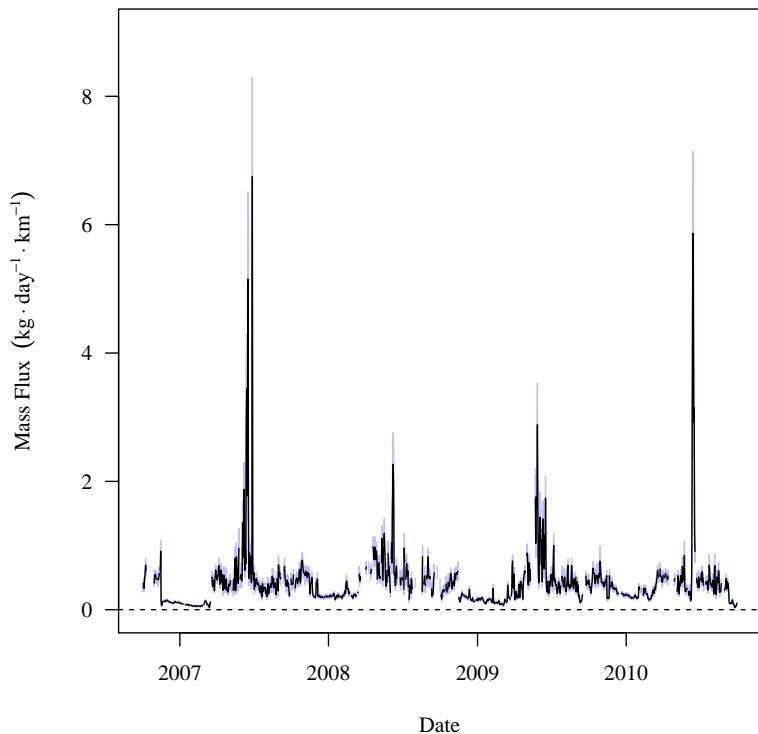


(b) Stochastic Model.

Figure 5.26 (Cont). USR tributary and irrigation canal stream gauge deterministic and stochastic dissolved selenium mass transport time-series.



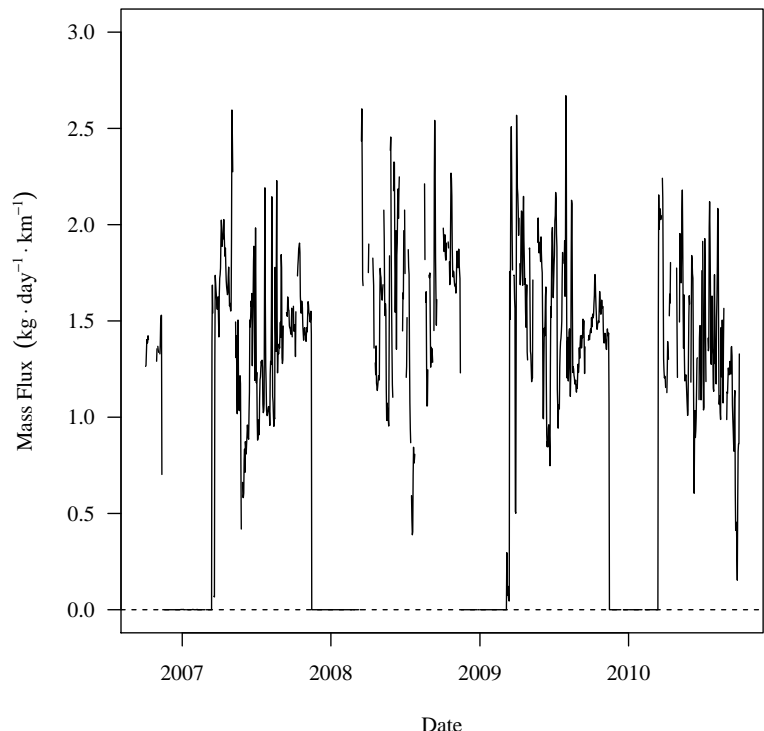
(a) Deterministic Model.



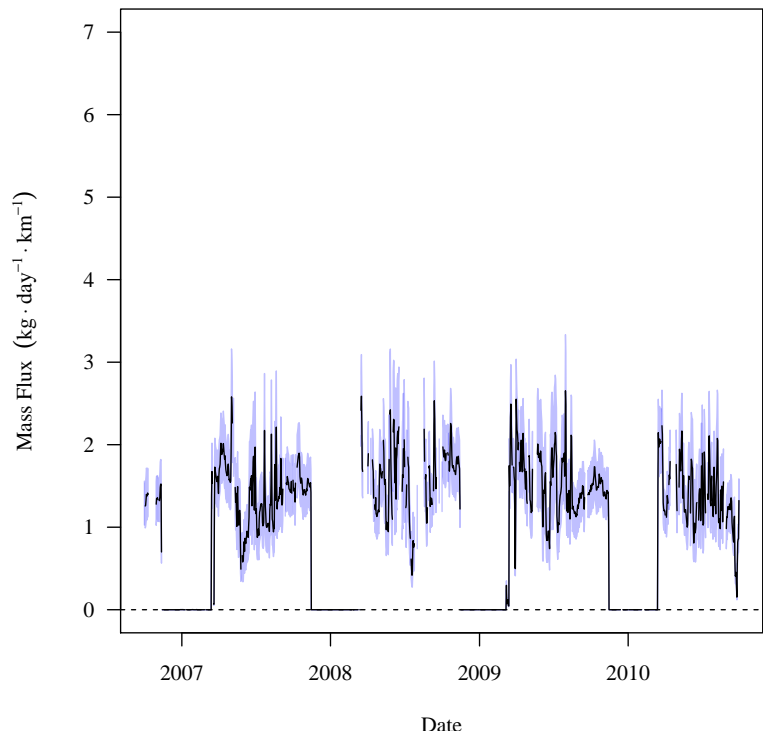
(b) Stochastic Model.

Figure 5.26 (Cont). USR tributary and irrigation canal stream gauge deterministic and stochastic dissolved selenium mass transport time-series.

$L_{CONDITCO}$

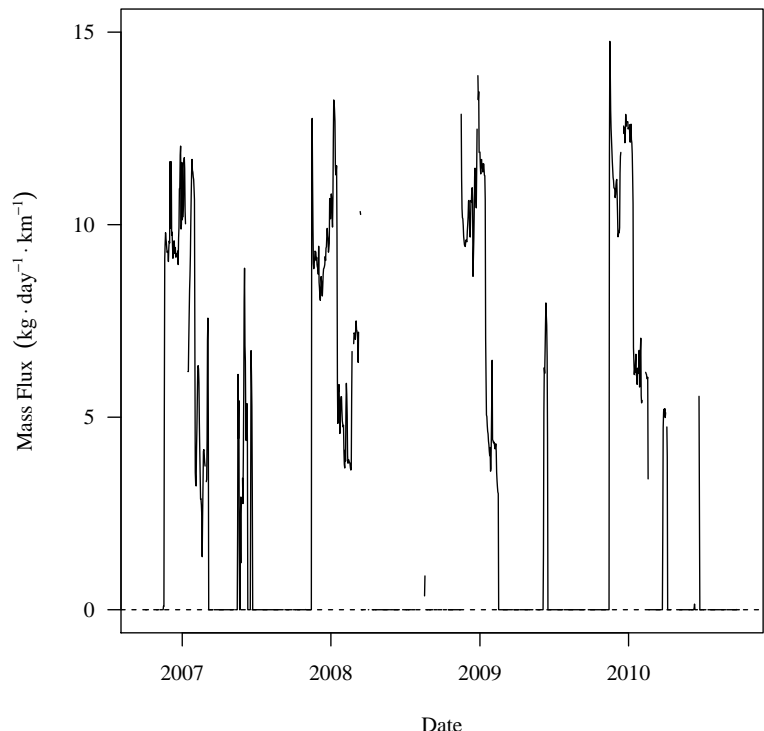


(a) Deterministic Model.

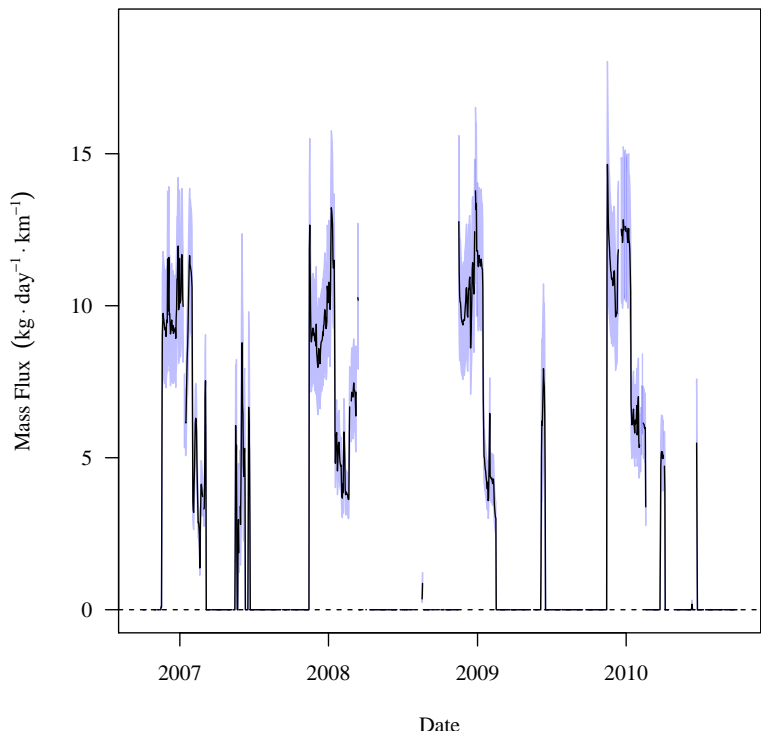


(b) Stochastic Model.

Figure 5.26 (Cont). USR tributary and irrigation canal stream gauge deterministic and stochastic dissolved selenium mass transport time-series.

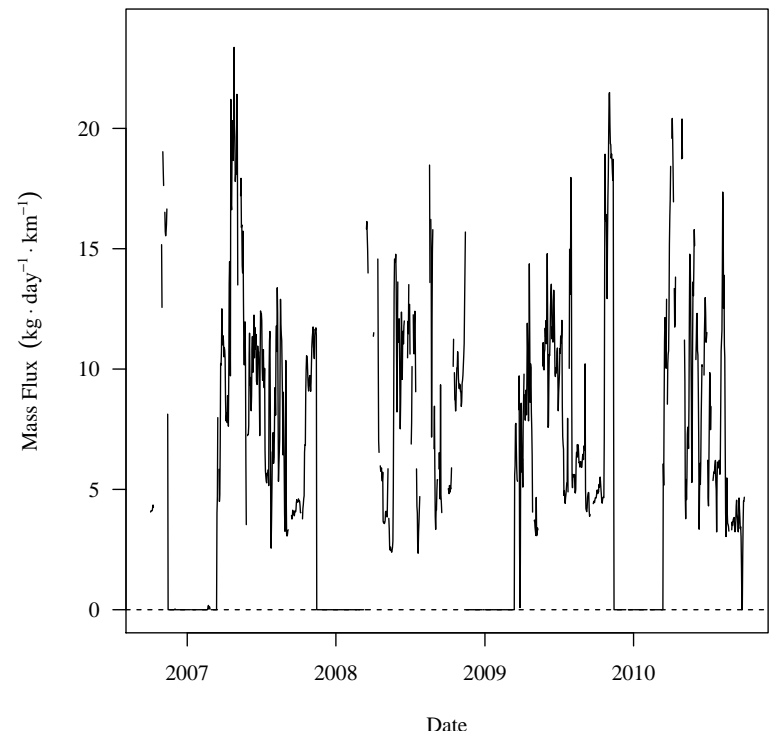


(a) Deterministic Model.

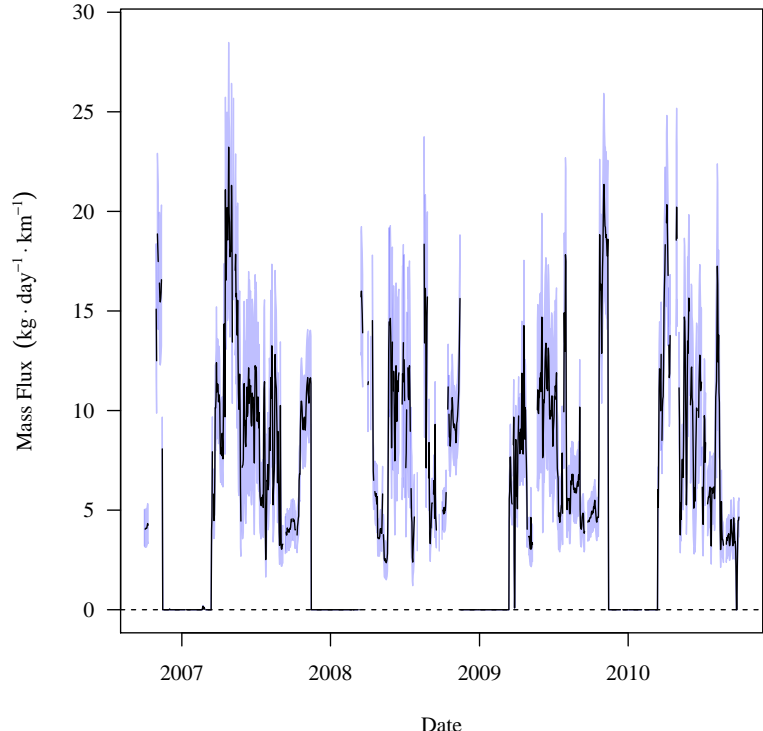


(b) Stochastic Model.

Figure 5.26 (Cont). USR tributary and irrigation canal stream gauge deterministic and stochastic dissolved selenium mass transport time-series.

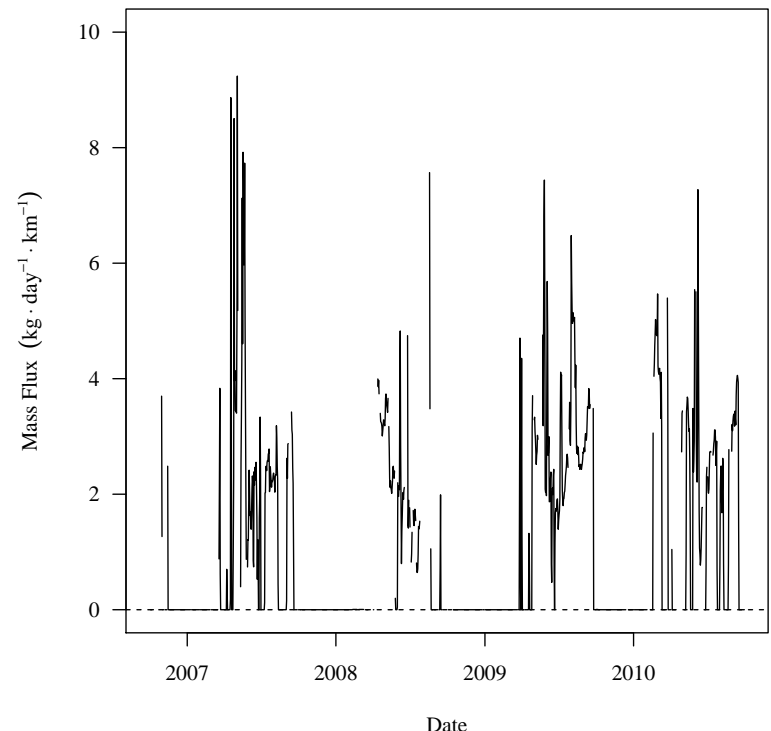


(a) Deterministic Model.

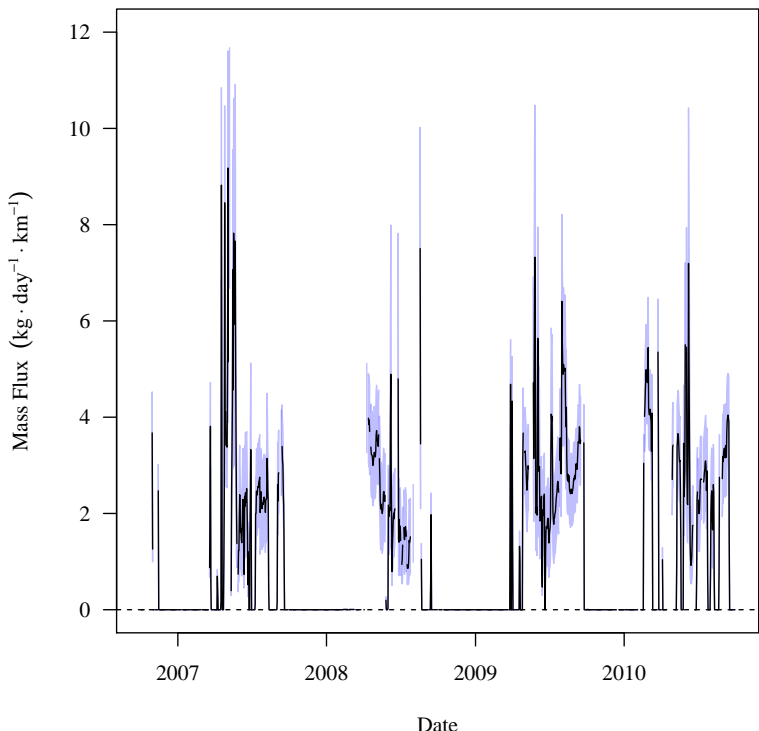


(b) Stochastic Model.

Figure 5.26 (Cont). USR tributary and irrigation canal stream gauge deterministic and stochastic dissolved selenium mass transport time-series.

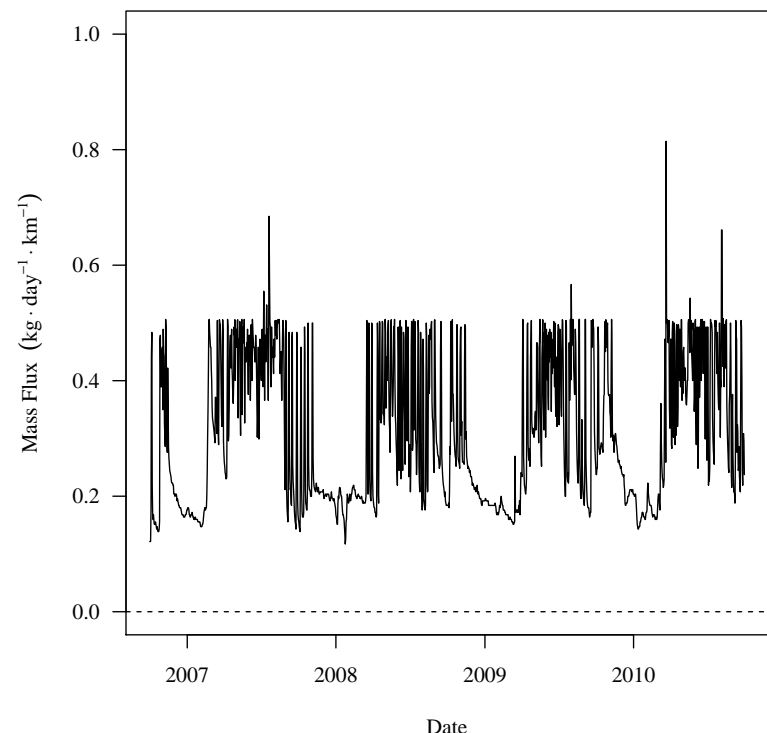


(a) Deterministic Model.

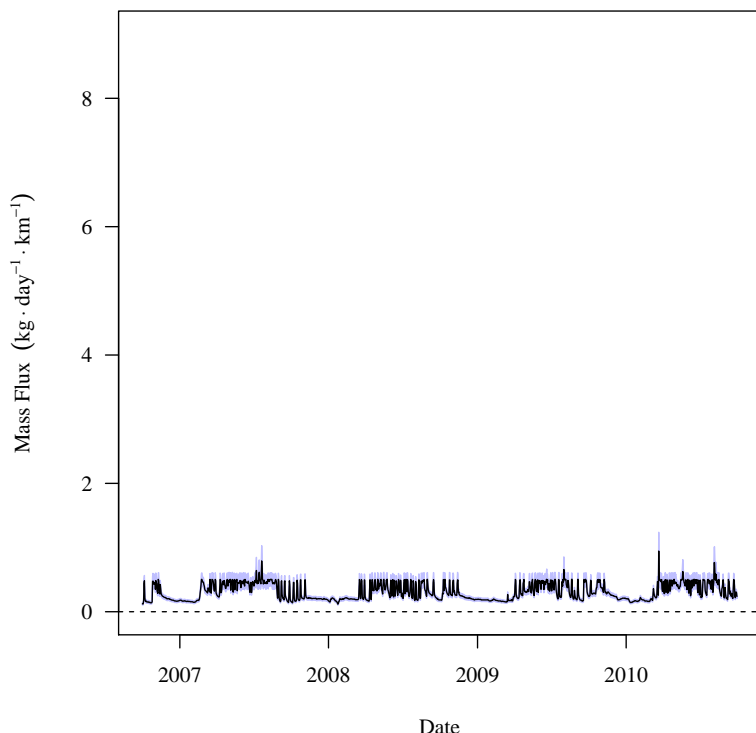


(b) Stochastic Model.

Figure 5.26 (Cont). USR tributary and irrigation canal stream gauge deterministic and stochastic dissolved selenium mass transport time-series.

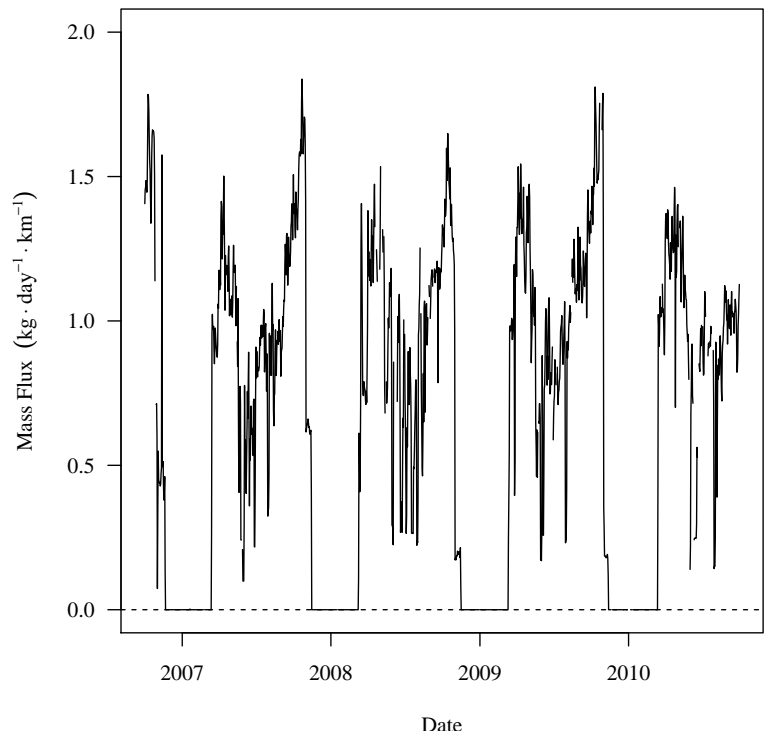


(a) Deterministic Model.

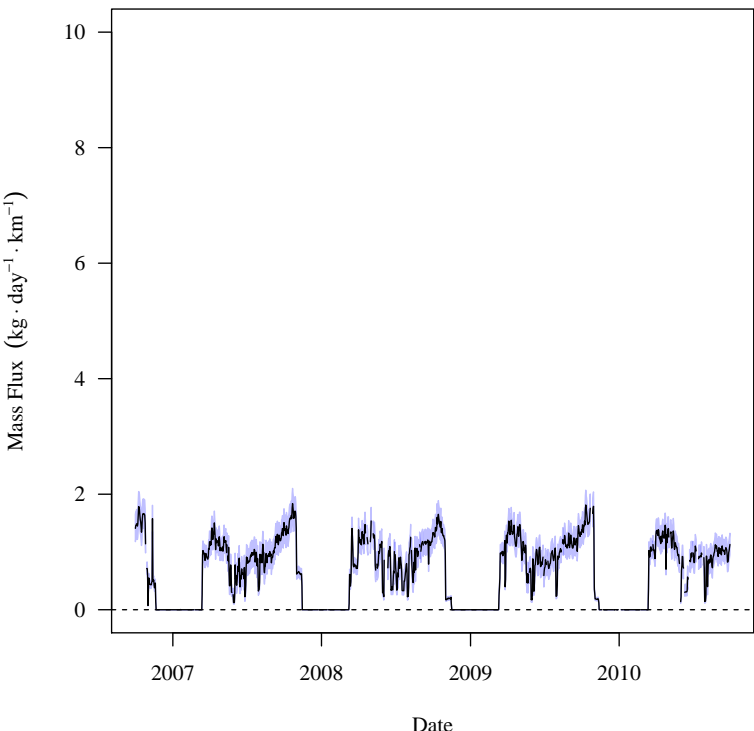


(b) Stochastic Model.

Figure 5.26 (Cont). USR tributary and irrigation canal stream gauge deterministic and stochastic dissolved selenium mass transport time-series.

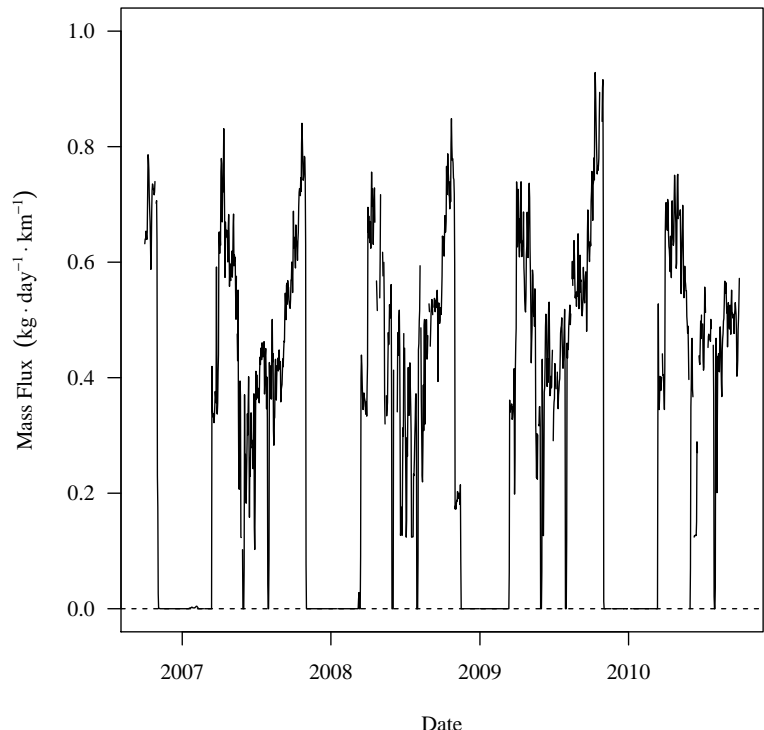


(a) Deterministic Model.

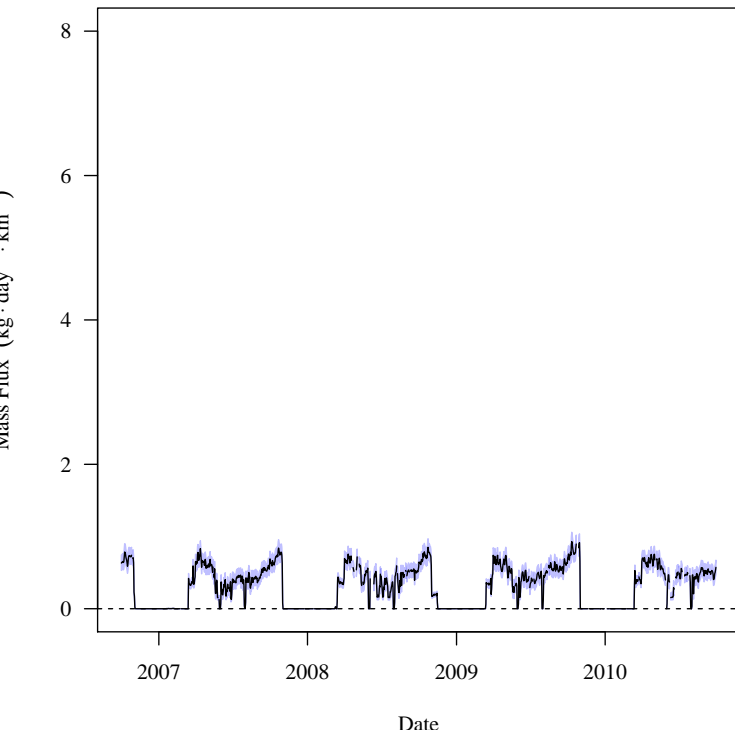


(b) Stochastic Model.

Figure 5.26 (Cont). USR tributary and irrigation canal stream gauge deterministic and stochastic dissolved selenium mass transport time-series.

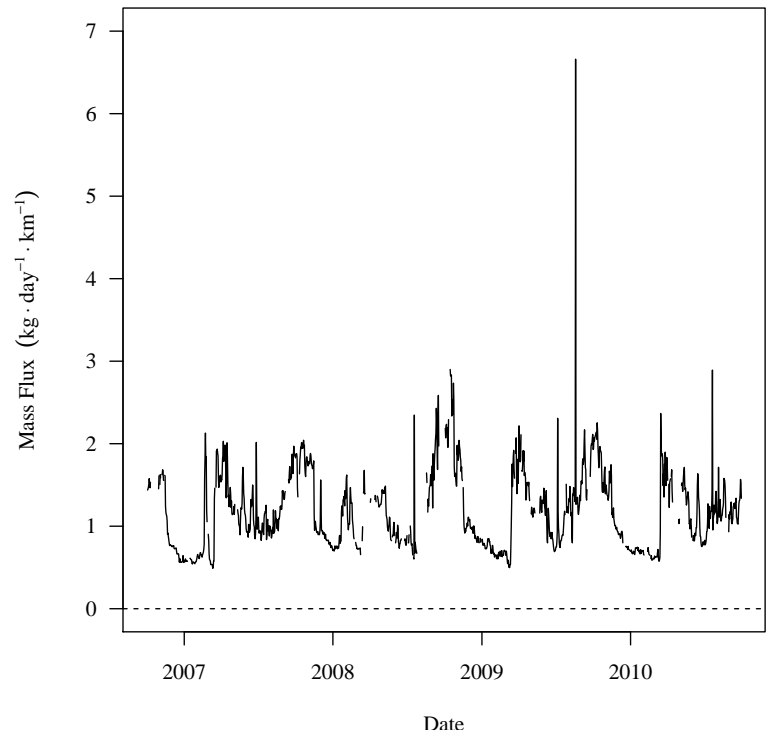


(a) Deterministic Model.

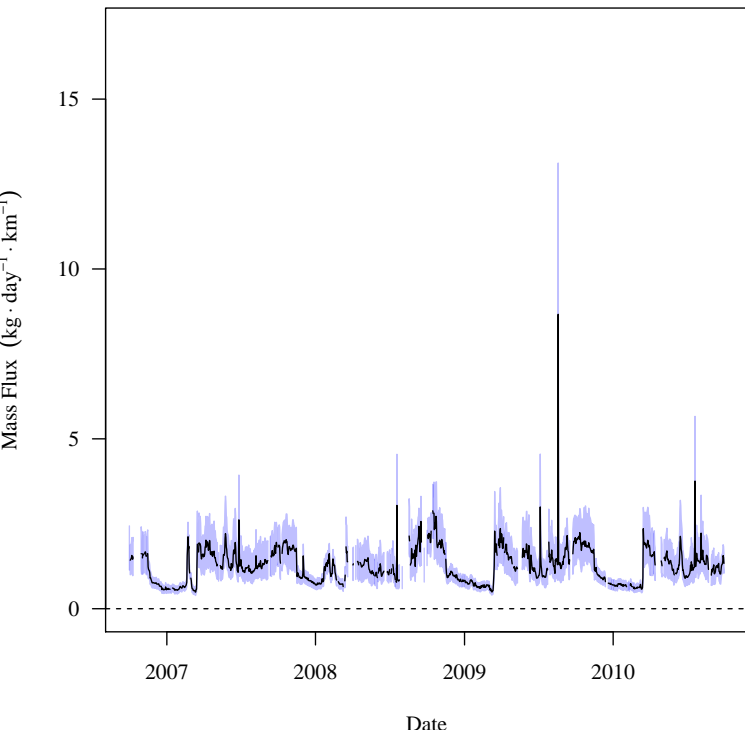


(b) Stochastic Model.

Figure 5.26 (Cont). USR tributary and irrigation canal stream gauge deterministic and stochastic dissolved selenium mass transport time-series.



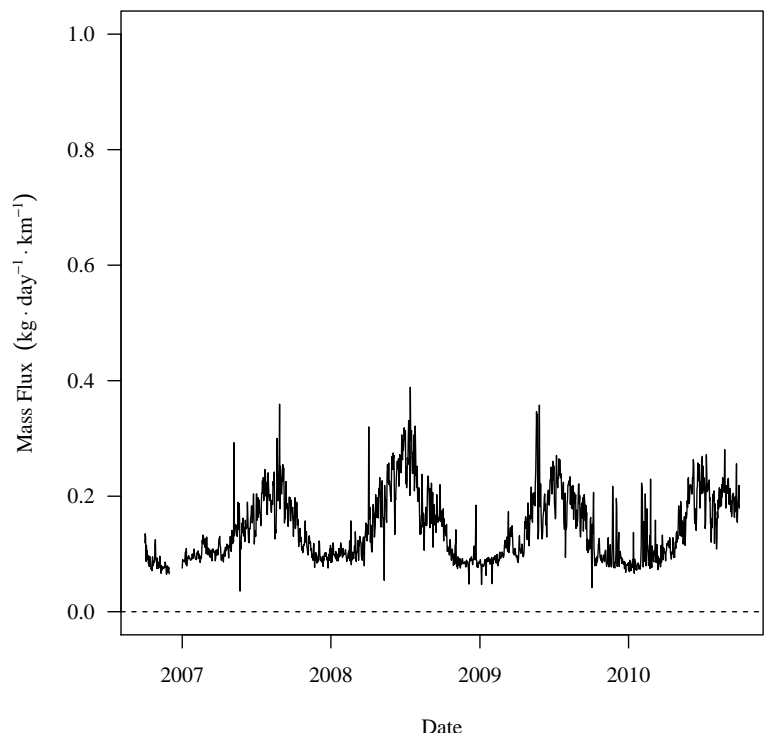
(a) Deterministic Model.



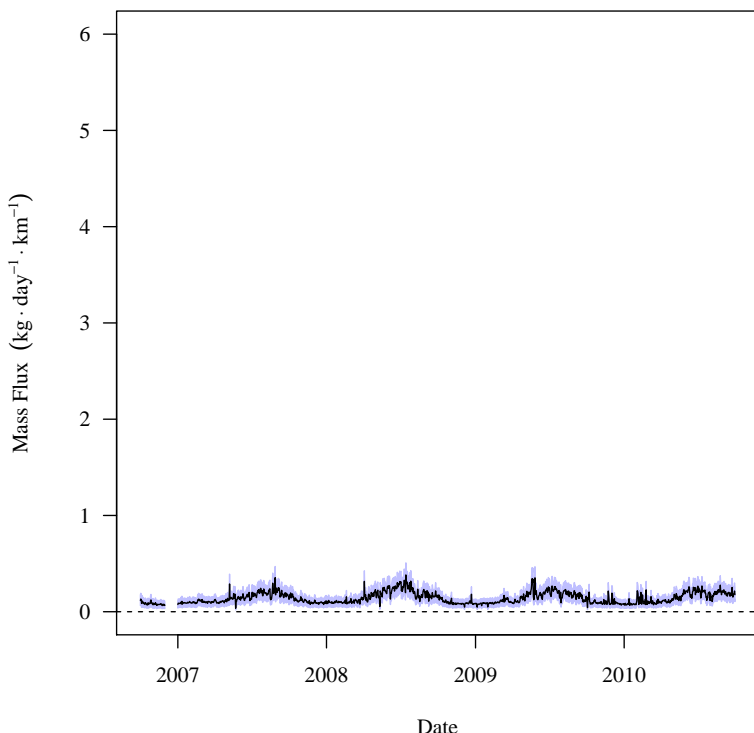
(b) Stochastic Model.

Figure 5.26 (Cont). USR tributary and irrigation canal stream gauge deterministic and stochastic dissolved selenium mass transport time-series.

$L_{LAJWWTP}$

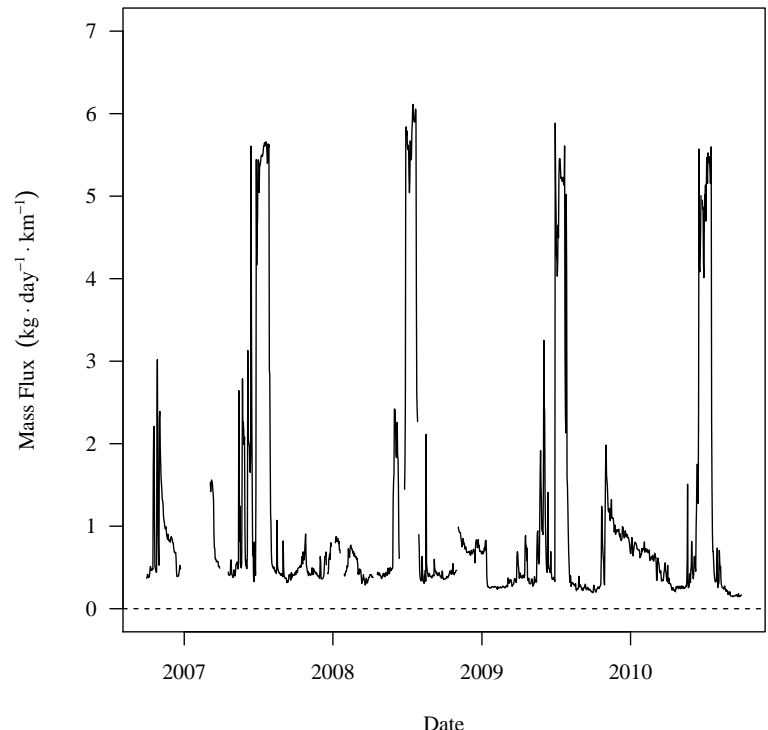


(a) Deterministic Model.

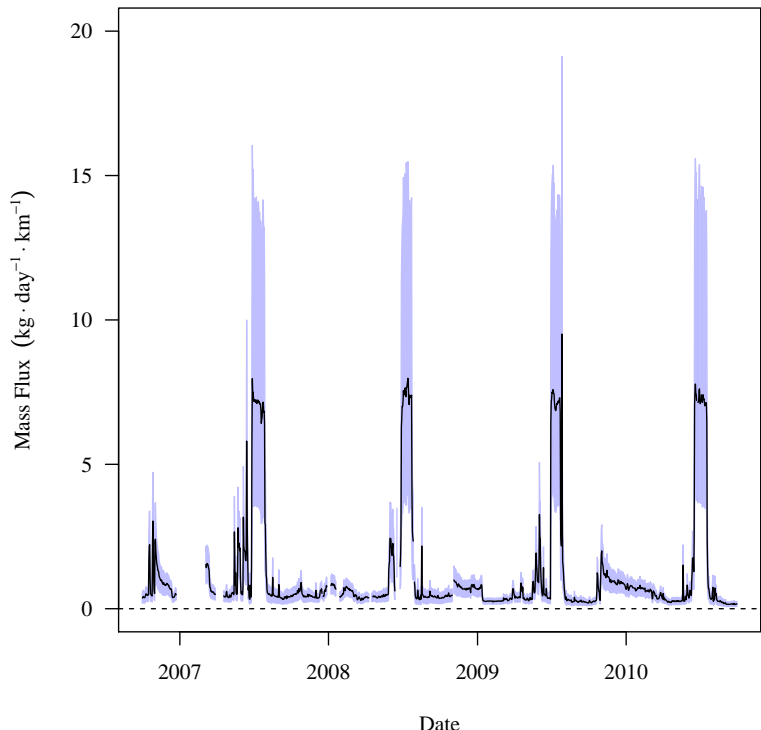


(b) Stochastic Model.

Figure 5.26 (Cont). USR tributary and irrigation canal stream gauge deterministic and stochastic dissolved selenium mass transport time-series.

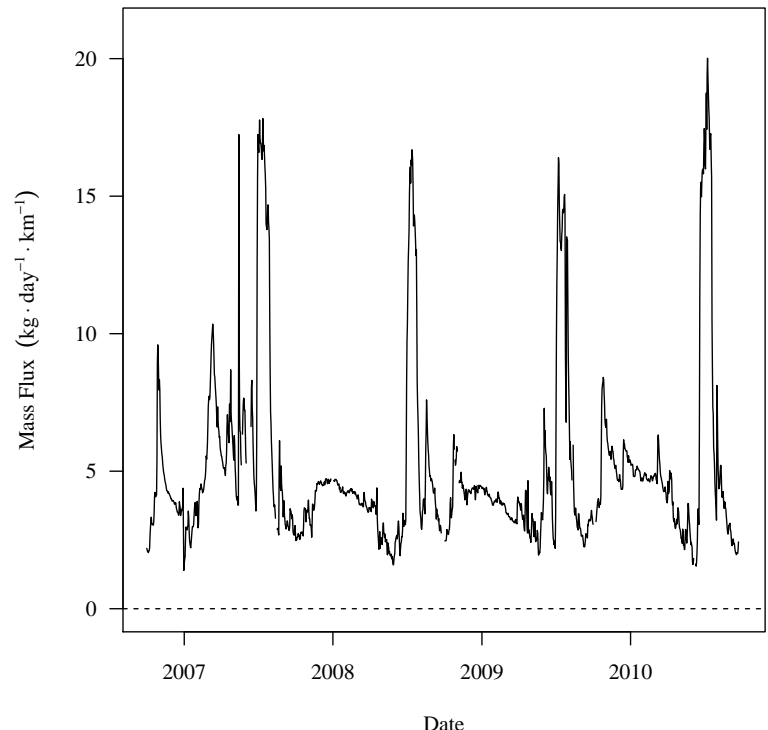


(a) Deterministic Model.

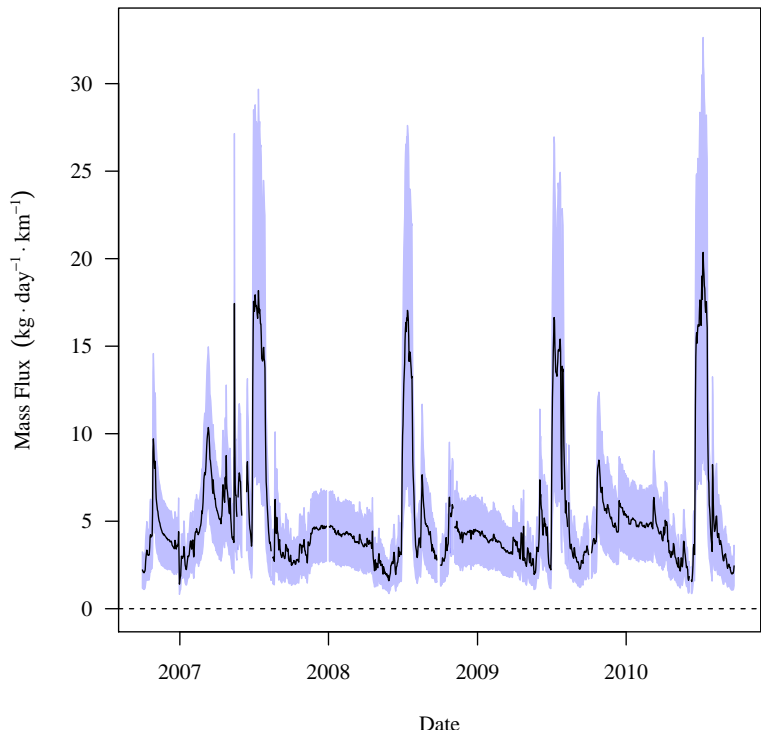


(b) Stochastic Model.

Figure 5.27. DSR tributary and irrigation canal stream gauge deterministic and stochastic dissolved selenium mass transport time-series. For the stochastic model, the line is the mean of the realizations and the blue band is the 97.5th CIR.

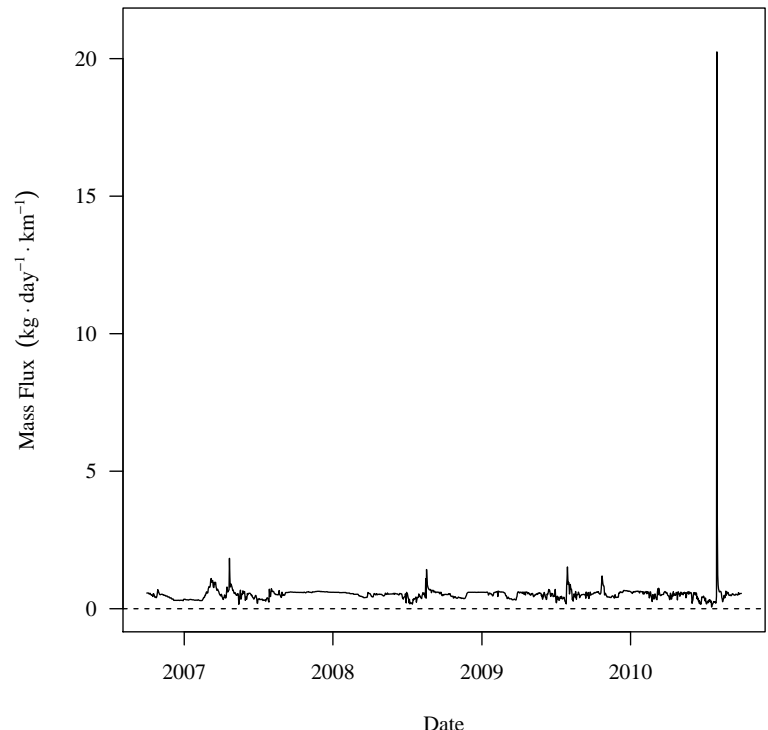


(a) Deterministic Model.

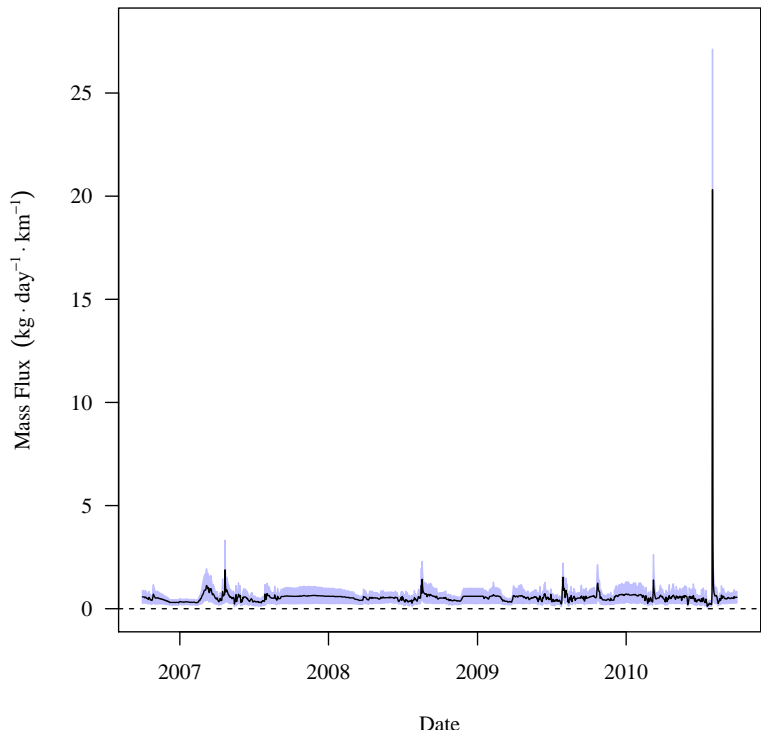


(b) Stochastic Model.

Figure 5.27 (Cont). DSR tributary and irrigation canal stream gauge deterministic and stochastic dissolved selenium mass transport time-series.

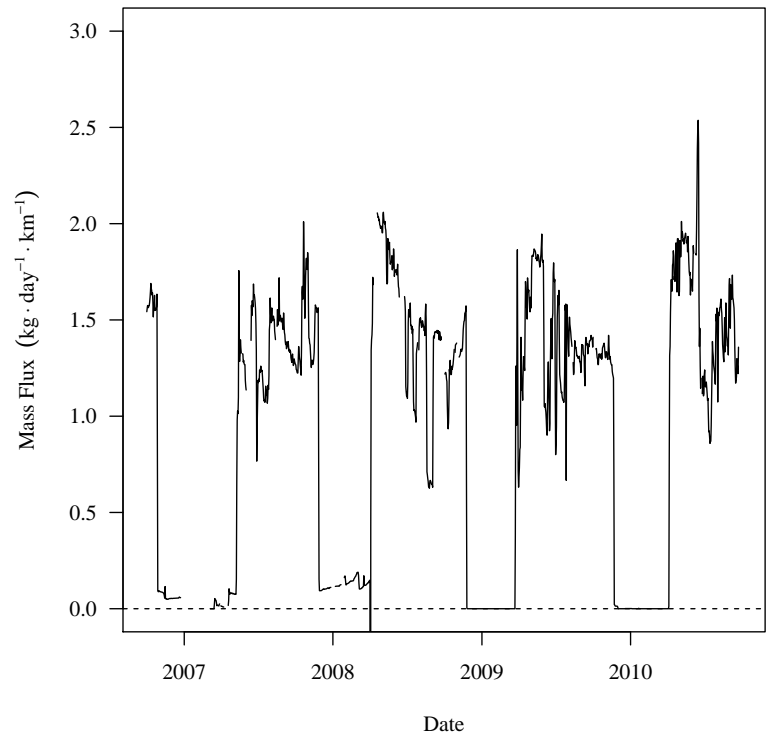


(a) Deterministic Model.

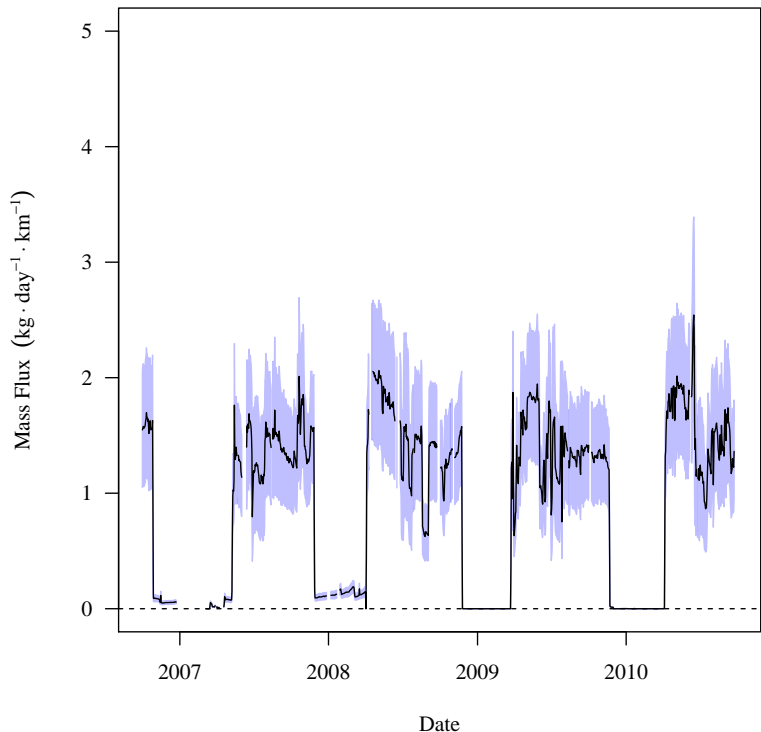


(b) Stochastic Model.

Figure 5.27 (Cont). DSR tributary and irrigation canal stream gauge deterministic and stochastic dissolved selenium mass transport time-series.

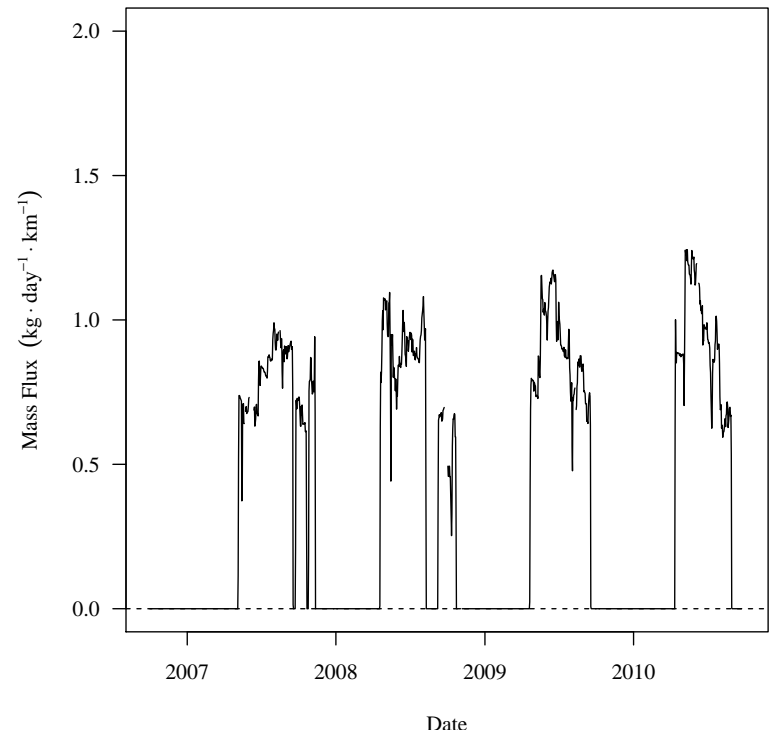


(a) Deterministic Model.

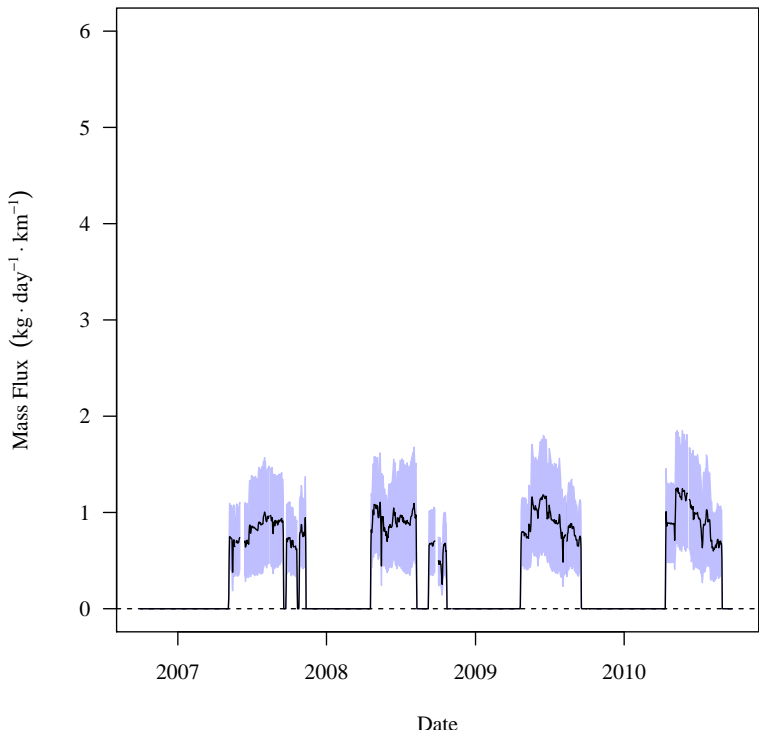


(b) Stochastic Model.

Figure 5.27 (Cont). DSR tributary and irrigation canal stream gauge deterministic and stochastic dissolved selenium mass transport time-series.



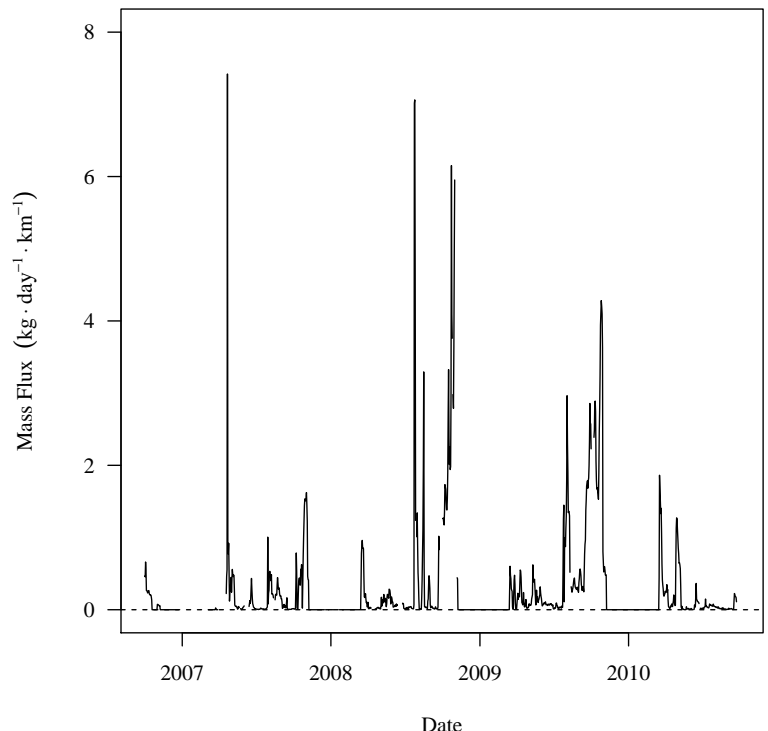
(a) Deterministic Model.



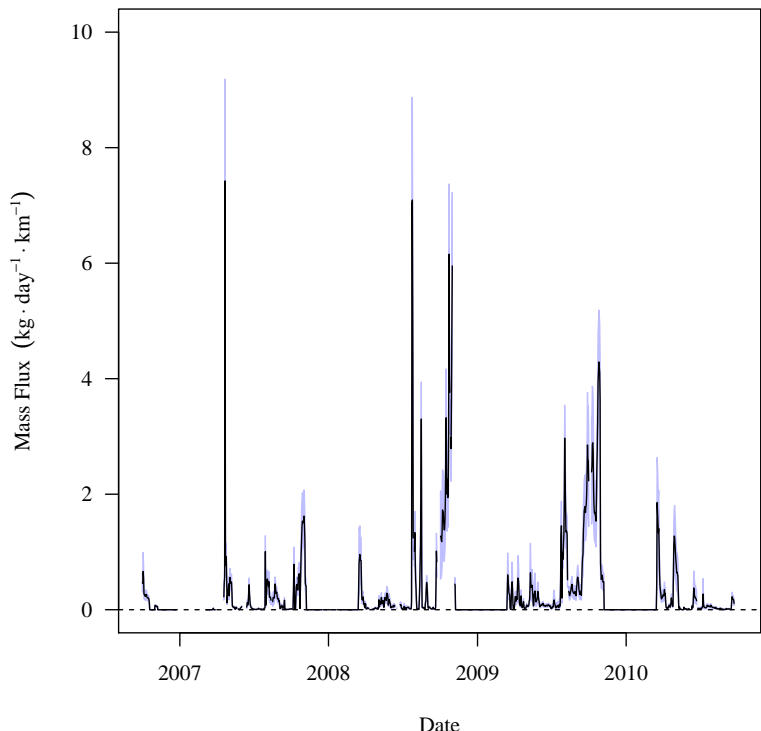
(b) Stochastic Model.

Figure 5.27 (Cont). DSR tributary and irrigation canal stream gauge deterministic and stochastic dissolved selenium mass transport time-series.

$L_{WILDHOCO}$



(a) Deterministic Model.



(b) Stochastic Model.

Figure 5.27 (Cont). DSR tributary and irrigation canal stream gauge deterministic and stochastic dissolved selenium mass transport time-series.

Figures 5.26 and 5.27 show that there is a definite seasonal variation $\sum L_{Surface}$ in both the USR and DSR. This temporal relationship follows the same pattern identified with $\sum Q_{Surface}$. There is a visual relationship between $\sum Q_{Surface}$ and $\sum L_{Surface}$. This is to be expected since $\sum Q_{Surface}$ is the prime contributor to $\sum L_{Surface}$. These figures show also 5 that uncertainty with the $\sum L_{Surface}$ component is very large at many of the flow gauges. This is to be expected since the mass balance models contain all of the uncertainty from the water balance model and the selenium concentration estimation linear models. The magnitude of the flow component uncertainty is comparable to the magnitude of the storage component uncertainty. This is expected since both model components use many of the 10 same input variables with their uncertainties.

The distribution of all realizations within each time step was analyzed to determine a distribution type. This analysis was performed to determine if the assumption that the deterministic model results were representative of the stochastic model. Testing was performed by comparing K-S statistics using the same method previously discussed. In the USR, 69.9% 15 of the time steps are normally distributed and 30.1% are best fit with a logistic distribution. In the DSR, 4.4% of the time-steps are normally distributed and 95.5% are best fit with a logistic distribution. This indicates that for both the USR and DSR, the distributions across the realizations are best fit with a logistic distribution, which has heavier tails than a normal distribution.

20 Tables 5.20 and 5.21 present the summary statistics for the deterministic model time-series and the three stochastic model summary statistics time-series for the results presented in Figures 5.26 5.27 which are for the USR and DSR, respectively. All values in these tables are in units of $\text{kg d}^{-1} \text{km}^{-1}$

Table 5.20. USR tributary and irrigation canal stream gauge deterministic and stochastic dissolved selenium mass transport time-series results tables. Values are in units of $\text{kg d}^{-1} \text{ km}^{-1}$.

LARKCATCO

Deterministic Model Time Series

2.5th Percentile	Mean	97.5th Percentile
1.87 (4.12)	9.56 (21.1)	22.8 (50.3)

Stochastic Model Summary Statistics Time Series

Time Series	2.5th Percentile	Mean	97.5th Percentile
97.5th Percentile	2.09 (4.61)	11 (24.3)	27.3 (60.2)
Mean	1.87 (4.12)	9.57 (21.1)	22.8 (50.3)
2.5th Percentile	1.67 (3.68)	8.18 (18)	18.3 (40.3)
Pearson Correlation = 0.9999			

LARKLASCO

Deterministic Model Time Series

2.5th Percentile	Mean	97.5th Percentile
1.03 (2.27)	5.2 (11.5)	10.3 (22.7)

Stochastic Model Summary Statistics Time Series

Time Series	2.5th Percentile	Mean	97.5th Percentile
97.5th Percentile	1.18 (2.6)	6.31 (13.9)	13.4 (29.5)
Mean	1.03 (2.27)	5.24 (11.6)	10.3 (22.7)
2.5th Percentile	0.875 (1.93)	4.24 (9.35)	7.92 (17.5)
Pearson Correlation = 0.9952			

The difference between the deterministic model time-series mean and the stochastic model mean time-series mean is very low. This indicates that the deterministic model is representative of the stochastic model expected value. The fairly low differences between the

Table 5.20 (Cont). USR tributary and irrigation canal stream gauge deterministic and stochastic dissolved selenium mass transport time-series results tables.

L_{CANSWKCO}

Deterministic Model Time Series

2.5th Percentile	Mean	97.5th Percentile
0.0631 (0.139)	0.411 (0.906)	1.19 (2.62)

Stochastic Model Summary Statistics Time Series

Time Series	2.5th Percentile	Mean	97.5th Percentile
97.5th Percentile	0.0735 (0.162)	0.494 (1.09)	1.45 (3.2)
Mean	0.063 (0.139)	0.413 (0.911)	1.19 (2.62)
2.5th Percentile	0.0525 (0.116)	0.338 (0.745)	0.969 (2.14)
Pearson Correlation = 0.9998			

L_{CONDITCO}

Deterministic Model Time Series

2.5th Percentile	Mean	97.5th Percentile
0 (0)	0.94 (2.07)	2.17 (4.78)

Stochastic Model Summary Statistics Time Series

Time Series	2.5th Percentile	Mean	97.5th Percentile
97.5th Percentile	0 (0)	1.17 (2.58)	2.69 (5.93)
Mean	0 (0)	0.934 (2.06)	2.15 (4.74)
2.5th Percentile	0 (0)	0.706 (1.56)	1.67 (3.68)
Pearson Correlation = 1			

deterministic model time series and the stochastic model mean time series at the 2.5th and 97.5th percentile indicate that there is still a small range of uncertainty contained within the stochastic model that the deterministic model cannot replicate.

Table 5.20 (Cont). USR tributary and irrigation canal stream gauge deterministic and stochastic dissolved selenium mass transport time-series results tables.

$L_{FLSCANCO}$

Deterministic Model Time Series

2.5th Percentile	Mean	97.5th Percentile
0 (0)	2.85 (6.28)	12.2 (26.9)

Stochastic Model Summary Statistics Time Series

Time Series	2.5th Percentile	Mean	97.5th Percentile
97.5th Percentile	0 (0)	3.43 (7.56)	14.5 (32)
Mean	0 (0)	2.84 (6.26)	12.1 (26.7)
2.5th Percentile	0 (0)	2.28 (5.03)	9.95 (21.9)
Pearson Correlation = 1			

$L_{FLYCANCO}$

Deterministic Model Time Series

2.5th Percentile	Mean	97.5th Percentile
0 (0)	5.57 (12.3)	18.4 (40.6)

Stochastic Model Summary Statistics Time Series

Time Series	2.5th Percentile	Mean	97.5th Percentile
97.5th Percentile	0 (0)	7.13 (15.7)	22.6 (49.8)
Mean	0 (0)	5.53 (12.2)	18.3 (40.3)
2.5th Percentile	0 (0)	4.02 (8.86)	14.4 (31.7)
Pearson Correlation = 0.9999			

Figures 5.28 and 5.29 show the $\sum L_{Surface}$ values for the USR and DSR, respectively.

Within the stochastic model sub-figure, the black line is the mean of all realizations for each time step and the blue band is the 95% CIR for all realizations for each time step.

Table 5.20 (Cont). USR tributary and irrigation canal stream gauge deterministic and stochastic dissolved selenium mass transport time-series results tables.

L_{HOLCANCO}

Deterministic Model Time Series

2.5th Percentile	Mean	97.5th Percentile
0 (0)	1.03 (2.27)	5.01 (11)

Stochastic Model Summary Statistics Time Series

Time Series	2.5th Percentile	Mean	97.5th Percentile
97.5th Percentile	0 (0)	1.37 (3.02)	6.54 (14.4)
Mean	0 (0)	1.02 (2.25)	4.97 (11)
2.5th Percentile	0 (0)	0.693 (1.53)	3.46 (7.63)
Pearson Correlation = 0.9997			

L_{HRC194CO}

Deterministic Model Time Series

2.5th Percentile	Mean	97.5th Percentile
0.151 (0.333)	0.308 (0.679)	0.506 (1.12)

Stochastic Model Summary Statistics Time Series

Time Series	2.5th Percentile	Mean	97.5th Percentile
97.5th Percentile	0.173 (0.381)	0.365 (0.805)	0.61 (1.34)
Mean	0.151 (0.333)	0.31 (0.683)	0.504 (1.11)
2.5th Percentile	0.131 (0.289)	0.26 (0.573)	0.41 (0.904)
Pearson Correlation = 0.9952			

Table 5.20 (Cont). USR tributary and irrigation canal stream gauge deterministic and stochastic dissolved selenium mass transport time-series results tables.

$L_{RFDMANCO}$

Deterministic Model Time Series

2.5th Percentile	Mean	97.5th Percentile
0 (0)	0.659 (1.45)	1.58 (3.48)

Stochastic Model Summary Statistics Time Series

Time Series	2.5th Percentile	Mean	97.5th Percentile
97.5th Percentile	0 (0)	0.787 (1.74)	1.83 (4.03)
Mean	0 (0)	0.662 (1.46)	1.59 (3.51)
2.5th Percentile	0 (0)	0.544 (1.2)	1.36 (3)
Pearson Correlation = 0.9999			

$L_{RFDRETCO}$

Deterministic Model Time Series

2.5th Percentile	Mean	97.5th Percentile
0 (0)	0.309 (0.681)	0.762 (1.68)

Stochastic Model Summary Statistics Time Series

Time Series	2.5th Percentile	Mean	97.5th Percentile
97.5th Percentile	0 (0)	0.368 (0.811)	0.879 (1.94)
Mean	0 (0)	0.31 (0.683)	0.763 (1.68)
2.5th Percentile	0 (0)	0.255 (0.562)	0.656 (1.45)
Pearson Correlation = 0.9999			

Table 5.20 (Cont). USR tributary and irrigation canal stream gauge deterministic and stochastic dissolved selenium mass transport time-series results tables.

$L_{TMSWICO}$

Deterministic Model Time Series

2.5th Percentile	Mean	97.5th Percentile
0.57 (1.26)	1.17 (2.58)	2.12 (4.67)

Stochastic Model Summary Statistics Time Series

Time Series	2.5th Percentile	Mean	97.5th Percentile
97.5th Percentile	0.678 (1.49)	1.72 (3.79)	2.97 (6.55)
Mean	0.568 (1.25)	1.25 (2.76)	2.15 (4.74)
2.5th Percentile	0.457 (1.01)	0.913 (2.01)	1.6 (3.53)
Pearson Correlation = 0.9581			

$L_{LAJWWTP}$

Deterministic Model Time Series

2.5th Percentile	Mean	97.5th Percentile
0.0753 (0.166)	0.143 (0.315)	0.269 (0.593)

Stochastic Model Summary Statistics Time Series

Time Series	2.5th Percentile	Mean	97.5th Percentile
97.5th Percentile	0.114 (0.251)	0.202 (0.445)	0.364 (0.802)
Mean	0.0741 (0.163)	0.14 (0.309)	0.266 (0.586)
2.5th Percentile	0.0374 (0.0825)	0.0816 (0.18)	0.172 (0.379)
Pearson Correlation = 1			

Table 5.21. DSR tributary and irrigation canal stream gauge deterministic and stochastic dissolved selenium mass transport time-series results tables. Values are in units of $\text{kg d}^{-1} \text{ km}^{-1}$.

LARKLAMCO

Deterministic Model Time Series

2.5th Percentile	Mean	97.5th Percentile
0.197 (0.434)	1.02 (2.25)	5.57 (12.3)

Stochastic Model Summary Statistics Time Series

Time Series	2.5th Percentile	Mean	97.5th Percentile
97.5th Percentile	0.296 (0.653)	2.04 (4.5)	14.3 (31.5)
Mean	0.198 (0.437)	1.19 (2.62)	7.34 (16.2)
2.5th Percentile	0.0989 (0.218)	0.624 (1.38)	3.73 (8.22)
Pearson Correlation = 0.986			

LARKCOOKS

Deterministic Model Time Series

2.5th Percentile	Mean	97.5th Percentile
2.04 (4.5)	5.07 (11.2)	16.4 (36.2)

Stochastic Model Summary Statistics Time Series

Time Series	2.5th Percentile	Mean	97.5th Percentile
97.5th Percentile	3.01 (6.64)	7.66 (16.9)	27 (59.5)
Mean	2.04 (4.5)	5.12 (11.3)	16.6 (36.6)
2.5th Percentile	1.13 (2.49)	2.68 (5.91)	7.35 (16.2)
Pearson Correlation = 1			

Table 5.21 (Cont). DSR tributary and irrigation canal stream gauge deterministic and stochastic dissolved selenium mass transport time-series results tables.

$L_{BIGLAMCO}$

Deterministic Model Time Series

2.5th Percentile	Mean	97.5th Percentile
0.242 (0.534)	0.53 (1.17)	0.841 (1.85)

Stochastic Model Summary Statistics Time Series

Time Series	2.5th Percentile	Mean	97.5th Percentile
97.5th Percentile	0.435 (0.959)	0.865 (1.91)	1.48 (3.26)
Mean	0.303 (0.668)	0.545 (1.2)	0.882 (1.94)
2.5th Percentile	0.144 (0.317)	0.256 (0.564)	0.376 (0.829)
Pearson Correlation = 0.9967			

$L_{BUFDITCO}$

Deterministic Model Time Series

2.5th Percentile	Mean	97.5th Percentile
0 (0)	0.916 (2.02)	1.95 (4.3)

Stochastic Model Summary Statistics Time Series

Time Series	2.5th Percentile	Mean	97.5th Percentile
97.5th Percentile	0 (0)	1.24 (2.73)	2.55 (5.62)
Mean	0 (0)	0.921 (2.03)	1.95 (4.3)
2.5th Percentile	0 (0)	0.617 (1.36)	1.37 (3.02)
Pearson Correlation = 0.9862			

Table 5.21 (Cont). DSR tributary and irrigation canal stream gauge deterministic and stochastic dissolved selenium mass transport time-series results tables.

L_{FRODITKS}

Deterministic Model Time Series

2.5th Percentile	Mean	97.5th Percentile
0 (0)	0.358 (0.789)	1.14 (2.51)

Stochastic Model Summary Statistics Time Series

Time Series	2.5th Percentile	Mean	97.5th Percentile
97.5th Percentile	0 (0)	0.551 (1.21)	1.71 (3.77)
Mean	0 (0)	0.362 (0.798)	1.15 (2.54)
2.5th Percentile	0 (0)	0.183 (0.403)	0.612 (1.35)
Pearson Correlation = 1			

L_{WILDHOCO}

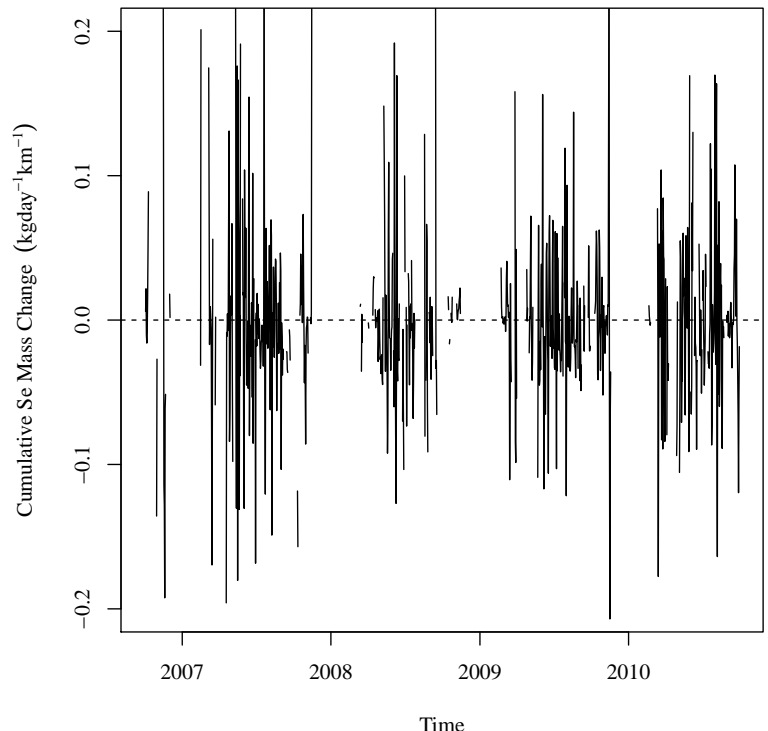
Deterministic Model Time Series

2.5th Percentile	Mean	97.5th Percentile
0 (0)	0.285 (0.628)	2.46 (5.42)

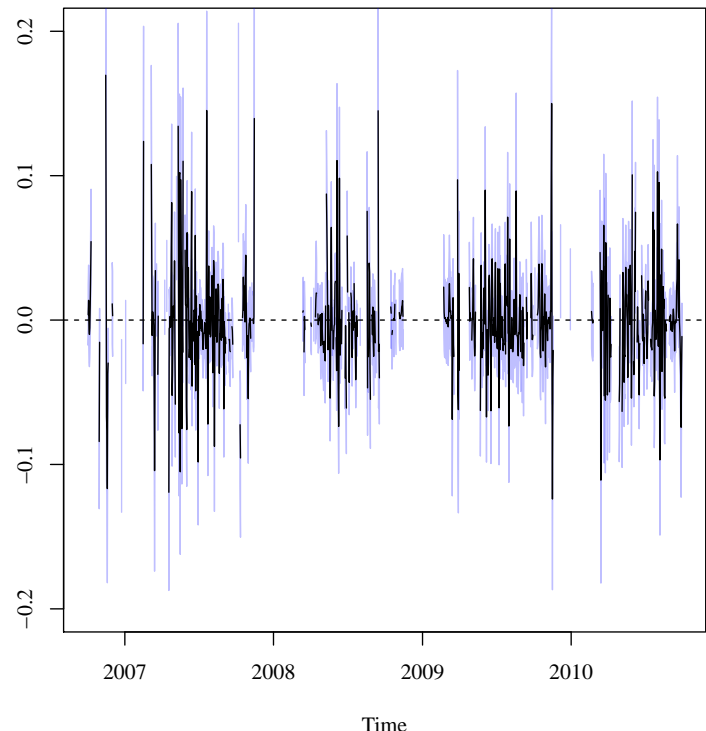
Stochastic Model Summary Statistics Time Series

Time Series	2.5th Percentile	Mean	97.5th Percentile
97.5th Percentile	0 (0)	0.38 (0.838)	3.32 (7.32)
Mean	0 (0)	0.287 (0.633)	2.46 (5.42)
2.5th Percentile	0 (0)	0.2 (0.441)	1.73 (3.81)
Pearson Correlation = 0.9998			

$L_{Surface,USR}$



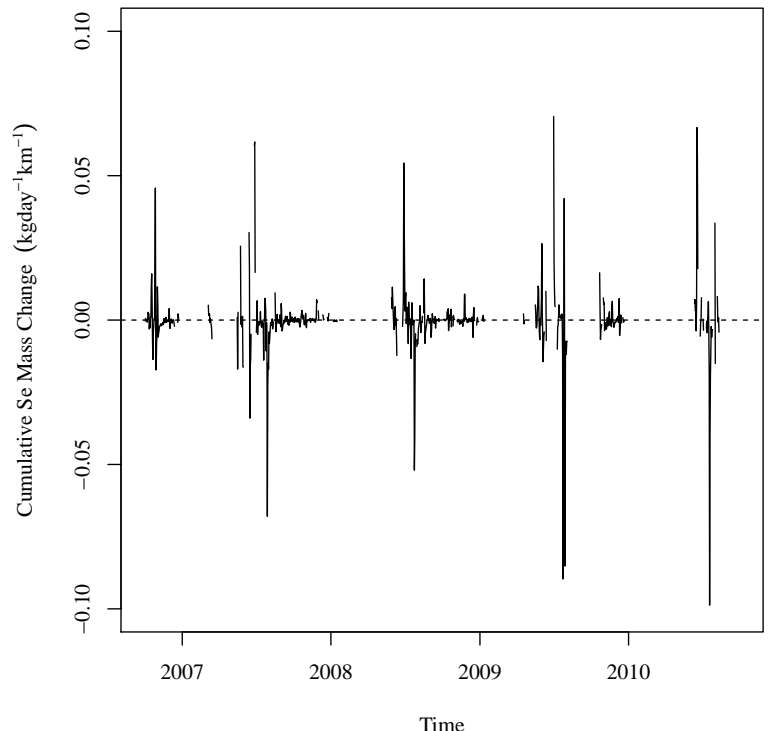
(a) Deterministic Model.



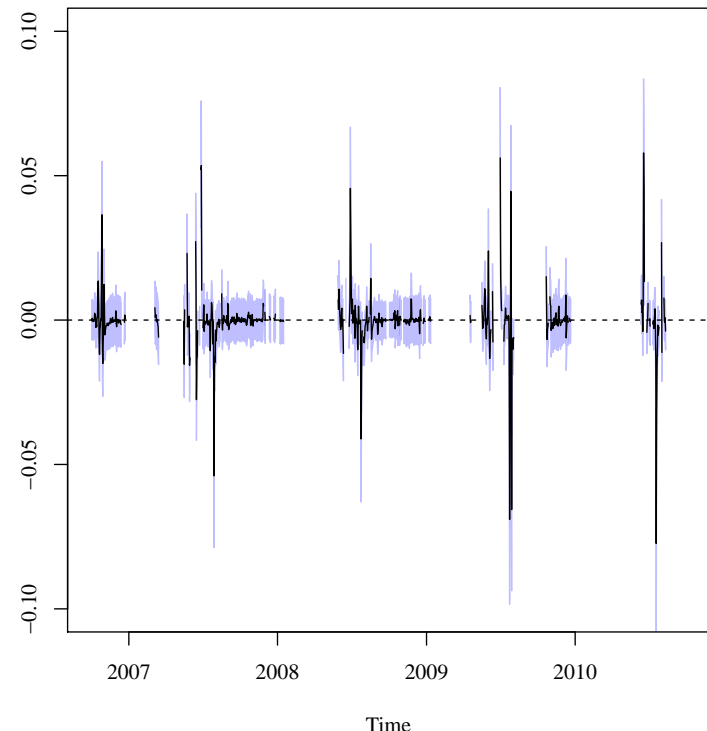
(b) Stochastic Model.

Figure 5.28. USR deterministic and stochastic dissolved selenium mass transport time-series. For the stochastic model, the line is the mean of the realizations and the blue band is the 97.5th CIR.

$$L_{Surface, DSR}$$



(a) Deterministic Model.



(b) Stochastic Model.

Figure 5.29. DSR deterministic and stochastic dissolved selenium mass transport time-series. For the stochastic model, the line is the mean of the realizations and the blue band is the 97.5th CIR.

Figures 5.28 and 5.29 show that there is a definite seasonal variation $\sum L_{Surface}$ in both the USR and DSR. This is to be expected since $\sum L_{Surface}$ is the sum of the individual surface water loadings. These figures show also that the total mass loading in the USR is significantly larger than in the DSR.

5 The distribution of all realizations within each time step was analyzed to determine a distribution type. This analysis was performed to determine if the assumption that the deterministic model results were representative of the stochastic model. Testing was performed by comparing K-S statistics for the best fit normal, log-normal, logistic, exponential, gamma, and Weibull distributions. In the USR, 69.9% of the time-steps were normally distributed
10 and 30.1% were best fit by a logistic distribution. In the DSR 4.39% of the time-steps were normally distributed and 95.6% were best fit by a logistic distribution. This indicates that the DSR stochastic model distribution within the time-steps more heavily favor the tails
15 than in the USR.

Tables 5.22 and 5.23 present the summary statistics for the deterministic model time-series and the three stochastic model summary statistics time-series for the results presented
15 in Figures 5.28 5.28 which are for the USR and DSR, respectively. All values in these tables are in units of $\text{kg d}^{-1} \text{km}^{-1}$

The difference between the deterministic model time-series mean and the stochastic model mean time-series mean is very low. This indicates that the deterministic model is
20 representative of the stochastic model expected value. The fairly low differences between the deterministic model time series and the stochastic model mean time series at the 2.5th and 97.5th percentile indicate that there is still a small range of uncertainty contained within the stochastic model that the deterministic model cannot replicate.

Table 5.22. USR deterministic and stochastic dissolved selenium mass transport time-series results tables. Values are in units of $\text{kg d}^{-1} \text{ km}^{-1}$.

$$L_{\text{Surface}, \text{USR}}$$

Deterministic Model Time Series

2.5th Percentile	Mean	97.5th Percentile
-0.124 (-0.273)	-0.0441 (-0.0972)	0.0434 (0.0957)

Stochastic Model Summary Statistics Time Series

Time Series	2.5th Percentile	Mean	97.5th Percentile
97.5th Percentile	-0.0775 (-0.171)	-0.0139 (-0.0306)	0.0833 (0.184)
Mean	-0.118 (-0.26)	-0.043 (-0.0948)	0.0349 (0.0769)
2.5th Percentile	-0.175 (-0.386)	-0.0726 (-0.16)	0.00603 (0.0133)
Pearson Correlation = 0.9963			

Table 5.23. USR deterministic and stochastic dissolved selenium mass transport time-series results tables. Values are in units of $\text{kg d}^{-1} \text{ km}^{-1}$.

$$L_{\text{Surface}, \text{DSR}}$$

Deterministic Model Time Series

2.5th Percentile	Mean	97.5th Percentile
-0.207 (-0.456)	-0.0734 (-0.162)	-0.0313 (-0.069)

Stochastic Model Summary Statistics Time Series

Time Series	2.5th Percentile	Mean	97.5th Percentile
97.5th Percentile	-0.0564 (-0.124)	-0.0242 (-0.0534)	0.0352 (0.0776)
Mean	-0.184 (-0.406)	-0.0713 (-0.157)	-0.0303 (-0.0668)
2.5th Percentile	-0.37 (-0.816)	-0.119 (-0.262)	-0.0565 (-0.125)
Pearson Correlation = 0.983			

5.4. RESULTS OF CALCULATED UNACCOUNTED FOR RETURN LOADING

Figures 5.30 and 5.31 depict the final results for the USR and DSR mass balance models, respectively. These figures show the calculated average daily selenium loading rate between the aquifer and the river channel for the deterministic and stochastic models using
5 Equation 37 applied to the two study reaches. The blue bands in the stochastic model sub-figures depict the 95% CIR for the calculated time steps. Positive values indicate that water is moving into the river channel from the aquifer.

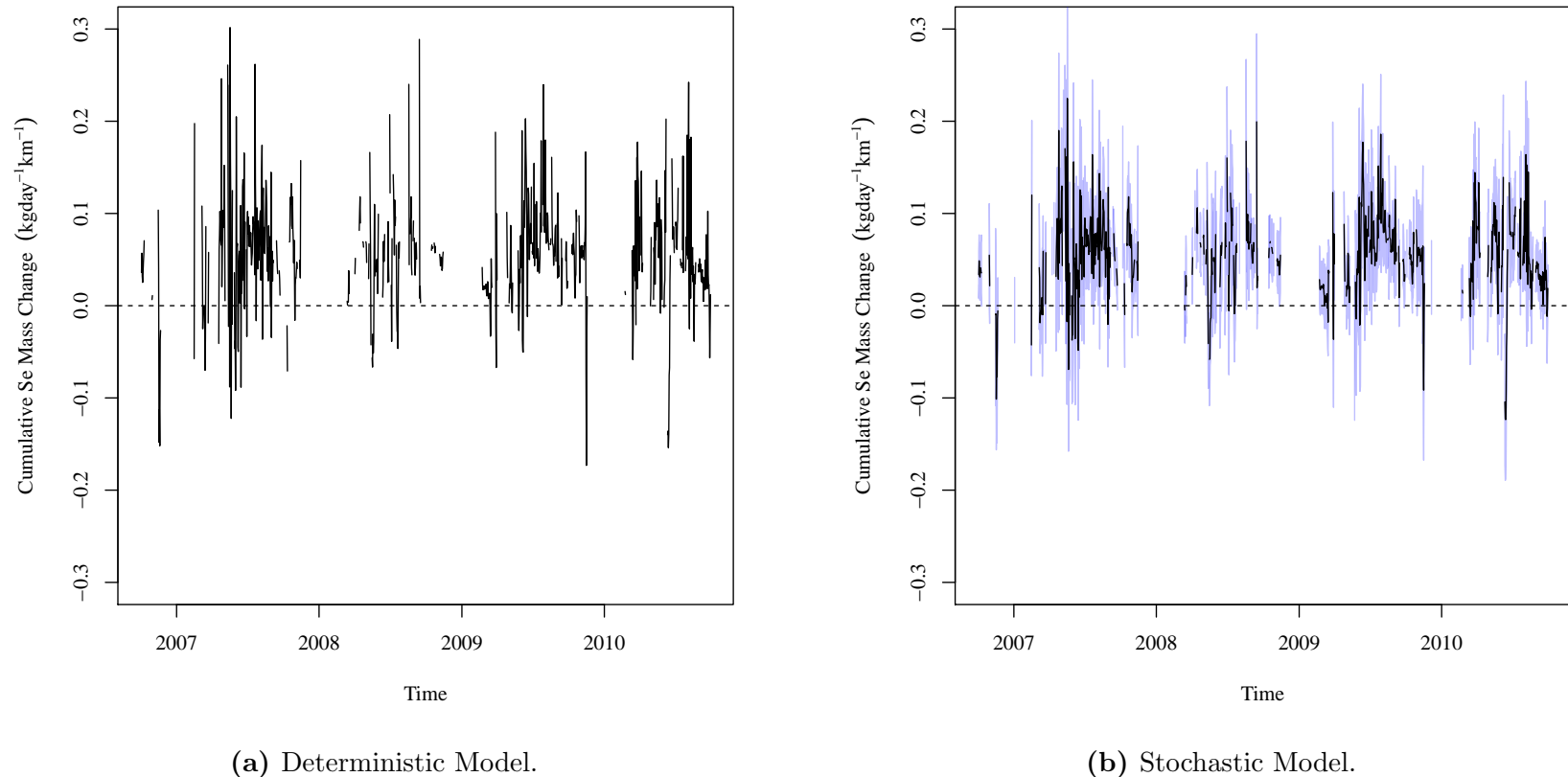


Figure 5.30. USR deterministic and stochastic dissolved selenium unaccounted for loading time-series. For the stochastic model, the line is the mean of the realizations and the blue band is the 97.5th CIR.

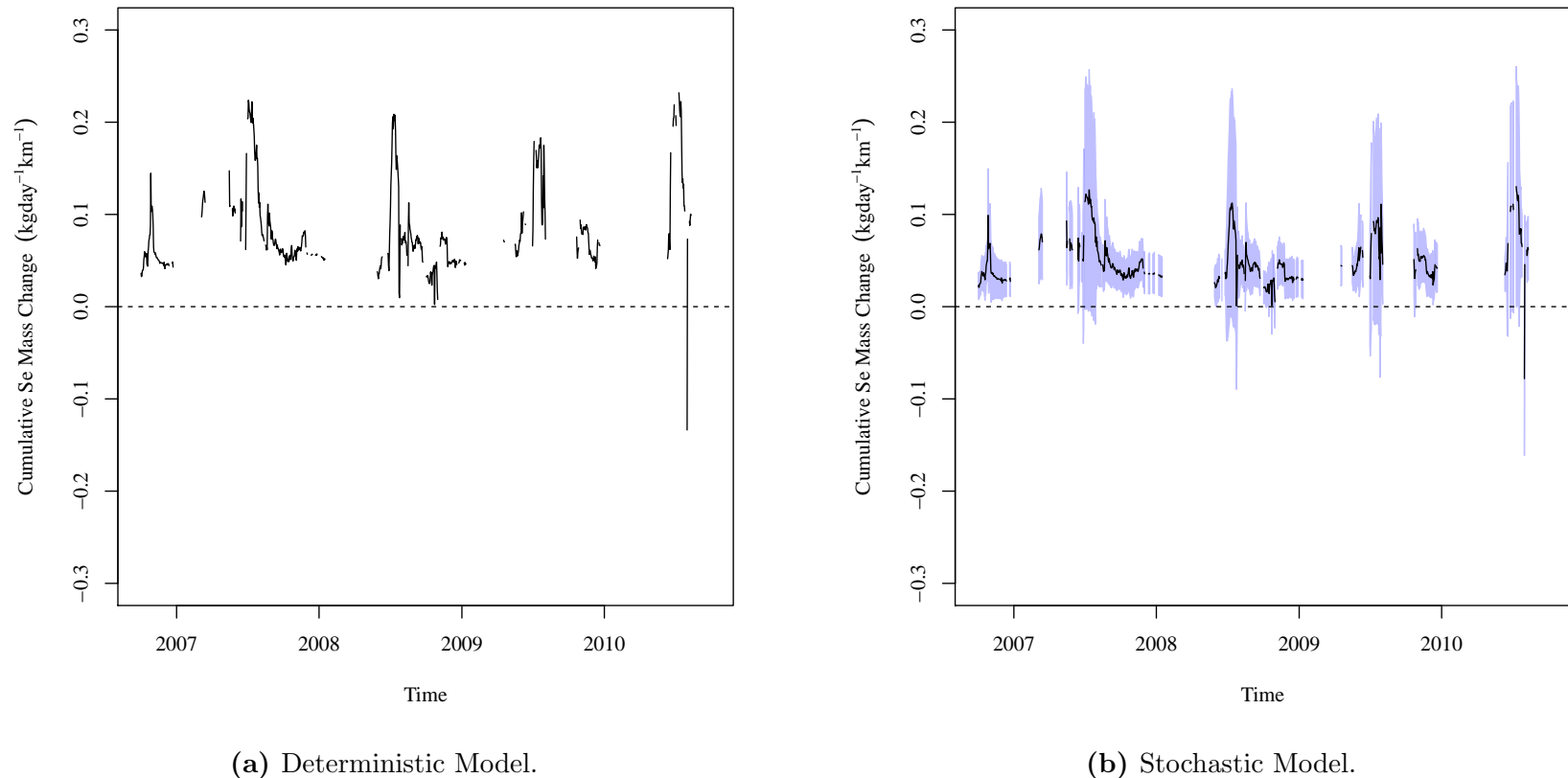


Figure 5.31. DSR deterministic and stochastic dissolved selenium unaccounted for loading time-series. For the stochastic model, the line is the mean of the realizations and the blue band is the 97.5th CIR.

As anticipated with the study reach intermediate results, Figures 5.30 and 5.31 indicate that there is seasonable variability with the transport of selenium. The figures show that the USR and DSR receive a significant quantity of selenium from unaccounted for sources. There is a very short period during midyear where the unaccounted for selenium transport 5 flows are a sink for mass being lost from the Arkansas River in the USR. The DSR nearly always receives water from unaccounted for non-point sources throughout the year.

The distribution of all realizations within each time step was analyzed to determine a distribution type. This analysis was performed to determine if the assumption that the deterministic model results were representative of the stochastic model. Testing was performed by comparing K-S statistics for the best distribution using the same methodology 10 used previously. In the USR, 72.6% of the time-steps are normally distributed and 27.4% are best fit by a logistic distribution. In the DSR, 12.7% of the time-steps are normally distributed and 87.3% are best fit by a logistic distribution. This indicates that the values 15 within each time-step for the DSR stochastic mass loading model are more heavily weighted toward the tails than in the USR stochastic mass loading model.

Tables 5.24 and 5.25 presents summary statistics of the deterministic and stochastic unaccounted for mass balance models. Values are presented in units of $\text{kg d}^{-1} \text{ km}^{-1}$. These tables present the mean, 97.5th percentile, and 2.5th percentile for the deterministic model time series and the mean, 97.5th percentile, and 2.5th percentile for each of the stochastic 20 model summary statistics time series.

Tables 5.24 and 5.25 show that the deterministic model time series is representative of the stochastic model mean time series. The mean value of the two time series are similar and the values 95% CIR of the two time-series, although different, are similar enough to call the deterministic model a reasonable representation of the stochastic model. Both the

Table 5.24. USR deterministic and stochastic dissolved selenium unaccounted for loading time-series results tables. Values are in units of $\text{kg d}^{-1} \text{ km}^{-1}$.

$L_{UNPS,USR}$

Deterministic Model Time Series

2.5th Percentile	Mean	97.5th Percentile
-0.0692 (-0.153)	0.0556 (0.123)	0.189 (0.417)

Stochastic Model Summary Statistics Time Series

Time Series	2.5th Percentile	Mean	97.5th Percentile
97.5th Percentile	0.0238 (0.0525)	0.101 (0.223)	0.214 (0.472)
Mean	-0.04 (-0.0882)	0.0543 (0.12)	0.145 (0.32)
2.5th Percentile	-0.107 (-0.236)	0.00817 (0.018)	0.0822 (0.181)
Pearson Correlation = 0.9401			

Table 5.25. DSR deterministic and stochastic dissolved selenium unaccounted for loading time-series results tables. Values are in units of $\text{kg d}^{-1} \text{ km}^{-1}$.

$L_{UNPS,DSR}$

Deterministic Model Time Series

2.5th Percentile	Mean	97.5th Percentile
0.0279 (0.0615)	0.0822 (0.181)	0.208 (0.459)

Stochastic Model Summary Statistics Time Series

Time Series	2.5th Percentile	Mean	97.5th Percentile
97.5th Percentile	0.0604 (0.133)	0.14 (0.309)	0.375 (0.827)
Mean	0.033 (0.0728)	0.0783 (0.173)	0.184 (0.406)
2.5th Percentile	-0.0496 (-0.109)	0.0172 (0.0379)	0.0498 (0.11)
Pearson Correlation = 0.9611			

figures and tables indicate that the USR and DSR are gaining selenium from unaccounted for non-point sources. The exact location of these sources is not known, but considering the low magnitude of the observed, but unaccounted for flows, the assumption can be made that the majority of these unaccounted for loadings are from the riparian aquifer.

Comparing the USR and DSR mass loading model results shows that the unaccounted for flow are relatively equal between the study regions. The results show that the DSR receives 38.3% more selenium from unaccounted for sources than the USR. This difference is roughly $0.0263 \text{ kg d}^{-1} \text{ km}^{-1}$ ($0.058 \text{ lb d}^{-1} \text{ mi}^{-1}$) which isn't very large considering the magnitude of the values. When these results are applied to both regions, the difference is magnified.

The USR and DSR receive approximately 5.52 kg d (7.59 lb d^{-1}) and 5.12 kg d (7.04 lb d^{-1}), respectively. Given that the Arkansas River in the DSR is approximately 37% shorter than in the USR we can take an initial guess that the selenium concentration in the DSR unaccounted for mass loading is higher than in the USR.

This guess is directly observable in the DSR where the flow rate at the upstream end of the reach is visibly typically less than or equal to the flow rate at the downstream end. It has also been observed that there are flows present at the upstream end of the DSR when John Martin Reservoir, which is approximately 16 km (10 mi) upstream, is not actively discharging water to the river. There are no points along the river between the reservoir and the upstream end of the DSR where water is discharged into the river channel. The water passing the upstream end of the DSR must be coming from groundwater sources.

The difference between the study region mass loading model results is low. This allows us to conclude that the selenium dissolution and transport processes that are active in the USR are equal or approximately equal in magnitude to those in the DSR.

The estimated average daily selenium loading concentration from unaccounted for sources was compared to the selenium concentration values collected from riparian wells near the river. The estimated average daily selenium loading concentration values were calculated by converting Equation 34 to solve for the concentration. The calculation was performed for 5 each time step and summary statistics were calculated. An appropriate conversion factor was used to convert the resultant average daily concentration values to $\mu\text{g L}^{-1}$.

Figures 5.32 and 5.33 present the estimated average daily selenium loading concentration model for the USR and DSR, respectively. The left sub-figure is the results of the deterministic model time series and the right sub-figure is the result of the stochastic model. 10 The black line in the stochastic model is the mean of all realizations for each time step. The blue band is the 2.5th and 97.5th percentile for each time step. Positive concentrations indicate the concentration entering the river channel. The absolute value of the negative concentrations in these two figures is the concentration that is leaving the river channel.

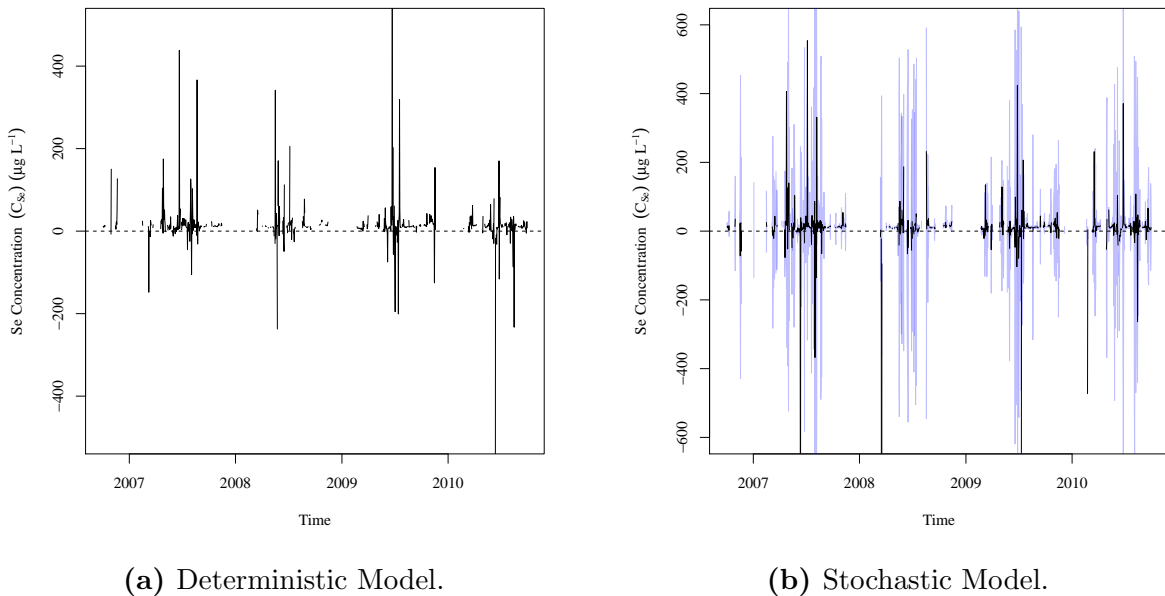
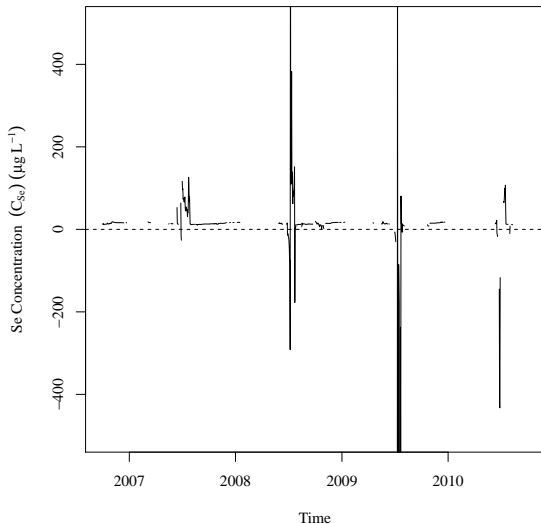
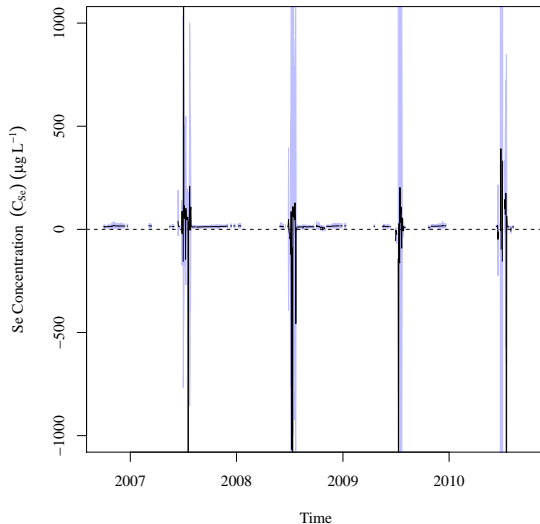


Figure 5.32. Time series of the calculated concentration of USR unaccounted for mass loading. For the stochastic model, the line is the mean of the realizations and the blue band is the 97.5th CIR.



(a) Deterministic Model.



(b) Stochastic Model.

Figure 5.33. Time series of the calculated concentration of USR unaccounted for mass loading. For the stochastic model, the line is the mean of the realizations and the blue band is the 97.5th CIR.

Figures 5.32 and 5.33 show that there is a large degree of uncertainty in the values as can be seen by comparing the deterministic and stochastic sub-figures for each study reach. In spite of the uncertainty, we can see that the concentration of unaccounted for loading to and from the river peaks during the middle of the year. This is when the use of irrigation water on crops is at its highest. Analysis of the distribution of realizations within each time step was not performed. The goal of this analysis was to determine the loading concentration and to determine if there was any temporal relationship.

Tables 5.32 and 5.33 present the summary statistics for the deterministic model time-series and the three stochastic model summary statistics time-series. All values are presented in units of $\mu\text{g L}^{-1}$.

We can only speculate on the source of the higher dissolved selenium concentration. Discussions with others familiar with the LARB selenium issue have added to the pool of possible sources. There is the possibility that John Martin Reservoir may be a combined

Table 5.26. USR deterministic and stochastic dissolved selenium unaccounted for loading calculated concentration time-series results tables. Values are in units of $\text{kg d}^{-1} \text{ km}^{-1}$.

$$C_{UNPS,USR}$$

Deterministic Model Time Series

2.5th Percentile	Mean	97.5th Percentile
-32	14.3	104

Stochastic Model Summary Statistics Time Series

Time Series	2.5th Percentile	Mean	97.5th Percentile
97.5th Percentile	3.93	93.6	504
Mean	-57.5	4.41	102
2.5th Percentile	-505	-67.2	12
Pearson Correlation = 0.003341			

Table 5.27. DSR deterministic and stochastic dissolved selenium unaccounted for loading calculated concentration time-series results tables. Values are in units of $\text{kg d}^{-1} \text{ km}^{-1}$.

$$C_{UNPS,DSR}$$

Deterministic Model Time Series

2.5th Percentile	Mean	97.5th Percentile
-108	60	136

Stochastic Model Summary Statistics Time Series

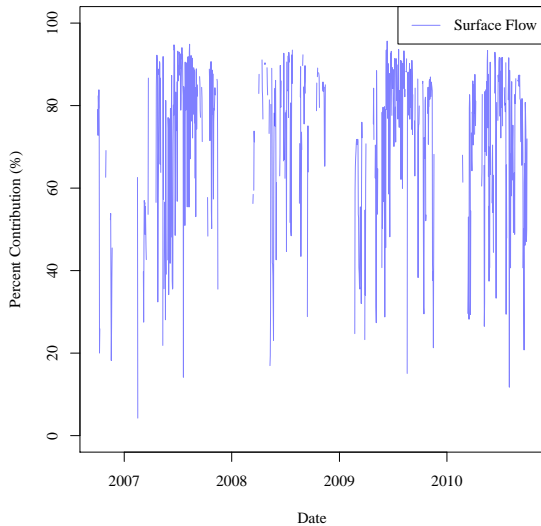
Time Series	2.5th Percentile	Mean	97.5th Percentile
97.5th Percentile	13.6	121	1310
Mean	-95	2.46	102
2.5th Percentile	-1420	-86.1	8.61
Pearson Correlation = 0.08137			

source and sink. Selenium may be dissolved from the USR, concentrated within the reservoir through evaporation of water, and discharged at a higher concentration to the DSR. This has a couple problems as the reservoir is normally not discharging water to the DSR. There is the possibility that the concentrated solution may be seeping through the ground under the dam
5 and into the DSR riparian aquifer. Another possibility is that the higher concentration may be a cumulative effect of evaporation as water moves down the LARB from the USR to the DSR. Some have even speculated that sediment transport may play a significant role. Others have suggested that the bedrock beneath the riparian aquifer, which is the ultimate source of selenium in the LARB, may be more rich in selenium in the DSR than the USR.

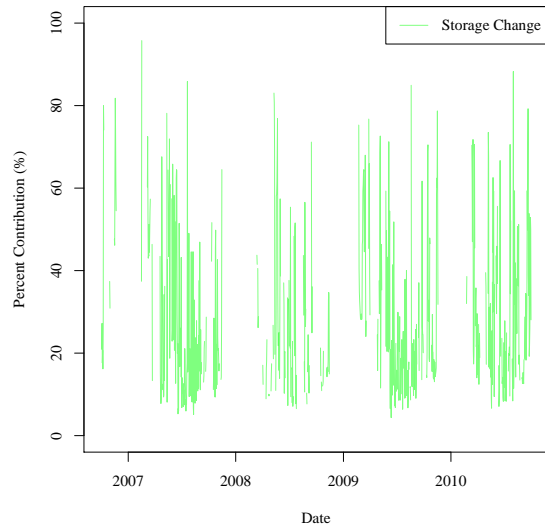
10 Figures 5.34 and 5.35 present the deterministic model results as fractions of the components of the USR and DSR water balance, respectively. Values are presented as percent of the total. Total values are calculated as the sum of the respective constituent components. The combined sub-figure combines the other sub-figures as a overlapping comparison.

These figures show that the surface flow component of the water balance model
15 $(\sum Q_{Surface})$ is the most significant portion in both the USR and DSR. They also show that the storage component $(\frac{\Delta S}{\Delta t})$, is more significant in the USR than the DSR. Both figures show that the storage change component of the mass loading model cannot be ignored and must be included. These figures also seem to show an inverse relationship between the contribution of the flow portion and the contributions of the storage. The mechanism of this
20 relationship is not understood at this time.

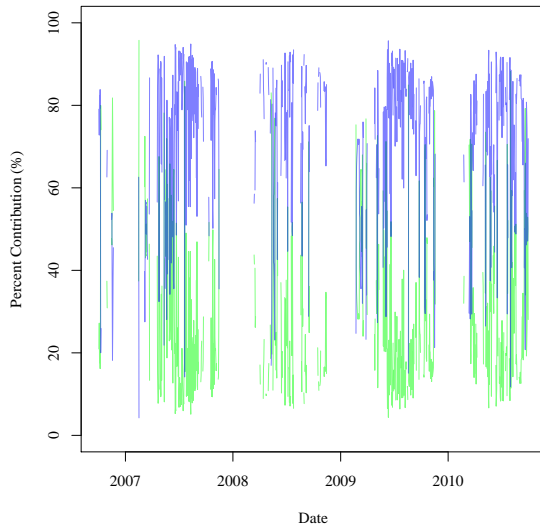
Tables 5.28 and 5.29 present the numerical results associated with the contribution analysis. These tables show that the mass storage change component of the mass loading model is more significant in the USR than in the DSR. Since water volume change is one of the two components of this value, we can compare this to field observations of the flow rates



(a) Surface Water Portion.



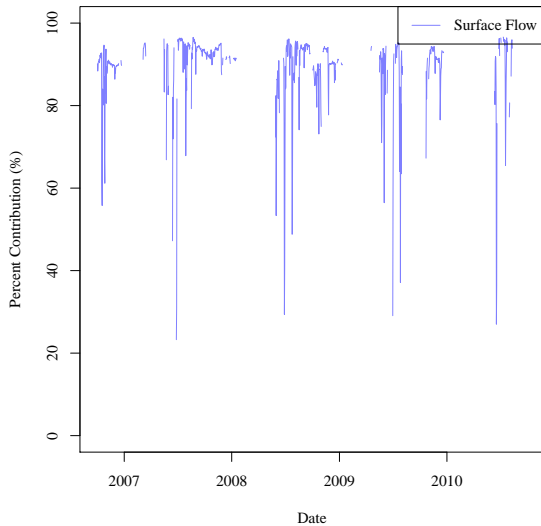
(b) Storage Change Portion.



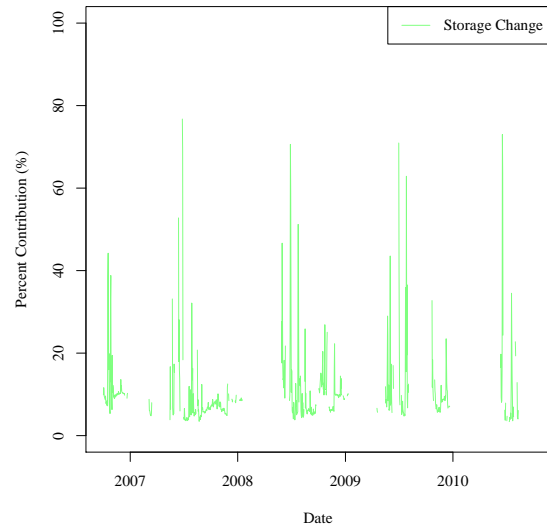
(c) Combined Contributions.

Figure 5.34. Time series of the major USR Arkansas River contributions to the mass loading model.

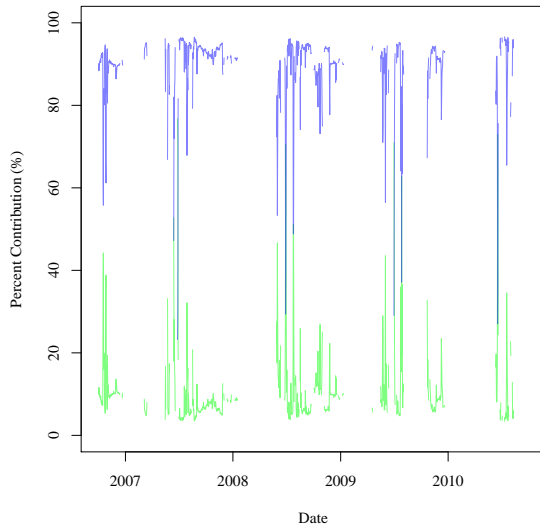
in the DSR. These flow rates are relatively constant throughout the year. Most likely due to flow regulation from John Martin Reservoir such that flow rates into Kansas comply with court mandated minimums.



(a) Surface Water Portion.



(b) Storage Change Portion.



(c) Combined Contributions.

Figure 5.35. Time series of the major DSR Arkansas River contributions to the mass loading model.

The typical method for calculating a river mass loading includes negating daily storage changes. This study assumed that these assumptions were false for the LARV and included major portions of the total effort to calculating daily changes in storage. Neglecting the

Table 5.28. Major portion contributions to the USR mass loading models.

Model Portion	2.5%	Mean	97.5%
$\frac{\Delta S_M}{\Delta t}$	8.33	28.7	55.6
$\sum L_{Surface}$	44.4	71.3	91.7

Table 5.29. Major portion contributions to the DSR mass loading models.

Model Portion	2.5%	Mean	97.5%
$\frac{\Delta S_M}{\Delta t}$	1.6	10.6	30.1
$\sum L_{Surface}$	69.9	89.4	98.4

storage change component of the USR mass loading balance causes a large change in the resultant unaccounted for mass loading values and should not be neglected.

CHAPTER 6

SENSITIVITY ANALYSIS

6.1. SENSITIVITY ANALYSIS PURPOSE, SCOPE, AND METHODOLOGY

Sensitivity analyses serves as a means to determine the degree to which each input variable affects the model. The results of this analyses serves to assist with future model development and refinement. Input variables which are not found to significantly affect 5 the complete model can be considered for removal from the model after determining if the variable is significant for a portion of the model. A variable may be insignificant for the whole model, but may be significant for a intermediate value in the model.

For this thesis, we are only analyzing the sensitivity of the water and mass loading models to the input variables. Many of the variables are used in multiple intermediate 10 calculations and cannot reasonably be removed from the models. The uncertainty range was of primary concern. Each variable was perturbed such that the new value was at the ends of the estimated uncertainty range. Additionally, the average daily reported flow depth values were perturbed four times, once each for uncertainty ranges of 0.0030 m, 0.0152 m, 0.0304 m and 0.0762 m (0.01 ft, 0.05 ft, 0.1 ft and 0.25 ft). The additional analyses were performed 15 on the average daily reported flow depth to determine the extent of the water balance and mass loading models sensitivity to these values. Reported average daily flow depth values are directly used to calculate water surface area used in the evaporation and precipitation calculations and to calculate river volume change.

Sensitivity analyses were only performed on the deterministic models. Since the 20 scope of the sensitivity analysis included testing the ends of the uncertainty distributions,

two trials were run for each input variable. One trial tests the upper bound of the uncertainty distribution and the second tests the lower bound.

6.2. SENSITIVITY ANALYSIS RESULTS

Tables 6.1 and 6.2 list the results from the sensitivity analyses for both the water

balance and mass loading models in the USR and DSR, respectively. The results are given as the mean of all the calculated results in each of the two deterministic time series models and as the percent difference from the base model. The base model is calculated without perturbing any of the input variables. Those variables with "0" are either not significant to the model or are not part of the model.

10

Table 6.1. USR Sensitivity Analysis Results. The results columns are the mean of the average daily unaccounted for water balance or mass loading, as appropriate. The difference column indicates the percent difference between the trial result and the baseline result. The Base trial was run without any changes to input variables.

Trial	Water Balance		Mass Loading	
	Result ($\text{m}^3 \text{s}^{-1} \text{km}^{-1}$)	Difference (%)	Result ($\text{kg d}^{-1} \text{km}^{-1}$)	Difference (%)
Base (no change)	0.0532	--	0.0556	--
$Q_{ARKCATCO} +10\%$	0.0327	-38.6	0.0452	-18.6
$Q_{ARKCATCO} -10\%$	0.0738	38.6	0.0659	18.6
$EC_{ARKCATCO} +10\%$	0.0532	0	0.0556	0
$EC_{ARKCATCO} -10\%$	0.0532	0	0.0556	0
$T_{ARKCATCO} +5^\circ\text{C}$	0.0532	0	0.0556	0
$T_{ARKCATCO} -5^\circ\text{C}$	0.0532	0	0.0556	0
$Q_{ARKLASCO} +10\%$	0.0675	26.9	0.0648	16.7
$Q_{ARKLASCO} -10\%$	0.0389	-26.9	0.0463	-16.7
$EC_{ARKLASCO} +10\%$	0.0532	0	0.0556	0
$EC_{ARKLASCO} -10\%$	0.0532	0	0.0556	0
$T_{ARKLASCO} +5^\circ\text{C}$	0.0532	0	0.0556	0
$T_{ARKLASCO} -5^\circ\text{C}$	0.0532	0	0.0556	0
$Q_{HOLCANCO} +20\%$	0.0594	11.6	0.0587	5.63
$Q_{HOLCANCO} -20\%$	0.047	-11.6	0.0524	-5.63
$Q_{RFDMANCO} +20\%$	0.0558	4.85	0.0573	3.13
$Q_{RFDMANCO} -20\%$	0.0507	-4.85	0.0538	-3.13

Table 6.1. USR Sensitivity Analysis Results. (continued)

Trial	Water Balance		Mass Loading	
	Result ($\text{m}^3 \text{s}^{-1} \text{km}^{-1}$)	Difference (%)	Result ($\text{kg d}^{-1} \text{km}^{-1}$)	Difference (%)
$Q_{FLSCANCO} +20\%$	0.0551	3.44	0.0568	2.14
$Q_{FLSCANCO} -20\%$	0.0514	-3.44	0.0544	-2.14
$Q_{RFDRETCO} +20\%$	0.052	-2.29	0.0548	-1.46
$Q_{RFDRETCO} -20\%$	0.0545	2.29	0.0564	1.48
$Q_{TIMSWICO} +15\%$	0.0496	-6.91	0.0537	-3.44
$Q_{TIMSWICO} -15\%$	0.0569	6.89	0.0575	3.44
$Q_{FLYCANCO} +20\%$	0.0785	47.4	0.072	29.6
$Q_{FLYCANCO} -20\%$	0.028	-47.4	0.0391	-29.6
$Q_{CANSWKCO} +15\%$	0.0523	-1.69	0.0548	-1.4
$Q_{CANSWKCO} -15\%$	0.0541	1.69	0.0564	1.42
$Q_{CONDITCO} +20\%$	0.0569	6.8	0.0582	4.77
$Q_{CONDITCO} -20\%$	0.0496	-6.8	0.0529	-4.77
$Q_{HRC194CO} +20\%$	0.0525	-1.43	0.0548	-1.33
$Q_{HRC194CO} -20\%$	0.054	1.43	0.0563	1.33
$Q_{LAJWWTP} +15\%$	0.0531	-0.263	0.0553	-0.45
$Q_{LAJWWTP} -15\%$	0.0534	0.263	0.0558	0.45
$P +25\%$	0.0531	-0.319	0.0556	0
$P -25\%$	0.0534	0.319	0.0556	0
$ET_{Ref} +0.98\text{mm}$	0.0544	2.24	0.0556	0
$ET_{Ref} -0.98\text{mm}$	0.052	-2.24	0.0556	0
$u_2 +0.5\text{ m s}^{-1}$	0.0532	-0.0939	0.0556	0
$u_2 -0.5\text{ m s}^{-1}$	0.0533	0.0939	0.0556	0
$RH_{min} +2\%$	0.0532	0	0.0556	0
$RH_{min} -2\%$	0.0532	0	0.0556	0
$\beta_1 +10\%$	0.054	1.37	0.0554	-0.234
$\beta_1 -10\%$	0.0525	-1.37	0.0557	0.234
$\beta_2 +10\%$	0.0531	-0.244	0.0556	0.018
$\beta_2 -10\%$	0.0534	0.244	0.0556	-0.018
$d_A +0.01 \text{ ft}$	0.0532	0	0.0556	0
$d_A -0.01 \text{ ft}$	0.0532	0	0.0556	0
$d_B +0.01 \text{ ft}$	0.0532	0	0.0556	0
$d_B -0.01 \text{ ft}$	0.0532	0	0.0556	0
$d_C +0.01 \text{ ft}$	0.0532	0.0188	0.0556	0
$d_C -0.01 \text{ ft}$	0.0532	-0.0376	0.0556	0
$d_D +0.01 \text{ ft}$	0.0533	0.0376	0.0556	0
$d_D -0.01 \text{ ft}$	0.0532	-0.0376	0.0556	0.018
$d_E +0.01 \text{ ft}$	0.0532	0.0188	0.0556	0
$d_E -0.01 \text{ ft}$	0.0532	-0.0188	0.0556	0
$d_A +0.05 \text{ ft}$	0.0533	0.0376	0.0556	0
$d_A -0.05 \text{ ft}$	0.0532	-0.0376	0.0556	0

Table 6.1. USR Sensitivity Analysis Results. (continued)

Trial	Water Balance		Mass Loading	
	Result (m ³ s ⁻¹ km ⁻¹)	Difference (%)	Result (kg d ⁻¹ km ⁻¹)	Difference (%)
d_B +0.05 ft	0.0532	0.0188	0.0556	0
d_B -0.05 ft	0.0532	-0.0188	0.0556	0
d_C +0.05 ft	0.0533	0.131	0.0556	0
d_C -0.05 ft	0.0532	-0.15	0.0556	0
d_D +0.05 ft	0.0533	0.15	0.0556	-0.036
d_D -0.05 ft	0.0532	-0.169	0.0556	0.036
d_E +0.05 ft	0.0533	0.0563	0.0556	0
d_E -0.05 ft	0.0532	-0.0751	0.0556	0
d_A +0.1 ft	0.0533	0.0563	0.0556	0
d_A -0.1 ft	0.0532	-0.0751	0.0556	0.018
d_B +0.1 ft	0.0532	0.0188	0.0556	0
d_B -0.1 ft	0.0532	-0.0376	0.0556	0
d_C +0.1 ft	0.0534	0.244	0.0556	0
d_C -0.1 ft	0.0531	-0.319	0.0556	0
d_D +0.1 ft	0.0534	0.301	0.0556	-0.054
d_D -0.1 ft	0.053	-0.394	0.0556	0.09
d_E +0.1 ft	0.0533	0.131	0.0556	0
d_E -0.1 ft	0.0532	-0.15	0.0556	0
d_A +0.25 ft	0.0533	0.15	0.0556	-0.018
d_A -0.25 ft	0.0538	0.977	0.0568	2.25
d_B +0.25 ft	0.0533	0.0563	0.0556	0
d_B -0.25 ft	0.0548	2.87	0.0578	3.98
d_C +0.25 ft	0.0535	0.563	0.0556	-0.036
d_C -0.25 ft	0.0585	9.88	0.0623	12.1
d_D +0.25 ft	0.0536	0.676	0.0555	-0.144
d_D -0.25 ft	0.0553	3.79	0.0554	-0.378
d_E +0.25 ft	0.0534	0.282	0.0556	0
d_E -0.25 ft	0.0528	-0.751	0.0555	-0.216

Table 6.1 shows that the USR water balance model is most sensitive to the variables

$Q_{ARKCATCO}$, $Q_{ARKLASCO}$, $Q_{HOLCANCO}$, and $Q_{FLYCANCO}$ with sensitivity to other variables

to a lesser extent. Flow rate measurement uncertainty distributions for $Q_{ARKCATCO}$ and

5 $Q_{ARKLASCO}$ are at the smallest possible available in the LARV. Flow rate measurements

represented by $Q_{HOLCANCO}$ and $Q_{FLYCANCO}$ should be improved to make the model more

accurate. The input variables $EC_{ARKCATCO}$, $T_{ARKCATCO}$, $EC_{ARKLASCO}$, and $T_{ARKLASCO}$ are not used in the water balance model and therefore show no change from the base model.

It was expected that the percent difference for the upper bound trial and the lower bound trial would have different signs but the same magnitude. In almost all cases, this is true.

- 5 The reported average daily flow depths that were perturbed by $\pm 0.0152\text{ m}$ ($\pm 0.05\text{ ft}$) or more were not symmetrical. This is due to the lower bound of the perturbed flow depths being less than zero, which is the lower bound of acceptable flow depths. Since the perturbed average daily flow depths were altered such that no values were below zero, we expect that the difference between the particular trial and the base trial would not be symmetrical.

- 10 This table also shows that the USR mass loading model is most sensitive to $Q_{ARKCATCO}$, $Q_{ARKLASCO}$, $Q_{HOLCANCO}$, and $Q_{FLYCANCO}$ with sensitivity to other variables to a lesser extent. Note that these are the same variables to which the USR water balance model is also most sensitive to. The USR mass loading model is more sensitive to changes in flow depth than the water balance model which is evident in the difference values. Input variables P ,
- 15 ET_{Ref} , u_2 , and RH_{min} are not used in the mass loading model and therefore show no change from the base model. As with the water balance model, the differences between the upper and lower limits for each variable are symmetrical for all variables except the reported average daily flow depths. These are not symmetrical for the same reason as described for the water balance model.

Table 6.2. DSR Sensitivity Analysis Results. The results columns are the mean of the average daily unaccounted for water balance or mass loading, as appropriate. The difference column indicates the percent difference between the trial result and the baseline result. The Base trial was run without any changes to input variables.

Trial	Water Balance		Mass Loading	
	Result ($\text{m}^3 \text{s}^{-1} \text{km}^{-1}$)	Difference (%)	Result ($\text{kg d}^{-1} \text{km}^{-1}$)	Difference (%)
Base (No Change)	0.0299	0	0.0516	0
$Q_{ARKLASCO} +10\%$	0.0266	-11.1	0.0501	-3.02
$Q_{ARKLASCO} -10\%$	0.0332	11.1	0.0532	3.04
$EC_{ARKJMRCO} +10\%$	0.0299	0	0.0516	0
$EC_{ARKJMRCO} -10\%$	0.0299	0	0.0516	0
$T_{ARKJMRCO} +5^\circ\text{C}$	0.0299	0	0.0516	0
$T_{ARKJMRCO} -5^\circ\text{C}$	0.0299	0	0.0516	0
$Q_{ARKCOOKS} +10\%$	0.0378	26.3	0.0608	17.8
$Q_{ARKCOOKS} -10\%$	0.0221	-26.3	0.0424	-17.8
$EC_{ARKCOOKS} +10\%$	0.0299	0	0.0516	0
$EC_{ARKCOOKS} -10\%$	0.0299	0	0.0516	0
$T_{ARKCOOKS} +5^\circ\text{C}$	0.0299	0	0.0516	0
$T_{ARKCOOKS} -5^\circ\text{C}$	0.0299	0	0.0516	0
$Q_{BIGLAMCO} +20\%$	0.0292	-2.41	0.0505	-2.15
$Q_{BIGLAMCO} -20\%$	0.0307	2.44	0.0527	2.15
$Q_{WILDHOCO} +20\%$	0.0295	-1.3	0.051	-1.24
$Q_{WILDHOCO} -20\%$	0.0303	1.34	0.0523	1.26
$Q_{BUFDITCO} +20\%$	0.0322	7.75	0.0537	4.11
$Q_{BUFDITCO} -20\%$	0.0276	-7.72	0.0495	-4.11
$Q_{FRODITKS} +20\%$	0.0307	2.54	0.0525	1.72
$Q_{FRODITKS} -20\%$	0.0292	-2.51	0.0507	-1.72
$P +25\%$	0.0299	-0.0334	0.0516	0
$P -25\%$	0.03	0.0668	0.0516	0
$ET_{Ref} +0.98 \text{ mm}$	0.0301	0.434	0.0516	0
$ET_{Ref} -0.98 \text{ mm}$	0.0298	-0.401	0.0516	0
$u_2 +0.5 \text{ m s}^{-1}$	0.0299	0	0.0516	0
$u_2 -0.5 \text{ m s}^{-1}$	0.0299	0.0334	0.0516	0
$RH_{min} +2\%$	0.0299	0.0334	0.0516	0
$RH_{min} -2\%$	0.0299	0	0.0516	0
$\beta_1 +10\%$	0.03	0.301	0.0516	-0.0387
$\beta_1 -10\%$	0.0298	-0.267	0.0516	0.0387
$\beta_2 +10\%$	0.0299	-0.0334	0.0516	0.0194
$\beta_2 -10\%$	0.03	0.0668	0.0516	-0.0194
$d_F +0.01\text{ft}$	0.0299	0.0334	0.0516	0
$d_F -0.01\text{ft}$	0.0299	0	0.0516	0.0194
$d_G +0.01\text{ft}$	0.0299	0.0334	0.0516	0
$d_G -0.01\text{ft}$	0.0299	0	0.0516	0
$d_F +0.05\text{ft}$	0.03	0.1	0.0516	-0.0387

Table 6.2. DSR Sensitivity Analysis Results. (continued)

Trial	Water Balance		Mass Loading	
	Result ($\text{m}^3 \text{s}^{-1} \text{km}^{-1}$)	Difference (%)	Result ($\text{kg d}^{-1} \text{km}^{-1}$)	Difference (%)
d_F -0.05ft	0.0299	-0.1	0.0516	0.0387
d_G +0.05ft	0.03	0.1	0.0516	0.0194
d_G -0.05ft	0.0299	-0.0668	0.0516	0
d_F +0.1ft	0.03	0.2	0.0516	-0.0581
d_F -0.1ft	0.0299	-0.2	0.0517	0.0775
d_G +0.1ft	0.03	0.167	0.0516	0.0194
d_G -0.1ft	0.0299	-0.134	0.0516	-0.0194
d_F +0.25ft	0.0301	0.434	0.0515	-0.155
d_F -0.25ft	0.022	-26.4	0.0793	53.6
d_G +0.25ft	0.03	0.368	0.0516	0.0387
d_G -0.25ft	0.0298	-0.368	0.0516	-0.0387

Table 6.2 shows that the DSR water balance model is most sensitive to the variables $Q_{ARKLASCO}$, $Q_{ARKCOOKS}$, $Q_{BUFQUITCO}$, and d_F with sensitivity to other variables to a lesser extent. Sensitivity to the d_F input variable is only significant when the flow depth is perturbed by -0.0762 m (-0.25 ft). This isn't a likely uncertainty range, but it should be noted that this is most likely due to the β_1 and β_2 shape parameters. Flow rate measurement uncertainty distributions for $Q_{ARKLASCO}$ and $Q_{ARKCOOKS}$ are at the smallest possible available in the LARV. Flow rate measurements represented by $Q_{BUFQUITCO}$ should be improved to make the model more accurate. The input variables $EC_{ARKJMRCO}$, $T_{ARKJMRCO}$, $EC_{ARKCOOKS}$, and $T_{ARKCOOKS}$ are not used in the water balance model and therefore show no change from the base model. It was expected that the percent difference for the upper bound trial and the lower bound trial would have different signs but the same magnitude. In almost all cases, this is true. The reported average daily flow depths were not symmetrical. This is due to the same effect noted in the USR.

This table also shows that the DSR mass loading model is most sensitive to $Q_{ARKLASCO}$, $Q_{ARKCOOKS}$, $Q_{BUFQUITCO}$, and d_F with sensitivity to other variables to a lesser extent. Note that these are the same variables to which the USR water balance model is also most sensitive to. The USR mass loading model is more sensitive to changes in flow depth than the water balance model which is evident in the difference values. Input variables P , ET_{Ref} , u_2 , and RH_{min} are not used in the mass loading model and therefore show no change from the base model. As with the water balance model, the differences between the upper and lower limits for each variable are symmetrical for all variables except the reported average daily flow depths. These are not symmetrical for the same reason as described for the water balance model.

Refining reported flow rate uncertainty may improve the models but is not an acceptable solution. Flow rate uncertainty is not solely based on measuring equipment or methodology, but also on the channel being measured. The Arkansas River in the LARV is a sandy bed variable channel where the only method to improve measurements is to perform more frequent gauge calibration. This is a cost that is borne by the CDWR and USGS, both of which are perpetually struggling to justify the existing stream gauge system.

Model improvement can be realistically performed by improving the characterization of the river channel. River cross section surveys should be performed at a more frequent spatial interval along the river with each cross section tied to a benchmark. Surveys should also be performed at the same location to determine a temporal relationship. While more complicated to set up, this effort should be easy to routinely re-accomplish with high accuracy GPS survey equipment.

CHAPTER 6

CONCLUSION AND RECOMMENDATIONS

6.1. UNACCOUNTED FOR RETURN FLOW CONCLUSIONS

The following list summarizes the results of the USR deterministic unaccounted for return flow model:

- (1) Water storage changes in the main stem of the river accounted for $0.000\ 534\ \text{ha m km}^{-1}$ ($0.0374\ \text{ac ft mi}^{-1}$) loss from the main channel.
- (2) Water storage changes accounted for approximately 33.6% of the water balance model.
- (3) Water flows through active gauges accounted for $0.3095\ \text{m}^3\ \text{s}^{-1}\ \text{km}^{-1}$ ($2.42\ \text{cfs mi}^{-1}$) loss from the main channel.
- (4) Water flows through active gauges accounted for approximately 59% of the water balance model.
- (5) The combined effects of precipitation and evaporation accounted for $0.007\ 77\ \text{m}^3\ \text{s}^{-1}\ \text{km}^{-1}$ ($0.544\ \text{cfs mi}^{-1}$) loss from the main channel.
- (6) The combined effects of precipitation and evaporation accounted for approximately 7.4% of the water balance model
- (7) Unaccounted for return flows accounted for $0.0532\ \text{m}^3\ \text{s}^{-1}\ \text{km}^{-1}$ ($3.73\ \text{cfs mi}^{-1}$) gain to the main river channel.

The following list summarizes the results of the USR stochastic unaccounted for return flow model:

- (1) Water storage changes in the main stem of the river accounted for $0.000\ 282\ \text{ha m km}^{-1}$ ($0.0198\ \text{ac ft mi}^{-1}$) loss from the main channel.

- (2) Water flows through active gauges accounted for $0.0395 \text{ m}^3 \text{ s}^{-1} \text{ km}^{-1}$ (2.42 cfs mi^{-1}) loss from the main channel.
- (3) The combined effects of precipitation and evaporation accounted for $0.00474 \text{ m}^3 \text{ s}^{-1} \text{ km}^{-1}$ ($0.332 \text{ cfs mi}^{-1}$) loss from the main channel.
- 5 (4) Unaccounted for return flows accounted for $0.0504 \text{ m}^3 \text{ s}^{-1} \text{ km}^{-1}$ (3.53 cfs mi^{-1}) gain to the main river channel.

The following list summarizes the results of the DSR deterministic unaccounted for return flow model:

- (1) Water storage changes in the main stem of the river accounted for $0.000117 \text{ ha m km}^{-1}$ ($0.0082 \text{ ac ft mi}^{-1}$) loss from the main channel.
- (2) Water storage changes accounted for approximately 12.7% of the water balance model.
- (3) Water flows through active gauges accounted for $0.0469 \text{ m}^3 \text{ s}^{-1} \text{ km}^{-1}$ (3.29 cfs mi^{-1}) loss from the main channel.
- 15 (4) Water flows through active gauges accounted for approximately 83.6% of the water balance model.
- (5) The combined effects of precipitation and evaporation accounted for $0.00131 \text{ m}^3 \text{ s}^{-1} \text{ km}^{-1}$ ($0.0918 \text{ cfs mi}^{-1}$) loss from the main channel.
- (6) The combined effects of precipitation and evaporation accounted for approximately 3.7% of the water balance model
- 20 (7) Unaccounted for return flows accounted for $0.0475 \text{ m}^3 \text{ s}^{-1} \text{ km}^{-1}$ (3.33 cfs mi^{-1}) gain to the main river channel.

The following list summarizes the results of the DSR stochastic unaccounted for return flow model:

- (1) Water storage changes in the main stem of the river accounted for $0.000\ 119\ \text{ha m km}^{-1}$ ($0.008\ 34\ \text{ac ft mi}^{-1}$) loss from the main channel.
- (2) Water flows through active gauges accounted for $0.0469\ \text{m}^3\ \text{s}^{-1}\ \text{km}^{-1}$ ($3.29\ \text{cfs mi}^{-1}$) loss from the main channel.
- 5 (3) The combined effects of precipitation and evaporation accounted for $0.001\ 78\ \text{m}^3\ \text{s}^{-1}\ \text{km}^{-1}$ ($0.125\ \text{cfs mi}^{-1}$) loss from the main channel.
- (4) Unaccounted for return flows accounted for $0.0479\ \text{m}^3\ \text{s}^{-1}\ \text{km}^{-1}$ ($3.36\ \text{cfs mi}^{-1}$) gain to the main river channel.

The following list enumerates the conclusions reached after analysis of the USR and

10 DSR deterministic and stochastic models:

- (1) Storage changes within the channel cannot be ignored.
- (2) Evaporation and precipitation cannot be ignored.
- (3) Both the USR and DSR deterministic water models are representative of the respective stochastic models.

6.2. UNACCOUNTED FOR RETURN MASS LOADING CONCLUSIONS

The following list summarizes the results of the USR deterministic unaccounted for return mass loading model:

- (1) Mass storage changes in the main stem of the river accounted for $0.001\ 31\text{ kg d}^{-1}\text{ km}^{-1}$
 $(0.002\ 89\text{ lb d}^{-1}\text{ mi}^{-1})$ loss from the main channel.
 - (2) Mass storage changes accounted for approximately 28.8% of the water balance model.
 - (3) Mass loadings passing through active stream gauges accounted for $0.0441\text{ kg d}^{-1}\text{ km}^{-1}$
 $(0.0972\text{ lb d}^{-1}\text{ mi}^{-1})$ loss from the main channel.
 - (4) Mass loadings passing through active stream gauges accounted for approximately 71.2% of the water balance model.
 - (5) Unaccounted for return mass loading accounted for $0.0556\text{ kg d}^{-1}\text{ km}^{-1}$ ($0.123\text{ lb d}^{-1}\text{ mi}^{-1}$)
gain to the main river channel

The following list summarizes the results of the USR stochastic unaccounted for return

15 mass loading model:

- (1) Mass storage changes in the main stem of the river accounted for $0.000\,772 \text{ kg d}^{-1} \text{ km}^{-1}$
 $(0.0017 \text{ lb d}^{-1} \text{ mi}^{-1})$ loss from the main channel.
 - (2) Mass loadings passing through active stream gauges accounted for $0.043 \text{ kg d}^{-1} \text{ km}^{-1}$
 $(0.0948 \text{ lb d}^{-1} \text{ mi}^{-1})$ loss from the main channel.
 - (3) Unaccounted for return mass loading accounted for $0.0543 \text{ kg d}^{-1} \text{ km}^{-1}$ ($0.12 \text{ lb d}^{-1} \text{ mi}^{-1}$)
gain to the main river channel.

The following list summarizes the results of the DSR deterministic unaccounted for return mass loading model:

(1) Mass storage changes in the main stem of the river accounted for $0.000\ 302\ \text{kg d}^{-1}\ \text{km}^{-1}$
($0.000\ 666\ \text{lb d}^{-1}\ \text{mi}^{-1}$) loss from the main channel.

(2) Mass storage changes accounted for approximately 10.6% of the water balance
model.

5 (3) Mass loadings passing through active stream gauges accounted for $0.0734\ \text{kg d}^{-1}\ \text{km}^{-1}$
($0.162\ \text{lb d}^{-1}\ \text{mi}^{-1}$) loss from the main channel.

(4) Mass loadings passing through active stream gauges accounted for approximately
89.4% of the water balance model.

(5) Unaccounted for return mass loading accounted for $0.0819\ \text{kg d}^{-1}\ \text{km}^{-1}$ ($0.181\ \text{lb d}^{-1}\ \text{mi}^{-1}$)
gain to the main river channel.

The following list summarizes the results of the DSR stochastic unaccounted for return
mass loading model:

(1) Mass storage changes in the main stem of the river accounted for $0.000\ 346\ \text{kg d}^{-1}\ \text{km}^{-1}$
($0.000\ 763\ \text{lb d}^{-1}\ \text{mi}^{-1}$) loss from the main channel.

15 (2) Mass loadings passing through active stream gauges accounted for $0.0712\ \text{kg d}^{-1}\ \text{km}^{-1}$
($0.157\ \text{lb d}^{-1}\ \text{mi}^{-1}$) loss from the main channel.

(3) Unaccounted for return mass loading accounted for $0.782\ \text{kg d}^{-1}\ \text{km}^{-1}$ ($0.172\ \text{lb d}^{-1}\ \text{mi}^{-1}$)
gain to the main river channel.

The following list enumerates the conclusions reached after analysis of the USR and
20 DSR deterministic and stochastic models:

(1) Storage changes within the channel cannot be ignored.

(2) Both the USR and DSR deterministic water models are representative of the re-
spective stochastic models.

- (3) The selenium concentration in the unaccounted for return flows is higher in the DSR than in the USR.

6.3. UNACCOUNTED FOR RETURN FLOW AND MASS LOADING HYPOTHESES

The following Hypotheses:

(1) The bed of John Martin Reservoir might be a significant source of selenium in the

DSR.

(2) The selenium concentration in the unaccounted for return flows is significantly lower

than the reported concentration from nearby test wells. There are processes in
the riparian zone of the river that are significant and should be investigated. We
suspect the primary process is biomethylation through the native and non-native
plant species.

6.4. RECOMMENDATIONS

The Arkansas R. is gaining water and selenium from unknown sources. Groundwater is most likely the largest component of these sources. The models presented in this paper were formulated from the best available data and the most reasonable assumptions, yet 5 there are essential pieces of information missing that can allow us to have a clearer picture of selenium transport and fate in the LARB. Selenium volatiliztion and other transport pathways are not completely understood. We do not know if there are spatial, temporal, or physical relationships with volatiliation.

Many assumptions were made in the analyses presented in this thesis. Most of which 10 are accounted for. There are many ways to improve the study contained in these pages. Of the concepts discussed, there are a few that deserve further study. These include, but are not limited to, the following:

- (1) Improve the methodology for measuring and estimating river geometry values.
- (2) Improve the concentration estimating linear models for the tributaries. These linear 15 models showed the largest uncertainty.
- (3) Improve the estimation of evaporation. Determine a method to calculate evaporation from a river by using reference ET values calculated for locations distant from the river channel.
- (4) Perform studies on selenium volatalization and boimethylation by riparian vegetation. These contributors to selenium loss were not included in this thesis due to the 20 lack of sufficient information to make even the most elementary of calculations.
- (5) Determine a method by which the groundwater flow rate into and out of the river channel can be measured. This will provide a measureable check to the values calculated in this thesis.

Future studies in the LARB should include further surface water sampling as described in this thesis. Additional data will only improve the selenium concentration estimation models. This data may also shed light on temporal patterns not recognized at this time.

5 The Lower Arkansas River Basin is valuable to the State of Colorado as a source of agriculture and history. Life and progress may appear to move slowly to those who pass through the region, but change does happen. Changes in the region have lead to an increase in water availability to residents of the LARB in Colorado and Western Kansas. This change has caused agriculture to spread throughout the valley. Increase irrigation
10 has released naturally occurring pollutants into the groundwater which returns to the river. Understanding the interaction between the aquifer and the river with increased focus on the riparian area should help residents and water managers improve water quality in the Lower Arkansas River Basin.

REFERENCES

- Abbott, P.O. (1985). *Description of water-systems operations in the arkansas river basin, colorado. Water resources Investigations report 85-4092.* Tech. rep. U.S. Geological Society.
- Allen, Richard G., Luis S. Pereira, Terry A. Howell, et al. (2011). “Evapotranspiration information reporting: I. Factors governing measurement accuracy.” In: *Agricultural Water Management* 98.6, pp. 899–920. issn: 0378-3774.
- Allen, Richard G., Luis S. Pereira, Dirk Raes, et al. (1988). *Crop Evapotranspiration - guideguide for computing crop water requirements.* FAO Irrigation and Drainage Paper No. 56. Food and Agriculture Organization of the United Nations.
- Andales, A.A., T.A. Bauder, and N.J. Doesken (2009). *The Colorado Agricultural Meteorological Network (CoAgMet) and Crop ET Reports.* Fact Sheet No. 4.723. Colorado State University.
- Bailey, R. T., E. C. Romero, and T. K. Gates (2015). “Assessing best managment practices for remediation of selenium loading in groundwater streams in an irrigated region.” In: *Journal of Hydrolog* 521, pp. 341–359.
- Bailey, Ryan T. (2012). “Regional Selenium Cycling In An Irrigated Agricultural Groundwater System: Conceptualization, Modeling, And Mitigation.” Ph.D. Colorado State University.
- Bailey, Ryan T, William J Hunter, and Timothy K. Gates (2012). “The influence of nitrate on selenium in irrigated agricultural groundwater systems.” In: *Journal of environmental quality* 41.3, pp. 783–792.

- Besser, John M. et al. (1989). "Distribution and Bioaccumulation of Selenium in Aquatic Microcosms." In: *Environmental Pollution* 62, pp. 1–12.
- Buhman, Daniel L., Timmothy K. Gates, and Chester C. Watson (2002). "Stochastic Variability of Fluvial Hydraulic Geometry: Mississippi and Red Rivers." In: *Journal of Hydraulic Engineering* 128.4, pp. 426–437.
- Cain, Doug (1985). *Quality of the Arkansas River and irrigation-return flows in the lower Arkansas River Valley, Colorado*. Tech. rep. United States Geological Survey.
- Christophersen, N. and R.F. Wright (1981). "Sulfate budget and a model for sulfate concentration in stream water at Birkenes, a small forested catchment in southernmost Norway." In: *Water Resources Research* 17 (2), pp. 377–389.
- Clifford, W Austin and Nolan J Doesken (2009). *Detecting trends in evapotranspiration in Colorado*. Colorado Water Institute, Colorado State University.
- Clifton, Daphne G. and Robert J. Gilliom (1989). *Sources and concentrations of dissolved solids and selenium in the San Joaquin River and its tributaries, California, October 1985 to March 1987*. Water-Resources Investigations Report 88-4217. U.S. Geological Survey.
- Cobb, Ernest D. (1989). *Programs and Plans—Policy Statement on Stage Accuracy*. USGS. URL: <http://water.usgs.gov/admin/memo/SW/sw89.08.html>.
- Cody, Brent M. (2010). "Sources, Occurrence, And Mobilization Of Selenium In Colorado's Lower Arkansas River Valley." PhD thesis. Colorado State University.
- Colorado Climate Center (2012). *About CoAgMet*. Colorado State University. URL: <http://www.coagmet.colostate.edu/about.php>.
- D'Agostino, Ralph B. and Michael A. Stephens, eds. (1986). *Goodness-of-fit-techniques (Statistics: a Series of Textbooks and Monographs, Vol. 68)*. 1st ed. Dekker. ISBN: 9780824774875.

Darton, Nelson Horatio (1906). *Geology of the Bighorn Mountains*. Vol. 51. US Government Printing Office.

Delignette-Muller, Marie Laure and Christophe Dutang (2014). “fitdistrplus: An R Package for Fitting Distributions.” In:

Donnelly, Joseph P and Timothy K. Gates (2005a). “Assessing irrigation-induced selenium and iron in the Lower Arkansas River Valley in Colorado.” In: *Impacts of Global Climate Change*. ASCE, pp. 1–12.

— (2005b). “Assessing irrigation-induced selenium and iron in the Lower Arkansas River Valley in Colorado.” PhD thesis. Colorado State University.

Elder, J.F. (1985). “Nitrogen and phosphorus speciation and flux in a large Florida river wetland system.” In: *Water Resources Research* 21 (5), pp. 724–732.

Gates, Timmothy K. and Muhammad A. Al-Zahrani (1996). “Spatiotemporal Stochastic Open-Channel Flow. I: Model And Its Parameter Data.” In: *Journal of Hydraulic Engineering* 122.11, pp. 641–651.

Gates, Timothy K. et al. (2009). “Assessing selenium contamination in the irrigated stream-aquifer system of the Arkansas River, Colorado.” In: *Journal of environmental quality* 38.6, pp. 2344–2356.

Gersberg, Richard M. (2006). *Selenium in the New River and an Evaluation of Human Health Risk Reduction by the Brawley and Imperial Constructed Wetlands Demonstration Project*. Summary and Final Report W-06-3. Southwest Consortium for Environmental Research, Policy, and San Diego State University.

Gillespie, Robert B and Paul C Baumann (1986). “Effects of high tissue concentrations of selenium on reproduction by bluegills.” In: *Transactions of the American Fisheries Society* 115.2, pp. 208–213.

Haan, C. T. (1989). "Parametric Uncertainty in Hydrologic Modeling." In: *Transactions of the ASAE* 32.1, pp. 0137–0146.

Haan, Charles Thomas (2002). "Statistical methods in hydrology." In:

Hamilton, S.J. and A.D. Lemly (1999). "Water-sediment controversy in setting environmental standards for selenium." In: *Ecotoxicology and Environmental Safety* 44.3, pp. 227–35.

ISSN: 0147-6513.

Harmel, R Daren and Patricia K Smith (2007). "Consideration of measurement uncertainty in the evaluation of goodness-of-fit in hydrologic and water quality modeling." In: *Journal of Hydrology* 337.3, pp. 326–336.

Herschy, RW (2002). "The uncertainty in a current meter measurement." In: *Flow Measurement and Instrumentation* 13.5, pp. 281–284.

Herting, Alexander W. and Timothy K. Gates (2006). "Assessing and modeling irrigation-induced selenium in the stream-aquifer system of the Lower Arkansas River Valley, Colorado." In: *Colorado State University Hydrology Days, Colorado State University, Fort Collins, Colorado*.

ISO (2008). "Guide to the Expression of Uncertainty in Measurement, (1995), with Supplement 1, Evaluation of measurement data, JCGM 101: 2008." In: *Organization for Standardization, Geneva, Switzerland*.

Jain, C. K. (1996). "Application of chemical mass balance to upstream-downstream river monitoring data." In: *JOURNAL OF HYDROLOGY -AMSTERDAM-* 182, pp. 105–115.
ISSN: 0022-1694.

Jensen, L. (1999). "History and importance of selenium for poultry." In: *A.L.Moxon Honorary Lecture*.

Johnson, Paula I et al. (2009). "The fate of selenium in the Imperial and Brawley constructed wetlands in the Imperial Valley (California)." In: *Ecological Engineering* 35.5, pp. 908–913.

Johnson, Richard A. and Dean W Wichern (2007). *Applied Multivariate Statistical Analysis*. 6th. Pearson.

Kansas Department of Health and Environment (2014). *2014 Kansas 303(d) List*.

Konikow, Leonard F and John D Bredehoeft (1974). "Modeling flow and chemical quality changes in an irrigated stream-aquifer system." In: *Water Resources Research* 10.3, pp. 546–562.

Lalvani, Shashi B. (2004). *SELENIUM REMOVAL FROM AGRICULTURAL DRAINAGE WATER: LAB SCALE STUDIES*. Tech. rep. Miami University.

Latimer, J.S. et al. (1988). "Water quality in the Pawtuxet river: Metal monitoring and geochemistry." In: *Water Resource Bulliten* 24.4, pp. 791–800.

Lawson, N.M. and R.P. Mason (2001). "Concentration of mercury, methylmercury, cadmium, lead, arsenic, and selenium in the rain and stream water of two contrasting watersheds in western Maryland." In: *Water research* 35.17, pp. 4039–52. ISSN: 0043-1354.

Lemly, A. Dennis (1993). "Metabolic stress during winter increases the toxicity of selenium to fish." In: *Aquatic Toxicology* 27, pp. 133–158. ISSN: 0166-445X.

Lemly, A Dennis (2002). "Symptoms and implications of selenium toxicity in fish: the Belews Lake case example." In: *Aquatic Toxicology* 57.1, pp. 39–49.

Lemly, A.D. and G.J. Smith (1988). *Aquatic cycling of selenium: implications for fish and wildlife*.

Luoma, Samuel N. et al. (2000). *Forecasting selenium discharges to the San Francisco Bay-Delta Estuary: ecological effects of a proposed San Luis Drain extension*. US Department of the Interior, US Geological Survey.

McMahon, Gerard and Michael D Woodside (1997). "NUTRIENT MASS BALANCE FOR THE ALBEMARLE-PAMLICO DRAINAGE BASIN, NORTH CAROLINA AND VIRGINIA, 19901." In: *JAWRA Journal of the American Water Resources Association* 33.3, pp. 573–589.

Miller, Lisa D. et al. (2010). *Occurrence and Distribution of Dissolved Solids, Selenium, and Uranium in Groundwater and Surface Water in the Arkansas River Basin from the Headwaters to Coolidge, Kansas, 1970-2009: U.S. Geological Survey Scientific Investigation Report 2010-5069*. Tech. rep. US Geological Survey.

Moore, John E and Leonard A Wood (1967). "Data Requirements and Preliminary Results of an Analog-Model Evaluation—Arkansas River Valley in Eastern Coloradoa." In: *Groundwater* 5.1, pp. 20–23.

Morway, Eric D. et al. (2013). "Modeling variably saturated subsurface solute transport with MODFLOW-UZF and MT3DMS." In: *Groundwater* 51, pp. 237–251.

MSE Technology Applications, Inc. (2001). *Selenium Treatment/Removal Alternatives Demonstration Project. Mine Waste Technology Program Activity III, Project 20*. Tech. rep. National Risk Management Research Laboratory and Federal Energy Technology Center.

Mueller-Price, Jennifer and Timmothy K. Gates (2008). "Assessing uncertainty in mass balance calculation of river nonpoint source loads." In: *Journal of Environmental Engineering* 134.4, pp. 247–258. ISSN: 0733-9372.

Naftz, David L et al. (2008). "Estimation of selenium loads entering the south arm of Great Salt Lake, Utah." In: *US Geological Survey scientific investigations report 5069*.

Nagler, Pamela L. et al. (2010). "Distribution and Abundance of Saltcedar and Russian Olive in the Western United States." In: U.S. Geological Survey. Chap. 2, pp. 7–32.

Navarro-Alarcón, M. and M.C. López-Martínez (2000). “Essentiality of selenium in the human body: relationship with different diseases.” In: *Science of the Total Environment* 249.1, pp. 347–371.

Ohlendorf, Harry M. et al. (1986). “Embryonic mortality and abnormalities of aquatic birds: Apparent impacts of selenium from irrigation drainwater.” In: *Science of The Total Environment* 52, pp. 49–63. ISSN: 0048-9697.

Oliver, Wade et al. (2009). “Estimating selenium removal by sedimentation from the Great Salt Lake, Utah.” In: *Applied Geochemistry* 24.5, pp. 936–949.

Oram, Libbie L. et al. (2008). “Macro- and Microscale Investigation of Selenium Speciation in Blackfoot River, Idaho Sediments.” In: *Environ. Sci. Technol. Environmental Science & Technology* 42.18, pp. 6830–6836. ISSN: 0013-936X.

Painter, Edgar Page (1940). *The Chemistry And Toxicity Of Selenium Compounds, With Special Reference To The Selenium Problem*. North Dakota State University.

Palmer, W.C. (1965). *Meteorological drought resource paper*. Tech. rep. US Weather Bureau.

Plummer, L.N. and W. Back (1980). “The mass-balance approach: Application to interpreting the chemical evolution of hydrologic systems.” In: *American Journal of Science*.

Rantz, S. E. et al. (1982a). *Measurement and Computation of Streamflow: Volume 1. Measurement of Stage and Discharge*. Geological Survey Water-Supply Paper 2175. USGS.

— (1982b). *Measurement and Computation of Streamflow: Volume 2. Computation of Discharge*. Geological Survey Water-Supply Paper 2175. USGS.

Rayman, Margaret P (2000). “The importance of selenium to human health.” In: *The Lancet* 356.9225, pp. 233–241.

Rohwer, Carl (1931). “Evaporation From Free Water Surfaces. Technical Bulletin No. 271.” In: *Bureau of Agricultural Engineering*.

Roman, Marco, Petru Jitaru, and Carlo Barbante (2014). “Selenium biochemistry and its role for human health.” In: *Metallomics* 6.1, pp. 25–54.

Saiki, Michael K., Mark R. Jennings, and William G. Brumbaugh (1993). “Boron, Molybdenum, and Selenium in Aquatic Food Chains from the Lower San Joaquin River and Its Tributaries, California.” In: *Archives of Environmental Contamination and Toxicology* 24, pp. 307–319.

Sauer, Vernon B. and D. Phil Turnipseed (2010). *Stage Measurement at Gaging Stations, Techniques and Methods 3-A7*. Tech. rep. USGS.

Schwarz, Klaus and Calvin M Foltz (1957). “Selenium as an integral part of factor 3 against dietary necrotic liver degeneration.” In: *Journal of the American Chemical Society* 79.12, pp. 3292–3293.

Scott, ML (1973). “The selenium dilemma.” In: *The Journal of nutrition* 103.6, pp. 803–810.

Scott, ML et al. (1967). “Selenium-responsive myopathies of myocardium and of smooth muscle in the young poult.” In: *The Journal of nutrition* 91.4, pp. 573–583.

Smith, David B. et al. (2014). *Geochemical and Mineralogical Maps for Soils of the Continental United States, Open-File Report 2014-1082*. Tech. rep. U.S. Geological Survey.

Sorensen, Mary A., David R. Parker, and John T. Trumble (2009). “Effects of pollutant accumulation by the invasive weed saltcedar (*Tamarix ramosissima*) on the biological control agent *Diorhabda elongata* (Coleoptera: Chrysomelidae).” In: *Environmental Pollution Environmental Pollution* 157.2, pp. 384–391. ISSN: 0269-7491.

Spallholz, Julian E and David J Hoffman (2002). “Selenium toxicity: cause and effects in aquatic birds.” In: *Aquatic Toxicology* 57. State of Science and Future Needs for Selenium Aquatic Criteria, pp. 27–37. ISSN: 0166-445X.

Spiess, Andrej-Nikolai and Natalie Neumeyer (2010). “An evaluation of R₂ as an inadequate measure for nonlinear models in pharmacological and biochemical research: a Monte Carlo approach.” In: *BMC pharmacology* 10.1, p. 6.

State of Colorado (2012). *5 CCR 1002-93. Regulation No. 93 - Colorado’s Section 303(d) List of Impaired Waters and Monitoring and Evaluation List.*

- (2013). *5 CCR 1002-31. Regulation No. 31 - The basic standards and methodologies for surface water.*
- (2014). *5 CCR 1002-32. Regulation No. 32 - Classifications and numeric standards for Arkansas River Basin.*

Sutherland, P Lorenz and John A Knapp (1988). “The impacts of limited water: A Colorado case study.” In: *Journal of Soil and Water Conservation* 43.4, pp. 294–298.

Takayanagi, Kazufumi and George T.F. Wong (1984). “Total selenium and selenium (IV) in the James River estuary and southern Chesapeake Bay.” In: *Estuarine, Coastal and Shelf Science Estuarine, Coastal and Shelf Science* 18.1, pp. 113–119. ISSN: 0272-7714.

Thomas, H.A. et al. (1983). *Methodology for water resource assessment, Report NTIS 84124163.* Tech. rep. U.S. Geological Survey, National Technology Information Service.

Thomson, CD and MF Robinson (1996). “The changing selenium status of New Zealand residents.” In: *European journal of clinical nutrition* 50.2, pp. 107–114. ISSN: 0954-3007.

Thorntwaite, C.W. and J.R. Mather (1955). *The water balance.* Tech. rep. Drexel Institute of Technology, Laboratory of Climatology.

Tinggi, Ujang (2003). “Essentiality and toxicity of selenium and its status in Australia: a review.” In: *Toxicology Letters* 137, pp. 103–110. ISSN: 0378-4274.

USBoR (2008). *Programmatic Biological Assessment: Gunnison River Basin, Colorado: Operations Of The Wayne N. Aspinall Unit; Operations And Depletions Of Existing Reclamation Projects; And Operations And Depletions Of Non-federal Water Development*. Tech. rep. US Bureau of Reclamation.

USDA, Agricultural Research Service (2006). *Selenium-Accumulating Plants*. USDA. URL: <http://www.ars.usda.gov/Research/docs.htm?docid=9979>.

USDA and USDHHS (2010). *Dietary Guidelines for Americans, 2010*. 7th. U.S. Government Printing Office.

USEPA (1992). *Specifications and Guidance for Contaminant-Free Sample Containers*. Publication 9240.0-05A, EPA540/R-93/051, PB93-953316. U.S. Government Printing Office.

– (2009). *National Recommended Water Quality Criteria*. Tech. rep. USEPA.

– (2014a). *Coal Combustion Residual Beneficial Use Evaluation: Fly Ash Concrete and FGD Gypsum Wallboard*. Tech. rep. USEPA.

– (2014b). *External Peer Review Draft Aquatic Life Ambient Water Quality Criterion for Selenium – Freshwater 2014*. Ed. by USEPA. U.S. Government Printing Office.

USGS (2006). *National Water Information System data available on the World Wide Web (USGS Water Data for the Nation)*. URL: <http://waterdata.usgs.gov/nwis/>.

– (2007). *National Water Information System data available on the World Wide Web (USGS Water Data for the Nation)*. U.S. Geological Society. URL: <http://waterdata.usgs.gov/nwis/>.

– (2008). *National Water Information System data available on the World Wide Web (USGS Water Data for the Nation)*. U.S. Geological Society. URL: <http://waterdata.usgs.gov/nwis/>.

- USGS (2009). *National Water Information System data available on the World Wide Web (USGS Water Data for the Nation)*. URL: <http://waterdata.usgs.gov/nwis/>.
- (2010). *National Water Information System data available on the World Wide Web (USGS Water Data for the Nation)*. URL: <http://waterdata.usgs.gov/nwis/>.
- (2011). *National Water Information System data available on the World Wide Web (USGS Water Data for the Nation)*. URL: <http://waterdata.usgs.gov/nwis/>.
- (2012). *National Water Information System data available on the World Wide Web (USGS Water Data for the Nation)*. URL: <http://waterdata.usgs.gov/nwis/>.
- Venables, William N and Brian D Ripley (2002). *Modern applied statistics with S*. Springer Science & Business Media.
- Vicens, Guillermo J., Ignacio Rodríguez-Iturbe, and John C Schaake (1975). “Bayesian generation of synthetic streamflows.” In: *Water Resources Research* 11.6, pp. 827–838.
- Walter, Ivan A et al. (2000). “ASCE’s standardized reference evapotranspiration equation.” In: *Proc. of the Watershed Management 2000 Conference, June*.
- Wanielista, Martin, Robert Kersten, Ron Eaglin, et al. (1997). *Hydrology: Water quantity and quality control*. John Wiley and Sons.
- Wolock, D.M. (2003). *Infiltration-excess overland flow estimated by TOPMODEL for the conterminous United States: U.S. Geological Survey Open-File Report 03-310*. USGS. URL: <http://water.usgs.gov/GIS/metadata/usgswrd/XML/ieof48.xml>.
- World Health Organization et al. (1996). “Trace elements in human nutrition and health.” In:
- Yang, GQ et al. (1983). “Endemic selenium intoxication of humans in China.” In: *The American journal of clinical nutrition* 37.5, pp. 872–881.

Yuretich, R.F. and G.L. Batchelder (1988). "Hydrogeochemical cycling and chemical denudation in the Fort River Watershed,. Central Massachusetts: An approach of mass-balance studies." In: *Water Resources Research* 24.1, pp. 105–114.

Zielinski, RA, Sigrid Asher-Bolinder, and AL Meier (1995). "Uraniferous waters of the Arkansas River valley, Colorado, USA: a function of geology and land use." In: *Applied geochemistry* 10.2, pp. 133–144.

Zielinski, RA, S Asher-Bolinder, et al. (1997). "Natural or fertilizer-derived uranium in irrigation drainage: A case study in southeastern Colorado, USA." In: *Applied Geochemistry* 12.1, pp. 9–21.